ZANCO Journal of Pure and Applied Sciences
The official scientific journal of Salahaddin University-Erbil
https://zancojournals.su.edu.krd/index.php/JPAS

ISSN (print):2218-0230**, ISSN (online):** 2412-3986**, DOI: http://dx.doi.org/10.21271/zjpas**

RESEARCH PAPER

Improved Mixed Neighborhood Tabu Search by Random Selection for Combinatorial Interaction Testing

Imad H. Hasan , Moayad Y. Potrus

Department of Software and Informatics Engineering, College of Engineering , Salahaddin University-Erbil, Kurdistan Region, Iraq.

A B S T R A C T:

Combinatorial interaction testing (CIT) is a technique used to find minimal test suite among configuration options of a System Under Test (SUT) that uses a Covering Array (CA) as a combinatorial structure. CIT is very effective for reducing the costs of the testing process that uses a sampling technique instead of exhaustive testing. This paper proposes the modification of Mixed Neighborhood Tabu Search (RMiTS) algorithm using the random selection strategy. The base MiTS algorithm is originally used for generating t-way Mixed Covering Array (MCA). The modification improves the algorithm performance (running time) to cover all possible input configuration combinations to produce the optimal or near-optimal test suites. The modified algorithm is evaluated through a comparison against the base MiTS algorithm to confirm the performance improvements. Also, it is compared to a state-of-the-art algorithm known as Advanced Combinatorial Test Tool (ACTS) to confirm its efficiency. The experimental results confirm the effectiveness of the modifications that improved the performance for all applied benchmarks, and also it shows that RMiTS is more efficient than ACTS.

KEY WORDS: Combinatorial Interaction Testing, Covering Array, Combinatorial Optimization, Software Testing
DOI: http://dx.doi.org/10.21271/ZJPAS.32.5.1
ZJPAS (2020) , 32(5);1-19 .

1. INTRODUCTION

Software Testing is a very important stage in the process of Software Development Life Cycle (SDLC). A high-quality software needs an exhaustive testing process and large test suites to detect most of the bugs in the developed software. However, exhaustive testing may require higher cost budget and longer development time (Ahmed, 2016).

Instead of exhaustive testing, a sampling technique is used to minimize the size of the test suites. This means, generating a high-quality test suite is a game-changer, that reduces the testing time and development costs without affecting the quality of the software. Eventually, it can detect most of the bugs in less effort. Recently, the demand for high customizable software systems has increased. These type of systems reuses the ready components from a set that belongs to one core to produce newly developed software. Thus, the highly-configurable systems are becoming the direction and the future of software development. Significant reusability of highly-configurable systems notably reduced the development cost (Lin *et al.*, 2016). The highly-configurable systems comprise many ready components that

* **Corresponding Author:**
Imad H. Hasan
E-mail: imad.hadi@su.edu.krd
Article History:
Received: 07/09/2019
Accepted: 07/01/2020
Published: 13/10 /2020

can interact with each other. Each component has many input configurations options. Evidence revealed that software bugs occur during the small number of the interaction of these input configuration options (Kuhn *et al.*, 2013). As mentioned by Cohen *et al.* (2007), the high-configurable systems made the software testing a threat to the quality of software than before, which forces the software tester to exhaustively test the combination of all input options. Therefore, this leads to more time consuming on the testing process that increases the development costs too. Testing all the combinations of parameter values is not always feasible. Instead, a sampling technique is used to detect faults from parameter combinations. This technique called Combinatorial Interaction Testing (CIT) (Cohen *et al.*, 1997, Cohen et al., 2007). It reduces the size of the exhaustive test suite dramatically, in such a way, that cover all possible value combinations at least once.

The CIT techniques are considered as an NP-hard problem (Nie and Leung, 2011). Thus, many approaches have been proposed in the literature to solve this problem. Most two popular approaches are meta-heuristic and greedy, the approaches are either constrained or unconstrained, the systematic literature studies including Nie and Leung (2011) that summarizes an overview of CIT approaches and applications. The book by Kuhn et al. (2013) covers a practical aspect and definitions of CIT.

The above-mentioned studies categories the CIT approaches based on generation strategies into greedy algorithms, meta-heuristic algorithms and mathematical methods. The upcoming paragraph highlights the most relevant works of the first two popular categories.

First, greedy algorithms are widely used algorithms for solving CIT problems. Basically, there are two generation strategies in greedy algorithm one-parameter-at-a-time (OPTAT) and one-test-at-a-time (OTAT). An example of OPTAT is in-parameter-order IPO algorithm that starts by generating CA with only t parameters, then the algorithm extends the CA by adding one parameter at each iteration, there are two types of CA extension of horizontally and vertically consequently, this process is repeated until all t-tuples are covered. The IPO algorithm originally proposed by Lei and Tai (1998) for generating 2-way CA, but it was generalized for t-way CA generator as in-parameter-order-general (IPOG) by Lei *et al.* (2007).

A Combinatorial Test Generation Tool (ACTS) is a tool that presented by Yu *et al.* (2013) that composed of IPOG, IPOG-D, IPOG-F, and IPOG-F2 algorithms; this tool can handle large SUT models including large constraint sets with high interaction strength $t \in \{2-6\}$ that known as the state-of-the-art greedy algorithm.

Another OTAT greedy strategy that constructs CA by generating one test at each iteration until all t-tuple are covered, the purpose of using such a strategy is to cover more t-tuples at each iteration. A popular tool of this strategy is Automatic Efficient Test Generator (AETG) that firstly proposed by Cohen et al. (1997) which was the first greedy algorithm that adopted OTAT strategy and a general framework of OTAT algorithm initiated by Bryce *et al.* (2005). Also, the proposed method uses a greedy OTAT strategy in the initial solution and test case generation as described section in 3.2.1.

Second, the meta-heuristic algorithms which use random guess and evolving solutions with each cycle to reach a solution or best solution (Potrus, 2016), such as Genetic Algorithm (GA) (Ghazi and Ahmed, McCaffrey), Simulating Annealing (SA) (Cohen *et al.*, 2003b, Cohen *et al.*, 2003a, Cohen *et al.*, 2003c), Tabu Search (TS) (Gonzalez-Hernandez and Torres-Jimenez) and Particle Swarm Optimization (PSO) (Ahmed and Zamli, 2011, Ahmed *et al.*, 2012, Kalaee and Rafe, 2016, Ahmed *et al.*, 2017), that have a similar strategy for generating CA, usually starts by constructing a partial or incomplete CA then applies modifications or transformations to it, until it covers all the t-tuples. At each iteration, the algorithm moves toward an unexplored region so that it tries to cover all possible missed t-tuples as much as possible.

Cohen et al. (2003b) used the meta-heuristic Simulating Annealing (SA) algorithm to construct covering arrays for $t \in \{2-3\}$. The SA algorithm first generates an initial solution randomly as an N by k matrix. Then the temperature reduced by a constant value close to one, the cost of the evaluation function is the number of uncovered t-tuples. Within that year, Cohen et al. (2003a) integrated an algebraic construction technique to SA, this approach called Augmented Simulated Annealing.

Gonzalez-Hernandez and Torres-Jimenez (2010) used a tabu search algorithm for generating MCA and their contribution was using the mixture of three neighborhood functions called MiTS, that selects the functions based on a random probability. However this work is improved later in (Gonzalez-Hernandez, 2015), they changed a way of using MiTS to generate smaller MCAs than the best found so far, for interaction strength $t \in \{2-6\}$. The improvements included a parameter tuning based on statistical tests identified the values that significantly affect the performance of MiTS. To verify the efficiency of the proposed improvements, the results of MiTS was compared and analyzed statistically against popular approaches included the best bound MCAs for interaction strength $t \in \{2-6\}$ that have been reported to date in the literature for SA and IPOG algorithms, and others. The improved MiTS showed that there were notable differences between the obtained solutions and the best previously reported bounds.

Besides, Avila-George *et al.* (2012) used the mixed neighborhood functions with SA to construct MCA with $t \in \{2-3\}$. The MCA generation process begins with an initial solution that uses the maximum Hamming-distance among many candidate test cases, in the algorithm uses two neighborhood functions to optimize the MCA matrix.

Ahmed et al. (2012) proposed a Particle Swarm Test Generator (PSTG) to construct a covering array for $t \in \{2-6\}$. PSTG randomly generates test cases and chooses the one that has a maximum interaction coverage that utilizing the PSO with a greedy strategy for identifying the test cases. The main problem of the PSO based algorithms is related to PSO that needs many parameter tunings.

However, the improved MiTS in (Gonzalez-Hernandez, 2015) reported the best bounds (minimum possible test suite sizes). But it still suffers from low performance (long running time). Thus, in this work, we modified the MiTS using random selection strategy into random MiTS (RMiTS), the major modifications targeted the neighborhood functions N_2 and N_3 to improve the performance (reducing running time) of the neighborhood functions with random selection techniques instead of normal sequential selection. However, one of the downsides of the tabu search algorithm is suffering from local minima (Ahmed et al., 2012). To overcome this problem, one of the neighborhood functions is optimized in which the behavior of the evaluation function is modified from local best evaluation into a global best evaluation, that helped the tabu search to diversify the search.

The reminder sections of this paper are structured as follows: Section 2 starts with an example to introduce the combinatorial interaction testing and shows the mathematical notion of CA. Section 3 presents the proposed modifications of the base MiTS algorithm. Section 4 shows the design of experiments and discusses the efficiency and performance evaluation of the proposed method. The final section concludes this paper.

2. MATERIALS AND METHODS

This section presents an overview of the theoretical backgrounds on CIT and how to model the system under test. Alongside that, it explains the general concepts and mathematical notation of combinatorial data structures.

2.1. Combinatorial Interaction Testing

To illustrate the concept of CIT assume there is a System Under Test (SUT) that has a set of k input parameters or configurations such that $P = \{p_1, p_2, .., p_k\}$ and each parameter has a set of n values or options such that $Vp_i = \{v_1, .., v_n\}$ equivalents to the domain of p_i. For this purpose, let us consider Figure 1 as a SUT which is a user interface of Tesla car autopilot settings.

For example, Table 1 shows a model of the SUT, that takes eight configuration parameters, the first five parameters have two values or options, the seventh parameter has three options, and the last parameter has four options. If all the parameter options of the current SUT are exhaustively tested together it will produce $26 \times 31 \times 41 = 768$ test cases, imagine if the only parameter with four options is added to the SUT, the number of test cases will increase to $768 \times 4^1 = 3072$ the test suite size will growth exponentially, which is impossible to apply due to time and budget constraints. Though, a sampling technique such as CIT should be applied to overcome this problem.

CIT is a combination of parameter values, with a specific interaction strength usually denoted as t and the value of $t \in \{2-6\}$. CIT sampling techniques will reduce the number of test cases dramatically for example in the current SUT instead of applying all 768 test cases to cover all possible value combinations it needs only 12 test cases to

cover all possible t-tuple value combinations at least once as shown in Table 2. To understand the interaction strength *t*, let's consider given SUT that receives three parameters each with two values, such that $P = \{P_1, P_2, P_3\}$, and *X* be a function that takes *t* parameter combinations, then computes the cartesian product of their possible values that produces t-tuple sets, for example when $t = 2$ it means the $2 - way$ combination of parameters which is pairwise combination such that $X(P_1,P_2)$, $X(P_1,P_3)$, $X(P_2,P_3)$ as demonstrated in Figure 2.

Table 2 shows a test suite that equivalents to $2-way$ CIT of the SUT in Figure 1 which means the combination of parameters is pairwise, where each column represents an input parameter that contains only values from its domain, and each row represents a test case. This combination structure is called Covering Array (CA) as defined in the next subsection.

2.2. Covering Array (CA)

A Covering array is a mathematical object denoted by $CA(N;t,k,v)$ that is *N* rows by *k* columns (parameters) array. The key feature of a CA is that for every $N \times t$ sub-array, all possible value combination t-tuple sets appear at least once and they considered as covered tuples. where *N* represents the number of tests, *k* is the number of parameters, and each parameter has *v* values, *t* is the interaction strength

A Mixed Covering Array (MCA) denoted by $MCA(N;t,k,Vp_1 \ldots Vp_k)$ is an extended version of CA, the only difference with CA is that domains of the parameters in MCA are non-unified since the domains of the parameters in CA are unified. The values in the i^{th} column belong to the V_{pi} set. for example according to MCA definitions the test suite in Table 2 can be represented as $MCA(12,2,8,2^6 3^1 4^1)$.

3. THE PROPOSED METHOD

This section presents the details and implementation of the proposed method and highlights the improvements and modification to the original mixed neighborhood tabu search. In the upcoming subsections, first, the concept of tabu search algorithm and its properties are explained briefly. Then, it illustrates the steps of the test case generation. Finally, the modifications for the neighborhood functions are implemented.

Algorithm 1: A pseudo-code of a typical Tabu Search algorithm

```
1  T ← φ      // empty tabu list
2  s ∈ S      // candidate solution
3  s_best ← s // assume s is the best soliution
4  T ← s
5  while f(s_best) > 0 do
6      s' ← N(s, T)
7      if f(s') ≤ f(s_best) then
8          s_best ← s'
9      T ← s'
10     s ← s'
```

3.1. Tabu Search

The Tabu Search (TS) algorithm originally proposed by Glover (1986). The TS is a meta-heuristic local search algorithm, the principle idea of TS is the combination of memory to the search algorithm called tabu list (Glover and Laguna, 1999). The tabu list has a queue data structure that keeps a given number of the latest moves carried out to change a current solution s to a new solution s'. When a new solution is obtained, the TS algorithm avoids the moves in the tabu list, then the current move is queued to the tabu list and the very old move is dequeued from the tabu list so that the current move is banned as it lives in the tabu list. However, sometimes the TS allows the moves that live in the tabu list which can produce better solutions than the current best, this is another feature of the TS algorithm known as aspiration criteria. Other two important features of the TS algorithm are intensification and diversification for search strategies, the details can be found here (Glover, 1998). The intensification is a strategy that intensively searches a region where the best solutions found so far to find better solutions. Whereas, the diversification strategy is exploring the unvisited regions from the search space looking forward to a new solution that may vary from those solutions seen before .

The pseudo-code of a very basic TS algorithm is shown in Algorithm 1 that includes the main components of the TS including: 1) initialization s is subset of search space; 2) tabu list queue T; 3) neighborhood function $N(s,T)$ that by which TS moves from current solution s to another new solution s'; 4) the evaluation function $f(s)$; 5) the stop criteria $f(s_{best}) > 0$, in this case, is minimization function. Note that the words move and transformation are used interchangeably in the following sections.

Algorithm 2: An overview pseudo-code of the proposed test generation algorithm

```
Input: SUT(P, V_p, C), strength t, initial CMCA size N, iteration I
Output: complete CMCA M
1 S ← search_space_contruction(SUT(P,V_p,C),t);
2 M ← initialization(N);
3 while not all t-tuple in S are covored do
4     for i ← I to 0 do
5         M ← Tabu_Search(M,I);
6         if all t-tuple in S are covored then
7             stop;
8     if M is not optimized for some iterations then
9         M ← new_row_with_hamming_distance(M);
```

3.2. Test case generation algorithm

An overview of the proposed algorithm can be summarized in Figure 3, at first the algorithm receives the SUT model files, the coverage strength t and initial size of the test suite N, the SUT models files are parameters model file which refers to P and V_p.

Then, the algorithm constructs the search space S which is a two-level hash-table data structure, the first level is the parameters combinations and the second level is the combination or cross-product of their values in the form of t-tuple sets.

Next, the algorithm initializes the partial MCA M matrix of size N from Algorithm 2 see line 6 that calls the initialization function that explained in detail in section 3.2.1. Finally, the tabu

search will start to optimize the initial *M* for *I* iterations and after each tabu search call the algorithm checks for t-tuple coverage, if all t-tuple are covered then the algorithm will stop, otherwise the algorithm will add new random row to *M*, the new row is generated based on Hamming distance to diversify the search see the line 13 and section 3.3.3 for the details, this process is repeated until it covers all the t-tuples in *S* then the algorithm will stop and produces the complete MCA, see lines 7-13. It is worth to mention that the tabu search algorithm uses two neighborhood function to optimize the matrix *M*, the neighborhood functions are selected based on a random probability to explore the search space see section 3.2for the internal steps of each neighborhood function and how the algorithm optimizes the initial *M*.

3.2.1. Initialization

Initialization function takes an initial size of test suite *N* and initializes an empty partial MCA *M* matrix, As the proposed method uses one-test-at-a-time (OTAT) as test generation strategy, the initialization function generates test cases based on the two modes **random generation** and **random t-tuple selection** until the size of the initialized MCA *M* reaches *N* rows. Lastly, it passes the generated MCA *M* for optimization. the following paragraphs describe the two modes of initial generation in detail.

$$hd(r_s) = \sum_{i=1}^{s-1} \sum_{j=1}^{k} g(m_{i,j}, m_{s,j}) \quad (1)$$

$$where \quad g(m_{i,j}, m_{s,j}) = \begin{cases} 1 & m_{i,j} \neq m_{s,j} \\ 0 & otherwise \end{cases}$$

In **random generation** mode, the very first row of the matrix *M* is randomly generated in a way that each value for the parameters p_i is randomly chosen from the V_{pi} set, after that the new row is added to the matrix *M*. Then from the second row, the initialization function generates two new random rows known as candidate rows using the same way as for the first row, but the only difference here is the two candidate rows will not directly be added to the matrix *M* instead the initialization function relies on the hamming distance to choose one of the candidate rows, as demonstrated in Table 3, hamming distance can be computed using Equation 1, which is the summation of a number of different symbols between the candidate row and all current rows in the matrix *M*, so the initialization function computes a hamming-distance for the candidate rows, then a candidate row that has maximum hamming-distance is inserted to matrix *M* with the purpose of diversifying the values in the newly added row from current rows in the matrix, so that to cover as much t-tuples as

Algorithm 3: Initialization function of the proposed Algorithm

```
   Input: N
   Output: partial MCA M
1  let CTuples() = No. of covered t-tuples in S;
2  let UTuples() = No. of uncovered t-tuples in S;
3  let HD(R) = hamming distance from R to M;
4  let random_row() = creates a valid random row;
5  M ← random_row();
6  for i ← 0 to N do
       // random mode
7      if UTuples() < CTuples() then
8          C1 ← random_row();
9          C2 ← random_row();
10         if HD(C1) > HD(C2) then
11             M ← C1;
12         else
13             M ← C2;
14     else
           // selection mode
15         temp_row ← {−1} ∗ size(P);
16         let param_combinations = {set of paramter combinations};
17         while temp_row contatins -1 do
18             foreach combination ∈ param_combinations do
19                 t_tuple ← select_t_tuple(combination);
20                 temp_row[combination] ← t_tuple;
21         M ← temp_row;
```

possible to visit the unexplored regions in the search space, the initialization function repeats this process for a specific number of iterations based on some heuristics such as number of covered and uncovered t-tuples, from the Algorithm 3 see the lines 7-13 that refers to this random mode and the rest of iterations will be generated based on the second mode.

In **random t-tuple selection** mode, this mode in initial solution generation is very simple, first, it initializes a row of -1s, then the selection mode replaces the current -1s from the row with the selected uncovered t-tuples from search space *S*, each time a t-tuple is selected and it will be replaced with *t* -1s in the new row until no -1 will remain in it. This process is repeated until the size of the matrix *M* reaches to *N* rows, see the lines between 15-21.

Algorithm 4: Th second neighborhood function N_2 of base MiTS Algorithm

Input: partial M
Output: optimized M

1 $R_{best} \leftarrow +\infty$;
2 $c \leftarrow select\ random\ column\ 0\ to\ k$;
3 $r \leftarrow 0$;
4 **while** $r < size_o f(M)$ **do**
5 $\quad R \leftarrow M[r]$;
6 $\quad R[c] \leftarrow randomly\ choose\ a\ value\ from\ V_{p_c} \setminus R[c]$;
7 $\quad$ **if** $F(R) \leq F(R_{best})$ **then**
8 $\quad\quad R_{best} \leftarrow f(R)$;
9 $\quad\quad$ **if** $F(R_{best}) = 0$ **then**
10 $\quad\quad\quad$ stop the algorithm;
11 $\quad r \leftarrow r + 1$;

3.2.2. The base neighborhood functions

The mixed neighborhood tabu search MiTS is first proposed by Gonzalez-Hernandez and Torres-Jimenez (2010). The original algorithm uses three neighborhood functions each one has a specific moving strategy as follows: the first one N_1 randomly changes only a value of one cell of the matrix M at each call; the second function N_2 as shown in Algorithm 4, changes the values of randomly selected column for the entire rows at each call that helps the algorithm to move toward a better solution; the third function N_3, firstly it searches for uncovered t-tuples from the search space and selects it, then it replaces the selected t-tuple with the corresponding t-tuple in the matrix M for the entire rows.

The man goal of using such neighborhood functions in tabu search algorithm is to explore the search space that at each function call, it moves from current best solution to a better solution that navigates the search space to find unexplored regions.

In general, N_2 and N_3 takes the partial MCA M as input and tries to transform the rows in M based on their strategy, after each transformation the algorithm evaluates the movement if the search goes toward better solution it is accepted otherwise is rejected. In this case, the evaluation function $F(R)$ is a minimization function. The evaluation is based on the number of covered t-tuple the tabu search continues this process until all t-tuple are covered. The most effective neighborhood functions for exploring the search space and convergence to the final solution are the second N_2 and the third one N_3, but the main problem of them is that they require to mutate the entire rows in the matrix M at each call. However, based on statistical analysis changing the all the rows in matrix M at each call will not guarantee that all the changed rows will produce a better solution see line 7 in Algorithm 4, as a result, this will lead to more time consuming and slow convergence that affects the performance of the algorithm.

To boost the convergence and reducing the running time, naturally, we asked what if randomly a specific number of rows in M are selected to transform instead of the changing entire rows sequentially as shown in Algorithm 4. The analysis of the results showed a notable boost in performance as compared with the base algorithm. The next subsection explains the modifications in detail.

3.3. The Modification

In the proposed method RMiTS the tabu search algorithm only uses the two effective neighborhood function N_2 and N_3 that are modified with random selection strategy, to explore the search space and to move from one state to another state, the tabu search selects one of the neighborhood functions based on the random probability during the search. The next subsection explains the modifications for each neighborhood

function in detail.

Algorithm 5: The improved second neighborhood function N_2 of the proposed RMiTS Algorithm

Input: partial M, number of rows I_{rows}
Output: optimized M

```
1  c ← select random column 0 to k;
2  r ← select random row 0 to N;
3  R_global_best ← the numer of uncovered t − tuples;
4  i ← 0;
5  while i < I_rows do
6      R ← M[r];
7      R[c] ← randomly choose a value from V_pc \ R[c];
8      if F(R) ≤ F(R_global_best) then
9          R_global_best ← f(R);
10         if F(R_best) = 0 then
11             stop the algorithm;
12         i ← i + 1;
13     r ← (r + 1) mod N;
```

3.3.1. Improved second neighborhood function N_2

The N_2 function in RMiTS receives the partial MCA matrix M and the number of rows I_{rows} for modifications (movements). Firstly, The N_2 initializes random row index r and random column index c then the function starts with the r^{th} row R and changes the value of c^{th} column $R[c]$ in a way that randomly chooses a value from V_{pc} except for the current value. Later, the movement R is evaluated if the fitness value is less than or equal to the best global solution, the movement R is accepted and it will be a new global best solution $R_{gloabl\ best}$ otherwise the row index r is sequentially incremented but the column index c is fixed. Finally, the process is repeated for I_{rows} iterations see the Algorithm 5, sometimes the function may converge to zero then it will stop and returns the complete MCA M see the lines (9 to 10).

It is necessary to highlight the modifications here, The first improvement is that the function to starts from a random row and modifies I_{rows} rows see the lines 2,5,6, and 13, instead of starting from the first row and modifying all the rows as shown in Algorithm 4, using this random selection strategy boosted the performance of this function.

The second contribution is that we modified the locality property of the tabu search that allows the search return to the previous or explored regions which means it accepts the moves that worse than R_{best} found from previous function calls see lines 1 and 7 in Algorithm 4, but we modified the N_2 that does not allow the search to return to the worse moves which means a global search and the evaluation function is based globally found $R_{global\text{-}best}$ the total number of uncovered t-tuples among every function calls see the modification at lines 3,8 and 9 in Algorithm 5.

Algorithm 6: The improved third neighborhood function N_3 of the proposed RMiTS Algorithm

Input: partial M, number of rows I_{rows}
Output: optimized M

```
1  T ← {empty tabu list};
2  r ← 0;
3  R_best ← +∞;
4  i ← 0;
5  while i < I_rows do
6      r ← select random row 0 to N \ {T};
7      R ← M[r];
8      R[(t − tuple)] ← randomly choose uncovered t − tuple from S;
9      if F(R) ≤ F(R_best) then
10         R_best ← f(R);
11         if F(R_best) = 0 then
12             stop the algorithm;
13         i ← i + 1;
14     T ← T ∪ {r};
```

3.3.2. Improved third neighborhood function N_3

The third neighborhood function N_2 in RMiTS takes the partial MCA matrix M and the number of rows I_{rows} for movements, Algorithm 6 shows the steps of this function, first N_2 selects a random index or row r except for the indices currently in the tabu list, then the function N_2 starts with the r^{th} row and replaces the randomly selected uncovered t-tuple from the search space S with the corresponded t-tuple indices from R see the line 7, later the new move R is evaluated if the fitness value is less than or equal to the local best solution the move R is accepted and it will be a new local best solution R_{best} and the current row index r is added to the tabu list and it will be a tabu for this function call, for the next iteration a new random row is selected and the process is repeated for I_{rows} iterations, the function N_2 may converge to zero then it will stop and returns the complete MCA M.

The main modification done on this function is based the random selection (random sampling) strategy, the function N_3 randomly select I_{row} rows in matrix M for modifications see the lines 5, 6, 7 and 14 in Algorithm 6, instead of modifying all the rows sequentially. This improvement is very effective to diversify the search process, as a result, the tabu search converged faster than the base algorithm.

4. EVALUATION OF RESULTS AND DISCUSSION

This section is first, describes the benchmarks used to evaluate the efficiency of the proposed method. Second, specifies the tools and approaches that the proposed method is compared against. Then it shows the settings of the experiments. Next, it presents the evaluation of the experiment results. Finally, it presents the effectiveness of the generated test suites through an imperial case study.

4.1. Benchmarks

In the experiments of evaluating the proposed method, we use a specific number of real-world system benchmarks some of them are the exact benchmarks used by Gonzalez-Hernandez (2015) for evaluating the MiTS that found the best bounds so far for unconstrained CIT problem. The most popular benchmarks that are the model of real-world systems including:

1. **Bugzilla** a bug-tracking system.
2. **SPINV** a verifier for SPIN model checker.
3. **SPINS** a simulator for SPIN.
4. **GNU Gzip** which is a popular data compression program in the GNU project.
5. **Android** is an open-source mobile phone operating system.
6. **RFID** is a radio-frequency identification uses electromagnetic fields to automatically identify and track tags attached to objects.
7. **Tesla,** we modelled this benchmark which is taken from autopilot settings of Tesla electric car.
8. **TCAS** a traffic collision avoidance system which is an aircraft collision avoidance system designed to reduce the incidence of mid-air collisions between aircraft.

4.2. Experiment Settings

To perform a fair evaluation, the modified MiTS algorithm and the original MiTS algorithm are both implemented in C# language and compiled with .NET Core version 2.0. We conducted exhaustive experiments for t-way testing, for most of the benchmarks in the experiment we set different values for the control parameters of the tabu search including initial test suite (MCA) size N and the number of rows I_{rows} for the neighborhood functions.

To evaluate the proposed method RMiTS we conduct two set of experiments, in the first set experiment the RMiTS is compared the original MiTS to confirm the efficiency (test suite size) and performance (running time) improvements based on the proposed modifications, the second set experiments the RMiTS is compared to a state-of-the-art t-way CIT generator called Advanced Combinatorial Test Tool (ACTS) proposed by Yu et al. (2013) that implemented in Java language to prove the efficiency (test suite size) of the RMiTS.

All the experiments are executed 20 times for both RMiTS and MiTS but ACTS only executed once as it is a deterministic algorithm that produces the same result in every run. The experiments are executed under macOS environment on a machine with 2.6 GHz Intel Core i7 process and with 16 GB memory.

It is important to note that, for all the experiments, the iteration I of the tabu search algorithm is fixed to 100 for both MiTS and RMiTS. However, the best bounds that found by MiTS as reported in (Gonzalez-Hernandez, 2015), the iteration of the tabu search was set to 1000, as iteration increases the algorithm takes longer running and smaller results. Some of the results of the original MiTS that reported in this paper may not compatible with those reported in (Gonzalez-Hernandez, 2015) because due to lack of similar running environment as the original MiTS was executed in a hybrid cluster with 256 processing nodes with 1056 CPU cores, 2112 GB of memory RAM, but the experiments in this work as mentions above are executed in a personal computer, which this shows another strength of work as achieved many similar results with much more lower cost.

4.3. Results and discussion

This section presents the results of both sets of experiments including the performance and efficiency assessments and discusses the outcomes to evaluate the modifications done in the new algorithm. Table 4 shows the results of the first set of experiments which is an efficiency and performance comparisons between original MiTS and the improved RMiTS, the first column in the table indicates the identification (ID) of the benchmark average execution with a specific strength for both tools MiTS and RMiTS. The second column represents the SUT model and configurations of the real-word benchmarks, the third column is k which is a number of input parameters for each corresponding configuration. The values in column 5 are the average of test suite sizes N of 20 runs of the original MiTS algorithm and column 6 contains the average values of the running times (in seconds) required by the MiTS algorithm to

generate the test suites sizes on column 5. Similarly, the columns 7 and 8 are the average of the test suite size *N* of 20 runs and running time (in seconds) values of the improved algorithm RMiTS. The last two columns represent differences in the size and time respectively between MiTS and RMiTS. In general, the values in the table that are in bold indicate the improvements either in size or in time, the values with a symbol (*) indicate the theoretical best bound and can't be optimized further which is the optimal test suite size.

As mentioned before, this study aimed to improve the performance (reducing running time) of the original MiTS. So, according to the results reported in Table 4, the modified algorithm RMiTS outperforms MiTS in performance for all the benchmarks with different interaction strength *t* without exception as all the values in column 8 in bold, however when the strength $t = 2$ for the benchmarks Mobile Phone, SPINS, Android, RFID, gzip and Tesla the differences of the average running times between MiTS and RMiTS were very small amount of time because for such interaction strength the search space size is very small if compared with the search spaces for higher strengths, thus both algorithms were very fast in generating test suites. As interaction strength goes higher the difference amount of time goes higher too as shown in the last column, especially when interaction strength $t \geq 4$ the percentage of performance improvements between 50% to 75% and the average performance improvements for all the interaction strengths is 52%.

Usually improving the performance of a combinatorial problems costs the efficiency degradation, but the test suites generated with RMiTS as shown in the Table 4 confirm that the efficiency of RMiTS is enhanced for 9 benchmark instances out of 34 as compared with the original MiTS with better performance see the benchmark instances 9, 15, 16, 20, 25, 27, 29 and 34, the positive values in column 9 indicates the difference of test suites sizes between MiTS and RMiTS for the benchmark instances for which the efficiency was enhanced and the enhanced test suite sizes are in bold text in column 7. Remember, RMiTS matched MiTS for 12 benchmark instances that generated the same results but with higher performance especially for benchmark instances 23,24 and 28. Also, both MiTS and RMiTS generated the theoretical best bound test suite sizes for 10 instances that marked with (*) symbol. For the remaining tests, the RMiTS showed poor efficiency as compared with MiTS for 13 benchmark instances but the differences in average test suite sizes between the MiTS and RMiTS is very small, as the differences of 8 benchmark instances out of the 13 benchmark instances are less than one see the column 9 the negative values indicate the poor results, however, the differences are relatively small but don't forget that the RMiTS results have almost higher performance.

The second set of experiments which is a comparison of efficiency only between the improved algorithm RMiTS and a state-of-the-art greedy algorithm ACTS to evaluate the improvements in the efficiency of the modified algorithm. Table 4 shows the comparison of the average test suite sizes generated by RMiTS with test suite sizes generated by the greedy algorithm ACTS for the same benchmarks used in the first set of experiments, the first column in the table represents the benchmark instance identification, the second column is SUT model, the column 3 and 4 indicate the number of inputs parameters and interaction strength respectively, column 5 contains the size *N* of test suite generated by one run of ACTS tool, column 6 represents the average of test suite sizes *N* generated by 20 runs of the improved algorithm RMiTS, and the last column is the differences in size between the two competitors.

The observed results in Table 4 show that the improved RMiTS algorithm generated smaller test suites than ACTS for 23 benchmark instances out of 34 as in bold text in column 6, surprisingly the differences of test sizes between ACTS and RMiTS are incredibly high for interaction strengths $t \geq 4$ see the benchmarks instances 14, 15, 16, 19, 20, 25, 28, 29, 32, 33 and 34 in which the

RMiTS generated significantly smaller test suites. ACST generated smaller test suites only for benchmark instances 8 and 22, but the difference in the size of benchmark instance 22 is very small it is less than 0.5, thus only the benchmark instance 8 can be considerable. The RMiTS and ACTS generated similar results for 9 benchmark instances see the last column the value 0 indicates the similarity of test suite sizes generated by both tools. It is important to be noted, 8 instances of the 9 similar results generated by both tools are the theoretically best bounds that can't be optimized further, thus if we ignore these 8 similar instances, we can say that the RMiTS efficient than ACTS for the 88% of applied benchmark instances.

7. CONCLUSION

In this paper, we present an improvement for mixed neighborhood functions tabu search which is a meta-heuristic search algorithm, for generating t-way mixed covering array (MCA), the main contributions of this research are using random selection strategy for the two neighborhood functions N_2 and N_3 to explore the search space more thoroughly and rapidly.

For evaluating the proposed algorithm, in the experiments, we used different real-world systems with t-way testing to measure the quality of generated test cases. The results showed that RMiTS improved in performance for all the interaction strengths for about 52% as compared with original MiTS. Where running time is reduced without significant effects in the efficiency, also the efficiency of RMiTS still competitive and the test suites generated by RMiTS are significantly higher-quality than one state-of-the-art tool such as ACTS for about 88% of the applied benchmark instances. The result of both sets of experiments showed that the improvements in performance and efficiency are mainly targeted the higher interaction strength $t \geq 4$. As a result, we can say that the aim of this work is met.

As technology growth alongside many real-world system growths too that includes constraints among input configuration, therefore CIT is shifting toward constraints. The main future challenges for this research are investigating the search space and time optimizations with the presence of constraints. It is worth to mention that our approach is unable to generate the MCA for benchmarks that have more than 100 parameters for interaction strengths $t \geq 4$ due to the full memory footprint, many strategies that can be used to reduce the memory occupation of the MCA data structure, such as compression techniques or using different strategy for storing the t-tuples sets. However, this might affect the running time but there is a possibility to optimize the running time by implementing our approach in a parallel computing environment such as Compute Unified Device Architecture (CUDA) (Ploskas *et al.*, 2016) which is C/C++ language based framework runs on NVIDA Graphics Processing Unit (GPU), or using GPU programming with Matlab (Schmidt *et al.*, 2018).

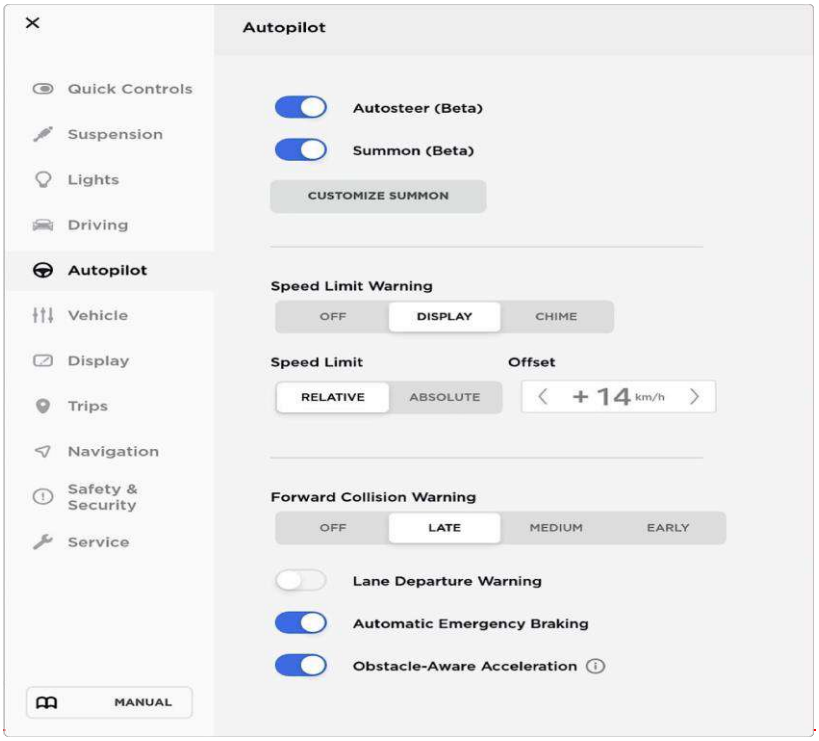

Figure 1: GUI of Tesla electric car autopilot settings

Table 1: Input parameters and their values of Tesla electric car autopilot settings

#	**Parameter**	**Values**
1	Autosteer	off, on
2	Summon	off, on
3	Lane Departure Warning (LDW)	off, on
4	Automatic Emergency Breaking (AEB)	off, on
5	Obstacle-Aware Acceleration (OAA)	off, on
6	Speed Limit (SL)	relative, absolute
7	Speed Limit Warning (SLW)	off, display, chime
8	Forward Collision Warning (FCW)	off, late, medium, early

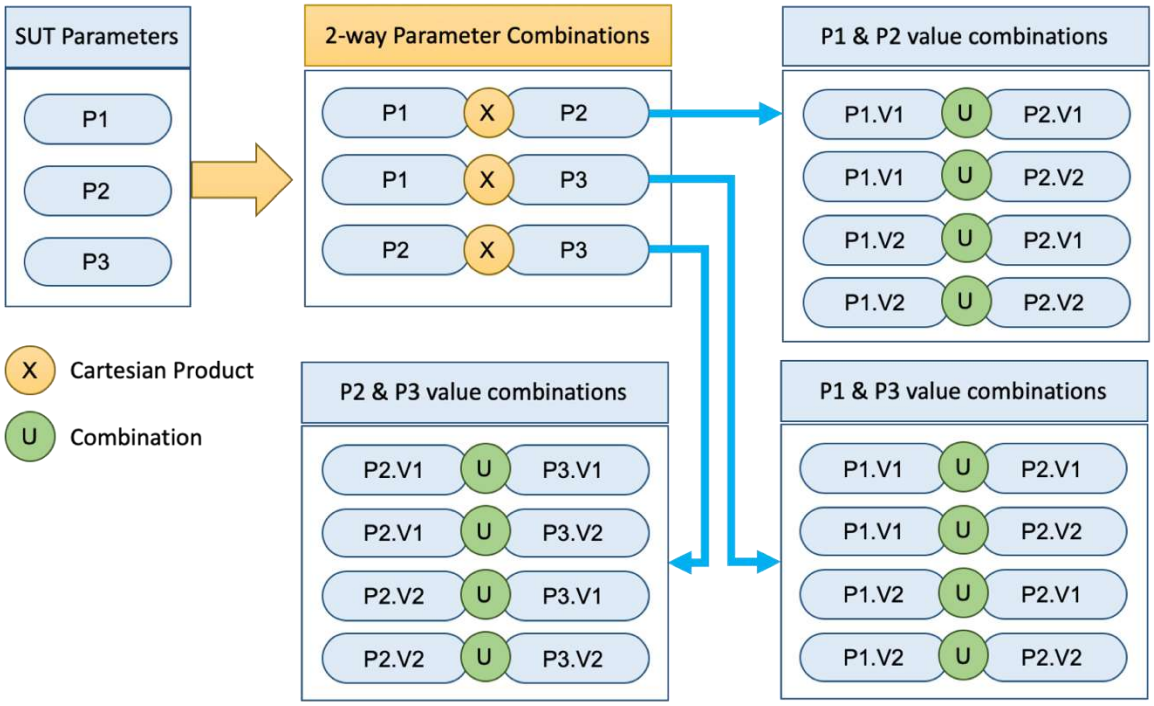

Figure 2: Modeling a 2-way CIT

Table 2: 2-way test suite of Tesla electric car autopilot settings

#	Autosteer	Summon	LDW	AEB	OAA	SL	SLW	FCW
1	on	on	off	off	on	absolute	chime	Medium
2	off	off	on	on	on	absolute	display	Late
3	on	on	on	on	on	absolute	off	Off
4	on	on	off	off	off	relative	chime	Late
5	off	off	on	on	on	absolute	chime	Early
6	off	on	off	on	off	relative	display	Early
7	off	off	on	off	off	relative	off	Medium
8	off	off	off	on	off	relative	chime	Off
9	off	off	on	on	off	relative	display	Medium
10	on	off	off	off	off	absolute	off	Early
11	on	on	on	off	on	relative	display	Off
12	on	on	off	off	off	relative	off	Late

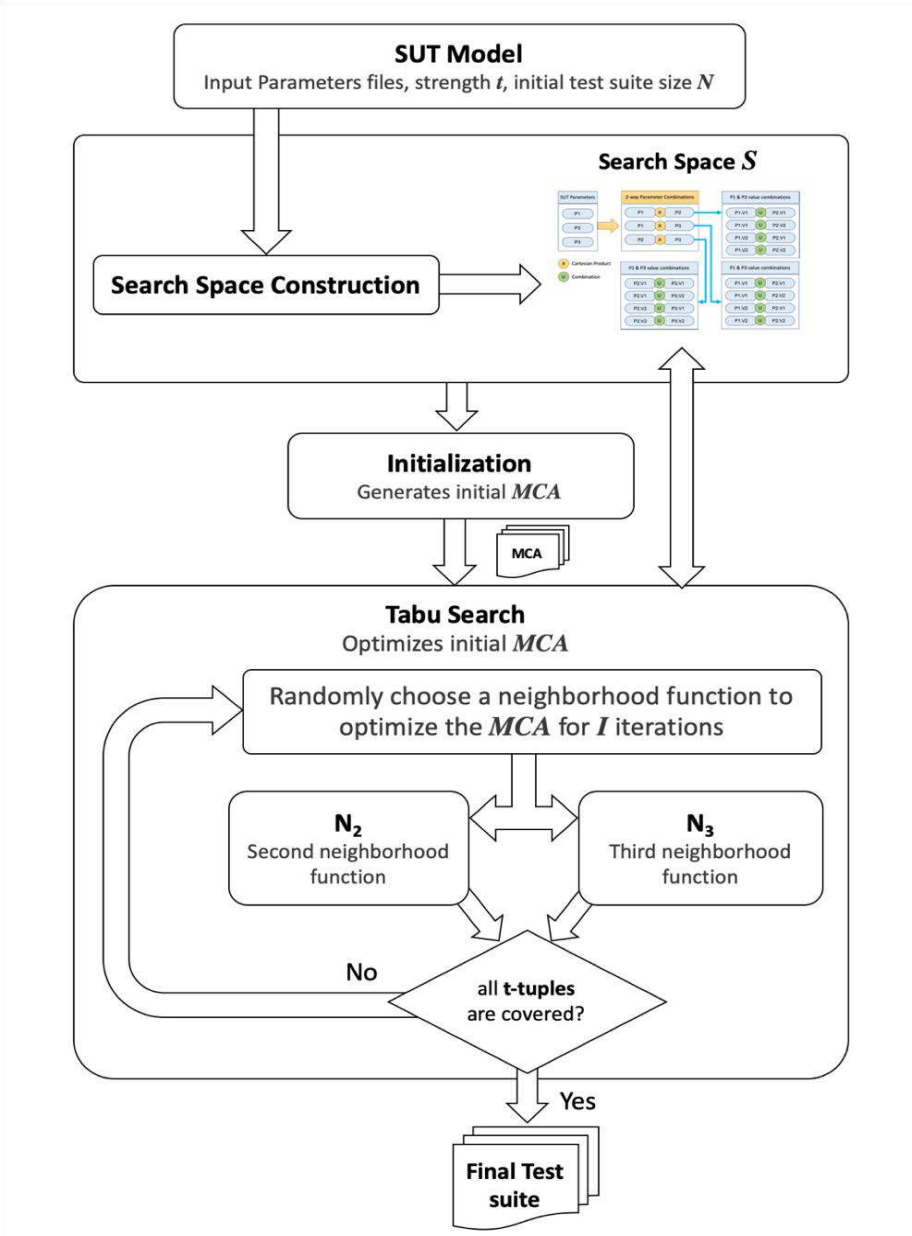

Figure 3: An overview block diagram of the proposed method

Table 3: Computing Hamming Distance for candidate rows

Test	P1	P2	P3	
R1	0	1	0	
C1	1	1	0	$hd(C1) = 1$
C2	0	0	1	$hd(C1) = 2$
R2	0	0	1	$C2$ is selected as a next row

Table 4: Efficiency(size) and performance(time in seconds) comparison between original MiTS and modified RMiTS, ***k*** refres to a number of paarameters in the benchmarks and ***t*** is an interaciton strength.

#	Benchmarks	k	t	Base MiTS		Improved RMiTS		Δ size	Δ time(s)
				Avg. size	Avg. time(s)	Avg. size	Avg. time(s)		
1	Mobile Phone	5	2	9*	0.04	9*	**0.03**	0	0.01
2	$3^3 2^2$		3	27*	0.40	27*	**0.22**	0	0.18
3			4	54*	0.34	54*	**0.17**	0	0.17
4			5	108*	1.20	108*	**0.41**	0	0.79
5	Bugzilla	52	2	17.50	4.86	**16.75**	**1.43**	0.75	3.43
6	$4^2 3^1 2^{49}$		3	59.80	2415.98	60.40	**1092.64**	-0.60	1323.34
7	SPIN simulator	18	2	18.60	0.89	19	**0.53**	-0.40	0.36
8	$4^5 2^{13}$		3	87.25	150.10	88.60	**62.57**	-1.35	87.53
9			4	345	14712.20	**337**	**4797.25**	8	9914.95
10	SPIN verifier	55	2	28	19.17	28.25	**12.05**	-0.25	7.12
11	$4^1 13^2 2^4 2$		3	151	4820.82	154.50	**2967.75**	-3.50	1853.07
12	Android	9	2	25.40	0.45	25.60	**0.25**	-0.20	0.20
13	$5^2 4^4 3^3$		3	131.20	54.48	132	**22.41**	-0.80	32.07
14			4	593.50	910.12	596.40	**472.50**	-2.90	437.62
15			5	2449.50	16087.85	**2426**	**7813.74**	23.50	8274.12
16			6	8308	144976.62	**8236**	**46652.35**	72	98324.27
17	RFID	11	2	33.60	1.14	34.80	**0.68**	-1.20	0.46
18	$5^7 2^4$		3	212	103.49	216	**62.29**	-4	41.20
19			4	1124.67	5649.59	1132.50	**4080.29**	-7.83	1569.30
20			5	5332	239766.95	**5316**	**119330**	16	120436.95
21	gzip	8	2	90*	3.48	90*	**2.67**	0	0.80
22	$10^1 9^1 2^6$		3	180*	21.87	180.20	**8.78**	-0.20	13.09
23			4	540	378.72	540	**209.86**	0	168.86
24			5	1080	1164.93	1080	**418.59**	0	746.34
25			6	1924.50	1601.92	**1911.67**	**400.85**	12.83	1201.07
26	TCAS	12	2	100*	6.36	100*	**1.48**	0	4.88
27	$10^1 4^1 3^2 2^7$		3	401.8	150.33	**400***	**32.81**	1.80	117.52
28			4	1206	7744.95	1206	**3221.52**	0	4523.43
29			5	3800	216248.35	**3754**	**58242.54**	46	158005.81
30	Tesla	8	2	12*	0.13	12*	**0.09**	0	0.04
31	$4^1 3^1 2^6$		3	28*	1.50	28*	**1.18**	0	0.32
32			4	72*	21.50	72*	**11.71**	0	9.79
33			5	144	30.47	144.50	**11.23**	-0.50	19.24
34			6	257.25	31.93	**257.20**	**9.43**	0.05	22.51

Table 5: Efficiency(size) comparison between RMiTS and state-of-the-art tool ACTS, k refers to a number of parameters in the benchmarks and t is an interaction strength

#	Benchmarks	k	t	ACTS	RMiTS	Δ size
				size	Avg. size	
1	Mobile Phone	5	2	9*	9*	0
2	$3^3 2^2$		3	27*	27*	0
3			4	54*	54*	0
4			5	108*	108*	0
5	Bugzilla	52	2	18	**16.75**	1.25
6	$4^2 3^1 2^{49}$		3	67	**60.40**	6.60
7	SPIN simulator	18	2	24	**19**	5
8	$4^5 2^{13}$		3	**79**	88.60	-9.60
9			4	343	**337**	6
10	SPIN verifier	55	2	33	**28.25**	4.75
11	$4^1 13^2 2^4 2$		3	159	**154.50**	4.50
12	Android	9	2	29	**25.60**	3.40
13	$5^2 4^4 3^3$		3	139	**132**	7
14			4	631	**596.40**	34.60
15			5	2582	**2426**	156
16			6	9107	**8236**	871
17	RFID	11	2	45	**34.80**	10.20
18	$5^7 2^4$		3	239	**216**	23
19			4	1292	**1132.50**	159.50
20			5	6030	**5316**	714
21	gzip	8	2	90*	90*	0
22	$10^1 9^1 2^6$		3	**180***	180.20	-0.20
23			4	634	**540**	94
24			5	1080	1080	0
25			6	2520	**1911.67**	608.33
26	TCAS	12	2	100*	100*	0
27	$10^1 4^1 3^2 2^7$		3	400*	400*	0
28			4	1359	**1206**	153
29			5	4233	**3754**	479
30	Tesla	8	2	12*	12*	0
31	$4^1 3^1 2^6$		3	32	**28***	4
32			4	92	**72***	20
33			5	172	**144.50**	27.50
34			6	336	**257.20**	78.80

References

AHMED, B. S. 2016. Test case minimization approach using fault detection and combinatorial optimization techniques for configuration-aware structural testing. *Engineering Science and Technology, an International Journal*, 19**,** 737-753.

AHMED, B. S., GAMBARDELLA, L. M., AFZAL, W. & ZAMLI, K. Z. 2017. Handling constraints in combinatorial interaction testing in the presence of multi objective particle swarm and multithreading. *Information and Software Technology*, 86**,** 20-36.

AHMED, B. S. & ZAMLI, K. Z. 2011. A variable strength interaction test suites generation strategy using Particle Swarm Optimization. *Journal of Systems and Software*, 84**,** 2171-2185.

AHMED, B. S., ZAMLI, K. Z. & LIM, C. P. 2012. Constructing a t-way interaction test suite using the particle swarm optimization approach. *International Journal of Innovative Computing, Information and Control*, 8**,** 431-452.

AVILA-GEORGE, H., TORRES-JIMENEZ, J., HERNÁNDEZ, V. & GONZALEZ-HERNANDEZ, L. 2012. Simulated Annealing for Constructing Mixed Covering Arrays. Springer, Berlin, Heidelberg.

BRYCE, R. C., COLBOURN, C. J. & COHEN, M. B. A framework of greedy methods for constructing interaction test suites. 2005 New York, New York, USA. ACM Press, 146-146.

COHEN, D. M., DALAL, S. R., FREDMAN, M. L. & PATTON, G. C. 1997. The AETG system: an approach to testing based on combinatorial design. *IEEE Transactions on Software Engineering*, 23**,** 437-444.

COHEN, M. B., COLBOURN, C. J. & LING, A. C. H. Augmenting simulated annealing to build interaction test suites. 2003 2003a. IEEE, 394-405.

COHEN, M. B., DWYER, M. B. & SHI, J. Interaction testing of highly-configurable systems in the presence of constraints. 2007 2007 New York, New York, USA. ACM Press, 129-129.

COHEN, M. B., GIBBONS, P. B., MUGRIDGE, W. B. & COLBOURN, C. J. Constructing test suites for interaction testing. 2003 2003b. IEEE, 38-48.

COHEN, M. B., GIBBONS, P. B., MUGRIDGE, W. B., COLBOURN, C. J. & COLLOFELLO, J. S. A variable strength interaction testing of components. 2003 2003c. IEEE Comput. Soc, 413-418.

GHAZI, S. A. & AHMED, M. A. Pair-wise test coverage using genetic algorithms. 2003. IEEE, 1420-1424.

GLOVER, F. 1986. Future paths for integer programming and links to artificial intelligence. *Computers and Operations Research*, 13**,** 533-549.

GLOVER, F. 1998. Tabu Search: A Tutorial. *Interfaces*, 20**,** 74-94.

GLOVER, F. & LAGUNA, M. 1999. *TABU search*, Kluwer Academic Publishers.

GONZALEZ-HERNANDEZ, L. 2015. New bounds for mixed covering arrays in t-way testing with uniform strength. *Information and Software Technology*, 59**,** 17-32.

GONZALEZ-HERNANDEZ, L. & TORRES-JIMENEZ, J. 2010. MiTS: A new approach of tabu search for constructing mixed covering arrays. 2010. Springer, Berlin, Heidelberg, 382-393.

KALAEE, A. & RAFE, V. 2016. An Optimal Solution for Test Case Generation Using ROBDD Graph and PSO Algorithm. *Quality and Reliability Engineering International*, 32**,** 2263-2279.

KUHN, D. R., KACKER, R. N. & LEI, Y. 2013. *Introduction to combinatorial testing*, CRC Press.

LEI, Y., KACKER, R., KUHN, D. R., OKUN, V. & LAWRENCE, J. 2007. IPOG: A general strategy for T-way software testing. 2007/03//. IEEE, 549-556.

LEI, Y. & TAI, K. C. 1998. In-parameter-order: A test generation strategy for pairwise testing. 1998/11//. IEEE Comput. Soc, 254-261.

LIN, J., LUO, C., CAI, S., SU, K., HAO, D. & ZHANG, L. TCA: An efficient two-mode meta-heuristic algorithm for combinatorial test generation. 2016/11// 2016. IEEE, 494-505.

MCCAFFREY, J. D. Generation of Pairwise Test Sets Using a Genetic Algorithm. 2009. IEEE, 626-631.

NIE, C. & LEUNG, H. 2011. A survey of combinatorial testing. *ACM Computing Surveys*, 43**,** 1-29.

PLOSKAS, N., SAMARAS, N., PLOSKAS, N. & SAMARAS, N. 2016. Introduction to GPU programming in MATLAB. *GPU Programming in MATLAB***,** 71-107.

POTRUS, Y. M. 2016. Maintenance Scheduling Optimization for Electrical Grid Using Binary Gray Wolf Optimization Technique. *ZANCO Journal of Pure and Applied Sciences*, 28.

SCHMIDT, B., GONZÁLEZ-DOMÍNGUEZ, J., HUNDT, C., SCHLARB, M., SCHMIDT, B., GONZÁLEZ-DOMÍNGUEZ, J., HUNDT, C. & SCHLARB, M. 2018. Compute Unified Device Architecture. *Parallel Programming***,** 225-285.

YU, L., LEI, Y., KACKER, R. N. & KUHN, D. R. ACTS: A combinatorial test generation tool. 2013/03//. IEEE, 370-375.

ZANCO Journal of Pure and Applied Sciences
The official scientific journal of Salahaddin University-Erbil
https://zancojournals.su.edu.krd/index.php/JPAS

ISSN (print):2218-0230**, ISSN (online):** 2412-3986**, DOI: http://dx.doi.org/10.21271/zjpas**

RESEARCH PAPER

Power Quality Measures of Non-Ideal 3-phase Diode Rectifiers and Smoothing Circuits

Faraidun W Ahmad[1], Farhad M. Mahmood[1]

[1]Department of Physics, College of Science, University of Halabja-Halabja, Kurdistan Region, Iraq

A B S T R A C T:

The study of the rectifier LC smooth circuit to minimize the total harmonic distortion (THD) of three phase of non-ideal diode rectifier has been proposed. The input line current has a non- sinusoidal shape and contains harmonic, which has a negative effect on the input power quality and it makes much stress on the load. According to the International Electrotechnical Commission (IEC61000) standards, variety harmonic limitations are defined to be regulated. In this paper, the cost effective solutions such as changing different parameters including load resistance, DC capacitance and inductance and input AC inductance, on the rectifier performance in terms of V load mean, ripple, diode and Capacitor RMS current, fundamental current and considering relevant harmonics up to 1 kHz and the load side voltage (mean value and ripple) have been investigated to find a best way to reduce ripple voltage stress and harmonics. It has been founded that the best way to obtain high V_{load} mean and fewer ripple is increasing the DC-link Inductance. The major purpose here is to reduce the Total Harmonic Distortion (THD) of the line current under different load conditions (from 61.33% to 26.87%).

KEY WORDS: Three phase rectifier, Total Harmonic Distortion (THD), Ripple, Power quality
DOI: http://dx.doi.org/10.21271/ZJPAS.32.5.2
ZJPAS (2020) , 32(5);20-25 .

1. INTRODUCTION

In last decades, the request for devices which convert AC-DC signals have been increased rapidly, in particularly demands for using power converters in the field of High Voltage Direct Current (HVDC) and high-power machine drives (Mohan, N. and Undeland, T.M., 2007, Hui et al. 2000). Converters can be used for control frequency and voltage deviation, and decreasing total harmonic distortion (THD) (Mohan, N. and Undeland, T.M., 2007).

The main issues in such low power converter is how to minimizing the THD and ripple while increasing the mean load voltage [Hui et al. 2000 and Singh et al. 2004], therefore in recent years, researchers have focused on improving power quality of the rectifier by reducing total harmonic distortion (THD) throughout changing circuit's parameters as a reliable solution [Krismadinata et al 2009, Ivensky, G. and Ben-Yaakov, S., 2001, and Du et al. 2011]. Recently a huge developments and control techniques have been presented to reduce THD [Ameen, H.F. and Ibrahim, Aula, F.T., 2016, B.S., 2016, Ivensky, G. and Ben-Yaakov, S., 2001, and Du et al. 2011]. In this paper an analysis have been done to minimize the total harmonic distortion (THD) of three phase of non-ideal diode rectifier to an acceptable value by changing different parameters such as, Load

* **Corresponding Author:**
Faraidun W Ahmad
E-mail: faraidun.ahmad@uoh.edu.iq
Article History:
Received: 19/11/2019
Accepted: 01/03/2020
Published: 13/10 /2020

resistance, DC capacitance, AC side inductance and DC inductance. In addition the output signal of each case will be assessed individually based on that mentioned criteria.

Power simulation programing (PSIM Version 12.0.3.0.564) has been used to design the Circuit diagram of three phase non-ideal rectifier. PSIM software is a powerful computer programing for designing and simulation of all electrical and electronic circuits which helps researchers to be able to analyze results in various scenarios through changing parameters value according to the circuit's requirements [Mehar, H. 2013, Kamiriski et al. 2004]. Authors have investigated Rectifier at full load, Rectifier at reduced load, Increasing DC capacitance, Increasing AC side inductance (Capacitive Smooth Only), Increasing DC inductance, and Increasing AC Inductance, moreover; summary of each case has been explained in the performances of all the cases.

2. Circuit Diagram Of The Rectifier

The circuit diagram of the three phase non-ideal diode rectifier is shown in the fig. (1), the circuit is designed through PSIM Simulation tools.

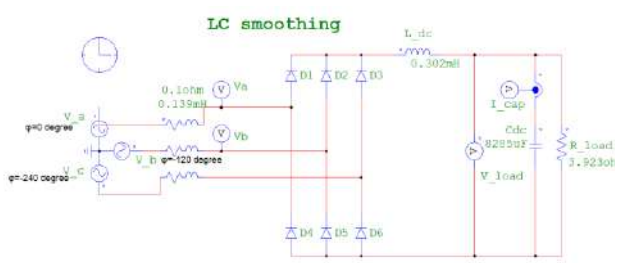

Figure 1: Three phase non-ideal diode rectifier

The above circuit diagram with the input line voltage of 338.4 V while the frequency is 50 Hz contains AC and DC inductances, and DC capacitance, based on that circuit, from the time domain analysis the following parameters have been calculated namely; the load voltage (mean voltage), load ripple voltage, diode peak current, and RMS grid current at the frequency of 300 Hz, while from the Fast Fourier Transform (FFT), the fundamental current up to 19th harmonics will be shown, simultaneously by using that parameters distortion factor and THD can be found, as well as the others. To provide more details and to be concise only three major expressions have been included apart from case A, which full details have been given, therefore; following sections will clarify each case individually.

A- Rectifier at full load

For the circuit as shown in figure (1) with the input voltage (338.4 V, 50 Hz) and output load (R=3.923 ohm, C=8285µF).

From the time domain analysis

1-V load (mean) = $\frac{V\ peak\ (Max)+V\ peak\ (Min)}{2}$

V load mean = $\frac{531.0106+526.207}{2}$ = **528.6088 V**

2-V load (Ripple) =

V peak (Max) − V peak (Min)

V load (Ripple) = 531.0106 − 526.207 = **4.8036 V**

3- Diode Peak Current[A] = **168.929[A]**

4- Cdc (300Hz) RMS Grid Current [A] = **36.704 A.**

From **FFT** Analysis

5- Fundamental RMS Grid Current Line A [Ia] = **105.834 A**

Fundamental peak Grid Current Line A [Ia] = **149.6734A**

nth Harmonic current [%] = [nth Harmonic current (A)/Fundamental current (A)] ∗ 100

3rd Harmonic Current [%] = **0.29360%**

5th Harmonic Current [%] = **30.1041%**

7th Harmonic Current [%] = **9.4677%**

9th Harmonic Current [%] = **0.1346%**

11th Harmonic Current [%] = **7.1077%**

13th Harmonic Current [%] = **4.0085%**

15th Harmonic Current [%] = **0.1213%**

17th Harmonic Current [%] = **3.2888%**

19th Harmonic Current [%] = **2.3962%**

To calculate Total Harmonic Distortion [THD]

$THD=100\sqrt{1-DF^2}$, $DF=\frac{\text{Fundamental RMS current}}{\text{Total RMS Current}}$

Fundamental RMS current input = 149.6734/ $\sqrt{2}$ = **105.8350 A**

Total RMS input current = **111.5095 A**

DF = (105.8350 / 111.5095) = 0.9491

$THD=100\sqrt{1-DF^2} = 100\sqrt{1-0.9491^{\,2}}$ = **31.4974%**

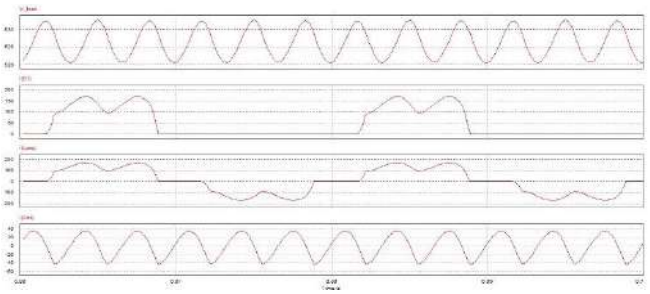

Figure 2: Time domain wave form of (V load, Ia Diode, Ia line, I Cdc) CASE A

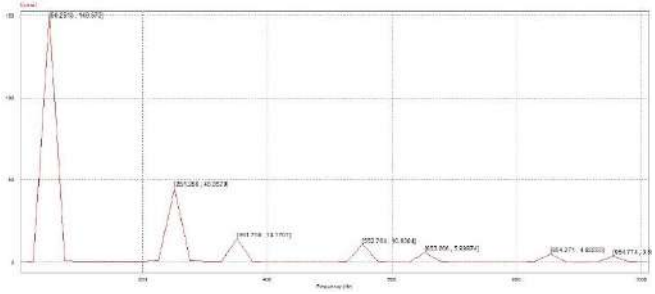

Figure 3: FFT wave form of (Ia line) CASE A

As it can be seen from the fig.2, there is a remarkable ripple, which is calculated around 4.8036 V that makes a problem for the power quality. High ripple means low power quality [Lee et al. 2017]. on another hand, Fig (3) shows that the 5th harmonic value is very high compared with the fundamental harmonic, and then this leads to increase the THD which is 31.4974%. This is due to the fact of having capacitor and inductor in the circuit which are increasing reactive power and it cannot be canceled out [Zobaa, A.F. et al, 2018], therefore we are moving to another case to resolve that problems.

B- Resistance (R) load reduced

When $R\ load\ reduced\ = \frac{R\ load\ at\ full\ load}{5}$, the both ripple voltage and average voltage across the load will change accordingly, due to the short space in this paper, only three significant expression have been presented in this section:

V load (Ripple) = **3.9449 V**

V load (mean) = **555.0998 V**

THD= **61.3364 %**

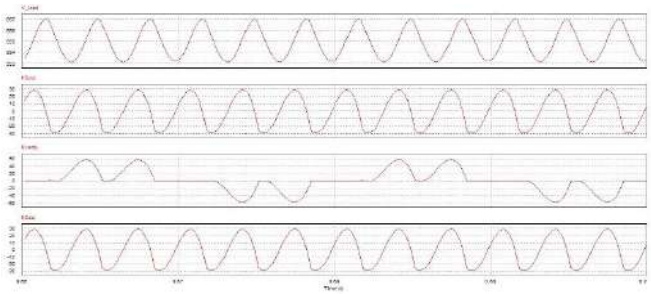

Figure 4: Time domain wave form (V load, Ia Diode, Ia line, I Cdc) CASE B

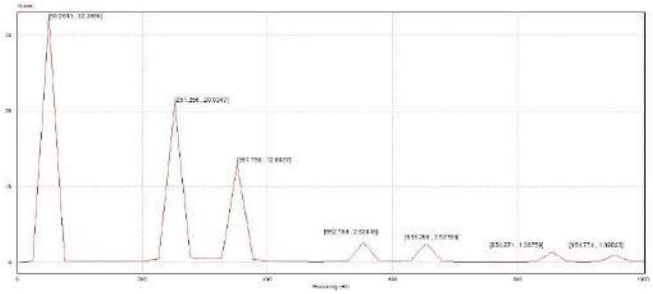

Figure 5: FFT wave form of (Ia line) CASE B

the above figures (fig. 4 and fig.5) shows that, when the load is reduced (increase resistance), the load current reduces as well. Thus, the ripple voltage decreases from 4.8036V at case A to 3.9449V. Similarly, reducing load current is also proportional to the line voltage drop. In another word, ripple voltage of the line decreases and the V load (mean) increases to 555.1V. However, the power quality is appearing to be very bad THD = 61.3364%, which is not desired.

C- Increasing DC-link Capacitance

This time the value of DC capacitance will be four times the values of this capacitance at full load case ($Cdc\ new\ = 4\ Cdc\ at\ case\ A$), the parameters will modify as follows:

V load (Ripple) = **1.759 V**

V load (mean) = **528.4983 V**

THD= **31.0724 %**

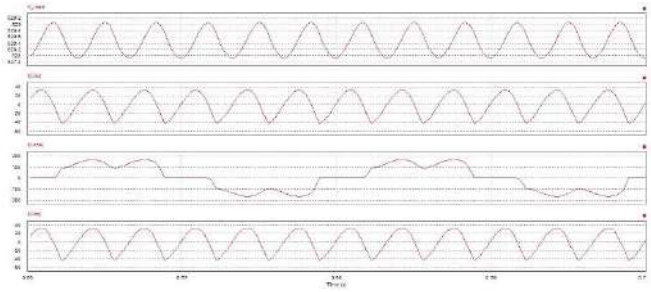

Figure 6: Time domain wave form (V load, Ia

Diode, Ia line, I Cdc) CASE C

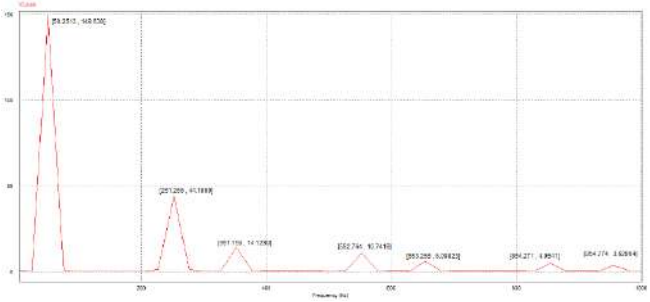

Figure 7: FFT wave form of (Ia line) CASE C

The capacitor always attempts to smooth the output voltage (Mayordomo et al. 2014); it means (fewer ripples). By increasing the capacitance, the ripple reduces from **4.8036V** at case A to **1.759V**, and the capacitor RMS current is also decreasing. The V load (mean) and the diode current is the same as case A, with a better THD=**31.0724 %**

D- ALL Inductance ONLY on AC side

In this occasion, the DC side inductance will be eliminated (Ldc=0), and AC side inductance will be increased by half the ratio of the DC link inductance ($Lac - new = Lac\ at\ case\ A + 0.5 * Ldc\ at\ case\ A$), then the results will appear as below.

V load (Ripple) = **5.579 V**

V load (mean) = **522.6375 V**

THD= **34.9865 %**

It is obvious that most of the ripple voltage is indirectly drops across (Ldc). When Ldc is not connected, the ripple voltage rises to **5.579V.** The diode current is slightly higher than Case A, while capacitor RMS current is still lower. And increasing (Lac) means more line voltage drop. Hence, the V load mean decreases to **522.638V** compared to case A. THD= **34.9865%,** which is higher than case A.

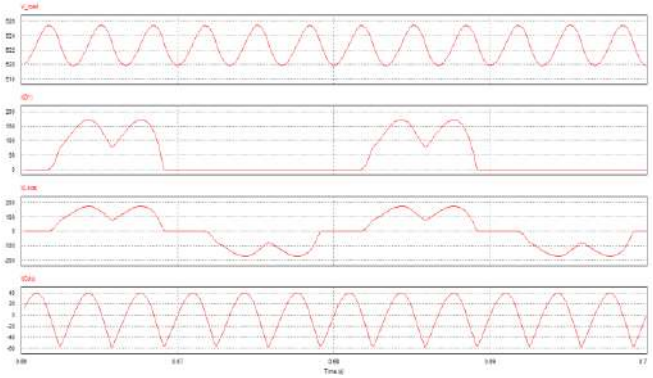

Figure 8: Time domain wave form (V load, Ia Diode, Ia line, I Cdc) CASE D

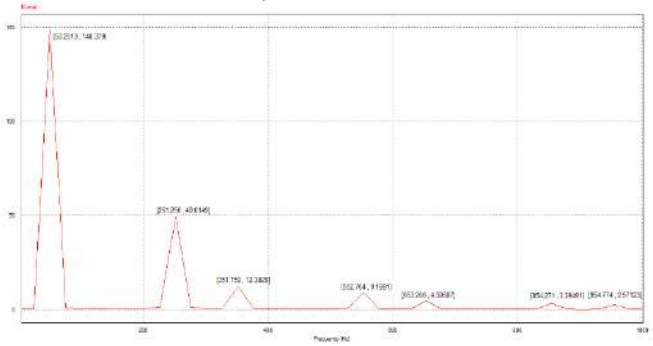

Figure 9: FFT wave form of (Ia line) CASE D

E- Increasing DC-Link Inductance

This case, the new DC side inductance will be three times the DC side inductance (Ldc –new= 3*Ldc at case A), the values for the previous expressions will be as:

V load (Ripple) = **2.2454 V**

V load (mean) = **528.6661 V**

THD= **26.8785 %**

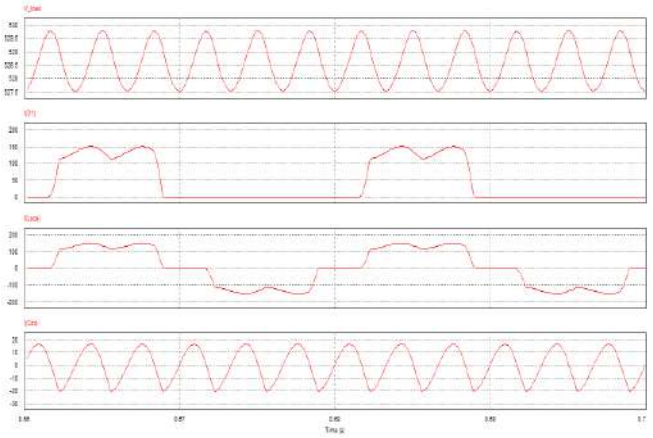

Figure 10: Time domain wave form (V load, Ia Diode, Ia line, I Cdc) CASE E.

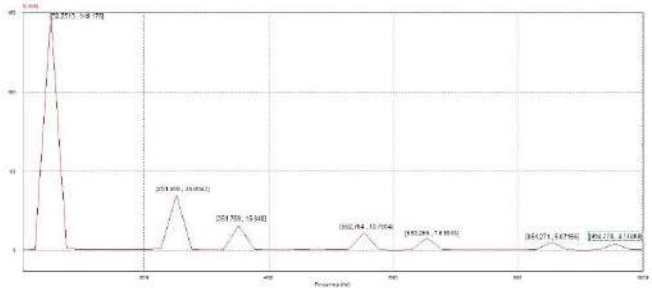

Figure 11: FFT wave form of (Ia line) CASE E.

More ripple voltage drop is obtained by increasing (Ldc), The ripple voltage is reduced to **2.2454 V** which is less than A&D. The diode and capacitor RMS current is less than A&D, and Vload (mean) is the same as A because the Voltage does not drop on Ldc [Prakash et al. 2018, Ertl, H. and Kolar, J.W., 2005]. The power quality is improved and THD=**26.8785%,** which is much better than case A&D.

F- Increasing AC Side Inductance

In the last case AC inductance values will be changed as

(Lac-new= Lac at case A + Ldc at case A), then the three major parameters will change as its shown:

V load (Ripple) = **2.7532 V**

V load (mean) = **517.2288 V**

THD= **26.0773 %**

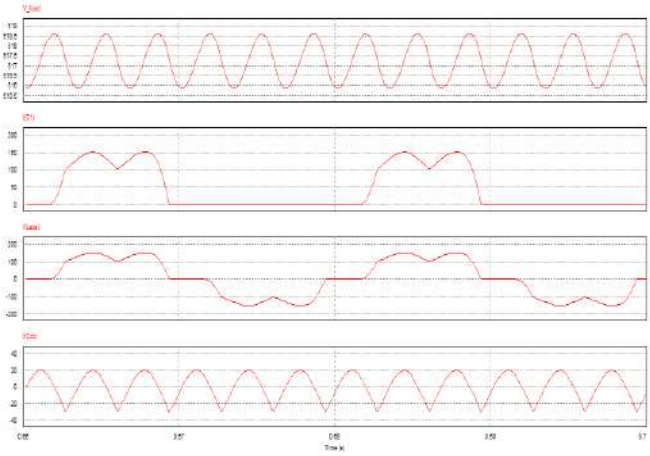

Figure 12: Time domain wave form (V load, Ia Diode, Ia line, I Cdc) CASE F.

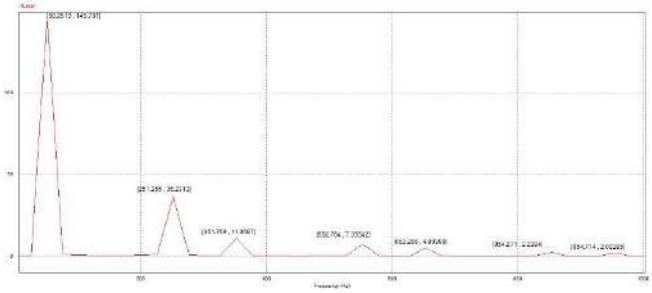

Figure 13: FFT wave form of (Ia line) CASE F.

The higher the value of AC side inductance, leads to the lower the Vload mean=**517.2288 V**, because of the high line voltage drops, and ripple is also lower **2.7532 V** than A, D and greater than E, due to high line inductance. Similarly, the diode current is much lower than A, D and the same as E. Capacitor RMS current is higher than E. THD=**26.0773 %,** which is the lowest value compared to other cases. However, the low Vload mean is not desirable.

3. Performances of analysis

Determining the best case among (A-F) will be based on input power quality and load performance. Results have shown that the voltage does not drop on DC link inductor, and most of the ripple voltage falls on DC Inductor. In another word, high Vload mean and fewer ripples can be obtained by increasing the DC-link Inductance, which is highly preferable by the designers to improve TDH. Therefore, results have proved that increasing the DC-link inductance **(as indicated in CASE E)** is the best way to improve the input power quality, the load voltage and ripple simultaneously. In addition, using DC inductor seems to be cheap economically rather than using AC inductor. Furthermore, the diode current is low and low diode rate for current is required, which is cheaper than high diode current rate.

4. Conclusion

This paper has concerned with reducing THD and Ripple voltage. Several cases have been tested throughout changing circuit's parameters to determine the best way to reduce THD in terms of simplicity and cost effectiveness. Results have shown that V_{load} mean is highly depending on AC side inductance. This means that high AC inductance leads to less V_{load} mean as indicated in Case D&F. According to the obtained results, the ripple voltage also depends on the value of load

resistance, DC inductance, AC inductance, and DC capacitance. High value of (R_{load}, L_{dc}, L_{dc} *and* C_{dc}) less ripple as in case C,E and F. Although the input power quality in Case F is lower than its value in other cases there is much voltage drop due to high AC inductance which is not advantageous. Total Harmonic Distortion (THD) of the line current has been decreased (from 61.33% to 26.87%) under different load conditions. It is highly preferred to replace passive smoothing inductor L by a small power electronic unit such as dc/dc converter.

Acknowledgments

We would like to thank the editors and reviewers for their valuable comments.

References

Ameen, H.F. and Ibrahim, B.S., 2016. The Current Control Regulator Parameters Effect based on PI+ MR of DFIG WT under Grid Voltage Distortion at PCC. ZANCO Journal of Pure and Applied Sciences, 28(2).

Aula, F.T., 2016. Optimal Control Scheme for Flicker Mitigation in Large-Scale PMSG based Wind Energy Conversion Systems. ZANCO Journal of Pure and Applied Sciences, 28(3), pp.55-66.

Du, X., Zhou, L., Lu, H. and Tai, H.M., 2011. DC link active power filter for three-phase diode rectifier. IEEE Transactions on Industrial Electronics, 59(3), pp.1430-1442.

Ertl, H. and Kolar, J.W., 2005. A constant output current three-phase diode bridge rectifier employing a novel" Electronic Smoothing Inductor". IEEE Transactions on Industrial Electronics, 52(2),pp.454-461.

Hui, S.Y., Chung, H.S.H. and Yip, S.C., 2000. A bidirectional ac-dc power converter with power factor correction. IEEE Transactions on Power Electronics, 15(5), pp.942-948.

Ivensky, G. and Ben-Yaakov, S., 2001. A novel three-phase rectifier with reduced THD. In 2001. IEEE 32nd Annual Power Electronics Specialists Conference (IEEE Cat. No. 01CH37230) (Vol. 2, pp. 672-677). IEEE.

Kamiriski, B., Wejrzanowski, K. and Koczara, W., 2004, June. An application of PSIM simulation software for rapid prototyping of DSP based power electronics control systems. In 2004 IEEE 35th Annual Power Electronics Specialists Conference (IEEE Cat. No. 04CH37551) (Vol. 1, pp. 336-341). IEEE.

Krismadinata, C., Selvaraj, J. and Rahim, N.A., 2009, December. A novel topology and PWM single-phase three-level rectifier. In 2009 International Conference for Technical Postgraduates (TECHPOS) (pp. 1-6). IEEE.

Lee, J.U., Baek, S.W., Cho, K.Y. and Kim, H.W., 2017, December. Fault detection of three phase diode rectifier based on harmonic ratio of dc-link voltage ripples. In 2017 IEEE 12th International Conference on Power Electronics and Drive Systems (PEDS) (pp. 386-391). IEEE.

Mayordomo, J.G., Beites, L.F., Carbonero, Á., Yang, X. and Xu, W., 2014. An analytical procedure for calculating harmonics of three-phase uncontrolled rectifiers under non ideal conditions. IEEE Transactions on Power Delivery, 30(1), pp.144-152.

Mehar, H., 2013. The Case Study of Simulation of Power Converter Circuits Using PSIM Software in Teaching. American Journal of Educational Research, 1(4), pp.137-142.

Mohan, N. and Undeland, T.M., 2007. Power electronics: converters, applications, and design. John wiley & sons.

Prakash, P.S., Kalpana, R., Singh, B. and Bhuvaneswari, G., 2018. Power Quality Improvement in Utility Interactive Based AC–DC Converter Using Harmonic Current Injection Technique. IEEE Transactions on Industry Applications, 54(5), pp.5355-5366.

Singh, B., Singh, B.N., Chandra, A., Al-Haddad, K., Pandey, A. and Kothari, D.P., 2004. A review of three-phase improved power quality AC-DC converters.IEEE Transactions on industrial electronics, 51(3),pp.641-660.

Zobaa, A.F. and Bihl, T.J. eds., 2018. *Big Data Analytics in Future Power Systems*. CRC Press.

ZANCO Journal of Pure and Applied Sciences
The official scientific journal of Salahaddin University-Erbil
https://zancojournals.su.edu.krd/index.php/JPAS

ISSN (print):2218-0230**, ISSN (online):** 2412-3986**, DOI: http://dx.doi.org/10.21271/zjpas**

RESEARCH PAPER

REDUCING OIL POLLUTION IN KAWERGOSK OIL REFINERY EFFLUENT

Cheeman Abdulkarim Qarani*[1], Mohammed Jawdat Barzanjy [2], Ziyad Jamil Talabany [3]

[1&2]Department of chemical and petrolchemical Engineering, College of Engineering, Salahaddin University-Erbil Kurdistan Region, Iraq
[3]Department of Petroleum Engineering, college of Engineering, Knowledge University, Erbil, Kurdistan Region, Iraq.

A B S T R A C T:

The present work deals reducing the oil spill pollution by the treatment of oily wastewater in Kawergosk oil refinery. This research evaluates the efficacy of dissolved air flotation in treating manufactured water samples attained from Kawergosk oil refinery. Percent removal into effluent before and after treatment concerning oil content, COD and BOD are determined. Process factors administering the execution of dissolved air flotation in the reducing of oil and grease are initial oil concentration, pH, and flow rate is investigated. In the dissolved air flotation experimentations, highest oil removal is 85%. The optimum pH for maximum percent removal is 9 with flow rate of 88 m^3/hr, and 92 m^3/hr. Related to COD and BOD maximum percent removal obtained when pH values are 8–9. In addition, the results indicated that the parameters as initial oil concentration, pH and flow rate have a direct effect on the air flotation process in the handling of wastewater.

KEY WORDS: Wastewater; Oil and grease; Separation; Dissolved air flotation.
DOI: http://dx.doi.org/10.21271/ZJPAS.32.5.3
ZJPAS (2020) , 32(5);26-35 .

1. INTRODUCTION

The risk of oil pollutants will increase thru the evolution of oil survey and manufacturing processes, besides the industrial improvement around the world. The research at the handling of oily wastewater is a crucial problem to ecological safety such as oil brought on troubles to the wastewater treatment offerings (Wahi et al., 2013). Natural toxic waste oil and grease in water results in lower dissolved oxygen levels within the water.

Then made trouble for oxygen particles to be oxidative for bacterial on hydrocarbon particles and cause biology harms to water forms (Ite et al., 2013). The acceptable hydrocarbons and its products that release into water forms in Iraqi protection law are set 20 mg/L (Law, 2011)

1.1 Objective of study

The main objective of this study is to estimate the efficiency of DAF in removing oil and grease from refinery wastewater. Additional purposes involved the following:

1. In Erbil city, external runoff from each aspects of greater-Zab River blends through the river water. Formed effluent from Kawergosk oil refinery can also blend through surface runoff and far ahead input to the river; otherwise it might also blends at once through aquatic assets.

* **Corresponding Author:**
Cheeman Abdulkarim Qarani
E-mail: cheeman.qarani@su.edu.krd
Article History:
Received: 03/02/2020
Accepted: 08/03/2020
Published: 13/10 /2020

2. Classification of wastewater produced at the Kawergosk refinery.
3. To investigate the influences of the processing factors on removal efficiency of oil and grease, COD, BOD and TDS in the Kawergosk waste water treatment site.

1.2 Refinery Overview

Erbil Kawergosk oil refinery is the first most crucial refinery inside the northern of Kurdistan about 30 km far from Erbil City. Kawergosk refinery is the fourth biggest in Iraq, the biggest private part one and native investment in Kurdistan. It obtained its first oil in 2009. Its produced wastewater disposed to characterize through the attendance of massive amounts of crude oil yields, greases, polycyclic and aromatic hydrocarbons, phenol, sulfides, naphthenic acids, and different chemical substances (Aziz, 2017). If manufactured wastewater from oil refiners inclined to the surroundings, it might harm to the water assets (Fakhrey, 2016).

The oily effluent in the Kawergosk oil refinery will be separated and removed through these steps shown in figure (1).

1.3 Principles of Air Flotation

In the dissolved air flotation, the pressurized stream is saturated with a gas commonly below 2.7bar-4bar. Upon the discharge of pressure, the air is above of the atmosphere saturation concentration is discharge from solution evolving bubbles almost 30µ to 120µ in diameter. The bubbles produce on the exteriors of the postponed particles otherwise are interested in the particles via surface energies. The most significant electrical property of the colloidal and suspended particles is their surface charge. This charge makes the particles to stay in suspension deprived of collecting for long times. Surface water particle suspensions are thermodynamically unsteady and given sufficient time; they will flocculate and settle. For most particles in water, the sign of the charge is negative (McCave, 1984). Therefore, an aggregate is formed who is a mean density is much less than that of water will rise to the surface, which follows the same laws as sedimentation but in an inverse field of pressure." The governing equation in air flotation separation, as in all gravity controlled approaches, is Stokes Law, that's used to calculate the rising rate of bubble flocks, agglomerates, and bubble-oil accumulation (Alwared and Faraj, 2015).

$$Vt = \frac{gd^2(\rho\alpha - \rho o)}{18\,\mu} \quad \ldots\ldots \quad (1)$$

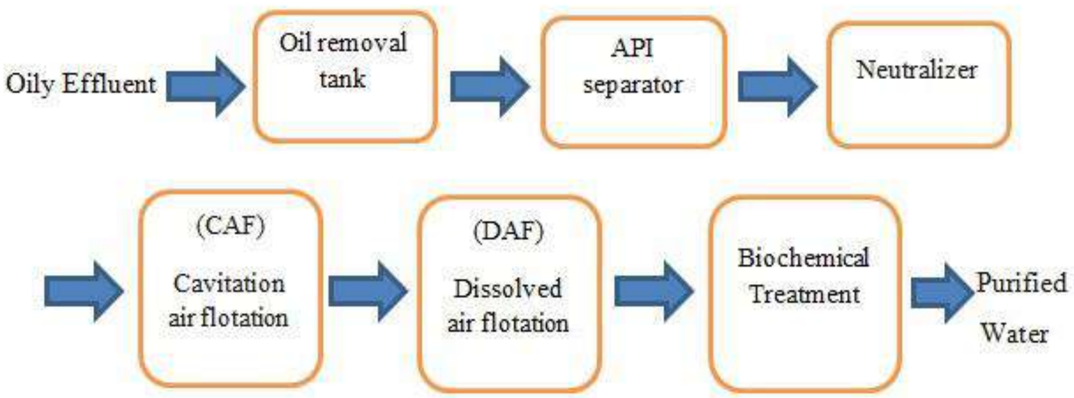

Figure (1) Kawergosk refinery wastewater treatment plant

2. LITERATURE REVIEW

(Painmanakul et al., 2010) the removal of oil mixture in wastewater via the induced air flotation on the research of the consequence of bubble size and chemical coagulant and chemical amount for the handling of greasy wastewater has been developed on this study. The pH value within the range of pH 8-10 is the efficient value for removing oil emulsion using alum as a chemical coagulant.

(Saththasivam, Loganathan, & Sarp, 2016) air flotation is one of the practical devices to remove oil components from oily wastewater. DAF is reducing oil concentration from about 10 ppm to 1000 ppm by prior adding of coagulants-flocculants. Oil bubble attachment by using of full encapsulation gives the greatest percent removal.

(e Silva, e Silva, da Silva, et al., 2018) applying bio surfactants and the dimensionless number of Damköhler (Da) in a prototype of DAF yields the removal efficiency around 90%. It was detected it is probable to estimate the flotation chamber volume based on the desired value of removal efficiency.

(Tetteh and Rathilal, 2018) DAF is less affected by rising saturator pressure and rising rate, as compared with raising the air-water ratio. The accumulation of the oil precipitations is depended only on the poly aluminum sulfate (PAS) amount to weaken the oil drops. The DAF removal efficiency presented above 80% at optimal circumstances of pH of 5, PAS dosage of 10 mg/L, the rising rate of 15 minutes, air saturator pressure of 300-500 kpa, and the air-water ratio of 5-15%. The most significant factor is the PAS dosage.

(Varjani et al., 2019) have reviewed different types of petroleum waste water treatment technologies such as adsorption, coagulation, opposite osmosis, ultrafiltration, chemical destabilization, flocculation, dissolved air flotation (DAF). In this analysis, they similarly offer technical works on information fissures also futurity investigation that orders to estimate the impacts of several treatment technologies existing.

3. MATERIALS AND METHODS

3.1 Oil and Grease

The process applied for the oil and grease test was improved by Standard Methods for the Analysis of Water and Wastewater which is investigation way for oil and grease petroleum hydrocarbons in water (ASTM D3921-96, 2011). During visits to the Kawergosk refinery in December 2018, January and February 2019, effluent water samples were collected from air flotation treatment unit. Input sampling point is shown in figure (2 a) and (2 b) shows the output sampling point. The samples are daily collected during the visiting to the site. Poly Aluminum Chloride (PAC) is used as a coagulant. The process parameters such as oil content, pH and flow rate was different in each sample. The refinery ranges for parameters are shown in table (1) these parameters have been changed to determine the effect of each parameter on the DAF during the treatment of oily waste water. Input oil contents are changed depend on the crude oil that refined in the site so in every two hours the oil content was determined.

Table1: characteristics of refinery wastewater

Parameter	Range
Wastewater Temperature (°C)	25 – 32
pH	6- 10
Input oil content (Cin) mg/l	10 -100
Flow rate m^3/hr	75 - 120
Pressure (bar)	1.5-2.5

(a) (b)

Figure (2) wastewater sample (a) DAF input wastewater. (b) DAF output wastewater

3.1.1 Experimental procedure

1. Five hundred milliliter of sample composed in a clean 1000 ml separator funnel.
2. A distillation flask of 125ml dried and cleaned. The weight of the flask was recorded.
3. Adding 4 milliliters of 1:1 HCL to the separatory funnel for pH adjustment via a pipette also pipette filler.
4. Fifty milliliters of CCL4 added to the separator funnel to achieve the extraction between the water and oil.
5. The funnel was closed then reversed to discharge the vapors thru the stopcock. So, the funnel was intensely shaken for 2 minutes. To discharge vapors from the separatory funnel, reverse and wobble it formerly very hard and point the delivery tube in as safe way beneath a hood and gradually open the stopcock to discharge all vapor.
6. Leaving the funnel for at least 10 minutes to approve the separation. This procedure was repeated two more times on the produce water solution that remained.
7. The solvent was drip exhausted into the distilling flask which is pre-weighted thru a funnel.
8. The distilling flask including the solvent was placed in the hot water bath on the top of the heater to 85℃ interior the hood. The flask was detached from the water bath after finishing evaporation of solvent.
9. The flask was located in the desiccator for 30 minutes.
10. The flask was weighted by an analytical balance.

In all the tests oil content was determined before and after treatment. The procedure was repeated for samples having different oil contents at the same conditions, so as to investigate the influence of oil content on the flotation manner.

3.1.2 Oil and Grease %Removal

The amount of oil and grease removed from refinery waste water is calculated by using the following equation:

$$\text{mg oil and grease/l} = (B1 - B2) \times 1000/\text{ml sample} \quad \text{..... (2)}$$

$$\%\ \text{oil and grease removal} \ \frac{\text{initial concentration}\left(\frac{\text{mg}}{\text{l}}\right) - \text{finalconcentration}\left(\frac{\text{mg}}{\text{l}}\right)}{\text{initial concentration}\left(\frac{\text{mg}}{\text{l}}\right)} \quad \text{..... (3)}$$

3.2 Chemical Oxygen Demand (COD)

COD of wastewater was evaluated thru usage of COD photometer device. The suitable dosage of wastewater (2ml) was presented into absorption solution (MR-Rang: 150-1500mg/l) including potassium hydroxide, sulfuric acid, and mercuric sulfate. Then the combination moved to COD reactor (model RD-125), for 120 min at 150°C., The COD concentration was displayed on the screen after completing oxidation.

3.3 Biochemical Oxygen Demand (BOD)

BOD was measured via usage of the respirometric system. Each incubation bottle is associated to a pressure sensor in a locked process which called air incubator. Microorganisms devour oxygen in the wastewater, the pressure in the bottle headspace drops. This varying in the pressure relates straight to BOD. Through determining pressure variations alternatively of dissolved oxygen levels, the necessity for inquiries and titrations is removed. One Nutrient buffer pillows and 5tabs of potassium hydroxide absorber added to the bottle. The measured BOD value is displayed as (mg O2/l) on screen.

4. RESULTS AND DISCUSSION

4.1Effect of pH on Oil and Grease Removal, COD and BOD

The influence of pH shows a significant character in the eliminating of oil and grease through flotation process. Values of pH changed daily with produced water also in the rainy days pH value was low. To know the influence of pH on the DAF dissimilar values of pH have been tested.

Figure (3) represents the effect of pH on the removal of oil and grease at a constant flow rate (78m³/hr) and different oil content. The graph displays that the amount of oil deletion increased with increasing pH until achieved its highest percent removal value at pH (7.5) which recommends that the revulsion among bubbles and oil particles are lost and the adhesion between them is motivated. The figure also shows pH (6.5 and 9.3) are giving the same oil removal at this flow rate. The highest oil and grease removal at flow tare (92m³/hr) and at pH (9.2) is approximately 90%; it can be seen in figure (4).

Figure (5) explain the influence of pH on the oil and grease removal at constant initial oil concentration (14mg/l) and (32 mg/l) with different flow rate. It shows that the oil removal decreases at first, then it is beginning to rise gradually through increasing pH.

Figure (6) and (7) show the relation between pH and COD and BOD. The graph clearly specifies the highest BOD and COD were observed between the pH values of 8–9. That because the adhesion between bubble and oil droplets promoted at this range.

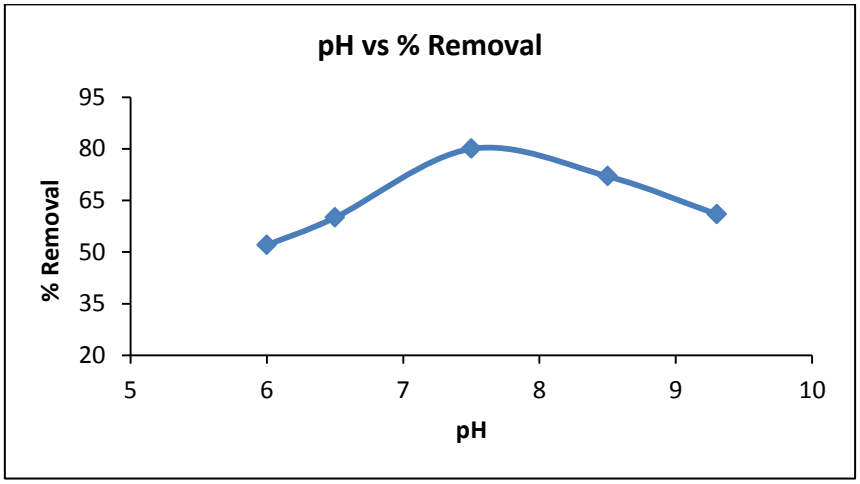

Figure (3) Effect of pH on the oil and grease removal at flow rate= 78m³/hr

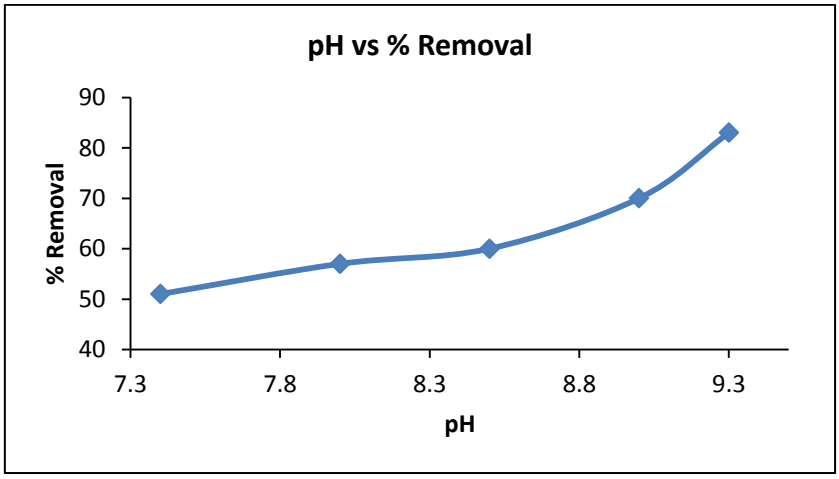

Figure (4) Effect of pH on the oil and grease removal at flow rate= 92m³/hr

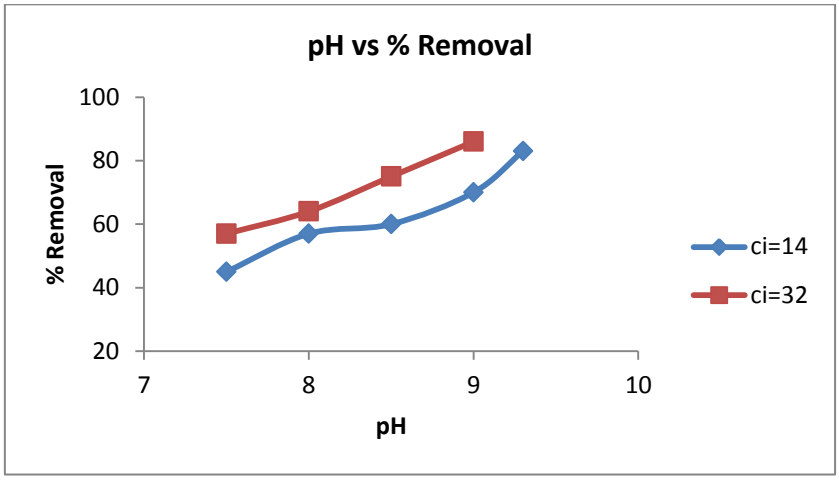

Figure (5) Effect of pH on the oil and grease removal at Different oil content

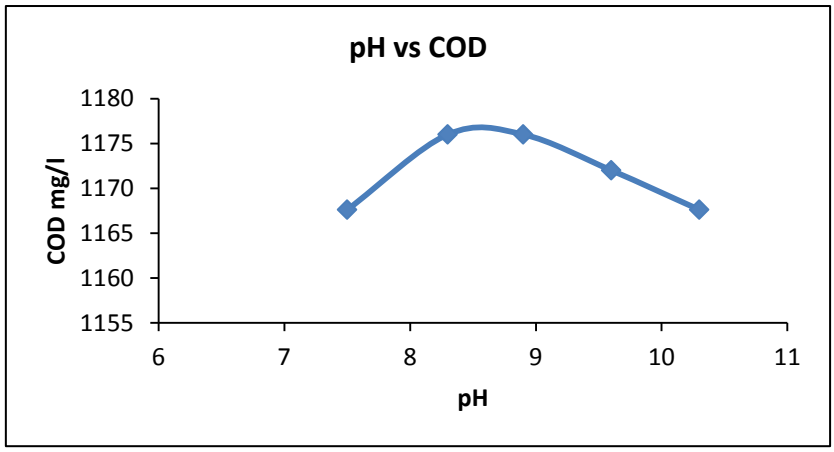

Figure (6) Effect of pH on the COD at oil content= 64.2 mg/l, flow rate=88 m³/hr

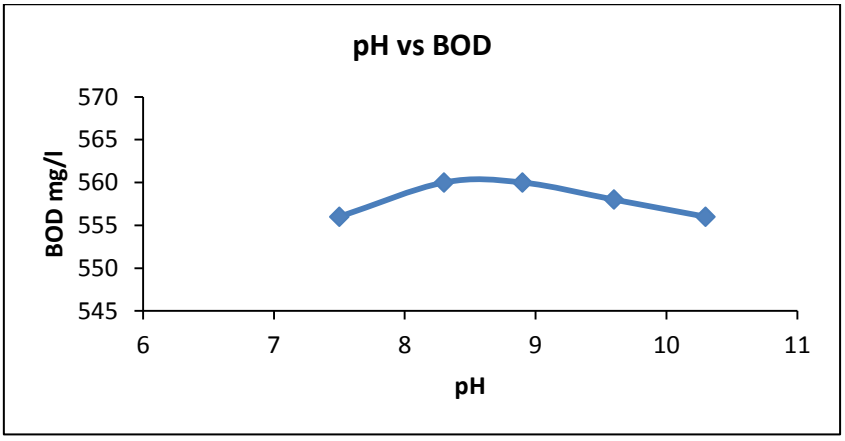

Figure (7) Effect of pH on the BOD at oil content= 64.2 mg/l, flow rate=88 m³/hr

4. 2 Effect of Initial Oil Concentration on Oil and Grease Removal, COD and BOD

Figure (8) demonstrates the consequence of increasing percent removal of oil and grease within constant pH (8.9) and flow rate (88m³/hr). The graph shows increasing of initial oil concentration will result in increasing oil and grease removal because the interaction between an air bubble and oil precipitations will increase while the initial concentration of oil increased. Wherein the oil content is more significant than (25mg/l) with pH (7.5) there is no apparent increase in the oil removal, so at this region. Hence there is an average oil and grease removal (75%).

Figure (9) and (10) demonstrate the influence of increasing initial oil concentration on COD and BOD. The graph indicate increasing of initial oil concentration results rising in COD and BOD because while the input oil content augmented the requirement for air bubble for oxidation reaction is increased.

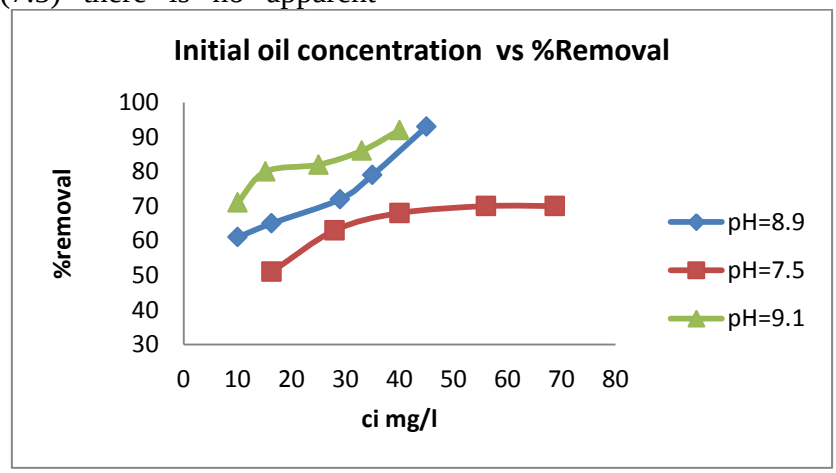

Figure (8) Effect of initial oil concentration on the removal of oil and grease at different pH

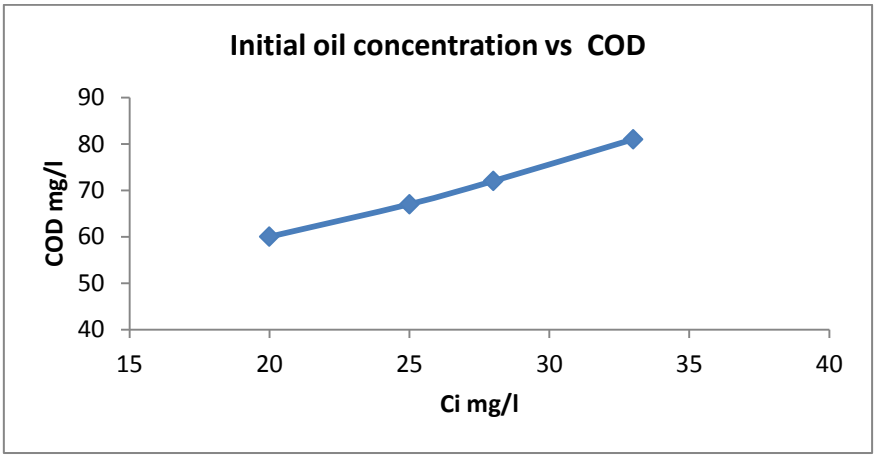

Figure **(**9**)** Effect of initial oil concentration on the COD removal

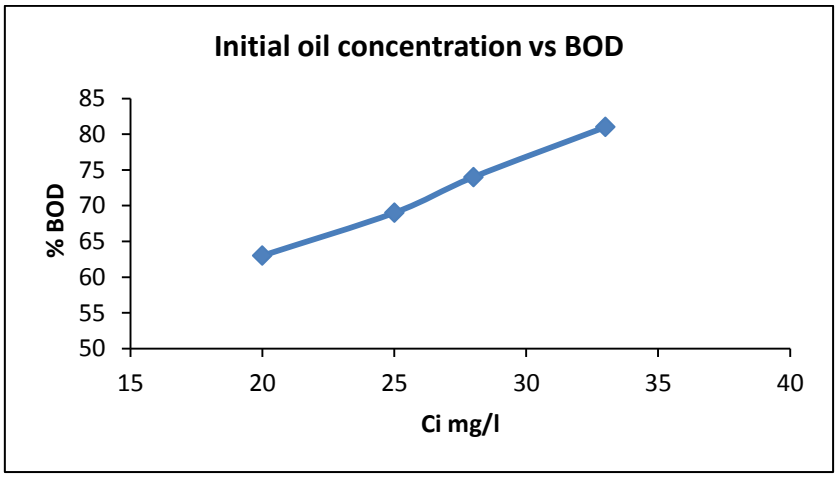

Figure (10) Effect of initial oil concentration on the BOD

4.3 Effect of Flow Rate on Oil and Grease Removal

Figure (11) presents the relationship between flow rate and oil removal. The figure indicates the percent removal of oil decreases as flow rate increases for constant pH (6), the lowest oil removal is achieved at a flow rate of ($120m^3/hr$). The maximum oil removal at constant pH (8) is obtained at lowest flow rate ($78m^3/hr$) figure (12).

Figure (13) illustrate the influence of flow rate on the oil removal. The graph demonstrates the increasing of flow rate which is significant at ($88m^3/hr$) and the optimum flow rate for removing oil and grease at pH (9), where the minimal removal yielded at flow rate ($75m^3/hr$) because at this flow rate the probability of impact between bubbles and oil droplets results to reduction in the separation efficiency.

Figure (14) shows the relation between flow rate and percent oil removal at constant oil content (33mg/l) there is no apparent increase in the oil removal, so at this oil content, the amount of oil removal does not much affected by flow rate.

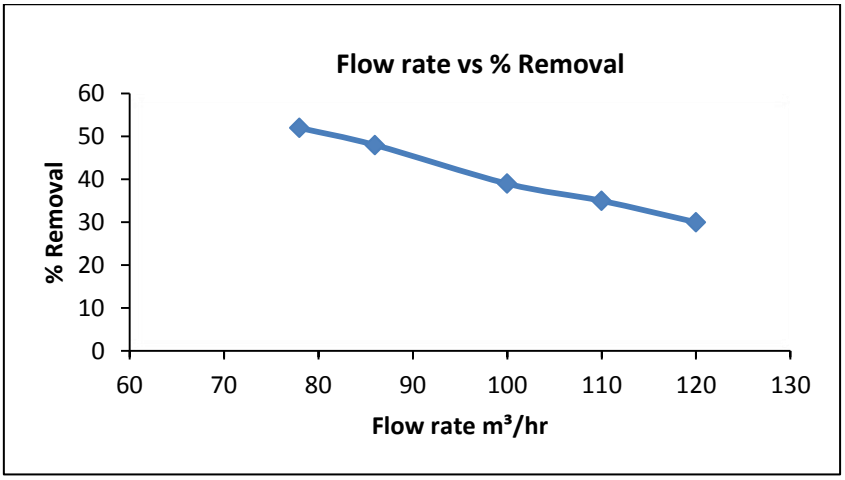

Figure (11) Effect of flow rate on the oil and grease removal pH=6

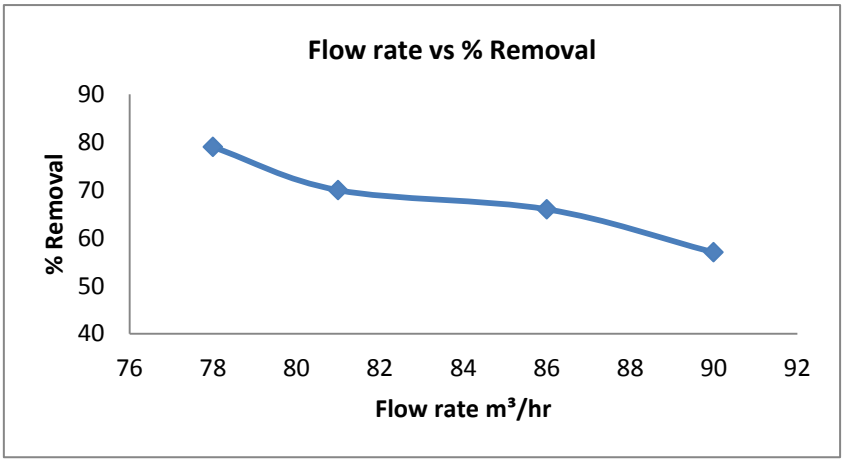

Figure (12) Effect of flow rate on the oil and grease removal at pH=8

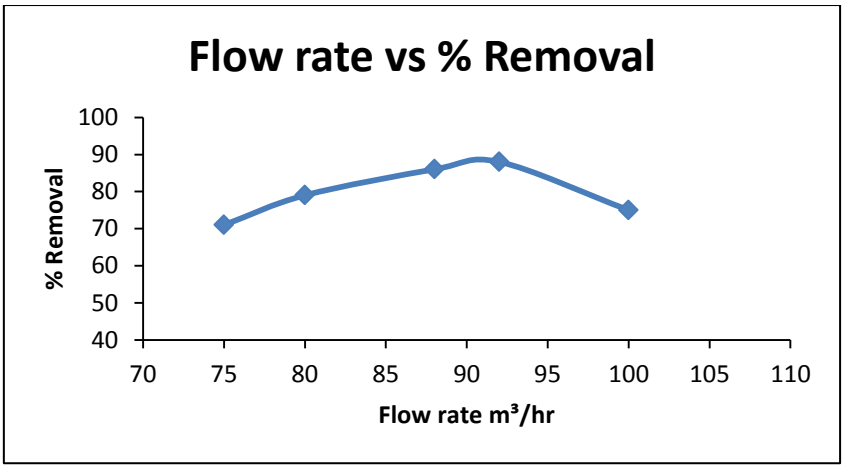

Figure (13) Effect of flow rate on the oil and grease removal at pH=9.2

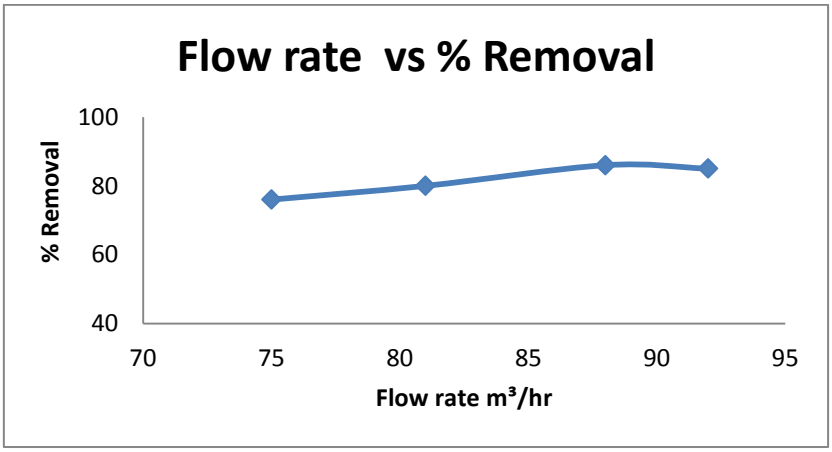

Figure (14) Effect of flow rate on the oil and grease removal at oil content = 33 mg/l

5. CONCLUSION

On the Basis of influences of the three processing parameters on the removal effectiveness of Oil and Grease, COD and BOD by using refinery wastewater, various observations were attained:

1. The wastewater that produced from the Kawergosk oil refinery contained high levels of oil and grease.
2. The best percent removal of oil and grease was 85% at pH 9.
3. From experimental data are obtained direct proportional between initial oil content and oil and grease percent removal, COD and BOD.
4. From the experimental tests obtained the rise in the flow rate results decreasing in the oil deletion, the appropriate flow rate is 88m³/hr gives optimal percent removal.
5. Overpressures have a negative effect on the elimination of Oil and grease because of the incidence of turbulent flow, which disturbs the fluid in the column and eliminates floc creation.

REFERENCES

Alwared, A. I. & Faraj, N. S. 2015. Coagulation-Flotation Process for Removing Oil from wastewater using Sawdust+ Bentonite. Journal of Engineering, 21**,** 62-76.

Aziz, Shoukr Qarani, 2017. Optimization of Aeration Style and Cycle Time for Treatment of Oil Refinery Wastewater Using Powdered Activated Carbon and Sequential Batch Reactor, ZANCO Journal of Pure and Applied Sciences,29, 140-153.

e Silva, F. C. P. R., e Silva, N. M. P. R., da Silva, I. A., Brasileiro, P. P. F., Luna, J. M Rufino, R. D., . . . Sarubbo, L. A. (2018). Oil removal efficiency forecast of a Dissolved Air Flotation (DAF) reduced scale prototype using the dimensionles number of Damköhler. Journal of Water Process Engineering, 23, 45-49 .

Fakhrey, S. Q. A. A. E. S. A. 2016. The Effect of Kawergosk Oil Refinery Wastewater on Surrounding Water Resources. ZANCO Journal of Pure and Applied Sciences, 28**,** 656-667.

Iraqi preservation Law 2011.Total Allowable hydrocarbons in Wastewater.

ITE, A. E., IBOK, U. J., ITE, M. U. & PETTERS, S. W. 2013. Petroleum exploration and production: Past and present environmental issues in the Nigeria's Niger Delta. American Journal of Environmental Protection, 1**,** 78-90.

MCCAVE, I. 1984. Size spectra and aggregation of suspended particles in the deep ocean. Deep Sea Research Part A. Oceanographic Research Papers, 31, 329-352.

Painmanakul, P., Sastaravet, P., Lersjintanakarn, S. & Khaodhiar, S. 2010. Effect Of Bubble Hydrodynamic And Chemical Dosage On Treatment of oily wastewater by induced air flotation (IAF) process. Chemical Engineering Research and Design, 88**,** 693-702.

Saththasivam, J., Loganathan, K., & Sarp, S. (2016). An overview of oil–water separation using gas flotation systems. Chemosphere, 144, 671-680 .

Tetteh, E. K. & Rathilal, S. Investigating Dissolved Air Flotation Factors For Oil Refinery Wastewater Treatment. CBU International Conference Proceedings, 2018. 1173-1177.

Varjani, S., Joshi, R., Srivastava, V. K., Ngo, H. H. & Guo, W. 2019. Treatment of wastewater from petroleum industry: current practices and perspectives. Environmental Science and Pollution Research**,** 1-9.

Wahi, R., Chuah, L. A., Choong, T. S. Y., Ngaini, Z. & Nourouzi, M. M. 2013. Oil removal from aqueous state by natural fibrous sorbent: an overview. Separation and Purification Technology, 113**,** 51-63.

ZANCO Journal of Pure and Applied Sciences
The official scientific journal of Salahaddin University-Erbil
https://zancojournals.su.edu.krd/index.php/JPAS

ISSN (print):2218-0230**, ISSN (online):** 2412-3986**, DOI: http://dx.doi.org/10.21271/zjpas**

RESEARCH PAPER

Boltzmann equation studies on electron swarm parameters for oxygen plasma by using electron collision cross – sections

Mohammad M. Othman, Sherzad A. Taha , Saeed Rasool Hussein
Department of Physics, College of Education, Salahaddin University- Erbil, Kurdistan Region, Iraq.

A B S T R A C T:

The Boltzmann transport equation has been solved using a two-term approximation method in pure electronegative gas oxygen to evaluate the electron energy distribution function (EEDF) and electron transport parameters for a wide range of E/N varying from 0.1 to 1000 Td (1 Td=10^{-17} V.cm^2). These parameters, are "electron drift velocity, mean electron energy, characteristic energy, diffusion coefficients, electron mobility, attachment and ionization coefficients, effective *ionization coefficient and critical reduced electric field strength* $(E/N)_{crt}$*".. The* dependence of second kind collision (super-elastic collision) and electron energy distribution function on E/N are explained (where E is electric field and N is neutral number density). The present calculated results are in good agreements as compared, with the previous experimental and theoretical results. A group of electron/molecule collision (elastic and inelastic) cross-sections are collected for oxygen gas to evaluate transport parameters over the entire E/N range. In addition, the energy lost by different types of electron/molecule collision processes are computed as a function of E/N.

KEY WORDS: Boltzmann equation, Electron energy distribution function (EEDF), Electron transport parameters, Critical field strength, Electric discharge.
DOI: http://dx.doi.org/10.21271/ZJPAS.32.5.4
ZJPAS (2020) , 32(5);36-53 .

1. INTRODUCTION

Oxygen molecule (O_2) is a strongly electro negative gas, is an electron attaching gas ($O_2 + e \rightarrow O + O^-$) and it decreases with the electrical discharge, which gives oxygen an excellent dielectric strength (McNevin, 1990). Oxygen is the one of the main combinations of the earth's atmosphere (20.8%) and is the third most numerous elements in the Universe after hydrogen and helium gases. Oxygen is an environmentally clean, nontoxic, nonflammable, colorless, orderless diatomic gas and non-reactive but an oxidizer, and it can be toxic at elevated partial pressure (more than 160mmHg). It has a high critical temperature (-154.6K) and has high critical pressure (49.8 atm).

At low temperature plasma oxygen molecule with noble gases and molecules are used in application of various fields such as: material processing properties which used as an arc quenching medium. (Harthney et al., 1989) biomedical purposes (Graves, 2014) environmental /energy application (Tatarova, et al., 2014) in material processing, such as photoresist aching, surface modification, chemical vapor deposition (VCD) and oxidation. Plasma discharges of Cl_2 and O_2 mixtures were used in application thin film etching silicon (McNevin, 1990) and deposition in microelectronic device fabrication (Thorsteinsson. and Gudmundsson, 2010). In addition, industrial oxygen mixed with pure CF_4 plasma to control the production of fluorocarbon (CF) molecules which were

* **Corresponding Author:**
Mohammad M. Othman
E-mail: sherzad.taha@su.edu.krd
Article History:
Received: 20/11/2019
Accepted: 29/04/2020
Published: 13/10 /2020

generally used for etching of Si and SiO_2 (Lu et al., 2012). Because of its industrial importance and for understanding plasma phenomena a set of electron/molecule cross- sections for pure oxygen evaluated by (Phelps, 1985; Jeon, 2003). The electron swarm parameters were studied experimentally and theoretically by variety of investigators as a function of electric field strength E/N. For example (Settaouti, 2007) calculated electron swarm parameters over the range 100 Td -1000 Td, ($1Td=10^{-17}$ $V.cm^2$). The attachment and ionization coefficients are experimentally measured by (Jeon et al,, 1997). At low electric field strength electron swarm parameters in N_2, O_2 and H_2 are theoretically calculated by (Ridenti et al., 2015) using homogenous Boltzmann equation. For the purpose of abbreviation, previous literatures of electron swarm parameters in pure oxygen are collected in table 1.

The Monte-Carlo simulation method used by (Leyla et al., 2011) to evaluate the mean electron energy, ionization and attachment coefficients as functions of time for an electrical discharge in pure oxygen molecule and (Settaouti, 2018) studied the point plane corona discharge by using an equivalent method. The electron energy distribution function (EEDF) plays a crucial role in calculating electron swarm parameters and physical properties of plasma, (Nighan, 1970; Engelhardt and Phelps, 1963; Jiang and Economou, 1993) theoretically calculated the electron swarm parameters using (EEDF) by two-term approximation solution of Boltzmann equation under dc field. Electron swarm parameters in oxygen were also calculated in binary gas mixtures O_2-Ar (Jeon and Nakamura, 1998), SF_6-O_2 (Hernandez-Avila and Urquijo, 2006; Linsheng et al., 2014), Cl_2-O_2 (Tuan,2014), O_2-CO (Price and Moruzzi, 1973), N_2-O_2 (Dujko et al., 2011; Pancheshnyi, 2013; Guerra et al., 2019), TMS-O_2 (Hien, et al., 2012), TEOS-O_2 (Yoshida et al., 1996; Tuan and Jeon, 2012), CO_2-O_2 (Yousfi et al., 2009) and TRIES-O_2 gas mixtures (Tuoi et al., 2018). The ternary mixtures of CF_4/Ar/O_2 were analyzed by (Nikitovic et al., 2010; Nikitovic et al., 2011) Furthermore, ternary mixtures of $C_5F_{10}O$/CO_2/O_2 was used in gas-insulated high-voltage switchgear (GIS) (Bousoltane et al., 2018) and C_4F_7N or $C_5F_{10}O$ mixtures with CO_2 and O_2 were used as insulating and switching media in the case of high and medium voltage (Eguz et al., 2019).

Electrical breakdown voltage and critical field strengths $(E/N)_{crt.}$ were calculated at condition that reduced ionization coefficient (α/N) and reduced attachment coefficient (η/N) are in equilibrium, therefore the effective ionization coefficient equal to zero ($\bar{\alpha}$ = (α/N)-(η/N) =0), this method was used by (Láska et al., 1984; Brand and Kopainsky, 1979; Itoh et al., 1980; Zhao et al., 2017) to calculate electrical breakdown voltage using two-term approximation solution of Boltzmann equation. Critical field strength have been studied by both theoretical calculations (Tanaka, 2004; Rong et al., 2014; Zhao and Lin, 2016; Zhao et al., 2017) and experimentally to find new gases with high dielectric field strength which used in electrical insulator, for example, experimentally (Xiao et al., 2018) reported that small addition of oxygen O_2 reduced breakdown voltage of the c-C_4F_8/N_2 mixed gas. (Beaty, et al. 1979 and Dutton, 1975) published a large data on the electron swarm parameters in number gases over a wide range of electric field strength E/N. We previously reported a detailed explanation to calculate electron swarm parameters by using two-term approximation method of the Boltzmann equation (Othman, et al. 2018; Othman, et al. 2019a).

In the present work, the electron swarm parameters and critical field strength $(E/N)_{crt}$. for a wide range of E/N varying from 0.1Td to 1000 Td in pure oxygen gas are calculated using a two-term approximation of the Boltzmann equation. Since 1970, several numerical techniques have used to calculate electron, energy distribution, function and electron swarm parameters. BOLTZ code (Thomson and Smith, 1976), NOMAD code (Rockwood and Greene, 1980), ELENDIF code (Morgan and Penetrante, 1990), METHES code (Rabie and Franck, 2016), and LoKI-B (Tejero-del-Caz, et al., 2019). NOMAD and ELENDIF code are containing electron attachment coefficient which are not considered by BOLTZ code. In the present study one chooses the NOMAD code, because it's more limited by available of electron energy collision cross-sections as compared to ELENDIF code.

Table 1. Summary of previous theoretical work (Boltzmann equation & Monte-Carlo method)

Investigator	*E/N range (Td)*	v_d *cm/s*	<u> eV	u_k eV	η/N cm^2	α/N cm^2	*f(x)* $eV^{-3/2}$
Hake and Phelps, 1967	0.01-150	x		x	x	x	x
Myers, 1969	0.003-200		x	x			x
Wanger, 1971	90-50				x	x	
Nelson & Davis, 1972	≥1.3	x					
Lucas et al., 1973	15-152	x	x		x	x	x
Crompton & Elford, 1973	0.8-12	x					
Mašek, 1975	1-140	x	x	x		x	x
Mašek et al., 1977a	1-200	x	x	x			x
Mašek et al., 1977b	10-200				x		x
Taniguchi et al., 1978	1-30				x		
Reid & Crompton, 1980	0.14-1.4	x					
Roznerski and Leja,1984	50-250	x					
Al-Amin et al., 1985	14.1-5650	x	x	x		x	
Gousset et al., 1991	0-130	x	x	x		x	x
Liu and Govinda Raju, 1992	20-5000	x	x	x	x	x	x
Liu and Govinda Raju, 1993	20-2000	x	x			x	
Jeon, 2003	1-1000	x		x	x		
Rabie & Frank, 20016	≥200	x	x				
Alves et al., 2016	10^{-3}-1000			x	x	x	
Mašek, 1975	1-140	x	x	x		x	x

2. Theory

2.1 The Boltzmann Equation

The electron energy distribution function (EEDF) derived from the solution of the Boltzmann equation. This parameter used to calculate reaction rates and electron swarm parameters in pure gases/mixtures. The general form of Boltzmann equation written as follows, (Morgan and Penetrante, 1990; Govinda Raju, 2017).

$$\frac{\partial f(v)}{\partial t} + V.\nabla f(v) - \frac{e}{m}\bar{E}.\nabla_v f(v) = \left(\frac{\partial f}{\partial f}\right)_{coll} \quad (1)$$

where *f(v)* is the electron energy distribution function, *V* is the velocity, m is the electron mass, $\bar{E}$ is the dc electric field and ∇_v is the velocity-gradient operator. The right part of the equation denotes the rate of change in the electron distribution due to elastic and inelastic collisions. To solve the Boltzmann transport equation the electron distribution function is expanded in two-terms of Legendre polynomials, $f(\bar{v}) = f_o(v) + f_1(v)\cos\theta$, where $f_o(v)$ is the isotropic part and $f_1(v)$ is anisotropic part of the distribution function where $f_1(v) << f_o(v)$. The two-term approximation is used to deduce the swarm equations by filling them into the Boltzmann equation. (Govinda-Raju, 2006 and 2012) collected a large literatures on the solution of Boltzmann equation by the numerical method.
),

2.2. The Transport Parameters

The electron transport coefficient in gases is calculated by using a two-term approximation solution of the Boltzmann equation are functions of E/N the gas temperature (T_g) and electron/molecule (atom) cross-sections. The relation between E/N and E/p is E/N [Vcm^2] =$1.036x10^{-19}$ T_g [K].E/P [$Vcm^{-1}Torr^{-1}$], where T_g is gas temperature, for example at T_g=273K, E/P=1Vcm^{-1}Torr then E/N=2.823 Td, (1 Td=10^{-17} Vcm^2). The electron energy distribution function is the important parameter used for calculating electron swarm parameters, for thermal equilibrium the electron distribution function is given by Maxwellian distribution as follows, (Fridman, 2008),

$$f(u) = 2*\left(\frac{u}{\pi(K_B*T_e)^3}\right)^{1/2}\exp\left(\frac{-u}{K_B T_e}\right) \quad (2)$$

where T_e is electron temperature, this leads to an electron mean energy of,

$$\langle u\rangle = \int_0^\infty u f_0(u) du = \frac{3}{2}T_e \quad (3)$$

where T_e is expressed in electron volts.

However, in many cases, deviations occur and non-thermal plasma often possess, the distribution follows a non-Maxwellian shape (Hagelaar and Pitchford, 2005). In this case, the electron energy distribution function (EEDF) derived analytically is the main coefficient to calculate the electron swarm parameters, that is. the electron drift velocity v_d and the transverse diffusion coefficient D_T as follows (Thomson and Smith, 1976; Al-Amin and Lucas, 1988),

$$v_d = -\frac{1}{3}\sqrt{\frac{2e}{m}}\frac{\bar{E}}{N}\int_0^\infty \frac{u}{Q_m^T(u)}\frac{\partial f_0(u)}{\partial u}du \quad (4)$$

$$D_T = \frac{1}{3N}\sqrt{\frac{2e}{m}}\int_0^\infty \frac{u}{Q_m^T(u)} f_0(u)du \tag{5}$$

(Sakai et al., 1977) measured longitudinal diffusion coefficient experimentally using time-of-flight method.

The electron mobility, $\mu_e = v_d \overline{E}$ and the mean electron energy $\langle u \rangle$, in terms of the electron energy distribution function (EEDF) (Smith and Thomson, 1978; Simith and Thomson, 1978; Hagelaar and Pitchford, 2005; Ridenti and Amorim, 2012), are expressed as follows,

$$\mu_e = -\frac{1}{3N}\sqrt{\frac{2e}{m}}\int_0^\infty \frac{u}{Q_m^T(u)} \frac{\partial f_0(u)}{\partial u} du \tag{6}$$

$$\langle u \rangle = \frac{2}{3}\int_0^\infty u^{3/2} f_0(u)du \tag{7}$$

here, $Q_m^T(u) = Q_m(u) + \sum_j Q_k(u) + Q_i(u) + Q_a(u)$ represent the total effective momentum transfer cross section. Where $Q_m(u)$, $Q_k(u)$, $Q_i(u)$ and $Q_a(u)$ are momentum transfer, excitation (vibration/ electronic), ionization, and attachment cross sections respectively.

The definition of characteristic energy u_k is given by combining equations (5) and (6), (Makabe and Petrovic, 2015) which yields:

$$u_k = e\frac{D_T}{\mu_e} = e\frac{D_T}{v_d}\overline{E} \tag{8}$$

whereas for the thermal equilibrium,

$$u_k = \frac{2}{3}\langle u \rangle \tag{9}$$

where $u_k = \frac{3}{2}K_B T_g$, the following relation obtained,

$$\frac{D_T}{\mu_e} = \frac{K_B T_g}{e} \tag{10}$$

This is also known as Einstein's relation.

By using the drift velocity v_d equation, the reduced ionization and attachment coefficients are calculated as follows, (Lucas et al., 1973; Láska, et al. 1984; Loureiro and Amorim, 2016; Othman, et al., 2019b),

$$\frac{\alpha}{N} = \frac{1}{v_d}\left(\frac{2e}{m}\right)^{1/2}\int_{u_i}^\infty u\ Q_i(u) f_0(u)du \tag{11}$$

$$\frac{\eta}{N}=\frac{1}{v_d}\left(\frac{2e}{m}\right)^{1/2}\int_{u_a}^{\infty}u\ Q_a(u)f_0(u)du \qquad (12)$$

Where, $Q_i(u)$, $Q_a(u)$ are ionization and attachment cross section, here, u_i is the ionization threshold energy for oxygen which is equal to 12.2 eV, and u_a is attachment threshold energy of 4.4 eV. The reduced critical electric field strength $(E/N)_{crt.}$ is calculated when reduced ionization coefficient (α/N) and the reduced attachment coefficient (η/N) are in balance, in this case, the effective ionization coefficient ($\bar{\alpha}=0$) equal to zero (Láska et al, 1984; Li et al., 2012).

$$\bar{\alpha}=\frac{\alpha}{N}-\frac{\eta}{N}=\frac{\alpha-\eta}{N}=0 \qquad (13)$$

The rate constant of excitation for the j^{th} inelastic collision cross-sections is obtained from information of cross- sections and electron energy distribution function by the following formula (Nakamura and Lucas, 1978)

$$R_{sj}=\left(\frac{2e}{m}\right)^{1/2}\int_{0}^{\infty}uNQ_{sj}(u)f(u)du \qquad (14)$$

where Q_{sj} is electron cross-sections of excitation of level j in species, s.

The electron energy loss P_j during inelastic collision process is calculated as follows,

$$P_j=\frac{u_j R_{sj}}{e\bar{E}v_d} \qquad (15)$$

Where u_i is the onset energy for the excitation.
The neutral number density for pure gas calculated as follows,

$$N=\frac{\rho N_A}{M_w} \qquad (16)$$

where ρ represents gas density, M_w is molecular weight and N_A is Avogadro number.

3. The Cross Section

The electron/molecule collision cross-sections (Phelps, 1985) are necessary in order to calculate the EEDF and electron swarm parameters in oxygen gas. The oxygen molecule includes 14 sets of collisional cross-sections: one momentum transfer cross-sections (Q_m), eight vibrational excitation (Q_{v1}, Q_{v2}, Q_{v3}, Q_{v4}, Q_{v5}, Q_{v6}, Q_{v7}, Q_{v8}) with threshold energy 0.37, 0.56, 0.75, 0.93, 1.12, 1.3, 1.47 and 1.46 eV, respectively, three electronic excitation (Q_{ex1}, Q_{ex2}, Q_{ex3}) cross-sections with threshold energy of 4.4, 8.0 and 9.7 eV, respectively, and one attachment cross-sections (Q_a) with threshold energy 4.4 eV are taken from (Hake and Phelps, 1967), and one dissociation ionization cross-sections with threshold energy of 12.2 eV is taken from (Rapp and Englander-Golden, 1965).

4. Results and Discussion

There are several literatures published of the electron swarm parameters in pure oxygen gas, however it is impossible to display all the previous experimental and theoretical data. For comparison with the present results one shows only selected data with an emphasis on more recent results. The major objective of this research is the calculation of the reduced critical electric field strength and electron swarm parameters for pure oxygen in the range 0.1 Td to 1000 Td by using two term solution of Boltzmann equation.

Normalized electron energy distribution function (EEDF) for various reduced electric field strength E/N in pure oxygen molecule at temperature 300K and pressure 1 atm are shown in figure (1). When the electron energies ≤ 4.4 eV, the EEDF decreases as the reduced electric field strength E/N increases, the tail of the distribution is decreasing and there are only small number of electrons that have energies greater than the ionization potential. Moreover, due to inelastic collision there are few electrons with energies, greater than the excitation energy. At low electron energy the shape of the energy distribution function depends on the momentum transfer cross-sections, but for electron energies >4.4 eV, the EEDF increases with increasing E/N, then the electrons gain at highers kinetic energy, and the tail extends to energies above the ionization potential. As E/N increases degree of ionization increase and then increases the number of particles with energies higher than excitation, energy tends to spread energy due to collisions, at high energies the distribution function influenced by electron collisions so the distribution approaching to straight line becomes more nearly of the Maxwellian form, with a slope of, $(-1/k_BT)$.

Figures (2a) and (2b) are shown the influence of second kind collisions (super-elastic collisions) from metastable electronic states on EEDF at electric field strength 0.5 Td and 10 Td with and without super-elastic collision respectively. Figure (2b) shows, that super-elastic collisions are not important at higher reduced electric field strength E/N.

The electron drift velocity as a function of E/N is shown in figure (3) which increases with increasing E/N values, the results are compared with the theoretical and experimental results are also illustrated in the same figure, a good agreement is obtained when compared with experimental results of (Roznerski and Leja, 1984; Al-Amin et al., 1985; Jeon et al., 1997). While the theoretical results calculated by (Liu and Govinda-Raju, 1992, Liu and Govinda-Raju, 1993; Jeon, 2003; Settaouti and Settaoutim 2007 and Tuoi and Tuan, 2018) are observed to be in good agreement over the common E/N range. Figure (4) illustrates the mean electron energy in range of 0.12 eV-19.39 eV for different values of E/N varying from the range 0.1 Td to 1000 Td. The variation of mean electron energy progressives exponential the electrons gain energy from the electric field, comparison has been made with the theoretical values of (Liu and Govinda Raju, 1992, 1993; Settaouti and Settaouti, 2005 and Dujko et al., 2011) a good fit has been observed. Figure (5) shows the calculated characteristic energy as a function of E/N, during inelastic collision process E/N ≥40 Td, the ionization processes occur and then the characteristic energy starts to increase with increasing E/N. In comparison the present results are found to be in good fit with theoretical results of (Hake and Phelps, 1967; Jeon, 2003) and experimental results of (Al-Amin et al., 1985). Otherwise the experimental values of (Jeon and Nakamura, 1998) and theoretical values of (Toui and Tuan, 2018) are lower than the present results at the range E/N≥ 1 Td, the variation of present results gives rise by large momentum transfer cross - section.

Figure (6) is comparison between the present results for electron mobility with theoretical results of (Alves et al., 2016) at room

temperature, the present results agree well with theoretical results. The transverse diffusion coefficient, DN for electrons in pure oxygen, as a function of E/N varying from 0.1 Td to 1000 Td is illustrated in figure (7), together with theoretical multi term solution results obtained from (Dujko, et al., 2011) for comparison. It indicates the good agreement between present results and theoretical results of (Dujko, et al., 2011).

Figure (8) shows the Townsend, ionization coefficient α/N (also known as reducedionization coefficient) is calculated for the rang $40 \leq E/N \leq 1000$ Td. The ionization coefficient increases as E/N increases, good agreement has been obtained with the theoretical values of (Liu and Govinda Raju, 1993; Settaouti and Settaouti, 2007 and Tuoi and Tuan, 2018) and the experimental results of (Al-Amin et al., 1985 and Yoshida et al., 1996). The attachment coefficient, is the probability that an electron will attach with the molecule in traveling a unit distance in electric field, is only a function of E/N. The calculated Townsend reduced, attachment coefficient, η/N (also known as attachment, reduced coefficient), for the pure oxygen molecule as a function of E/N is shown in figure (9). The present calculation i found tso be in a good agreement with theoretical results of (Jeon, 2003; Hien et al., 2012 and Alves et al., 2016) and experimental results of (Huxley et al., 1959). An electron avalanche can occur when the effective ionization-coefficient $(\alpha-\eta)/N > 0$.

The reduced effective ionization coefficient $(\alpha-\eta)/N$ as a function of E/N in pure oxygen is shown in figure (10) which calculated from the results of α/N and η/N. The critical reduced electric field strength, $(E/N)_{crt.}$ is described, as the value of E/N at $(\alpha-\eta)/N = 0$, calculated from the results of the effective ionization coefficient $(\alpha-\eta)/N$ which describes variations of free electrons in oxygen.. Critical reduced electric field strength, $(E/N)_{crt}$ is important coefficient for the purpose of identification the insulation performance of electronegative gases. The $(E/N)_{crt}$ value is shown in figure (10), at which $\alpha/N = \eta/N$, in the present calculation $(E/N)_{crt}$ equal to (119 Td), in agreement for comparison with the results of (Laska et al., 1984), 110 Td, (Tuan, 2014), 118.5 Td and (Zhao et al., 2017), 120.5 Td. The reduced effective ionization coefficient is zero, since α/N are balanced with η/N, when $E/N < (E/N)_{crt.}$ attachment processes dominants, in this case negative values for the effective ionization coefficient as E/N is decreased, on the other hand, for $E/N > (E/N)_{crt.}$ the effective ionization coefficient increases with increasing E/N values where the ionization collisions dominants, in this case, the effect of the attachment processes is not important at high E/N values.

Figure (11) illustrates the percentage energy losses by elastic and inelastic processes. At high E/N=600 Td, 25% energy lost through ionizing collisions, 74% to electronic excitation, and 1% to attachment collisions. While at Lowest E/N (E/N=1 Td), 10% energy lost through momentum transfer (elastic) collisions and 90% to vibrational collisions. Maxima for vibrational excitation loss occurs at E/N= 2 Td. At high E/N the energy transfer to attachment is very small, only electronic and ionization fraction are dominates.

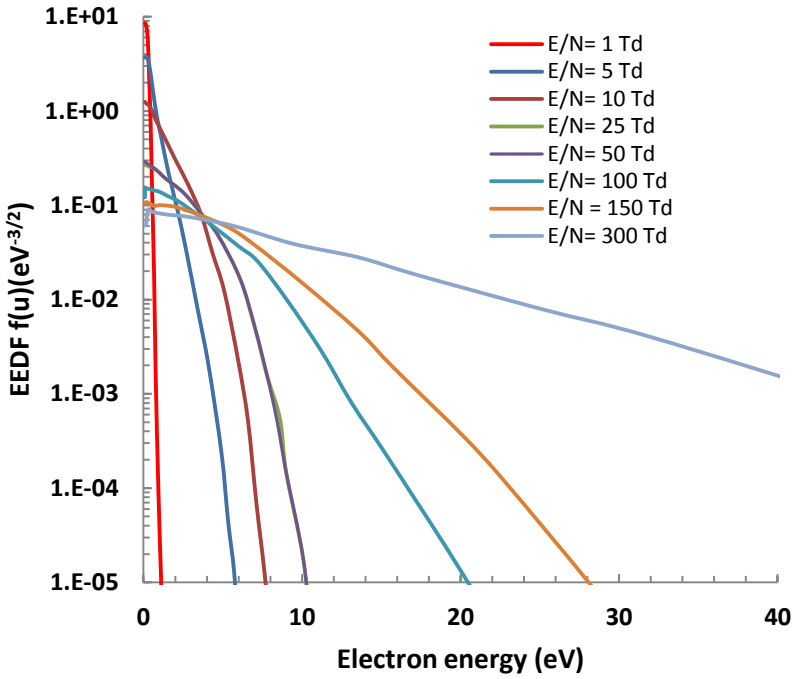

Figure 1. Variation of the electron energy distribution function with the electron energy for pure oxygen.

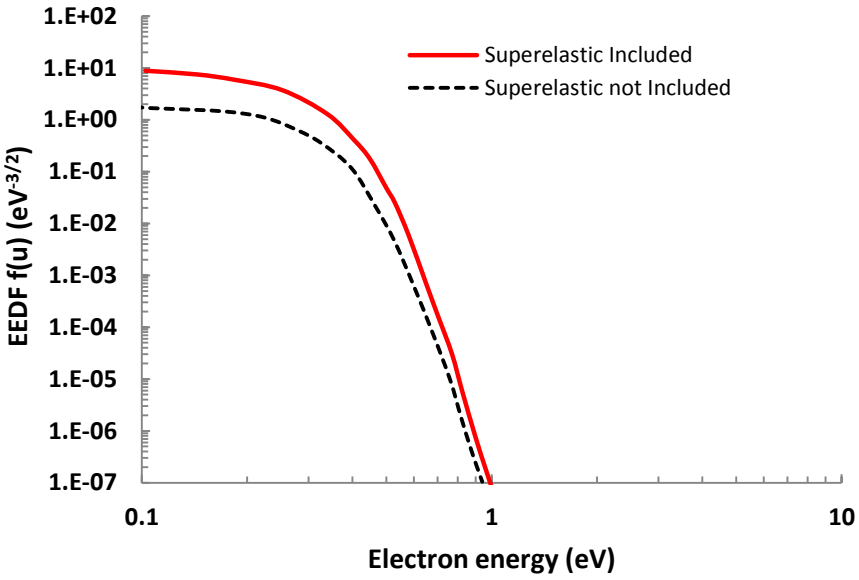

Figure 2a. The electron energy distribution function in oxygen at E/N= 0.5 Td, with and without the superelastic process.

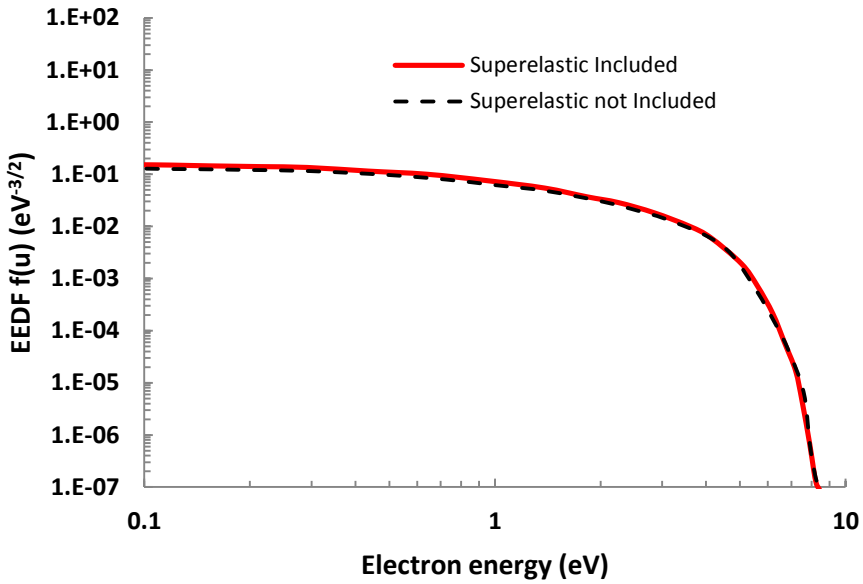

Figure 2b. The electron energy distribution function in oxygen at E/N= 10 Td, with and without the super-elastic process.

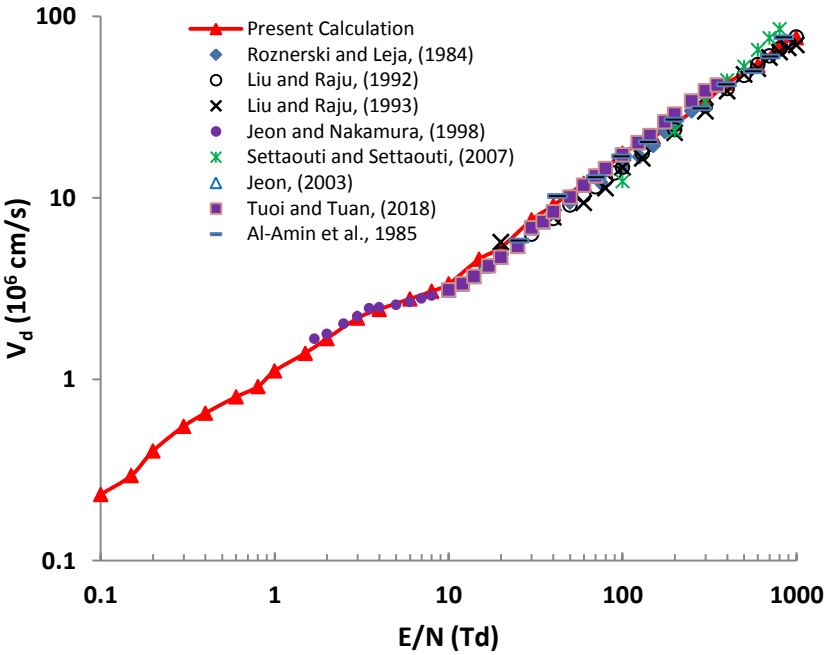

Figure 3. Variation of the drift velocity with E/N values for pure oxygen.

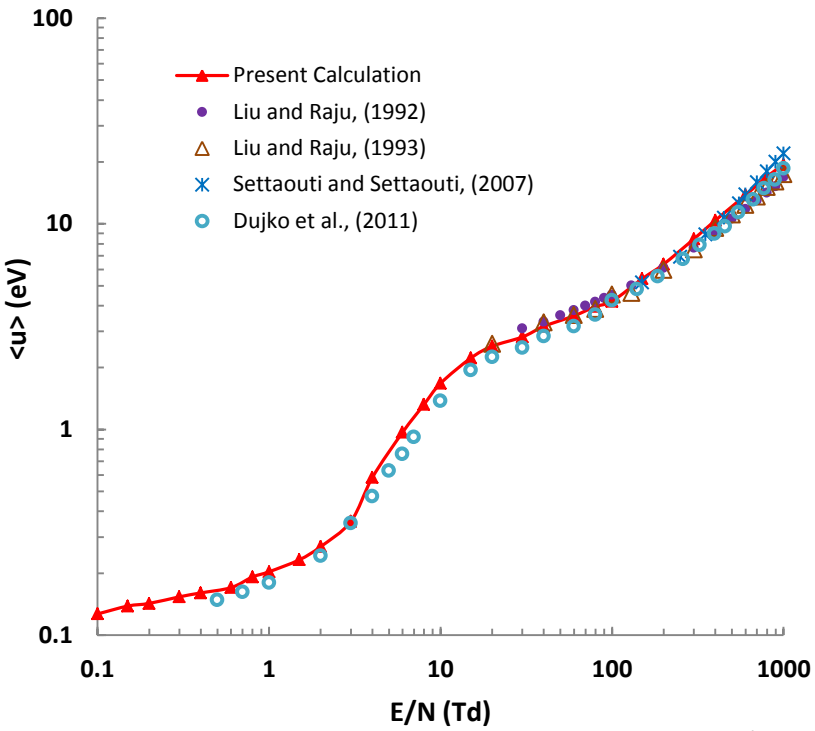

Figure 4. Variation of the mean electron energy with E/N valus for pure oxygen.

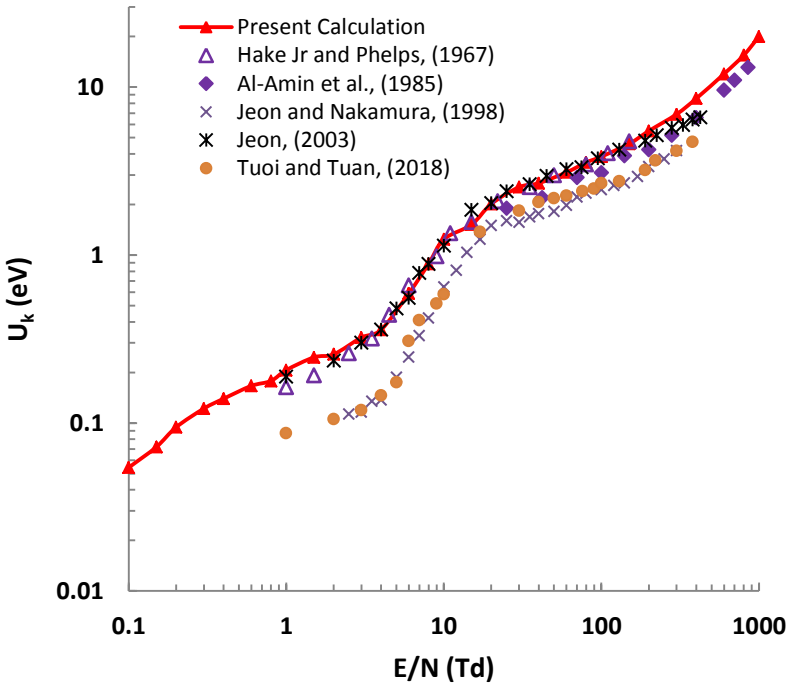

Figure 5. Variation of the characteristic energy with E/N values for pure oxygen.

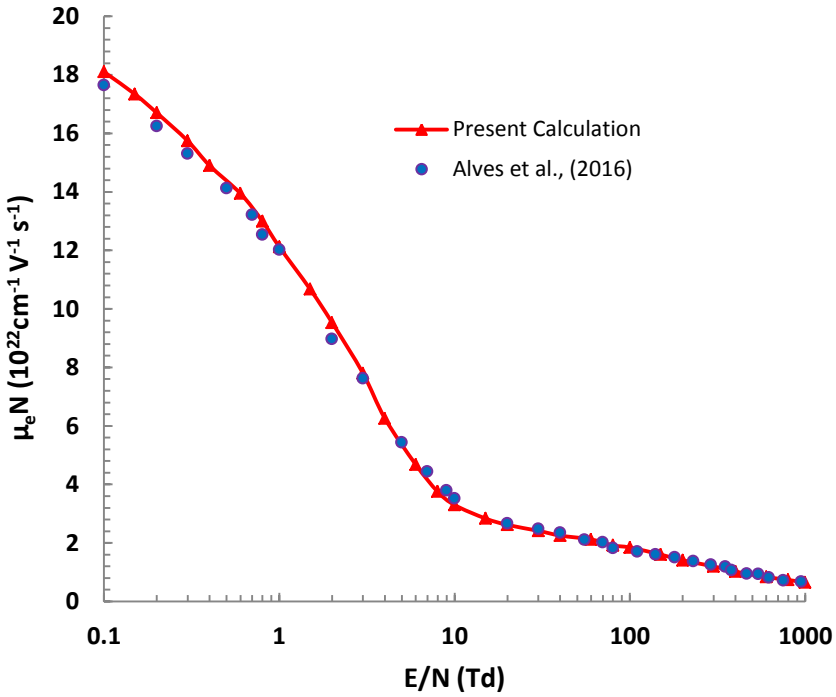

Figure 6. Variation of the reduced electron mobility with E/N values for oxygen.

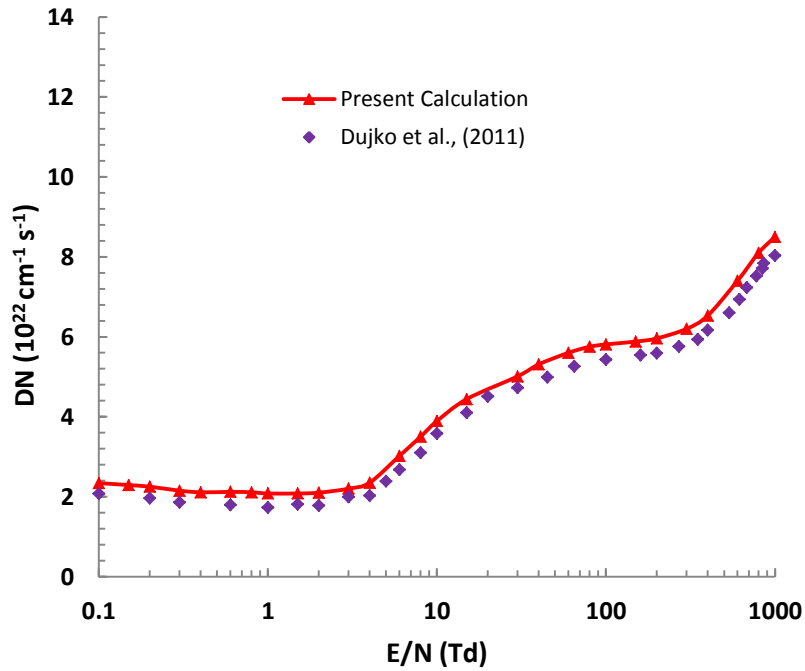

Figure 7. Variation of the density normalized diffusion coefficient with E/N values for oxygen.

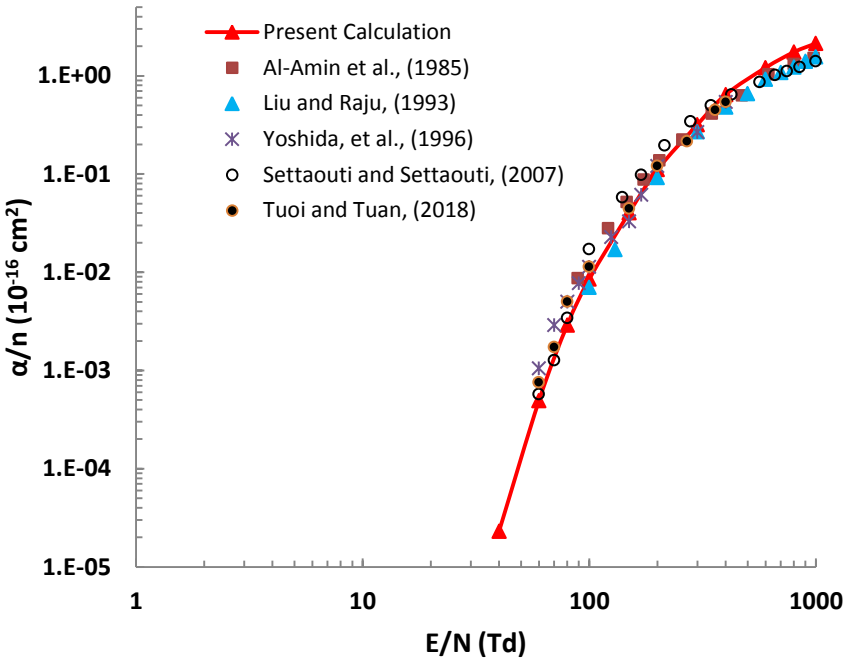

Figure 8. Variation of the reduced ionization coefficient with E/N values for oxygen.

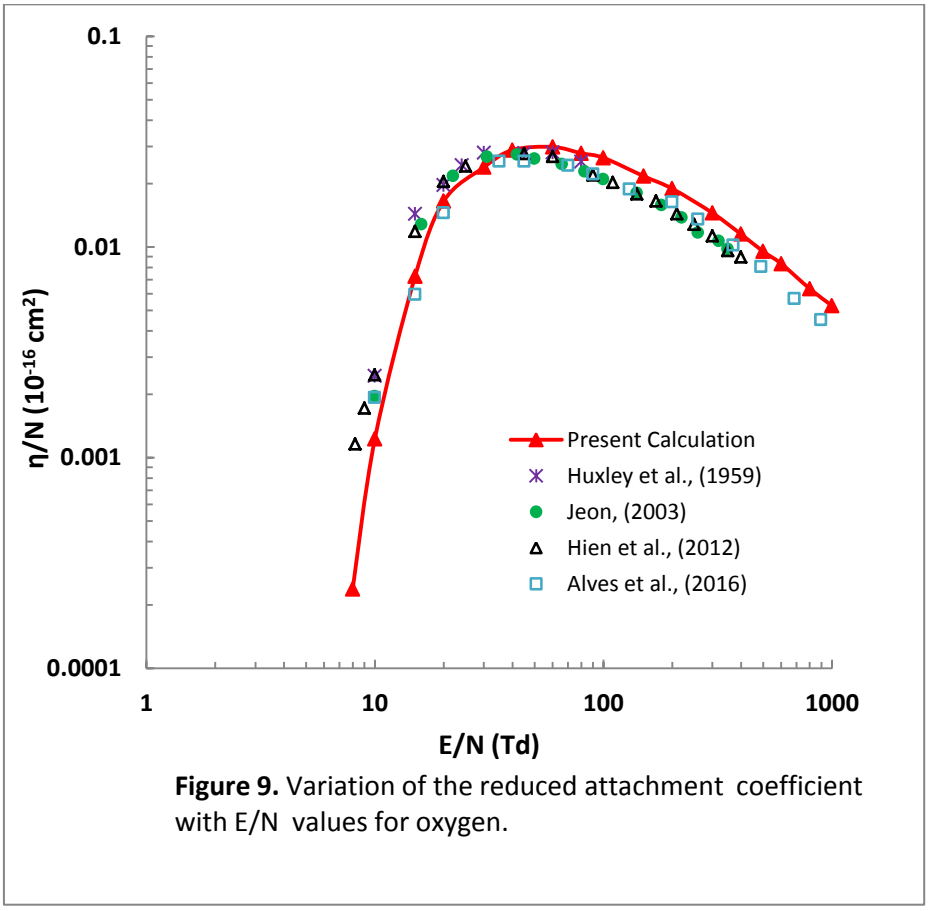

Figure 9. Variation of the reduced attachment coefficient with E/N values for oxygen.

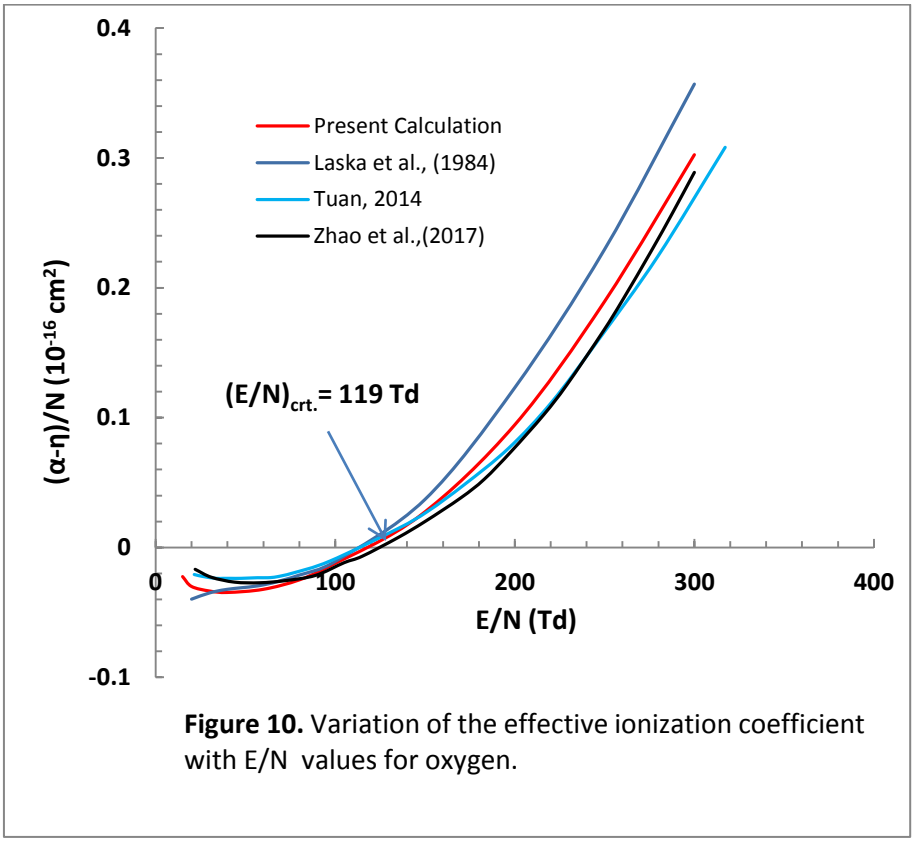

Figure 10. Variation of the effective ionization coefficient with E/N values for oxygen.

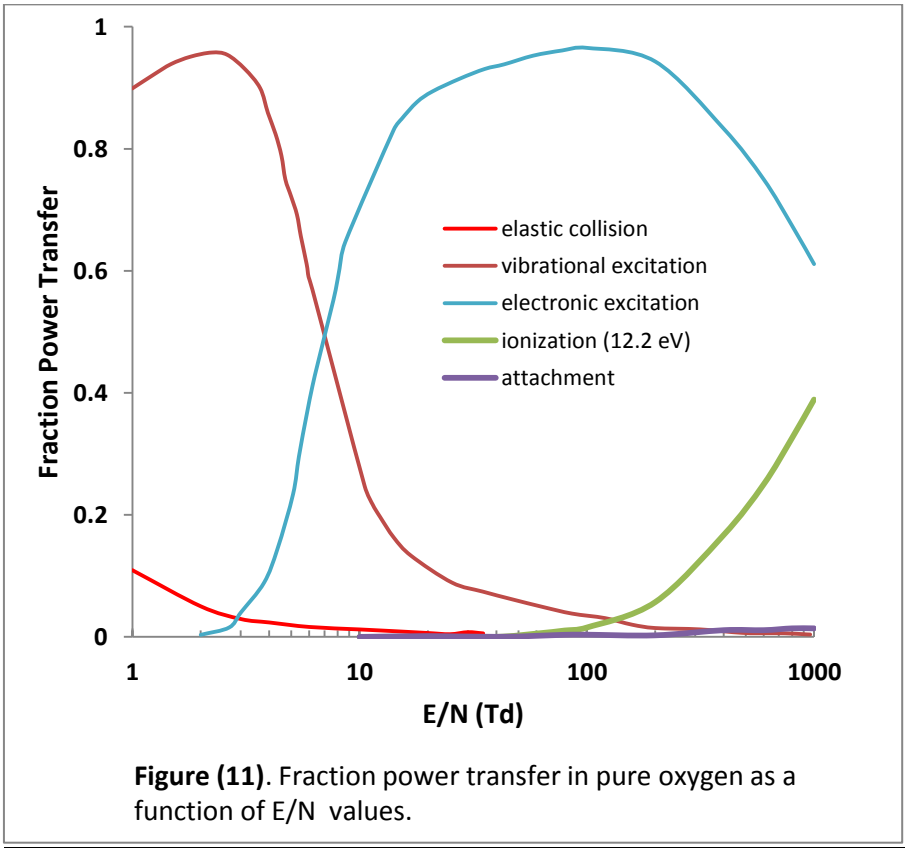

Figure (11). Fraction power transfer in pure oxygen as a function of E/N values.

4. Conclusion

The electron swarm parameters in pure oxygen has been calculated and analyzed over a wide range of E/N varying from 0.1 Td to 1000 Td, using two-term solution of Boltzmann equation, where the effect of the ionization coefficient would be considered. A set of electron/molecule cross-sections has been used to calculate electron energy distribution function (EEDF) and swarm parameters namely, electron drift velocity, mean electron energy, characteristic energy, electron mobility, diffusion coefficient, ionization and attachment coefficient. The distribution function strongly effected by changing the electric field strength E/N, whereas, the effect of second kind collision (super-elastic collision) is not important at high E/N. The calculated swarm parameters are agree well with previous experimental and theoretical values. Moreover, the reduced critical electric field strength $(E/N)_{crt}$ is calculated using effective, ionization curves. Furthermore, the energy losses by different types of elastic and inelastic collision have been explained.

REFERENCES

Al-Amin, S. A. J., Kucukarpaci, H. N. and Lucas, J. (1985), Electron swarm parameters in oxygen and methane. *J. Phys. D: Appl. Phys.*, 18(9), pp. 1781-1794.

Al-Amin, S. and Lucas, J. (1988). Electron swarms in mixtures of metal vapour and argon gas. *Journal of Physics D: Applied Physics*, 21(8), pp.1261-1270.

Alves, L. L., Coche, P., Ridenti, M. A. and Guerra, V. (2016). Electron scattering cross sections for the modeling of oxygen-containing plasmas. *Eur. Phys. J. D*, 70, pp.124-13.

Beaty, E. C., Dutton J. and Pichford, L. C. 1979. A bibliography of electron swarm data. *JILA (Joint Institution for Laboratory Astrophysics). Information Center Report No. 20*.

Bousoltane, K. and Kieffel, Y. (2018). Investigation on the influence of the O_2 content in fluoronitrile/CO_2/O_2(g3) mixtures on the breaking in high voltage circuit breakers. *In International Conference on Gas Discharges and their Applications.*

Brand, K. P. and Kopainsky, J. (1979). Breakdown field strength of unitary attaching gases and gas mixtures. *Appl. Phys*. 18(4), pp. 321-333.

Crompton, R. W. and Elford, M. T. (1973). The drift velocity of electrons in oxygen at 293K. *Ast. J. Phys.*, 26, pp. 771-782.

Dujko, S., Ebert, U., White, R. D., and Petrovic, Z. L. (2011). Boltzmann equation analysis of electron transport in a N_2-O_2 streamer discharge. *Japanese Journal of Applied Physics*, 50, 08JC01 (6pp).

Dutton, J. 1975. A survey of electron swarm data. J. Phys. Chem. Ref. Data, 4(3), pp. 577-856.

Eguz, E. A., Chachereau, A., Hosl, A. and Franck, C. M. (2019). Measurements of swarm parameters in $C_4F_7N/O_2/CO_2$, $C_5F_{10}O/O_2/CO_2$ and $C_5F_{10}O/O_2/N_2$ mixtures. *The 19th International Symposium on High Voltage engineering*, Budapest, Hungary, August, 26-30.

Engelhardt, A. G. and phelps, A. V. (1963). Elastic and inelastic collision cross sections in hydrogen and deuterium from transport coefficients. *Phys. Rev*., 131(5), pp. 2115-2128.

Fridman, A. 2008. *Plasma chemistry*. 2nd ed., Cambridge University Press, Drexel.

Govinda-Raju, G. 2006. *Gaseous Electronics: Theory and practice*, Taylor and Francis LLc, Boca Raton, USA.

Govinda-Raju, G. 2012. *Gaseous Electronics, Tables, Atoms, Molecules*, Taylor and Francis LLc, Boca Raton, USA.

Govinda-Raju, G. 2017. Analysis of discharge parameters for applications in plasma devices. Progress *In Electromagnetics Research Symposium*, Fall (PIERS-FALL), Singapore, 19-22 November.

Gousset, G., Ferreira, C. M., Pinheiro, M., Sa, P. A. Touzeau, M., Vialle, M. and Loureiro, J. (1991). Electron and heavy-particle kinetics in the low pressure oxygen positive column. *J. Phys. D: Appl. Phys.*, 24(3), pp. 290-300.

Graves, D. (2014). Low temperature plasma biomedicine: A tutorial review, Phys. *Plasmas* **21**, 080901(11pp).

Guerra, V., Rejero-del-Caz, A., Pintassllgo, C. D. and Alves, L. L. (2019). Modelling N_2-O_2 plasmas: volume and surface kinetics. *Plasma Sources Sci. Technol*. 28, 073001 (38pp).

Hake Jr, R. D. and Phelps, A. V. (1967). Momentum transfer and inelastic collision cross sections for electrons in O_2, CO and CO_2. *Phys. Rev*., 158(1), pp. 70-84.

Hangelaar, G. J. M. and Pichford, L. C. 2005. Solving the Boltzmann equation to obtain electron transport coefficients and rate coefficients for fluid models. *Plasma Sources Sci. Technol*., 14(4), pp. 722-733.

Hartney, M. A., D. W. Hess, and D. S. Soane (1989). Oxygen plasma etching for resist stripping and multilayer lithography. *J. Vac. Sci. Technol. B*, 7 (1), 1–13.

Hernandez-Avila, J. L. and Urquijo, J. D. (2006). Measurement of electron transport and effective ionization in SF_6-air and SF_6-O_2 mixtures. *J. Phys. D: Appl. Phys.*, 39(4), pp. 647-651.

Hien, P. X., Tuan, D. A. and Jeon, B. H. (2012). Electron collision cross sections for the TMS molecule and electron transport coefficients in TMS-Ar and TMS-O_2 mixtures. *Journal of the Korean Physical Society*, 61(1), pp. 62-72.

Huxley, L. G. H., Crompton, R. W. and Bagot, C. H. 1959. A new method for measuring the attachment of slow electrons in gases. Australian Journal of Physics, 12(3), pp. 303-308.

Itoh, H., Shimozuma, M. and Tagashira, H. (1980). Boltzmann equation analysis of the electron swarm development in SF_6 and nitrogen mixtures. *J. Phys. D: Appl. Phys*., 13(7), pp. 1201-1209.

Jeon, B. H., Ha, S. C., Paek, S. K. and Nakamura, Y. (1997). Momentum transfer cross section for oxygen molecule by electron transport coefficients in the O_2-Ar mixtures and in pure O_2 molecule. *Proceeding of the 5th International Conference on Properties and Applications of Dielectric Materials, May 25-30*, Seol, Korea.

Jeon, B. H. and Nakamura, Y. (1998). Measurement of drift velocity and longitudinal diffusion coefficient of electrons in pure oxygen and in oxygen-argon mixtures. *J. Phys. D: Appl. Phys.*, 31(17), pp. 2145-2150.

Jeon, B. H. (2003). Determination of electron collision cross sections for oxygen molecule by using an electron swarm study. *Journal of the Korean Physical Society*, 43(4), pp. 513-525.

Jiang, P. and Economou, D. J. (1993). Temporal evolution of the electron energy distribution function in oxygen and chlorine gases under dc and ac fields. *J. Appl. Phys*., 73(12), pp. 8151-8160.

Láska, L., Mašek, K., Krasa, J. and Perina, V. (1984). Dielectric properties of SF_6 mixtures containing oxygen and other gases. *Czech. J. Phys. B*, 34, pp. 1038-1047.

Leyla, Z., Leila, M. and Mebarek, D. (2011). Monte-Carlo Simulation for an electrical discharge in O_2. *Advanced Materials Research*, 337, pp. 211-214.

Li X., Zhao H. and Jia S. (2012). Dielectric breakdown properties of SF_6–N_2 mixtures in the temperature range 300–3000K. *J. Phys. D: Appl. Phys.*, 45(44), 445202(7pp).

Linsheng, W., Min, Xu. and Dingkun, Y. (2014). Electron transport coefficients and ionization coefficients in SF_6-O_2 and SF_6-air mixtures using Boltzmann analysis. *Plasma Science and Technology*, 16(10), pp. 941-947.

Liu, J. and Govinda Raju, R. G. (1992). Calculation of electron swarm parameters in oxygen using a rigorous Boltzmann equation analysis. *Can. J. Phys*., 70, pp. 216-224.

Liu, J. and Govinda Raju, R. G. (1993). Electron swarm parameters in nitrogen oxygen and air. *IEEE Transactions on Electrical Insulation.* 28(1), pp. 154-156.

Loureiro, J. and Amorim, J. 2016. *Kinetics and Spectroscopy of Low Temperature Plasmas*. Springer.

Lu, X. Laroussi, M. and V Puech, V. 2012. On atmospheric-pressure non-equilibrium plasma jets and plasma bullets, *Plasma Sources Sci. Technol*. 21(3), 034005 (17pp).

Lucas, J., Price, D. A. and Moruzzi, J. L. (1973). The calculation of electron energy distributions and attachment coefficient for electron swarm in oxygen. *J. Phys. D: Appl. Phys*., 6(12), pp. 1503-1513.

Makabe, T. and Petrovic, Z. L. 2015. *Plasma Electronics Applications in Microelectronic Device Fabrication*, 2nd ed., CRC Press Taylor & Francis Group.

Mašek, K. (1975). An analytical approach to the distribution functions of electrons in the molecular oxygen discharge, Czech. *J. Phys. B,* 25(6), pp. 686-700.

Mašek, K., Růžička, T. and Láska, L. (1977a). Electron gas in molecular oxygen discharge. *Czech. J. Phys. B*, 27(8), pp. 888-898.

Mašek, K., Láska, L. and Růžička, T. (1977b). Dissociative attachment coefficient in oxygen. *J. Phys. D: Appl. Phys.*, 10, L25-L28.

McNevin, S. C. (1990). Radio frequency plasma etching of Si/Sio_2 by Cl_2/O_2 : Improvements resulting from the time modulation of the processing gases. *J. Vac. Sci. Technol. B*, 8(6), pp. 1185-1191.

Morgan, W. L. and Penetrante, B. M. (1990). ELENDIF: A time dependent Boltzmann solver for partially ionized plasmas. *Computer Physics Communications*, 58(1-2), pp. 127-152.

Myers, H. (1969). Analysis of electron swarm experiments in oxygen. *J. Phys. B: Atom. Molec. Phys*., 2(2), pp. 393-402.

Nakamura, V. and Lucas, J. 1978. Electron drift velocity and momentum cross-section in mercury, sodium and thallium vapors. II. Theoretical, *J. phys. D: Appl. Phys*., 11(3), 337-345.

Nelson, R. D. and Davis, F. J. (1972). Thermal and near thermal electron transport coefficients in O2 determined with a time-of- light swarm experiment using Drift Dewell . *J. Chem. Phys*., 56(10), pp. 4079-4084.

Nighan, W. L. (1970). Electron energy distributions and collision rates in electrically excited N_2, CO, and CO_2. *Phys. Rev*., 2(5), pp. 1989-2000.

Nikitovic, Z., Stojanovic, V. and Petrovic Z. (2010). Transport coefficients for electron scattering in mixtures of CF_4, Ar and O_2. *Publ. Astron. Obs. Belgrade*, 89, pp. 75-78.

Nikitovic, Z., Stojanovic, V. and Radmilovic-Radjenovic, M. (2011). Transport coefficients for electron in mixtures $CF_4/Ar/O_2$ and CF, CF_2 or CF_3 radicals. *Acta Physica Polonica* A, 120(2), pp. 289-291.

Othman, M. M., Taha, S. A., Mohammad, J. J. and Karem, A. S. 2018. Electron swarm parameters in Germane – Argon mixtures using Boltzmann equation. *ZANCO Journal of Pure and Applied Sciences*, 30 (1), pp. 34-43.

Othman, M. M., Taha, S. A. and Salih, I. H. 2019a. Analysis of electron transport coefficients in SiH_4 gas using Boltzmann equation in the presence of applied electric field. *ZANCO Journal of Pure and Applied Sciences*, 31 (1), pp. 77-88.

Othman, M. M., Taha, S. A. and Salih, I. H. 2019b. Solving of the Boltzmann transport equation using two - term approximation for pure electronegative gases (SF_6, CCl_2F_2). *ZANCO Journal of Pure and Applied Sciences*, 31 (s4), pp. 7-25.

Pancheshnyi, S. (2013). Effective ionization rate in nitrogen-oxygen mixtures. *J. Phys. D: Appl. Phys.*, 46(15), 155201 (8pp).

Phelps, A. (1985). Tabulations of collision cross sections and calculated transport and reactions coefficients for electron collisions with O_2. *JILA Information Center Report No.28*, university of Colorado, Colorado.

Price, D. A. and Moruzzi, J. L. (1973). Ionization in mixtures of oxygen and carbon monoxide. *J. Phys. D: Appl. Phys.*, 6(2), pp. L17-L19.

Rapp, D. and Englander-Golden, P. (1965). Total Cross Sections for Ionization and Attachment in Gases by Electron Impact. I. Positive Ionization. *J. Chem. Phys.*, 43(5), pp. 1464-1479.

Rabie, M. and Franck, C. M. (2016). METHES: A Monte Carlo collision code for the simulation of electron transport in low temperature plasma. *Computer physics communication*, 203, pp. 268-277.

Reid, I. D. and Crompton, R. W. (1980). The drift velocity of low energy electrons in oxygen at 293K., Aust. J. Phys., 33, pp. 215-226.

Ridenti M. A. and Amorim J., (2012), A numerical solver for the homogeneous Boltzmann Equation" *Physics Proceeding, XI Young Researchers Meeting*, pp.6-5.

Ridenti, M. A., Alves, L. L., Guerra, V. and Amorim, J. (2015). The role of rotational mechanisms in electron swarm parameters at low reduced electric field in N_2, O_2 and H_2. *Plasma Sources Sci. Technol*., 24, 035002(16 pp).

Rockwood, S. D. and Greene, A. E. (1980). Numerical solutions of the Boltzmann transport equation. *Computer Physics Communications*, 19(3), pp. 377-393.

Rong, M., Sun, H., Fei Yang, F., Wu, Y., Chen, Z., Wang, X. and Wu, M. (2014). Influence of O_2 on the dielectric properties of CO_2 at the elevated temperatures. *Physics of Plasmas*, 21(11), 112117 (13pp).

Roznerski, W. and Leja, K. (1984). Electron drift velocity in hydrogen, nitrogen, oxygen, carbon monoxide, carbon dioxide and air at moderate E/N. *J. Phys. D: Appl. Phys.*, 17(2), pp. 279-285.

Rapp, D. and Englander-Golden, P. (1965). Total Cross Sections for Ionization and Attachment in Gases by Electron Impact. I. Positive Ionization. *J. Chem. Phys.*, 43(5), pp. 1464-1479.

Sakai Y., Tagashira H. and Sakamoto S. (1977). The development of electron avalanches in argon at high E/N values: I. Monte Carlo simulation. *J. Phys. D: Appl. Phys.*, 10(7), pp. 1035-1049.

Settaouti, A. and Settaouti L. (2007). Monte Carlo simulation of electron swarm parameters in O_2. *Eur. Phys. J. Appl. Phys*., 37, pp. 335-341.

Settaouti, A. (2018). Characterization of point-plane corona discharge in oxygen with Monte Carlo method. *Physics Journal*, 4(1), pp. 1-8.

Smith K. and Thomson R. M. (1978). *Computer Modeling of Gas Lasers*, Plenum Press.

Tanaka, Y. (2004). Prediction of dielectric properties of N_2/O_2 mixtures in the temperature range of 300-3500K. *J. Phys. D: Appl. Phys*., 37(6), pp. 851-859.

Taniguchi, T, Tagashira, H., Okada, I. and Sakai, Y. (1978). Three-body attachment in oxygen. **.** *J. Phys. D: Appl. Phys.*, 11(16), pp. 2281-2284.

Tatarova, E., Bundaleska, N. Sarrette, J. Ph. and Ferreira, C. M. (2014). Plasmas for environmental issues: from hydrogen production to 2D materials assembly, *Plasma Sources Sci. Technol*. **23**, 063002 (52pp).

Tejero-del-Caz, A., Guerra , V., Gonçalves , D., Lino da Silva, M., Marques, L., Pinhão, N., Pintassilgo, C. D. and Alves, L. L. (2019). The LisbOn KInetics Boltzmann solver. *Plasma Sources Sci. Technol.*, 28(4), 043001 (21pp).

Thomson, R. M. and Smith, K. (1976). Boltz: A code to solve the transport equation for electron distributions and then calculate transport coefficients and vibrational excitation rates in gases with applied fields. *Computer Physics Communications*, 11(3), pp. 369-383.

Thorsteinsson, E. G. and J. T. Gudmundsson (2010). The low pressure Cl_2/O_2 discharge and the role of ClO. *Plasma Sources Sci. Technol*. 19 (5), 055008 (17pp).

Tuan, D. A. and Jeon, B. H. (2012). Electron collision cross sections for the tetraethoxysilane molecule and electron transport coefficients in tetraethoxysilane–O_2 and tetraethoxysilane–Ar mixtures. *Journal of the Physical Society of Japan*, 81, 064301 (8pp).

Tuan, D. A. (2014). Calculations of electron transport coefficients in Cl_2-Ar, Cl_2-Xe and Cl_2-O_2 mixtures. *Journal of the Korean Physical Society*, 64(1), pp. 23-29.

Tuoi, P. T., Tuan, D. A. and Hien, P. X. (2018). Electron collision cross sections for the TRIES molecule and electron transport coefficients in TRIES-Ar and TRIES-O_2 mixtures. *Journal of the Physical Society of Japan*, 73(12), 1855-1862.

Wagner, K. H. (1971). Ionization, electron attachment, detachment, and charge transfer in oxygen and air. *Z. Phys*., 241, pp. 258-270.

Xiao, S., Tian, S., Cressault, Y., Zhang, X., Tang, J., Li, Y. and Deng. Z. (2018). Study on the influence of O_2 on the breakdown voltage and self-recovery characteristics of c-C_4F_8/N_2 mixture. *AIP Advances*, 8(8), 085121 (10pp).

Yoshida, K., Tagashira, H., Ohshima, T., Ohuchi, H. and Kishimoto, Y. (1996). Measurement of the Townsend first ionization coefficient in tetraethoxysilane and oxygen mixtures. *J. Phys. D: Appl. Phys.*, 29(8), pp. 2124-2128.

Yousfi, M., Urquijo, J. D., Juárez, A., Basurto, E. and Hernández-Ávila, J. L. (2009). Electron Swarm Coefficients in CO_2–N_2 and CO_2–O_2 Mixtures. *IEEE Transactions on Plasma Science*, 37(6), pp. 764-772.

Zhao, H. and Lin, H. (2016). Dielectric breakdown properties of N_2–O_2 mixtures by considering electron detachments from negative ions. *Physics of Plasmas*, 23(7), 073505 (7pp).

Zhao, H., Deng, Y. and Lin, H. (2017). Study of the synergistic effect in dielectric breakdown property

of CO_2-O_2 mixtures. *AIP Advances*, 7(9), 095102 (21pp).

Zhao, H., Tian, Z., Deng, Y., Li, X. and Lin, H. (2017). Study of the dielectric breakdown properties of CO_2–O_2 mixtures by considering electron detachments from negative ions. *Journal of Applied Physics* 122(23), 233303 (8pp).

ZANCO Journal of Pure and Applied Sciences
The official scientific journal of Salahaddin University-Erbil
https://zancojournals.su.edu.krd/index.php/JPAS

ISSN (print):2218-0230**, ISSN (online):** 2412-3986**, DOI: http://dx.doi.org/10.21271/zjpas**

RESEARCH PAPER

Preliminary Cost Estimation Modeling for School Buildings in Sulaimani Governorate

DalyaFarhadAbubakr[1;] Noori Sadiq Ali[2]
[1] construction Eng. At University of Sulaimani, Iraq.
[2] Civil Engineering department-university of Cihan- Erbil

A B S T R A C T:
Cost estimation for any construction projects at the early stage is a significant attempt, which has a main role in the success of the construction projects, because estimation at the early stage before design is very desired for decision maker to decide whether to start or not according to available budget. All parties involved in construction work as (owners, engineers, contractors and others) pay a great attention to this stage where limited information is available with no drawings or designs even no specifications. The objective of this research is to derive a model relating the cost of project as awarded with several independent variables (parameters) which are; site area, building area, duration(days), earthwork, area of doors and windows, number of floors, number of columns, distance from the city center(km), by utilizing linear regression techniques. The research methodology consists of data collection of 52 school building projects from public sectors which carried out between 2007 and 2014 in Sulaimani governorate. The models have been developed by applying Excel program and Minitab 19 software, then the models have been summarized and best one has been selected. Also, several statistical procedures have been conducted such as R^2, R^2- adjusted and two sample t-test were used to select more reliable equation. To find out the accuracy of each developed model, the author calculated mean absolute percentage error (MAPE). The range was between 25.3% and 46%. The R^2 was between 0.87 and 0.977 and also the ρ-value from two sample t- test was between 0.891 and 0.991.

KEY WORDS: Cost; Estimation; Model; Pre-Design; Regression.
DOI: http://dx.doi.org/10.21271/ZJPAS.32.5.5
ZJPAS (2020) , 32(5);54-61 .

1. INTRODUCTION

Early stage cost estimation is a cost measuring which is used for prediction of the cost of a project before planning and design phase (Alumbugu et al.,2014). Early cost estimation is a systematic process which has a great impact on the new construction projects. Estimating is an essential part of the engineer's work; therefore, a great interest will be received over the years (Mahamid et al., 2010).

* **Corresponding Author:**
DalyaFarhadAbubakr
E-mail: Dalya.abubakr@univsul.edu.iq
Article History:
Received: 03/03/2020
Accepted: 05/06/2020
Published: 13/10 /2020

The conceptual cost estimation has a great effect on the future of the project success. This process depends on the background, which enters the taking out of different relationships between cost and its effect factors (Adel et al., 2016). Cost is one of the main principles for making decisions at the early stages of a building design process (Gunaydın et al., 2004). Any successful project is known by gathering three criteria, which are fitting cost with budget, implementing on time and quality as specified by the owner (Rezaian, 2011) (Shehatto, 2013). Wrong budget estimation or incorrect scheduling can simply switch and invert a predictable profit to loss (Cheng et al, 2010). In today's global competitive world, moving back profit limits and decreasing market stocks, cost control plays a major role for being competitive while maintaining high quality levels (Gunaydın et al., 2004). Therefore, effective

estimating is one of the most important factors of a construction project attainment (Al-Shanti, 2003). The cost of a building is influencing expressively by decisions made at the design phase. While this effect decreases through all stages of the building project, which allows owners and planners to evaluate project option and control costs successfully. Due to the great role of cost estimate in early stage and incomplete information during the early phase of a project, construction managers generally use their knowledge, practice and standard estimate procedures to measure project costs. Therefore, such perception plays important part in helping project owners and planners in their early decisions. Researchers have worked hard to find out best way to develop cost estimate techniques that maximize the applied value of limited information in order to improve the exactness and dependability of cost estimation work (Cheng et al., 2010). Thus, many methods and techniques have been investigated either traditional or artificial intelligence methods to predict and estimate preliminary cost of the project at early stage.

2. Literature review

Cost estimating is a decisive part of construction projects, where cost is considered as one of the most important criteria in decision making at the early stages of building design process (Gunaydın et al., 2004). Numerous projects tolerate suffering and possible profit loss because of unsystematic cost and schedule following practices as well as erroneous data collection and estimates (Al Jawhar & Araji, 2016). The reliability of estimation is an important factor in the success of any construction project, since cost overruns are a main problem, especially with recent weight on firm budgets. Certainly, cost overruns can lead to end up of a project. In some cases, a possible overrun may result in cancellation of a project (Feng et al., 2010). One of the most important problems facing the construction management process is the occurrence of change orders, which became expected in every construction project and the magnitude of these variations differs from project to project. Considerably causing different effects to the project like changes in cost, time, quality, and completion schedule. One of the most significant causes of the change order come to poor cost estimation (Khalil Ismail & Saber, 2019). Many studies have been done about preliminary cost estimation for construction projects. (Lawther et al., 2001) Investigated in their study a statistical analysis techniques for evaluating historical data by regression analysis. The evaluation started at specifying the main parameters then find out the mathmatical relationships between those parameters in the format of an algebric equation. From 1970s till now continuously regression model is applying for determining cost. "The purpose of linear regression is to use the linear relationship between a dependent variable (e.g. estimated final cost) and independent variables (e.g. location, size) to predict or explain the behavior of the dependent variable. Multiple regression analysis is generally represented in the form: $Y = \beta o + \beta 1X1 + \beta 2X2 + \ldots \beta nXn$. Where Y is the total estimated cost; βo is a constant or line intercept; and X1, X2, etc. are the measures of variables that may help estimate y; and β1, β2 …etc. are the coefficients estimated by regression analysis. The regression equation can then be used to predict the value of a dependent variable once the values of the independent variables are inserted". (Merrow and Yarossi (1990) cited by (Baccarini, 2005)) used y as the measured cost/real cost and x as main parameters.

(Shehatto, June 2013) Focused in developing a model for cost estimation of building projects in pre-design stage with a high degree of accuracy by Artificial Neural Networks. The percentage of accuracy of his modified model was more than (94 %). The sensitivity analysis of the study presented that the area of typical floor and number of floors are the most significant parameters in building cost.

(Lowe, 2006) used 286 sets of historical project data for developing a linear regression models for estimating the cost of building projects. The researcher worked on 41 independent parameters for developing a regression model. The study indicated that five of the independent parameters such as gross internal floor area, building function, duration, mechanical installations, and piling, had a great impact on the total cost.

*(*Kim et al., 2004) examined of three techniques for developing cost estimation models, the examinations are based on multiple regression analysis (MRA), neural networks (NNs), and case-based reasoning (CBR) of the data of 530

historical costs. the result of their study showed that the more accurate model for estimating new projects in future was (NN), then (CBR) was better than (MRA) for predicting new projects.

(Kim et al., 2013) focused on exploring the most dependable and exact cost estimation for school construction projects by comparing the accuracy result of three used techniques (regression analysis (RA), neural network (NN), and support vector machine techniques (SVM)) using historical cost data, for developing the three different models. The result of their study clearly showed that the most reliable models for estimating new projects was NN than the RA and SVM models. Subsequently, it is determined that to more accurate estimation, NN model is most appropriate techniques especially to school building projects.

(Barakchia et al., 2017) investigated different methods and their application for estimating total cost of transport projects. The study was depended on literature review and a quantitative data analysis was examined to find out the regularity of each method, as a result among 12 cost estimation methods according to accuracy; usability/application and acceptance, the parametric, artificial neural network and unit cost methods were the most used methods along the transport infrastructure.

3. Research Methodology

Regression analysis was used to develop a model for estimating the construction costs of school building in Sulaimani Governorate. By reviewing the literature, eight parameters were defined for developing a model such as, duration (days), site area (m^2), building area (m^2), number of floors, number of columns, earthwork (m^3), area of doors and windows (m^2) and distance from the city center (km). several statistical analyses were conducted then the models were developed and summarized. Before choosing the best model the accuracy of each model was checked.

3.1 Data Collection

The data gathered in administrative public sectors including construction firms, institutions and government branch ministries in Sulaimani Governorate. The collected data consists of 52 school building projects which implemented between 2007 and 2014. The main parameters involved the cost of the projects are eight parameters; table.1 shows the summarized characteristic of data collected.

Table.1. Characteristic of data collection.

	Variables	Description	Min.	Max.	Average
Input	X1	Site area (m^2)	732	8400	4834
	X2	Building area (m^2)	182	5550	1516
	X3	No. of floor	1	2	
	X4	No. of columns	0	57	28.5
	X5	Duration (days)	115	529	255
	X6	Earthwork (m^3)	258	16350	3720
	X7	Area of Door & Window (m^2)	62	916	275
	X8	Distance (Km)	0	184	76
Output	Y	Total construction cost (ID)			

3.2 Model Development

MiniTab software version 19 and Excel program have been used for developing regression models, data and variables have been recognized, a sequence of mathematical models has been developed. The typical model is shown below:

$$Y = \beta_o + \beta_1 X_1 + \beta_2 X_2 \ldots\ldots\ldots\beta_n X_n \ldots\ldots\ldots\ldots\ldots\ldots\ldots\ldots (1)$$

Where;

Y…. is the dependent variable which refers to the Total Cost of the project

X_1 …X_n …..are the independent variables, which refers to the site area (m^2), Building area (m^2)… etc.

β_i's……. are regression estimated parameters.

4. Result and Discussion

Linear regression techniques were used for developing a set mathematical model and the results for all tests prove the capability of the tests which are shown in the Table (2):

Table.2. Criterions Results.

N (Number of Projects)	52
R^2	0.92
Adjusted R^2	0.90

The following sections shows eight different regression models that developed to forecast the total cost of the school building projects as below:-

1. Cost-Duration Model(days)

The entire cost of the school building projects utilized as the dependent variable and actual duration in days utilized as the independent variable, C= f(D). The regression model was developed and the result is shown in Table (3).

Table.3. Total cost- Actual duration model.

Model	Independent variables	coefficients	ρ-value	Adjusted R^2(R^2used only for one Variable)
1	(Constant)	-490345504.71	0.00	0.76
	Actual duration (days)	4618929.18	0.00	

The model relating cost of project with duration of execution is as follow:

Total Cost = (4618929.18*Actual Duration)-49034550..... (2)

2. Cost estimating model depends on Actual Duration (days) and Site Area (m^2)

The entire cost of the school building projects utilized as the dependent variable and actual duration in days with site area in square meter utilized as the independent variables, C= f (D, SA). The result of developed regression model is shown in Table (4).

Table.4. Total Cost- Actual Duration and Site Area

Model	Independent variables	coefficients	ρ-value	R^2 - Adjusted
2	(Constant)	-644513031.45	0.000	0.82
	Actual duration (days)	3464587.69	0.000	
	Site area (m^2)	91378.398	0.000	

By inserting second parameter relating total cost of project which is site area with duration the model will be in the form shown below: -

Total Cost = (3464587.69*D) +(91378.398* SA)-644513031.45…….....(3)

3. Cost estimating model depends on Actual Duration (days), Site Area (m^2) and Building Area (m^2)

The whole cost of the school building projects utilized as the dependent variable and actual duration in days, site area in square meter and building area in square meter utilized as the independent variables, C= f (D, SA, BA).The result of developed regression model is shown in Table (5).

Table.5. Total Cost- Actual Duration, site Area and Building Area

Model	Independent variables	coefficients	ρ-value	R^2 - Adjusted
3	(Constant)	-373439225	0.0042	0.86
	Actual duration (days)	2447413.913	0.000	
	Site area (m^2)	38723.23017	0.156	
	Building area (m^2)	160823.6813	0.001	

By inserting third parameter relating total cost of projects which is Building area with duration and site area the model will be in the form shown below: -

Total Cost =(2447413.913*D)+(38723.23017*SA) +(160823.6813*BA) 373439225…….... (4)

4. Cost estimating model depends on Actual Duration (days), Site Area (m^2), Building Area (m^2) and Number of floors.

In the fourth model, the whole cost of the school building projects utilized as the dependent variable and actual duration in days, site area in square meter, building area in square meter and numbers of floors utilized as the independent variables, C= f (D, SA, BA, NF). The result of developed regression model is shown in Table (6).

Table.6. Total Cost-Actual duration, Site area, Building Area and Numbers of floors.

Model	Independent variables	coefficients	ρ-value	R^2 - Adjusted
4	(Constant)	-305797571.2	0.063	0.86
	Actual duration (days)	2593949.35	0.000	
	Site area (m^2)	39471.29	0.152	
	Building area (m^2)	185945.95	0.004	
	Nos. of floors	-108333902.1	0.509	

By inserting fourth parameter relating total cost of project which is number of floors with duration,

site area and building area the model will be in the form shown below: -

Total Cost = (2593949.35*D) +(39471.29*SA) +(185945.95*BA) -(108333902.1*FN)-305797571.2 …… (5)

5. Cost estimating model depends on Actual Duration (days), Site Area (m^2), Building Area (m^2), Numbers of floors and No. of Columns.

The whole cost of the school building projects used in this relationship as the dependent variable and actual duration in days, site area in square meter, building area in square meter, numbers of floors and No. of Columns utilized as the independent variables, C= f (D, SA, BA, FN, NC). The regression model was developed and the result is shown in Table (7).

Table.7. Total Cost- Actual duration, Site area, Building area, No. of floors and No. of columns.

Model	Independent variables	coefficients	ρ-value	R^2 - Adjusted
5	(Constant)	-274657045.1	0.110	0.86
	Actual duration (days)	2689583.76	0.000	
	Site area (m^2)	36748.3799	0.189	
	Building area (m^2)	204120.1588	0.004	
	Nos. of floors	-149629956.2	0.398	
	No. of columns	-1997551.064	0.505	

By inserting fifth parameter relating total cost of project which is No. of columns with duration, site area, building area, No. of floor the model will be in the form shown below:

Total Cost = (2689583.76*D) +(36748.3799*SA) +(204120.1588*BA) -(149629956.2*FN.) -(1997551.064*NC.)-274657045.1

..... (6)

6. Cost estimating model depends on Actual Duration (days), Site Area (m^2), Building Area (m^2), Numbers of floors, No. of Columns and Earthwork (m^3).

The cost of the school building projects used in this relationship as the dependent variable and actual duration in days, site area in square meter, building area in square meter, numbers of floors, No. of Columns and Earthwork used as the independent variables, C= f(D, SA, BA, FN, NC, E).The result of developed regression model is shown in Table (8).

Table.8. Total Cost- Actual duration, site area, Building area, No. of floors, No. of Columns and Earthwork.

Model	Independent variables	coefficients	ρ-value	R^2 - Adjusted
6	(Constant)	-228378117.7	0.194	0.86
	Actual duration (days)	2544598.69	0.000	
	Site area (m^2)	32459.37	0.249	
	Building area (m^2)	209383.80	0.003	
	Nos. of floors	-185607666.2	0.303	
	No. of columns	-2181587.198	0.467	

By inserting sixth parameter relating total cost of project which is earthwork with duration, site area, building area, No. of floors and No of columns the model will be in the form shown below:

Total Cost = (2544598.69* D) +(32459.37*SA)

+(209383.80*BA) -(185607666.2*FN) -(2181587.198*

NC) +(13691.73*E)-228378117.7

.....(7)

7. Cost estimating model depends on Actual Duration (days), Site Area (m^2), Building Area (m^2), Numbers of floors, No. of Columns, Earthwork (m^3) and Area of Doors and Windows (m^2).

The cost of the school building projects used in this relationship as the dependent variable and actual duration in days, site area in square meter, building area in square meter, numbers of floors, No. of Columns, Earthwork and area of doors and windows used as the independent variables, C= f(D, SA, BA, NF, E, NC, ADW).The result of developed regression model is shown in Table (9).

Table.9. Total Cost- Actual duration, Site area, Building area, No. of floors, No. of columns, earthwork, Area of doors and windows.

Model	Independent variables	coefficients	ρ-value	R^2 - Adjusted
7	(Constant)	-60476606.87	0.684	0.90
	Actual duration (days)	1422584.841	0.017	
	Site area (m^2)	45335.58077	0.057	
	Building area (m^2)	99809.16566	0.112	
	Nos. of floors	-340358596.7	0.031	
	No. of columns	-3951600.279	0.120	
	Earthwork	15400.24977	0.150	

	Area of doors and windows	1613924.91	0.000

By inserting seventh parameter relating total cost of project which is area of doors and windows with duration, site area, building area, no. of floors, no. of columns and earthwork the model will be in the form shown below: -

Total Cost = (1422584.841* D) +(45335.58077*SA) +(99809.16566*BA) -(340358596.7*NF) - (3951600.279*CN) +(15400.24977*E) +(1613924.91*ADW)-60476606.87 ……. (8).

8. Cost estimating model depends on Actual Duration (days), Site Area (m^2), Building Area (m^2), Numbers of floors, No. of Columns, Earthwork (m^3), Area of doors and windows and Distance from the city center (km).

The cost of the school building projects in total used in this relationship as the dependent variable and actual duration in days, site area in square meter, building area in square meter, numbers of floors, No. of Columns, Earthwork, area of doors and windows and distance from the city center used to be independent variables, C= f(D, SA, BA, NF, CN, E, ADW, Di). The result of regression model is shown in table (10).

Table.10. Total Cost- Actual duration, Site area, Building area, No. of floors, No. of columns, earthwork, area of D&W, Distance from the city center.

Model	Independent variables	coefficients	ρ-value	R^2 - Adjusted
8	(Constant)	-12794469.66	0.933	0.90
	Actual duration (days)	1437130.47	0.016	
	Site area (m^2)	40168.06	0.095	
	Building area (m^2)	85235.72	0.179	
	Nos. of floors	-284795798.8	0.081	
	No. of columns	-3270639.33	0.207	
	Earthwork	14961.24	0.161	
	Area of doors and windows	1514231.65	0.000	
	Distance from the city center (km)	-716289.53	0.267	

By inserting eightieth parameter relating total cost of project which is distance from city center with duration, site area, building area, number of floors, number of columns, earthwork and area of doors and windows the model will be in the form shown below: -

Total Cost = (1437130.47* D) +(40168.06*SA) +(85235.72*BA) -(284795798.8*NF) - (3270639.33*NC) +(14961.24*E) +(1514231.65*ADW) -(716289.53* Di)-12794469.66 .....(9)

9. Mean absolute percentage error (MAPE)

Excel program has been used to find the percentage of error of each model by calculating mean absolute percentage error (MAPE). Below is the rule for calculating (MAPE):

$$MAPE = \frac{\sum_{i=1}^{n} \left| \frac{Ce - Ca}{Ca} \right|}{\mathrm{N}} * 100 \qquad (10)$$

Where

MAPE= mean absolute percentage error,

Ce= estimated cost,

Ca= actual cost,

N= no. of tested data

Ce-Ca= error.

For checking the reliability of equations, 13 of collected data was used to calculate MAPE and R^2 between actual and estimated cost as shown in table.11. The dependability of each equation was conducted by using 13 data from historical collected data to compute MAPE and R^2 between actual and estimated. To select best model among eight obtained models, minimum MAPE% and maximum R^2 were required. Model #8 had minimum MAPE% which was 25.3%, since maximum R^2 was taken by model #7 which was 0.977. therefore, it was confusing indication to choose best model by MAPE% and R^2 only. Further evaluation has been done to measure the presentation of the eight equations. Nonparametric two sample test was made, in first step the normality of the result from the equations were studied. Conditional on normality of the actual and estimated cost data, then the statistical tests were used to check the dependability of equations. The statistical results (actual and estimated cost) were normally distributed. F-test to compare the variance of both actual and estimated cost data has been performed to check equality of variances and two-sample t-test was used to compute p-value. Table.12 shows the p-value from two sample t-test with equal variance. Therefore, the best model is model 8, it can be applied to estimate cost for school building projects. If comparing this result to the study of (kim, et al, 2013) which focused on the cost estimation modeling for school building. The author of that study used mean absolute error

rates (MAERs) for measuring performance of each models and got 10% if compared to our study which was 25.3%, the difference happened depends on the following points:

1. Different place of working.
2. The range of years, which the author took only three years from 2004 to 2007, while we used wide range from 2007 to 2014.
3. Number of data, the author used 197 data set for developing the regression model while the current data just 52 data.
4. Different input parameters.

Table.11. Results of evaluation criteria for equations of Actual cost compared to Estimated cost data.

		Evaluation Criteria	
NO.	Equation Number	MAPE %	R^2
1	Eq.2	33.85	0.871
2	Eq.3	46.03	0.908
3	Eq.4	29.83	0.921
4	Eq.5	31.44	0.926
5	Eq.6	29.6	0.935
6	Eq.7	29.39	0.939
7	Eq.8	27.33	0.977
8	Eq.9	25.3	0.969

Table.12. Results of two sample t-test with equal variance.

	Normality test		P-value from two
Equation No.	Actual Cost	Estimated Cost	sample t-test
Eq.2	>0.005	> 0.005	0.942
Eq.3	> 0.005	> 0.005	0.949
Eq.4	> 0.005	> 0.005	0.958
Eq.5	> 0.005	> 0.005	0.973
Eq.6	> 0.005	> 0.005	0.931
Eq.7	> 0.005	> 0.005	0.891
Eq.8	> 0.005	> 0.005	0.965
Eq.9	> 0.005	> 0.005	0.991

5. Conclusion and recommendation

In this study, eight regression models were developed to estimate total cost of school building project. The models were checked by a part of historical collected data. The following conclusions can be shown:

- According to previous studies that have studied in the same arena displays that the estimate accuracy in the early stage of construction project process is between ±25% and ±50%.
- The accuracy of the models MAPE are between 25.3%-46%.
- The value of coefficients (R^2) and (adjusted- R^2) for the formed models are between 0.871 and 0.977 which tell us that the relation between dependent and independent parameters are strong enough to be relied on.
- Depend on the study magnitude of $R^2$of the models increase with increasing number of variables.
- It is recommended to choose model 9 which its MAPE= 25.3% and R^2=0.969 and depends on more parameters compared to other models.

Reference

Adel, Kareem and Elyamany, Ahmed and Belal, Adel Mahmoud and Kotb, Akram Soltan, 2016. Developing parametric model for conceptual cost estimate of highway projects. *International Journal of Engineering Science*, Volume 6, pp. 1728--1734.

Al-Shanti, Y., 2003. A Cost Estimate System for Gaza Strip Construction Contractors,.

Alumbugu, Polycarp Olaku and Ola-awo, Wasiu Adeniran and Saidu, Ibrahim and Abdullahi, Mustapha Muhammed and Abdulazeez, Abdulmumin, 2014. Assessment of the factors affecting accuracy of pre-tender cost estimate in Kaduna state, Nigeria. *IOSR Journal of Environmental Science, Toxicology and Food Technology*, Volume 8, pp. 19--27.

Anon., n.d. s.l.:s.n.

Baccarini, D., 2005. *Estimating project cost contingency-Beyond the 10% syndrome. in Australian Institute of Project Management National Conference.* Australia, Australian Institute of Project Management.

Cheng, M.-Y., Tsai, H.-C. & Sudjono, E., 2010. Conceptual cost estimates using evolutionary fuzzy hybrid neural network for projects in construction industry.. 4224–4231.(6).

Feng, W., Zhu, W. & Zhou, Y., 2010. The Application of Genetic Algorithm and Neural Network in Construction Cost Estimate.. Volume 51-155.

Gwang-Hee Kim, Jae-Min Shin, Sangyong Kim, Yoonseok Shin, 2013. Comparison of School Building Construction Costs Estimation Methods Using Regression Analysis, Neural Network, and Support Vector Machine. *Journal of Building Construction and Planning Research*, Issue 1, pp. 1-7.

Gwang-Hee Kim, Sung-Hoon An , Kyung-In Kang, 2004. Comparison of construction cost estimating models based on regression. *Elsevier Ltd.*, Volume 39, pp. 1235-1242.

H. Murat Gunaydın, S. Zeynep Dogan, 2004. A neural network approach for early cost estimation of. Volume 22, p. 595–602.

Husam D. Al-Jawhar , Sura Z. Araji, 2016. Management of the cost overrun of Baghdad University projects using Earned Value Management (EVM) and Value Engineering (VE).. *ZANCO Journal of Pure and Applied Sciences.*, 28(2), pp. 240-250.

Khalil Ismail Wali and Nazik Imad Saber, 2019. An Analysis of Causes and Factors Affecting Change Orders Occurrence in Construction Projects in Iraq.. *ZANCO Journal of Pure and Applied Sciences.*, 31(6), pp. 1-12.

Lawther, P.M. and P.J. Edwards, 2001. Design cost modelling-the way forward. Construction Economics and Building. Volume 32-42.

Lowe, D. M. E. a. A. H., 2006. Predicting construction cost using multiple regression techniques. *Journal of construction engineering and management*, Volume 132(7), pp. 750-758.

Mahamid, Ibrahim and Brul, Amund and Bruland, Amund, 2010. Preliminary cost estimating models for road construction activities.

Moein Barakchia, Olav Torp, Alemu Moges Belay, 2017. Cost Estimation Methods for Transport Infrastructure: A Systematic Literature Review. *ELSEVIER*, 196(270-277).

Rezaian, A., 2011. Time-Cost-Quality-Risk of Construction and Development Projects or Investment.. 218-223(10(2).

Shehatto, M., June 2013. Cost estimation for building construction projects in Gaza Strip using Artificial Neural Network (ANN).

Verlinden, B., Duflou, R., Collin, D. & Cattrysse, D., 2007. Cost estimation for sheet metal parts using multiple regression and artificial neural networks: A case study... 127(2)(93-100).

Weckman, G. e. a., 2010. Using neural networks with limited data to estimate manufacturing cost. Journal of Industrial and Systems Engineering.. 257-274(3(4)).

ZANCO Journal of Pure and Applied Sciences
The official scientific journal of Salahaddin University-Erbil
https://zancojournals.su.edu.krd/index.php/JPAS

ISSN (print):2218-0230**, ISSN (online):** 2412-3986**, DOI: http://dx.doi.org/10.21271/zjpas**

RESEARCH PAPER

Aspect Ratio Consideration in Flat Plate Concrete Slab Deflection

Sarkawt Asaad Hasan[*1], Bahman Omar Taha[2]

[1,2] Department of Civil Engineering, Erbil Engineering Technical College, Erbil Polytechnic University

A B S T R A C T:

This paper addresses the effect of the aspect ratio (long span/short span), concrete strength grade and live load on the long-term deflection of uniformly loaded corner flat plate floor panels without edge beams. It outlines in particular the effects of not considering the aspect ratio parameter in five national codes of practice provisions for the minimum slab thickness and tries to search for the "slab reference span" along which the calculated actual relative deflection and the maximum permissible deflection are determined. The calculations of deflections have been done by the finite element SAFE software through a parametric study with variable long span length, aspect ratio, thickness as recommended by ACI 318-14, concrete grade and live load.

The results showed that, for the range of concrete grade and live load studied, the slab panel aspect ratio parameter has the largest effect on the long-term deflection; the parameter which is overlooked by all the five codes of practice. In spite of this effect, the applicability of the ACI 318-14 provisions for thickness of flat plat floors without beams seemed to be adequate for the L/360 limit, L/240 limit for typical spans and concrete strength grade but showed to be inadequate in many cases to satisfy the L/480 limit. Further, the results showed that the relative deflection along the long span could be recommended for deflection control in flat plate floors without edge beams.

KEY WORDS: Flat Plate, Aspect Ratio, Long Term Deflection, Permissible Deflection.
DOI: http://dx.doi.org/10.21271/ZJPAS.32.5.6
ZJPAS (2020) , 32(5);62-77 .

1. INTRODUCTION

In flat plate/slab floors, the main challenge in the structural design is the deflection control. Excessive deflections of a flat plate floor/roof may render a structure unusable considering both an esthetical and a functional point of view; noticeable deflections may create an impression of faulty construction work or may give a sense of instability. Nevertheless, the major effect of large deflections is usually to cause damage to construction carried by the floor not to the floor itself. Such damage could be seen though cracking of brittle partitions, jamming and miss-alignment of doors.

* **Corresponding Author:**
Sarkawt Asaad Hasan
E-mail: sarakot.hasan@epu.edu.iq
Article History:
Received: 02/03/2020
Accepted: 10/07/2020
Published: 13/10 /2020

The current paper claims that ACI 318-14 code (2014) deflection provisions for flat plate floor panels without edge beams might lack: i) the inclusion of the aspect ratio; ii) assigning explicitly the L/480 long-term deflection (*LTD*) limit to floors supporting masonry partitions; and iii) specifying clearly the span direction (short, long or diagonal) that is required to be used in calculating/checking the permissible maximum deflection.

The current research conducted a nonlinear cracked analysis to obtain the *LTD* for 600 flat plate corner panel cases using finite element SAFE software, for the range of concrete strength (20-40 MPa) and live load (2.4-5 kN/m^2) used in practice and for aspect ratios ranging from 1 to 2. For each panel, three LTD deflections have been

recorded at the middle of each of the short, long and diagonal spans resulting in having a record of 1800 deflection values to evaluate. To this limit, the scope of the current study is to:

- Evaluate the ACI 318-14 code provisions for deflection considering varied aspect ratio, concrete strength grade, live load;
- Determine the "*Slab Reference Span*" for deflection control; for this purpose, the current paper evaluates the relative deflection along all three slab panel directions (short, long and diagonal).
- Recommend a proper LTD limit for floors supporting masonry walls;

1.1 ACI Provisions for Flat Plate Panel Deflection Control.

For slab panels (including flat plate panels), ACI 318 (2014) recommends two alternative procedures for control of deflection. Deflection is controlled by specifying minimum thickness as a ratio of the long span of the slab (maximum span-to-depth ratio). This provision is attractive as a mean of deflection control due to its simplicity; however, it has been criticized by many researchers (Scanlon and Lee (2010), Bondy (2005), Hwang and Chang (1996), Hilbert (1985)) for not providing an allowance for the actual load level, concrete strength, steel quantities, and the desired deflection limit.

Furthermore, there is another dispute in the slab's recommended minimum thickness, which is not having any inclusion for the slab panel aspect ratio. For example, for slab panels between 4x8 m to 8x8 m (keeping the long span constant), ACI 318-14 recommends the same *l/d*, as only the long span (***l)*** is included in the code provisions. The current paper tries to investigate the impact of the slab aspect ratio on the calculated *LTD* in flat plate slabs.

Thompson and Scanlon (1988) conducting Finite Analysis of 300 slabs considering many variables including the slab aspect ratio; Scanlon concluded that for square slab panels, the ACI minimum thickness should be increased by 10 %. In Further, as an inclusion for the flat slab aspect ratio in the recommended minimum thickness, Bondy (2005) suggested basing the limiting span for deflection on the panel diagonal dimension. This is because of the fact that the maximum deflection of the center of the slab panel is an additive function of the spans of both orthogonal directions (Bondy, 2005).

In the 2nd procedure for determination of flat plate panel thickness (which is applicable to all two-way slab types), the theoretical calculated deflection along a "slab reference span" needs to be compared with a maximum calculated permissible deflection. ACI 318 (2014) is silent about the slab reference span direction (short span, long or diagonal span) that is required to be used. Bondy (2005) suggested the use of the diagonal span for this purpose and advised adding a statement in the ACI 318 about this span direction.

The authors made a survey for the "*slab reference span*" direction used for checking of deflection, see **Table 1**. As seen, in spite of having an agreement about the span direction "***Lc***" that the theoretical deflection is calculated along it, there is an extensive disagreement about the span direction "***Lr***" that the maximum calculated permissible deflection is calculated along it. As a matter of functionality to prevent damage to partitions, the purpose of the deflection control is to minimize its variation along a line; therefore, it is an inaccurate to compare deflections calculated along the diagonal span with the maximum permissible deflection calculated along another span {long span [as it is the case in ACI 435 (2003) MacGregor and Wight (2012), ACI SP17 (2015)] or the short span [as it is the case in Nilson et al (2016)]}.

The authors believe that Regan (1981)'s approach is the realistic one considering the slab function in limiting cracks in partitions, as it considers the relative deflection along any line, while in the other approaches, the relative deflection along the long and short spans are neglected, and in some approaches, the mid-panel (diagonal) deflection is compared with a permissible deflection based on other spans (long or short). In the current paper, Regan's approach is selected to be used, where the relative deflection calculated along any span (short, long or diagonal) needs to be compared with the maximum permissible deflection based on the same span aiming to determine the span direction "slab reference span" along which the critical relative deflection occurs.

Table 1: Two-way slab span directions "Slab Reference Span" used for deflection checking against ACI 318 code provisions.

Slab Type	Author	Span "Lc" used for calculating the deflection	Span "Lr" used for determining the maximum permissible deflection
Flat Plate	(ACI 435R-95, 2003, pp. ,66)	*Mid-panel*	***Diagonal span***
	(ACI SP-17(14): Volume 2, 2015, pp. ,139)	*Mid-panel*	***Diagonal span*** *(based on ref* (ACI 435R-95, 2003) *)*
		Mid-panel	***Long span*** *(as another possibility)*
	(MacGregor, J G. and Wight, J K., 2012, pp. ,762)	*Mid-panel*	***Long span***
	(Regan, 1981, pp. ,45)		***Diagonal span*** (for the absolute maximum deflection at the mid-panel); ***Long/short span*** (when the deflection check is made for the sake of the partitions). In this case, the relative deflection in the partition span (mostly Long or Short span) under consideration is calculated.
Slabs with supporting beams	(ACI 435R-95, 2003, pp. ,65), (Nawy, 2009, pp. ,532)	*Mid-panel*	***Long span***
	(Nilson, A., Darwin, D., Dolan, C., 2016, pp. ,444)	*Mid-panel*	***Short span***

1.2 Slab Aspect Ratio in International Codes

ACI 318-14 and CSA A23.3-14 codes considers the aspect ratio in determining the minimum slab thickness only in the case of edge-supported slabs with beams having beam /slab relative stiffness not less than 0.2, while in flat plates/flat slabs floors, no consideration is taken for the aspect ratio. On the other hand, AS 3600 (2018), BS 8110 (1997) and EN 1992 (2004) codes do not include the aspect ratio in determining the slab thickness in all slab types (with/without edge supports).

1.3 Deflection Limitation Affecting Masonry Partitions in International Codes

As a measure to avoid large deflections in slabs and consequently preventing noticeable cracks and functional and esthetic problems in non-structural elements including masonry partitions, the codes of practice have set limits (see **Table 2**) on that part of the total deflection occurring after the installation of the non-structural elements; this deflection part (LTD) is the sum of the *long-term effect* of the sustained loads and the immediate deflection due to any additional live load. This limit is *L*/500 (*L*:Span) in BS8110-97 and EN 1992-04, *L*/500 *(floors supporting masonry partitions where provision is made to minimize the effect of movement) or L/1000 (other cases) in* AS 3600, while in ACI 318-14 and CSA A23.3-14, it could be either *L*/240 or *L*/480 as the term "*not likely (or likely) to be damaged*" stated in the code to specify the use of any of them is ambiguous with respect to floor slabs supporting masonry partitions. Thus, in order to match other codes of practice, the current paper urges to add a definite inclusion of such floors in ACI 318 and CSA A23.3.14, and to consider them as non-structural elements likely to be damaged with excessive deflection.

Considering the "Slab Reference Span" for *LTD* control, among all the five codes of practice, only CSA A23.3-14 and AS3600-18 have a definition for it. As this definition is not stated in ACI 318-14, the current paper search for such a definition for the "Slab Reference Span" in flat plates. AS3600-18 presents a sophisticated approach for the spans that the deflection is checked along it, where it states:

"In general, deflection limits should be applied to all spanning directions. This includes, but is not limited to, each individual member and the diagonal spans across each design panel. For flat slabs with uniform loadings, only the column strip deflections in each direction need be checked."

Table 2: Long term deflection limits and Slab Reference Span in different codes (applicable also to floors supporting partitions)

Code	Long term deflection limit		Slab Reference Span for check
(ACI 318 , 2014)	L/240 floor slabs supporting non-structural elements not likely to be damaged with excessive deflection	L/480 otherwise	**Not specified**
(CSA A23.3-14, 2014)	L/240 floor slabs supporting non-structural elements not likely to be damaged with excessive deflection	L/480 otherwise	Long clear span
(AS 3600-18, 2018)	L/500 floors supporting **masonry partitions** where provision is made to minimize the effect of movement	L/1000 otherwise	-All spans (short, long and Diagonal) for slabs with beams, -Long/Short clear span in flat slab case.
(BS EN 8110-1-97, 1997)	L/500 ≤ 20 mm		**Not specified**
(EN 1992-1-1-04, 2004)	L/500		**Not specified**

1.4 Deflection Calculations

In the current paper, the deflection of a uniformly loaded flat plate corner panel has been determined by two methods: i) SAFE software, with finite element slab mesh of 0.5 m; ii) Theoretical calculation based on the equivalent frame approach.

SAFE is a software produced by CSI (Computers & Structures, Inc.) (2016); it is a special purpose analysis, design, and detailing software for concrete slab systems. For the current slab deflection analysis, the slabs have been modelled using 4-nodded thin shell bending elements with six degree of freedoms per node (three rotation and three displacements); The shell elements capture out-of-plane bending and shear behavior, as well as in-plane deformations with no inclusion of transverse shear deformation. The *LDT* is calculated as (using nonlinear cracked analysis type in SAFE):

$LDT = L_1 + S_1 - S_2$, Where,

L_1: Long-term deflection of 25% live load and 100% self-weight, super imposed deal

S_1: Immediate deflection of 100% live load and 100% self-weight, super imposed deal

S_2: Immediate deflection of 100% live load and 25% self-weight, super imposed deal

In the theoretical calculation, the deflection is calculated using the equivalent frame method for the first interior design frames, with dividing the slab panel into column and middle strips in each direction (ACI 435R-95 (2003), Nilson et al (2016)). **Figure 1** shows actual deformed shape of a slab panel; In this approach, the equivalent frame method is used to analyze the slab in two directions, then to take the average deflection of two parallel column strips and to add the deflection of the middle strip spanning orthogonally to obtain an approximation for the maximum deflection at the center of the slab panel (Crossing-Beam Approach) using Branson effective moment of inertia approach (ACI 318 , 2014) for cracked concrete. The calculated LTD included:

- Deflection affecting construction/equipment installed on the slab, which is equal to the long term nonlinear cracked deflection under full self-weight, superimposed dead and 25 % live load plus the short term nonlinear cracked deflection for 75% of the live load.

- Nonlinear Cracked deflection under full live load;

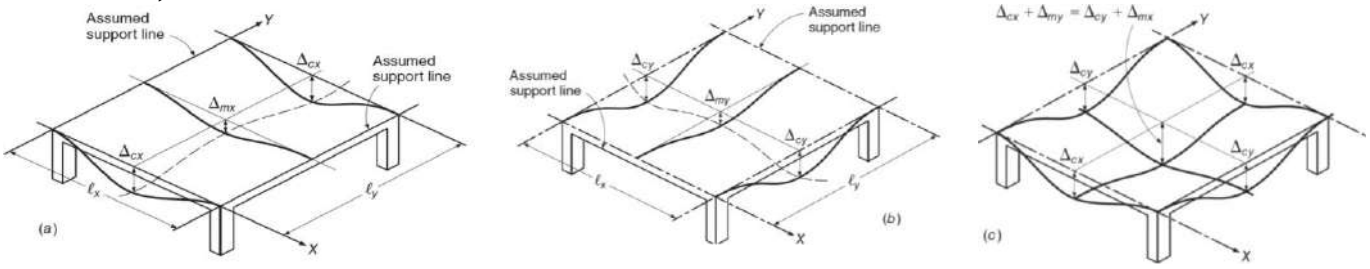

(A) X- DIRECTION BENDING; (B) Y- DIRECTION BENDING (C) COMBINED BENDING

Figure (1) Basic of equivalent frame method deflection analysis (from Nilson et al (Nilson, A., Darwin, D., Dolan, C., 2016))

2. PARAMETRIC STUDY

A parametric study has been performed for the slab deflection evaluation, taking one-story prototype structure consisting of 3 x 3 reinforced concrete flat plate panels without edge beams, having same span length in each direction, designed according to ACI 318-14, taking the ***corner*** panels as the studied panel, as they experience the largest deflection in the studied model. The study program is divided into six main groups as detailed in **Table 3**, and taking the below as constant, in both the SAFE analysis and the theoretical calculation:

- Modulus of rupture is based on ACI-specified value of 0.62 √ f_c' (ACI 318-14, section 19.2.3.1)
- Slab tension reinforcement ratio for cracking analysis= 0.0018,
- Slab compression reinforcement ratio for cracking analysis= 0.0,
- The modulus of elasticity of concrete= 4700 √ f_c' (ACI 318-14, section 19.2.2.1);
- Combined creep and shrinkage time dependent factor = 2 (ACI 318-14, section 24.2.4.1.3);
- Yield strength of reinforcement: 420 MPa;
- Superimposed dead load (SDL) = 2.4 kN/m^2 (including an allowance for partitions)
- Columns: 0.4 x 0.4 m, 3.5 m height, fixed at bottom.

In summary, each group consisted of 100 cases with different slab aspect ratio, live loads and concrete strength grades. The selected range of long spans (5 to 10 m) and concrete strength grades (20 – 40 MPa) are those typically encountered in practice; the lowest live load value taken (2.4 kN/m^2) as this given by ASCE/SEI 7 (2010) provisions for offices.

Table 3: Parametric Study Variables Summary

Group	Slab thick, mm	Span			Concrete compressive strength, MPa	Slab live loads, kN/m^2
		Long span (*L1*), m	Short span (*L2*) cases, m	Aspect ratio range cases		
C05	153.3	5	2.5,3.0,3.5,4.0,5.0	2 to 1	20, 25, 30, 35, 40	2.4, 3.0, 4.0, 5.0
C06	186.7	6	3.0,3.5,4.5,5.5,6.0	2 to 1	20, 25, 30, 35, 40	2.4, 3.0, 4.0, 5.0
C07	220.0	7	3.5,4.0,5.0.6.0.7.0	2 to 1	20, 25, 30, 35, 40	2.4, 3.0, 4.0, 5.0
C08	253.3	8	4.0,5.0,6.0,7.0,8.0	2 to 1	20, 25, 30, 35, 40	2.4, 3.0, 4.0, 5.0
C09	286.7	9	4.5,6.0,7.0,8.0,9.0	2 to 1	20, 25, 30, 35, 40	2.4, 3.0, 4.0, 5.0
C10	320.0	10	5.0,6.0,7.0,9.0,10.0	2 to 1	20, 25, 30, 35, 40	2.4, 3.0, 4.0, 5.0

3. RESULTS AND DISCUSSION

3.1 Long Term Deflection Along all Span Directions (Short, Long, Diagonal)

Figure 2 presents the results of the parametric study including the *absolute LTD* (measured in mm) along three directions (Diagonal span, Interior column strip along each of the short and long span) of the flat plate corner panels. In total, there are 1800 deflection values divided into six long span groups; each group has 300 deflection values (100 deflection values at each direction).

As could be seen in **Figure 2**, in spite of the fact that ACI 318-14 provisions make no difference between all the flat slab cases of the same long span (each group in the current paper), it is clear that there is a noticeable variation in the *LTD* in all directions (short, long and diagonal); this variation increases with the increase of the long span length. This variation is ignored by ACI 318-14 provisions, due to not having any allowance for concrete grade, aspect ratio or live loading in flat plate floors.

As an overview of the rate of variation in the *LTD* within each group, **Table 4** lists the minimum and maximum *LTD* along the long span (*L1*) within the groups. As could be seen, within each group, the lowest LTD value occurred at the case of rectangular panels (aspect ratio of 2), lowest live load (2.4 kN/m^2) and largest concrete grade (40 MPa), while the highest LTD value occurred at the case of square panels (aspect ratio of 1), highest live load (5.0 kN/m^2) and lowest concrete grade (20 MPa). This variation in the *LTD* values within each group along the long span ranged from the largest in group C10 (35.4 mm equal to *L1*/282.5) to the smallest in group C05 (11.3 mm equal to *L1*/442.5).

Table 4: Long-term deflection variation along the long span within each group

Group	Long span (*L1*), mm	Group	Deflection within group, mm		Variation, mm	L1 / variation ratio
			Minimum	Maximum		
C05	5000	C05	3.8	15.1	11.3	442.5
C06	6000	C06	5.5	19.6	14.1	425.5
C07	7000	C07	7.7	27.0	19.3	362.7
C08	8000	C08	10.2	35.6	25.4	315.0
C09	9000	C09	14.0	44.7	30.7	293.2
C10	10000	C10	18.3	53.7	35.4	282.5

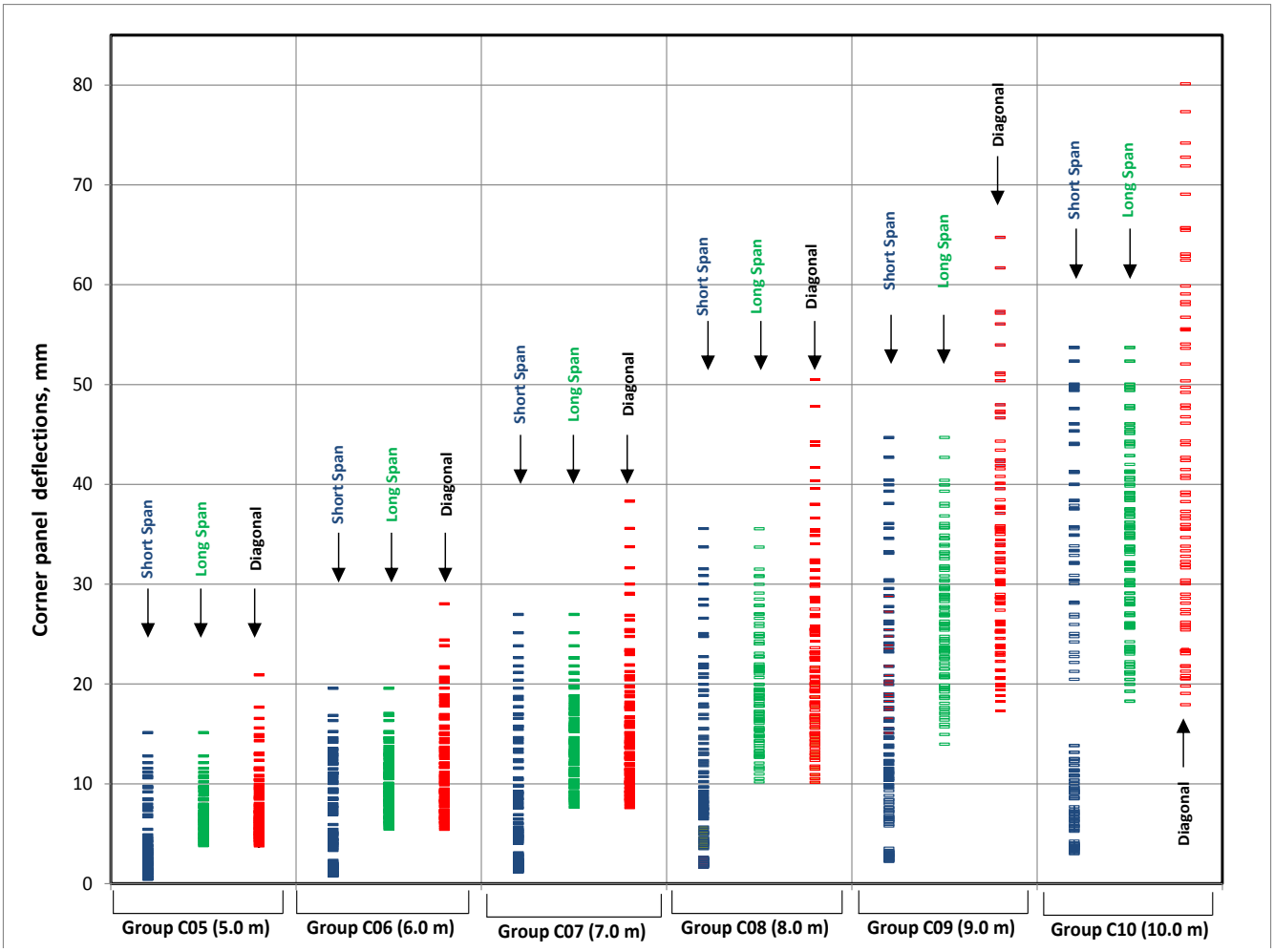

Figure (2) Variation of the corner flat slab panel absolute LTD within the tested groups

3.2 Slab Panel Maximum Relative Deflection

The absolute *LTD* along panel spans (short, long and diagonal) of **Figure 2** are re-presented in **Figure 3** as a ratio of *LTD* to the span that the deflection is measured along it. As could be seen, as the long span is getting larger, the number of cases exceeding the *L*/240 and *L*/480 limits is increasing, as detailed in **Table 5**. As seen, up to 7 m long span, ACI 318 (2014) provisions for the minimum slab thickness are sufficient to assure that the long-term deflections are not exceeding the *L*/240 limit; however, these provisions resulted in long term deflections exceeding the *L*/480 limit in all the long span values.

The relative *LTD* deflection occurred along the long direction in almost all the cases (592 cases out of 600 cases (or 98.7%)), except at 10 x 10 m square panels with low concrete grade (*fc'* = 20, 25 MPa), where the maximum relative deflection occurred at the diagonal direction; even in these cases, the difference did not exceed L/20. Based on that, and consistent with CSA A23.3-14 code (2014), this observation suggests adopting the long span direction in the calculation and evaluation of the *LTD*.

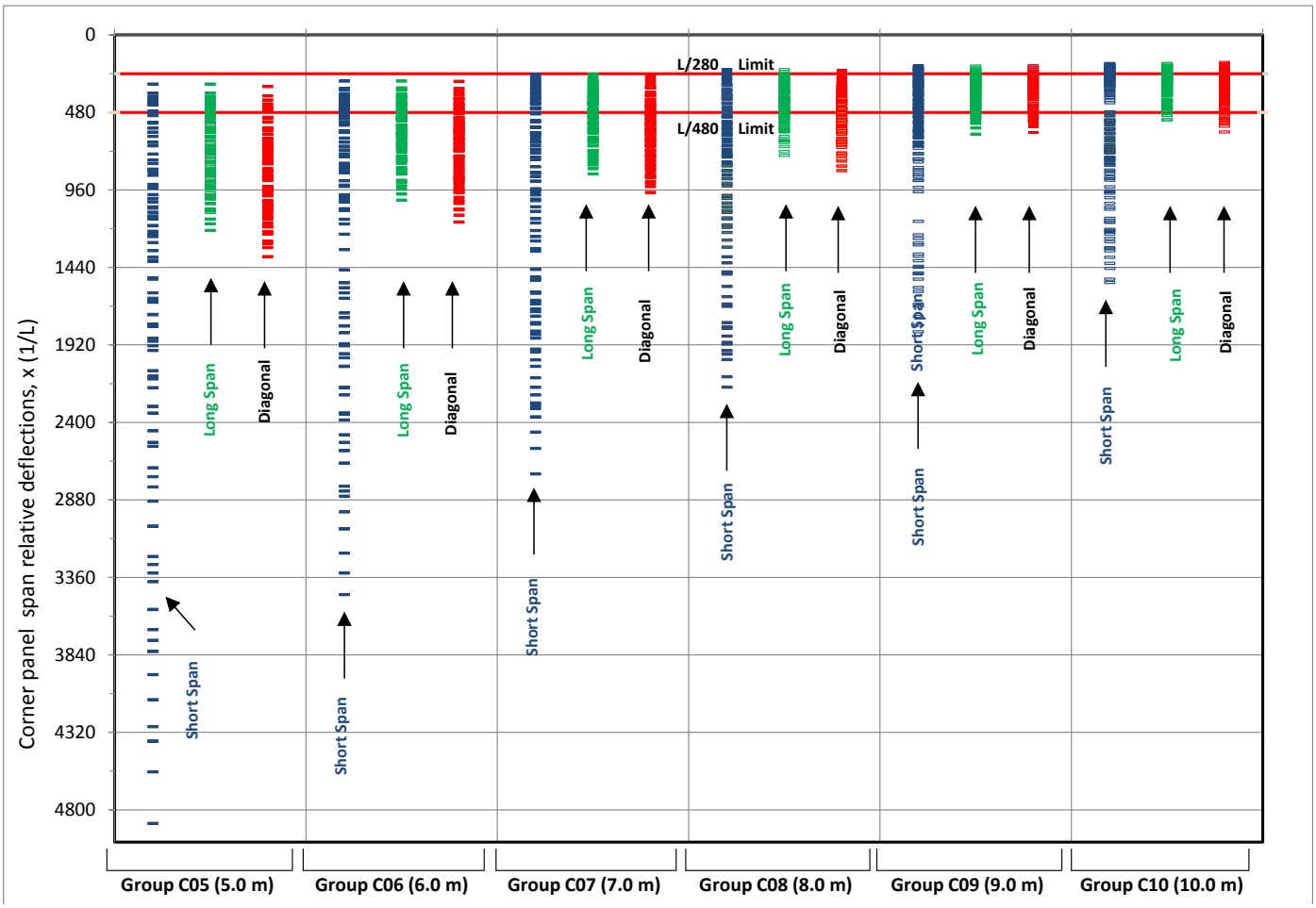

Figure (3) Variation of the corner flat slab panel relative LTD within the tested groups

Table 5: Cases of relative LTD along long span exceeding ACI 318 (2014) limits

Group (each group consists of 100 cases)	Number of cases with relative LTD exceeding L/240			Number of cases with relative LTD exceeding L/480		
	Short Span	Long Span	Diagonal Span	Short Span	Long Span	Diagonal Span
C05	0	0	0	10	11	07
C06	0	0	0	18	27	20
C07	0	0	0	23	46	30
C08	2	2	2	31	71	53
C09	7	11	7	43	90	75
C10	14	24	17	41	97	87

3.3 Slab Panel Relative Deflection Along the Long Span

As the relative *LTD* along the long span appeared to the critical in 98.7 % of the cases, as detailed in the previous section, the deflection results along this span is presented in full in **Table 6.** Hence, the increase in the slab deflection is a combined effect to the three tested variables; the individual effects for each variable are listed in **Table 7**, where the range of the individual effect for each variable (live load, concrete strength, aspect ratio) are reported within each group. As seen, the aspect ratio and the concrete had the largest effect on the *LTD* deflection followed by the live load with the effects being more pronounced at larger spans. The live load had a lesser effect on the LTD deflections compared to the concrete strength due to the status of the applying the live loads, where only 25% of the live load is considered to have long term effect while the other 75% of the live load is considered to have only the short-term effect (immediate deflection). Further, the effect of the concrete strength on the deflection is pronounced through the modulus of elasticity of concrete which is proportional to the square root of compressive strength.

Figure 4 shows the trend of the change in maximum *LTD* along the long span as a function of the panel aspect ratio, where the length "*L*" is taken as the clear long span length. This trend is compared with ACI 318-14 provisions for *LTD* part for panels not attached to normal non-structural elements (*L*/240) and for panels attached to non-structural elements likely to be damaged by large deflection (*L*/480). As could be seen, for the *L*/240 limit, the slabs of long span up to 7.0 m conformed to ACI 318-14 maximum permissible deflection provisions. For higher long span lengths, the non-conformity appeared at cases of low concrete grade and high live load. On the other side, for the *L*/480 limit, the slabs did not perform well in most of the cases. This observation (for slabs with minimum reinforcement ratio) conforms Scanlon and Lee (2010) finding that "*the ACI values (deflection provisions) for flat plates (and flat slabs) seem to be adequate for the L/240 limit for typical spans and loading but may be inadequate in many cases to satisfy the L/480 limit*".

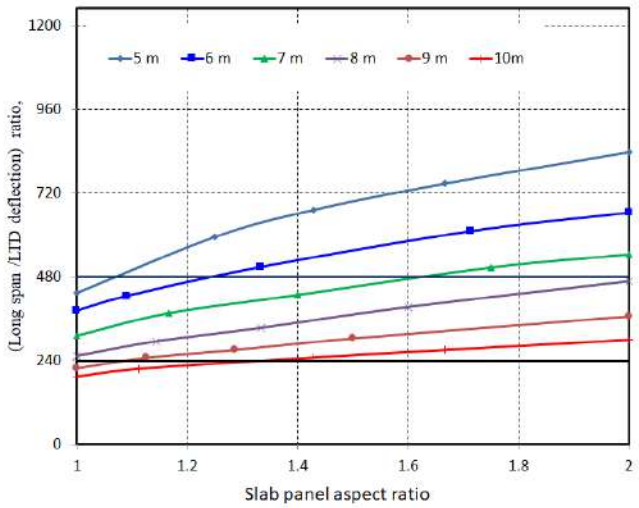

a) Concrete grade of 20 MPa, live load of 2.4 kN/m²

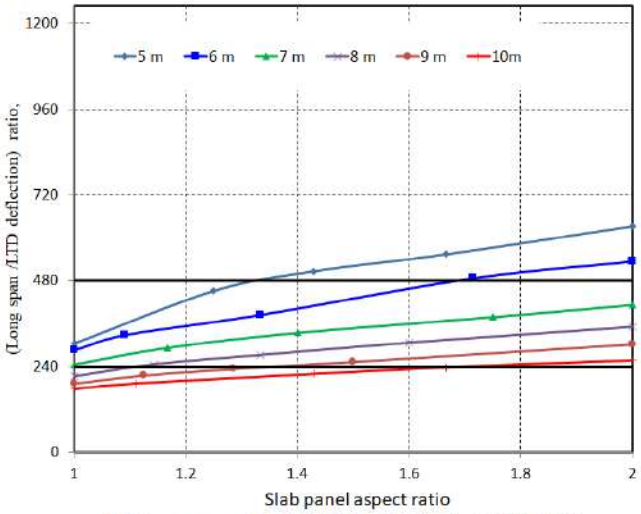

b) Concrete grade of 20 MPa, live load of 5.0 kN/m²

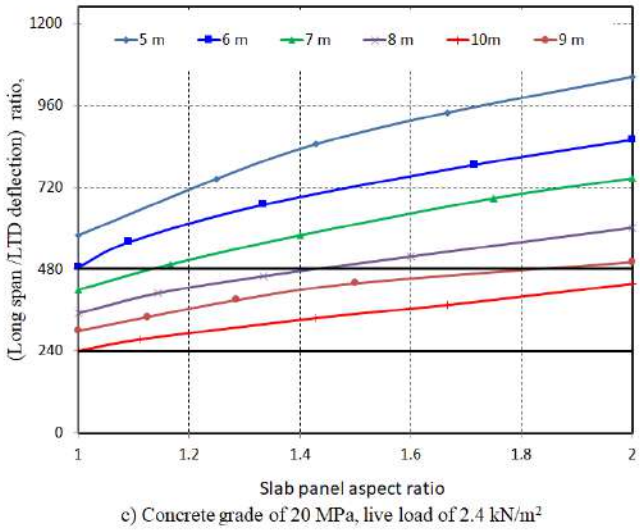

c) Concrete grade of 20 MPa, live load of 2.4 kN/m²

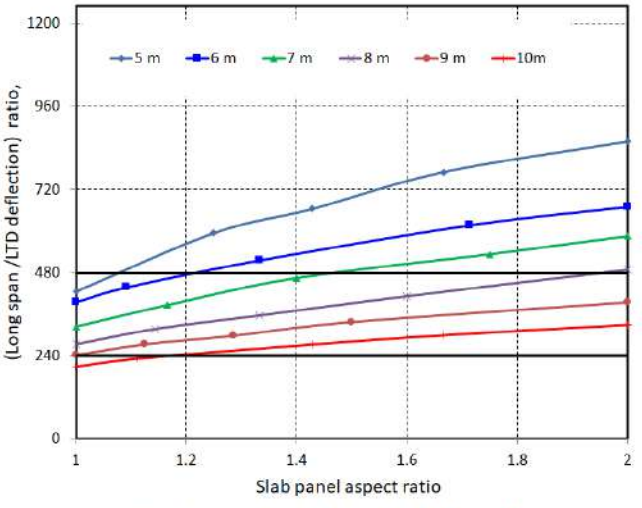

d) Concrete grade of 30 MPa, live load of 5.0 kN/m²

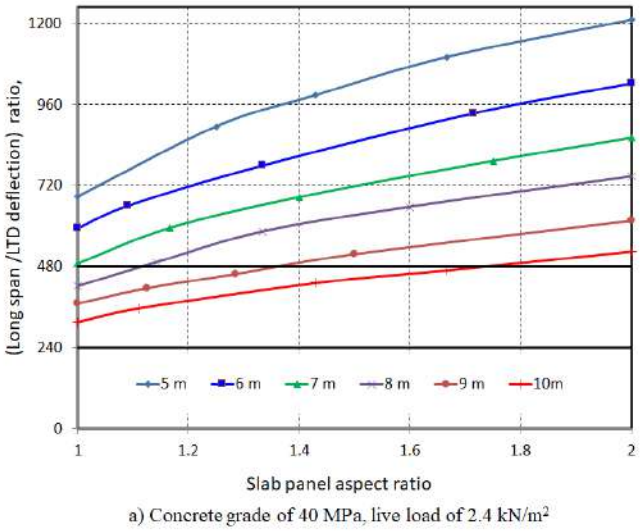

a) Concrete grade of 40 MPa, live load of 2.4 kN/m²

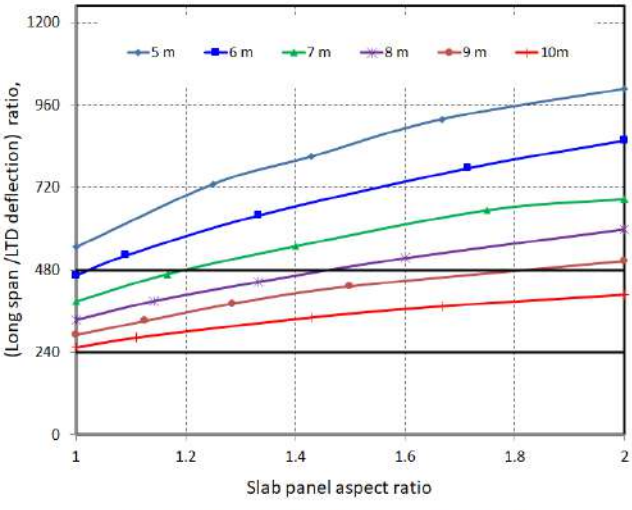

f) Concrete grade of 40 MPa, live load of 5.0 kN/m²

Figure (4) Flat slab floor panel aspect ratio versus (long span/LDT deflection) Ratio

Table 6: Long-Term Deflection along the long span

Group	Long Span, m	Short Span, m	Aspect ratio	Slab thick, mm	Long Term Deflection part, mm																			
					f_c'=20 MPa				f_c'=25 MPa				f_c'=30 MPa				f_c'=35 MPa				f_c'=40 MPa			
					Live load, kN/m^2				Live load, kN/m^2				Live load, kN/m^2				Live load, kN/m^2				Live load, kN/m^2			
					2.4	3	4	5	2.4	3	4	5	2.4	3	4	5	2.4	3	4	5	2.4	3	4	5
C05	5	2.5	2	153.3	5.5	5.9	6.5	7.3	4.8	5.1	5.6	6.2	4.4	4.6	4.9	5.4	4.0	4.2	4.6	4.9	3.8	3.9	4.3	4.6
		3.0	1.67	153.3	6.2	6.5	7.3	8.3	5.4	5.7	6.1	6.9	4.9	5.2	5.7	6.0	4.5	4.7	5.1	5.5	4.2	4.4	4.7	5.0
		3.5	1.43	153.3	6.8	7.3	8.2	9.0	6.1	6.4	7.0	7.6	5.4	5.8	6.2	6.9	5.0	5.3	5.8	6.2	4.7	4.9	5.3	5.7
		4.0	1.25	153.3	7.7	8.4	9.4	10.2	6.7	7.0	7.9	8.8	6.2	6.4	7.0	7.7	5.7	6.0	6.4	7.0	5.1	5.4	6.0	6.3
		5.0	1	153.3	10.6	11.6	12.8	15.1	9.2	9.8	11.1	12.1	8.0	8.5	9.6	10.8	7.3	7.6	8.5	9.6	6.7	6.9	7.6	8.4
C06	6	3.0	2	186.7	8.4	9.0	9.9	10.5	7.1	7.4	8.2	9.3	6.5	6.8	7.3	8.3	5.9	6.2	6.6	7.2	5.5	5.7	6.1	6.5
		3.5	1.71	186.7	9.2	10.0	10.8	11.5	7.7	8.1	9.1	10.0	7.1	7.4	8.2	9.1	6.5	6.8	7.3	7.9	6.0	6.2	6.7	7.2
		4.5	1.33	186.7	11.0	11.9	12.6	14.6	9.4	1.1	11.2	11.8	8.4	8.8	9.9	10.8	7.8	8.1	8.7	9.7	7.2	7.5	7.9	8.8
		5.5	1.09	186.7	13.2	13.8	15.1	17.0	11.3	12.0	12.9	14.6	10.0	10.8	12.0	12.8	9.2	9.6	10.6	11.6	8.5	8.9	9.6	10.7
		6.0	1	186.7	14.6	15.2	16.9	19.6	12.9	13.5	14.4	16.3	11.5	12.4	13.4	14.2	10.8	11.0	12.1	13.1	9.4	10.0	11.1	12.0
C07	7	3.5	2	220.0	12.1	12.7	14.4	16.0	10.2	10.9	12.0	13.1	8.9	9.2	10.4	11.3	8.2	8.5	9.1	10.1	7.7	8.0	8.5	9.6
		4.0	1.75	220.0	13.0	13.7	15.8	17.4	11.0	12.1	13.0	14.3	9.6	10.2	11.4	12.4	8.8	9.2	9.9	11.1	8.3	8.6	9.2	10.1
		5.0	1.40	220.0	15.4	16.0	18.2	19.8	13.1	14.0	15.4	17.1	11.4	12.1	13.3	14.2	10.4	10.8	12.0	13.1	9.6	9.9	10.9	12.0
		6.0	1.17	220.0	17.5	18.8	21.1	22.6	15.4	16.2	18.0	19.8	13.4	14.2	15.2	17.1	12.0	12.8	14.1	15.5	11.1	11.6	13.0	14.1
		7.0	1	220.0	21.2	22.6	25.1	27.0	18.5	19.6	21.8	23.8	15.8	16.6	17.7	20.4	14.6	15.5	17.0	18.8	13.5	14.4	15.7	17.0
C08	8	4.0	2	253.3	16.2	17.8	20.0	21.7	14.3	14.8	16.7	18.9	12.6	13.2	14.3	15.5	11.0	11.7	12.9	13.8	10.2	10.5	11.4	12.7
		5.0	1.6	253.3	19.3	21.3	23.1	24.8	16.4	17.2	19.4	21.3	14.7	15.3	16.4	18.5	12.8	13.6	14.8	16.1	11.6	12.1	13.3	14.8
		6.0	1.33	253.3	22.8	24.3	26.1	27.9	18.3	19.4	21.7	24.0	16.6	17.3	18.5	21.3	15.0	15.6	16.8	18.9	13.0	14.1	15.4	17.1
		7.0	1.14	253.3	25.8	27.0	29.1	30.8	21.2	22.7	25.0	27.0	18.5	19.1	21.0	24.0	17.0	17.8	18.8	21.5	15.4	16.3	17.8	19.5
		8.0	1	253.3	30.0	31.5	33.7	35.5	25.1	26.6	28.5	30.9	21.6	22.0	24.7	27.9	19.4	19.9	21.8	24.8	18.0	18.9	20.6	22.7
C09	9	4.5	2.00	286.7	23.4	24.8	26.9	28.5	19.2	20.6	22.6	24.5	17.2	18.1	19.9	21.9	15.7	16.4	17.7	19.7	14.0	14.9	16.0	17.0
		6	1.50	286.7	28.3	29.6	31.8	34.0	23.7	25.7	27.6	29.7	19.6	20.9	23.4	25.6	18.5	19.4	21.0	23.3	16.7	17.5	18.7	19.9
		7	1.29	286.7	31.7	32.8	34.9	36.8	26.9	28.6	30.8	32.6	22.1	23.7	26.9	28.9	20.7	21.5	23.6	26.1	18.8	19.5	20.7	22.5
		8	1.13	286.7	34.6	35.9	37.8	40.0	29.8	31.4	33.8	35.7	25.4	27.3	29.4	31.6	23.1	24.4	27.0	29.0	20.7	21.5	22.8	26.0
		9	1.00	286.7	39.3	40.4	42.7	44.7	34.6	36.1	38.1	40.0	28.8	30.4	33.1	35.6	26.3	27.8	30.3	33.2	23.2	24.1	26.0	29.6
C10	10	5	2.00	320.0	32.1	33.5	35.6	37.4	26.9	27.9	30.4	32.2	22	23.8	26.1	29.1	20	21.2	23.7	25.8	18.3	19.3	21	23.5
		6	1.67	320.0	35.6	36.7	38.7	40.4	29.9	31.5	33.8	35.9	25.6	27.1	29.9	32	21.7	23.3	26	28.3	20.4	21.2	23.2	25.6
		7	1.43	320.0	38.6	39.8	42	43.8	33.2	34.7	37	38.9	28.6	30	33	35.1	24.2	26.1	29.1	31.3	22.2	23	25.7	28
		9	1.11	320.0	44.3	45.7	47.9	49.7	39.1	40.7	42.9	45.1	35.1	36.2	39.2	41.3	30	32	34.6	37.1	26.9	28.6	31.5	33.8
		10	1.00	320.0	49.4	49.8	52.3	53.7	44	45.4	47.6	50	40	41.3	44.1	46.1	33.4	35.7	38.4	41.2	30.4	32.1	34.9	37.6

Table 7: Maximum Live load, concrete grade, aspect ratio individual contribution to the *LDT* variation along long span within each group (while keeping the other two variables constant)

Group	*L1*, m	combined LDT variation, mm	*L1* / LDT variation ratio	*LDT* variation due to live load		*LDT* variation due to concrete grade		*LDT* variation due to aspect ratio	
				mm	*L1*/variation	mm	*L1*/variation	mm	*L1*/variation
C05	5	11.3	442.5	4.6	1087.0	6.7	746.3	7.9	632.9
C06	6	14.1	425.5	5.0	1000.0	7.5	666.7	9.1	549.5
C07	7	19.3	362.7	5.8	862.1	10.0	500.0	11.0	454.5
C08	8	25.4	315.0	6.3	793.7	13.1	381.7	13.9	359.7
C09	9	30.7	293.2	7.0	714.3	16.7	299.4	16.2	308.6
C10	10	35.4	282.5	7.0	714.3	19.0	263.2	18.0	277.8

3.4 Live Load Deflection

The instant deflection under the live load is required by the ACI 318-14 code to be less than the maximum permissible deflection of L/360 (for floors supporting non-structural elements likely to be damaged by large deflection, the critical case). For Group C10, and taking the long span direction as the "reference span", this limit would be 27.78 mm. **Table 8** presents the short term cracked deflections under live load for Group C10; the reported are less than the limits, conforming to ACI 318-14 requirements. The results of the other groups (C05 to C09) showed the same trend of results.

Table 8: Short term cracked concrete deflection under live load for group C10 (long span = 10 m, slab thickness = 320 mm)

Short Span, m	Aspect ratio	Short term deflection, mm																			
		f_c'=20 MPa				f_c'=25 MPa				f_c'=30 MPa				f_c'=35 MPa				f_c'=40 MPa			
		LL, kN/m²				*LL, kN/m²*				*LL, kN/m²*				*LL, kN/m²*				*LL, kN/m²*			
		2.4	3	4	5	2.4	3	4	5	2.4	3	4	5	2.4	3	4	5	2.4	3	4	5
5	2.00	11.3	12.6	14.6	16.4	8.7	10.2	12.3	14.1	6.2	7.9	10.2	12.3	4.4	5.6	8.2	10.4	3.7	4.6	6.2	8.7
6	1.67	12.4	13.8	16.0	18.0	9.8	11.3	13.5	15.6	7.3	9.0	11.4	13.5	5.1	6.7	9.3	11.6	4.4	5.2	7.4	9.8
7	1.43	13.6	15.0	17.4	19.4	10.9	12.4	14.7	16.9	8.4	10.0	12.5	14.7	5.9	7.7	10.4	12.8	5.0	5.9	8.5	11.0
9	1.11	15.7	17.5	19.9	22.0	13.1	14.8	17.2	19.6	10.9	12.4	15.0	17.4	8.3	10.3	12.9	15.3	6.8	8.2	11.1	13.5
10	1.00	18.3	20.1	22.4	23.9	15.4	17.1	19.8	22.2	12.7	14.6	17.3	19.8	10.1	11.9	15.1	17.7	8.3	10.0	13.0	15.8

3.5 Theoretical Calculation for Deflection

As a check for the *LTD* calculated by SAFE, five flat plate floor cases from group C8 have been re-analyzed theoretically using equivalent frame method for the deflection calculation (ACI 318 , 2014); these deflections are compared with the corresponding *LTD* obtained from the SAFE analysis in **Table 9**. The SAFE models produced larger deflection in square panels; as the aspect ratio decreases (smaller panels), the theoretical approach produced larger deflection. This is attributed mainly to the fact that SAFE model is capable of modelling the degradation in the slab moment of inertia due cracking for every 0.5 x 0.5 m slab elements, this is in contrast to the theoretical approach in calculating the moment of inertia of a concrete member based on the

weighted-average properties for the sections at the maximum positive and negative average moments. As could be seen in **Table 9**, in the ACI-318 (2014) approach, the aspect ratio has a limited effect on the deflection of the long direction column strip (from 24.5 mm to 22.7 mm for aspect ratio of 1 to 2), while the aspect ratio affects the deflection of the middle strip deflection (perpendicular to the long direction), and consequently affecting the diagonal deflection, which is the sum of the long span column strip deflection plus the short span middle strip deflection (refer to Figure 1.C). This might be the reason for not considering the aspect ratio in the ACI 318 provisions for deflection control as it might have been believed that only the deflection along long direction are required to be checked and it is not affected by the aspect ratio. In contrast, SAFE results (**Table 9)** showed that there around 77% increase in the long span column strip in panels of square panels compared with panels of aspect ratio of 2. This observation indicates that the ACI 318 approach in dealing with aspect ratio might be not quite accurate, urging the need for an inclusion of the aspect ratio in the code of practice deflection provisions.

Table 9: Comparison between SAFE and theoretical long-term deflection (C8 group, live load= 3 kN/m^2, SDL = 2.4 kN/m^2, slab thickness = 253.3 kN/m^2, f_c' = 20 MPa)

aspect ratio	SAFE deflection, mm		Theoretical calculated deflection, mm			Ratio (SAFE /hand calculation)	
	long span col. strip	Diagonal	long span col. strip	Middle strip	Summation (diagonal)	long span col. strip	diagonal
2.00	17.82	17.71	22.66	0.90	23.6	0.786	0.754
1.60	21.26	21.24	24.52	2.19	26.7	0.867	0.794
1.33	24.29	25.46	25.63	4.40	30.0	0.948	0.847
1.14	26.96	32.18	25.93	7.49	33.4	1.040	0.964
1.00	31.51	44.31	24.51	14.42	38.9	1.286	1.139

3.6 Scanlon and Lee Unified Slab Thickness Equation

Scanlon and Lee (2006) proposed a unified span-to-depth ratio minimum thickness equation for one-way, two-way non-prestressed slab floors and beams, considering the amount of the applied load (dead & live load), aspect ratio (but for edge-supported slabs only), concrete strength grade (through the modulus of elasticity) using effective moment of inertia, I_e, equal to 0.52 I_g (gross moment of inertia). In addition, this equation accounts for the long-time deflection multiplier, the moment continuity at the panel edges, drop panels, beams and LDT limits. Scanlon and Lee (2006) reported that the use of this unified equation for flat slabs results in slab thickness in large spans compared to what ACI 318-05 values.

$$\frac{l_n}{h} = \beta \left[\left(\frac{\Delta_{inc}}{l}\right)_{allow} \frac{0.0167\ k_{DP}\ E_c\ b}{\kappa\ k_{AR}\ k_{SS}\ (\lambda\ W_S + W_{L\,(add)})} \right]^{1/3}$$

W_S: sustained load (kN/m^2), equal to the self-weight, superimposed dead load plus 25% of the live load. As self weight depends on the slab thickness, there is a need for an estimated slab thickness. In the current paper calculation, this estimated thickness is based on ACI 318 provisions.

$W_{L(add)}$: additional live load (kN/m^2); 75% of the live load

β: for slab without edge supports = 1, for edge-supported slabs β= long span / short span;

κ: end-support condition coefficient

(both ends continuous=1.4, one end continuous = 2, both ends discontinuous = 5.0)

$\left(\frac{\Delta_{inc}}{l}\right)_{allow}$: required/targeted incremental deflection limit (LDT)

k_{DP}= 1, except k_{DP}= 1.35 for slab with drop panels;

k_{SS}= 1, except k_{SS}= 1.35 for column-supported two-way slabs;

k_{AR}= 1, except k_{AR}= 0.2 + 0.4 ß for edge-supported slabs;

Ec: Modulus of elasticity of concrete, $4700\sqrt{fc'}$ (ACI 318-14, section 19.2.2.1);

b = 1000 mm; λ : time-dependent factor for sustained loads (ACI 318-14, Section 24.2.4.1.3)

Scanlon and Lee (2006)'s equation has been used in the current study to estimate the slab thickness and compare it with the ACI 318-14 provisions (for the cases of *fc'* of 20, 30 and 40 MPa) for a targeted LDT of L/480, as detailed in **Table 10**. The calculations have been made in 2 iterations; in the 1st one, the slab thickness was estimated using ACI- provisions (l/30); in the 2nd one, the slab thickness of the 1st iteration has been used. As could be seen, Scanlon and Lee's equation proposes larger slab thickness compared with the ACI 318-14 provisions; the difference increases as the *fc'* getting smaller, live load getting larger and the long spans getting larger. This trend of requiring larger slab thickness is corresponding to the results of the current paper, the need to increase slab thickness as the concrete grade getting smaller, and the live load getting larger. However, this equation, does not account for aspect ratio because the equation account for it in edge-supported slabs only. This means that even this equation produces same slab thickness for panels of 8 x 8 m and 8 x 4 m, the concern that the current paper aim to raise. It could be expected that the use of Scanlon and Lee (2006)'s equation will limit the deflection in flat plate slabs within the L/480, but not accounting for the aspect ratio might produce non-economical thickness at rectangular panels. This matter could be evaluated more in further studies evaluating the equations for the cases studied in the current paper

Table 10: Slab thickness as per Scanlon and Lee (2006)'s unified equation

A) 1st iteration, using ACI 318 proposed slab thickness

Group	Long span, m	Aspect ratio	Slab thick as per ACI, mm	Scanlon and Lee 2006 slab thickness, mm											
				f_c'=20 MPa				f_c'=30 MPa				f_c'=40 MPa			
				Live load, kN/m²				*Live load, kN/m²*				*Live load, kN/m²*			
				2.4	**3**	**4**	**5**	**2.4**	**3**	**4**	**5**	**2.4**	**3**	**4**	**5**
C05	**5**	**1-2**	**153.3**	176.0	178.8	183.4	187.7	164.5	167.1	171.4	175.5	156.8	159.3	163.4	167.2
C06	**6**	**1-2**	**186.7**	221.5	224.8	230.0	235.0	207.0	210.1	215.0	219.6	197.3	200.2	204.9	209.4
C07	**7**	**1-2**	**220**	269.1	272.7	278.6	284.1	251.5	254.9	260.4	265.6	239.8	243.0	248.2	253.1
C08	**8**	**1-2**	**253.3**	318.6	322.6	328.9	335.1	297.8	301.5	307.4	313.2	283.9	287.4	293.1	298.5
C09	**9**	**1-2**	**286.7**	370.0	374.2	381.1	387.7	345.8	349.8	356.2	362.4	329.6	333.4	339.5	345.4
C10	**10**	**1-2**	**320**	423.0	427.5	434.8	441.9	395.3	399.5	406.4	413.0	376.8	380.8	387.4	**393.7**

B) 2nd iteration, using slab thickness of 1st iteration

Group	Long Span, m	Aspect ratio		Scanlon and Lee 2006 slab thickness, mm											
				f_c'=20 MPa				f_c'=30 MPa				f_c'=40 MPa			
				Live load, kN/m²				*Live load, kN/m²*				*Live load, kN/m²*			
				2.4	**3**	**4**	**5**	**2.4**	**3**	**4**	**5**	**2.4**	**3**	**4**	**5**
C05	**5**	**1-2**		180.1	183.3	188.4	193.2	166.4	169.4	174.2	178.8	157.3	160.3	164.9	169.3

C06	**6**	**1-2**	228.6	232.3	238.2	243.7	211.0	214.5	220.0	225.3	199.3	202.7	208.0	213.1
C07	**7**	**1-2**	280.2	284.3	290.8	297.0	258.3	262.2	268.4	274.2	243.8	247.6	253.5	259.2
C08	**8**	**1-2**	334.5	339.0	346.2	353.0	308.1	312.3	319.1	325.6	290.7	294.8	301.3	307.5
C09	**9**	**1-2**	391.5	396.4	404.1	411.5	360.3	364.9	372.2	379.2	339.8	344.2	351.3	358.0
C10	**10**	**1-2**	451.1	456.2	464.5	472.4	414.9	419.8	427.6	435.1	391.0	395.7	403.3	**410.5**

Sample calculation for the case of 10 x10 m slab, *fc'*=40 MPa, live load = 5 kN/m^2

- *SDL* = 2400 N/m^2
- Live Load = 5000 N/m^2
- Clear span, long, l_n = 10 – 0.4 = 9.6 m
- Width, b = 1000 mm
- Estimate slab thickness:
  $h = l/30$ = (10-0.4)/30 = 0.32 m
- Slab self-weight =
  (0.32 m) × 24000 N/m3= 7680 N/m^2
- Sustained load
  Ws = 7680+2400 + 0.25 x 5000 = 11330 N/m^2
- Additional live load,
  $WL_{(add)}$ = 0.75 x 5000 N/m^2 = 3750 N/m^2

- E= 4700 √ *40 x 1000000* = 29.73 E9 N/m^2
- β = 1.0, k_{DP} = 1.0, κ = 2.0, k_{AR} = 1.0, k_{SS} = 1.35,
- Deflection limit = 1/480

$$\frac{l_n}{h} = \beta \left[\left(\frac{\Delta_{inc}}{l}\right)_{allow} \frac{0.0167\ k_{DP}\ E_c\ b}{\kappa\ k_{AR}\ k_{SS}\ (\lambda\ W_S + W_{L\ (add)})} \right]^{1/3}$$

$$h = \frac{9.6}{1\left[\left(\frac{1}{480}\right)_{allow} \frac{0.0167\ x\ 1\ x\ 29.73\ \text{E9 x } 1000}{2\ x\ 1\ x\ 1.35\ (2\ (11330) + 3750)} \right]^{1/3}} = 0.393$$

in the 2nd iteration, using this thickness (0.393 m) for estimating the self-weight, the thickness would be 0.410 m.

4.CONCLUSIONS:

The conclusions drawn from the current study could be summarized as below:

1- ACI 318-14 and CSA A23.3-14 deflection provisions do not specify explicitly L/240 or L/480 as the long term deflection limit for floors supporting masonry walls; therefore, based on the other three codes of practice (AS 3600 (2018), BS 8110 (1997) and EN 1992 (2004)), the current research believes that the L/480 limit needs to be considered.

2- Within each group (constant long span), the slab panel aspect ratio and concrete strength had the largest effect on the slab *LTD* followed by the live load with the effects being more pronounced at larger spans

2- ACI 318-14 provisions for flat plates seem to be adequate for the *L*/240 limit for slab floor panels up to long span of 7.0 m, but they are inadequate in most of the cases to satisfy the *L*/480 limit

3- There is a need for the code of practice provisions for flat plat panel thickness to include the panel aspect ratio effect; the effect which is even not accounted for in Scanlon and Lee (2006)'s unified equation.

4- As an accurate practice, the actual relative deflection calculated along a span should be compared with the corresponding maximum permissible deflection calculated along the same span direction

5- The long span is suggested to be taken as the "***slab reference span***" for flat plate slabs, along which the calculated actual relative deflection and the maximum permissible deflection are determined.

REFERENCES

ACI 318 . (2014). *Building Code Requirments for Reinforced Concrete (ACI 318-14) and Comentray.* Detroit: American Concrete Institute, Farmington Hills.

ACI 435R-95. (2003). *Control of Deflection in Concrete Structures (ACI435R-95).* Detroit: American Concrete Institute.

ACI SP-17(14): Volume 2. (2015). *"The Reinforced Concrete Design Handbook" An ACI Handbook; A Companion to ACI 318-14.* Detroit: American Concrete Institute, Farmington Hills.

AS 3600-18. (2018). *Australian Standard for Concrete Structures.* Sydney: Standards Australia.

ASCE/SEI 7-10. (2010). *Minimum Design Loads for Buildings and Other Structures.* Virginia: American Society of Civil Engineers.

Bondy, K. B. (2005). ACI Code Deflection Requirements - Time for a Change ? Serviceability of Concrete: A Symposium Honoring Dr. Edward G. Nawy,. *ACI Special Publications. SP-225-06*, 133-145 pp.

BS EN 8110-1-97. (1997). *British Standard Code: Design of Concrete Structures.* London,: British Standards Institution.

CSA A23.3-14. (2014). *Design of Concrete Structures.* Ontario, Canada: Canadian Standards Association.

CSI. (2016). *SAFE 2016, Key Features and Termnology.* USA: Computers & Structures, Inc.

EN 1992-1-1-04. (2004). *Eurocode 2: Design of Concrete Structures. General Rules and Rules for Buildings - Part 1-1 : General rules and rules for buildings.* London: British Standards Institution.

Gilbert, R. I. (1985). "Deflection Control of Slabs using Allowable Span to Depth Ratios". *ACI Journal, 82*(01), 67-72 pp.

Hwang, Sh. J. and Chang, K. Y. (1996). Deflection Control of Two-way Reinforced Concrete Slab. *ASCE, Journal of Structural Engineering*, pp 160-169.

MacGregor, J G. and Wight, J K. (2012). *Reinforced Concrete: Mechanics & Design* (6th ed.). New Jersey, USA: Pearson Education, Inc.

Nawy, E. G. (2009). *Reinforced Concrete: A Fundemental Approach* (6th Edition. ed.). New Jersey: Pearson International Edition.

Nilson, A., Darwin, D., Dolan, C. (2016). *Design of Concrete Structures* (15th Edition ed.). New York: McGraw-Hill Company.

Regan, P. I. (1981). *"Behaviour of Reinforced Concrete Flat Slabs"*. The Construction Industry Research and Information Association (CIRIA). London: CIRIA Report 89.

Scanlon, A. and Lee, Y. H. (2010). Comparison of One- and Two-Way Slab Minimum Thickness Provisions in Building Codes and Standards. *ACI Structural Journal, 107*(2), pp 157-163.

Scanlon, A., and Lee, Y. H. (2006). Unified Span-to-Depth Ratio Equation for Nonprestressed Concrete Beams and Slabs. *ACI Structural Journal, V. 103*(No. 1, Jan.-Feb), pp. 142-148.

Thompson, D.P., and Scanlon, A. (1988). Minimum Thickness Requirements for Control of Two-Way Slab Deflections. *ACI Structural Journal, V. 85*(No. 1, Jan.-Feb), pp 12-22.

ZANCO Journal of Pure and Applied Sciences
The official scientific journal of Salahaddin University-Erbil
https://zancojournals.su.edu.krd/index.php/JPAS

ISSN (print):2218-0230**, ISSN (online):** 2412-3986**, DOI: http://dx.doi.org/10.21271/zjpas**

RESEARCH PAPER

Detection of Coronavirus Phishing Emails using Echo State Neural Network

Omar Younis Abdulhammed

Department of computer, College of Science, Garmian University, Kurdistan Region, Iraq

A B S T R A C T:

E-mail is an important and fast mean of conveying information among people, banks, companies and organizations, that information is often important, sensitive and secret, this make it worthy to attackers who can use it for harmful purposes. Spread of coronavirus in most countries of the world and the huge amount of media coverage surrounding this virus led to emergence phishing emails by exploiting coronavirus pandemic. Phishing emails are scam messages used by fraudsters to take out secret information from persons by pretending that it is from official sources. In this paper a novel method has been proposed to detect the coronavirus phishing emails and distinguish them from legitimate mails by using Echo state neural network(ESN), after preprocessing the emails, features are selected from the header and body of it, these features are given as fed to the (ESN) algorithm to classify emails as malicious or legitimate. The results showed the efficiency and accuracy of the algorithm used in the detection of coronavirus phishing emails, where the rate of accuracy, precision, recall and F-measure are 99.392, 98.892, 99888, and 99.387 respectively with low required processing time (0.00092 msec.) for testing and (165.19 msec.) for training.

KEY WORDS: Coronavirus, Phishing, email, ESN, Features, Legitimate.
DOI: http://dx.doi.org/10.21271/ZJPAS.32.5.7
ZJPAS (2020), 32(5); 78-85 .

1. INTRODUCTION

Internet and e-mail has become a daily activity that is used by people. Due to rapid development of technologies, internet, mobile technology and online services, there has been increased interest with security of information against threats and dangers likely to be faced by users during the use of these technologies (Sonmez et al, 2018). Phishing is electronic attack carried out by using electronic email via the internet on people to persuade them to implement some procedures such as entering the password or credit card number that are boon of the attacker .

The attacker send s socially engineered message that give victim user illusion that he needs to perform such action, such as warning the user about account suspension or that the website admin is requesting him to reset his password (Yasin and Abuhasan, 2016).

Phishing is a criminal technique using both social engineering and technical subterfuge to theft use's information to obtain financial and banking accounts or sometimes it is used to bargain the user victim (Yang et al, 2019) Phishing emails are categorized as spam messages, one of the most common methods used by phishing scams is by sending messages to the victim user's e-mail which it is claims from a legitimate world health organization or bank and asking the victim user to follow an embedded link. The link will redirect the user to a fake website that requests sensitive and important information. The cycle of phishing

* **Corresponding Author:**
Omar Younis Abdulhammed
E-mail: omar.y@garmian.edu.krd
Article History:
Received: 27/05/2020
Accepted: 03/09/2020
Published: 13/10 /2020

mechanism shows in figure (1) (Almomani et al, 2013).

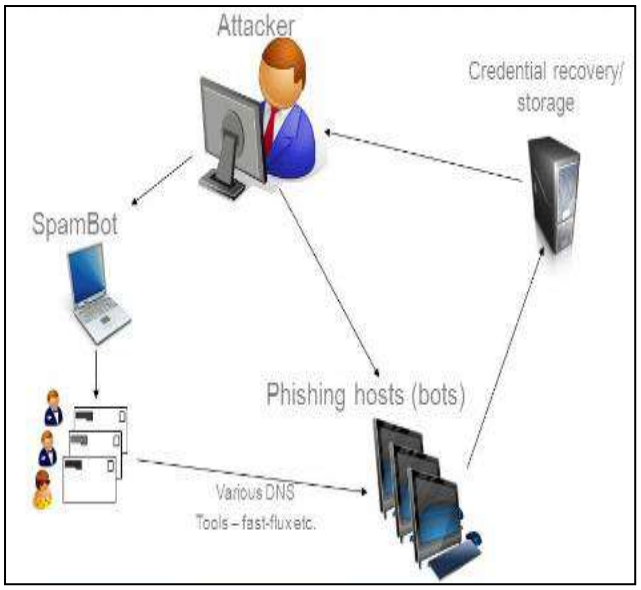

Figure 1: Cycle of phishing techniques.

2. LITERATURE REVIEW

This section introduces some of the previous methods for detecting malicious mails. The authors in (Pandey and Ravi, 2012) proposed a method for classifying the emails by relying on the 23 features extracted from the email's body, the method was tested by using several algorithms which are support vector machine, logistic regression and genetic programming, the results showed that the genetic programming gave the best results with accuracy 98.12%. The authors in (Nizamani et al, 2014) proposed a method to detect the scams email by using advance feature choice and several classification techniques such as J84, support vector machine and cluster based classification model, the accuracy ratio for this method was 96%. In paper (Mohammed and George ,2013) propose a schema to disclosure deceptive email by using FF neural networks where 18 features are extracted from contents of email, the identification rate for this method was 98.72%. The authors in (Form, 2105) used SVM's algorithm to classify the emails as legitimate and malicious through using 9 features extracted from the emails, the accuracy ratio for this method was 97.25%. In paper (Moradpoor et al, 2017) a method to detecting phishing scams was proposed through using neural network based model, where a large dataset of multiple levels of difficulty were used for training and testing phase, the results showed the efficiency and effectiveness of this method. In paper (Rathod and Pattewar, 2015) the Bayesian algorithm has been proposed to classify emails as legitimate and malicious, the results showed the efficiency and accuracy of this method. In paper (Montazer and Yarmohammadi, 2015) proposed a method to detect the phishing email of the Iranian electronic banking, method merge two algorithm which are fuzzy logic and rough sets which a rough used to minimize the size of the data. Then, fuzzy logic was applied to convert the input data into linguistic variables, the results prove the effectiveness of this method. In paper (Lallie et al, 2020) analyses the COVID-19 pandemic from a cyber-crime perspective and highlights the range of cyber-attacks experienced globally during the pandemic. Cyber-attacks are analyzed and considered within the context of key global events to reveal the modus-operandi of cyber-attack campaigns. The analysis shows how following what appeared to be large gaps between the initial outbreak of the pandemic in China and the first COVID-19 related cyber-attack. The analysis proceeds to utilize the UK as a case study to demonstrate how cyber-criminals leveraged key events and governmental announcements to carefully craft and design cyber-crime campaigns. The main contribution of this paper is proposed new system that can quickly detect phishing emails with low false positive rate through depending on the two points, first point, extract a new 15 features from content and structure of coronavirus phishing emails to test each coming emails to identify whether it is phish email or not, second point, using ESN algorithm to categorize the email samples into phish or ham category. It is worth mentioning the algorithm and the dataset used is a novel and has not used previously in this field due to the novelty of the subjects, also the ESN algorithm has achieved impressive results and proved its accuracy and strength compared to the algorithms that are used in previous work.

3. ECHO STATE NETWORK

Artificial Neural Networks is software rely on the nervous structure of the human brain and try to simplify and simulate brain behavior. Due to its ability to learn from entered data, updating the network structure and communication weights so it is considered a good system in many fields such as predication and classification.

The ANN have several types such as FF Neural Network Artificial Neuron, Radial Basis Function Neural Network, Kohonen Self Organizing NN and Recurrent Neural Network (RNN), Convolutional Neural Network. Recently, the Echo State Network (ESN) has been introduced as a novel approach for designing RNNs [12]. Echo state networks (ESNs) were proposed as a inexpensive and quick supervised learning method and are therefore proposed to be beneficial in solving real problems. The basic idea is to convert the low dimensional temporal input into a higher dimensional echo state, and then train the output connection weights to make the system output the desired information [13]. Because only the output weights are altered, training is typically quick and computationally efficient compared to training of other recurrent neural networks [14].

Echo state network (ESN) is a recurrent discrete-time neural network with K input units, N internal (reservoir) units, and L output units. The activation of the input, internal, and output units at time step t are denoted by: $s(n) = (s_1(t), ..., s_K(t))^T$, $x(t) = (x_1(t), ..., x_N(t))^T$, and $y(t) = (y_1(t), ..., y_L(t))^T$ respectively. The connections between the input units and the internal units are given by an N × K weight matrix V , connections between the internal units are collected in an N ×N weight matrix W, and connections from internal units to output units are given in L × N weight matrix U. The internal units are updated according to:

$$x(t+1)=f(V_s(t+1)+W_x(t)+z(t+1)) \quad (1)$$

Where f is the reservoir activation function; z(t+1) is an optional uniform noise. The linear readout is computed as:

$$y(t+1)=U_x(t+1) \quad (2)$$

Elements of W and V are fixed prior to training with random values drawn from a uniform distribution over a (typically) symmetric interval. To account for ESP, the reservoir connection matrix W is typically scaled as $W \leftarrow \alpha W/|\lambda_{max}|$, where $|\lambda_{max}|$ is the spectral radius of W and $0 < \alpha < 1$ is a scaling parameters. Figure (2) shows the architecture of ESN [15].

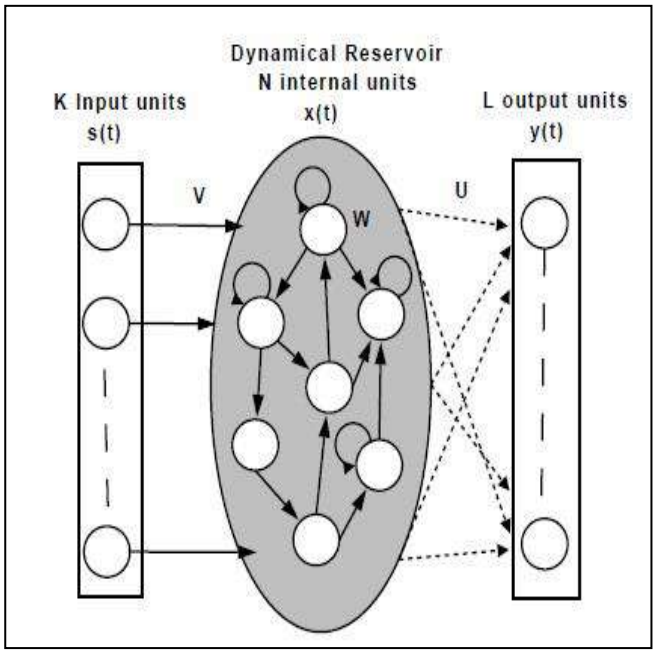

Figure 2: Architecture of ESN

4. PROPOSED METHOD

This paper proposed a method to detect coronavirus phishing emails through applying ESN algorithm on the data set that was taken from several legitimate websites, the number of email samples used to train and test the ESN is 4550 phish and ham emails. 3185 emails were used to train the ESN and 1365 emails were used to test the system performance.

Two types of messages were used in this method which are coronaviruses phishing email and ham email. A set of 15 features that appeared in the coronaviruses phishing email have been used in the spoofing detection method and represented as binary value. Table (1) shows the features and their descriptions. The proposed system was implemented in four phases, namely, preprocessing, feature extracting, training and testing, the figure (3) shows the block diagram of the proposed method.

Table (1) Features used in emails classification

Features	Descriptions
F1	Binary feature that returns 1 if the email contains World Health Organization logo image otherwise 0
F2	Binary feature that returns 1 if the email subject contains @ symbols otherwise 0
F3	Binary feature that returns 1 if the email body contains words"N95","masks", "goggle", "instructions" and "vaccine" otherwise 0
F4	Binary feature that returns 1if the email contain links start with http; and not https: otherwise 1
F5	Binary feature that returns 1 if the email contain links include "coronavirus" "CDC" or "covid-19" otherwise 0
F6	Binary feature that returns 1 if the email contain "Dear valued member", Dear account holder" or" Dear customer" otherwise 0
F7	Binary feature that returns 1 if the email request "Passwords", "Credit card" and "Tax numbers" otherwise 0
F8	Binary feature that returns 1 if the email contain two or more hyperlinks
F9	Binary feature that returns 1 if the domain name of have three dots or more than otherwise 0
F10	Binary feature that returns 1 if the email contains link like "rar", outbreak", "advice" and "spread"
F11	Binary feature that returns 1 if detect the difference between the sender and reply-to email address otherwise 0
F12	Binary feature that returns 1 if the email labeled as phishing email by spam assassin otherwise 0
F13	Binary feature that returns 1 if the sender email is "@who-pc.com", "@who-safety.org", "@cdc-gov.org" and "@cdcgov.org" otherwise 0
F14	Binary feature that returns 1 if the subject include "safety measures" otherwise 0
F15	Binary feature that returns 1 if the mail sender from "Covid-19@" otherwise 0

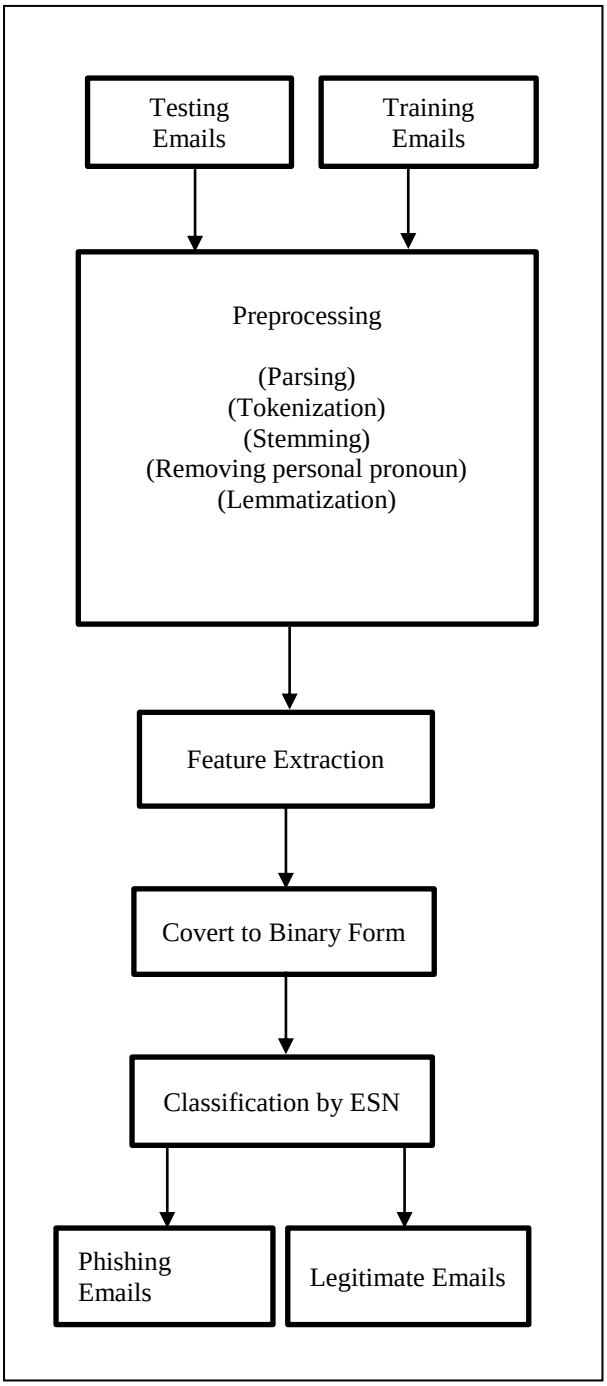

Figure 3: Proposed system

4.1 Preprocessing

The aim of this phase is to decrease the training time, reducing the amount of memory required, removing noise and invaluable data and enhance the performance of the proposed method, where email's contents are parse and tokenized into tokens and each token is stem, also during this stage all personal pronouns are deleted and obtaining the base form of the words (Lemmatization).

4.2 Features Extraction

It is considered to be one of the most important phases, in this method a list of 15 binary features are selected from the email's header and body and it coded with binary form, where 1 value reference to presence of feature in the tested email and 0 values to the absence of it.

4.3 Training phase

After coding the features to binary form are given to train the echo state network (ESN) algorithm. Where the number of hidden layer is three, where the first and second layers consists of 4 nodes while the third layer consist of 3 nodes, the number of output layer is one with one node. The 70% of samples had been prepared to train and 30% of the samples had been used to test the system by using ESN. The steps of training phase are shown in the following algorithm:

Input: 3185 phish and ham emails
Output: phish or ham emails
Step1: Recurrent neural network is generated
Step2: Produce weight for input Win, internal weight W, weight for output Wback
Step3: Given feature input and target output to the ESN
Step4: Compute the internal units according to eq. (1)
Step5: Compute the output unit according to eq. (2)
Step6: compare the actual output with target output
Step7: Update the output weight if the mean square traing error (MSE) between the actual and target output is maximum.

4.4 Testing phase

After the training phase is finished, 30% samples of emails is given as fed to the ESN algorithm to classify it. The ESN produces output in the forms 0 or 1, 1 means it is coronavirus phish email and 0 means it is legitimate.

5- Results

This section presents the results that had been obtained from the proposed method for the fifteen features which have been extracted from email's

header and body. The performance metrics are used for evaluating proposed method are:

A- Accuracy: it computed as $accuracy = (TP + TN)/Tp + TN + FP + FN$, where TP (true positive) is the percentage of malicious emails in the training dataset that are correctly classified as malicious emails, TN (True negative) is the percentage of ham emails in the training dataset that are correctly classified as ham emails, FP (False positive) is the percentage of ham emails that are incorrectly classified as malicious emails and the FN (False negative) is the percentage of malicious emails that are incorrectly classified as ham emails.

B- Precision: it computed as $precision = TP/(TP + FP)$

C- Recall: it calculate as $recall = TP/(TP + FN)$

D- F-measure: It is calculate as$F - measure = 2 * (Precision * Recall)/(Precision + Recall)$.

Table (2) and figure (4) shows the values of TN, TP, FN and FP using ESN algorithm with different number of neurons in hidden layer, the case of 11 neurons in the hidden was selected to build the module because it gave us the best FP value.

Table (3) and figure (5) shows the values of accuracy, precision, recall and f-measure of the proposed algorithm, where the higher accuracy value was using 11 neurons in the hidden layer with the value 99.392.

Table (2) Result of TP, TN, FP and FN metrics

No. of hidden layer node	TP	TN	FP	FN
1	0.959	0.954	0.013	0.0017
2	0.944	0.957	0.014	0.0025
3	0.944	0.958	0.041	0.0026
4	0.951	0.972	0.017	0.0026
5	0.954	0.974	0.013	0.0029
6	0.953	0.961	0.012	0.0021
7	0.933	0.978	0.018	0.0002
8	0.981	0.979	0.016	0.0018
9	0.941	0.984	0.013	0.0017
10	0.994	0.988	0.012	0.0017
11	0.982	0.998	0.011	0.0011
12	0.921	0.989	0.012	0.0019
13	0.926	0.981	0.015	0.0028
14	0.923	0.932	0.013	0.0019
15	0.959	0.954	0.013	0.0017

Table (3) Result of accuracy, precision, recall and f-measure metrics

No. of hidden layer node	Accuracy %	Precision %	Recall %	F-measure %
1	99.237	98.662	99.823	99.239
2	99.139	98.538	99.735	99.133
3	97.759	95.837	99.725	97.742
4	98.991	98.243	99.727	98.980
5	99.182	98.655	99.696	99.173
6	99.268	98.756	99.780	99.265
7	99.056	98.107	99.978	99.034
8	99.100	98.395	99.816	99.100
9	99.242	98.637	99.819	99.224
10	99.313	98.807	99.829	99.315
11	99.392	98.892	99.888	99.387
12	99.277	98.713	99.794	99.251
13	99.111	98.405	99.773	99.048
14	99.075	98.405	99.698	99.199
15	99.203	98.611	99.794	99.239

Table (4) shows testing time for single email and training time for different number of neurons in the hidden layer, Figure 6 shows the relation between the number of neurons in hidden layer and the training time for the ESN. Figure 7 shows the relation between the number of neurons in hidden layer and test time required for a single email.

Table (4) Training and testing time with different neurons

No. of hidden layer node	Training time (msec.)	Testing time (msec.)
1	35.09	0.00056
2	47.92	0.00058
3	62.48	0.00059
4	71.56	0.00063
5	88.77	0.00070
6	97.42	0.00075
7	109.5	0.00077
8	124.4	0.00082
9	137.54	0.00084
10	149.67	0.00089
11	165.19	0.00092
12	175.38	0.00093
13	189.77	0.00101
14	205.12	0.00104
15	228.45	0.00107

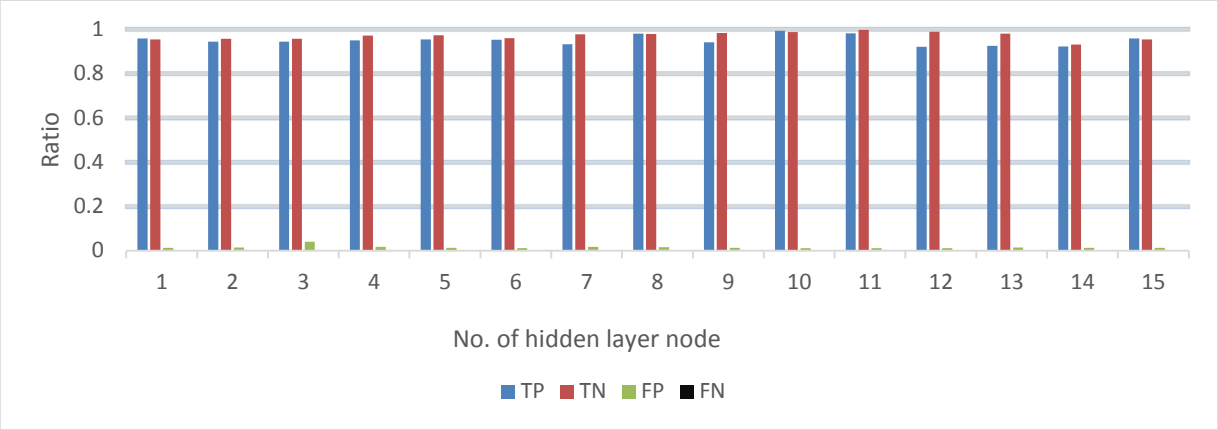

Figure 4: Result of TP, TN, FP and FN

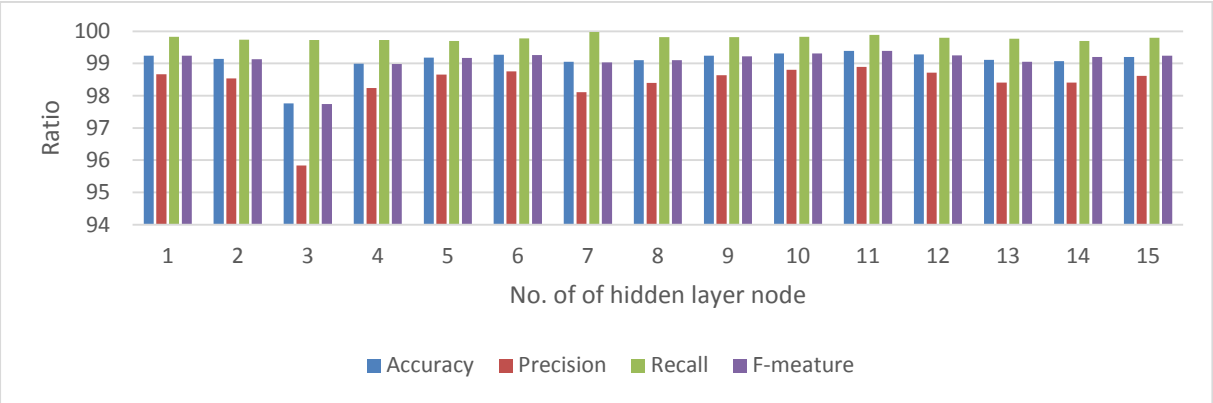

Figure 5: Result of accuracy, precision, recall and f-measure

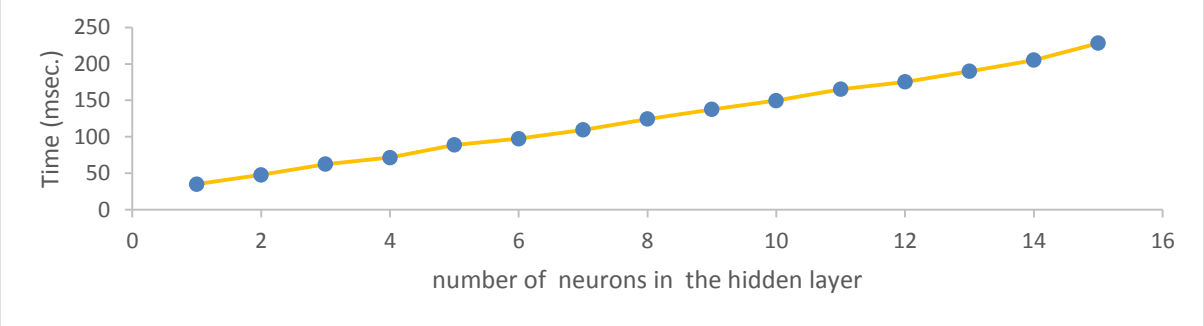

Figure 6: the relation between the number of neurons in hidden layer and the training time

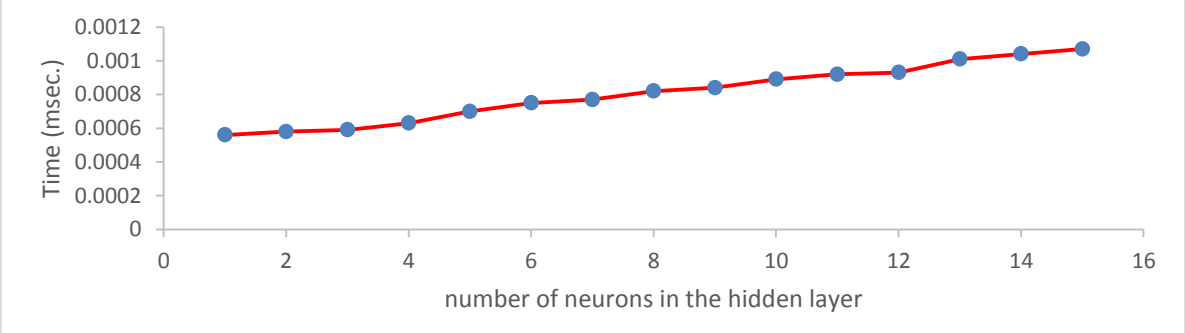

Figure 7: The relation between the number of neurons in hidden layer and test time required for a single email.

6- Conclusion

Corona phishing emails have become widespread and pose a threat to all companies, organizations and internet users nowadays, therefore the proposed method used to discover those emails. In this method ESN's algorithm was used to detect the coronavirus phishing emails by using fifteen email's features selected from email's content with eleven nodes in the hidden layer and one node in the output layer. Empirical results prove that proposed method has accuracy equal to 99.392, precision equal to 98.892, recall equal to 99.888 and F-measure equal to 99.387 with short required time (0.00092 msec.) for testing and (165.19 msec.) for training when using 11 neurons in the hidden layer as shown in table (3) and figure (5), also the proposed method of training had achieved very low FN and low FP as shown in table (2) and figure (4), this indicates that the proposed algorithm was very efficient and accurate in the classify the emails into phish and ham. The conclusion from table (5), figures 6 and 7, the training and test time will increase when the number of neurons in the hidden layer increases.

References

Abdulfattah A. and Salih L. (2016). Speaker Recognition Using Discrete Wavelet Transform and Artificial Neural Networks. ZANCO Journal of Pure and Applied Sciences, 78-85.

Almomani A., B. B. Gupta, Atawneh S., M. A. and Almomani E. (2013). A Survey of Phishing Email Filtering Techniques, Ieee Communications Surveys & Tutorials, Vol. 15, No. 4, Fourth Quarter, 1-21.

Dai, Venayagamoorthy and Harley. (2009). an introduction to the echo state network and its applications in power system. International conference on intelligent system applications to power system, 1-7

Form L. N, Chiew K. L., and Tiong. (2015). email detection technique by using hybrid features. 9th International Conference on IT in Asia (CITA), 1-5.

Lallie H.S., Shepherd L.A., Nurse J. R (2020). Cyber security in the age of COVID-19: a timeline and analysis of cyber-crime and cyber-attacks during the pandemic, arXiv: 2006. 11929 v1 [cs.CR], 1-20.

Løvlid R.A. (2013). A novel method for training an echo state network with feedback error learning. Advances in Artificial Intelligence journal, 1-10.

Mohammed N. G, George L. E, (2013). Detection of phishing emails using feed forward neural network, International Journal of Computer Applications, 10- 16.

Moradpoor N., Clavie B.and Buchanan B. (2017). Employing machine learning techniques for detection and classification of phishing emails. Computing Conference, 1-8.

Montazer and Yarmohammadi. (2015). Detection of phishing attacks in Iranian e-banking using a fuzzy–rough hybrid system. Appl. Soft Computer, 482-492.

Nizamani S., Memon N., Glasdam M. and Nguyen D. D. (2014). Detection of fraudulent emails by employing advanced feature abundance. Egyptian Informatics Journal, 169-174.

Pandey M., Ravi V. (2012). Detecting phishing e-mails using Text and Data mining", IEEE International Conference on Computational Intelligence and Computing Research, 1-6.

Rathod S.B and Pattewar T.M. (2015). Content Based Spam Detection in Email using Bayesian Classifier. International Conference on Communications and Signal Processing (ICCSP), 1257-1261.

Rodan A., Tino P. (2016). Minimum complexity echo state network. IEEE Transactions on Neural Networks journal, 131-144.

Saeedd I. (2019). Artificial Neural Network Based on Optimal Operation of Economic Load Dispatch in Power System. ZANCO Journal of Pure and Applied Sciences, 94-102.

Sonmez, Y., Tuncer, T., Gokal, H., & Avci, E. (2018). Phishing web sites features classification based on extreme learning machine.6th International Conference on Digital Forensic and Security (ISDFS), 1-6.

Tuong and Peters. (2011). Model learning for robot control: a survey. Cognitive Processing journal, 319– 340.

Yasin A., Abuhasan A. (2016). An intelligent classification model for phishing email detection. International Journal of Network Security & Its Applications (IJNSA) Vol.8, No.4, 55-72.

Yang Z., Qiao C., Kan W. and Qiu J. (2019). Phishing email detection based on hybrid features", IOP Conf. Series: Earth and Environmental Science 252, 1-11.

ZANCO Journal of Pure and Applied Sciences
The official scientific journal of Salahaddin University-Erbil
https://zancojournals.su.edu.krd/index.php/JPAS

ISSN (print):2218-0230**, ISSN (online):** 2412-3986**, DOI: http://dx.doi.org/10.21271/zjpas**

RESEARCH PAPER

Synthesis and characterization of bis (5-phenyl-1,3,4-oxadiazole-2-ylthio) mercury complexes with Pd(II) and Pt(II) metal ions

Beriwan M. H. Ameen,Hikmat A. Mohamad

Department of chemistry, College of education, University of Salahaddin-Hawler, Erbil, Kurdistan Region, Iraq.

A B S T R A C T:
A complexes of Pd(II) and Pt(II) have been synthesized from a reaction of one mole of (5-phenyl-1,3,4-oxadiazole-2-ylthio)mercury (HgL_2) with two mole of $PdCl_2$ and $PtCl_2$ to give the colored complexes with general formula $[M_2Cl_4(HgL_2)]$ [where M=Pd(II) or Pt(II)]. The results of identification indicated that all complexes have square planer shapes, which the metal coordinates to the ligand through Nitrogen, and Sulfur atoms of ligand (HgL_2). Characterization have been done by using FT- IR Spectroscopy, H^1-NMR spectroscopy, UV-visible spectra, melting point and CHNS analysis.

KEY WORDS: $PdCl_2$(II),$PtCl_2$(II), 1,3,4-oxadiazole-2-thiol, spectral data.
DOI: http://dx.doi.org/10.21271/ZJPAS.32.5.8
ZJPAS (2020), 32(5); 86-91 .

1. INTRODUCTION

The compounds that contain two nitrogen and one oxygen atoms in five membered ring are called Oxdiazole. It has four different types isomers, 1,3,4-oxadiazole is the most common isomers of the oxadiazole (Abbasi et al., 2018), (Srivastav and Pandeya 2011).

1,3,4-Oxadiazoles have a broad spectrum of biological activities include anti-inflammatory, antifungal, antitumor, **P**-Glycoprotein Inhibitors, pesticides and insecticides, Inhibitors, anticonvulsant activity etc (Roy et al., 2017). In addition to the oxadiazoles derivatives displayed an electrochemical, electro-optical, Luminescence and photo physical properties(Abbas et al., 2017).

* **Corresponding Author:**
Beriwan Mohamad Hamad Ameen
E-mail: Birewan.hamadamin@su.edu.krd
Article History:
Received: 03/10/2019
Accepted: 07/02/2020
Published: 13/10 /2020

There are several methods have been reported to synthesis 1,3,4-oxadiazols, for example cyclization of acid hydrazides with a different reagents such as thionyl chloride, phosphorous oxychloride and sulfuric acid, under reaction conditions. Since current years several efficient methods have been engaged for the synthesis of 1,3.4-oxadiazoles, from presented carboxylic and hydrazides acid (Aryanasab et al., 2011).There are wide recent research records highlighting the potential of the complexes of 1,3,4–oxadiazole dyes, liquid crystals, and inorganic light-emitting diodes (Aydogan et al., 2002.(Crystallography reports) (Mohamad et al., 2020). In this current work a new complexes of bis(5-phenyl 1,3,4-oxadiazole-2-ylthio) mercury (HgL_2) with Pd(II),and Pt(II) have been synthesized. Our interest aim is synthesize of new complexes in which binding with the central metal through nitrogen and sulfur atoms coordination to the central metal ions that they play important role biological and medical fields.

2. MATERIALS AND METHODS

2.1 Experimental Notes:

All chemical are of reagent grade, and used as supplied (Fluka), (Merk) ,(Alpha), or (B.D.H). Shimadzu FT-IR. 8400 spectrometer was used to recorded infrared spectra in the (400-4000) cm^{-1} range. Melting Point-MPD-100Pixel Technology CO., Limited was used to measured melting point. UV-Visible spectra were obtained using a Perkin-Elmer 330.The elemental analyses for Carbon, Hydrogen, Nitrogen and Sulfur atoms were performed by Innovation at the Nelson Mandela Metropolitan University for CHNS analysis.^{1}H-NMR, ^{13}C-NMR spectra of complexes were recorded by Bruker ultra shield 300 MHz with TMS as internal reference, in (Al-ALBayt) University Central Labs (Jordon).

2.2 Preparation of the Complexes

A clear solution of bis(5-phenyl 1,3,4-oxadiazole-2-ylthio) mercury (HgL_2) (0.5mmole) in ethanol (10ml) was added to a suspended solution of MCl_2 (M= Pd(II), Pt(II)) (1mmole) in (10ml) ethanol, the brown precipitate was formed after stirring for 12hrs. The precipitate was filtered and wished by diethyl ether. Analytical calculated % for $[C_{12}H_{12}S_2N_2Pd_2Cl_4$: C (21.12) , H (1.10), N (6.16), S (7.04),M (23.39) Found: C 20.76 , H 0.98, N 5.15, S 6.85 , M (23.04) and for Analytical calculated.% for $C_{12}H_{12}S_2N_2Pt_2Cl_4$ C (17.67) , H (0.92), N (5.15) , S (5.89) , M (35..89) Found: C 17.28 , H 0.68, N 4.59,. S 5.29, M 35.28.

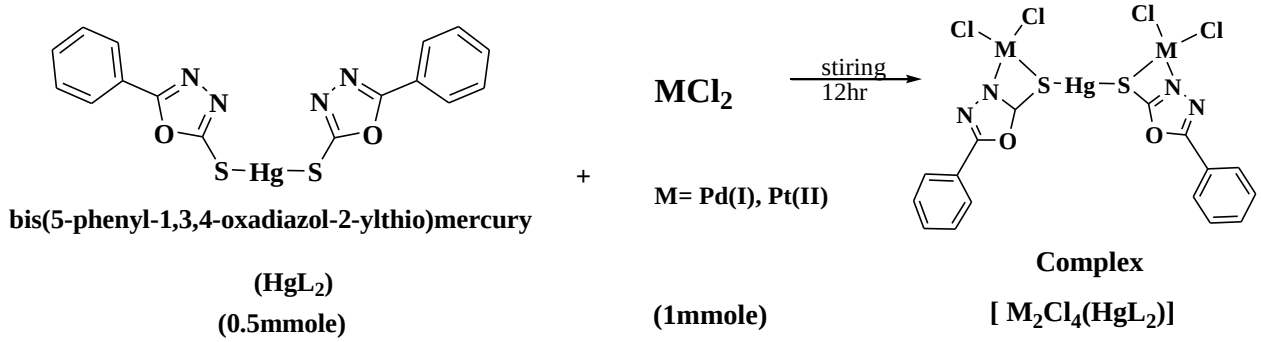

bis(5-phenyl-1,3,4-oxadiazol-2-ylthio)mercury

(HgL_2)

(0.5mmole)

(1mmole)

Complex

[$M_2Cl_4(HgL_2)$]

3. RESULTS AND DISCUSSION

3.1 Reactions of the preparation $[M_2Cl_4(HgL_2)]$

Complexes:

3.2 FT-IR spectra for complexes: The band of ν (C=N) shifted to 1608cm^{-1} , this shifting to a higher frequency from the (HgL_2) indicated the coordination of nitrogen to metal ions of Pd(II) and Pt(II) (Jawdat et al., 2017). Upon complexion the stretching vibration of ν (C-O-C)in the free ligand shifted to a higher frequency appears at 1078cm^{-1} in the complexes. The ν (C-S) band of the free ligand was displayed at 704cm^{-1} , this band was observed within (698)cm^{-1} for complexes of Pd(II), Pt(II) ,the shifting to lower frequency from free ligand indicated to the coordination of (C-S) to the metal ions (Ameen et al, 2018).

3.3^{1}H-NMR, spectra for complexes : The ^{1}H-NMR, spectra for a new complexes of (HgL_2)were taken in DMSO-d^6 solvent . ^{1}H NMR (295K, ppm, d^6-DMSO) for**[$Pd_2(HgL_2)Cl_4$]** :6.73-7.85 (d, 1H, H2); and7.43-7.85 (d, 1H, H (4)..
^{1}H NMR (295K, ppm, d^6-DMSO) for**[$Pt_2(HgL_2)Cl_4$]** : 6.64-6.98 (d, 1H, H2); and7.65-7.95 (d, 1H, H (4)(Aziz et al.,2017) .

3.4 UV-Visible spectra of complexes: The UV-visible spectrum of **[$Pd_2(HgL_2)Cl_4$]**,
The band at 22321cm^{-1}, which attributed to transition $^{1}A_1g \rightarrow {}^{1}Eg$ other high energy bands observed at 31251cm^{-1},35087cm^{-1} which assigned to $Pd^{+2} \rightarrow$ C=N charge transfer transitions, it's reasonable to assigned square planner geometry(Hassan, 2014)
The UV-Visible spectrum of **[$Pt_2(HgL_2)Cl_4$]** shows three bands at 25000cm^{-1},30769 ,36363cm^{-1}, the bands at 30769cm^{-1} 36363 cm^{-1} may assign to M-L charge transfer transition, while the band

at 25000cm^{-1}, is donated to $^{1}A_1g \rightarrow {}^{3}B_2g$, these transitions value were indicated to square planner geometry(Amin , 2011).

5. CONCLUSION

The main work in this research includes the synthesis of new Palladium(II) and platinum(II) complexes with (HgL_2) ligand. According to the IR, H^1-NMR , UV-visible spectroscopy , melting point and CHNS analysis, both complexes of **$[Pd_2(HgL_2)Cl_4]$, $[Pt_2(HgL_2)Cl_4]$** have a square planer geometry and the metal ions coordinates to the ligand through Nitrogen, and Sulfur atoms of the ligand (HgL_2).

6. ACKNOWLEDGMEN

The authors are great thanks and respects to all members of the staff in Chemistry Department, College of Education for their particular and continuous help during performing our work.

Table 1: Yield%,Colors, molecular weight, , melting points and elemental analysis for the synthesized complexes(CHNS)

No.	Complexes	Yield%	Color	M.Wt	M.P(°C)	(Calculated) Found %				
						C	H	N	S	M
1	$[Pd_2(HgL_2)Cl_4]$	58	Brown	909.56	>300	(21.12) 20.76	(1.10) 0.98	(6.16) 5.79	(7.04) 6.85	(23.39) 23.04
2	$[Pt_2(HgL_2)Cl_4$	65	Greenish-brown	1086.90	258	(17.67) 17.28	(0.92) 0.68	(5.15) 4.59	(5.89) 5.29	(35.89) 35.28

Table.2 Infrared spectral and Electronic spectral bands of the prepared complexes

No.	Complexe	IR spectra cm^{-1}				Band Absorption		Assignment
		C=N	C-O-C	C-S	M-N	cm^{-1}	nm	
1	$[Pd_2(HgL_2)Cl_4]$	1608	1078	698	530	35087	285	C.T
						31250	320	C.T
						22321	440	$^{1}A_1g \rightarrow {}^{1}Eg$
2	$[Pt_2(HgL_2)Cl_4]$	1608	1078	698	570	36363	275	C.T
						30769	325	C.T
						25000	400	$^{1}A_1g \rightarrow {}^{3}B_2g$

Table(3): ^{1}H-NMR data for synthesized complexes

No.	Complexe	^{1}H-NMR(ppm)	
		(d, 1H, H2)	(d, 1H, H4)
1	$[Pd_2(HgL_2)Cl_4]$	6.73-7.85	7.43-7.85
2	$[Pt_2(HgL_2)Cl_4]$	6.64-6.68	7.65-7.95

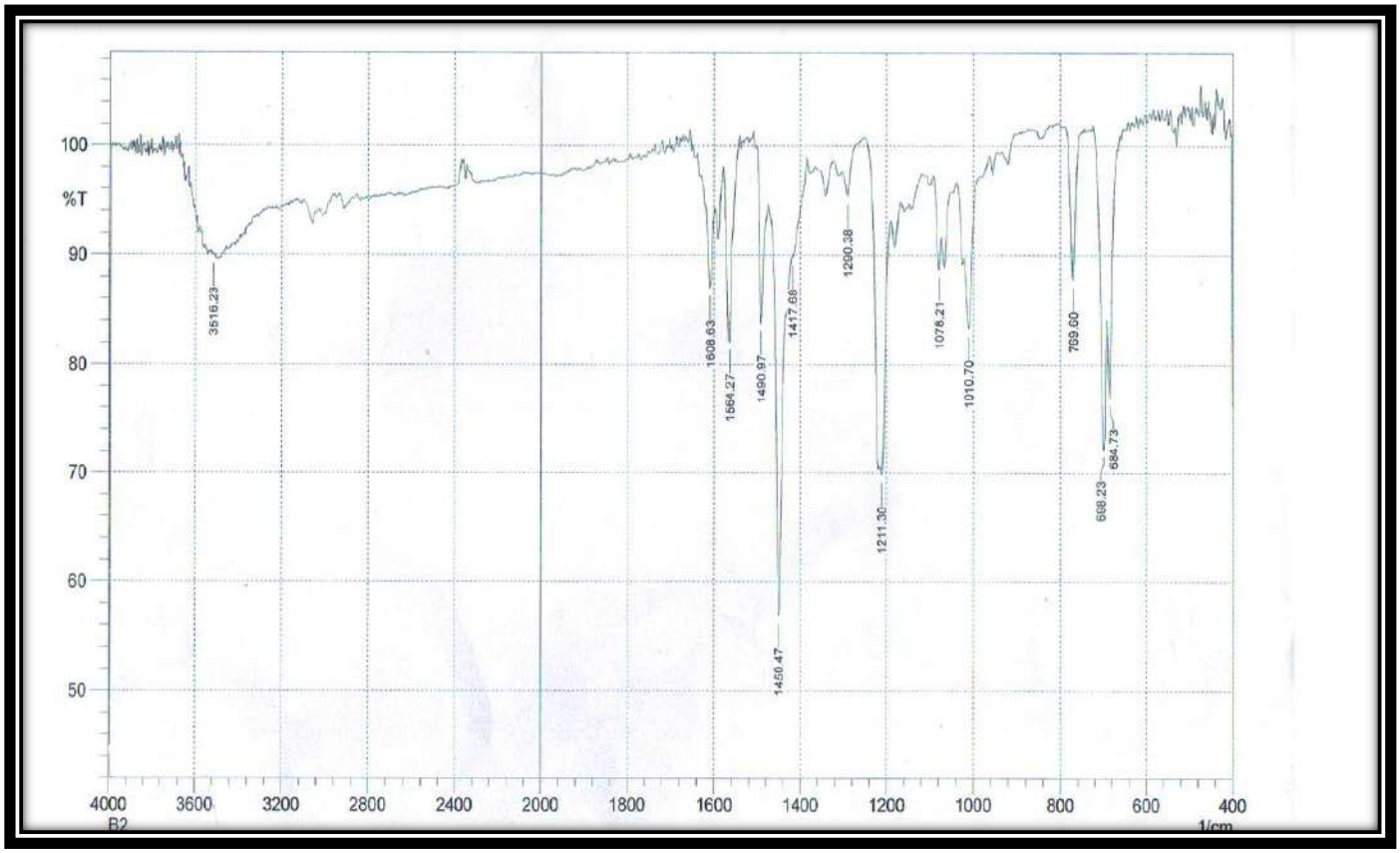

Fig(1): The Infrared spectrum of $[Pt_2 (HgL_2)Cl_4]$

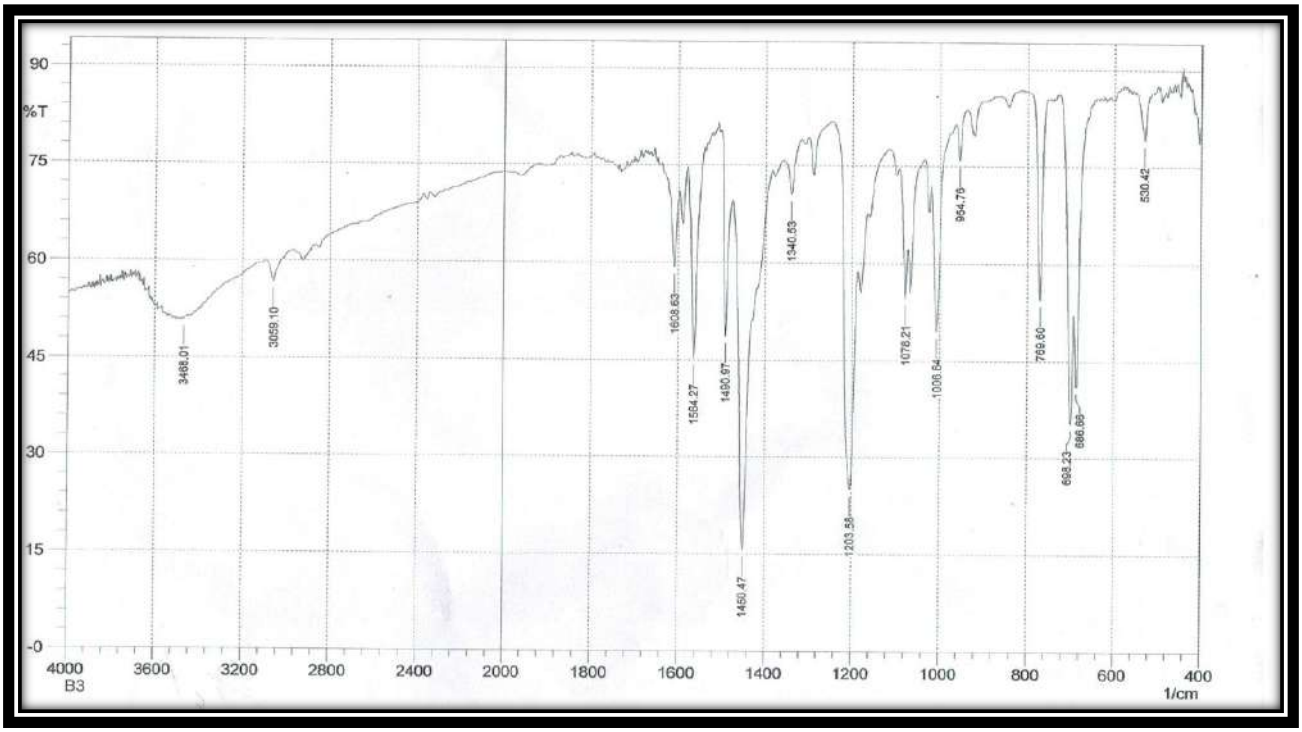

Fig(2): The Infrared spectrum of $[Pd_2 (HgL_2)Cl_4]$

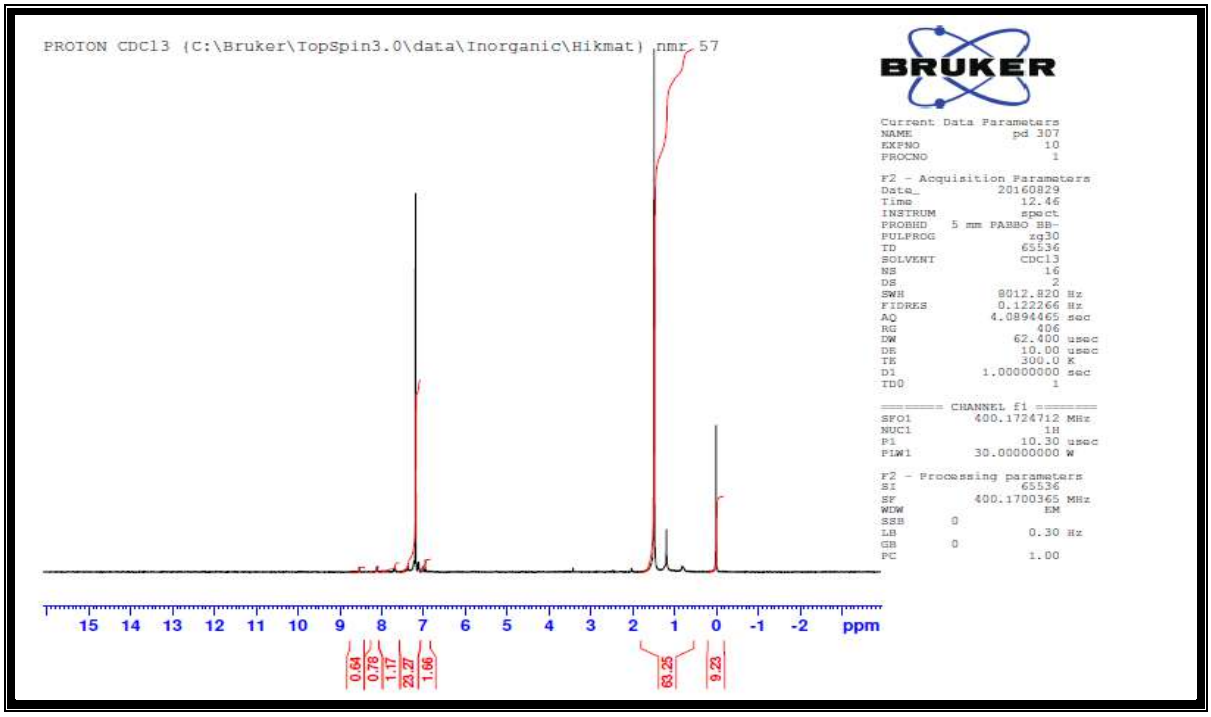

Fig(3): The ^{1}H-NMR for $[Pd_2 (HgL_2)Cl_4]$

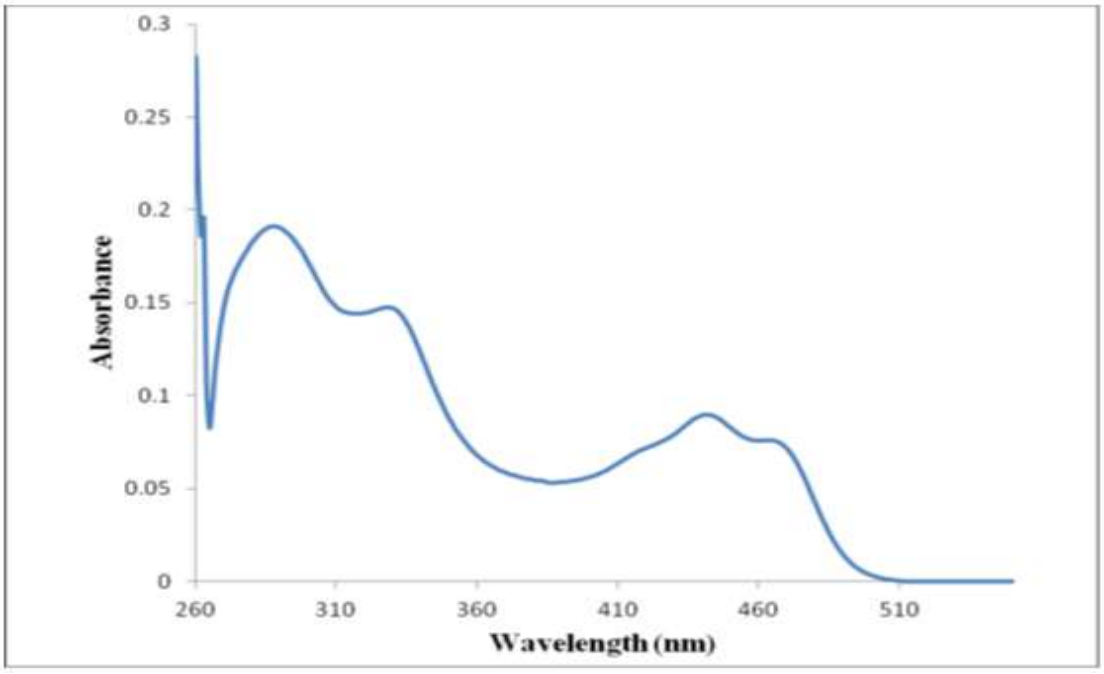

Fig.(4): UV-visible spectrum for $[Pd_2 (HgL_2)Cl_4]$

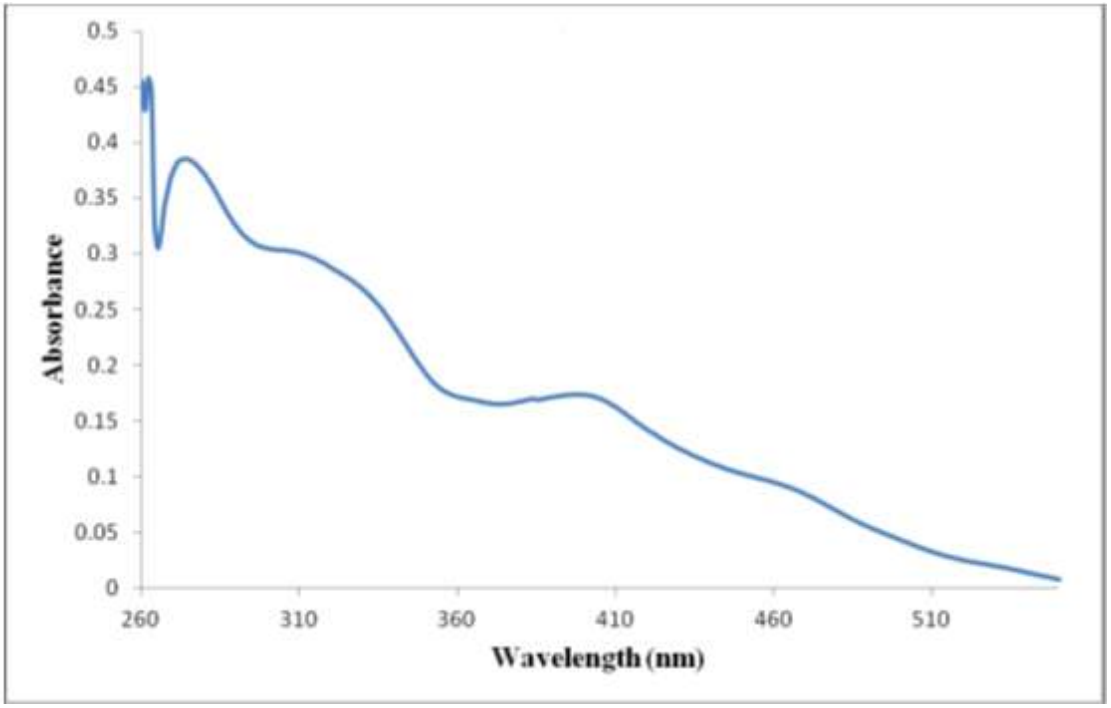

Fig(5): UV-visible spectrum for the $[Pt_2 (HgL_2)Cl_4]$

REFERENCES

Abbas Z. M., Hussain D. F. and Shakir. M. R., 2017. Synthesis of Some New Heterocyclic Fused Rings Compounds Based on 5-Aryl-1,3,4-OxadiazoleIbn AL-Haitham J. for Pure and Appl. Sci., 30(2) , pp. 161-176.

Abbasi M. A., Rehman A. U., Siddiqui S. Z., Ali Shad S. A.,2018. Synthesis and Bioactivity of Novel Tri-Heterocyclic Molecules: {4-[3-({[5-(Substituted)-1,3,4-Oxadiazol-2-Yl] Sulfanyl}Methyl) Benzoyl]-1-Piperazinyl}(2-Furyl)Methanones . Arc.Org. Inorg.Chem. Sci. 1(2), pp.57-64 .

Ameen B. M. H. Mohamad A.H. ,2018. Synthesis and characterization of Pd(II) and Pt(II) complexes with bis [Hg (2-apt)].Kirkuk. U. J. S.S. , 13(3), pp.(12-22).

Amin K.F.M., 2011. Synthesis and characterization of tetranuclear metal complexes of the type [$M_2(bztzS)_4M'_2Cl_4$]. M.Sc., Thesis, Sulamani University.

Aryanasab F., Malike H. and Saidi R. M., 2011. A Novel One-Pot Synthesis of 2-Alkylthio-1,3,4-oxadiazoles in Water J. Iranian chem. Soc., 8(2), pp. 525-530.

Aydogan F., Turgut Z., and Ocal N., 2002. Synthesis and Electronic Structure of New Aryl- and Alkyl-Substituted 1,3,4-Oxadiazole-2-thioneDerivatives Turk. J. Chem., 29, pp.159-169.

Aziz M.Y.,Bayiz Y. K. and Hawaiz F. E., 2017. One-pot Three Component Synthesis of Some NewAzo-PyrazolineCompounds

Derived From 5-((3-chloro-4-methylphenyl)diazenyl)-2-hydroxybenzaldehyde, Z. J. of Pure and Applied Sciences, 29(4), PP. 134-139.

Hassan N. H., 2014. Synthesis and characterization of some complexes of bis (2-mercaptobenzimidazole)mercury (II) with Ni(II),Pd(II), Ag(I), Pt(II),Pb(II) and their adducts. M.Sc., Thesis, Salahaddin University.

Jawdat H.A., Maha S. H. and Dardaa A. I. , 2017. Synthesis, Characterization and Study of Biological Activity of Some 1, 3, 4 – Oxadiazole Derivatives and Complexes with Some Metals and Transition MetalsDiyala J. for pure Sc., 13(2),pp. 92-110.

Mohamad H., Gerber T. I. and Hosten E., 2020. The Reaction of (1,3,4-Oxaadiazole-Thiolato)Mercury(II)with Triphenyl Phosphine, Crystallography Reports, 65(7),pp.1117-1120.

Roy P. P., Bajaj S. , MaityT.K. , and Singh J.2017. Synthesis and Evaluation of Anticancer Activity of 1, 3, 4-Oxadiazole Derivatives against Ehrlich Ascites Carcinoma Bearing Mice and Their Correlation with Histopathology of Liver .Ind. J. Pharm. Edu. and Resc.51,pp. 260-269.

Srivastavs S. and Pandeya S.N. , 2011. Various Approaches for Synthesis of Oxadiazole derivatives. Tnter. J. Res. Ayru. Pharm. , 2(2), pp.459-468.

ZANCO Journal of Pure and Applied Sciences
The official scientific journal of Salahaddin University-Erbil
https://zancojournals.su.edu.krd/index.php/JPAS

ISSN (print):2218-0230**, ISSN (online):** 2412-3986**, DOI: http://dx.doi.org/10.21271/zjpas**

RESEARCH PAPER

Specification and Evaluation of Diesel Fuel used in Electricity Generation in Erbil

Hawar M. Ali, Kasim S. Hadi, and Sangar S. Ahmed *

Department of Chemistry, College of Science, Salahaddin University-Erbil, Kurdistan Region, Iraq.

A B S T R A C T:

Two sets of diesel samples, which include fifty samples in both winter and summer seasons, from electricity generators in different locations in Erbil city (Kurdistan reign-Iraq) were investigated. Another additional diesel sample, which was obtained from the directly fractional distillation of Khurmala oilfield near Erbil city was also investigated. The samples were evaluated and compared their sulfur content, flash point, density (API), pour point, aniline point, cetane number and distillation curves with worldwide guidelines. It was observed from the evaluation of these samples that most of the diesel samples have higher sulfur content, lower flash point, higher pour point, lower cetane number, naphthenic character and have low IBP, low 10% distillation temperature, normal 50% distillation temperature and Final Boiling point (FBP). While the diesel fuel obtained from the fractional distillation of Khurmala crude oil gave acceptable values in all specification tests according to Iraqi guideline.

KEY WORDS: Diesel, Khurmala oilfield, API, Flash Point, Cetane number.
DOI: http://dx.doi.org/10.21271/ZJPAS.32.5.9
ZJPAS (2020), 32(5); 92-105 .

1. INTRODUCTION

Due to larger efficiency, reliability, high energy output and gasoline economy, the commercial transportation sector and electric producer station utilize diesel fuels which are the most dominant oils (Nadeem *et al.*, 2006). Whereas, the distillation of crude oil makes Diesel fuel that is totally complicated of a mixture of hydrocarbons. There are hydrocarbons in diesel fuels consisting of four types which are paraffin, naphthenic, olefin, and aromatics The carbon numbers of these fractions are in the ranges between C_9 to C_{20} (Naman *et al.*, 2017) (Demshemino S. Innocent *et al.*, 2013) (Romano *et al.*, 2010).

The primary sources of diesel fuels from refinery streams are immediately run middle distillation atmospheric within the range of between 160 to 350 °C and vacuum distillation towers. In contrast, diesel fraction can be mixed with the diesel pond containing heavy cracker naphtha and light Coker oil (Meyers, 2000) (Anjana Srivastava and Ram Prasad, 2000). Moreover, a high substance of sulfur compounds is the most trouble in the usage of diesel oil as a fuel. After combustion, it changed over to sulfur oxides (SOx) and radiated to air as essential contamination. Thus, it led to a large number of diseases for example; emphysema, asthma and bronchitis (Meyers, 2000) (Abdulsalam and Luqman O. Hamasalih, 2013).

The aim of this paper is to evaluate the diesel fuel that has been used in the electric generators of Erbil city in Kurdistan Region-Iraq in two seasons (summer and winter). Therefore, the outcomes of this study are compared with the diesel fuel

* **Corresponding Author:**
Sangar S. Ahmed
E-mail: sangar.ahmad1@su.edu.krd
Article History:
Received: 11/12/2019
Accepted: 25/03/2020
Published: 13/10 /2020

specifications of some countries and Khurmala diesel product.

2.Material and Methods:

2.1Sampling:

Two series of fifty diesel fuel samples in two seasons {winter (W) and summer (S)} were collected directly from the electric generator owner's located different places in Erbil city. To assess the variation between various seasons, the samples were taken and tested at both winter and summer seasons from the same places as shown in **Table 1**. Moreover, the crude oil sample was also taken from Khurmala field, which is located in Erbil city and fractionally distilled to obtain fresh diesel fuel which is distilled at range (170-330 °C). This diesel fuel was taken as a standard for comparison with collected diesel samples.

2.2ASTM Specifications and Equipment

According to the American Society of Testing and Materials (ASTM), the samples were analyzed for specification and evaluation. All tests except cetane number and fractional distillation curve, which provided by petroleum lab from the Ministry of Natual Resource-KRG and green PCB Company-Erbil, were carried out in the Chemistry Department/ College of Sciences/ Salahaddin University, Erbil-Iraq.

Moreover, the total sulfur content of oils was analyzed by utilizing an X-ray sulfur meter, RX-360SH, Japan using (ASTM D4294, 2020). The fractional distillation curve was analyzed using an automated distillation tester, AD-6, Japan according to (ASTM D86, 2020). Moreover, Density determined at 60 °F (15.5 °C) using a pycnometer according to standard method (ASTM D1217-93, 2020), Flashpoint according to (ASTM D92, 2020), Aniline point according to (ASTM D611, 2020), Pour point according to (ASTM D97, 2020). Finally, Cetane number was determined depending on (ASTM D613, 2020) by applying the octane number Zeltex, ZX-101XL, U.S.A.

3 .Results and Discussion:

Today, diesel fuel has become one of the most important petroleum products in the world. Diesel is used worldwide for transportation, manufacturing, power generation, construction and agriculture. All those uses of diesel fuel of cores because of their reliability, efficiency and high power output. Therefore, countries around the world need diesel fuel with higher quality to keep our environment safe and cleaner and to reduce the negative effects of polluted emission of these fuels on our societies. Recently, the demand for diesel fuel over the world is extremely increased, and the amount of polluted emission increased accordingly. Many international organizations interested in improving the environment provide regulations and standards for fuel qualities and periodically make more restriction on applying these regulations and standards (Pirouzfar and Fayyazbakhsh, 2016) .

Generally in our country, especially in Erbil city which was taken as an example, the demand for diesel fuel is in increase especially for the production of electricity beside other sectors. Furthermore, the official refiners are unable to produce enough amount of diesel fuel to cover needs for this sector and thereby different sources appear for marketing through importing diesel fuel from other countries or preparation diesel fuel by blending other petroleum products outside quality controls. According to these considerations, the evaluation of diesel fuel in the electricity sector was more interesting and must take more attention.

For more additional consideration, it was preferred to achieve diesel fuel directly from the fractional distillation of a crude oil sample taken from Khurmala field near Erbil city. The distillation was carried out at a standard range of boiling point for diesel fuel fraction between (170°C-340°C). The same tests were applied for this diesel fuel sample as applied for all diesel samples taken from electricity generation. Generally, for specification and evaluation of diesel fuel, the following tests must be carried out; sulfur amount, density and API gravity, flash point, aniline point, pour point, distillation curve and cetane number. Each of these tests provides indications about the quality of diesel fuel and the overall results used to evaluate and qualifying the diesel fuel.

The evaluation of the diesel fuels samples under the test was carried out by comparison with guidelines and standards of some industrial and

gulf countries beside Iraqi standards which, is shown in **Table 2**. Moreover, the results in **Table 3** illustrate that the specification of the Khurmala diesel sample, which was obtained by fractional distillation of Khurmala crude oil and it was useful for providing an additional guideline for evaluation of diesel samples.

3.1Sulfur Content:

The acid rain containing sulphuric acid is resulted from the reaction of released SO_2 with water . Acid rain and particulate matter production are the major environmental concerns of sulfur pollution. Acid rain has many negative impacts on the environment; including water acidification, soil acidity, and vegetation damage (Mohammed K. Younis and Sherwan Mohammed Simo, 2015).
As shown in **Figure 1**, the sulfur content (wt %) for diesel samples taken in summer season was higher than those taken in the winter season. The sulfur content for the summer sample was ranged between (1.7-3.0 wt %), while the sulfur content of the winter sample was lower and ranged between (1.0-2.5 wt %) with some exceptions. Comparing the sulfur content of diesel fuels in Erbil city with those of worldwide surveyed in 2018 as shown in **Table 2**, it was observed that the sulfur content was out the range of (0.0004 – 0.0007 wt %) in industrial countries, and for gulf countries in the range of (0.02-0.1 wt %) and in Iran is (0.5 wt %), whereas, Iraqi diesel fuel is 0.840 wt %. Moreover, the results demonstrate how much difference was between diesel fuel in Erbil city and those of industrial countries and even gulf countries. The sulfur content of diesel fuel obtained from the fractional distillation of Khurmala crude oil was only (0.5 wt %). As it was seen in **Table 3**, which was acceptable according to Iraqi guideline. Besides, the sulfur content of Khurmala diesel was (2-6) folds lower than those used in the electricity generator sector. In addition to that, as it is shown in Figure 1 and Figure 2 the high sulfur content of diesel fuel samples in Erbil city in both summer and winter season especially summer samples may be attributed to that, the diesel fuels in Erbil city prepared by blending of heavy oil products which already contain a higher level of sulfur compounds.

3.2 Density

Density of diesel fuel provides important an information about the composition of diesel fuels. Low density indicates that diesel fuel has lighter components in its composition. The acceptable value for the diesel fuel density is around (0.83 g/ml) at 15.5 °C. As shown in **Figure 3**, there isn't samples among the overall (50) samples of diesel fuels collected in both winter and summer seasons have a density in the normal density, almost it has a higher density, which ranged between (0.87-0.9) g/ml. Furthermore, Diesel samples in the winter season from (1-7) and (32-46) have densities around (0.84-0.86) g/ml and they are near the normal value as shown in **Figure 3**, while samples from (13-30) have densities between (0.86-0.88) g/ml.
On the other hand, all the diesel fuel samples taken in summer season have higher densities, it was more than (0.88 g/ml) and some samples like (8, 10, 12, 14 and 17) have densities near (0.89 g/ml). These results confirm that the diesel fuels in Erbil city were prepared by blending of different oil products in random ratios without using scientific procedures and standard methods. Accordingly, it was noted that each diesel sample was different than the others in the specification and almost all the samples were obeyed the standard guidelines. However, the density of diesel sample obtained directly from the fractional distillation of Khurmala crude oil was (0.825 g/ml), and it was acceptable according to Iraq, Iran, Kuwait guidelines (**Table 2**, **Table 3,** and **Table 4**).

3.3 Flash Point:

The flashpoint affects the handling and storage of fuel, the low value of flashpoint is an indication of fire hazard. The low flash purpose of diesel oil is that the root of the explanation for several tragic fireplace accidents of diesel storages. (J. Thilagan and R. Gayathri, 2014).
The flashpoint of diesel fuels used in most countries around the world lies between 50 to 60 °C (**Table 5**). While the flashpoint of some diesel fuel samples, which have been used in Erbil, was below room temperature (below 25 °C) and the others were between (30 – 40) °C (**Figure 4**). The flashpoint of diesel samples was lower than those listed in and this may cause difference

risks during storage and transportation, also may be evaporated to the atmosphere and cause additional air pollution.It was observed that the flashpoint of summer samples was generally higher than those of winter samples, as it was illustrated in **Figure 4**.

3.4 Aniline Point:

The Aniline point is the lowest temperature at which the same volume of aniline and oil is completely miscible (clear). The aniline point (AP) is roughly correlated with the amount and type of aromatic hydrocarbons in the oil sample. The low AP is an indication of higher aromatics content and vice versa. Diesel oil with AP below 120 ° F (49 °C) is likely to be hazardous to use. The lower the Aniline point, the higher the solvency or reactivity of the oil, which in turn gives an aromatic indication of the oil. For example, for aromatic oil with a 75% aromatic content, the aniline point would be between 32 °C and 49 °C. For naphthenic form with a 40% aromatic composition, it would be between 66 °C and 77 °C, and for paraffin oil with a 15% aromatic content, it would be between 93 °C and 126 °C. (Rajesh Kanna *et al.*, 2017).
With respect to these values, and according to the determined aniline point of diesel samples, which were utilized in this study, as shown in **Figure 5**, the most of the diesel samples contain less than 40% aromatic and have naphthenic character. An exception was observed for samples (5,16 and 48), which have aniline point near $90C^{o,}$ that is the indication for lower aromatic content (15-204 wt %) and have paraffinic characters.

3.5 Pour point:

Pour point provides information about waxy materials in the diesel fuel, which refers to the presence of long-chain aliphatic hydrocarbons. Normally, by increasing the weight ratios of these long-chain hydrocarbons the pour point accordingly increases. At low temperature especially at cold weather, the waxes will separate from the diesel and then coagulate forming bulky layer cause difference problem to the internal combustion engines during working (Saeedi Dehaghani and Rahimi, 2019).

As it was explained in **Table 2**, the pour point of diesel in industrial countries which already have cold weather ranged between (-23 °C to -33 °C), while in Gulf countries the pour point arises to the range between (-3 °C to -6 °C). Even according to Iraqi guideline the pour point is (-9 °C) because these countries have relatively hot weather and the wax under these conditions will not separates from the diesel fuel. The results in **Figure 6** shows a wide range of fluctuation ranged between (+9 °C to -15 °C) in winter diesel samples and (+10 °C to +5 °C) in summer diesel samples. Moreover, the samples (32, 33, 35) in both winter and summer seasons have fixed and acceptable pour point, which was -15 °C, whereas, it was about -9 °C for sample 34 in both seasons. Besides, the rest samples have pour point above 0.0 °C either in both seasons or summer season and all were not acceptable according to even to Iraqi guideline (see **Table 2**).
On the other hand, the pour point of diesel, which obtained from the fractional distillation of Khurmala crude oil was (-15 °C) which is acceptable according to Iraqi even to worldwide diesel fuel guideline. As it was mentioned earlier the an acceptable pour point of commercial diesel fuel in Erbil city referred to random procedures, which have used for the blending process between different types of diesel and other oil products.

3.6 Distillation Curve:

Distillation curves gives knowledge that enables quality to be associated with the efficiency of the engine. The temperature of 10% of the recovered volatilized gas fraction represents the case of vaporization, while the temperature of 90% of this fraction suggests the presence of high molecular weight compounds that will be difficult to vaporize entirely, preferring the emission of particular matter (PM) and unburned hydrocarbons (HCs) (Cataluña and da Silva, 2012).
Set of seven samples (6,17, 23, 32, 34, 35, and 49) in both seasons were chosen from both winter and summer seasons to evaluate their distillation curves as are illustrated in **Figure 7** and **Figure 8**. In this set, there was no sample completely field in all fractional ranges with standard distillation curves, but a few samples like 34S and 35W have distillation curves similar to the standard

distillation curves (see **Table 2**). Other samples like 32S, 32W, 35S and 35W have similar IBP, 10%, and 50%distillation temperature, but their 90% and FBP appear at lower temperature and this means that these samples contain higher levels of light petroleum fractions.
Moreover, the distillation curve of Khurmala diesel sample as it was explained in **Table 3** was in similar temperature ranges as for standard distillation curve provided as guideline survey 2018 (**Table 2**).

3.7 Cetane Number:

Cetane number is an associate degree empirical parameter related to associate degree ignition delay time of diesel fuels. Low CN means longer lag time causes an increase in the emission of unburned hydrocarbons and particulate matter Cetanus number (C.N.) also affects direct fuel consumption, with a propensity to decrease fuel consumption as CN rises due to higher combustion cycle temperatures and improves engine thermal performance. (Cataluña and da Silva, 2012).
A set of samples, which were included (6, 16, 17, 32, 33, 34, 35 and 49) for both winter and summer seasons were taken to determine their cetane number as are presented in **Figure 9**. The cetane number of the samples was between (44.3 to 47.8), while the acceptable value of cetane number is above 50 as mentioned in **Table 2**. The cetane number of Khurmala diesel sample was (51) as in **Table 3**.

4 Conclusion:

1- The sulfur content of diesel samples in the winter season was relatively lower than those of the summer season. But the sulfur content of diesel samples of both winter and summer season was very high with respect to worldwide guidelines.
2- The density of the summer season samples was relatively higher than those of the winter samples and all the samples have higher density according to guidelines.
3- Flash point of most diesel samples was below room temperature and others were between (30-40) °C.
4- From aniline point, it was concluded that most of the diesel samples were naphthenic character.
5- Pour point of some samples was above zero temperature and only 25% of the samples have pour point between (-9 to -15) °C.
6- The cetane number of all the samples was lower than 50 and it was around 40.
7- The distillation curve of selected samples provide an indication that the sample has a low temperature of IBP, 10% distillation and normal range temperature of 50%, 90% and FBP.
7- The diesel sample obtained from the fractional distillation of Khurmala crude oil gave acceptable results according to Iraqi guideline.
Therefore, the overall conclusion observed from the evaluation of diesel samples, which have been used in electricity generator section has low quality according to guidelines because the diesel fuel for this sector was prepared by blending of different petroleum product not by professional persons using uncorrected procedures without quality control. An accepting was observed from the specification of diesel fuel used by Teammart group for their electricity generators. This group brought a large quality of diesel fuel produced directly from Kar, Hawler and Kirkuk refineries or from Iran. Besides, the diesel obtained from them directly fractional distillation of Khurmala crude oil also has acceptable quality according to Iraqi guideline.

Table 1: sample code and locations:

Sample code	Location	Place
1D	36.164028, 44.028283	Andaziaran – Wafai park
2D	36.191328, 44.012026	Swrchyan street
3D	36.162664, 44.024823	Andaziaran
4D	36.151111,44.047515	Galawezh

5D	36.181564,44.029233	Mamostaian 1
6D	36.157939, 44.017528	Mantkawa- near Chihan Bank
7D	36.215332, 44.023044	Ulama – Shix Najmadin Mosque
8D	36.209765, 44.019949	Near Shorsh Stadium
9D	36.184680, 44.037141	Near Langa bazar
10D	36.189443,44.036679	40 meter street –near Top Med Laboratory
11D	36.153923,44.031306	99 Zanko – near Dli Kurdistan School
12D	36.169620 , 43.989301	Gulan street – Muhammad Bajalan Hospital
13D	36.169523,44.030675	Badawa – near Perezhn Mosque
14D	36.170891,44.025740	Near Mufty
15D	36.176431,44.012574	40 meter street – near Hawler School for Girl
16D	36.168860,43.985578	Kurdistan street- near Sharawany 6
17D	36.163682,44.067321	Near Haji Ali Shakr Mosque
18D	36.149412,44.032381	Zanko village
19D	36.168097,44.995290	Kuran
20D	36.173000,43.984301	Kurdistan street – near Safa & Marwa Mosque
21D	36.192702,44.065882	Hiran city
22D	36.176281,43.970729	Nawroz street – near Shahed Abdullqadr Mosque
23D	36.124181, 44.055163	Daratw – near Mala Nwri mosque
24D	36.156059,44.063909	Farmanbaran – near Galawezh School
25D	36.148973,44.060433	Farmanbaran – near Shahed & Anfalkrawakan Mosque
26D	36.174005,43.980299	Nawroz
27D	36.158433,44.059296	Farmanbaran – near Bnasllawa street
28D	36.158086,44.071827	Farmanbaran – near Brwadaran Mosque
29D	36.151833, 44.023266	92\Mhabad – near Shanga beri school
30D	36.156580, 44.022804	92\Mhabad – near Haji Yahia Mosque
31D	36.140733, 44.033864	Mamostayan 2 – near Frdaws Mosque
32D	----------	Kar diesel for Teammart Group
33D	----------	Hawler diesel for Teammart Group
34D	----------	Iran diesel for Teammart Group

35D	----------	Kirkuk diesel for Teammart Group
36D	36.168346, 44.019387	Runaky – near School Activity
37D	36.170671, 44.026020	Mufty – Flower nursery Chihan
38D	36.149347,44.042978	Mamostayan
39D	36.172258,44.014766	Komare – Near Haji Salam Mosque
40D	36.146491,44.020478	Mhabad – near 92-Apartments
41D	36.163911,43.991075	Opposite Walee Dewana School
42D	36.156519,44.043095	Sharawani
43D	36.170758,44.032404	Mufty
44D	36.146842,44.056399	Farmanbaran – 6000
45D	36.158382,44.026559	92 Mhabad – near Ahmadi khane High School
46D	36.179690,44.025753	Malafande street – near Shex Maarwf Graveyard
47D	36.159136, 44.031441	Zanko – near Hamid Sian Mosque
48D	36.166696, 44.022254	Runaky – near Runaky High School
49D	36.169970, 44.022458	Runaky – near Sharawany 5
50D	36.173001, 44.025602	Mufty – near Eskan Police Station

Table 2: Worldwide Diesel Fuel Quality Survey 2018 (Infineum International Limited, 2018).

Country	Sulfur Content (Wt%)	Density 15.5 °C g/ml	Cetane Number	Pour point	Distillation IBP °C	%10	%20	%50	%90	%95	FBP
Germany	0.0007	0.835	54	-30	172	207	224	273	336	352	361
France	0.0007	0.836	52	-26	163	196	215	269	337	356	361
UK	0.0007	0.836	52	-24	170	205	223	268	333	354	361
Japan	0.0007	0.823	50	-28	161	193	210	254	319	335	351
USA-W	0.0004	0.828	53	-23	172	211	223	258	321	337	350
Russia	0.0007	0.824	50	-33	162	196	211	251	314	332	344
Kuwait	0.1029	0.845	51	-6	193	231	249	290	350	368	378
Qatar	0.0221	0.831	58	-6	204	245	256	282	343	368	375
Turkey	0.0004	0.830	57	-24	165	209	233	281	344	363	368

Saudi Arabia	0.0381	0.835	53	-13	187	219	232	271	338	350	367
Iran	0.5	0.847	N/A	-3	N/A	N/A	N/A	N/A	N/A	N/A	N/A
Iraq	1.0000	0.840	53	-9	N/A	N/A	N/A	N/A	N/A	N/A	N/A

Table 3: the test results for Khurmale diesel fuel.

Test		Result
Density at 15.5 °C (g/ml)		0.825
Sulfur content (wt %)		0.5140
Flash point (°C)		43
Pour point (°C)		Below -15
Aniline point (°C)		62
Cetane number		51
Distillation curve	Initial B.P.	170 °C
	10%	192 °C
	50%	268 °C
	90%	324 °C
	95%	338 °C
	Final B.P.	346 °C

Table 4: Classification of sulfur content (wt.-) from lower to higher diesel samples

Sample Group	Sample number							Sulfur content (wt %)
Group 1	6	34	35	32	17			(0.0-1.0) wt %
Group 2	12	10	8	45	44	39	41	(1.0-2.0) wt %
		46	38	43	40	37	4	
		3	2	1	33	14	23	
		7	9	5	25	22	29	
		24	21	26				
Group 3	42	36	47	11	48	28	13	(2.0-3.0) wt %
		50	19	27	30	31	15	
			20	18	49	16		

Table 5: Standard Flash point values of some country (J. Thilagan and R. Gayathri, 2014):

Country	Australia	China	Germany	Japan	Malaysia	Norway	U.K.	U.S.A.
Diesel flash point (°C)	61	66	56	50	60	60	56	54

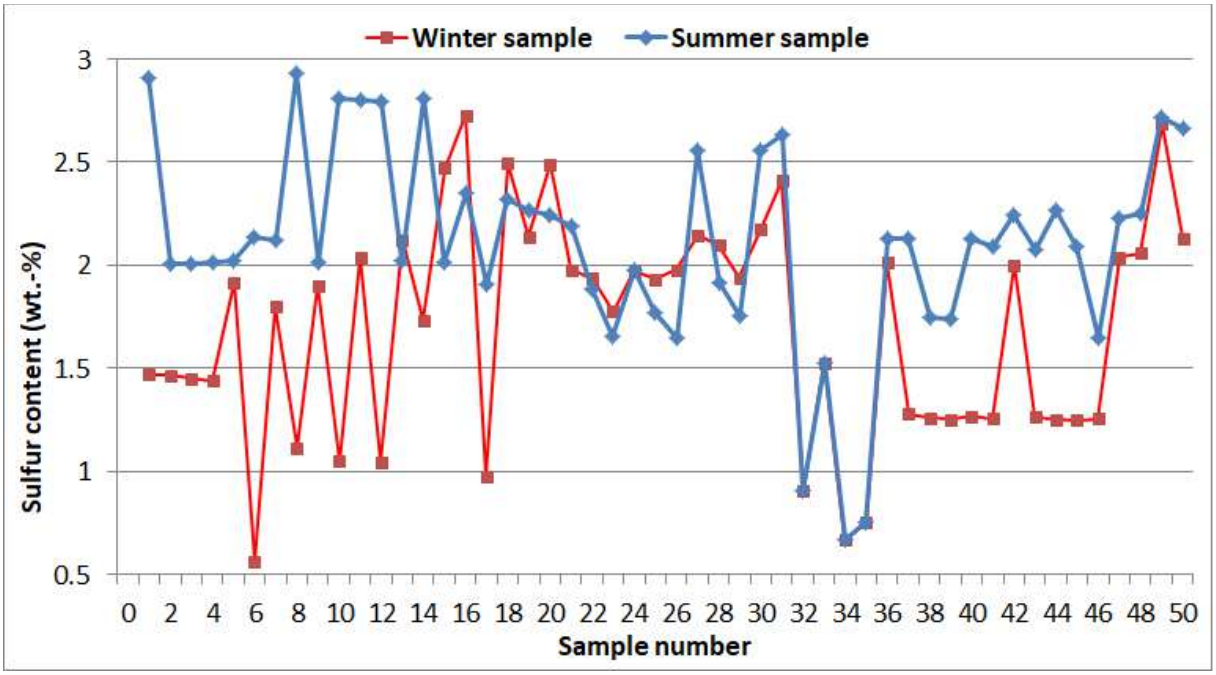

Figure 1: sulfur content in diesel sample

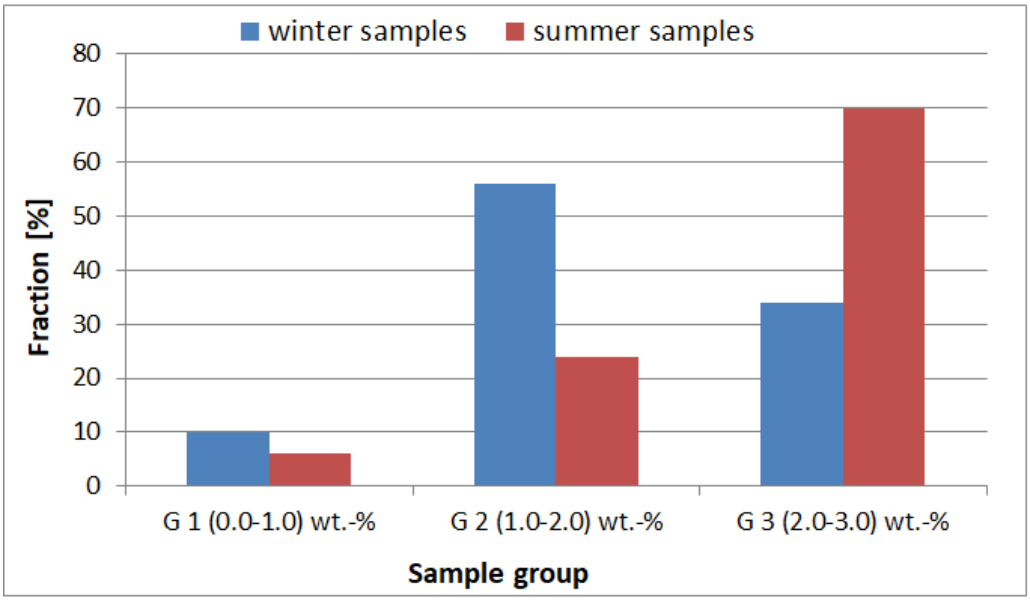

Figure 2: Classification of sulfur content (wt.-) of diesel samples

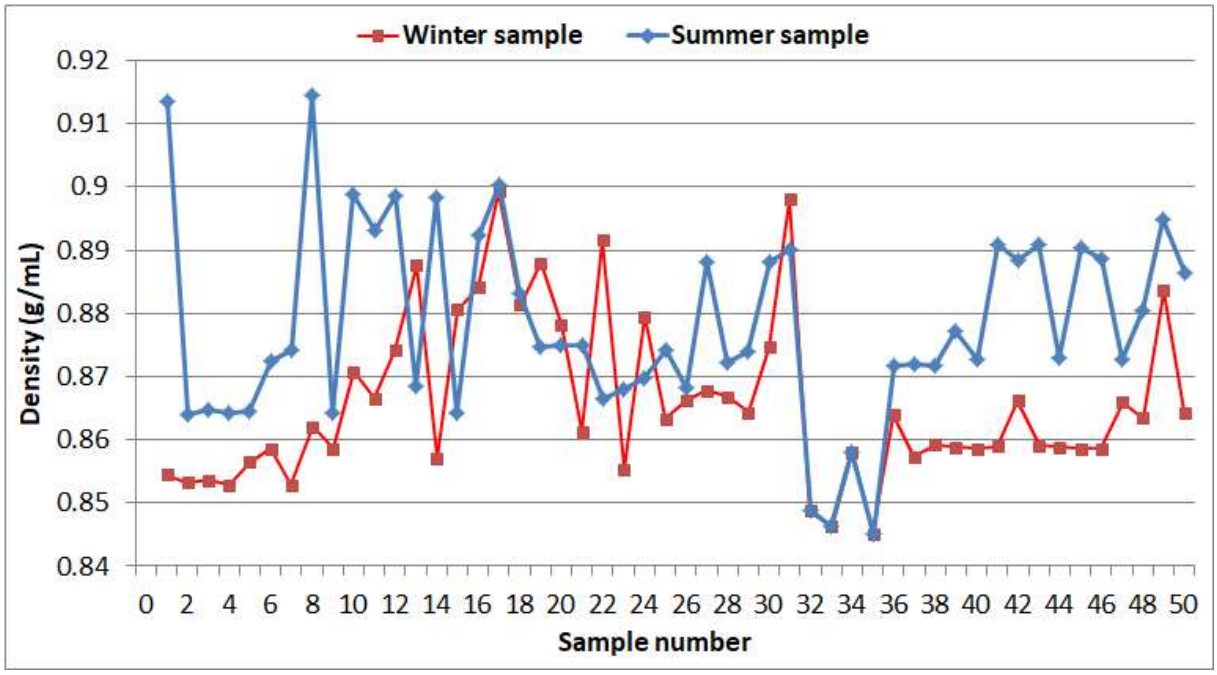

Figure 3: Density of diesel sample

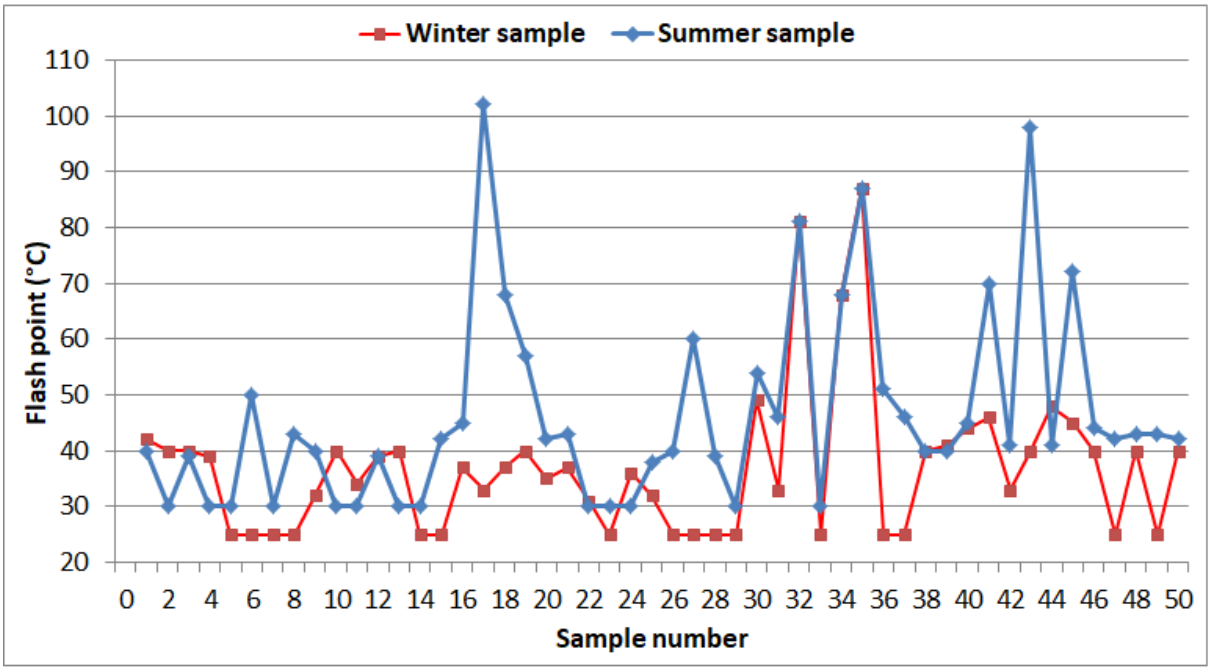

Figure 4: Flashpoint of diesel samples

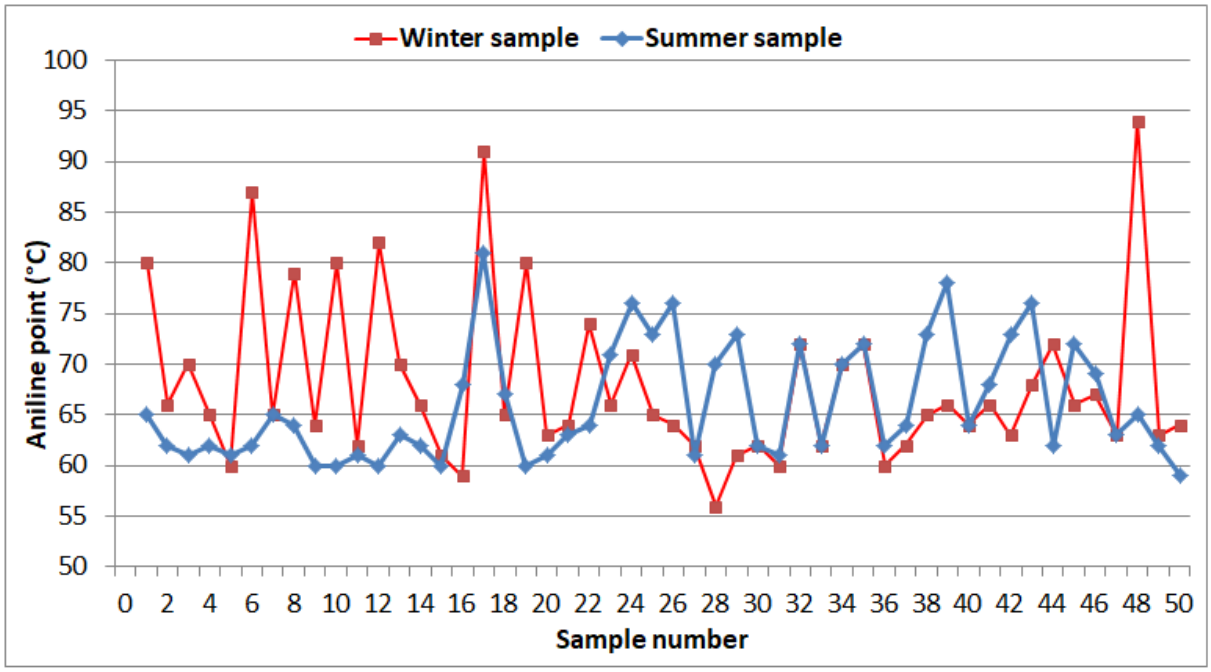

Figure 5: Aniline point of diesel samples

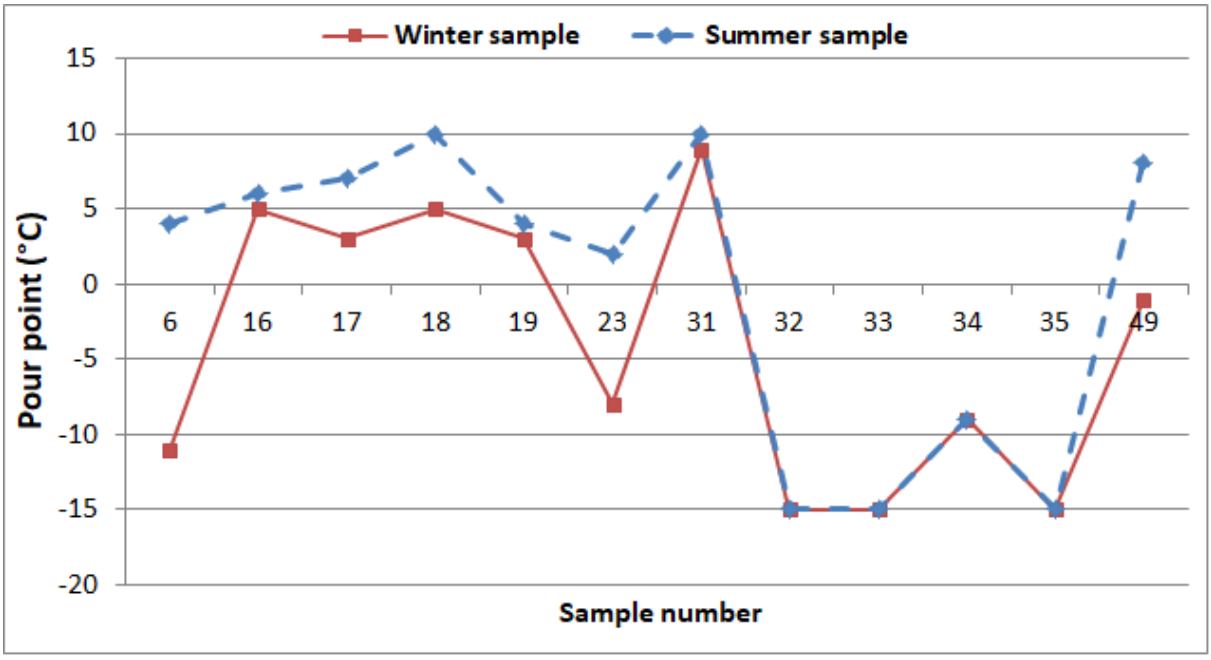

Figure 6: Pour point of diesel samples

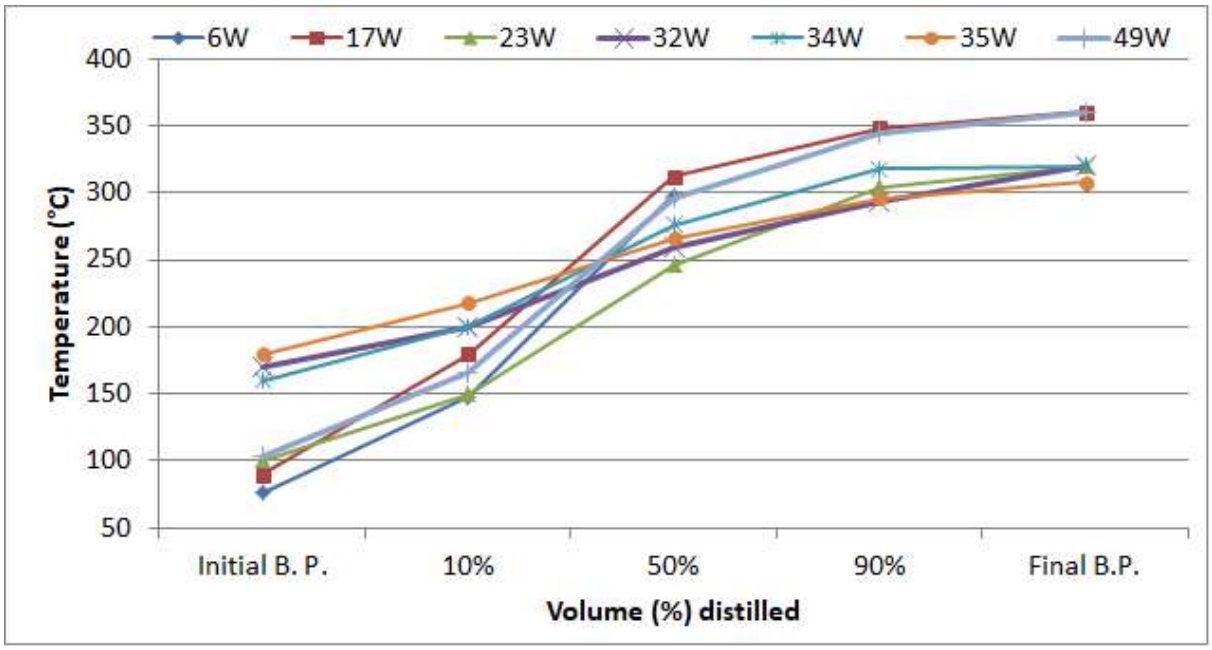

Figure 7: Distillation curve for diesel samples in the winter season.

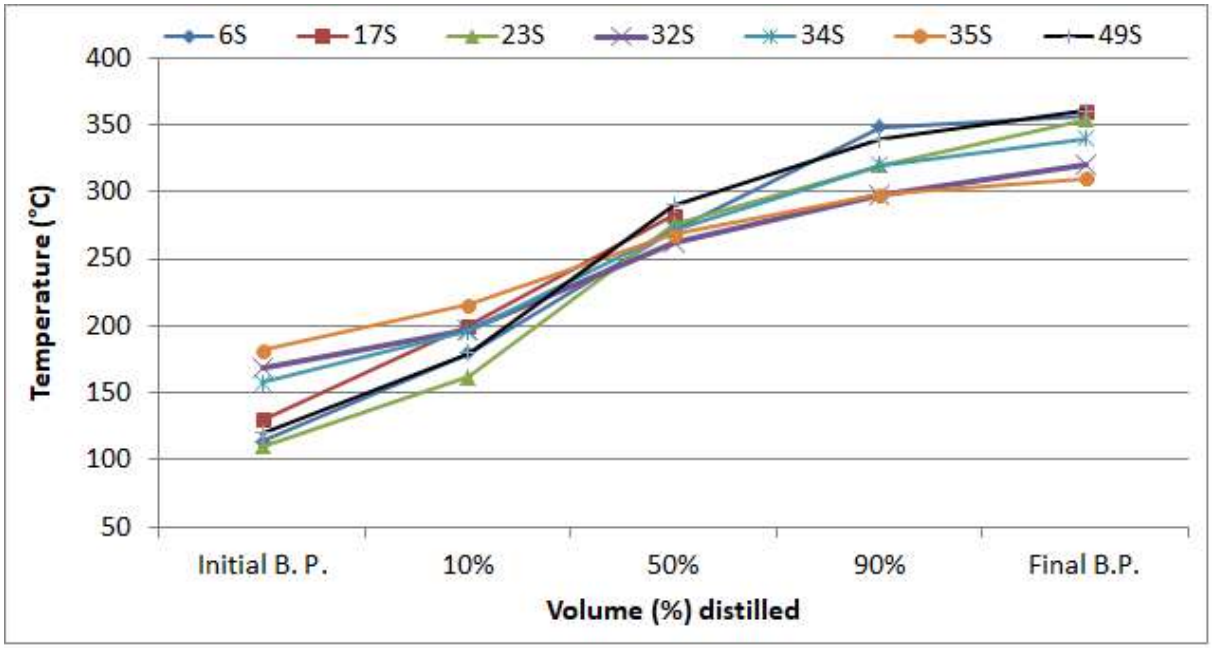

Figure 8: Distillation curve for diesel samples in the summer season.

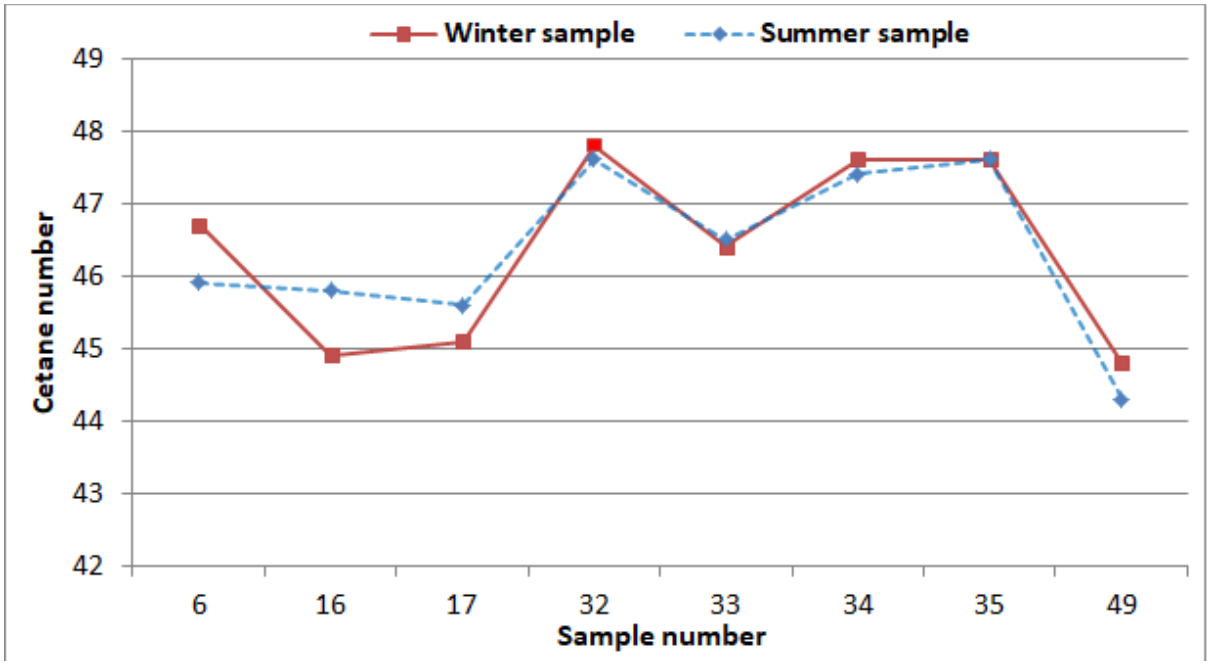

Figure 9: Cetane number of diesel samples

References

Abdulsalam, R.K. and Luqman O. Hamasalih (2013), "Production and Evaluation of some Gas Oil Fractions from Taq-Taq Crude Oil and Their Structural Group Analysis", *International Journal of Engineering and Innovative Technology*, Vol. 3 No. 2, pp. 278–282.

Anjana Srivastava and Ram Prasad (2000), "Triglycerides-based diesel fuels", *Renewable and Sustainable Energy Reviews*, Vol. 4, pp. 111–113.

ASTM D1217-93 (2020), "Standard Test Method for Density and Relative Density (Specific Gravity) of Liquids by Bingham Pycnometer", available at: https://www.astm.org/DATABASE.CART/HISTORICAL/D1217-93R07.htm.

ASTM D4294 (2020), "Standard Test Method for Sulfur in Petroleum and Petroleum Products by Energy Dispersive X-ray Fluorescence Spectrometry", available at: https://www.astm.org/Standards/D4294.htm.

ASTM D611 (2020), "Standard Test Methods for Aniline Point and Mixed Aniline Point of Petroleum Products and Hydrocarbon Solvents", available at: https://www.astm.org/Standards/D611.htm.

ASTM D613 (2020), "Standard Test Method for Cetane Number of Diesel Fuel Oil", available at: https://www.astm.org/Standards/D613.

ASTM D86 (2020), "Standard Test Method for Distillation of Petroleum Products and Liquid Fuels at Atmospheric Pressure", available at: https://www.astm.org/Standards/D86.

ASTM D92 (2020), "Standard Test Method for Flash and Fire Points by Cleveland Open Cup Tester", available at: https://www.astm.org/Standards/D92.

ASTM D97 (2020), "Standard Test Method for Pour Point of Petroleum Products", available at: https://www.astm.org/Standards/D97.htm.

Cataluña, R. and da Silva, R. (2012), "Effect of Cetane Number on Specific Fuel Consumption and Particulate Matter and Unburned Hydrocarbon Emissions from Diesel Engines", *Journal of Combustion*, Vol. 2012 No. 3, pp. 1–6.

Demshemino S. Innocent, O'Donnell P. Sylvester, Muhammad F. Yahaya and Isioma Nwadike (2013), "Comparative Analysis of Biodiesel and Petroleum Diesel", *International Journal of Education and Research*, Vol. 1 No. 8, pp. 1–8.

Infineum International Limited (2018), "Worldwide Winter Diesel Fuel Quality Survey 2018", available at: https://www.infineuminsight.com/en-gb/resources/winter-diesel-fuel-quality-survey/2018-winter-diesel-fuel-survey/.

J. Thilagan and R. Gayathri (2014), "Low flash point of Diesel in India and fire accidents in transport vehicles - An analysis", *International Journal of Green and Herbal Chemistry*, Vol. 3 No. 2, pp. 532–535.

Meyers, R.A. (2000), *Encyclopedia of analytical chemistry: Applications, theory and instrumentation / edited by R.A. Meyers*, John Wiley, Chichester.

Mohammed K. Younis and Sherwan Mohammed Simo (2015), "Desulphurization of Tawke Diesel Fuel by Adsorption on Na-Y Type Zeolite, Local Clay and Active Carbon", *International Research Journal of Pure & Applied Chemistry*, Vol. 10 No. 1, pp. 1–7.

Nadeem, M., Rangkuti, C., Anuar, K., Haq, M.R.U., Tan, I.B. and Shah, S.S. (2006), "Diesel engine

performance and emission evaluation using emulsified fuels stabilized by conventional and gemini surfactants", *Fuel*, Vol. 85 No. 14-15, pp. 2111–2119.

Naman, S., Ali, M. and Simo, S. (2017), "Evaluation and Improvement of Diesel Cut from Tawke Crude Oil Wells, Zakho", *Science Journal of University of Zakho*, Vol. 5 No. 1, pp. 93–100.

Pirouzfar, V. and Fayyazbakhsh, A. (2016), *Diesel Fuel Additives*, 1. Auflage, LAP LAMBERT Academic Publishing, Saarbrücken.

Rajesh Kanna, Nandhu M, Jossy Joy, Sreekuttan Vijayan and Johnast PC, N. (2017), "Determination of aniline point of petroleum sample", *International Refereed Journal of Engineering and Science*, Vol. 6 No. 3, pp. 18–21.

Romano, J.A., Lukey, B.J. and Salem, H. (2010), *Chemical warfare agents: Chemistry, pharmacology, toxicology, and therapeutics*, Second edition, Informa Healthcare, New York, London.

Saeedi Dehaghani, A.H. and Rahimi, R. (2019), "An experimental study of diesel fuel cloud and pour point reduction using different additives", *Petroleum*, Vol. 5 No. 4, pp. 413–416

ZANCO Journal of Pure and Applied Sciences
The official scientific journal of Salahaddin University-Erbil
https://zancojournals.su.edu.krd/index.php/JPAS

ISSN (print):2218-0230**, ISSN (online):** 2412-3986**, DOI: http://dx.doi.org/10.21271/zjpas**

RESEARCH PAPER

The Main Bioactive Constituents of Traditional Kurdish Plant *Achellia oligocephala* DC.; their Antiproliferative and Antioxidant Activities.

Hawraz Ibrahim M. Amin[1,2]

[1]Department of Chemistry, College of Science, Salahaddin University-Erbil, Kurdistan Region, Iraq
[2]Department of Pharmacy, Paitaxt Technical Institute-Private, Erbil, Kurdistan Region, Iraq

A B S T R A C T:
Achellia oligocephala DC. , which grows in the mountains, is very popular as wound healing and gastrointestinal complaints. This research article reports the first study of the phytochemical investigation and biological properties of bioactive secondary metabolites from the traditional Kurdish plant *Achellia oligocephala*. (+) - Luteolin-6-C-glucoside (AO1) and Lupeol (AO2) were isolated from aerial parts for the first time from this plant. The antiproliferative activity was measured against three human tumour cell lines, MCF7, SkBr3, and BG-1 cancer cells by using the MTT assay. Notably, the (+) - Luteolin-6-C-glucoside showed significant antiproliferative activity against MCF7 cancer cell line, IC_{50} value (10 µg/mL). The antioxidant activity of AO1 and AO2 were evaluated on total antioxidant capacity (TOAC) test. Interestingly, its showed a remarkable antioxidant activity compared to standard antioxidant. This study confirms that (+) - Luteolin-6-C-glucoside can be considered a natural anticancer and antioxidant compound.

KEY WORDS: *Achellia oligocephala* DC., (+) - Luteolin-6-C-glucoside (isoorientin), Traditional medicinal plant, Antiproliferative and Antioxidant activity.
DOI: http://dx.doi.org/10.21271/ZJPAS.32.5.10
ZJPAS (2020) , 32(5);106-117 .

1. INTRODUCTION

A large number of higher plants have been used by local inhabitants all over the world as ethnobotanical healings; many of them have yielded important pharmaceutical lead compounds after recent scientific investigations. The Middle East region of the Asian continent is particularly rich in medicinal plants, and most of them have not been investigated yet for their metabolite contents (Mükemre et al., 2015).

The region of Iraqi Kurdistan is a particularly little studied zone as concerns ethnobotanical and phytochemical investigation. Several plants are currently used by local people for their medicinal properties. (Braiem et al., 2017).

Approximately 140 species in the world represent *Achillea* species (Asteraceae). In folk medicine, these species are used as herbal remedies due to their anti-inflammatory, analgesic, antispasmodic, digestive, wound healing, hemostatic and cholagogue effects (Şabanoğlu et al., 2017).

Achellia oligocephala DC. which grows on mountains around choman in Erbil city of Iraq, especially on Halgurd Mountain (Amin et al.,

* **Corresponding Author:**
Hawraz Ibrahim M. Amin
E-mail: hawraz.mohammedamin@su.edu.krd
Article History:
Received: 04/01/2020
Accepted: 30/03/2020
Published: 13/ 10/2020

2016); It is commonly used by local people for treating wound healing and gastrointestinal complaints: yet the phytochemical constituents and the evaluation of biological properties of *Achellia oligocephala* have not been investigated.

To this aim, In this research article, I report the main bioactive constituents of the non-volatile fractions from the aerial parts, and the evaluation of their cytotoxic activity on three human cancer cell lines, as well as their antioxidant in vitro activity for the first time.

.

Figure 1: *Achellia Oligocephala DC.*

2. MATERIALS AND METHODS

2.1. General

For most general experimental techniques and procedures see (Gilardoni et al., 2015), all solvents that have been used in this research were of HPLC and the analytical grade was purchased from Carlo Erba (Milano, Italy). Thin-layer chromatography was performed with both reversed phase: TLC on Merck 60 RP-18 on aluminum plates with 0.2 mm, and direct phase: TLC on silica gel Fluka on aluminum plates with 0.2 mm, (Germany), and stained with 5 % H_2SO_4 in MeOH before heating. Ultraviolet (UV) lamp: fluorescent lamp at 254 and 366 nm; cammag (Italy). Rotavapor: IKA rotation instrument. ^{1}H-NMR and ^{13}C-NMR spectra were recorded with Bruker instrument (300 and 400 MHz), chemical shifts (δ, ppm) of AO1 were reare relative to deuterated MeOH signals at δ 3.27 (central line of a quintuplet) and at d(C) 49.0 (central line of a septuplet), respectively. Moreover, AO2 referenced against solvent signals (^{1}H-NMR: $CDCl_3$ δ=7.26; ^{13}C-NMR: $CDCl_3$ δ=77.02). Preparative middle pleasure liquid chromatography (MPLC) separations were carried out on a Biotage one Isolera instrument (Sweden).

2.2. Plant Material Collection

Aerial parts of *Achellia oligocephala* DC. for this study were collected on Halgurd Mountain-Erbil on the beginning of April 2018. The plant was identified and classified (accession number 7236) by Professor Abdulhussain Al-Khayyat in Erbil, Iraq (Amina et al., 2016).

2.3. Extraction, Purification and Isolation

The collected aerial parts of *A. oligocephala* were allowed to dry for three weeks in the well-ventilated shade. Then, the air-dried samples were grinding into fine particles. *Achellia oligocephala* powdered aerial parts (500 g) was extracted exhaustively at ventilated room temperature by maceration with 1 L of MeOH for 10 days with occasional shaking and followed by filtration. The methanol filtrate was concentrated to yield the methanol extract (8.9 g). This was partitioned with liquid-liquid extraction between distilled water and ethyl acetate (1:1) to afford an EtOAc fraction (2.55 g) as the organic phase. The aqueous layer (non-organic) was further partitioned against n-butanol to give a soluble fraction in n-BuOH (2.3 g). For this work, only EtOAc soluble fraction was used because of the antioxidant activity of this fraction (Gilardoni et al., 2015) . 1 g of ethyl acetate fraction was separated by a medium pressure liquid chromatography (MPLC) “Isolera ONE” (Biotage) instrument on a direct phase column. A linear gradient was applied from an 80:20 A/B mixture (A = n-hexane and B = ethyl acetate), to 100% solvent B (ethyl acetate), over 40 minutes, at a flow rate of 30 mL/minute, and the wavelength has been detected at UV 254-366 nm. Repeated Coloum chromatography and MPLC on both direct and reversed-phase columns of the chlorophyll-free ethyl acetate extract of aerial parts, afforded AO1 (42.6 mg) and AO2 (29.1 mg).

2.4. Identification of Bioactive Compound (AO1)

Yellow powder; $[\alpha]^{D}_{20}$+1.90 (c=0.021, Methanol); ESI-MS (negative ion mode, m/z): 447 [M-H]- for $C_{21}H_{20}O_{11}$; and its melting point is 244–245°C (Kumazawa et al., 2000). ^{1}H-NMR Spectral Data (300 MHz, CD_3OD): δ 6.49 (1H, s, H-8), 6.55 (1H, s, H-3), 6.91 (1H, d, J=8.5 Hz, H-5′), 7.37 (1H, dd, 1.5 Hz, J=8.5, H-6′), 7.38 (1H, m, H-2′). Sugar moiety; 3.46 (1H, m, H-3″), 3.49 (2H, m, H-4″), 3.50 (2H, m, H-5″), 3.75 (1H, m, H-6a″), 3.90 (1H, dd, J=12.0, 2.0 Hz, H-6b″), 4.19 (1H, t, J=9.0 Hz, H-2″), 4.91 (1H, d, J=9.0 Hz, H-1″). Moreover, ^{13}C-NMR (75 MHz, CD_3OD) δ: 95.47 (C-8), 104.20 (C-3), 105.50 (C-10), 109.46 (C-6), 114.44 (C-2′), 117.08 (C-5′), 120.62 (C-6′), 123.83 (C-1′), 147.34 (C-3′), 151.35 (C-4′), 158.99 (C-9), 162.34 (C-5), 165.16 (C-7), 166.55 (C-2), 184.30 (C-4). Sugar moiety; 63.18 (C-6″), 72.09 (C-4″), 72.87 (C-2″), 75.59 (C-1″), 80.42 (C-3″), 82.94 (C-5″).

2.5. Identification of Bioactive Compound (AO2)

White amorphous powder; ESI-MS [M]+ m/z 426 (Jash et al., 2013), for $C_{30}H_{50}O$; IR (NaCl) λmax 3350, 2946, 1455, 1380, 1265, 739 cm^{-1} and its melting point is 214°C (Gallo and Sarachine, 2009a); ^{1}H-NMR Spectral Data (200 MHz, $CDCl_3$): δ 0.70 (1H, m, H-5), 0.77 (1H, s, H-24), 0.80 (1H, s, H-28), 0.84 (1H, s, H-25), 0.93 (1H, m, H-1b), 0.94 (1H, m, H-15b), 0.95 (1H, s, H-27), 0.98 (1H, s, H 23),1.04 (1H, s, H-26), 1.11 (1H, m, H-12b), 1.18 (1H, m, H-22), 1.26 (1H, m, H-21), 1.30 (1H, m, H-11b), 1.31 (1H, m, H-9), 1.36 (1H, m, H-7), 1.40 (1H, m, H-6b), 1.42 (1H, m, H-18), 1.44 (1H, m, H-11a), 1.48 (1H, m, H-16), 1.57 (1H, m, H-6a), 1.60 (1H, m, H-15a), 1.61 (1H, m, H-2), 1.62 (1H, m, H-13), 1.64 (1H, m, H-1a), 1.68 (1H, m, H-12a), 1.69 (1H, s, H-30), 2.38 (1H, m, H-19), 3.19 (1H, dd, J = 10.1; 5.2 Hz, H-3), 4.57 (1H, br s, H-29b), 4.70 (1H, br s, H-29a). Moreover, ^{13}C-NMR (100 MHz, CD_3OD) δ: 38.7 (C-1), 27.5 (C-2), 79.0 (C-3), 38.9 (C-4), 55.3(C-5), 18.3(C-6), 34.3(C-7), 40.8(C-8), 50.5(C-9), 37.1(C-10), 21.0(C-11), 25.2(C-12), 38.1(C-13), 43.0(C-14), 27.4(C-15), 35.6(C-16), 42.8(C17), 48.0(C-18), 48.3(C-19), 151.0(C-20), 29.9(C-21), 40.0(C-22), 28.0(C-23), 15.4(C-24), 16.1(C-25), 16.0(C-26), 14.6(C-27), 18.0(C-28), 109.3(C-29), 19.3(C-30).

2.6. Anti-Proliferative Activity

2.6.1. Cell Culture

The lung cancer cell line 549 and MCF-7 breast cancer cell line has been kept in DMEM/F-12 medium which augmented with 5% fetal bovine serum (FBS), 2 mM L-glutamine, and 100 mg/mL streptomycin/penicillin. Moreover, BG-1 ovarian cancer was cultured in RPMI-1640 medium supplemented with 100 mg/mL streptomycin/penicillin, 10% FBS, and 2 mM L-glutamine, all the materials that mentioned above have been ordered from Invitrogen, Gibco, Milan, Italy. Then the cells were switched to medium without FBS the day before experiments and subsequently they treated in medium supplemented with less percentage of FBS, which was 2.5%.

2.6.2. Cell Proliferation Assay

The isolated compounds (AO1 and AO2) has been tested on the three cancer cell lines proliferation ability. The cell viability was evaluated by MTT [3-(4,5-dimethylthiazol-2-yl)-2,5-diphenyltetrazolium bromide] assay, the base of this assay depends on the conversion of the MTT [3-(4,5-dimethylthiazol-2-yl)-2,5-diphenyltetrazolium bromide] to MTT-formazan the special mitochondrial enzyme. In regular growth condition, the tumour cells were seeded in 96-well plates as a quadruplicate and grown until they reach 70% confluency. Subsequently, the gown cells were washed by a physiological buffer solution (PBS) twice once they had attached. After that, they attend to with decimally increasing in concentrations (1–100 μM) of each isolated compound and incubated under humidifying condition 5% CO_2, 37ºC for 48hrs in cell culture medium augmented with 2% FBS. Cancer cell viability was fixed by MTT assay according to the manufacture's protocol (Sigma-Aldrich, Milan-Italy). For each AO1 and AO2 dose exposure, the mean absorbance was determined as a % of the cells treated with plotted sample drug concentration and vehicle absorbance. The drug concentrations was represented by IC_{50} values, that reduced the mean absorbance at 570 nm to 50% of those in the control condition or untreated wells (Mosmann, 1983).

2.7. Antioxidant Activity (Total Antioxidant Power)

The suitable concentration of the isolated compound standards (1, 3, 5, 7 and 10 mg/mL), have been prepared by dissolving the powder of each AO1 and AO2 in distilled water. 0.35 mL of each aliquots were mixed with 3.5 mL of the Antioxidant assay reagent solutions including; (28 mM of sodium phosphate, 0.6 M of H_2SO_4, and 4 mM ammonium molybdate). The solution containing tubes were incubated at 95 ^{0}C for 1 hr and 30 mints as described in detail in (Gülçin et al., 2010, Büyükokuroğlu et al., 2001). Then, the heated tubes were cooled down to room temperature, then the absorbance of each sample was measured at 695 nm against the blank. Total antioxidant capacity was expressed as equivalents of ascorbic acid as descibed else were (Sun et al., 2011, Umamaheswari and Chatterjee, 2008).

2.8. Statistical Analysis

The IC_{50} for all the values in each experiment was determined by linear regression analysis through equation (y=(value)x+(value); where y is 50% inhibition, and X is the value of IC_{50} for each given y value). The data were shown as mean±SD; all the data on both types of antioxidant property tests are the average of three independent experiments. The data has been analysed statically by GrapghPad Prism software program.

3. RESULTS AND DISCUSSION

3.1. Phytochemical Investigation

Achellia oligocephala aerial parts have been collected on Halgurd Mountain in Kurdistan region of Iraq. The chlorophyll-free methanol extract of aerial parts have been partitioned between distilled water and ethyl acetate. Repeated normal coloum chromatography and MPLC of the residue on both reversed (C-18) and silica gel phases afforded two main bioactive compounds; (+) - Luteolin-6-C-glucoside (isoorientin) (AO1) and lupeol (AO2) (see figure 2), and structures were established on the basis of their melting point, IR, ESI-MS, ^{1}HNMR, ^{13}CNMR, 2DNMR data and comparison with literature data (Oliveira et al., 2013, Jash et al., 2013) (figures 5-12 in supplementary material). However, this is the first report of these constituents in traditionally used plant *A. oligocephala* DC.

The homogeneity of compound AO1, was proved by a single spot in TLC using R-C18 as adsorbent, TLC (MeOH/H_2O 65:35): R_f= 0.64. AO1 got it as a yellow powder, the ESI-MS spectrum (negative ion mode) showed the molecular ion peak [M]- at 447 *m/z* (Jash et al., 2013), suggesting the formula $C_{21}H_{20}O_{11}$. Moreover, In the ^{1}H-NMR spectrum, the singlet at δ 6.49 (1H, H-8) and the signal at δ 109.46 (quaternary carbon) were attributed to H-6 and C-6 of the 5,6,7- trisubstituted A-ring system of a flavonoid compounds. Moreover, (8H, 4 (OH) of flavone at position 5, 7, 3′, 4′ and 4 (OH) of sugar moiety at position 2″, 3″, 4″, 6″). Thus, the C-7 OH at 7.39 ppm shows cross peaks with carbons C-7 (165.2 ppm), C-8 (95.5 ppm) and C-6 (109.5 ppm), while the other OH group cannot be distinguished from the baseline due to rapid chemical exchange between hydroxyl groups and protic solvents especially in case if you have used MeOH-d as a solvent but Proton exchange rates in alcohol –OH groups can be reduced by dissolving in DMSO-d6 or by supercooling aqueous solutions or by using organic co-solvents. Kontogianni and co-workers investigated in detail correlations between hydrogen bonds and solvent effects of phenol –OH chemical shifts for numerous phenolic acids, flavonoids and oleuropein derivatives (Kontogianni et al., 2013). The C-5 OH resonance in DMSO-d6 is more deshielded in the presence of a C-2–C-3 double bond: luteolin, and apigenin, compared to those molecules without a C-2–C-3 double bond e.g., eriodictyol, and naringenin. This was attributed to the extensive conjugation of the C-2–C-3 double bond and the ring C with the OC-4 carbonyl group which results in a more polarizable CO bond and, thus, a stronger intramolecular hydrogen bond (Charisiadis et al., 2014). On the basis of the melting point, ESI-MS, ^{1}H-NMR,^{13}C-NMR and 2DNMR spectral data (figures 5-9 in supplementary material) and comparison with the literature data (Oliveira et al., 2013, Çalış et al., 2006), component AO1 was identified as luteolin-6-*C*-glycoside, as known as (isoorientin) (figure 2).

Compound 2 was obtained as a white amorphous powder. ESI showed the molecular ion peak [M]+ at *m/z* 426 (Jash et al., 2013),

corresponding to the $C_{30}H_{50}O$ as a molecular formula, [21H ($7CH_3$ group at position C23, C24, C25, C26, C27, C28, C30)], [22H ($11CH_2$ group at position C1, C2, C6, C7, C11, C12, C15, C16, C21, C22, C29)], [6H (6CH group at position C3, C5, C9, C13, C18, C19)], and IH (OH group at position 3). The ^{1}H-NMR spectrum indicated the presence of characteristic protons of seven methyl groups [δH 0.78, 0.81, 0.85, 0.97, 0.99, 1.05 and 1.70], all of them on quaternary carbons. The double doublet at δH 3.21 (1H, *dd*, *J* = 5.2 Hz and 10.1) in the spectrum of AO2 was typical for a triterpenoid compound with a 3-hydroxy substituent. The exocyclic double bond protons resonances were observed at δH 4.59 and 4.71 (1H each, br, singlets). Thus, the structure of compound AO2 was identified as lup-20(29)-en-3β-ol (Lupeol) was definitely confirmed by the close similarity of the melting point with (Gallo and Sarachine, 2009a); IR, ^{1}H-NMR and ^{13}C-NMR with the literature (Garcia et al., 2015, Jash et al., 2013, Adzu et al., 2015) (figures 10, 11 and 12 in supplementary material).

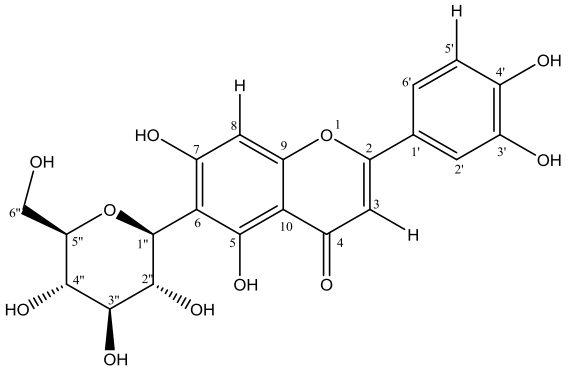

(AO1)

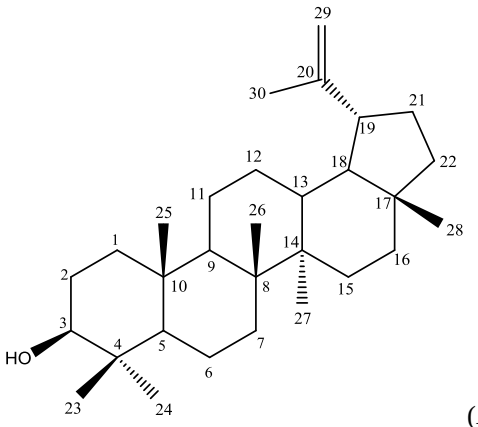

(AO1)

Figure 2: Isolated compounds from *Achellia oligocephala* DC.: (AO1) = - (+) - Luteolin-6-C-glucoside; (AO2) = lupeol.

To the best of our knowledge we determined, for the first time, the structures of two secondary metabolites from *A. oligocephala*: (+) - Luteolin-6-C-glucoside (isoorientin) and lupeol. Metabolites of those classes occur in nature in several families of plants. In addition to many other plants, according to the data reported previously, isoorientin and lupeol has been isolated from the other *Achillea* species; isoorientin isolated from *Achelia nobilis* (Marchart et al., 2003, Krenn et al., 2003). On the other hand, lupeol isolated from *Achillea tenuifolia* Lam (Moradkhani et al., 2014), and *Achillea santolina* (Al-Snafi, 2013). Interestingly, isoorientin is one of the two bioactive compounds isolated from *A. oligocephala,* it is the component of many natural plant extracts, and many other researchers have proved its anti-inflammatory, anti-cancer and antioxidant effects (Kim et al., 2018, Kim et al., 2016, An et al., 2015).

3.2. Biological Activity

3.2.1. Antiproliferative Activity (MTT assay) and Antioxidant Activity (Total Antioxidant Power)

The effects of AO1 and AO2 on the proliferation of three human tumour cell lines, SkBr3, MCF7 breast and ovarian BG-1 cancer cells were evaluated in comparison with the well-known antitumor drug cis-diamminedichloroplatinum (II) (cisplatin) by the MTT assay. AO1 showed a novel cytotoxic activity due to its inhibition activity significantly higher than cisplatin against MCF7 cell line (Table 1). In addition, AO1 compound is more activite than AO2 against SkBr3, MCF7 breast cancer cells, in which the IC_{50} of AO1 was 10 ± (3) , and 24 ± (1) respectively (Table 1).

Table 1: Antiproliferative activity (MTT assay) of AO1 and AO2 from *Achellia Oligocephala*.

	IC_{50}(μM) ± S.D		
Compounds	**MCF7**	**SkBr3**	**TG-1**
AO1	10 (±3)	24 (±1)	>50
AO2	23 (±3)	>50	>50
Cisplatin	17 (±2)	10 (±2)	12 (±3)

The antioxidant properties of the AO1 and AO2 were evaluated by total antioxidant capacity in vitro (TOAC) test compared to the reference ascorbic acid, according to the procedures described in the kind of literature

(Gülçin et al., 2010, Umamaheswari and Chatterjee, 2008). As shown in figures 3 and 4, both bioactive compounds (AO1 and AO2) have antioxidant power and the IC_{50} values against Ascorbic acid standard. Interestingly, the higher activity was exhibited by AO1 were: (AO1, IC_{50} 2.565± 0.001, AO2, IC_{50} 3.72± 0.001 and Ascorbic acid, IC_{50} 0.869± 0.001).

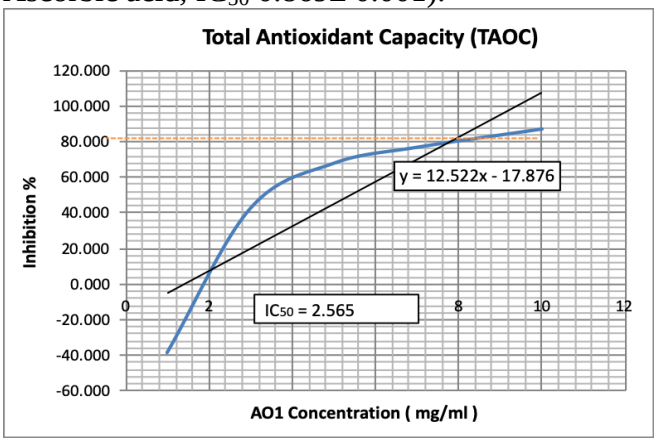

Figure 3: Total antioxidant capacity of AO1, IC_{50} value expressed in mg/mL.

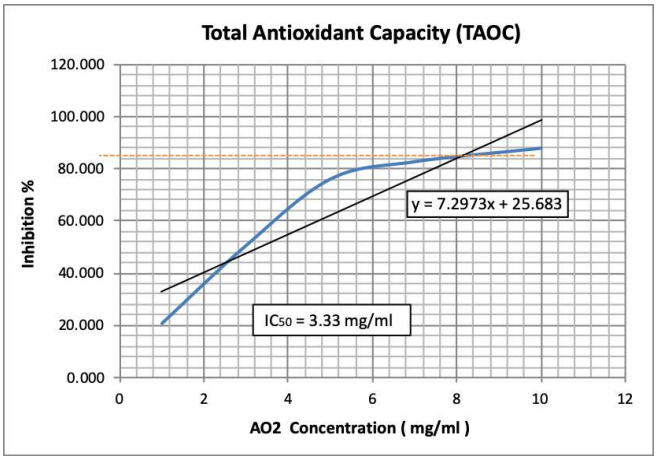

Figure 4: Total antioxidant capacity of AO2, IC_{50} value expressed in mg/mL.

It has been reported that isoorientin showed anti-inflammatory effects by treatment significantly reduces the expression of TNF-α and IL-1β in a concentration dependent manner. NF-$\kappa\beta$ is known to control the expression of cell survival genes, cytokines and proinflammatory markers. Moreover, isoorientin inhibited the LPS induced translocation of NF-$\kappa\beta$/p65 as evidenced by Western blotting (Anilkumar et al., 2017). In addition, Nam and co-workers have reported that isoorientin in KIOM-2015EW may contribute to its anti-inflammatory properties (Nam et al., 2017). According to the literature data, also lupeol was found to possess significant anti-inflammatory activity; Lupeol has been shown to exhibit various pharmacological activities under in vitro and in vivo conditions. These include its beneficial activity against inflammation, cancer, arthritis, diabetes, heart diseases, renal toxicity and hepatic toxicity (Saleem, 2009, Geetha and Varalakshmi, 2001, Agarwal and Rangari, 2003, Gallo and Sarachine, 2009b). Thus, the biological activities of the two isolated pure compounds (AO1 and AO2) corroborated the biological activities of this plant and validate the traditional use of *Achillea oligochephala* in Kurdistan.

1. CONCLUSIONS

This is the first scientific investigation study on the secondary metabolites of *Achellia oligocephala* DC., both from phytochemical and pharmacological points of view. The plant was collected in Kurdistan Region, where it is used as a herbal remedy, especially against wound healing and gastrointestinal complaints. Two bioactive compounds have been isolated from *A. oligocephala*: (+) - isiorientin for the first time from this plant. AO1 showed remarkable cytotoxic activity due to inhibition effects higher than cisplatin against MCF7 human tumour cell line. In addition, AO1 and AO2, showed significant total antioxidant activity compared to standard antioxidant. In conclusion, the current investigation confirms that AO1 can be considered as a potential natural chemotherapeutic agent. Moreover, the biological properties determined for the isolated compounds from aerial parts of *A. oligocephala*, have validated the traditional uses of this plant in Kurdistan.

Acknowledgements

Thanks to Prof. Abdul Hussain Al Khayyat for the botanical classification and identification.

Conflict of Interest (Nothing)

SUPPLEMENTARY MATERIALS:

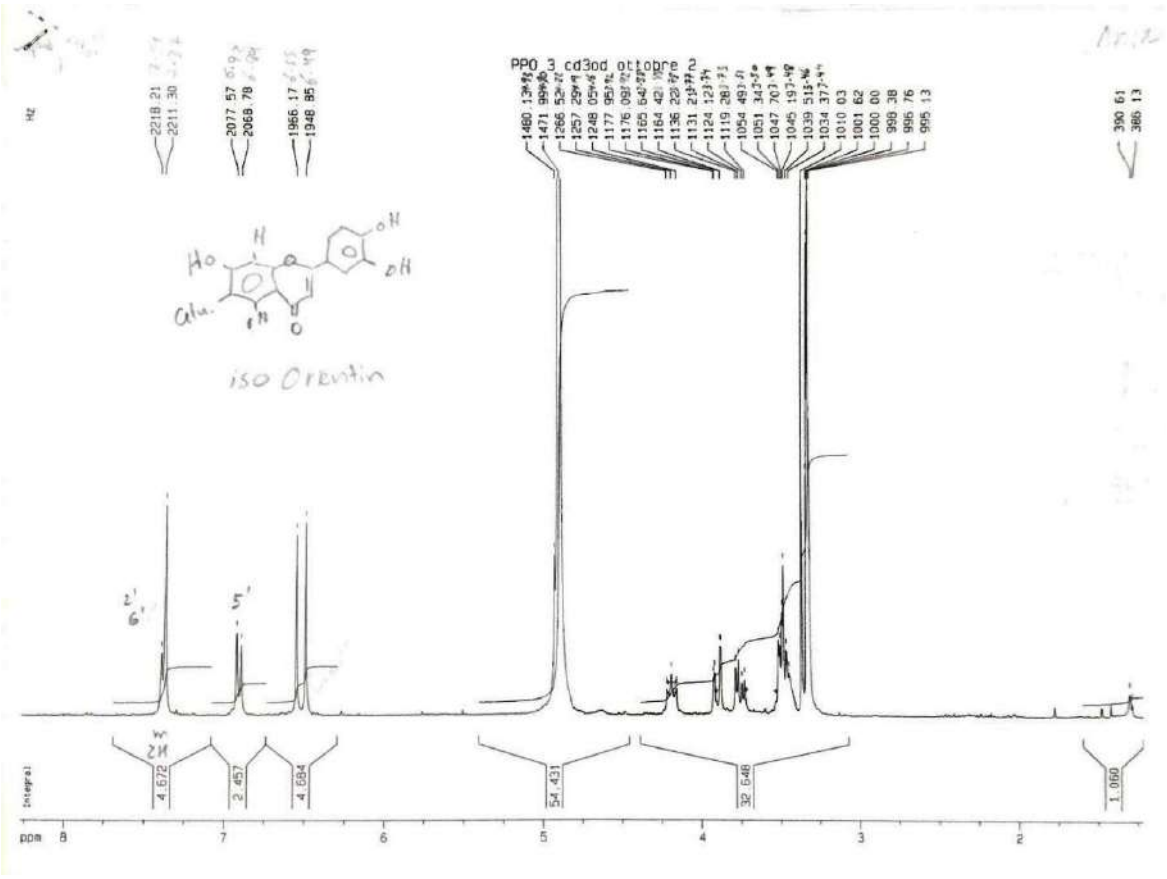

Figure 5: ^{1}H-NMR spectrum (300 MHz) of compound AO1 (in CD_3OD).

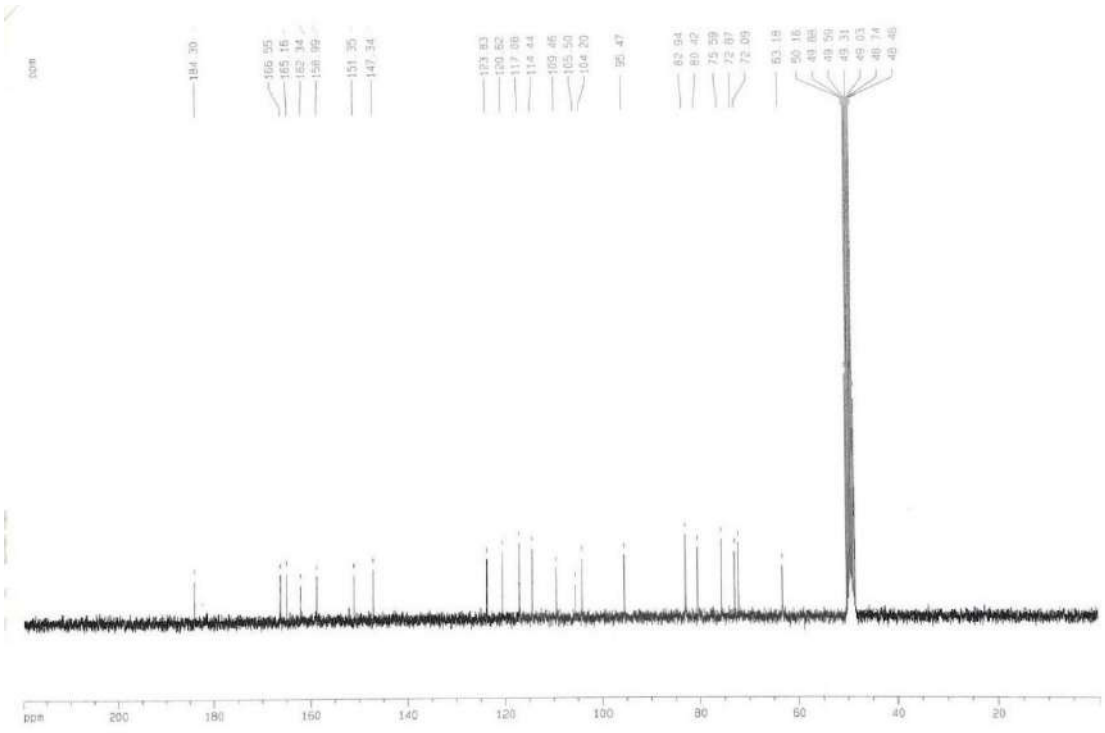

Figure 6: ^{13}C-NMR spectrum (75 MHz) of compound AO1 (in CD_3OD).

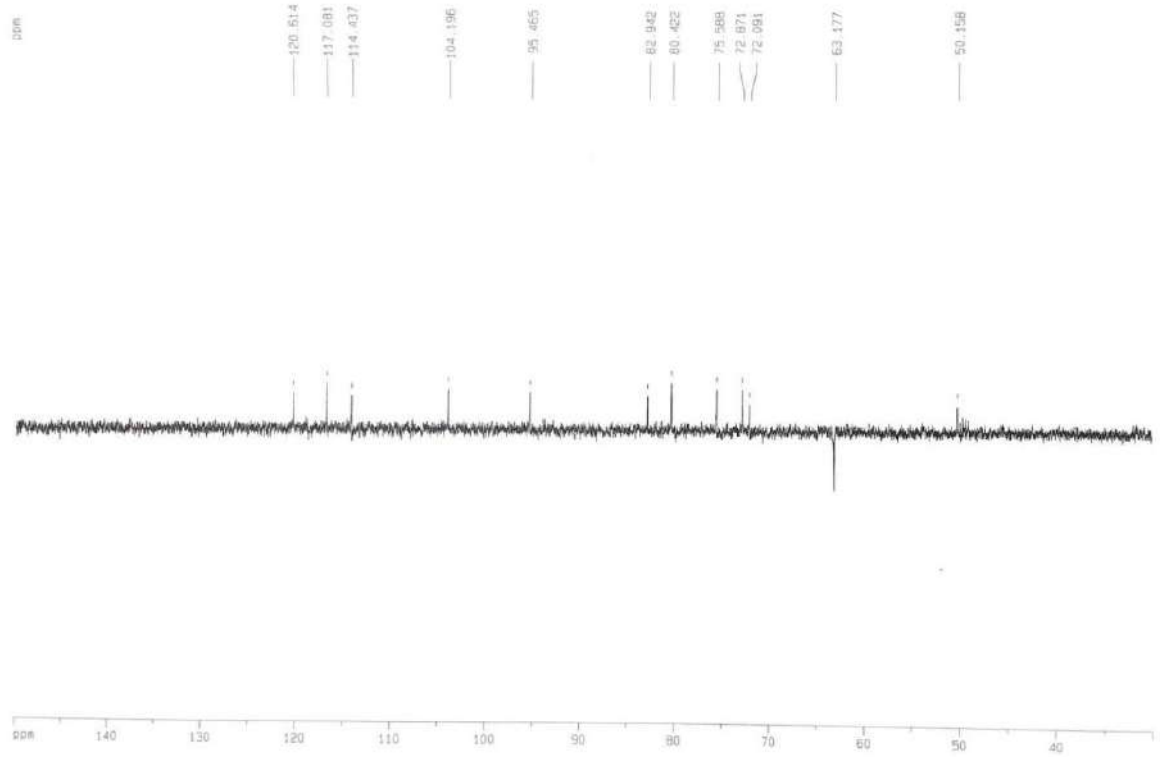

Figure 7: DEPT spectrum (75 MHz) of compound AO1 (in CD_3OD).

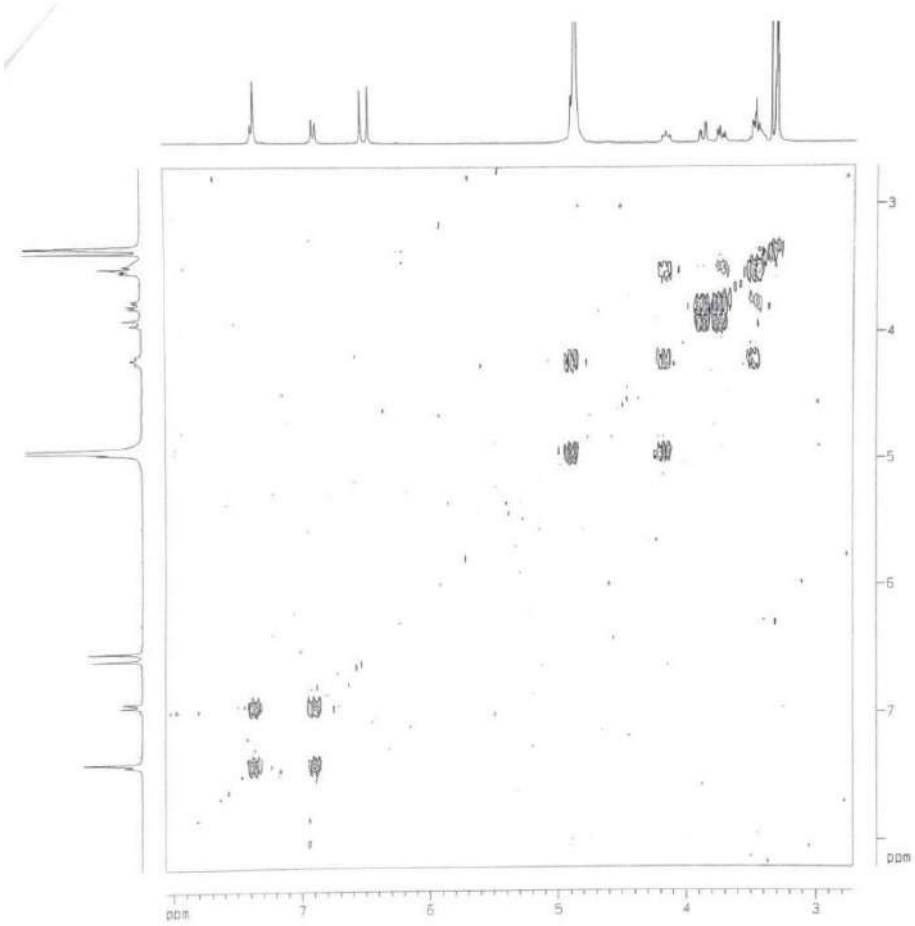

Figure 8: COSY spectrum (300 MHz) of compound AO1 (in CD_3OD).

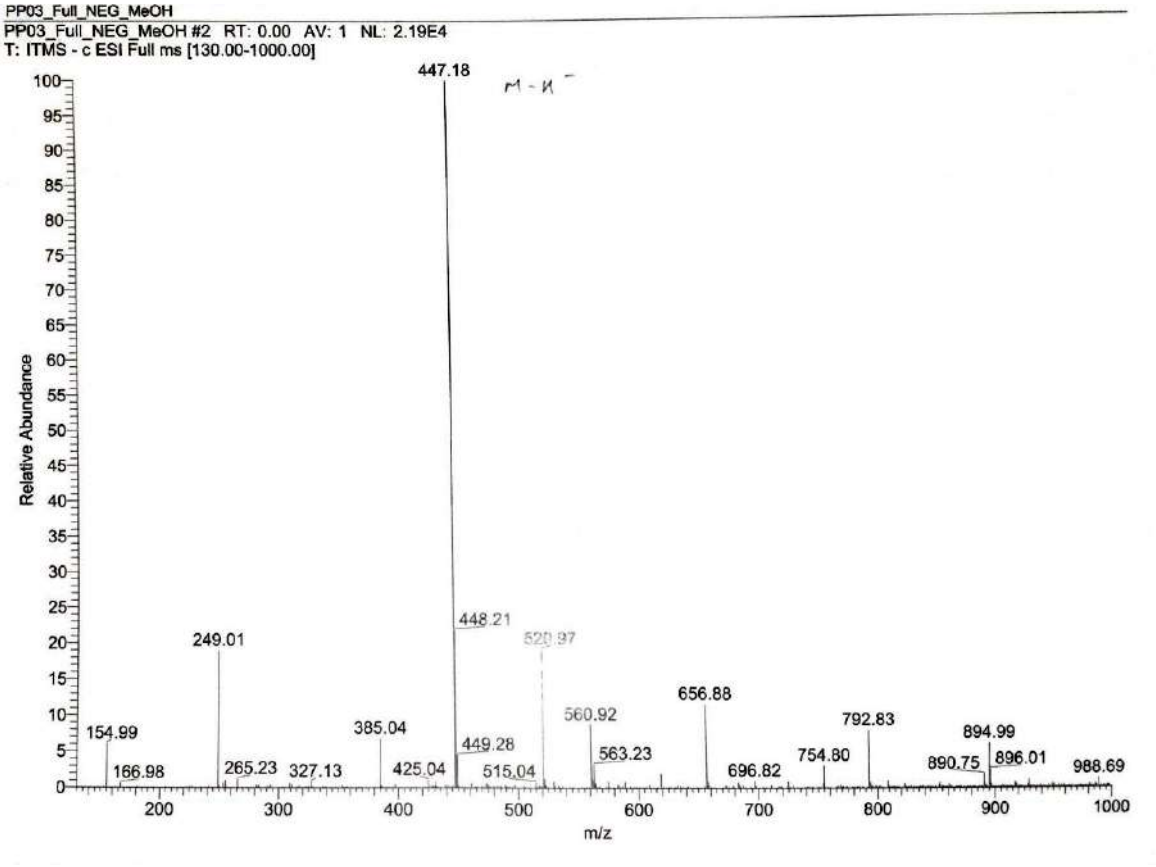

Figure 9: LC-ESI-MS spectrum of compound AO1 measured in negative ion mode.

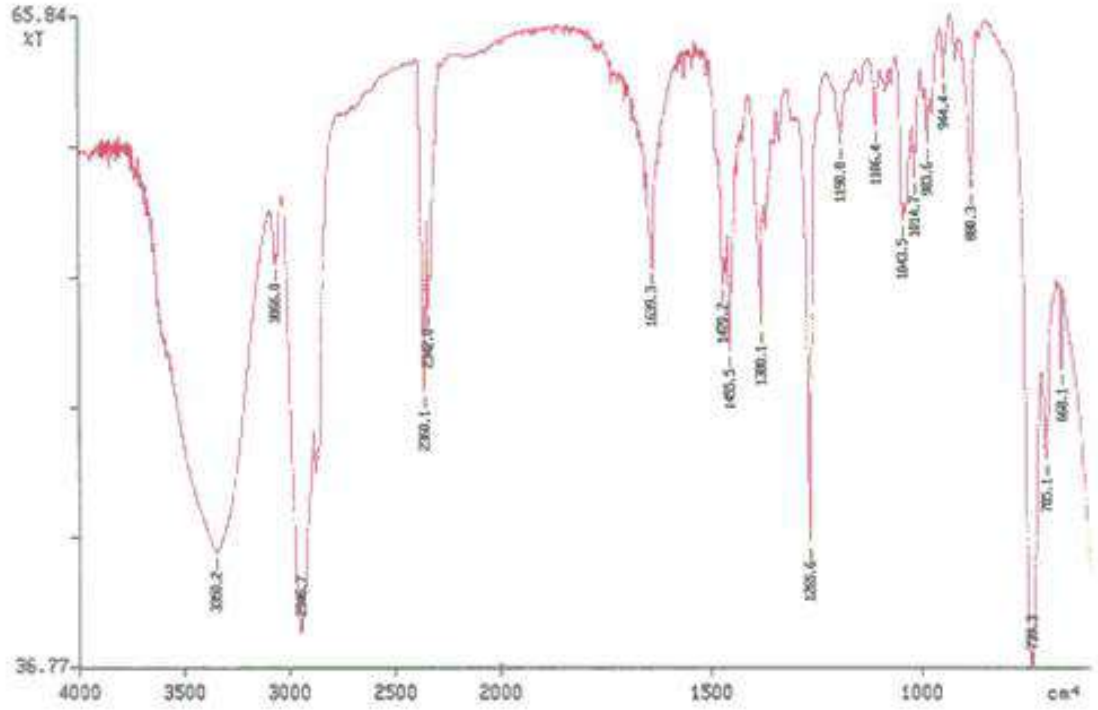

Figure 10: FT-IR spectrum of compound AO2.

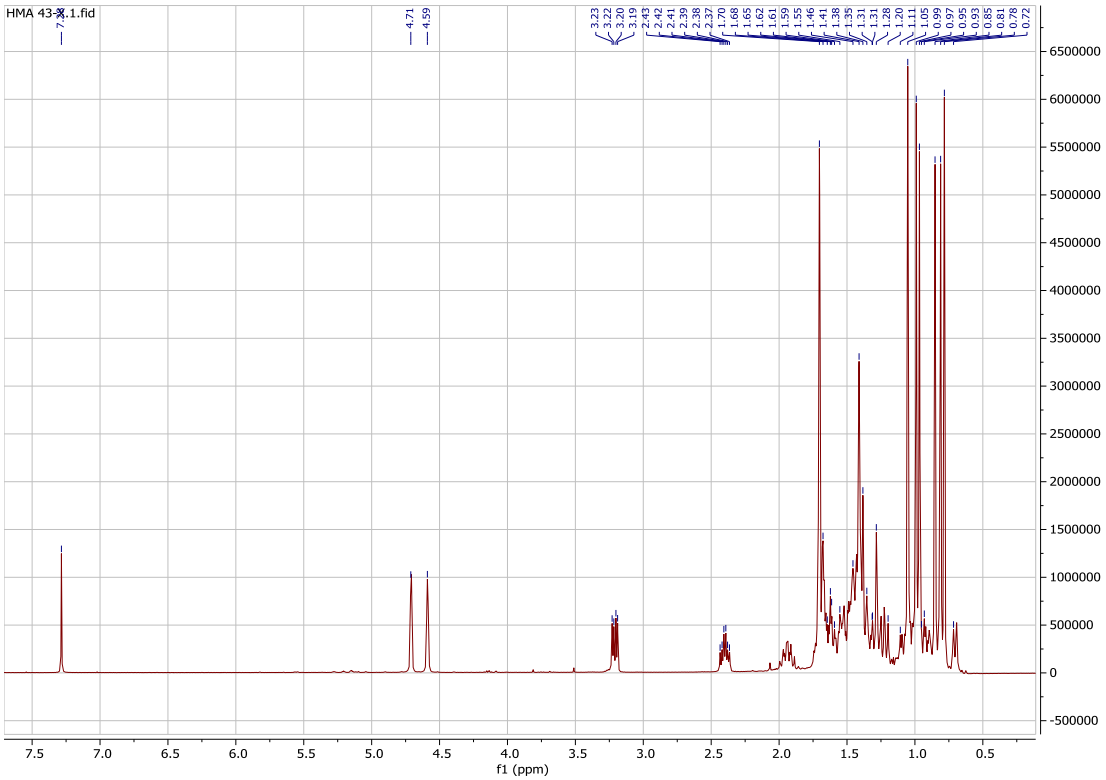

Figure 11: ^{1}H-NMR spectrum (400 MHz) of compound AO2 (in $CDCl_3$).

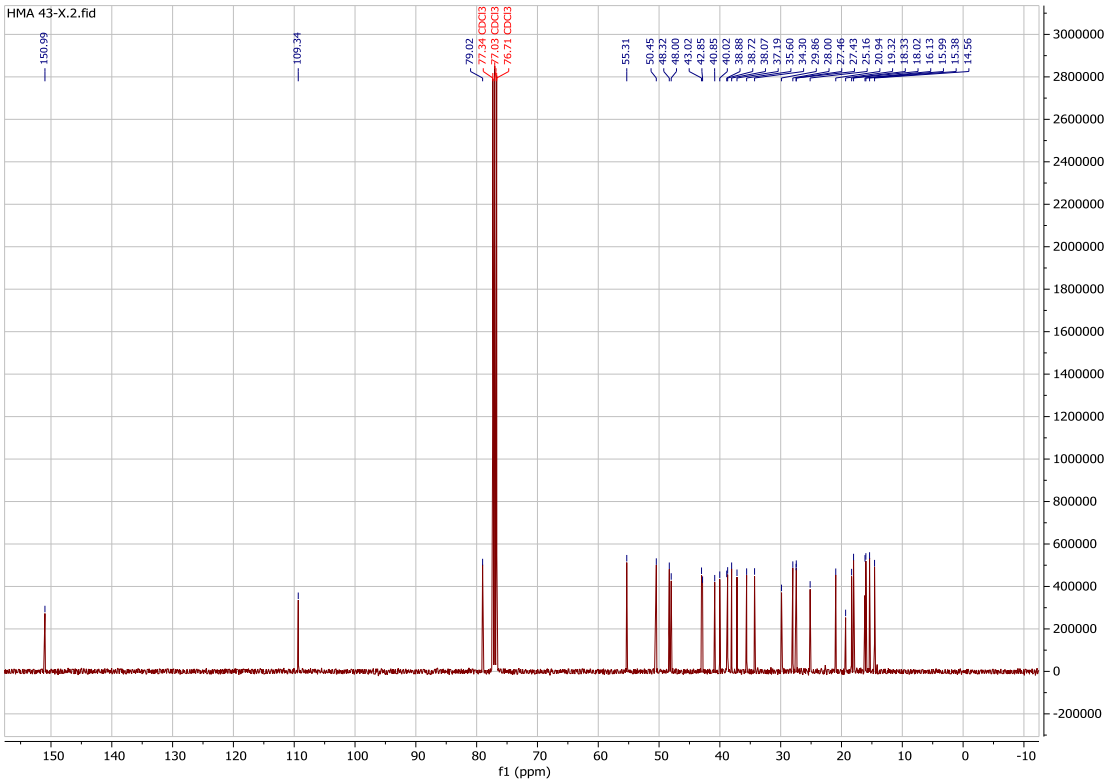

Figure 12: ^{13}C-NMR spectrum (100 MHz) of compound AO2 (in CD_3OD).

References

ADZU, B., CHINDO, B. A., TARFA, F. D., SALAWU, O. A. & IGOLI, O. J. 2015. Isolation and analgesic property of lupeol from *Diospyros mespiliformis* stem bark. *Journal of Medicinal Plants Research,* 9**,** 813-819.

AGARWAL, R. & RANGARI, V. 2003. Antiinflammatory and antiarthritic activities of lupeol and 19 alpha-H lupeol isolated from *Strobilanthus callosus* and *Strobilanthus ixiocephala* roots. *Indian Journal of Pharmacology,* 35**,** 384-387.

AL-SNAFI, A. E. 2013. Chemical constituents and pharmacological activities of Milfoil (*Achillea santolina*)-A Review. *International Journal of PharmTech Research,* 5**,** 1373-1377.

AMIN, H. I. M., IBRAHIM, M. F., HUSSAIN, F. H., SARDAR, A. S. & VIDARI, G. 2016. Phytochemistry and ethnopharmacology of some medicinal plants used in the Kurdistan region of Iraq. *Natural product communications Journal,* 11**,** 1934578X1601100306.

AMIN, H. I. M., HUSSAIN, F. H. S. & VIDARI, G. V. 2016. Characterization and quantification of some esters of fatty acids from *Iris persica* L. Bulbs by GC-MS analysis. *ZANCO Journal of Pure Applied Sciences,* 28**,** 32-36.

AN, F., WANG, S., TIAN, Q. & ZHU, D. 2015. Effects of orientin and vitexin from *Trollius chinensis* on the growth and apoptosis of esophageal cancer EC-109 cells. *Oncology Letters,* 10**,** 2627-2633.

ANILKUMAR, K., REDDY, G. V., AZAD, R., YARLA, N. S., DHARMAPURI, G., SRIVASTAVA, A., KAMAL, M. A. & PALLU, R. 2017. Evaluation of Anti-Inflammatory Properties of Isoorientin Isolated from Tubers of *Pueraria tuberosa*. *Oxidative Medicine Cellular Longevity,* 2017**,** 5498054.

BRAIEM, R. R., AMIN, H. I. M. & HUSSAIN, F. H. 2017. Free Radical Scavenging Activity of Methanolic Root Extract of *Iris postii* Mouterde, a Kurdish Herbal Remedy. *ZANCO Journal of Pure and Applied Sciences,* 29**,** 146-149.

BÜYÜKOKUROĞLU, M., GÜLÇIN, I., OKTAY, M. & KÜFREVIOĞLU, O. 2001. In vitro antioxidant properties of dantrolene sodium. *Pharmacological Research,* 44**,** 491-494.

ÇALıŞ, I., BIRINCIOĞLU, S. S., KıRMıZıBEKMEZ, H., PFEIFFER, B. & HEILMANN, J. 2006. Secondary metabolites from *Asphodelus aestivus*. *Zeitschrift für Naturforschung B,* 61**,** 1304-1310.

CHARISIADIS, P., KONTOGIANNI, V. G., TSIAFOULIS, C. G., TZAKOS, A. G., SISKOS, M. & GEROTHANASSIS, I. P. 2014. 1H-NMR as a structural and analytical tool of intra-and intermolecular hydrogen bonds of phenol-containing natural products and model compounds. *Molecules,* 19**,** 13643-13682.

GALLO, M. B. & SARACHINE, M. J. 2009a. Biological activities of lupeol. *International Journal of Biomedical and Pharmaciutical Science,* 3**,** 46-66.

GALLO, M. B. & SARACHINE, M. J. 2009b. Biological activities of lupeol. *International Journal of Biomedical and Pharmaciutical Science,* 3**,** 46-66.

GARCIA, G. R. M., HENNIG, L., SIELER, J. & BUSSMANN, R. W. 2015. Constituents of Corynaea crassa "*Peruvian Viagra*". *Revista Brasileira de Farmacognosia,* 25**,** 92-97.

GEETHA, T. & VARALAKSHMI, P. 2001. Anti-inflammatory activity of lupeol and lupeol linoleate in rats. *Journal of ethnopharmacology,* 76**,** 77-80.

GILARDONI, G., CHIRIBOGA, X., VITA FINZI, P. & VIDARI, G. 2015. New 3, 4-Secocycloartane and 3, 4-Secodammarane Triterpenes from the Ecuadorian Plant *Coussarea macrophylla*. *Chemistry and biodiversity Journal,* 12**,** 946-954.

GÜLÇIN, I., BURSAL, E., ŞEHITOĞLU, M. H., BILSEL, M. & GÖREN, A. C. 2010. Polyphenol contents and antioxidant activity of lyophilized aqueous extract of propolis from Erzurum, Turkey. *Food and Chemical Toxicology,* 48**,** 2227-2238.

JASH, S. K., GANGOPADHYAY, A., SARKAR, A. & GORAI, D. 2013. Phytochemical investigation of the hexane extract of stem bark of *Peltophorum pterocarpum* (DC.). *Der Pharma Chemica,* 5**,** 49-53.

KIM, A., IM, M., GU, M. J. & MA, J. Y. 2016. Ethanol extract of *Lophatheri Herba* exhibits anti-cancer activity in human cancer cells by suppression of metastatic and angiogenic potential. *Journal of Nutrients Scientific reports,* 6**,** 1-14.

KIM, Y.-H., OH, T. W., PARK, E., YIM, N.-H., PARK, K. I., CHO, W. K. & MA, J. Y. 2018. Anti-inflammatory and anti-apoptotic effects of *Acer palmatum* Thumb. extract, KIOM-2015EW, in a hyperosmolar-stress-induced In vitro dry eye model. *Nutrients,* 10**,** 282.

KONTOGIANNI, V. G., CHARISIADIS, P., PRIMIKYRI, A., PAPPAS, C. G., EXARCHOU, V., TZAKOS, A. G. & GEROTHANASSIS, I. P. J. M. 2013. Hydrogen bonding probes of phenol–OH groups. *Organic and biomolecular chemistry Journal,* 11**,** 1013-1025.

KRENN, L., MIRON, A., PEMP, E., PETR, U. & KOPP, B. 2003. Flavonoids from *Achillea nobilis* L. *Zeitschrift für Naturforschung C,* 58**,** 11-16.

KUMAZAWA, T., MINATOGAWA, T., MATSUBA, S., SATO, S. & ONODERA, J.-I. 2000. An effective synthesis of isoorientin: the regioselective synthesis of a 6-C-glucosylflavone. *Carbohydrate research Journal,* 329**,** 507-513.

MARCHART, E., HATTENBERGER, A., KRENN, L. & KOPP, B. 2003. Analysis of flavonoids in *Achillea nobilis* L. bv capillarv electrophoresis. *Scientia Pharmaceutica,* 71**,** 133-145.

MORADKHANI, S., KOBARFARD, F. & AYATOLLAHI, S. A. M. 2014. Phytochemical investigations on chemical constituents of *Achillea tenuifolia* Lam. *Iranian journal of pharmaceutical research,* 13**,** 1049.

MOSMANN, T. 1983. Rapid colorimetric assay for cellular growth and survival: application to proliferation and cytotoxicity assays. *Journal of immunological methods,* 65**,** 55-63.

MÜKEMRE, M., BEHÇET, L. & ÇAKıLCıOĞLU, U. 2015. Ethnobotanical study on medicinal plants in villages of Çatak (Van-Turkey). *Journal of ethnopharmacology,* 166**,** 361-374.

NAM, T. G., LIM, T.-G., LEE, B. H., LIM, S., KANG, H., EOM, S. H., YOO, M., JANG, H. W. & KIM, D.-O. 2017. Comparison of anti-inflammatory effects of flavonoid-rich common and tartary buckwheat sprout extracts in lipopolysaccharide-stimulated RAW 264.7 and peritoneal macrophages. *Oxidative medicine cellular longevity Journal,* 2017.

OLIVEIRA, D. M. D., SIQUEIRA, E. P., NUNES, Y. R. & COTA, B. B. 2013. Flavonoids from leaves of *Mauritia flexuosa*. *Revista Brasileira de Farmacognosia,* 23**,** 614-620.

ŞABANOĞLU, S., KHAZNEH, E., SALTAN, G., TEKIN, M., ERGENE, B. & ACIKARA, Ö. B. 2017. Secondary Metabolites of *Achillea sintenisii* HUB. MOR. *FABAD Journal of Pharmaceutical Sciences,* 42**,** 191-197.

SALEEM, M. 2009. Lupeol, a novel anti-inflammatory and anti-cancer dietary triterpene. *Cancer letters,* 285**,** 109-115.

SUN, L., ZHANG, J., LU, X., ZHANG, L. & ZHANG, Y. 2011. Evaluation to the antioxidant activity of total flavonoids extract from persimmon (*Diospyros kaki* L.) leaves. *Food and chemical toxicology,* 49**,** 2689-2696.

UMAMAHESWARI, M. & CHATTERJEE, T. 2008. In vitro antioxidant activities of the fractions of Coccinia grandis L. leaf extract. *African Journal of Traditional, Complementary Alternative Medicines,* 5**,** 61-73.

ZANCO Journal of Pure and Applied Sciences
The official scientific journal of Salahaddin University-Erbil
https://zancojournals.su.edu.krd/index.php/JPAS

ISSN (print):2218-0230**, ISSN (online):** 2412-3986**, DOI: http://dx.doi.org/10.21271/zjpas**

RESEARCH PAPER

Antinematicidal Potency of *Arum maculatum* L. (*Araceae*) to Control Macrocyclic Lactone Derivative-Resistant Gastrointestinal Roundworms in Ovine

Kareem Khoshnow Hamad*

*****Department of Biology, College of Science, Salahaddin University- Erbil, Kurdistan Region of Iraq

A B S T R A C T:

Antinematicidal resistance has been emerging between the gastrointestinal (GI) nematode populations in ovine to the popular broad-spectrum artificial drugs [say macrocyclic lactone (ML) derivatives] in most countries of the world including Kurdistan region of Iraq. Hence, the present study was designed to evaluate the efficacy of crude aqueous ethanol extract (CAEE) of native *Arum (A.) maculatum* L. (common name: snakehead) in eliminating ML derivative-resistant GI roundworms in ovine. The study was conducted on private sheep farms in Qushtapa district, Erbil governorate from October 2018 to March 2019. After confirmation of infestation with various GI nematodes (*Nematodirus* 37%, *Marshallagia* 42% and *Trichuris* 21%), the tentative animals were divided into six groups (n=15). One group was allotted for diagnosis of resistance against ML and one group for control. The faecal egg count reduction test (FECRT) has revealed the rampancy of resistance to the aforementioned antiparasitic. According to the RESO Computer Program, the calculated FECR% and lower confidence interval 95% were 69.83% and 48.4% respectively. For antiparasitic evaluation of the above phytomedicine, four groups (n=15) were exploited. The FECR% results post-therapy with 25, 50, 75, and 100 mg kg-^{1} BW of the *A. maculatum* CAEE were 21.13, 54.91, 73.28 and 96.27 respectively. According to these data and related references, the dose; 100 mg kg-^{1} BW was deemed effective, whilst other doses were ineffective. The ovicidal activity of the medicinal herb was also tested *in vitro* via executing egg hatch assay. The calculated LC_{50} value was 2.551µg ml^{-1} (range 2.454-2.647) after conduction of the assay. Having said, the same control group was employed because statistically, all the groups were belonged to the same population.

KEY WORDS: Medicinal herbs, antinematicidal resistance, ivermectin, alimentary tract nematodes, sheep
DOI: http://dx.doi.org/10.21271/ZJPAS.32.5.11
ZJPAS (2020) , 32(5);118-126 .

1. INTRODUCTION

Antinematicidal resistance (AR) has become an international phenomenon threatening sheep and goat resources since the last century (Kaplan and Vidyashankar, 2012; Karrow *et al.*, 2014; Kalkal *et al.*, 2019). Relatively, among the renowned broad-spectrum synthetic antinematicidals, macrocyclic lactone (ML) derivatives such as ivermectin is vulnerable to evolve resistance against it by the gastrointestinal (GI) nematodes of small ruminants, particularly in under-developed nations (Hamad, 2018).

It is noteworthy to mention that in some regions where small ruminants are being reared intensively, the resistance has reached a considerable level (Hamad, 2012) due to mutations (Beech and Silvestre, 2010). To overcome this dilemma, parasitologists and experts in the domain of livestock wellbeing have promoted some substitute policies such as pasture management, nutritional supplementations, biological control, immunization, and genetic approaches. Pragmatically, the aforementioned substitutions have not accomplished significant results in the field (Stear *et al.*, 2007) especially in under-developed states where livestock owners

* **Corresponding Author:**
Kareem Khoshnow Hamad
E-mail: kk_hamad@yahoo.com
Article History:
Received: 18/01/2020
Accepted: 03/05/2020
Published: 13/10 /2020

are not well-educated and unaware about the problem of AR (Hamad, 2014).

Alternatively, phytomedicines have been advocated in African, Asian, and South Latin American countries to be a sharp sward to control rampancy of antinematicidal-resistant GI roundworms of livestock (Jabbar *et al*., 2006). Having said, medicinal plant crude extracts comprise several active constituents which, in turn, preclude the emergence of AR by alimentary tract parasitic roundworms owing to targeting different dewormer receptors (Athanasiadou *et al*., 2007). In this regard, antinematicidal activity of *Arum* (*A.*) *maculatum* L. leaf extract, which has been mentioned in folk medicine (Adams *et al.*, 2011), was trialed *in vitro* and *in vivo* to assess its ovicidal and adulticidal efficacy utilizing reliable parasitological assays. Having said, this growing plant in spring season contains some agro-chemical secondary metabolites say cyanogenic glycosides, saponins, monoterpenes and alkaloids (Avato *et al.,* 2006).

2. Material and Methods

2.1. Allotment of experimental lambs

Animals (n=90) having 3-6 months age, which had not been deparasited for the last two months, were comprised in the research work. To choose tentative lambs, the five point check, lower eyelid paleness (anemia) assessed by FAMACHA (score 1-5) and bottle jaw (submandibular edema) were applied for haematophagous worm infestations, whilst for all GI nematode infections, back score condition (1-5) and coat condition were utilized. On the other hand, for scour worms, fecal soiling (dag score 0-5) was exploited. Moreover, determination of egg per gram of feces (EPG) was performed. The animals, selected for the trial, were marked and arbitrarily allotted into six groups:

Group 1: ML derivative (ivermectin) resistance detection group (n=15)

Group 2: *A. maculatum* dose (25 mg kg-^{1} BW) group (n=15)

Group 3: *A. maculatum* dose (50 mg kg-^{1} BW) group (n=15)

Group 4: *A. maculatum* dose (75 mg kg-^{1} BW) group (n=15)

Group 5: *A. maculatum* dose (100 mg kg-^{1} BW) group (n=15)

Group 6: infected non-treated group (n=15)

(Coles *et al.,* 1992; Macedo *et al.*, 2010)

The trialed lambs did not get any other remedy during the experiment period and routine clinical inspections were carried out as well (Kahn, 2005). The experimental animals were chosen from private sheep ranches in Qushtapa district, Erbil governorate, whilst the laboratory techniques were executed at the Department of Biology, College of Science, Salahaddin University-Erbil.

2.2. Preliminary assays to detect natural infestations with GI nematodes

●***Faecal examination***

Qualitative and quantitative parasitological tests were performed to determine natural infections with different alimentary tract parasitic roundworms and during conducting other steps of the study (Soulsby, 1982; Coles *et al*., 1992; Iqbal *et al*., 2006a).

●***Coprological method***

Coprocultures were also applied to detect the involvement of various digestive system helminths in whole natural worm infestations following MAAF (1986). Faecal samples of each group of tentative animals were pooled and cultured in plastic containers. Amphotericin B (5 µg g^{-1}) was added to prevent fungal contaminations. The cultures were incubated for seven days at 27±1ºC. After this time, the nematode larvae (L_3) were collected using Baermann apparatus.

●***Baermann technique***

This assay was performed to collect the parasite larvae (L_3) from the coproculture method. Approximately 15g of the incubated faeces were wrapped up in medical gauze and put in the Baermann apparatus funnel. Lukewarm water was added to stimulate larval motility to the end of collecting tube. The "Baermann" was left overnight and a small volume of water was collected and poured in a plastic container. Then the water sample transferred to a petridish, Lugol's iodine was added to the culture (Iqbal *et al*., 2006a) larvae were identified following MAAF (1986).

2.3. Studies on antinematicidal resistance

●***Fecal egg count reduction test (in vivo assay)***

Ivermectin 1% belongs to the macrocyclic lactone family and produced by Cherished Pharmac. (pvt) Ltd., was obtained from a reliable veterinary clinic. Lambs (n=15) in group 1 were injected

ivermectin subcutaneously at the regular dose (0.2 mg kg-^{1} BW); whilst group 6 served as infected non-dewormed control. Coproculture of animals (group 1 and control) were conducted at day 0 (pre-deworming) and day 14 (post-deworming) as pointed out formerly. Eggs per gram of faeces (EPG) were counted employing Whitlock Universal Egg Counting Slide (provided by JA Whitlock & Company, PO Box 51, EASTWOOD NSW 2122 AUSTRALIA). Post- therapy EPG and involvement of all parasitic roundworms in the natural infections were determined. EPG were computed by Whitlock slide using the formula below:

EPG= Total eggs in chamber 1, 2 and 3/3 x 50 (dilution factor)

Faecal egg count reduction percentage (FECR %) was estimated utilizing the following formula (Coles *et al.*, 1992):

FECR % = [1- (mean EPG treatment/mean EPG control)] x100

RESO computer program (CSIRO Animal Health Research Laboratory, Private Bag 1, Parkville, Vic. 3052, Australia) was exploited to calculate the arithmetic mean, variance of counts, FECR% and 95% confidence interval. According to Coles *et al*. (1992), resistance is rooted if (**i**) the FECR% is less than 95% (**ii**) the lower limit of 95% confidence interval is less than 90% (**iii**) If just one of the two norms is met, resistance is suspected. Moreover, Gill (1996) has suggested that any negative values obtained from FECR% and lower limit of confidence interval should be equal to zero, interpreting that the resistance is broadly prevalent and has reached the catastrophic level.

2. 4. Assessment of plant extract for using against resistant GI nematodes

●***Extraction* of *Arum maculatum* leaves**

Arum (A.) maculatum leaves were harvested naturally from South of Erbil governorate. Leaves were dried in shade at room temperature. After dryness, materials were powdered utilizing an electric grinding machine. The powder was solved in 70% aqueous ethanol by cold maceration at 25-30 Cº and the materials were mixed 2-3 times daily by a stirrer. After three days, the materials were filtrated through a portion of leaky textile and the filtrate was collected in a container. The aforementioned process was repeated thrice. The extract was evaporated to dryness at room temperature. The crude aqueous-ethanol extracts (CAEE) was kept at 4°C until used against the pathogenic nematodes (Gilani *et al*., 2004).

●***Fecal egg count reduction test (in vivo assay)***

The lambs in group 2, 3, 4 and 5 were drenched *A. maculatum* leaf CAEE at doses; 25, 50, 75 and 100 mg kg-^{1} BW respectively, whilst, group 6 utilized as control (infested untreated). Fecal examinations and coprocultures of the experimental lambs were conducted at day 0 (pre-therapy) and on day 14 (post-therapy) as mentioned previously. Post- therapy EPG and parasite infestations were recorded. FECR % was calculated using the undermentioned formula:

FECR% = [1-(mean EPG treatment/mean EPG control)] x100

●***Egg hatch assay (in vitro assay)***

This assay was performed to assess the inhibitory activity of various doses of the CAEE on egg hatching of the parasitic nematodes. The technique was done according to the protocol recommended by Coles *et al*. (1992) with slight changes by some parasitologists to be proper for evaluation of ethnobotanicals (Macedo *et al*., 2010). One gram of CAEE was dissolved in 10 ml of 70% acetone and this was reckoned as mother solution (100 mg ml^{-1}) which was serially diluted in a 24 multiwell plate. The egg samples were treated with 12 concentrations (100-0.048 mg ml^{-1}) of the extract. For positive control, 0.025 mg ml^{-1} of albendazole5% was dissolved in 0.3% Dimethylsulfoxide (DMSO). The well of negative control got just 1ml of 70% acetone. Plate was incubated at 27°C ±1 for 48 hours and 70% relative humidity. After incubation, two drops of Lugol's iodine was added.

At least 100 of the unhatched eggs (dead and embryonated) and hatched larvae were counted to calculate the hatching inhibition percentage. The subsequent formula was exploited to assess hatching inhibition (%):

Hatching inhibition (%) = P test/ P total x100

P test: number of unhatched or embryonated eggs.

P total: number of unhatched or embryonated eggs + Larvae (L_1).

LC_{50} values were calculated for the eggs by probit analysis.

2. 5. *Statistical analysis*

The RESO computer program was exploited to analyze the mean EPG for determination of resistance in treatment and control groups (14 days post-injection with ivermectin). The emergence of resistance was evaluated by this

program through calculating FECR% and lower limit of confidence interval 95%. For analysis of the data recovered from FECRT and assessment the influence of different doses of *A. maculatum* CAEE on reduction of EPG, one-way ANOVA was applied, followed by application of Tukey test for comparison between doses.

The data obtained from EHA for different concentrations of *A. maculatum* CAEE to evaluate their ovicidal efficacy against nematode eggs; one-way ANOVA was applied utilizing Graphpad Prism (version 7). Tukey as multiple comparison tests was used to compare among doses. All procured data were expressed as Mean±SE. For calculation of LC_{50} (µg ml^{-1}) at 95% confidence interval for preventing 50% of egg hatching, probit analysis of LC_{50} value on the EHA was applied.

3. Results

3.1. Contributing GI nematode species in infections

The larvae (L_3) of *Nematodirus* (37%), *Marshallagia* (42%) and *Trichuris* (21%) were identified following Soulsby (1982) and MAAF (1986) after execution of pre and post-deworming coproculture and Baermann technique (table 1).

3. 2. Trials on ivermectin resistance

●Faecal egg count reduction test

In accordance with the statistical analysis and RESO computer program, the post-treatment EPG mean, FECR% and lower confidence interval 95%, on day 14 post-deworming with ivermectin, were 22.47 (control mean EPG= 730.80), 69.83 and 48.4, respectively. The aforesaid data had verified that the resistance was emerged towards the previous synthetic dewormer.

3. 3. Antinematicidal influence of *A. maculatum* leaf CAEE against resistant GI nematodes

●Faecal egg count reduction test

Pre-treatment proportions (0 day) of nematode larvae (L_3), depending on the coprological assay, were displayed in table 2. The antinematicidal activity of *A. maculatum* leaf CAEE (four various dosages) against ivermectin-resistant worms in the experimental lambs naturally infested with GI nematodes in addition to comparison between influences of different doses of the plant extract on the egg reduction mean were analyzed statistically and exhibited in table 3 and 4. As evident from the data, obtained after performing the coprological assay (Table 3), group 5 was exposed to an efficacious dose (100 mg kg^{-1} BW) of *A. maculatum* leaf extract, so no parasite larvae (L_3) were recovered. On the other hand, the results of FECRT (Table 4) demonstrated the effectiveness of *A. maculatum* leaf extract in reducing faecal egg count (FECR% =96.27) in group 5 when exposed to100 mg kg^{-1} BW. Having said, other doses were not effective (FECR% <80). There was a significant difference ($P<0.05$) between all doses.

●Egg hatch assay

The analysis of variance (ANOVA) regarding the data collected from EHA in evaluating the ovicidal activity of different concentrations of *A. maculatum* leaf CAEE via hatching inhibition (%) calculation had revealed various impacts of different concentrations (dose-dependent ovicidal potency) (figure 1). The computed LC_{50} was 2.551 µg ml^{-1} (range 2.454-2,647) at the level of 95% confidence interval.

Table 1 Pre-deworming (0 day) and post-deworming (after 14 days) percentage of nematode larvae (L_3) in the tentative lambs selected for detection of resistance against ivermectin based on pooled faecal samples of groups 1 and 6 (control)

Groups	Pre-deworming L_3 (%) of nematodes		
	Nematodirus	*Marshallagia*	*Trichuris*
Group 1 (Ivermectin group)	46	37	17
Group 6 Control (untreated)	43	35	22
	Post-deworming L_3 (%) of nematodes		
Group 1			

(Ivermectin group)	43	33	24
Group 6			
Control (untreated)	41	38	21

Table 2 Pre-treatment proportions (0 day) of nematode larvae ($L_{3)}$ in the lambs chosen for evaluation of different doses of *Arum maculatum* CAEE based on pooled faecal specimens of groups 2, 3, 4, 5 and 6 (control)

Groups	*Nematodirus* %	*Marshallagia* %	*Trichuris* %
Group 2			
(25mg kg-^{1} BW)	44	36	20
Group 3			
(50 mg kg-^{1} BW)	42	33	25
Group 4			
(75 mg kg-^{1} BW)	48	34	18
Group 5			
(100 mg kg-^{1} BW)	45	32	23
Group 6			
Control (untreated)	44	37	19

Table 3 Post-treatment proportions (on day 14) of nematode larvae ($L_{3)}$ in the lambs chosen for evaluation of different doses of *arum maculatum* CAEE based on pooled faecal specimens of groups 2, 3, 4, 5 and 6 (control)

Groups	*Nematodirus* %	*Marshallagia* %	*Trichuris* %
Group 2			
(25mg kg-^{1} BW)	47	34	19
Group 3			
(50 mg kg-^{1} BW)	44	33	23
Group 4			
(75 mg kg-^{1} BW)	49	30	21
Group 5			
(100 mg kg-^{1} BW)	not recovered	not recovered	not recovered
Group 6 (control)	45	38	17

Table 4 Mean egg per gram of faeces and percentages of faecal egg count reduction in lambs on day 14 post-treatment with different doses of *Arum maculatum* CAEE

Groups	Mean EPG±SE	Mean FECR%
Group 2 (25 mg kg-^{1} BW)	647.8±15.11**C**	21.13
Group 3 (50 mg kg-^{1} BW)	370.3±12.42 **BC**	54.91
Group 4 (75 mg kg-^{1} BW)	219.4±7.34 **AB**	73.28
Group 5 (100 mg kg-^{1} BW)	36.6 ± 3.38 **A**	96.27
Group 6 (control)	821.4±71.99 **D**	-

Means sharing similar letters are statistically non-significant (P>0.05)

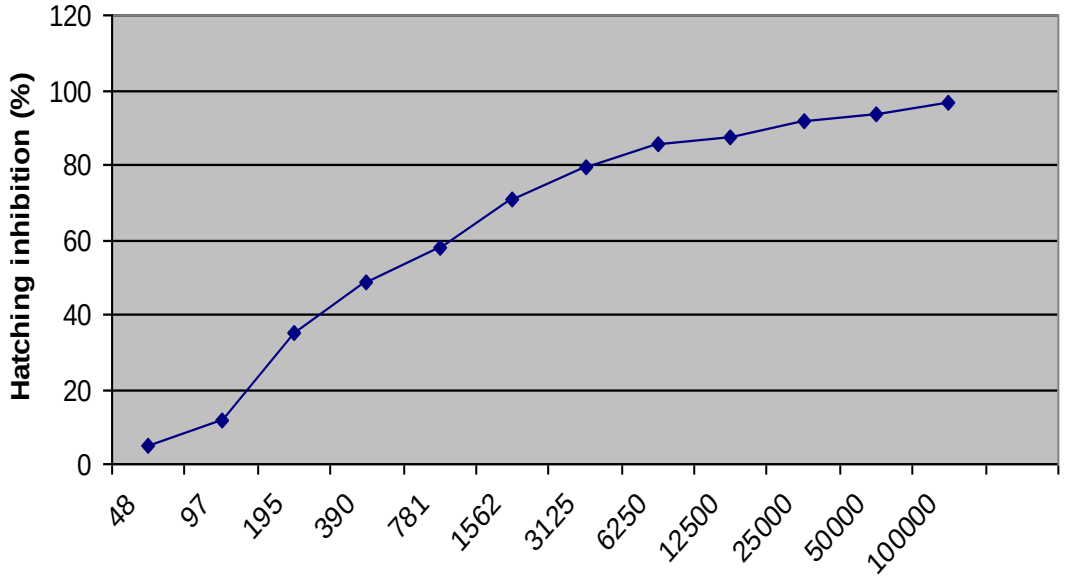

Figure 1 Correlation between the effects of various concentrations of *Arum maculatum* leaf extract and hatching inhibition (%)

4. Discussion

Definitely, recurrent annual use of ML derivative members has conduced to evolution and spread of AR between GI nematodes of sheep and goats every where (Waller, 2006; Hamad *et al*., 2017; Hamad *et al*., 2018). This dilemma has also become a menace to human beings (Beach and Silvestre, 2010). Certainly, GI nematodes of ovine and caprine have developed resistance dangerously against ML derivative members particularly in under-developed nations (Kaplan, 2004; Vercruysse *et al*., 2011). Therefore, this study, conducted in our region, had paid attention to the rampancy of resistance to ivermectin among GI nematode populations in naturally infected sheep using RESO computer program. The computed FECR% was (69.83), whilst the lower confidence interval was (48.4) which justify the emergence of resistance (Coles *et al*., 1992). It can be concluded that the resistance percentage between the GI nematode individuals of ovine in the study area was more than 25% and the worms were resistant to ivermectin. It is apparent that the AR could not be determined by these traditional

approaches if the resistance percentage is less than 25% between the GI nematodes (Martin *et al*., 1989).

The small ruminant owners are adapted to deparasite their livestock 2-3 times with ML derivative members yearly in the study zone (Veterinarian file in the research site). In this connection, Barnes *et al*. (1995); Waller *et al.* (1995); Kalkal *et al.* (2019) have stated that repeated annual use of an anthelmintic are closely related to the emergence and rampancy of resistance between alimentary tract roundworms. The study of Blackhall *et al.* (1998) has revealed that one allele of the putative ά-subunit gene is related to resistance against the dewormer. Nevertheless, Gill and Lacey (1998) have proposed that the mechanism of resistance to ivermectin might be unlike between various genera of parasitic nematodes. Having said, some investigators have also incriminated injecting low doses of the dewormer by shepherds, bad quality of the drug and storage conditions in under-developed countries as major predisposing factors enhancing emergence of resistance (Coles *et al*., 1995).

In contrast, absence of dependable commercialized substitutes to allopathic drugs at the present time, agrochemicals could be apposite alternatives to control GI nematodes in small ruminants particularly in sub-developed nations (Jabbar *et al*., 2006; Sindhu *et al*., 2014). Having said, medicinal plants contain many secondary metabolites which possess antinematicidal activity and their efficacy has been validated and documented in tropical and sub-tropical regions where nematodiasis is common (Hamad *et al.*, 2018). In continuation of the rare studies on phytomedicines, ivermectin-resistant GI nematodes were exposed to the native medicinal herb; *A. maculatum* leaf CAEE using *in vivo* and *in vitro* approaches. Obviously, several bioactive agrochemical substances have been extracted from *A. maculatum* leaves such as glycosides, flavonoids, alkaloids, fatty acids, and essential oils (Rahuman *et al*., 2008; Hussain *et al*., 2014). It is noteworthy mentioning that the efficacy of *A. maculatum* leaf CAEE has not been elaborated *in vitro* and *in vivo* against antinematicidal-resistant GI nematodes of small ruminants elsewhere, thus, it could be mentioned that this research work is a novel study in this domain. The FECR% results post-therapy with 25, 50, 75, and 100 mg kg-^{1} BW of the plant CAEE were 21.13, 54.91, 73.28 and 96.27 respectively. In this concern, it could be point out to the recommendations of W.A.A.V.P (second edition) edited by Wood *et al*. (1995) suggesting that any antiparasitic drug with FECR% (98) is counted highly effective; FECR% (80) and above is effective; whilst FECR% less than (80) is not encouraged to use in fighting pathogenic worms. Consequently, the dose; 100 mg kg-^{1} BW of the extract is effective (FECR% was 96.27). The study had also revealed that the highest doses were more efficacious as compared to the lowest doses. This therapeutic activity of ethnobotanicals was confirmed by several workers in the domain of herbology (Iqbal *et al*., 2006b; Hamad *et al*., 2013; Hamad, 2018; Ahmed *et al*., 2019).

5. Conclusions

Pursuant to the outcome of this research work, it may be concluded that the resistance proportion is above 25% between GI nematode individuals to ivermectin in ovine in Qushtapa district, Hawler governorate, where the study carried out. The likely cause beyond the rampancy of ivermectin resistance in the study zone is recurrent annual employment of ML derivatives. On the other hand, the highly effective dose of *A. maculatum* CAEE was 100 mg kg-^{1} BW which led to reduce mean EPG with percentage 96.27. This dose could be used in deparasiting sheep harboring ivermectin-resistant GI nematodes. Moreover, the EHA has demonstrated that the CAEE of *A. maculatum* can preclude egg hatching but not embryonations.

Acknowledgements

A lot of thanks go to the local veterinarian at Qushtapa district for the facilities he offered through connection with local farmers to conduct this study. The author appreciates the cooperation of sheep raisers in the study site.

Conflict of interest

The author attests that there is no conflict of interest regarding contents of the current research article.

6. References

Adams, M., Alther, W., Kessler, M. and Hamburger, M., 2011. Malaria in the Renaissance: remedies from European herbals from the 16th and 17th century. Journal of Ethnopharmacology, 133: 278-288.

Ahmed, C.N., Hamad, K.K. and Qadir, F.A., 2019. *Haemonchus contortus* as a model in assessing activity of *Citrullus colocynthis* fruit extract to control benzimidazole-resistant parasitic

nematodes. *ZANCO Journal for Pure and Applied Science*, (in press).

Avato, P., Bucci, R., Tava, A., Vitali, C., Rosato, A. and Bialy, Z., 2006. Antimicrobial activity of saponins from *Medicago sp.* Structure-activity relationship. Phytotherapy Resources, 20:454-457.

Barnes, E.H., Dobson, R.J. and Barger, I.A., 1995. Worm control and anthelmintic resistance: adventures with a model. *Parasitology Today*, 11: 56-63.

Beech, R.N. and Silvestre, A., 2010. Mutations associated with anthelmintic drug resistance. *Anti-infective agents in Medical Chem*istry, 9: 105-112.

Blackhall, W.J., Liu, H.Y., Xu, M., Prichard, R.K. and Beech, R.N., 1998. Selection at a P-glycoprotein gene in ivermectin-and moxidectin-selected strains of *Haemonchus contortus*. *Molecular and Biochemical Parasitology*, 95: 193-201.

Coles, G.C., Bauer, C., Borgsteede, F.H.M., Greets, S., Klei, T.R., Taylor, M.A. and Waller, P.J., 1992. World Association for the Advancement of Veterinary Parasitology (W.A.A.V.P.) methods for the detection of anthelmintic resistance in nematodes of veterinary importance. *Veterinary Parasitology*, 44: 35-44.

Coles, G.C., Papadopoulos, E. and Himonas, C.A., 1995. Tubulin, resistance and worms. *Parasitology Today*, 11: 183-185.

Gilani, A.H., Ghayur, M.N., Saify, Z.S., Ahmad, S.P., Choudary, M.I. and Khalid, A., 2004. Presence of cholinomimetic and acetylcholinesterase inhibitory constituents in betel nut. *Life Science*, 75: 2377-2389.

Gill, B.S., 1996. Anthelmintic resistance in India. *Veterinary Parasitology*, 63: 173-176.

Gill, J.H. and E. Lacey, 1998. Avermectin/milbemycins resistance in trichostrongyloid nematodes. *International Journal of Parasitology*, 28: 863-877.

Hamad, K.K., 2014. Combined strategies to control antinematicidal-resistant gastrointestinal nematodes in small ruminants on organized farms in Pakistan. *Pakistan Journal of Agricultural Science*, 51: 241-249.

Hamad, K.K., 2018. Assessment of *Azadirachta indica* seed kernel extracts to restrict the rampancy of antinematicidal-resistant *Haemonchus contortus* in ovine. *ZANCO Journal for Pure and Applied Science*, 30: 29-43.

Hamad, K.K., Iqbal, Z., Sindhu, Z.U.D. and Muhammad, G., 2013. Antinematicidal Activity of *Nicotiana tabacum* L. Leaf Extracts to Control Benzimidazole- Resistant *Haemonchus contortus* in Sheep. *Pakistan Veterinary Journal*, 33: 85-90.

Hamad, K.K., Qadir, F.A. and Hamad, H.O., 2017. Control of antinematicidal-resistant gastrointestinal nematodes in tamed small ruminants: achievements, trends and prospectives. *ZANCO Journal for Pure and Applied Science*, 29: 62-77.

Hamad, K.K., Ahmed, S.T., Ahmed, R.K. and Koyee, Q.M., 2018. Phytotherapeutics: As anticipating substitutes to synthetic drugs in combating antinematicidal-resistant gastrointestinal nematodes of small ruminants. *ZANCO Journal for Pure and Applied Science*, 30:102-114.

Hussain, A.I., Rathore, H.A., Sattar, M.Z.A., Chatha, S.A.S., Sarker, S.D. and Gilani, A.H., 2014. *Citrullus colocynthis* (L.) Schard (bitter apple fruit): A review of its phytochemistry, pharmacology, traditional uses and nutritional potential. *Journal of Ethnopharmacology*, 155: 54-66.

Iqbal, Z., Lateef, M., Jabbar, A., Ghayur, M.N. and Gilani, A.H., 2006b. *In vivo* anthelmintic activity of *Butea monosperma* against trichostrongylid nematodes in sheep. *Fitoterapia*, 77: 137-140.

Iqbal, Z., Sajid, M.S., Jabbar, A., Rao, Z.A. and Khan, M.N., 2006a. Techniques in Parasitology. Higher Education Commission, Islamabad, Pakistan, pp 198.

Jabbar, A., Iqbal, Z., Kerboeuf, D., Muhammad, G., Khan, M.N. and Afaq, M., 2006. Anthelmintic resistance: The state of play revisited. *Life Science*, 79: 2413-2431.

Kahn, C.M., 2005. The Merck Veterinary Manual, 9th Ed., Merck & Co., INC. Whitehouse Station, NJ., U.S.A., pp 2712.

Kalkal, H., Vohra, S., Singh, S., Gupta, S., Magotra, A. and Bangar, Y.C., 2019. Detection of moderate to severe anthelmintic resistance against fenbendazole in sheep and goat breeding farms, Hisar. *The Pharma Innovation Journal*, 8, 434-436.

Kaplan, R.M., 2004. Drug resistance in nematodes of veterinary importance: a status report. *Trends in Parasitology*, 20: 477-481.

Kaplan, R.M. and Vidyashankar, A.N., 2012. An inconvenient truth: global worming and anthelmintic resistance. *Veterinary Parasitology*, 186:70-76.

Karrow, N.A., Goliboski, K., Stonos, N., Schenkel, F. and Peregrine, A., 2014. Review: Genetics of helminth resistance in sheep. *Canadian Journal of Animal Science*, 94:1-9.

MAAF, 1986. *Manual of Veterinary Parasitological Laboratory Techniques*. *Tech. Bull.*, No.18. Ministry of Agriculture Fisheries and Food. Her Majesty's Stationary Office, London, UK.

Macedo, I.T.F., Bevilaqua, C.M.L., de Oliveira, L.M.B., Camurça-Vasconcelos, A.L.F., Viera, L. da S., Oliveira, F.R., Queiroz-Junior, E.M., Tome, A. da R. and Nascimento, N.R.F., 2010. Anthelmintic effect of *Eucalyptus staigeriana* essential oil against goat gastrointestinal nematodes. *Veterinary Parasitology*, 173: 93-98.

Martin, P.J., Anderson, N. and Jarrett, R.G., 1989. Detecting benzimidazole resistance with faecal egg count reduction tests and *in vivo* assays. *Australian Veterinary Journal*, 66: 236-240.

Rahuman, A.A., Venkatesan, P. and Gopalakrishnan, G., 2008. Mosquito larvicidal activity of oleic and linoleic acids isolated from *Citrullus colocynthis* (Linn.) Schard. *Parasitology Research*, 103: 1383-1390.

Sindhu, Z.U.D., Iqbal, Z., Ahmad, A. and Abbas, R.Z., 2014. *In vitro* Ovicidal and Wormicidal Activity of Six Medicinal Plants against *Haemonchus*

contortus. *International Journal of Agriculture and Biology*, 16: 1199-1203.

Soulsby, E.J.L., 1982. Helminths, Arthropods and Protozoa of Domasticated Animals.7th Ed., Bailliere Tindall, London, UK, pp. 248-250, 766-770.

Stear, M.J., Doligalska, M. and Donskov-Schmelter, K., 2007. Alternatives to anthelmintics for the control of nematodes in livestock. *Parasitology*, 134: 139-151.

Vercruysse, J., Albonico, M., Behnke, J.M., Kotze, A.C., Prichard, R.K., McCarthy, J.S., Montresor, A. and Levecke, B., 2011. Is anthelmintic resistance a concern for the control of human soil-transmitted helminths? *International Journal of Parasitology: Drugs and Drug Resistance*, 1: 14-27.

Waller, P.J., 2006. From discovery to development: Current industry prospectives for the development of novel methods of helminth control in livestock. *Veterinary Parasitology*, 139: 1-14.

Waller, P.J., Dash, K.M., Barger, A., Le Jambre, L.F. and Plant, J., 1995. Anthelmintic resistance in nematode parasites of sheep: learning from the Australian experience. *Veterinary Record*, 136: 411-413.

ZANCO Journal of Pure and Applied Sciences
The official scientific journal of Salahaddin University-Erbil
https://zancojournals.su.edu.krd/index.php/JPAS

ISSN (print):2218-0230**, ISSN (online):** 2412-3986**, DOI: http://dx.doi.org/10.21271/zjpas**

RESEARCH PAPER

Association of H. pylori infection indicated by their serum IgG antibodies with lymphoma malignancy

Zeki Ali Mohamed

MBchB, MRCP, FIBMS, consultant clinical hematologist, Director of hematology- oncology center.

Azadi teaching hospital.

Department of internal medicine, college of medicine,University of Duhok

A B S T R A C T:

Lymphoma is a type of lymphocyte malignancy that develops in different types of lymphoid tissues, many pathogens are expected to be implicated in the establishment of the disease including *Helicobacter pylori* (*H. pylori*). A total of 64 B-cells lymphoma patients recruited to oncology-hematology unit in Azadi Teaching Hospital in Duhok city and 60 sex and age matched apparently healthy individuals were involved in the current study. Serum samples were collected from all subjects and tested for detecting IgG antibodies against *H. pylori* as an indicator for *H. pylori* infections. The age average was (52.5±12.4) years for lymphoma cases and (56±12.5) years for controls. IgG anti-*H. pylori* antibodies were found in 11/64 (17.9%) of the lymphoma patients and in 8/60 (13.3%) of the control subjects. Lymphoma cases younger than 80 years had higher prevalence of IgG anti *H. pylori* antibodies (28.6%) as compared with all other age categories with a significant increase compared to both age groups <40 years (p= 0.008), 51-60 years (p=0.04) and 61-70 years (p=0.02) respectively. No significant difference was found in the IgG anti *H. pylori* antibodies prevalence between the lymphoma and control subjects (p=0.087), the gender had no significant effect on the IgG anti *H. pylori* antibodies prevalence in both of the lymphoma and control subjects respectively and between the two groups. Based on OR=1.34 (95% CI= 0.49-3.42) a very weak association of IgG anti *H. pylori* antibodies prevalence was observed with an overall increased risk of lymphoma. In conclusion, a week association of *H. pylori* infection with lymphoma was found due to non categorization of the lymphoma cases pathologically, the association might increases significantly if being categorized pathologically.

KEY WORDS: Lymphoma, Helicobacter pylori, MALT malignancy, H. pylori antibodies
DOI: http://dx.doi.org/10.21271/ZJPAS.32.5.12
ZJPAS (2020) , 32(5);127-133 .

1. INTRODUCTION

Lymphoma malignancy includes a large group of malignancies that usually develop from the lymph nodes (Kuppers 2009). The lymphocytes in the lymph nodes, undergo mutations or changes that lead in uncontrollable cell proliferation resulting in tumorigenesis. The cause of lymphoma remains argued, certain individuals are more susceptible to establishing the cancer. Some pathogens are reported to be significantly associated with the disease.

HIV-positive patients and people infected with several other viruses or bacteria including *Helicobacter pylori*, Epstein-Barr virus, and human T-lymphotropic virus are found to be more likely developing the disease (Engels 2007), in addition a genetic link or familial connection in lymphoma development has been suggested by Cerhan and Slager 2015. Also it has been speculated that gut colonizing fungi might have an role in some cancers, in a study conducted by Khidir A.K. and colleagues they retrieved Malssezia genus of fungi in high frequency from fecal samples of cancer patients (Khidir A.K. *et al*. 2017). Lymphoma can be

* **Corresponding Author:**
Zeki Ali Mohamed
E-mail: zeki.mohamed@uod.ac
Article History:
Received: 04/04/2020
Accepted: 09/05/2020
Published: 13/10 /2020

divided into two major categories, including non-Hodgkin lymphoma (NHL) and Hodgkin lymphoma (HL), they can be further categorized into more than 30 types of NHL and five types of HL (WHO Classification of Tumours, 2017). *Helicobacter pylori* (*H. pylori*), is a Gram negative, spiral-shaped, microaerophilic bacterium that inhabits the human stomach. According to records, it has been estimated to colonize more than half of the world's human population (Hatakeyama M . 2004). Due to its pathogenesis and multiple virulence factors, it has been recognized as a carcinogen and classified to be class I carcinogen and led to a new method for classifying gastric carcinoma (Wotherspoon *et al*. 1991). It has been shown that *H. pylori* infections trigger the gastric associated lymphoid tissues responses in a way to be a potential oncogenic factor leading to the development of gastric associated malignant lymphomas like mucosal associated lymphoid tissues (MALT) lymphoma and DLBCL (Amieva *et al*. 2016; Lee *et al*. 2016; Suzuki *et al*. 2006). The virulence factors of H. pylori involved in the mechanism of pathogenesis and potential ontogenesis are CagA, VacA and OipA, they have a significant role in lymphomagenesis which includes also host factors and environmental conditions. Cytotoxin-associated gene A (CagA) protein is the *H. pylori* virulence factor most intensively studied as an oncogen factor, it has the ability to cross the host cell membrane and induce intracellular cell signaling that might lead to oncogenesis (Murata-Kamiya et al, 2010). Evidences have proven that gastric associated lymphoma patients that are *H. pylori* sero-positive may show long-term survival and better prognoses ((Meimarakis *et al*. 2006; Marrelli *et al*. 2009; Postlewait *et al*. 2016). Because DLBCL (MALT) fails to respond to anti- *H. pylori* therapy, it is thought to be *H. pylori* status independent according to the WHO (World Health Organization) classification that differs from low-grade and *H. pylori*-dependent MALT lymphomas (MALT lymphoma) (Hussell *et al*. 1993; Neubauer *et al*. 1997; Swerdlow *et al*. 2008). Many other studies have demonstrated that an elevated rate of gastric DLBCL (MALT) is associated with *H. pylori* infections through responding effectively to *H. pylori* eradication (Chen *et al*. 2001; Morgner *et al*. 2001). The current study has aimed at estimating the prevalence of IgG anti- *H. pylori* antibodies among lymphoma patients as an indicator for H. pylori infection among them thereafter, the association of the *H. pylori* infection with the lymphoma malignancy.

2. SUBJECTS AND METHODS

2.1 **Subjects**

Patients involved in the current study were recruited to oncology-hematology unit in Azadi Teaching Hospital in Duhok city from January 2018 to February 2019. All of the cases were patients diagnosed with a lymphoid malignancy. The diagnosis of lymphoma was done locally based on serial complete blood count, peripheral blood smear examination, flourescent in situ hybridization, and bone marrow examination, at baseline in addition to histology and immunohistochemistry. Subjects with a diagnosis of uncertain malignant potential were excluded. Controls were apparently healthy individuals with age and sex matched. Severe immune-suppressed patients systemic infections, other than *Helicobacter pylori infection*, were excluded. Data on demographic, medical and family history, and environmental exposures were collected from each subject. . Informed consent was obtained from all subjects before enrollment. Blood samples were taken from the patients and controls.

2.2. Methods

serum anti- H. pylori IgG anti bodies

From each enrolled subject, 200 ul of serum sample was collected and preserved at -20 ^{o}C until processing in the laboratory. All samples were tested for in vitro qualitative and quantitative detection of IgG antibodies against *H. pylori* in duplicate using (MyBioSource, Inc. San Diego, USA) kit according to the manufacturer instructions, the sera samples were tested in duplicates. The enzyme immunoassay plate spectrophotomer reader was used to read the at absorbance of 450 nm. According to the kit supplier, the cut off value for the assay was 8 U/mL.

2.3. Statistical analysis

The comparison between lymphoma cases and IgG anti-*H. pylori* antibodies prevalence was done with a X^2 test. P values at level 0.05 and less were considered statistically significant. Regression was used to estimate the odds ratios and 95% confidence intervals (OR, 95% CI) to

measure association between anti-H. pylori IgG antibodies and the risk of lymphoma. The SPSS software was used for data analysis.

3. RESULTS AND DISCUSSION

There are scanty previous studies systematically reporting the potential role of *H. pylori* in lymphomagenesis, most of those studies have estimated no increased risk of lymphomas other than MALT associated lymphoma in the presence of *H. pylori* infection. In the current study, the IgG anti *H. pylori* antibody was estimated by serologic method as an indicator for the *H. pylori* infection of the subjects involved in the study, since IgG anti *H. pylori* has been demonstrated to be the best performance overall other serologic noninvasive diagnostic test for the detection of the *Helicobacter pylori* infection (Rosemary et al. 2009). A total of 64 B-cells lymphoma patients and 60 sex and age matched apparently healthy individuals were involved in the current case control study. Table 1 shows the demographic characteristics of the study subjects including the age and sex. The age average was 52.5 years for cases and 56 years for controls. There was no statistical difference in the distribution of the demographic characteristics (age and gender) between cases and controls (P value = 0.11), which is consistent with findings of Silvia *et al*. 2004 when they reported that no statistical differences were observed in the distribution of these characteristics between patients with lymphoma types and control subjects. The prevalence of IgG anti-*H. pylori* antibodies is indicated in table 2, the antibodies were found in 11/64 (17.9%) of the lymphoma patients, were as among the control subjects the IgG anti-*H. pylori* antibodies were detected in 8/60 (13.3%).

IgG anti *H. pylori* antibodies prevalence varied by age, subjects older than 80 years having higher prevalence of antibodies (28.6%) as compared with all other age categories. Regarding the age groups in lymphoma subjects, there was a significant increase in the IgG anti-*H. pylori* antibodies prevalence when the age group >80 years compared to both age groups <40 years (p= 0.008), 51-60 years (p=0.04) and 61-70 years (p=0.02) respectively. No significant difference was found in the IgG anti *H. pylori* antibodies prevalence between the lymphoma and control subjects (p=0.087). Also the gender had no significant effect on the IgG anti *H. pylori* antibodies prevalence in both of the lymphoma and control subjects respectively and between the two groups. Epidemiological studies on the general populations show a male preponderance in the infection rate by H pylori, although there are controversial reports representing comparable rates (Shi R *et al*. 2008; Dore MP *et al*. 2012), but Agah S *et al*. 2016 found that females are more vulnerable to develop gastric cancers after getting *H pylori* infection, in a time that males have shown higher risk of developing other related side effects associated with *H pylori* infection, including cancer, though more future prospective studies with large patient population are still needed to explain this disparity. As shown in table 3, a very weak association of IgG anti *H. pylori* antibodies prevalence was observed with an overall increased risk of lymphoma (OR=1.34, 95% CI= 0.49-3.42), of the 64 lymphoma patients, 11 had detectable IgG anti *H. pylori* antibodies in their sera. To some extent, these findings are consistent with those reported by Silivia *et al*. (2004), they found that *H. pylori* infection was not associated with an overall increased risk of lymphoma, within all lymphoma categories, they found that *H. pylori* was associated with an almost 4-fold increased risk of splenic MZL (OR = 3.97, 95% CI = 0.92-17.16, P value = 0.065). In contrast, in a study conducted on stomach cancer patients in Erbil city, Sulaiman K., found that most of the stomach cancer patients had *H. pylori* infection (Sulaiman K. 2016). This inconsistency in the results could be due to the lymphoma stratification, in the current study the lymphoma cases are not stratified into nodal, extranodal and MALT lymphomas, however, in a future study plan o the same samples of the same patients, the stratification will be considered and will be compared with the current findings to see the significance of lymphoma stratification. In the study conducted by Silivia *et al* (2004), the cases were stratified and the strongest association of *H. pylori* was found with MALT lymphomas, and they identified that 100% of the subjects with a gastric lymphoma categorized as MALT or as DLBCL histology had antibodies against *H. pylori* in agreement with the data reported by Nakamura *et al*. 2003. In the present study, if the MALT

associated lymphoma would of been studied separately, the association of *H. pylori* with the lymphoma might be much more stronger, this is supported by Anttila *et al.* (1998), they did not identify an increase in the seroprevalence of IgG anti-H. pylori among patients with non-Hodgkin's lymphomas (OR = 0.8 95% CI = 0.4-1.9). No data were presented by lymphoma subtype, and in contrast, when stratifying and categorizing the lymphoma cases the association will be increased as reported by Cuttner *et al*. (2001) when they found that *H. pylori* seroprevalence was significantly higher for MALT lymphomas as compared with other lymphoma types

It has been found that Gastric and MALT lymphoma is a rare type of non-Hodgkin lymphoma . This cancer represents approximately 12 percent of the extranodal (outside of lymph nodes) non-Hodgkin (Wu XC et al. 2009). On the other hand, even though the lymphoma patients are not categorized into extranodal lymphomas, the week association of the *H. pylori* infection with lymphoma in the current study could be due to the small sample size studied compared to others, because in some investigations it has been accepted that MALT lymphoma cells may disseminate into the splenic marginal zone through homing mechanisms since there has been no evidence of *H. pylori* playing a role in the development of lymphomas localized in the spleen with no evidence of gastric lymphoma (Cavalli *et al*. 2001). *H. pylori* virulence factors (e.g., CagA, VacA and OipA) have a significant role in lymphomagenesis which includes also host factors and environmental conditions. Cytotoxin-associated gene A (CagA) protein is the *H. pylori* virulence factor most broadly studied, it has the ability to cross the host cell membrane and induce intracellular cell signaling that might lead to oncogenesis (Murata-Kamiya et al, 2010). In other studies, researcher explored the significance of H. pylori infection in lymphoma oncogenesis and the significance of *H. pylori* eradication in lymphoma remission. It has been reported that *H. pylori* infection is significantly associated with lymphoma specifically Gastric lymphoma and MALT lymphoma, medicines used for the eradication of H. pylori are usually used as the first-line treatment for this disease particularly during the early stage of the disease (Nakamura et al. 2012; Fischbach et al. 2007), these data have been supported by researchers when they found a complete remission of diffused large B cell lymphoma DLBCL after *H. pylori* eradication (Sugimoto et al, 2003; Alsolaiman et al, 2003). Also, a large cohort study has validated the association of *H. pylori* infection with the de novo DLBCL (Kuo SH et al. 2012). Also it has been demonstrated that de novo gastric DLBCL *H. pylori*-positive is less aggressive than *H. pylori* negative and patients with primary gastric de novo DLBCL without *H. pylori* infection are more likely to have poor prognoses than patients with the infection; therefore, the patients without *H. pylori* may benefit from more aggressive treatment and more systematic follow-up (Cheng et al. 2019).

Table1. The demographic characteristics of the subjects included in the study

	Controls	**Lymphoma patients**	***P* value**
	***n* (%)**	***n* (%)**	
Age (years)			
<40	5(8.3)	6(9.4)	
41-50	9(15)	10(15.6)	
51-60	9(15)	9(14.1)	
61-70	13(21.7)	14(21.9)	0.11

71-80	10(16.7)	11(17.1)	
>80	14(23.3)	14(21.9)	0.23
Gender			
Males	32(53.3)	37(57.7)	
Females	28(46.7)	27(42.2)	
Total	60	64	

Table2. Seroprevalence of IgG anti H. pylori by demographic characteristics in Patients and control subjects

	Controls	**Lymphoma patients**	***P***
	IgG Anti- H. pylori+/Total *n* (%)	**IgG Anti- H. pylori+/Total *n* (%)**	**value**
Age			
(years)	1/5(20)	0/6(0)	
<40	0/9(0)	2/10(20)	0.008
41-50	2/9(22.2)	1/9(11.1)	
51-60	2/13(15.4)	1/14(7.14)	0.04
61-70	1/10(10)	3/11(27.3)	0.02
71-80	2/14(14.3)	4/14(28.6)	
>80			
Gender	4/32(12.5)	6/37(16.2)	
Males	4/28(14.3)	5/27(18.5)	
Females	8/60(13.3)	11/64(17.9)	
Total			

Table3. Association of IgG anti- *H. pylori* antibodies prevalence with the lymphoma cases.

	IgG Anti- H. pylori+/Total *n* (%)	%	OR (95% CI)
Controls	8/60	13.3	Reference
Lymphoma patients	11/64	17.9	1.34(0.49-3.42)

4. CONCLUSIONS

A week association of *H. pylori* infection with lymphoma was found due to pathologically non stratified and categorized cases of the lymphoma, if being categorized pathologically, the association might increased significantly since persistent infection of *H. pylori* has been reported to be associated with some types of lymphoma specifically gastric and MALT lymphomas. Clinically it is important to explore the *H. pylori* infection among lymphoma patients since eradication of the bacteria could improve the treatment because when caught early, lymphoma is highly treatable and often curable.

Acknowledgment: I would like to extend deep thanks to the team of Duhok medical research center at the college of medicine- university of Duhok and also the oncology- hematology unit team at Azadi teaching hospital for kind support and help.

Conflict of interests

Nothing to declare

REFERENCES

Agah S, Khedmat H, Ghamar-Chehreh ME, et al.2016. Female gender and Helicobacter Pylori Infection,the most important predisposition factors in a cohort of gastric cancer. A longitudinal study. *Caspian J Intern Med*. 7(2):136-141.

Alsolaiman MM, Bakis G, Nazeer T, et al. 2003. Five years of complete remission of gastric diffuse large B cell lymphoma after eradication of helicobacter pylori infection. *Gut.* 52:507–9.

Amieva M, Peek RM. 2016. Pathobiology of helicobacter pylori-induced gastric Cancer. *Gastroenterology*. 150:64–78.

Anttila TI, Lehtinen T, Leinonen M, et al. 1998. Serological evidence of an association between chlamydial infections and malignant lymphomas. *Br J Haematol*.103:150-6.

Cavalli F, Isaacson PG, Gascoyne RD, Zucca E. 2001. MALT lymphomas. *Hematology* (Am Soc Hematol Educ Program). 1:241-58.

Cerhan JR, Slager SL. 2015. Familial predisposition and genetic risk factors for lymphoma. *Blood.* 126(20):2265–2273. [PMC free article] [PubMed] [Google Scholar]

Chen LT, Lin JT, Shyu RY, et al. 2001. Prospective study of helicobacter pylori eradication therapy in stage I(E) high-grade mucosa-associated lymphoid tissue lymphoma of the stomach. *J Clin Oncol*. 19:4245–51.

Cuttner J, Werther JL, McGlynn P, et al. 2001.Seroprevalence of Helicobacter pylori infection in patients with lymphoma. *Leuk Lymphoma*. 40:591-7.

Dore MP, Fanciulli G, Tomasi PA, et al. 2012. Gastrointestinal symptoms and Helicobacter pylori infection in school-age children residing in Porto Torres, Sardinia, Italy. *Helicobacter*.17:369-73.

Engels EA. 2007. Infectious agents as causes of non-Hodgkin lymphoma. *Cancer Epidemiol Biomarkers Prev*. 16(3):401–404. [PubMed] [Google Scholar]

Fischbach W, Goebeler ME, Ruskone-Fourmestraux A, et al. 2007. Most patients with minimal histological residuals of gastric MALT lymphoma after successful eradication of helicobacter pylori can be managed safely by a watch and wait strategy: experience from a large international series. *Gut.* 56:1685–7.

Hatakeyama M. 2004. Oncogenic mechanisms of the helicobacter pylori CagA protein. *Nat Rev Cancer*.4:688–94.

Hussell T, Isaacson PG, Crabtree JE, et al. 1993.The response of cells from lowgrade B-cell gastric lymphomas of mucosa-associated lymphoid tissue to helicobacter pylori. *Lancet.* 342:571–4.

Khidir A.K, Ibrahim Hamad and Hiwa A. Ahmad. 2017. Fungal Diversity in Gut Microbiota in Patients with Cancer. *ZJPAS*. 29(5): 55-65

Kuo SH, Yeh KH, Wu MS, et al. 2012. Helicobacter pylori eradication therapy is effective in the treatment of early-stage H pylori-positive gastric diffuse large B-cell lymphomas. *Blood*. 119:4838–44.

Kuppers R. 2009. The biology of Hodgkin's lymphoma. Nat Rev Cancer. 9(1):15–27. [PubMed] [Google Scholar]

Lee YC, Chiang TH, Chou CK, et al. 2016. Association Between Helicobacter pylori Eradication and Gastric Cancer Incidence: A Systematic Review and Meta-analysis. *Gastroenterology*. 150:1113.

Marrelli D, Pedrazzani C, Berardi A, et al. 2009. Negative helicobacter pylori status is associated with poor prognosis in patients with gastric cancer. *Cancer*. 115:2071–80.

Meimarakis G, Winter H, Assmann I, et al. 2006. Helicobacter pylori as a prognostic indicator after curative resection of gastric carcinoma: a prospective study. *Lancet Oncol*.7:211–22.

Morgner A, Miehlke S, Fischbach W, et al. 2001. Complete remission of primary high-grade B-cell gastric lymphoma after cure of helicobacter pylori infection. *J Clin Oncol*. 19:2041–8.

Murata-Kamiya N, Kikuchi K, Hayashi T, et al. 2010. *Helicobacter pylori* exploits host membrane phosphatidylserine for delivery, localization, and pathophysiological action of the CagA oncoprotein. *Cell Host Microbe*.7:399–411.

Nakamura S, Matsumoto T, Jo Y, et al. 2003. Chromosomal translocation t(11;18)(q21;q21) in gastrointestinal mucosa associated lymphoid tissue lymphoma. *J Clin Pathol*. 56:36-42.

Nakamura S, Sugiyama T, Matsumoto T, et al. 2012. Long-term clinical outcome of gastric MALT lymphoma after eradication of helicobacter pylori: a multicentre cohort follow-up study of 420 patients in Japan. *Gut*. 61:507–13.

Neubauer A, Thiede C, Morgner A, et al. 1997. Cure of helicobacter pylori infection and duration of remission of low-grade gastric mucosa-associated lymphoid tissue lymphoma. *J Natl Cancer Inst*. 89:1350–5.

Postlewait LM, Squires MH, Kooby DA, et al. 2016. Preoperative helicobacter pylori infection is associated with increased survival after resection of gastric adenocarcinoma. *Ann Surg Oncol*. 23:1225–33.

Rosemary C. She, Andrew R. Wilson, and Christine M. Litwin. 2009. Evaluation of Helicobacter pylori Immunoglobulin G (IgG), IgA, and IgM Serologic Testing Compared to Stool Antigen Testing. *Clinical and Vaccine Immunology*. 16(8): p. 1253–1255

Shi R, Xu S, Zhang H, et al. 2008. Prevalence and risk factors for Helicobacter pylori infection in Chinese populations. *Helicobacter*. 13: 157-65.

S.H, Swerdlow,., E.Campo, , N.L.Harris, , E.S.Jaffe, , S.A.Pileri, , H.Stein, , J.Thiele, , J.W. Vardiman. 2017. *WHO Classification of Tumours of Haematopoietic and Lymphoid Tissues.* 4th edition(Vol 2). WHO Classification of Tumours.

Silvia de Sanjose, Andrew Dickie, Tomas Alvaro, Vicens Romagosa, Mercedes Garcia Villanueva, Eva Domingo-Domenech, Alberto Fernandez de Sevilla, and Emad El-Omar. 2004. *Helicobacter pylori* and Malignant Lymphoma in Spain. *Cancer Epidemiol Biomarkers Prev*. 13(6).

Sugimoto M, Kajimura M, Sato Y, et al. 2001. Regression of primary gastric diffuse large B-cell lymphoma after eradication of helicobacter pylori. *Gastrointest Endosc*. 54:643–5.

Sulaiman K. 2016. Cytogenetic study of Stomach cancer in Erbil City. ZJPAS. 28 (4): 56-65

Suzuki T, Matsuo K, Ito H, et al. 2006. A past history of gastric ulcers and helicobacter pylori infection increase the risk of gastric malignant lymphoma. *Carcinogenesis*. 27:1391–7.

Swerdlow SH, Campo E, Harris NL, et al. 2008. WHO classification of tumors of hematopoietic and lymphoid tissues. 4th ed. Lyon: IARC Press

Wotherspoon AC, Ortiz-Hidalgo C, Falzon MR, et al. 1991.Helicobacter pyloriassociated gastritis and primary B-cell gastric lymphoma. *Lancet*. 338:1175–6.

Wu XC, Andrews P, Chen VW, Groves FD. 2009. Incidence of extranodal non-Hodgkin lymphomas among whites, blacks, and Asians/Pacific Islanders in the United States: Anatomic site and histology differences. *Cancer Epidemiology*. 33(5):337–346.

Yuan Cheng, Yinan Xiao, Ruofan Zhou, Yi Liao, Jing Zhou and Xuelei Ma. 2019. Prognostic significance of helicobacter pylori-infection in gastric diffuse large B-cell lymphoma. *BMC Cancer*.19:842

ZANCO Journal of Pure and Applied Sciences
The official scientific journal of Salahaddin University-Erbil
https://zancojournals.su.edu.krd/index.php/JPAS

ISSN (print):2218-0230**, ISSN (online):** 2412-3986**, DOI: http://dx.doi.org/10.21271/zjpas**

RESEARCH PAPER

Estimation of Some Metals in Children's Colorful Modeling Clay Sold in the Markets of Erbil City, Kurdistan Region, Iraq

Aveen Faidhalla Jalal, Hawraz Sami Khalid*, Iman Tayib Yasin, Mhabat Rashid Xanamir

Department of Chemistry, College of Education, Salahaddin University-Erbil, Kurdistan Region, Iraq.

A B S T R A C T:

Toxic heavy metals are commonly introduced in the manufacturing of various children's products. In this study, nine different types of modeling clay brands collected from several markets in Erbil city were analyzed to assess the content of heavy metals including Cd, Cr, Cu, and Ni. The metals analyses were performed on different colors available in each of the purchased brands. Strong acids such as nitric acid (HNO_3 65%), and perchloric acid ($HClO_4$ 70%) were performed to digest samples. Concentrations of the selected metals were determined using a flame atomic absorption spectrophotometer (FAAS). Data showed that numbers of examined clays samples detected with Cr, Cd Cu, and Ni metals were 0, 5, 36, and 40 out of 54 examined clay samples, respectively. Ni and Cu were found in varying concentrations in most (detected in 8 brands out of 9 collected clay brands) of the examined clay brand samples. The total of the detected metals load in the nine analysed brands were as follows; Chinese-3 (221.41 mg/kg) > Italian (75.84 mg/kg) > Chinese-4 (68.00 mg/kg) > German (61.31 mg/kg) > Chinese-6 (58.67 mg/kg) > Turkish (54.05 mg/kg) > Chinese-5 (52.51 mg/kg) > Chinese-1 (23.7 mg/kg) > Chinese-2 (23.31 mg/kg). Data confirms that the concentrations of the selected metals in whole examined samples were below European Union permissible limits (EN 71-3:2013, Category-I) for the migratable metals in pliable clay toys except one clay sample (819.2 mg/kg of Cu in blue clay color). An analysis of variance (ANOVA) was applied to find the presence of significant differences among analysed brands of modeling clay samples.

KEY WORDS: AAS, Children toy, Heavy metals, Modeling Clay
DOI: http://dx.doi.org/10.21271/ZJPAS.32.5.13
ZJPAS (2020) , 32(5);134-145 .

1. INTRODUCTION

A toy is defined as any designed essential product for children's growth and development. Plying more time with toys by children is a great habit and has a vital role in a child's development (Kumar and Pastore, 2007, ISO, 8124-1. 2014). The most commonly used material to made soft children toys is polyvinyl chloride (PVC) which includes several additives.

* **Corresponding Author:**
Hawraz Sami Khalid
E-mail: hawraz.khalid@su.edu.krd
Article History:
Received: 03/4/2020
Accepted: 26/05/2020
Published: 13/10 /2020

Heavy metals and their compound are present and widely used from manufacturing children's toys as the necessary flexibility, stability, catalysts, coloring agents, brightness, softness, and many other additives (Belliveau and Lester, 2004, Guney and Zagury, 2012, Sindiku and Osibanjo, 2011). Cadmium and lead act as a stabilizer in toys and are also used in pigments to improve the attraction of toys visualization. Recent studies showed that both PVC and non-PVC children's toys included different concentrations of metals. Heavy metals are naturally 5 times denser than

water and cannot be metabolized by the body (Cui et al., 2015, Hillyer et al., 2014, Oyeyiola et al., 2017).

Due to beginning of industrialization, heavy metals have become a major health problem and observed in food, water, air, soils, drugs, plants, cosmetics, plastic toys, cookware, and other daily household tools (Kumar and Pastore, 2007, Kumar Das et al., 2011, Sindiku and Osibanjo, 2011, Abdullah et al., 2017, Amin et al., 2017, Darwesh, 2019, Bazzaz and Muhammad, 2018, Abd-Alhameed, 2019). In developing countries like China, it is known the rising number of children at risk for toxic heavy metals' exposure. It was revealed that the increased risk of several behavioural problems like anxiety, somatic complaints, withdrawn, thought problems, social problems, attention problems, delinquent and aggressive for school-aged children was associated with a polluted area with heavy metals' exposure (Bao et al., 2009). Heavy metals can cause unacceptable significant hazard risks and major disruption function problems in the human mental, nervous system, lungs, kidneys, and other organs (Duffus, 2002, Martin and Griswold, 2009).

Chemical exposure to children, especially leaching toxic heavy metals from plastic toys and painted materials, is an emerging concern. Child behaviours with plastic toys like stretching, chewing, sucking, licking, and swallowing can be seen as common and the impact source of heavy metal exposure due to leaching out toys component (Kumar and Pastore, 2007).

Exposure to a high concentration of heavy metals including cadmium (Cd), lead (Pb), chromium (Cr), nickel (Ni) and copper (Cu) can have several harmful health effects and problems (Cui et al., 2015, Martin and Griswold, 2009). Cadmium exposure at contents present in most countries can be harmful to early life and have an impact on child brain development (Kippler et al., 2012). It is also recognized to damage many organ functions, and increase cancer risk (Järup and Åkesson, 2009).

Even with the deserve attention and regulation of heavy metal contamination in children's toys, recent studies declared that more precaution is required through the production of children's toys and to limit the importing and handling of such child products into the markets. (Al-Qutob et al., 2014, Guney and Zagury, 2012, Ismail et al., 2017, Issa and Alshatteri, 2019). Varying concentrations of Cd and Pb and other toxic elements were recorded in several unbranded Indian soft plastic toys (Kumar and Pastore, 2007), 20 toys and children's jewellery bought on the North American market (Guney and Zagury, 2013), thirty different soft plastic toys collected from the Ghanaian markets (Kudjoe Gati et al., 2014), and over 100 of the collected vintage plastic toys (Miller and Harris, 2015). These toxic metals were recently detected in several PVC and non-PVC plastic toys (Oyeyiola et al., 2017) 200 second-hand plastic toys sourced in the UK (Turner, 2018), and different toy samples in Poznań city (Poland) (Karaś and Frankowski, 2018) and six infant care plastic products sold in markets of Kalar City, Kurdistan Region, Iraq (Issa and Alshatteri, 2019).

The Scientific Committee on Health and Environmental Risks (SCHER) mentioned that the average ingested daily intake toy materials are still appropriate as follows; 400 mg/d for liquid or sticky toy material, 100 mg/d for dry, brittle, powder-like or pliable toy material, and 8 mg/d for scraped-off toy material (EC, SCHER. 2016). However, in a worst-case assessment, ingestion values of different toy materials were found above permission standard limits for several toy products. Results confirmed that 739 and 151.8 mg/d average value were recorded as total ingested daily intake toys for liquid or sticky and dry, brittle, powder-like or pliable toy material, respectively (Danish, EPA. 2014).

Several methods for the assessment of bio-availability and Hazard Index (HI) with health risk characterization were recently recommended and applied to investigate metals health hazard exposure in various products of children's toys (Cui et al., 2015, Dahab et al., 2016, Guney et al., 2014, Guney and Zagury, 2014b, Oyeyiola et al., 2017). Last decades, scientists and physicians have extremely mentioned that no content of Cd or Pb metal in human blood is normal or considered harmless. They emphasized that what was 'safe' yesterday is no longer 'safe' today or tomorrow. Thus, the present 'safe' limits of heavy metals have been revised in blood, baby toys and

environments samples due to continuing scientific studies (Kudjoe Gati et al., 2014, Kumar and Pastore, 2007).

There is only one recent local study on the assessment of element contents in infant care plastic products sold in markets of Kalar City, Kurdistan Region, Iraq. The detected metals ranges for Cd, Cr, Cu, and Ni in six samples were (not detectable (ND)-0.10 mg/kg), (ND-71.12 mg/kg), (0.127-17.3 mg/kg), and (0.004-2.15 mg/kg) respectively. The detected contents of whole analyzed metals were lower than the world permissible limits while Cr contents were exceeded the permissible limit in most of the analysed samples (Issa and Alshatteri, 2019). However, few studies are available and have been recently examined for the assessment of heavy metals in colorful baby clay. According to the investigated study in Lebanon, inexpensive modeling clay is popular, and there is not good legislation to regulate such toys. The community survey declared that only 17 % of families in Lebanon were attentive to the health hazard of such toys and 82 % of parents try to purchase inexpensive and unbranded toys for their children (Korfali et al., 2013). Erbas et al. (2017) stated that the recorded contents (mg/kg) range of some metals in nine play dough samples were ND for Co, ND – 4.8 for Pb, 0.14 – 1.2 for Cd, 1.2 – 3.9 for Ni, 0.8 – 6.6 for Mn, and ND – 219 for Cu. Sogut and Ezer (2017) also reported that 13 different brands of children's play dough samples marketed in Turkey were investigated to determine elemental composition. The contents (mean±SD) of the analysed some elements were ND for Cd, 1.59 ± 0.76 mg/kg for Hg, 4.08 ± 1.89 mg/kg for As, 17.21 ± 18.43 mg/kg for Pb, 32.20 ± 19.44 mg/kg for Mn, 53.60 ± 16.72 mg/kg for Cu, and 63.16 ± 29.03 mg/kg for Zn.

In recent times, the maximum permissible content of migrated heavy metals in children toys have been regulated, declared and updated by many jurisdiction standards (Table 1) including European Union New Toy Safety Directive (EN, 71-3: 2006), European Toys Safety Directive (EC, 2009), International Standard (ISO, 8124-3. 2010), and European Union (EU) New Toy Safety Directive (EN, 71-3: 2013).

Table 1: Showing the country world permissible limits of migrated heavy metals (mg/kg) from children toy

Standards Jurisdiction	**Scope**	**Maximum acceptable metals migration from toy materials (**mg/kg**)**				
		Cu	**Ni**	**Cd**	**Cr (III)**	**Cr (VI)**
European Union (EN, 71-3: 2006)	For modeling clay and finger paints	--	--	50	25	--
European Union 2009/48/EC (EC, 2009)	Category I	622.5	75	1.9	37.5	0.02
	Category II	156	18.8	0.5	9.4	0.005
	Category III	7700	930	23	460	0.2
International Standard (ISO, 8124-3. 2010)	Any toy material given in clause I, except modeling clay and finger paint	--	--	75	60	--
	Modeling clay and finger paint	--	--	50	25	--
European Union (EN, 71-3: 2013)	**Category I**	**622.5**	**75**	**1.3**	**37.5**	**0.02**
	Category II	156	18.8	0.3	9.4	0.005
	Category III	7700	930	17	460	0.2

Category I: in dry, brittle, pliable or powder-like toy material, Category II: in liquid or sticky toy material, Category III: In scraped-off toy materials.

Toys and modeling clay must be safe and are essential for children's growth and development. To the best of our knowledge, there is no previous study addressed the amount contents of heavy metals in children modeling clay marketed in Erbil city/Iraq country. Thus, the main aim of this study was to evaluate the content of selected heavy metals in different brand samples of colorful modeling pliable clay collected in the markets of Erbil city. To know toys' product safety, the content of analysed metals can be compared with the recent international permissible limits (Category-I) for metals (EN, 71-3: 2013) due to none availability of the updated Iraqi standards for heavy metals in toys.

2. MATERIALS AND METHODS

2.1. Chemicals

Different chemicals including nitric acid (HNO_3 65%), and perchloric acid ($HClO_4$ 70%) were used with analytical grade throughout the experiment study for sample digestion. According to AAS manufacturer guideline (Whiteside and Milner, 1984), chromium nitrate [$Cr(NO_3)_3.9H_2O$] and nickel nitrate [$Ni(NO_3)_2.6H_2O$] were used and dissolved in distilled water throughout the experiments for the preparation of 1000 mg/kg of Cr and Ni stock solutions respectively. Chemicals such as CdO (dissolved in 5M diluted HCl) and Cu metal (dissolved in 5M HNO_3) were also used to prepare 1000 mg/kg of Cd and Cu stock solutions respectively. Then, serious working solutions for the selected of the metals ion were individually prepared from the stock solutions according to the instruments manufacturer guideline (Whiteside and Milner, 1984).

2.2. Instrumentation

Flame atomic absorption spectrometer (FAAS) (Pye-Unicam SP9 model flame AAS, Cambridge, CB, UK) accoutered with a hollow cathode lamp as the light source and acetylene-air flame burner was used to determine selected metal ions in whole sample solutions. The instrumental parameters and optimum conditions were those suggested by the manufacturer guideline (Whiteside and Milner, 1984). The wavelengths (nm) selected for the determination of the metals ion were as follows: Cd, 228.8 nm; Ni, 232.0 nm; Cu, 324.8 nm and Cr, 357.9 nm. Acetylene (C_2H_2) flow rate was 0.8-1.4 mL min^{-1} and air flow rate was 18-28 mL min^{-1}. The nebulizer uptake rate was 6 mL min^{-1}. The hallow cathode lamp currents were 5, 8, 12, and 15 mA for Cu, Cd, Cr, and Ni respectively.

2.3. Sample collection

During sampling, nine different brands of children modeling clay samples were obtained from local markets in Erbil city, Kurdistan Region (Iraq) during January 2018. The obtained samples were collected based on different brands name and origins. The collected samples included the following nine brand names (code); Glotto (Italian), Lyra (German), Lets Have Fun (Turkish), Play Doh (Chinese-1), 5D Mini Normal (Chinese-2), and 5D-Mini Soft (Chinese-3), Modeling Clay (Chinese-4), Play Dough (Chinese-5), and Tong Tong (Chinese-6). Seven main colorful clay samples for each of the collected brands were available except the Italian and German made brands.

2.4. Sample preparation and digestion for analysis

Sample digestion for metal analysis was carried out according to the published methods (Guney and Zagury, 2014b, Guney and Zagury, 2014a). Prior to analysis, digestion 1.0 g of a modeling clay sample was quantitatively subjected to strong wet acid digestion using nitric acid (HNO_3 65%) on digestion-heater, followed by perchloric acid ($HClO_4$ 70%). At first, a volume of 15 ml of concentrated HNO_3 was used to destruct the sample on digestion-heater until the brown fumes were appeared and liberated at about 150℃ temperature. After cooling, 5 ml of concentrated $HClO_4$ then was added to complete digestion until the white vapors of the acid were liberated (Figure 1). The digested sample solution was cooled, quantitatively transferred and then diluted into a 50 ml volumetric flask with distilled water. Finally, the last solution was labelled and stored until the final analysis and analyzed directly without any further dilution with distilled water. The above steps were repeated for blanks and each of the seven colors individually for each collected brand samples. Solution which contains only the digested acids or the reagents used to dissolve or digest the analyzed samples were individually prepared, used as blank and repeated three times for each of samples and working solutions. Blank solution is mainly used for calibration purposes or zeroed the absorbance of all the other presented components in the sample solution except the component of interest.

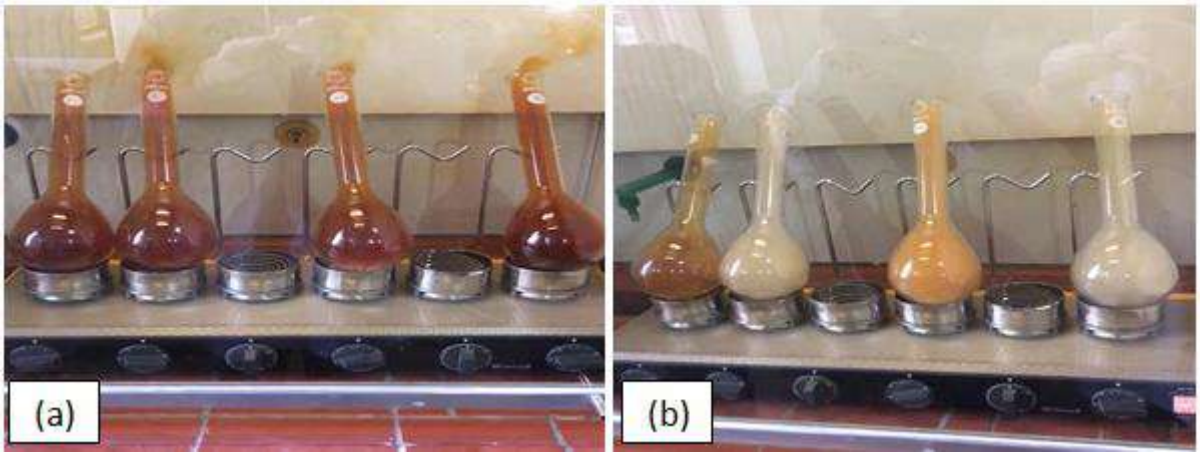

Figure (1): Wet digestion of the clay samples; (a) liberating brown fumes after addition concentrated HNO_3, (b) liberating white fumes after addition concentrated $HClO_4$

2.5. Sample analysis

Flame atomic absorption spectrometer (FAAS) was used and applied to determine the concentration of the selected heavy metals; chromium (Cr), nickel (Ni), copper (Cu), and cadmium (Cd) in seven main color clay samples from the collected brands. During analysis, some of the digested solutions were further diluted with distilled water when (necessary) concentration of analyzed metals in the sample solution was higher than the used metal linear range. Results were determined in mg/L (parts per million) in whole the digested solutions and converted into mg/Kg to find the contents of the selected metals in each of the colorful clay samples using dilution factor equation (Equation1) as follows:

$$\text{mg/Kg} = \frac{(\text{mg/L}) \times 50.0\ \text{mL}}{\text{accurate mass of 1.0 g sample}} \quad \ldots. \text{(Eq. 1)}$$

Results data were then used for the statistical data analysis.

2.6. Statistical analysis

This research was performed on nine different collected brands of modeling clay samples which included seven main colors for each brand. Several colors were selected for each brand to show the differences of the detected metal contents as heavy metals are broadly used in the manufacture of several industrial products such as colour pigment in paints (Järup, 2003). The results of this study were analyzed for statistical comparison using GraphPad Prism 6 and Microsoft Excel 2010 program software. An analysis of variance ANOVA was applied to assess differences in the mean concentration of the analyzed metals in modeling clay products. Data in tables and figures are shown in tabulated form as mean ± standard deviations (SD) and not detectable (ND) or below detection limit.

3. RESULTS AND DISCUSSIONS

The whole number of analyzed modeling clay brand was nine with different colors and brands. Seven main colors including white (W), black (Bk), yellow (Y), green (G), blue (B), red (R), and mixture (M) were available for each of the analyzed brands excepting the Italian and German made brands with few colors. Most of the available and selected brands were Chinese made. An adequate analytical estimation test was performed for assessment and finding the concentration of four heavy metals including chromium, nickel, copper, and cadmium in 54 examined colorful clay samples for the seven selected brands.

Detailed information including brands name, origin, color and the recorded metals content of the analyzed modeling clays are shown in Table 2. The finding results in the table confirms that Cr, Cd, Cu and Ni metals were presented and detected in 0, 5, 36, and 40 samples out of 54 examined colorful clay samples respectively. Both Cu and

Ni metals were recorded with a high amount in most of the 54 examined pliable colorful clay samples (Figure 2 and 3).

Columns diagram of the nickel and copper metal content in the entire main examined color including white, black, yellow, green, blue, red, and mixture color are individually illustrated for each of the collected brands in the Figure 2 and Figure 3, respectively. Figure 2 verifies that nickel metal was observed in at least five tested color available from each of the Turkish, Chinese-1, Chinese-3, Chinese-4, and Chinese-5 made brands. Based on ordering detected metals content in each pliable color, Cu metal was presented and recorded as the highest value in all the examined blue color clay followed by green color for each of the investigated brands excepting the Italian and German made brands (Figure 3).

Table 2: Concentration (mg/kg) of analyzed metals based on different colors modeling clay (n =2)

(Origin) Brand name	Code	Metal	Content of analyzed metals as ppm (mg/kg) in vary colorful modeling clay							
			(W)	(Bk)	(Y)	(G)	(B)	(R)	(M)	Mean±SD
(Italy) Glotto	Italian	Cu	40.6	NA	NA	NA	NA	25.00	25.00	30.20±9.00
		Cd	ND	NA	NA	NA	NA	ND	0.87	0.29±0.50
		Cr	ND	NA	NA	NA	NA	ND	ND	ND
		Ni	48.77	NA	NA	NA	NA	40.57	46.72	45.35±4.30
(Germany) Lyra	German	Cu	NA	NA	NA	NA	NA	ND	ND	ND
		Cd	NA	NA	NA	NA	NA	0.21	0.21	0.21±0.0
		Cr	NA	NA	NA	NA	NA	ND	ND	ND
		Ni	NA	NA	NA	NA	NA	61.10	61.10	61.10±0.0
(Turkey) Let's Have fun	Turkish	Cu	37.98	ND	37.98	47.59	62.01	35.57	36.77	36.84±18.80
		Cd	ND	ND	ND	ND	ND	ND	ND	ND
		Cr	ND	ND	ND	ND	ND	ND	ND	ND
		Ni	24.18	ND	15.98	15.98	24.18	20.08	20.08	17.21±8.30
(China) Play Doh	Chinese-1	Cu	ND	30.76	33.17	33.17	35.57	ND	33.20	23.70±16.20
		Cd	ND	ND	ND	ND	ND	ND	ND	ND
		Cr	ND	ND	ND	ND	ND	ND	ND	ND
		Ni	ND	ND	ND	ND	ND	ND	ND	ND
(China) 5D Mini Normal	Chinese-2	Cu	ND	ND	ND	ND	66.82	ND	ND	9.55±25.30
		Cd	ND	ND	ND	ND	ND	ND	ND	ND
		Cr	ND	ND	ND	ND	ND	ND	ND	ND
		Ni	ND	15.98	15.98	20.08	ND	28.28	15.98	13.76±10.40
(China) 5D Mini Soft	Chinese-3	Cu	ND	25.00	35.60	319.20	**819.20**	ND	230.2	204.2±298.9
		Cd	ND	ND	ND	ND	ND	ND	ND	ND
		Cr	ND	ND	ND	ND	ND	ND	ND	ND
		Ni	20.08	15.98	24.18	20.08	15.98	ND	24.18	17.21±8.3
(China) Modeling Clay	Chinese-4	Cu	30.76	37.98	ND	62.01	95.67	ND	30.76	36.74±33.9
		Cd	ND	ND	ND	ND	ND	0.21	0.20	0.06±0.1
		Cr	ND	ND	ND	ND	ND	ND	ND	ND
		Ni	32.38	36.47	28.28	36.47	32.38	15.98	36.47	31.20±7.37
(China) Play Dough	Chinese-5	Cu	35.57	35.57	33.17	40.38	66.82	35.00	42.78	41.33±11.70
		Cd	ND	ND	ND	ND	ND	ND	ND	ND

		Cr	ND	ND	ND	ND	ND	ND	ND	ND
		Ni	ND	15.98	ND	ND	15.98	15.98	30.33	11.18±11.60
(Chine) Tong Tong	**Chinese-6**	Cu	40.38	ND	ND	37.98	57.21	ND	42.78	25.48±24.60
		Cd	ND	ND	ND	ND	ND	ND	ND	ND
		Cr	ND	ND	ND	ND	ND	ND	ND	ND
		Ni	44.67	28.28	32.38	32.38	28.28	24.18	42.62	33.19±7.56

ND: Not Detectable, NA: Not Available, SD: Standard Deviation, W: White color, Bk: Black color, Y: Yellow color, G: Green color, B: Blue color, R: Red color, M: Mixture color, n: the sample repetition

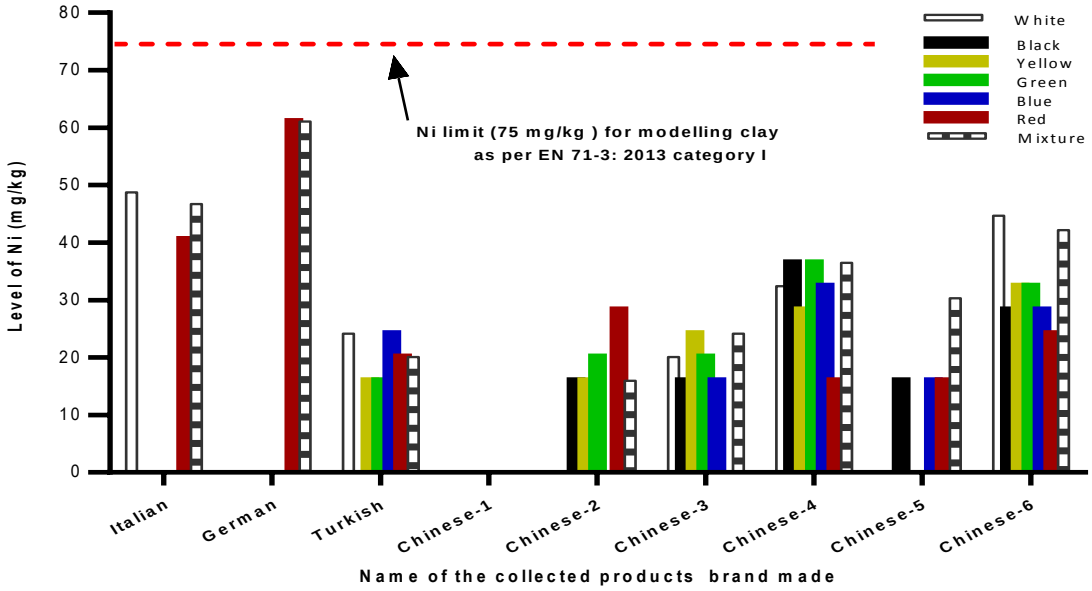

Figure (2) Concentration of nickel in the seven modeling clay colors collected from nine brands

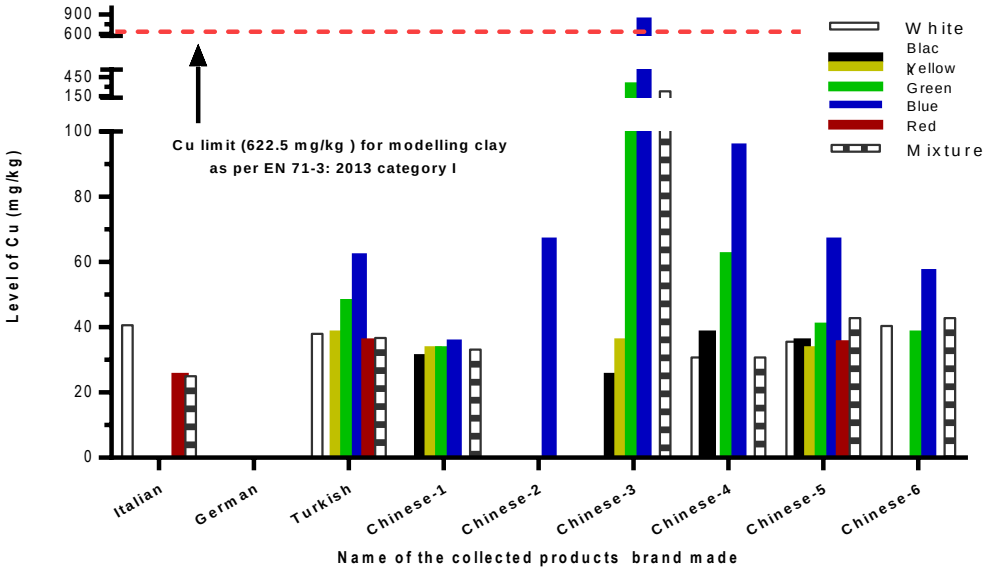

Figure (3) Concentration of copper in the different colorful modeling clay collected from nine brands

The summarized results of heavy metal concentration, the mean, range, standard deviation (SD), the available number of colorful samples per brands, number of samples detected with metals and a total of the detected metals load are presented in Table 3. Results show that the copper content ranged between ND - 819.2 mg/kg, while the nickel content ranged from ND - 61.10 mg/kg in different modeling clay. In addition, cadmium concentrations were only detected in 5 samples out of the whole (54) tested samples. The contents of the Cd metal in most of the chosen colorful clay sample were presented as non-detectable except the Italian (0.87 mg/kg in mixed color), German (0.21 mg/kg in red and mixture color), and Chinese-4 (0.21 mg/kg in red and 0.20 mg/kg in mixed color) brands. However, the total chromium concentration including Cr(III) and Cr(VI) was not detectable and also below the detection limit in the entire of the examined samples. Chromium's speciation which is Cr(III) and Cr(VI) was not performed and not identified in this study.

The total of the detected metals load in the entire nine analysed brands were recorded and ordered as follows in Table 3; Chinese-3 (221.41 mg/kg) > Italian (75.84 mg/kg) > Chinese-4 (68.00 mg/kg) > German (61.31 mg/kg) > Chinese-6 (58.67 mg/kg) > Turkish (54.05 mg/kg) > Chinese-5 (52.51 mg/kg) > Chinese-1 (23.7 mg/kg) > Chinese-2 (23.31 mg/kg).

Health risks of pliable clay can pose higher than usual children plastic toys because it is clear that modeling clay can be easily mouthed and chewed by children. Modeling clay toy relates to Category I which includes dry, brittle, pliable or powder-like materials that caused to leave a residue or trace on humans hands. Therefore, the permissible migration limits of toxic heavy metals in modeling clay (Category-I) were cautiously regulated to be stricter than those set for Child products including Category-III (scraped-off materials) (EN, 71-3: 2006, EN, 71-3: 2013). This is owing to the fact that brittle or pliable clay characterize a special toy category where the ingestion of higher amounts of these toy materials is imaginable during an exposure. Data for the selected metals concentrations in this study were evaluated and compared with recently standard permissible limits which regulated and highlighted by European Union (EU) New Toy Safety Directive (EN, 71-3: 2013) to stipulate the maximum permissible values of metals such as cadmium, lead, nickel and copper in toys. The permissible amounts are the boundary assessment between safety and danger for child products and must be below the content which could be harmful to children.

Table 3: Summarized metals content recorded in the vary colorful modeling clay from different brands (n=2)

Brands Name (Code)	**Metals**	**Metals content (**mg/kg)				**No. of colorful samples /brand**	**color samples detected with metals**	**Total of the detected metals load /brand (**mg/kg)
		Mini.	**Max.**	**Mean**	**±SD**			
Glotto (Italian)	Cu	25.00	40.60	30.20	9.00	3	W, R, M	75.84
	Cd	ND	0.87	0.29	0.50	3	M	
	Cr	ND	ND	ND	ND	3	None	
	Ni	40.57	48.77	45.35	4.27	3	W, R, M	
Lyra (German)	Cu	ND	ND	ND	ND	2	None	61.31
	Cd	0.21	0.21	0.21	0.00	2	R, M	
	Cr	ND	ND	ND	ND	2	None	
	Ni	61.10	61.10	61.10	0.00	2	R, M	
Let's Have fun (Turkish)	Cu	35.57	62.01	36.84	18.80	7	W, Y, G, B, R, M	54.05
	Cd	ND	ND	ND	ND	7	None	
	Cr	ND	ND	ND	ND	7	None	
	Ni	15.98	24.18	17.21	8.30	7	W, Y, G, B, R, M	
Play Doh	Cu	30.76	35.57	23.70	16.20	7	Bl, Y, G, B, M	23.70

(Chinese-1)	Cd	ND	ND	ND	ND	7	None	
	Cr	ND	ND	ND	ND	7	None	
	Ni	ND	ND	ND	ND	7	None	
5D Mini Normal	Cu	ND	66.82	9.55	25.30	7	B	23.31
	Cd	ND	ND	ND	ND	7	None	
	Cr	ND	ND	ND	ND	7	None	
(Chinese-2)	Ni	15.98	28.28	13.76	10.40	7	Bl, Y, G, R, M	
5D mini soft	Cu	25.00	**819.20**	204.20	298.90	7	Bl, Y, G, B, M	221.41
	Cd	ND	ND	ND	ND	7	None	
	Cr	ND	ND	ND	ND	7	None	
(Chinese-3)	Ni	15.98	24.18	17.21	8.30	7	W, Bl, Y, G, B, M	
Modeling Clay	Cu	30.76	95.67	36.74	33.90	7	W, Bl, G, B, M	68.00
	Cd	0.20	0.21	0.06	0.10	7	R, M	
	Cr	ND	ND	ND	ND	7	None	
(Chinese-4)	Ni	15.98	36.47	31.20	7.37	7	W,Bl,Y,G,B,R, M	
Play Doh	Cu	33.17	66.82	41.33	11.70	7	W, Bl, Y, G, B, R, M	52.51
	Cd	ND	ND	ND	ND	7	None	
	Cr	ND	ND	ND	ND	7	None	
(Chinese-5)	Ni	15.98	30.33	11.18	11.60	7	Bl, B, R, M	
Tong Tong	Cu	37.98	57.21	25.48	24.60	7	W, G, B, M	58.67
	Cd	ND	ND	ND	ND	7	None	
	Cr	ND	ND	ND	ND	7	None	
(Chinese-6)	Ni	28.28	44.67	33.19	7.56	7	W, Bl, Y, G, B, R, M	

ND: Not Detectable, NA: Not Available, SD: Standard Deviation, W: White color, Bk: Black color, Y: Yellow color, G: Green color, B: Blue color, R: Red color, M: Mixture color, n: the sample repetition

The data in this study proved that the detected concentrations of the investigated metals in all (54) of the analyzed colorful modeling clay samples were below the EU permissible limits for migrated metals (622.5 mg/kg for Cu, 75 mg/kg for Ni, 37.5 mg/kg for Cr (III), 0.02 mg/kg for Cr (VI), and 1.3 mg/kg for Cd) in pliable clay toys excepting one out of 54 examined colorful clay samples (blue color in Chinese-3 made brand). High content of copper (819.2 mg/kg) in blue color clay available in 5D Mini Soft product was detected in the Chinese-3 made brand and exceeded the permissible limit for copper. In this study, there is only one examined colorful sample which exceeded EN 71-3:2013 Category-I permissible limit for migrated Cu (622.5 mg/kg) metal in dry pliable children toys (EN, 71-3: 2013).

In Chinese-3 brand, the recorded Cu contents in analyzed mixture (230.20 mg/kg), green (319.20 mg/kg), and blue (819.20 mg/kg) color samples were largely higher than the detected Cu contents in white (ND), red (ND), black (25.00 mg/kg) and yellow (35.60 mg/kg) clay samples. In Chinese-4 brand, high concentrations of Cu were also detected in blue (95.67 mg/kg) and green (62.01 mg/kg) clay color samples (Table 2 & Figure 3). However, the highest Ni contents were detected in Chinese-6 (44.67 mg/kg), Italian (48.77 mg/kg) and German (61.10 mg/kg) brands (Table 2 & Figure 2). The presence of high contents of heavy metals could come from the used pigments from manufacturing children's toys as the necessary of coloring agents. Heavy metals which are known as the most polluting chemicals in the environment have been commonly encountered and used in paints component as pigments (Järup, 2003) and recorded with a high amount in various paint samples (Ogilo et al., 2017, Kameti, 2013, Apanpa-Qasim et al., 2016). The data of the metals mean in the Table 3 confirms that copper and nickel were detected in varying concentrations in most (8 out of 9) examined brand clay samples. It confirms that in most of the analyzed samples, the detected concentrations of Cu and Ni were higher than those in previously published studies on modeling clay (Guney and Zagury, 2013, Korfali et al., 2013).

An analysis of variance (ANOVA) two-factor without replications using a 95 % confidence level was also applied to find the presence of significant differences among whole analyzed brands of modeling clay samples in this study because the used data were the contents of the selected metals

mean (Table 3). The data of ANOVA showed that there is no statistically significant difference (p-value > 0.05) among means concentrations for seven examined clay brands including Turkish, Chinese-1, Chinese-2, Chinese-3, Chinese-4, Chinese-5, and Chinese-6 brands. P-value, F value, and $F_{(critical)}$ values were equal to 0.057, 3.14, and 3.287 respectively. However, both German and Italian clay brands were excluded in the ANOVA statistical analysis due to available few colors (white, red and mixture) modeling clay in these brands.

There are few studies for the assessment of heavy metals in colorful modeling clay. Korfali et al. (2013) investigated concentrations of some toxic metals in 23 different Far East colorful modeling baby clay toys of four brands imported into Lebanon. Korfali et al. (2013) reported that the recorded means ±SD (range) contents were 40.2±45 (ND–162) mg/kg for copper, 9.1±7 (ND–23) mg/kg for cadmium, 6.0±5.6 (ND–22) mg/kg for chromium, and 6.4±10.5 (ND–15) mg/kg for nickel in the analyzed clay samples. In a worst-case assessment, more than 15 (65%) of the analyzed clay samples recorded with a high amount of cadmium (9.1±7 mg/kg) and exceeded the Category-I permission limit for migration Cd metal (1.3 mg/kg) in children clay toys. However, each of Cu, and Ni content was far lower than the world permission level and also finding results in this study. Furthermore, Guney and Zagury (2013) also analysed the contents of several toxic metals in 18 different brittle or pliable clay toys. Results confirmed that only 1 (2.81±10 mg/kg of Cd) out of 18 brittle or pliable clay samples exceeded Category-I permission limits.

According to recent study by Erbas et al. (2017), the detected contents of Pb, Cd, Ni, Mn, Co and Cu metals in nine examined play dough samples were below the European Union permissible limits for the migratable metals in pliable clay toys excepting one sample. Data showed that high content of Pb metal (4.8±0.8 mg/kg) was detected in one of the examined green clay samples which was exceeded the permissible limit (3.4 mg/kg for Pb). Sogut and Ezer (2017) also reported that various concentrations of As, Hg and Pb toxic elements were detected in the same four play dough samples out of 13 examined samples marketed in Turkey while no Cd was determined in any of the analyzed samples. The recorded contents [mean± S.D. (detected in number of samples)] for As and Pb were 4.08±1.89 mg/kg (5) and 17.21± 18.43 mg/kg (8) and exceeded the recent EU permissible limits for the migratable metals. However, the detected contents for Cd and Cu were ND mg/kg (13) and 53.60±16.72 (12) and presented with good agreement with the recorded results in the present study.

In this study, the measured contents of selected heavy metals were generally low or below the world permissible limits (Category-I), modeling clay toys could still be harmful to children due to ingesting a high amount of modeling clay toys by children in a specific case. In addition, some toxic elements such as lead, mercury and arsenic remained, could be focused and analyzed to prove the safety of available clay toy in our country. These elements can cause several chronic health risks including pertaining to the central nervous system, the gastrointestinal tract (Markowitz, 2000), neurotoxic effects (Tolins et al., 2014), and acute and chronic intoxication at low levels of exposure (Bose-O'Reilly et al., 2010).

4. CONCLUSIONS

This study revealed that copper and nickel metal were detected in varying concentrations in most of the analyzed brand samples collected in Erbil city markets. In all cases the concentrations of copper in blue and green clay color is higher than that of copper in other colors. The recorded metal concentrations were below the permission limits except 1 out of 54 colorful pliable clay samples exceeded Category-I permission limit for copper.

5. RECOMMENDATIONS

Children product toys frequently contain varying amounts of toxic heavy metals. It is recommended that there should be continuous monitoring of all children products in the local markets.

REFERENCES

ABD-ALHAMEED, M. M. 2019. Spatial Distribution of Heavy Metals in Surface Soil Horizons Surrounding Erbil Steel Company (ESC) Areas. *ZANCO Journal of Pure and Applied Sciences,* 31**,** 32-38.

ABDULLAH, F. O., SAEED HUSSAIN, F. H. & VIDARI, G. 2017. Determination of some elements from wild Pterocephalus nestorianus Nab., growing in Kurdistan Region/Iraq using ICP-AES and ICP-MS. *ZANCO Journal of Pure and Applied Sciences,* 29**,** 83-89.

AL-QUTOB, M., ASAFRA, A., NASHASHIBI, T. & QUTOB, A. A. 2014. Determination of different trace heavy metals in children's plastic toys imported to the West Bank/Palestine by ICP/MS-environmental and health aspects. *Journal of Environmental Protection,* 5**,** 1104-1110.

AMIN, J. K. M., JALAL, S. S. & JARJEES, F. Z. 2017. The Elemental Composition of Atmospheric Particles and Dust Fall Rate in Erbil Governorate. *ZANCO Journal of Pure and Applied Sciences,* 29**,** 38-48.

APANPA-QASIM, A. F., ADEYI, A. A., MUDLIAR, S. N., RAGHUNATHAN, K. & THAWALE, P. 2016. Examination of lead and cadmium in water-based paints marketed in Nigeria. *Journal of Health and Pollution,* 6**,** 43-49.

BAO, Q.-S., LU, C.-Y., SONG, H., WANG, M., LING, W., CHEN, W.-Q., DENG, X.-Q., HAO, Y.-T. & RAO, S. 2009. Behavioural development of school-aged children who live around a multi-metal sulphide mine in Guangdong province, China: a cross-sectional study. *BMC public health,* 9**,** 217.

BAZZAZ, J. N. & MUHAMMAD, G. R. 2018. Some heavy metals assessment in frozen chicken meat sold in Erbil local markets. *ZANCO Journal of Pure and Applied Sciences,* 30**,** 96-101.

BELLIVEAU, M. & LESTER, S. 2004. PVC—Bad News Comes in Threes: The Poison Plastic, Health Hazards and the Looming Waste Crisis. *VA, USA: The Center for Health, Environment*.

BOSE-O'REILLY, S., MCCARTY, K. M., STECKLING, N. & LETTMEIER, B. 2010. Mercury exposure and children's health. *Current problems in pediatric and adolescent health care,* 40**,** 186-215.

CUI, X.-Y., LI, S.-W., ZHANG, S.-J., FAN, Y.-Y. & MA, L. Q. 2015. Toxic metals in children's toys and jewelry: coupling bioaccessibility with risk assessment. *Environmental Pollution,* 200**,** 77-84.

DAHAB, A. A., ELHAG, D. E. A., AHMED, A. B. & AL-OBAID, H. A. 2016. Determination of elemental toxicity migration limits, bioaccessibility and risk assessment of essential childcare products. *Environmental Science and Pollution Research,* 23**,** 3406-3413.

DANISH. EPA. 2014. *Survey and health assessment of preservatives in toys: Survey of chemical substances in consumer products* [Online]. The Danish Environmental Protection Agency 124. Available: https://www2.mst.dk/Udgiv/publications/2014/02/978-87-93178-07-6.pdf [Accessed 1 March 2020].

DARWESH, D. A. 2019. Heavy metals evaluation in soil of agricultural field around a pond of gas plant in the Kurdistan Region of Iraq. *ZANCO Journal of Pure and Applied Sciences,* 31**,** 28-35.

DUFFUS, J. 2002. Heavy metals" a meaningless term. IUPAC Technical Report). Pure App Chem. 74 (5), 793–807.

EC. 2009. *DIRECTIVE (2009)/48/EC of The European Parliament and the Council of the European Union on the safety of toys* [Online]. *Official Journal of the European Union,* L 170/1. Available: https://eur-lex.europa.eu/eli/dir/2009/48/oj [Accessed 1 Feb 2020].

EC. SCHER. 2016. *Final opinion on estimates of the amount of toy materials ingested by children* [Online]. Public Consultation on Toy Materials Ingested by Children: *Scientific Committee on Health and Environmental Risks*. Available: https://ec.europa.eu/health/scientific_committees/consultations/public_consultations/scher_consultation_10_fi [Accessed 20 Jan 2020].

EN. 71-3: 2013. *(British Standards) Safety of toys, Part 3: Migration of certain elements* [Online]. UK: British Standards Institution. Available: https://www.intertek.com/sparkles/2013/en-71-3-2013-published-in-uk/ [Accessed 13 Mar 2020].

EN. 71-3: 2006. *(British Standards) Safety of toys, Part 3: migration of certain elements* [Online]. European Committee of Standardization, Brussels. Available: https://issuu.com/fandomate/docs/en71-part3 [Accessed 20 Nov 2019].

ERBAS, Z., KARATEPE, A. & SOYLAK, M. 2017. Heavy metal contents of play dough, face and finger paint samples sold in turkish markets. *Talanta,* 170**,** 377-383.

GUNEY, M., NGUYEN, A. & ZAGURY, G. J. 2014. Estimating children's exposure to toxic elements in contaminated toys and children's jewelry via saliva mobilization. *Journal of environmental science and health, part A,* 49**,** 1218-1227.

GUNEY, M. & ZAGURY, G. J. 2012. Heavy metals in toys and low-cost jewelry: critical review of US and Canadian legislations and recommendations for testing. *Environmental science & technology,* 46**,** 4265-4274.

GUNEY, M. & ZAGURY, G. J. 2013. Contamination by ten harmful elements in toys and children's jewelry bought on the North American market. *Environmental science & technology,* 47**,** 5921-5930.

GUNEY, M. & ZAGURY, G. J. 2014a. Bioaccessibility of As, Cd, Cu, Ni, Pb, and Sb in toys and low-cost jewelry. *Environmental science & technology,* 48**,** 1238-1246.

GUNEY, M. & ZAGURY, G. J. 2014b. Children's exposure to harmful elements in toys and low-cost jewelry: characterizing risks and developing a comprehensive approach. *Journal of hazardous materials,* 271**,** 321-330.

HILLYER, M. M., FINCH, L. E., CEREL, A. S., DATTELBAUM, J. D. & LEOPOLD, M. C. 2014. Multi-technique quantitative analysis and socioeconomic considerations of lead, cadmium, and arsenic in children's toys and toy jewelry. *Chemosphere,* 108**,** 205-213.

ISMAIL, S. N. S., MOHAMAD, N. S., KARUPPIAH, K., ABIDIN, E. Z., RASDI, I. & PRAVEENA, S. M. 2017. Heavy metals content in low-priced toys. *JEAS,* 5**,** 1499-1509.

ISO. 8124-1. 2014. *Safety of Toys, Part 1: Safety aspects related to mechanical and physical properties* [Online]. ISO Technical Committee 181. Available: https://www.iso.org/standard/66626.html [Accessed 28 March 2020].

ISO. 8124-3. 2010. *Safety of Toys, Part 3: Migration of certain elements* [Online]. ISO Technical Committee 181. Available: https://www.iso.org/standard/43471.html [Accessed 28 March 2020].

ISSA, H. M. & ALSHATTERI, A. H. 2019. Second-Hand Infant Care Plastic Products Sold in Markets of Kalar City, Kurdistan Region, Iraq: Heavy Metals Contamination and Risk Assessment. *Journal of Garmian University,* 6**,** 8-17.

JÄRUP, L. 2003. Hazards of heavy metal contamination. *British medical bulletin,* 68**,** 167-182.

JÄRUP, L. & ÅKESSON, A. 2009. Current status of cadmium as an environmental health problem. *Toxicology and applied pharmacology,* 238**,** 201-208.

KAMETI, C. M. 2013. *Determination of lead and cadmium levels in decorative paints sold in Nairobi Kenya.* Master Thesis, Kenyatta University, Kenya.

KARAŚ, K. & FRANKOWSKI, M. 2018. Analysis of hazardous elements in children toys: Multi-elemental determination by chromatography and spectrometry methods. *Molecules,* 23**,** 1-17.

KIPPLER, M., TOFAIL, F., HAMADANI, J. D., GARDNER, R. M., GRANTHAM-MCGREGOR, S. M., BOTTAI, M. & VAHTER, M. 2012. Early-life cadmium exposure and child development in 5-year-old girls and boys: a cohort study in rural Bangladesh. *Environmental health perspectives,* 120**,** 1462-1468.

KORFALI, S. I., SABRA, R., JURDI, M. & TALEB, R. I. 2013. Assessment of toxic metals and phthalates in children's toys and clays. *Archives of environmental contamination and toxicology,* 65**,** 368-381.

KUDJOE GATI, L., BOKOR, L. & OFFOH, E. 2014. Assessment of level of lead and cadmium in selected plastic toys imported from china on the Ghanaian market. *Chem Mater Res,* 6**,** 62-68.

KUMAR, A. & PASTORE, P. 2007. Lead and cadmium in soft plastic toys. *Current Science***,** 818-822.

KUMAR DAS, S., SINGH GREWAL, A. & BANERJEE, M. 2011. A BRIEF REVIEW: HEAVY METAL AND THEIR ANALYSIS. *Organization,* 11**,** 13-18.

MARKOWITZ, M. 2000. Lead poisoning. *Pediatrics in Review,* 21**,** 327.

MARTIN, S. & GRISWOLD, W. 2009. Human health effects of heavy metals. *Environmental Science and Technology briefs for citizens,* 15**,** 1-6.

MILLER, G. Z. & HARRIS, Z. E. 2015. Hazardous metals in vintage plastic toys measured by a handheld X-ray fluorescence spectrometer. *Journal of Environmental health,* 77**,** 8-13.

OGILO, J., ONDITI, A., SALIM, A. & YUSUF, A. 2017. Assessment of Levels of Heavy Metals in Paints from Interior Walls and Indoor Dust from Residential Houses in Nairobi City County, Kenya. *Chemical Science International Journal***,** 1-7.

OYEYIOLA, A. O., AKINYEMI, M. I., CHIEDU, I. E., FATUNSIN, O. T. & OLAYINKA, K. O. 2017. Statistical analyses and risk assessment of potentially toxic metals (PTMS) in children's toys. *Journal of Taibah University for Science,* 11**,** 842-849.

SINDIKU, O. & OSIBANJO, O. 2011. Some priority heavy metals in children toy's imported to Nigeria. *J Toxicol Environ Health Sci [Internet],* 3**,** 109-15.

SOGUT, O. & EZER, M. 2017. DETERMINATION OF ELEMENTAL COMPOSITION OF VARIOUS CHILDREN'S PLAY DOUGH SAMPLES USING XRF SPECTROMETRY. *FRESENIUS ENVIRONMENTAL BULLETIN,* 26**,** 4277-4281.

TOLINS, M., RUCHIRAWAT, M. & LANDRIGAN, P. 2014. The developmental neurotoxicity of arsenic: cognitive and behavioral consequences of early life exposure. *Annals of global health,* 80**,** 303-314.

TURNER, A. 2018. Concentrations and migratabilities of hazardous elements in second-hand children's plastic toys. *Environmental science & technology,* 52**,** 3110-3116.

WHITESIDE, P. J. & MILNER, B. A. 1984. *Pye Unicam atomic absorption data book,* England, Pye Unicam Ltd.

ZANCO Journal of Pure and Applied Sciences
The official scientific journal of Salahaddin University-Erbil
https://zancojournals.su.edu.krd/index.php/JPAS

ISSN (print):2218-0230**, ISSN (online):** 2412-3986**, DOI: http://dx.doi.org/10.21271/zjpas**

RESEARCH PAPER

Optimization of biomass and some metabolites productivity of *Merismopedia tenuissima* and *Spirulina* (*Arthrospira*) *platensis* grown under stress conditions

Khalifa S.H. Eldiehy *[1], Mustafa A. Fawzy [2], Mohammed Rawway [1], Usama M. Abdul-Raouf [1]

[1]Botany and Microbiology Department, Faculty of Science, AL-Azhar University, Assiut 71524, Egypt
[2]Botany and Microbiology Department, Faculty of Science, Assiut University, Assiut, 71516 Egypt

A B S T R A C T:
The attention to using cyanobacteria as a nutrient supplement has increased due to their nutritional value and high bioactive metabolites contents. The reason behind designing such a study is to illustrate and clarify stress conditions effects like nitrogen and phosphorus supplementation and deficiency, salinity stress, and different pH values on the biomass, lipid, protein, amino acid, and carbohydrate productivities of *Merismopedia tenuissima* and *Spirulina* (*Arthrospira*) *platensis*. The obtained results revealed that an increase in sodium nitrate by 100% caused an improvement in biomass, protein, and amino acid's productivity of *S. platensis* and *M. tenuissima* by 7.02 % and 7.05, 9.2% and 47.5%, 11.8% and19.5, respectively while 100% nitrogen deficiency enhanced lipid productivity of *S. platensis* and *M. tenuissima* to 41% and 94%. Moreover, phosphorus limitation led to a reduction in biomass, protein, amino acid, and carbohydrate *S. platensis* to 24.3%, 21.1%, 43.3%, and 28.1%, respectively. However, phosphorus-free medium showed an increase in lipid productivity of *S. platensis* and *M. tenuissima* by 46.8% and 81.8%, respectively. The addition of 0.05 M NaCl concentration to *S. platensis* medium stimulates the biomass, protein, and carbohydrate productivity by 6%, 7.75%, and 18.1%, respectively, whilst, among all concentration, zero M NaCl (control) resulted in increasing biomass, protein, and amino acids, whilst, high concentration (0.3M) of NaCl enhanced lipid productivity to 125.9% and 153.5% at *S. platensis* and *M. tenuissima*, respectively. Applications of high alkalinity (pH 9) increased the productivities of all studied metabolites in *S. platensis* and reduction of all mention metabolites in *M. tenuissima*.

KEY WORDS: *Spirulina platensis*, *Merismopedia tenuissima*, Nutrients stress, pH, Metabolites, Productivity.
DOI: http://dx.doi.org/10.21271/ZJPAS.32.5.14
ZJPAS (2020), 32(5); 146-157.

1. INTRODUCTION:

Cyanobacteria, the blue-green algae, are gram-negative eubacteria widely distributed throughout the world. Besides the valuable metabolites produced by cyanobacteria, it represents a wide range of phytoplankton that helps in assessing the quality of the water system (Toma, 2019, Aziz and Yasin, 2019). Cyanobacteria are a treasure of valuable bioactive compounds where comprise high protein content, soluble, and non-soluble carbohydrates, lipids, mineral, antioxidant substances, and essentials vitamins essential and non-essential amino acids, the later have a feature of providing humans and animals with the essential one (Jung *et al.*, 2019). Because of its importance as a nutritional supplement and a fundamental source of food, cyanobacterial protein has gained global interest and consideration. Therefore, some *Spirulina* species (nowadays are named *Arthrospira*) for the high level of protein in addition to their fiber content, are being consumed as food supplements (Seghiri *et al.*, 2019). In general, cyanobacteria are rich of structurally novel and biologically active metabolites (De Morais *et al.*, 2015).

* **Corresponding Author:**
Khalifa, S.H. Eldiehy E-mail: khalifasaid@azhar.edu.eg
Article History:
Received: 01/05/2020
Accepted: 21/07/2020
Published: 13/10 /2020

Nowadays, the experimental trends are over-concerned with increasing the highly valuable compounds, and biomass contents using cultural stress strategies, manipulation the favorable conditions for the algae to grow and develop. Wherefore, as a kind of resistance, the algae either increase biomass or increase valuable metabolites. Among the stress strategies applied to microalgae cultures can be divided into two main groups: physical and nutrimental factors. The physical strategies are considered as variation in surrounding environmental parameter and operating conditions which overlap with the microalgae growth (pH, salinity, light intensities, an electromagnet), whilst nutrimental strategies are described as a change in the essential ingredients of culture growth media (nitrogen, phosphorus, carbon source, and iron deficiency). A recently conducted study has indicated that the phosphorus deficiency led to a remarkable improvement in the contents of carbohydrate and lipid of *Spirulina platensis* (Markou *et al.*, 2012). However, the productivity of carbohydrate and lipid contents in *Synechococcus* sp. PCC7942 has recorded an enhancement through increasing salinity concentration (Verma *et al.*, 2019). Setta *et al*. (2014) reported that the carbohydrate content was enhanced by more than 42% of dry weight under a nitrogen-free medium in *Synechococcus subsalsus*. The current study targeted isolating some cyanobacteria species from lakes and freshwater bodies of Assiut Governorate in Upper Egypt, and estimating the effects of manipulating the concentrations of phosphorus, nitrogen, and sodium chloride as well as different pH values on the biomass productivity and productivities of some metabolites of *S. platensis* and *M. tenuissima*.

2.MATERIALS AND METHODS

2.1. Isolation and Purification:

Cyanobacteria strains were isolated from aquatic habitats (freshwater bodies and lakes) in Assiut Governorate, Egypt (Figure 1). Isolation and purification of cyanobacterial species were done by common microbiological isolation methods through standard plating methods described by(Rippka, 1988), and identified as well as authenticated based on a standard manual (Prescott, 1959). Individual colonies were picked up under sterilized conditions and streaking at Petri dishes (9 cm diameter) containing a solidified medium. This was repeated until uni-algal colonies were established. Isolated and purified species of algae were cultured in Rippka modified medium (Rippka, 1992); (Table 1). *Merismopedia tenuissima* and *Spirulina platensis* were selected for this study based on their potential for biological activities (unpublished data). The purified *M. tenuissima* was inoculated into liquid Rippka, modified medium, and incubated under continuous illumination fluorescent light of 48.4 µmol.photon.m^{-2}.s^{-1} and 27±2ºC. The culture flasks were aerated with sterile air by using aquarium air pumps (3 W, Venus Aqua Air Pump Model AP-208 A, China). On the other hand, *S. platensis* was inoculated into liquid Zarrouk's medium (Zarrouk, 1966), and inoculated under the same mentioned conditions (Table 2).

Figure 1: Maps shows A: Map of Egypt, B: Map of Assiut Governorate and C: Sample collection sites (Googal Earth).

Figure 2: A photographic view of the cultivation cultures.

Table (1) Composition of liquid Rippka modified growth medium (Rippka, 1992).

Component	g/L
$NaNO_3$	1.5
K_2HPO_4	0.04
$MgSO_4.7H_2O$	0.075
$CaCl_2.2H_2O$	0.036
Citric acid	0.006
Ferric ammonium citrate	0.006
EDTA (disodium salt)	0.001
Na_2CO_3	0.02
Micronutrient solution (for 1 liter)	1 ml
H_3BO_3	2.86
$MnCl_2{\cdot}4H_2O$	1.81
$ZnSO_4{\cdot}7H_2O$	0.222
$NaMoO_4{\cdot}2H_2O$	0.39
$CuSO_4{\cdot}5H_2O$	0.079
$Co(NO_3)_2{\cdot}6H_2O$	0.049
Distilled water	1.0 L
PH to 7.1	

2.2 Algae strain and growth conditions

Cyanobacterial algae (*S. platensis* and *M. tenuissima*) were cultivated axenically as batch cultures in 500 ml Erlenmeyer flasks with Zarrouk's medium (Zarrouk, 1966) and Rippka modified medium (Rippka, 1992), respectively. Different nutrients effects, namely nitrogen [100% (2.5 and 1.5 g L^{-1}), - 50 % (1.25 and 0.75 gL^{-1}), -75%, (0.625 and 0.375 gL^{-1}), -100% (0 and 0 gL^{-1}) and +100% (5 and 3 gL^{-1}], phosphorus [100% (0.5 and 0.04 gL^{-1}), -50% (0.25 and 0.02 gL^{-1}), -75% (0.125 and 0.01 gL^{-1}), -100% (0 and 0 gL^{-1}) and +100% (1 and 0.08 gL^{-1}], sodium chloride [(control (0 g L^{-1}), 0.05M (2.92 gL^{-1}), 0.1M (5.84 gL^{-1}), 0.2M (11.68 gL^{-1}), 0.3M (17.52 gL^{-1})] and pH value [control (7), 5, 6, 8 and 9] on the growth, lipid, protein, amino acid and carbohydrate productivities of *S. platensis* and *M. tenuissima*, respectively, were studied (Figure 2).

2.3 Biomass assay

Two approaches were followed to monitor cyanobacterial growth, initially; a daily monitoring approach was done by using chlorophyll (A) according to Metzner *et al.* (1965), and optical density, according to Fatma *et al.* (1994), whilst the final approach was achieved through determining the cellular dry weight (CDW) after harvesting phase. The following equation illustrates the calculation of the productivity of biomass:

Biomass productivity (mg $CDWL^{-1}d^{-1}$) =

$$(CDW_L\text{-}CDW_E)/(t_L\text{-}t_E)$$

Where; CDW_E and CDW_L are representing the CDW (mgL^{-1}) at the start of the culture (t_E) and late exponential phase (t_L), respectively.

Table (2) Composition of Zarrouk's growth medium (Zarrouk, 1966).

Component	g/L
$NaHCO_3$	16.8
K_2HPO_4	0.5
$NaNO_3$	2.5
K_2SO_4	1.0
NaCl	1.0
$MgSO_4{\cdot}7H_2O$	0.2
$CaCl_2{\cdot}2H_2O$	0.04
$FeSO_4{\cdot}7H_2O$	0.01
$Na_2EDTA{\cdot}2H_2O$	0.08
Trace mineral mix A5	1.0 ml
H_3BO_3	2.86
$MnCl_2{\cdot}4H_2O$	1.81
$ZnSO_4{\cdot}7H_2O$	0.222
$NaMoO_4{\cdot}2H_2O$	0.39
$CuSO_4{\cdot}5H_2O$	0.079
$Co(NO_3)_2{\cdot}6H_2O$	0.0494
Distilled water	1.0 L
Trace mineral mix B6 Modified	1.0 ml
NH_4VO_3	0.23
$K_2Cr_2(SO_4)_4{\cdot}24H_2O$	0.096
$NiSO_4{\cdot}7H_2O$	0.0478
$Na_2WO_4{\cdot}2H_2O$	0.0179
$Ti_2(SO_4)_3$	0.04
Distilled water	1.0 L
pH to 9	

2.4. Estimation of total lipid:

The sulfophosphovanillin (SPV) technique was used to estimate the total lipid content (Drevon and Schmit, 1964).

2.5. Estimation of total protein:

The Lowry protein assay was used to measure the total protein, which is measured

spectrophotometrically at750 nm (Lowry *et al.*, 1951).

2.6 Estimation of total carbohydrate:

The anthrone-sulfuric acid technique described by Hedge and Hofreiter (1962)was used to determine the total carbohydrate content. Briefly, the processes of this method involve breaking down the polysaccharides using diluted HCL and turn them into simple sugar, which chemically interacts with anthrone-sulfuric acid as a result of this interaction a green color appears, which is measured spectrophotometrically at 630 nm. To specify the exact numeral values of the total carbohydrate, the calibration standard curve was prepared using glucose.

2.7. Estimation of free amino acids:

The ninhydrin method described by Lee and Takahashi (1966) was used to estimate free amino acids.

2.8. Productivities calculation

Productivities of lipid, protein, carbohydrate, and amino acid were calculated by:

Productivity ($mgL^{-1}d^{-1}$) = *Biomass productivity* × C_f

The abbreviation, C_f, is used to refer to amino acids, carbohydrates, lipids, or proteins' final contents.

2.9. Statistical Analysis

The data were obtained from four independent experiments and measured as a means±SE using Excel 2010 program. The statistical software SPSS (Version 16, Released 2007, SPSS Inc., Chicago, IL, USA) was applied to analyze the effect of various factors in this study. In the current study, the ANOVA table was consulted to determine significantly the various concentrations of different factors' effects on studied cyanobacterial metabolites. For comparison of the means, Duncan's multiple range tests ($p< 0.05$) were used.

3. RESULTS

In the initial work stage, from the three different freshwater bodies, samples were collected and eight genera (15 species) of cyanobacteria were identified (Table 3). Of cyanobacterial identified strains, two isolates viz., *S. platensis*, and *M. tenuissima* selected for this study based on their biological activity (unpublished data). The changes in growth patterns caused by applying different concentrations of nitrogen on the growth of *S. platensis* and *M. tenuissima* were recorded as Chlorophyll a (Chll a) and optical density for 10 days of incubation (Figure 3a, b, c, and d). The obtained results revealed that a decrease in sodium nitrate concentration led to a reduction in Chll a, optical density, and biomass productivity.

Table (3) List of cyanobacteria recorded (+) in water samples

Algal taxa	Water samples		
Cyanophyta	**S.1**	**S.2**	**S.3**
Chroococcus limneticus	+		
Chroococcus pallidus	+	+	+
Chroococcus sp.	+	+	
Chroococcus turgidus	+	+	+
Coelosphaerium sp.	+		+
Gomphosphaeria sp.		+	
Merismopedia convoluta	+	+	+
Merismopedia tenuissima	+	+	+
Microcystis aeruginosa	+	+	+
Microcystis sp.	+	+	+
Microcystis wesenbergii			+
Nostoc sp.	+		
Oscillatoria limosa		+	+
Oscillatoria sp.			+
Spirulina platensis			+

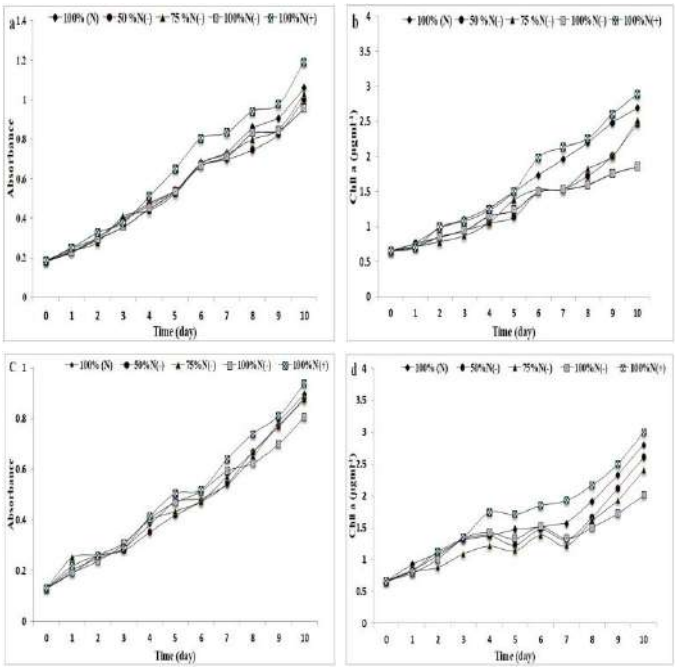

Figure 3: Effect of different concentrations of $NaNO_3$ on a) optical density of *S. platensis* b) chlorophyll a content of *S. platensis* c) optical density of *M. tenuissima* d) chlorophyll a content of *M. tenuissima*

Table (4) Effect of different nitrogen concentrations on biomass, lipids, proteins, amino acids, and carbohydrates productivities of *M. tenuissima* and *S. platensis*

		Productivities (mg/L/day)				
		Biomass	**Lipids**	**Proteins**	**Amino acids**	**Carbohydrates**
Merismopedia tenuissima	**100% N(C)**	61.53±3.34^{b}	5.35±0.43^{a}	4.25±0.3^{b}	1.79±0.12^{bc}	1.49±0.09^{a}
	50% N (-)	46.76±2.66^{a}	8.92±0.60^{b}	2.79±0.30^{a}	1.36±0.09^{b}	2.19±0.32^{a}
	75% N (-)	44.76±7.72^{a}	10.11±1.9^{b}	3.42±0.6^{ab}	1.48±0.24^{b}	1.82±0.33^{a}
	100% N (-)	38.76±3.62^{a}	10.38±1^{b}	3.18±0.2^{ab}	0.68±0.09^{a}	1.52±0.10^{a}
	100% N(+)	65.87±3.86^{b}	5.28±0.50^{a}	6.27±0.43^{c}	2.14±0.20^{c}	1.44±0.12^{a}
Spirulina platensis	**100% N(C)**	68.17±0.6^{bc}	8.39±0.10^{a}	10.9±0.2^{cd}	5.15±0.07^{c}	2.99±0.09^{b}
	50% N (-)	62.75±1.4^{ab}	9.35±0.12^{b}	7.77±0.38^{a}	3.84±0.47^{b}	1.41±0.07^{a}
	75% N (-)	59.79±2.87^{a}	9.71±0.24^{b}	8.65±0.6^{ab}	4.84±0.50^{bc}	1.75±0.22^{a}
	100% N (-)	56.13±1.56^{a}	11.83±0.4^{c}	9.8±0.23^{bc}	2.74±0.03^{a}	1.42±0.05^{a}
	100% N(+)	72.96±4.12^{c}	8.27±0.13^{a}	11.9±0.3^{d}	5.76±0.34^{c}	3.87±0.24^{c}

The data are given as averages of three replicates ± standard error. Values in each rows with different letters are significantly different at P≤0.05. Values in rows with same letters are not significantly different.

Table (5) Effect of different phosphorus concentrations on biomass, lipids, proteins, amino acids, and carbohydrates productivities of *Merismopedia tenuissima* and *Spirulina platensis*

		Productivities (mg/L/day)				
		Biomass	**Lipids**	**Proteins**	**Amino acids**	**Carbohydrates**
Merismopedia tenuissima	**100% P(C)**	66.42±6.8^{ab}	6.54±0.79^{a}	7.87±0.89^{b}	2.40±0.26^{b}	1.92±0.26^{a}
	50% P (-)	55.53±8.6^{ab}	9.67±1.87^{ab}	5.34±0.12^{a}	1.83±0.28^{ab}	2.50±0.11^{a}
	75% P (-)	52.20±8^{ab}	11.04±1.69^{b}	6.02±0.92^{ab}	1.79±0.29^{ab}	2.02±0.29^{a}
	100% P (-)	50.31±1.3^{a}	11.89±0.94^{b}	6.40±0.72^{ab}	1.13±0.02^{a}	2.10±0.38^{a}
	100%P (+)	70.53±1^{b}	5.97±0.44^{a}	9.85±0.15^{c}	3.22±0.23^{c}	1.90±0.07^{a}
Spirulina platensis	**100% P(C)**	73.3±4.38^{bc}	8.36±0.36^{a}	11.20±0.5^{b}	6.23±0.35^{c}	2.99±0.22^{c}
	50% P (-)	69.04±1.1^{b}	9.86±0.21^{b}	8.48±0.13^{a}	4.34±0.38^{ab}	1.23±0.09^{a}
	75% P (-)	61.42±1.6^{a}	10.34±0.31^{b}	8.72±0.40^{a}	4.97±0.33^{bc}	2.30±0.26^{b}
	100% P (-)	55.50±1.5^{a}	12.27±0.08^{c}	8.84±0.27^{a}	3.53±0.55^{a}	2.15±0.19^{b}
	100%P (+)	78.17±1.5^{c}	8.60±0.13^{a}	12.35±0.5^{b}	8.17±0.39^{d}	3.77±0.11^{d}

The data are given as averages of three replicates ± standard error. Values in each rows with different letters are significantly different at P≤0.05. Values in rows with same letters are not significantly different.

The most pronounced reduction in biomass productivity of *S. platensis* and *M. tenuissima* amounted to17.7% and 37%, respectively, at a 100% decrease in $NaNO_3$ (Table4). On the other hand, the biomass productivity was increased when cultured under testing has grown in a 100 % increase of nitrogen. The present study has proven that nitrogen starvation causes an increase in lipid productivity. The most distinct increase in lipid productivity of *S. platensis* and *M. tenuissima* were observed at a 100% decrease in $NaNO_3$, which amounted to 41 %, 94 %, respectively, compared to control (Table 4). However, the increase in nitrogen concentration by 100% decreased the lipid productivity of *S. platensis* and *M. tenuissima* by 1.4%, 1.3%, respectively. Increasing nitrogen concentration by 100% resulted in an increase of protein and amino acid productivities by 9.17%, 47.5%, and 11.8%,

19.5% in *S. platensis*, and *M. tenuissima*, respectively, whilst, the decrease in sodium nitrate led to a reduction in protein and amino acid productivities (Table 4). The increase or decrease of nitrogen concentration was not dependent on the carbohydrate productivity of *M. tenuissima.* In contrast, the carbohydrate productivity of *S. platensis* significantly increased to 29.4% under nitrogen-rich conditions (Table 4).

The changes in growth patterns caused by applying different concentrations of phosphorus on the growth of *S. platensis* and *M. tenuissima* that recorded as Chll a and optical density were studied for 10 days of incubation (Figure 4a, b, c, and d). The results in this study cleared that a decrease in phosphorus concentration led to a reduction in Chll a and optical density as well as biomass productivity.

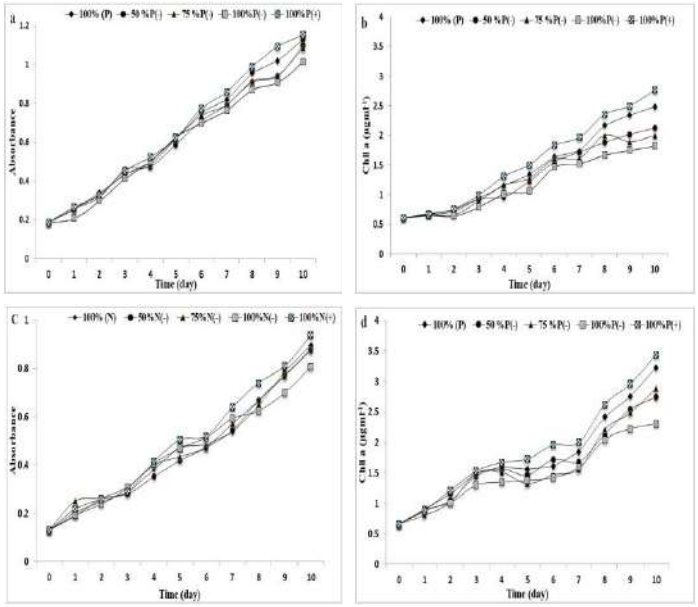

Figure 4: Effect of different concentrations of KH_2PO_4 on a) optical density of *S. platensis* b) chlorophyll a content of *S. platensis* c) optical density of *M. tenuissima* d) chlorophyll a content of *M. tenuissima*

The reduction in biomass productivity amounted to 24.28 and 24.25% in *S. platensis*, and *M. tenuissima*, respectively at a 100% decrease in phosphorus (Table 5). However, no significant change in biomass productivity when grown in a 100% increase in phosphorus concentration. Phosphorus free medium led to the enhancement of the productivity of lipid in *S. platensis*, and *M. tenuissima* by 46.8%, 81.8% respectively. On the other side, no significant effect appeared when an application of a high concentration of K_2HPO_4 (+100 %). Increasing phosphorus concentration by 100% resulted in an increase of protein and amino acid productivities by 10.2%, 25.1%, and 31.1, 34.1%% in *S. platensis*, and *M. tenuissima*, respectively.

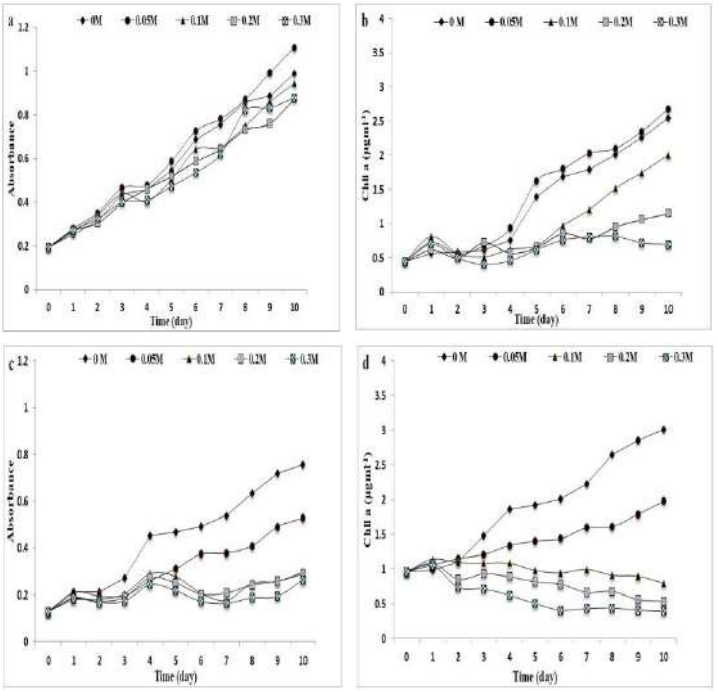

Figure 5: Effect of different concentrations of NaCl on a) optical density of *S. platensis* b) chlorophyll a content of *S. platensis* c) optical density of *M. tenuissima* d) chlorophyll a content of *M. tenuissima*

Whereas, when the *S. platensis* cultures were experienced to free phosphorus concentrations, the productivity of protein and the amino acid was put down by 21% and 43.3%, respectively, while phosphorus depletion resulted in shifting down amino acid productivity by 52.9% comparing to control.

The salinity effects on the growth pattern of *S. platensis* and *M. tenuissima* for 10 days of incubation are illustrated in Figure (5a, b, c, and d)**.** Results indicated that a remarkable increase in Chll a and optical density as well as biomass productivity of *S. platensis* and *M. tenuissima* at 0.05 M NaCl and zero M NaCl, respectively. High salinity concentrations (0.1, 0.2, and 0.3 M) significantly decreased biomass productivity (Table 6). The obtained results clarified that the increase in NaCl concentration increases the productivity of lipids (Table 6). At 0.3 M NaCl, *S. platensis* and *M. tenuissima* showed the most

pronounced increase in lipid productivity amounted to 125.9% and 153.5%, respectively.

Table (6) Effect of different sodium chloride concentrations on biomass, lipids, proteins, amino acids, and carbohydrates productivities of *M. tenuissima* and *S. platensis*

		Productivities (mg/L/day)				
	NaCl (M)	Biomass	Lipids	Proteins	Amino acids	Carbohydrates
Merismopedia tenuissima	**C. (0)**	75.09±2.39^{c}	4.26±0.28^{a}	6.51±1.5^{b}	2.07±0.13^{c}	0.62±0.09^{a}
	0.05	73.09±2.35^{c}	5.16±0.14^{a}	3.0±0.28^{a}	1.74±0.03^{bc}	0.82±0.09^{ab}
	0.1	62.53±0.77^{b}	6.74±0.41^{b}	2.87±0.7^{a}	1.38±0.001^{bc}	0.85±0.18^{ab}
	0.2	52.79±0.97^{a}	9.06±0.29^{c}	1.35±0.2^{a}	0.89±0.15^{a}	0.96±0.03^{ab}
	0.3	48.09±0.56^{a}	10.8±0.38^{d}	1.8±0.04^{a}	0.88±0.21^{a}	1.03±0.09^{b}
Spirulina platensis	**C. (0)**	86.8 ±0.7^{c}	5.18±0.34^{a}	12.9±0.5^{c}	7.26±0.05^{c}	3.14±0.05^{c}
	0.05	92±1.2^{c}	6.56±0.20^{ab}	13.9±0.3^{c}	7.52±0.06^{c}	3.71±0.31^{d}
	0.1	71.33±8.98^{b}	8.01±1.13^{bc}	9.02±0.5^{b}	5.50±0.74^{b}	2.53±0.15^{b}
	0.2	51.58±3.10^{a}	9.36±0.48^{c}	5.1±0.58^{a}	2.64±0.25^{a}	1.99±0.12^{ab}
	0.3	46.50±0.38^{a}	11.7±0.05^{d}	4.56±0.2^{a}	2.76±0.03^{a}	1.89±0.13^{a}

The data are given as averages of three replicates ± standard error. Values in each rows with different letters are significantly different at P≤0.05. Values in rows with same letters are not significantly different.

The protein and amino acid productivities were decreased with increasing salt concentration; the high concentration (0.3M) of NaCl resulted in 64.6%, 72.3%, and 62%, 57.4% reduction in protein, and amino acid productivity of *S. platensis* and *M. tenuissima*, respectively (Table 6). Moreover, promoting medium with 0.05 M NaCl concentration stimulates the carbohydrate productivity of *S. platensis* by 18.1%, whilst, application of 0.3 M NaCl concentration stimulates the carbohydrate productivity of *M. tenuissima* by 66.1%.

Table (7) Effect of different pH values on biomass, lipids, proteins, amino acids, and carbohydrates productivities of *Merismopedia tenuissima* and *Spirulina platensis*

		Productivities (mg/L/day)				
		Biomass	Lipids	Proteins	Amino acids	Carbohydrates
Merismopedia tenuissima	**C. (7)**	94.76±1.93^{c}	10.9±0.27^{a}	5.9±0.30^{b}	2.20±0.24^{d}	1.83±0.21^{a}
	5	73.20±6.74^{a}	9.65±0.95^{a}	7.96±0.31^{c}	1.15±0.10^{a}	1.89±0.11^{a}
	6	93.87±0.84^{bc}	9.65±0.38^{a}	7.81±0.16^{c}	1.86±0.03^{cd}	2.42±0.42^{a}
	8	82.09±3.95^{ab}	8.22±0.61^{a}	6.75±0.38^{b}	1.62±0.07^{bc}	2.08±0.13^{a}
	9	72.64±2.70^{a}	8.14±1.40^{a}	4.71±0.34^{a}	1.35±0.10^{ab}	1.83±0.52^{a}
Spirulina platensis	**C. (7)**	66±9.89^{a}	10±0.24^{bc}	8.92±0.07^{a}	5.95±0.03^{ab}	1.60±0.06^{a}
	5	62.17±0.44^{a}	5.71±0.26^{a}	10.1±0.43^{ab}	3.68±0.21^{a}	1.60±0.13^{a}
	6	69.58±2.72^{ab}	7.4±0.56^{ab}	12.1±0.4^{abc}	4.47±0.67^{a}	2.24±0.04^{ab}
	8	75.88±1.09^{ab}	11.1±0.19^{c}	13.7±0.34^{bc}	8.19±0.10^{bc}	2.92±0.28^{bc}
	9	84±0.89^{b}	13.4±2.27^{c}	15.1±2.37^{c}	8.59±1.50^{c}	3.03±0.40^{c}

The data are given as averages of three replicates ± standard error. Values in each rows with different letters significantly different at P≤0.05. Values in rows with same letters are not significantly different.

The data in table 7 and Figure (6 a, b, c, and d) shows that the best-suited pH value for the growth of *S. platensis* and *M. tenuissima* was 9 and 7, respectively, with a noticeable enhancement in the productivity of biomass. The alkaline pH value (pH 9) significantly increases the lipid, protein, amino acids and carbohydrate productivities in *S.*

platensis by 34%, 69.3%, 44.4% and 89.4 respectively and decrease protein and amino acids productivities in *M. tenuissima* by 20.2% and 38.6% (Table 7). However, the lipid and carbohydrate productivities in *M. tenuissima* are pH-independent, which means increasing or decreasing the value of the pH does not affect the increased lipid and carbohydrate.

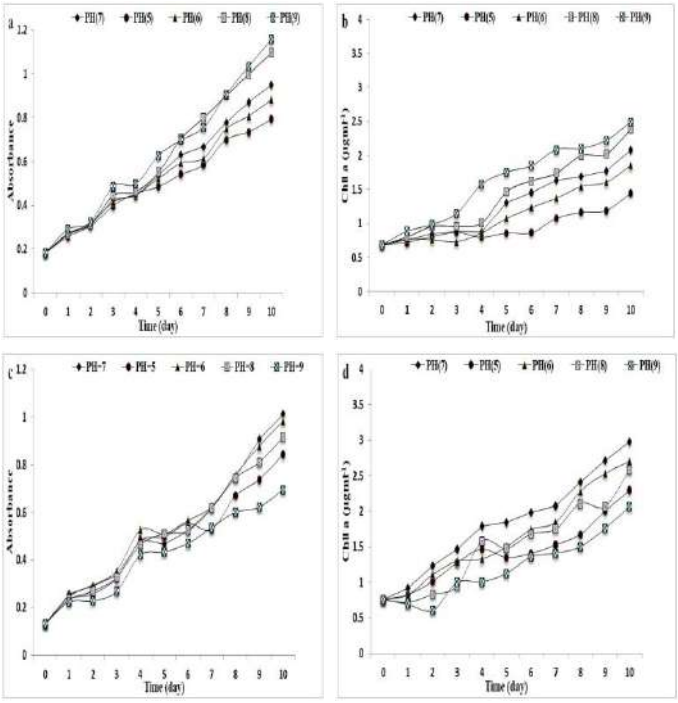

Figure 6: Effect of different pH values on a) optical density of *S. platensis* b) chlorophyll a content of *S. platensis* c) optical density of *M. tenuissima* d) chlorophyll a content of *M. tenuissima*

The increase and decrease of phosphorus concentration showed consistency in carbohydrate productivity of *M. tenuissima*, whilst, the culture of *S. platensis* grown in phosphorus limitation of K_2HPO_4 resulted in a decrease in carbohydrate productivity, furthermore, the 50% decrease in phosphorus concentration was followed by a reduction in productivity of carbohydrate by 58.9%, compared to the control. The most distinct increase in carbohydrate productivity was observed at a 100% increase in K_2HPO_4 amounted to 26.1% (Table5).

4. DISCUSSION

Cyanobacteria have gained importance as human food and pharmaceutical agent because it is rich with vitamins, protein, essential fatty acids carotenoids, lipids, and carbohydrates (De Morais *et al*., 2015); so many studies were established to optimize these critical compounds production. The previously mentioned experiment resulted that the concentrations of sodium nitrate inversely proportionate to the productivity of biomass and the growth parameters of the investigated strains. The same findings are recorded by Hifney *et al*. (2013), who observed completely removed nitrogen sources from medium caused a severe drop in the biomass of *Spirulina* sp. Yang *et al*. (2018) also observed that nitrogen-deficient conditions decreased the growth pattern for *Chlamydomonas reinhardtii*. Moreover, Menegol *et al*. (2017) noticed a reduction in algal biomass of *Heterochlorella luteoviridis* under low nitrate concentration. However, the biomass productivity of studied strains was improved when cultured under nitrogen enrichment conditions. It has been authorized that higher levels of nitrogen affect positively on the growth of cyanobacteria (Jonte *et al.*, 2013). Nitrogen has an influential role in the metabolism of fatty acids and lipids existing in different kinds of microalgae. Furthermore, as nitrogen is easily manipulated and cheap compared to other factors, it is intensively used for enhancing the lipid accumulation, which is used as a feedstock for biofuel production.

In the current study, nitrogen starvation caused an increase in lipid productivity of the studied cyanobacteria. This finding is in accordance with the observation of Fawzy, (2017) who noticed that the deficiency of nitrogen enriched the lipid content and productivity of *Asteromonas gracilis* by (29.26 % and 10.21 $mgl^{-1}d^{-1}$, respectively. Also, Yeesang and Cheirsilp (2011) reported that under nitrogen-starvation conditions, the lipid accumulation of microalgae increases as a result of their ability to store energy in form lipids, which serves as an essential carbon source, helping them to resist such conditions. On the other hand, De Bhowmick *et al*. (2015) reported that under nitrogen depletion conditions, the increase in the lipid content occurs as a result of the activation of acyl hydrolase, a decrease in the cellular content of the thylakoid membrane and stimulation of phospholipids hydrolysis. In the current study, the increase in nitrogen

concentration resulted in decreased lipid productivity of the studied cyanobacteria. The same findings are recorded by sassano *et al*. (2010), who recorded the negative effect of nitrogen-rich medium on the accumulation of lipids in the case of *Arthrospira platensis* . The supplementation of medium with 100% $NaNO_3$ followed by a remarkable enhancement in the productivity of amino acid and protein in the studied strains. An increase in biomass and protein production by increasing nitrogen concentration has been widely supported by various reports from *S. platensis* (Colla *et al.*, 2007), *Dunaliella viridis* (Loaiza *et al.*, 2010), and *Chlorella vulgaris* (Neha and Khan, 2016).

On the other hand, the decrease in sodium nitrate led to a reduction in protein and amino acid productivities. These findings were in correspondence to the results of Uslu *et al*. (2011) who studied the effects of nitrogen deficiency on the protein content of *Spirulina* cultivated on Zarrouk medium and recorded 67, 54, 6% of cellular dry weight protein for groups of control, 50% and 100% deficient nitrogen, respectively. The possible reason behind a decrease in protein contents in these conditions is that the cells might have neutralized intracellular nitrogen quota for their normal metabolic function through degrading the nitrogenous compounds (Imran *et al.*, 2014). Nitrogen and phosphorus play a critical role in most processes of cell metabolism, as the nitrogen contributes to structural, functional, and cellular processes of living cells while phosphorus plays a crucial role in energy transfer, signal transduction, respiration, photosynthesis, and macromolecular biosynthesis (Minhas *et al.*, 2016). Therefore, the manipulating in the concentration of nitrogen or phosphorus directly affects the biomass, the lipid content, and other metabolites.

The results in this study cleared that, a decrease in phosphorus concentrations led to a reduction in Chll a and biomass productivity of cyanobacterial species. The same results were also recorded in *Arthrospira platensis* cultured at very low phosphorus concentration in batch culture (Markou *et al*., 2012). From a different perspective, no significant change in biomass productivity was noticed when grown in a 100 % increase in phosphorus concentration. Similar results were reported by El-Shouny *et al*. (2015) who examined the effects of phosphorus concentration on biomass production content of *Arthrospira platensis* and recorded that, the increase of phosphorus concentration up to 50% and 100% didn't show any significant change in biomass production. The obtained data cleared that, in general, the phosphorus depletion led to an improvement in the lipid content and productivity of all studied cyanobacteria. However, the increase of phosphorus concentrations caused a non-significant reduction in lipid content and productivity of all studied cyanobacteria. Xin *et al*. (2010) noticed that by the time phosphorus concentration reduces from 2.0 to 0.1 mgl^{-1}, the lipid content of *Scenedesmus* sp. improves from 23 % to 53 %. In general terms, under nutrient limitation, microalgae accumulate lipids when photosynthesis process conditions such as carbon source (CO_2), energy source (light), and cellular mechanisms for this process are available (Courchesne *et al.*, 2009). The obtained results revealed that a decrease in phosphorus concentrations led to a decrease in protein productivity by all studied cyanobacteria. In this respect, Wang *et al*. (2018) observed that the limitation of phosphorus accessibility caused the soluble protein to decrease. They attributed the previously mentioned decrease to the repression of nonessential proteins' synthesis due to the affectation of the enzymes responsible for protein synthesis under these circumstances.

The current study revealed that high salinity concentrations significantly decreased biomass productivity. This observation is parallels the results of Hu *et al*. (2014), who illustrated that the biomass and Chll a production of *Scytonema javanicum* was reduced when exposed to high NaCl concentration. In an excessive salinity condition, the toxic ionic stress and salt osmotic cause the reduction of photosynthetic rate, which in turn will cause a decrease in chlorophyll contents (Moradi and Ismail, 2007). Wang *et al*.(2010, 2011)suggested that salinity stress may inhibit electron transport at the PSII donor site. In general, the high concentration of NaCl (0.3 M) caused a remarkable reduction in protein content and the productivity of all studied strains. Kirroliaa *et al*. (2011) clarified that the shortage in protein and chlorophyll contents is a direct outcome of cultivating the *Scenedesmus quadricauda* under intensive salinity concentration. Under the same conditions, a similar result in *Anabaena cylindrica* was observed (Sheikh *et al.*, 2006). The most

pronounced increase in lipid productivity for *S. platensis* and *M. tenuissima* was recorded at 0.3 M NaCl. This finding is in accordance with the findings of Church *et al*. (2017), who reported that the increase in total lipid content of *Chlorella vulgaris* from 11.5% to 16.1% when the culture under salinity stress. The carbohydrate content was enhanced by the treatment with different NaCl concentrations. The distinguished enhancement of carbohydrate synthesis was achieved in *Scenedesmus quadricauda* under stress conditions (Kirrolia *et al*., 2011). Gill *et al*. (2002) explained that during stress conditions and reproduction, the soluble carbohydrate is the key to the osmotic regulation of cells. The increase in the sugar content may be an adaptive measure under salinity conditions.

For maintaining the internal pH necessary for cell function, the cell consumes energy at high or low pH (Rai and Rajashekhar, 2016). The flourishing of cyanobacteria species is pH dependence; it has been suggested that pH can affect Chll a and biomass productivity of cyanobacteria. In acidic as well as alkaline conditions, the cultures of tested algae were able to grow, but the most appropriate pH value, which is needed for *M. tenuissima*, and *S. platensis* to grow were 7 and 9, respectively. According to former studies, the most suitable pH for cyanobacteria growth fluctuates from 7.4 to 8.0 (Thingujam *et al.*, 2016). Besides the ability of cyanobacteria to grow in a neutral medium, it can survive in a wide range of uncertain pH conditions (Burja *et al.*, 2002). Thornton (2009) indicated that the acidic environment caused the reduction in the efficiency rate of photosynthesis of *Chaetoceros muelleri*, while when the pH value is between 7.4 to 8.2 could not hold any reduction in the growth rate of diatom; rather at pH 6.8, the growth rate was remarkably decreased. The enhancement of triacylglycerol (TAG) accumulation and the reduction in membrane lipids of *Chlorella* CHLOR1 were achieved under alkaline pH stress without significant effect by carbon and nitrogen limitations (Sharma *et al.*, 2012). Based on morphological observations, alkaline pH inhibited the growth of microalgae, thus diverting the energy to form TAG. Change in pH facilitates changes in the net charge of the protein and also affects the partitioning behavior of the protein (Waghmare *et al.*, 2016).

5. CONCLUSION

In the current study, the protein, biomass, lipid, amino acid, and carbohydrate productivity of *S. platensis* and *M. tenuissima* grown under stress conditions was analyzed. In general, biomass productivity was passively affected by stress conditions. The best-suited pH value for the maximum biomass, protein, amino acids, and carbohydrate productivity of *S. platensis* was 9 with an increase of 27.3%, 69.3%, 44.4%, and 89.4, respectively compared to the control and other treatments. Whereas the treatment of *S. platensis* and *M. tenuissima* with high salinity concentration (0.3M NaCl) resulted in the highest lipid productivity amounted to 125.9% and 153.5%, respectively.

Conflict of interest:
The authors declare no conflict of interest.

REFERENCES

Aziz, F. H. and Yasin, S. A. 2019. Twenty-five new records of algae in eight artificial fish ponds in Erbil. *ZANCO Journal of Pure and Applied Sciences*, 31**,** 153-166.

Burja, A., Abou-Mansour, E., Banaigs, B., Payri, C., Burgess, J. and Wright, P. J. 2002. Culture of the marine cyanobacterium, *Lyngbya majuscula* (Oscillatoriaceae), for bioprocess intensified production of cyclic and linear lipopeptides. *Journal of microbiological methods*, 48**,** 207-219.

Church, J., Hwang, J.-H., Kim, K.-T., McLean, R., Oh, Y.-K., Nam, B., Joo, J. C. and Lee, W. H. 2017. Effect of salt type and concentration on the growth and lipid content of *Chlorella vulgaris* in synthetic saline wastewater for biofuel production. *Bioresource technology*, 243**,** 147-153.

Colla, L. M., Reinehr, C. O., Reichert, C., Costa, J. and Alberto, V. 2007. Production of biomass and nutraceutical compounds by *Spirulina Platensis* under different temperature and nitrogen regimes. *Bioresource technology*, 98**,** 1489-1493.

Courchesne, N. M. D., Parisien, A., Wang, B. and Lan, C. Q. 2009. Enhancement of lipid production using biochemical, genetic and transcription factor engineering approaches. *Journal of biotechnology*, 141**,** 31-41.

De Bhowmick, G., Koduru, L. and Sen, R. 2015. Metabolic pathway engineering towards enhancing microalgal lipid biosynthesis for biofuel application—a review. *Renewable Sustainable Energy Reviews*, 50**,** 1239-1253.

De Morais, M. G., Vaz, B. d. S., de Morais, E. G., Costa, J. and Alberto, V. 2015. Biologically active metabolites synthesized by microalgae. *BioMed research international,* 2015**,** 1-15.

Drevon, B. and Schmit, J. 1964. La réaction sulfophosphovanillique dans l'étude des lipides sériques. *Bull. Trav. Soc. Pharm. Lyon,* 8**,** 173-178.

El-Shouny, W., Sharaf, M., Abomohra, A. and Abo-Eleneen, M. 2015. Production enhancement of some valuable compounds of *Arthrospira Platensis* . *Journal of Basic Environmental Sciences,* 2**,** 74-83.

Fatma, T., Sarada, R. and Venkataraman, L. 1994. Evaluation of selected strains of Spirulina for their constituents. *Phykos,* 33**,** 89-97.

Fawzy, M. A. 2017. Fatty acid characterization and biodiesel production by the marine microalga *Asteromonas gracilis*: statistical optimization of medium for biomass and lipid enhancement. *Marine Biotechnology,* 19**,** 219-231.

Gill, P. K., Sharma, A. D., Singh, P. and Bhullar, S. S. 2002. Osmotic stress-induced changes in germination, growth and soluble sugar content of Sorghum bicolor (L.) Moench seeds. *Bulgarian Journal of Plant Physiology,* 28**,** 12-25.

Hedge, J. and Hofreiter, B. 1962. Determination of reducing sugars and carbohydrates. *In:* WHISTLER, R. L. A. W., M.L. (ed.) *Methods in Carbohydrate Chemistry.* New York: Academic Press.

Hifney, A. F., Issa, A. A. and Fawzy, M. A. 2013. Abiotic stress induced production of β-carotene, allophycocyanin and total lipids in *Spirulina* sp. *Journal of Biology and Earth Science,* 3**,** 54-64.

Hu, J., Jin, L., Wang, X., Cai, W., Liu, Y. and Wang, G. 2014. Response of photosynthetic systems to salinity stress in the desert cyanobacterium *Scytonema javanicum*. *Advances in Space Research,* 53**,** 30-36.

Imran, R., Hamid, A., Amjad, R., Chaudhry, C., Yaqub, G. and Akhtar, S. 2014. Evaluation of heavy metal concentration in the poultry feeds. *Journal of Biodiversity,* 5**,** 394-404.

Jonte, L., Rosales-Loaiza, N., Bermúdez-González, J. and Morales, E. 2013. Urea fed-batch cultures of the cyanobacterium *Phormidium* sp. as a function of the salinity and age of cultures. *Revista Colombiana de Biotecnología,* 15**,** 38-46.

Jung, F., Krüger-Genge, A., Waldeck, P. and Küpper, J.-H. 2019. *Spirulina Platensis* , a super food? *Journal of Cellular Biotechnology,* 5**,** 43-54.

Kirrolia, A., Bishnoi, N. and Singh, N. 2011. Salinity as a factor affecting the physiological and biochemical traits of *Scenedesmus quadricauda*. *Journal of Algal Biomass Utilization,* 2**,** 28-34.

Lee, Y. P. and Takahashi, T. 1966. An improved colorimetric determination of amino acids with the use of ninhydrin. *Analytical biochemistry,* 14**,** 71-77.

Loaiza, N. R., Avendaño, D., Otero, A. and Morales, E. 2010. Crecimiento, producción de pigmentos y proteínas de la microalga *Dunaliella viridis* (Chlorophyta) en cultivos semicontinuos. *Boletín del Centro de Investigaciones Biológicas,* 42.

Lowry, O. H., Rosebrough, N. J. and Farr, A. L. 1951. Randall RJ. Protein measurement with the Folin phenol reagent. *Journal of Biological Chemistry,* 193**,** 265-271.

Markou, G., Chatzipavlidis, I. and Georgakakis, D. 2012. Carbohydrates production and bio-flocculation characteristics in cultures of *Arthrospira* (*Spirulina*) *Platensis* : improvements through phosphorus limitation process. *BioEnergy research,* 5**,** 915-925.

Menegol, T., Diprat, A. B., Rodrigues, E. and Rech, R. 2017. Effect of temperature and nitrogen concentration on biomass composition of *Heterochlorella luteoviridis*. *Food Science,* 37**,** 28-37.

Metzner, H., Rau, H. and Senger, H. 1965. Untersuchungen zur synchronisierbarkeit einzelner pigmentmangel-mutanten von Chlorella. *Planta,* 65**,** 186-194.

Minhas, A. K., Hodgson, P., Barrow, C. J. and Adholeya, A. 2016. A review on the assessment of stress conditions for simultaneous production of microalgal lipids and carotenoids. *Frontiers in microbiology,* 7**,** 546.

Moradi, F. and Ismail, A. M. 2007. Responses of photosynthesis, chlorophyll fluorescence and ROS-scavenging systems to salt stress during seedling and reproductive stages in rice. *Annals of botany,* 99**,** 1161-1173.

Neha, K. and Khan, S. 2016. Effect of nitrogen, phosphorus concentrations, pH and salinity ranges on growth, biomass and lipid accumulation of *Chlorella vulgaris*. *International Journal of Pharmaceutical Sciences,* 7**,** 397-405.

Prescott, G. 1959. How to Know the Fresh Water Algae, Vol. 1. Cranbrook press, Michigan.

Rai, S. V. and Rajashekhar, M. 2016. Effect of pH, salinity and temperature on the growth of six species of cyanobacteria isolated from Arabian Sea coast of Karnataka. *International Journal of Biosciences,* 9**,** 1.

Rippka, R. 1988. Isolation and purification of cyanobacteria. *Methods in enzymology,* 167**,** 3-27.

Rippka, R. 1992. Pasteur culture collection of cyanobacterial strains in axenic culture. *Catalogue,* 1**,** 1-103.

Sassano, C., Gioielli, L., Ferreira, L., Rodrigues, M., Sato, S., Converti, A. and Carvalho, J. 2010. Evaluation of the composition of continuously-cultivated *Arthrospira* (*Spirulina*) *Platensis* using ammonium chloride as nitrogen source. *Biomass & BioEnergy research,* 34**,** 1732-1738.

Seghiri, R., Kharbach, M. and Essamri, A. 2019. Functional composition, nutritional properties, and biological activities of Moroccan Spirulina microalga. *Journal of Food Quality,* 2019.

Setta, B. R., Barbarino, E., Passos, F. B. and Lourenço, S. O. 2014. An assessment of the use fulness of the cyanobacterium *Synechococcus subsalsus* as a source of biomass for biofuel production. *Latin American Journal of Aquatic Research,* 42**,** 364-375.

Sharma, K. K., Schuhmann, H. and Schenk, P. M. 2012. High lipid induction in microalgae for biodiesel production. *Energies,* 5**,** 1532-1553.

Sheikh, T., Baba, Z. and Sofi, P. 2006. Effect of NaCl on growth and physiological traits of *Anabaena cylindrica* L. *Pakistan Journal of Biological Sciences,* 9**,** 2528-2530.

Thingujam, I., Keithellakpam, O. S., Oinam, A. S., Oinam, G., Nath, T. O. and Dutt, S. G. 2016. Optimization of Chlorophyll a Production of Some Cyanobacteria from Rice Paddies in Manipur, India Through Nutritional and

Environmental Factors. *Philippine Journal of Science,* 145**,** 373-383.

Thornton, D. C. 2009. Effect of low pH on carbohydrate production by a marine planktonic diatom (*Chaetoceros muelleri*). *International Journal of Ecology,* 2009.

Toma, J. J. 2019. Algae as indicator to assess trophic status in Dokan Lake, Kurdistan region of Iraq. *ZANCO Journal of Pure and Applied Sciences,* 31**,** 57-64.

Uslu, L., Içik, O., Koç, K. and Göksan, T. 2011. The effects of nitrogen deficiencies on the lipid and protein contents of *Spirulina Platensis* . *African Journal of Biotechnology,* 10**,** 386-389.

Verma, E., Singh, S. and Mishra, A. 2019. Salinity-induced oxidative stress-mediated change in fatty acids composition of cyanobacterium *Synechococcus* sp. PCC7942. *International Journal of Environmental Science,* 16**,** 875-886.

Waghmare, A. G., Salve, M. K., LeBlanc, J. G. and Arya, S. S. 2016. Concentration and characterization of microalgae proteins from *Chlorella pyrenoidosa*. *Bioresources Bioprocessing,* 3**,** 16.

Wang, G., Chen, L., Hao, Z., Li, X. and Liu, Y. 2011. Effects of salinity stress on the photosynthesis of *Wolffia arrhiza* as probed by the OJIP test. *Fresenius environmental bulletin,* 20**,** 432-438.

Wang, G., Hao, Z., Anken, R. H., Lu, J. and Liu, Y. 2010. Effects of UV-B radiation on photosynthesis activity of Wolffia arrhiza as probed by chlorophyll fluorescence transients. *Advances in Space Research,* 45**,** 839-845.

Wang, Y., Li, Y., Luo, X. and Gao, H. 2018. Effects of yttrium and phosphorus on growth and physiological characteristics of *Microcystis aeruginosa*. *Journal of Rare Earths,* 36**,** 781-788.

Xin, L., Hong-Ying, H., Ke, G. and Ying-Xue, S. 2010. Effects of different nitrogen and phosphorus concentrations on the growth, nutrient uptake, and lipid accumulation of a freshwater microalga *Scenedesmus* sp. *Bioresource technology,* 101**,** 5494-5500.

Yang, L., Chen, J., Qin, S., Zeng, M., Jiang, Y., Hu, L., Xiao, P., Hao, W., Hu, Z. and Lei, A. 2018. Growth and lipid accumulation by different nutrients in the microalga *Chlamydomonas reinhardtii*. *Biotechnology for biofuels,* 11**,** 40.

Yeesang, C. and Cheirsilp, B. 2011. Effect of nitrogen, salt, and iron content in the growth medium and light intensity on lipid production by microalgae isolated from freshwater sources in Thailand. *Bioresource technology,* 102**,** 3034-3040.

Zarrouk, C. J. 1966. *Contribution a l'etude d'une cyanobacterie: influence de divers facteurs physiques et chimiques sur la croissance et la photosynthese de Spirulina maxima (Setchell et Gardner) Geitler.* Ph.D., University of Paris, Paris.

ZANCO Journal of Pure and Applied Sciences
The official scientific journal of Salahaddin University-Erbil
https://zancojournals.su.edu.krd/index.php/JPAS

ISSN (print):2218-0230**, ISSN (online):** 2412-3986**, DOI: http://dx.doi.org/10.21271/zjpas**

RESEARCH PAPER

Essential Constituents of Truffle in Kurdistan Region

Pshtiwan Abdullah Yousif [1], Aveen Faidhalla Jalal [1*,] Kaeuis Aziz Faraj[2]

1- Department of Chemistry, College of Education, Salahaddin University-Erbil, Kurdistan Region, Iraq
2- Department of Medical Laboratory Science, Building B,Room206,Komar University for Science and Technology, Sulaymaniyah- Iraq

A B S T R A C T:

Essential constituents of truffle distributed in three different habitats of Kurdistan Region were investigated. Carbohydrates are the most abundant macronutrient ranged from 24.5% to 37%, the protein content was 4.4-5.0 %, fat 2-2.5 %, ash 3-3.2 % and moisture 73-75 %. High level of Chitin, a water insoluble polysaccharide was determined, (21-25 % of DM). The obtained results show high concentration of macro elements, potassium, Calcium, Magnesium and sodium, lower contents of essential elements iron, zinc, copper and chrome were found. Chemical constituents responsible for the antioxidant actions were examined as antioxidant activity (FRAP values), ascorbic acid, total phenolic, total flavonoids, β-carotene, tannin, lycopene and overall anthocyanins stated on a dry mass basis were (13-17 mmol Fe+2 equivalent/100g), (14-15.6 mg/100g), (14-20 mg/g DM), (6.19-8.41mg/100g), (1.55-2.16 mg/100g DM), (10.9-17.3 mg/g) (0.03-0.06mg/100g) and (10-15mg/100g DM) respectively. Total phenolics were the major antioxidant compounds as compared to β-carotene and ascorbic acid content.

KEY WORDS: Nutrient; Antioxidant Activity; Chitin; Macro Element; Hypogenous Fungi; Truffle; Kurdistan.
DOI: http://dx.doi.org/10.21271/ZJPAS.32.5.15
ZJPAS (2020) , 32(5);158-166 .

1. INTRODUCTION

Depended on their good nutritious value and characterized agreeable aroma, epigeous macro fungi (mushrooms) and hypogeous macro fungi (truffles) for millennia conceder as expensive food in many nations (El Enshasy et al., 2013). Truffles are seasonal grow wild and the number of truffles generally varies from season to season depending on the amount of precipitation (Al-Shabibi et al., 1982, Dahham et al., 2018). Truffles also known as "black diamonds," they are one of the Tuberaceae family as important underground eatable fungi (Gao et al., 2001).

It is hypogenic fungi and grows between 5 and 10 cm deep underground in combination with plant roots of both angiosperms and gymnosperms (Patel, 2012), forming ectomycorrhizas (ECM) (Mello et al., 2006, Splivallo et al., 2015) that form symbiotic relationships with well-groomed hosts in a variety of ecosystems including subtropical cloud forests, flood plains, boreal forests, forests temperate, tree nurseries, renovation and Mediterranean forests (Bonito et al., 2010). Tree species (beech, birch, hornbeam, hazel, oak , poplar ,and pine) (Segneanu et al., 2012). Truffle's etymological root is from tuber, meaning, and "lump". It is referred to by the Latin as Tuber, derived from the word tumor (to swell) that indicates the shape of the globoid. In scientific term, truffles are micro aerobic (AL-Damegh, 2014), they grow all over the world in

* **Corresponding Author:**
Pshtiwan Abdullah Yousif
E-mail: pshtiwan.yousif@su.edu.krd
Article History:
Received: 27/06/2020
Accepted: 19/09/2020
Published: 13/10/2020

temperate, humid climates; similar warm, dry summers, cold, wet winters, and alkaline soil (AL-Damegh, 2014, Segneanu et al., 2012), though one of the most expensive mushrooms. Visually, truffles have different physical characteristics which make them very easy to differentiate them from the more popular mushrooms that are eaten every day. Truffles usually don't have stalks and root (Wang and Marcone, 2011). Truffles are very prevalent in Italian and French cooking; summer truffles (Tuber aestivum Vittadini) are the most common (or one of these) truffle types in Middle Europe (Carpathian Basin). Their habitats are wide-spreading; they occur in different European countries (from Great Britain, Russia, Sweden up to Spain), North-Africa (Morocco), Israel, besides the Arab Peninsula countries Like Bahrain, Iraq, Jordan, Syria, Saudi Arabia and Kuwait (Khojasteh et al., 2013, Segneanu et al., 2012). Truffles (Tuber aestivum) occur on different habitats of Hungary mainly in the central chain of mountains but in Middle and South Hungary on the lowlands, too. Soil requirements of summer truffle are relatively wide: best are the loamy soils with pH: 6.1-7.4; content of organic substances 3.1-9.1 %; P_2O_5 and K_2O content are 200, 500 ppm respectively (Vetter, 2007, BRATEK, 2010).

Truffles are known for their biological properties in humans, such as anti-inflammatory, antimicrobial, antioxidant , anti-mutagenic, antiviral, hepatoprotective, immune-modulating and antitumor activity (Gülsen et al., 2018, Segneanu et al., 2012). The studies have shown that certain truffles contain steroids as important components of champignon fragrance as well as volatile organic compounds. In addition to; Tuber magnatum Pico (white truffle) and Tuber melanosporum Vitt (black truffle) are highly regarded for their unique fragrance of sulfur (Gao et al., 2001). The white truffle (Tuber magnatum pico) is a hypogean fungus that lives fully underground; it is most sought after among the roots and those among the oaks. It is renowned for its luscious, heady white truffle which was considered the finest in Italy due to its complicated aroma, and is also the best and most expensive (Segneanu et al., 2012). The black truffle widely known as the "diamond of black cuisine" is considered the most aromatic (Segneanu et al., 2012), dimethyl sulfide is the predominant sulphur compound in black truffle (Gao et al., 2001). For this purpose, a conservation method must be established to maintain the unique aroma and flavor of truffles intact. Black truffles are almost always served raw (they cannot tolerate cooking heat) while white truffles are softer and more perishable (Segneanu et al., 2012).

2. Materials and methods

2.1. Collection of samples

Summer truffle samples of three separate Kurdistan Region ecosystems were collected (sample No.1: truffle of Zumar, sample No.2: truffle of Qaraj and sample No.3: truffle of Shangal) beginning of March 2015. The location of truffles was identified on the soil surface from cracks that appeared above the truffles (Figure 1). The fresh truffles were thoroughly cleaned, sliced, carefully and immediately frozen with lyophilizes (Nohita, Japan) at 50 ˚C in an oven until constant weight (5 days). Then dried Samples were crushed by grinder (IKA Werke, Germany) and sieved to obtain a uniform particle (20 meshes). The finely pulverized powder was capped and stored at room temperature in a dry (in hermetically sealed plastic bags up to and until use in dark.

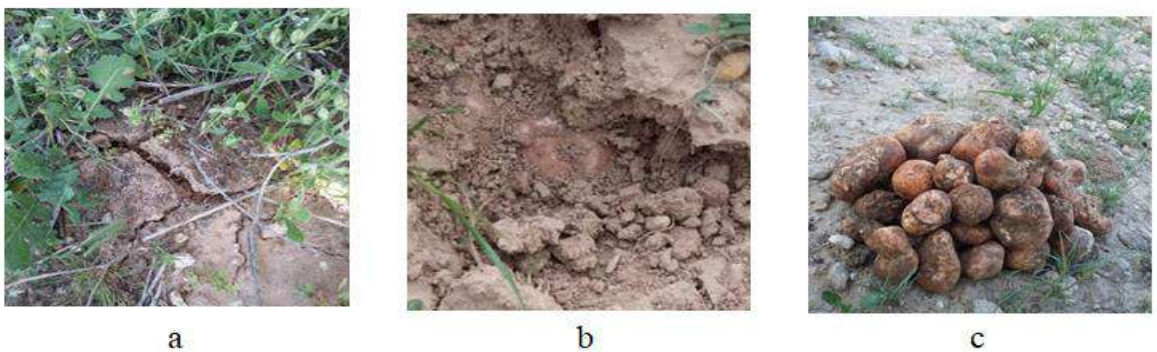

Figure 1. The species of *Truffles* from Kurdistan region of Iraq, a description of the organisms growing deep in the

earth and surrounding vegetation; b, c-Truffle ascocarps and deep soil truffles after removal of the surface soil.

2.2. Determination of primary metabolites

Truffle samples were analyzed according to the AOAC protocol for chemical composition (ash, starch, fat, moisture, and protein)(Horwitz and Latimer Jr, 2006). The humidity content was determined by drying samples in a 105 ˚C oven until constant weight was reached. The amount of ash was measured by burning the samples for 2.0 hours in a furnace at 600 µC in a crucible. The fat content at the solvent boiling point was estimated for 8.0 h with soxhlet extraction using hexane. Row chitin samples were treated at room temperature with 0.5 M HCL with a solid to acid solution ratio of 1:25 g/ml (w/v) for 2 h, and then washed with Distilled water. The acid treated solid was then treated at room temperature with a solution of NaOH in a ratio of 1:25 g/ml chitin to NaOH (0.5 M NaOH) ratio of (w/v) for 2 hours to obtain more pure chitin. Purified chitin was dried overnight at 55 ˚C (Vetter, 2007). The concentration of different mineral constituents was then analyzed separately using Flame Atomic Absorption Spectrometer (FAAS) , After the preparation of the sample solution when the summer truffle samples (0.25-0.26 g) weighed on the analytical balance, the samples were treated with 5.5 ml HNO3 14.6 M and digested for 15 minutes at 160 µC (Segneanu et al., 2012).

2.3. Determination of secondary metabolites

2.3.1. Ethanolic extraction of samples

10 g of each sample was cut into small pieces and then mixed with 100 ml of 50 percent (v/v) ethanol, then shaken at room temperature at 150 rpm for 24 hours, then centrifuged for 15 min at 12000 rpm. Under similar conditions the residue was re-extracted. The obtained extract was concentrated under vacuum at 40 ° C using the rotary evaporator and added 100 mL of 50 percent ethanol, well mixed, transferred to a dark plastic bottle and processed for analysis at -20 ° C (Boonsong et al., 2016).

2.3.2. Determination of Phenolic total content

Folin-Ciocalteu analysis was used, depending on the procedures, to determine total phenolic compounds in sample extracts described by Kaewnarin et al. (2016), (Keleş et al., 2011, Vamanu, 2014). In short, 1.0 ml of sample extracts transferred into volumetric flask containing 5.0 ml Folin-Ciocalteu reagent (1:10 Folin-Ciocalteu reagent: distilled water). After that 4.0 ml of sodium carbonate solution (7.5 percent, w/v) was added to the mixture and then the distilled water volume was completed to 10 ml. The volumetric flask permitted standing at room temperature for 60 min, then absorbance was read at 765 nm against blank. As standard, garlic acid was used in the same condition and standard curve of garlic acid ranging from 10-50 ppm. The quantity of phenolic compounds per gram of the sample extract was expressed as mg of garlic acid equivalent (GAE) (Aali et al., 2018).

2.3.3. Determination of Total Flavonoids Content

The Aluminum trichloride (AlCl3) method was used to estimate the total flavonoid compound of the sample extracts according to the method described by Gan et al. (2013), (Yan et al., 2017) with some modification. 0.75 ml of 10 percent Aluminum Trichloride (AlCl3) solution was applied after 5.0 min at room temperature, after the next 6.0 min 5.0 ml of 1.0 M NaOH was applied, then the volume of deionized water was completed to 25 ml. The mixture was shaken, and estimated at 510 nm against blank. Rutin was selected as a standard, with various concentrations. The results were expressed as mg rutin equivalent per gram of sample extract.

2.3.4. Determination of Vitamin C (Ascorbic acid)

The amount of vitamin C was taken by spectrophotometric process, the absorbance was measured at 515nm that described by Wahiba et al. (2016) with some modification. The collected sample was prepared by combining a appropriate quantity of samples with 10 ml of 1.0 per cent oxalic acid then centrifuged for 15 minutes, 5.0 ml of supernatant was combined with 9.0 ml of 0.2

mM of 2,4-dichlorophenol-indophenol then the amount completed with distilled water to 25 ml.

2.3.5. Determination of Tannin

When 0.05 ml of sample extracts is applied to 1.5 ml of 4.0 percent vanillin solution when prepared in methanol (w / v) and then mixed well, the dosage of tannin was determined. After adding 0.75 ml of hydrochloric acid, the mixture stayed to react for 20 min at room temperature. The absorbance was measured at 550 nm (Julkunen-Tiitto, 1985, Wahiba et al., 2016).

2.3.6. Determination of β-Carotene and Lycopene

The dried ethanol extraction (100 mg) was stirred continuously with 10 mL of a mixture of acetone-hexane (4:6) for 1 min to assess β-carotene and lycopene, and then filtered through whatman filter paper number 1. The contents for β-carotene and lycopene is calculated by the following equations:

Lycopene (mg/100 mL) = − 0.0458 ×A663 + 0.372 × $A505$ − 0.0806 × $A453$.

β-carotene (mg/100 mL)= 0.216 × $A663$ − 0.304 × $A505$ + 0.452 × $A453$.

Where A is absorbance of sample in this wavelength.

The results are expressed as mg of carotenoid/g of extract (Vamanu, 2014).

2.3.7. Determination of total anthocyanin's

To determine total anthocyanins, 0.05 g of dried truffle was mixed with 4.0 ml of distilled water (D.W), 3.0 min. sonicated in water bath, and 15 min. preserved at room temperature, with 10 min. continuous centrifugation mixing. 1.0 ml of pure solution was then mixed with 24 ml of buffer solution (KCl/HCl) pH 1.0. Subsequently 1.0 ml of the sample extract was mixed with 24 ml sodium acetate buffer (pH 4.5). The absorbance was read at 510 and 700 nm as well as the equation (Ab) was used to calculate the anthocyanin absorption as:

$Ab = (A_{510} - A_{700})$ pH 1.0 - $(A_{510} - A_{700})$ pH 4.5

Total anthocyanins (mg/100g) = $\frac{Ab}{\varepsilon} \times MW \times \left(\frac{V}{G}\right) 100$

Where ε is the coefficient of molar extinction taken as 26900, MW is the molecular weight of standard anthocyanins taken as 449,2, V is the final volume, and G is the gram sample weight (Al-Laith, 2010).

2.3.8. Ferric antioxidant capacity reduction assay (FRAP)

The FRAP value was calculated according to the methods described in Benzie and Strain (1996), (Gan et al., 2013, Vamanu, 2014) with some changes. The Ferric antioxidant capacity reduction reagent was prepared freshly by mixing (10:1:1 v/v/v) of 25 ml of 300 mM acetate buffer pH 3.6, 2.5 ml of (10 mM 2,4,6-tripyridyl-s-triazine (TPTZ) was prepared in 40 mM HCl) and 2.5 ml of 20 mM of $FeCl_3$. Then about 2.0 ml of FRAP reagent was applied to the test tube containing 100 µL of standard solution sample extraction or volume, and 900 µL of distilled water. At room temperature at 593 nm, the absorbance was assessed against blank for 30 min after incubation. Ferrous sulfate was used as standard in the same condition at different range (0-100 mM) and ascorbic acid was used as reference. Using the Fe^{+2} calibration curve, the value of FRAP was measured and expressed as mM Fe^{+2} equivalent per 100 g sample or µM Fe^{+2} equivalent / gram extracted.

2.3.9. Total Antioxidant Capability evaluation

The total antioxidant capacity of the extract was assessed using the phosphor molybdenum method. The evaluation is based on the reduction of Mo (VI) to Mo (V) in an acidic medium solution by the extract and subsequent development of a green phosphate / Mo (V) complex. Extract volume (20-100µg / ml) was mixed with a reagent of 1.0 ml (0.6 M sulfuric acid, 28 mM sodium phosphate and 4 mM ammonium molybdate). After cooling down to room temperature, the amount of deionized water was completed to 25 ml. The mixture was incubated for 90 min in a boiling water bath at 95° C. The blank solution prepared in the same condition without containing sample extraction. Using a spectrophotometer the solution absorbance was measured at 695 nm. Extract antioxidant capacity was compared to standard ascorbic acid within such a range (20-100 µg/ml) (Aguilar Urbano et al., 2013).

3. Results and discussion

Wilderness truffles are a rich source of amino acids, protein, fatty acids, carbohydrates and minerals (Al-Naama et al., 1988, Bokhary and Parvez, 1993, Bokhary et al., 1989, Bokhary et al., 1987). Table 1 illustrated the effects of the composition of the nutrients on a dry foundation. The fresh truffle's average moisture content was

74 % DM, which was in close agreement with those studies (Al- Laith, 2010, Al-Laith, 2014, Hamza et al., 2016b). The truffle ash content was 3.07-3.18 % DM, which was similar to that for other sand truffles such as a Tirmania and Terfezia claveryi (Gan et al., 2013), and lower than what has been reported by (Ahmed et al., 1981, Akyüz, 2013, Yildiz et al., 2006). Tests obtained have shown that truffle protein content (4.40-5 % DM) was low and not comparable with the results obtained for Tirmania nivea truffle rates by (Hamza et al., 2016a, and Truffle Terfezia boudieri from the arid region of Tunisia (Hamza et al., 2016b). Crude fat (2-2.5 percent of DM) is similar to other species of mushrooms (Vetter and Kruzselyi, 2014) but lower than truffle what has been reported. Compared to our results, Nivea truffle had a comparatively great fat content (6.78 g / DM) (Hamza et al., 2016a). The fat content varied between 2.81 to 7.42 percent DM for other desert truffles (Wang and Marcone, 2011). Carbohydrates are the most abundant macronutrients in truffle, in this study were ranged from 24.5 to 37% DM which is less than what has been reported earlier for truffle. Nivea truffle (57.83 g/DM) by Hamza et al. (2016a), and 60% of carbohydrates for other desert truffles (Kagan-Zur and Roth-Bejerano, 2008). Chitin level is high (21.35-24.85% of DM), this is in accordance with what has been earlier reported by Vetter (2007), Chitin level of truffle aestivum is high, higher than the average of other common cultivated mushrooms, also found that chitin content of summer truffle (22.03 % in average) seems to be higher than normally in common mushrooms (for example: in Pleurotus species 11 %) (Del Toro et al., 2006).

Table 1: The concentrations percentage contents of moisture, ash, protein, fat, carbohydrates and chitin in the dried truffle samples. (Sample number 1 is from Zumar, number 2 from Qraraj and number 3 from Shangal.

Sample	Moisture (%)	Ash (%)	Protein (%)	Fat (%)	Carbohydrate (%)	Chitin (%)
1	73.75 ± 1.08	3.18 ± 0.20	4.64 ± 1.18	2.05 ± 0.35	24.53 ± 0.58	22.36 ± 0.59
2	75.12 ± 0.69	3.07 ± 0.42	4.39 ± 2.52	2.48 ± 1.85	36.34 ±0.78	21.35± 0.77
3	73.63 ± 0.13	3.15 ± 0.35	5.16 ± 0.76	1.95 ± 0.98	36.89 ± 0.08	24.85± 0.25

The analytical methods used to characterize the samples indicated that the results obtained showed a high concentration of macroelements, potassium , calcium , magnesium and sodium, lower contents of iron, zinc , copper and chromium critical elements. Mineral spectrum of truffle fruit bodies is similar to composition of other edible mushrooms, i.e. they have high potassium and phosphorus contents, lower but important level from calcium, Magnesium and some microelements (Vetter and Kruzselyi, 2014). No traces of poison elements nickel, lead, cobalt and cadmium were detected; this is in accordance with (Akyüz, 2013). Accumulation (occurrence) of the problematic, "poisonous" elements (as Cd, As, Cr or V) was not established in truffle fruit bodies. According to Vetter and Kruzselyi (2014), several studies have also shown that truffles are a rich source of important minerals, such as Al, Cu, Na, Si, K, Ca, Mg, Mn, Fe and Zn (Darwesh, 2019, Nedelcheva et al., 2007). Truffle consumption contributes the highest percentage of the body's required mineral demands that shown in Table 2.

Table 2: Mineral concentrations in the truffle samples (mg/kg dry mass). (Sample number 1 is from Zumar, number 2 from Qraraj and number 3 from Shangal.

Sample	K	Ca	Mg	Na	Fe	Zn	Cu	Cr	Cd	Ni	Pb	Co
1	2462	1825	1751	1439	228.3	106.06	27.46	0.99	< d.I	< d.I	< d.I	< d.I
2	2525	1726	1600	2271	271.8	81.66	20.56	0.94	< d.I	< d.I	< d.I	< d.I
3	2583	1779	1489	1420	453.8	114.9	26.26	1.02	< d.I	< d.I	< d.I	< d.I

*< d.I: Under detections limit

This study investigated the chemical constituents that contribute to antioxidant activity in dessert truffle. The analyses of ascorbic acid, total phenolic, total flavonoids and total dry-mass anthocyanins were reported in Table 3.

Table 3: The concentration of ascorbic acid, total phenolics, total flavonoids and anthocyanins in total dried desert truffle (Sample number 1 is from Zumar, number 2 from Qraraj and number 3 from Shangal.

Sample	Extraction yield (g/100g dry weight)	Ascorbic acid (mg/100g)	Total phenolics (mg gallic acid/g extract)	Total flavonoids (mg rutin/g extract)	Total anthocyanins (mg/100g extract)
1	2.53	15.6 ± 0.07	14.25 ± 0.72	8.41 ± 1.01	10.02 ± 0.98
2	3.33	14.04 ± 0.62	18.32 ± 1.32	6.25 ± 0.09	15.03 ± 1.05
3	3.23	14.95 ± 0.54	19.95 ± 1.19	6.19 ± 0.81	15.03 ± 1.05

The chemicals responsible for the antioxidant activities have been established as ascorbic acid, anthocyanins, total esterified phenolics, total free phenolics and total flavonoids and total carotenoids (Patel, 2012).

The Results showed that the major antioxidant compounds is phenolics compound (14-20 mg/g DM), as compared to β-carotene (1.55-2.16 mg/100g), and ascorbic acid content (14.04-15.6 mg/100g)), (Table 3 & 4). The highest levels of phenolic compounds in desert truffles could be described by several harsh environmental conditions characterized by their natural habitat (Hamza et al., 2016b).There is a popular belief in Kurdistan about-truffle circumstances; there is a clear connection between thunderclap force and truffle production (number and size) of truffle. Hence, the ability of some plants or wild mushrooms to tolerate severe situations is probably due to their ability to neutralize the reactive oxygen species by increasing the level of antioxidants, specifically phenolic compounds (Al-Laith, 2014).

Table 4: Antioxidant activity (FRAP values), lycopene, of dried desert truffle samples (n=3). (Sample number 1 is from Zumar, number 2 from Qraraj and number 3 from Shangal.

Sample	Antioxidant activity (FRAP values) (mmol Fe^{+2} equivalent/100g)	Lycopene (mg/100g)	β-carotene (mg/100g)	Tannin (mg/g extract)
1	17.32 ± 3.06	0.0585 ± 0.28	2.12 ± 1.56	17.31 ± 2.38
2	13.08 ± 2.38	0.0865 ± 0.78	2.16 ± 1.28	10.94 ± 0.88
3	14.34 ± 2.07	0.0356 ± 0.93	1.55 ± 1.03	11.45 ± 1.58

Flavonoids (6.19-8.41mg/g DM) and anthocyanins (10-15mg/100g DM) (Table 3), they are well known as potentially protective substances, and work as antioxidants, having a scavenging effect on free radicals. Due to the antioxidant activity (Fig.2), it can be concluded that truffles has some medicinal properties. Therefore, it is consumed as food and for medicinal purposes as well. Total flavonoid concentration found in our desert truffle species in this study is higher than those in T. aestivum (0.093 mg/g DM) in Tirmenia nivea truffle. Truffles have a higher content of antioxidants including certain vitamin A, C, β-carotene and phenolic compounds that can scrounge peroxy radicals and chelate ferric ions, thus reducing lipid peroxidation (Al-Laith, 2010). The obtained results showed that ascorbic acid content (14.04-15.6mg /100gDM) is higher than Tirmenia nivea truffle (10.63 mg/100 g), whole carotenoids content (1.55-2.16 mg/100gDM g) is higher than Tirmenia nivea truffle (1.17 mg/100 g), and complete anthocyanins (10-15mg/100g DM) are lower than (29.1 mg/100 g) in Tirmenia nivea truffle reported earlier (Hamza et al., 2016a).

Total phenolic (14-20 mg/g DM) and flavonoid (6.19-8.41mg/g DM) contents of truffle in this study markedly higher than in Tirmenia nivea truffle samples 2.8 mg/g DM and 0.093 mg/g DM, for phenolic and flavonoids respectively (Hamza et al., 2016a). The highest content of tannins was recorded in sample number 1 from Zumar (17.31 mg/g extract), while the lowest content was recorded in sample number 2 that shown in (Table 4). The lycopene showed, respectively, for three samples, quantities of (0.0585 mg/100g), (0.0865 mg/100g) and (0.0356 mg/100g) that shown in (Table 4).

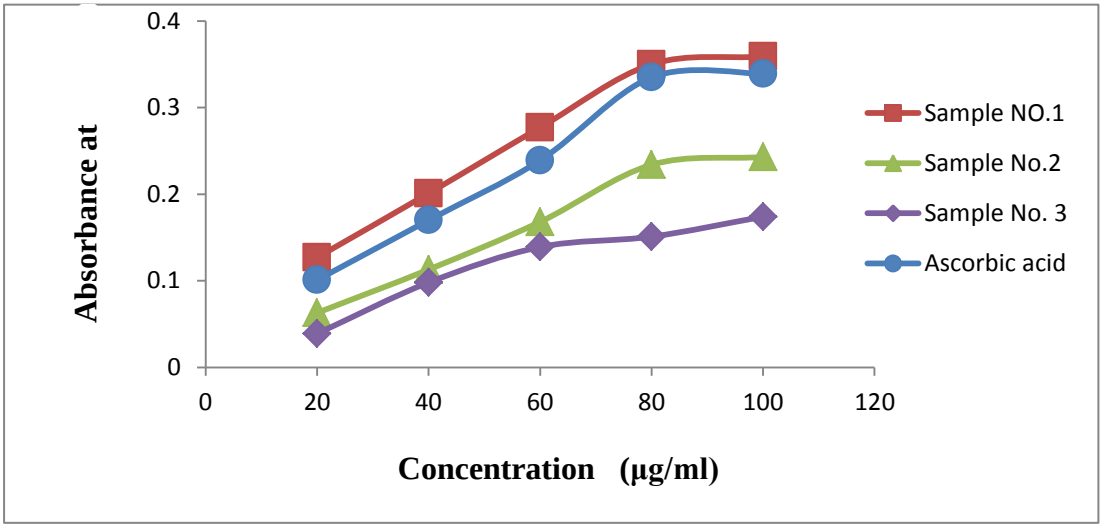

Figure (2): Full antioxidant strength of (●) for Ascorbic acid, (■) for *Truffle Sample No.1*, (▲) for *Truffle Sample No.2*, and (♦) for *Truffle Sample No.3.*

4.Conclusion

The present paper is contribution to the studies on the nutraceutical potential; primary metabolites, minerals and secondary metabolites of a wild edible desert truffle from Kurdistan region of Iraq. The results of this study, it is clearly indicated that the truffle was an excellent source of carbohydrate, protein fat and minerals compered than those of other truffles reported in literature. On the other hand, according to the results obtained from the study the protein content is significantly higher than most vegetables and fungi. The chemicals responsible for antioxidant activities were known as anthocyanins, ascorbic acid (Vitamin C), total esterified phenolic, complete free phe4.nolic, total flavonoids and total carotenoids. Throughout this analysis, the overall truffle content of phenolic and flavonoid was significantly higher than Tirmenia nivea truffle sample. More importantly, truffle seems to be a good source of several important nutrients and phytochemicals, such as phenolics, minerals and proteins. It could provide a healthy meat alternative that satisfied the nutritional requirements, especially for non-meat eaters.

Therefore, these finding provide evidences of truffle health benefits, owing it to it is antioxidant and nutrient properties which may be used nutraceutical or pharmaceutical industries.

References:

AALI, M. H., ISMAIEL, N. J. & MAJID, F. A. A. 2018. Antioxidant, and Antimicrobial Activities of Phenolic and Flavonoid Rich Medicinal Plants (Fritillaria zagrica and Tulipa kurdica) Bulbs Collected in Kurdistan Region of Iraq. *Zanco Journal of Pure and Applied Sciences,* 30**,** 1-16.

AGUILAR URBANO, M., PINEDA PRIEGO, M. & PRIETO, P. 2013. Spectrophotometric quantitation of antioxidant capacity through the formation of a phosphomolybdenum complex: specific application to the determination of vitamin E1.

AHMED, A. A., MOHAMED, M. A. & HAMI, M. 1981. Libyan Truffles "Terfezia Boudieri Chatin:" Chemical Composition and Toxicity. *Journal of Food Science,* 46**,** 927-929.

AKYÜZ, M. 2013. Nutritive value, flavonoid content and radical scavenging activity of the truffle (Terfezia boudieri Chatin). *Journal of soil science and plant nutrition,* 13**,** 143-151.

AL-DAMEGH, M. A. 2014. Tirmania (Zubaidi) and Terfezia (Khallasi) Fungi Preparation Method Modulates Body and Testicular Weights and Blood and Testicular TestosteroneConcentration in Albino Rats. *Journal of American Science,* 10.

AL-LAITH, A. A. A. 2010. Antioxidant components and antioxidant/antiradical activities of desert truffle (Tirmania nivea) from various Middle Eastern origins. *Journal of Food Composition and Analysis,* 23**,** 15-22.

AL-LAITH, A. A. A. 2014. Nutritional and antioxidant properties of the White Desert Truffle Tirmania nivea (Zubaidi). *Desert Truffles.* Springer.

AL-NAAMA, N., EWAZE, J. & NEMA, J. 1988. Chemical constituents of Iraqi truffles. *Iraqi Journal of Agricultural Sciences,* 6**,** 51-56.

AL-SHABIBI, M., TOMA, S. & HADDAD, B. 1982. Studies on Iraqi truffles. I. Proximate analysis and characterization of lipids. *Canadian Institute of Food Science and Technology Journal,* 15**,** 200-202.

BENZIE, I. F. & STRAIN, J. J. 1996. The ferric reducing ability of plasma (FRAP) as a measure of "antioxidant power": the FRAP assay. *Analytical biochemistry,* 239**,** 70-76.

BOKHARY, H. & PARVEZ, S. 1993. Chemical composition of desert truffles Terfezia claveryi. *Journal of Food Composition and Analysis,* 6**,** 285-293.

BOKHARY, H., SULEIMAN, A. & BASALAH, M. 1989. The Fatty Acid Components of the Desert Truffle" Al Kamah" of Saudi Arabia. *Journal of food protection,* 52**,** 668-669.

BOKHARY, H., SULEIMAN, A., BASALAH, M. & PARVEZ, S. 1987. Chemical composition of desert truffles from Saudi Arabia. *Canadian Institute of Food Science and Technology Journal,* 20**,** 336-341.

BONITO, G. M., GRYGANSKYI, A. P., TRAPPE, J. M. & VILGALYS, R. 2010. A global meta-analysis of Tuber ITS rDNA sequences: species diversity, host associations and long-distance dispersal. *Molecular Ecology,* 19**,** 4994-5008.

BOONSONG, S., KLAYPRADIT, W. & WILAIPUN, P. 2016. Antioxidant activities of extracts from five edible mushrooms using different extractants. *Agriculture and Natural Resources,* 50**,** 89-97.

BRATEK, Z. 2010. *Truffle cultivation. In: Győrfi, J. (ed.), Biology and cultivation of mushrooms (in Hungarian),* Budapest, Hungary, Mezőgazda Kiadó.

DAHHAM, S. S., AL-RAWI, S. S., IBRAHIM, A. H., MAJID, A. S. A. & MAJID, A. M. S. A. 2018. Antioxidant, anticancer, apoptosis properties and chemical composition of black truffle Terfezia claveryi. *Saudi journal of biological sciences,* 25**,** 1524-1534.

DARWESH, D. A. 2019. Heavy metals evaluation in soil of agricultural field around a pond of gas plant in the Kurdistan Region of Iraq. *Zanco Journal of Pure and Applied Sciences,* 31**,** 28-35.

DEL TORO, G. V., VEGA, R. C., GARÍN-AGUILAR, M. E. & LARA, H. L. 2006. Biological quality of proteins from three strains of Pleurotus spp. *Food Chemistry,* 94**,** 494-497.

EL ENSHASY, H., ELSAYED, E. A., AZIZ, R. & WADAAN, M. A. 2013. Mushrooms and truffles: historical biofactories for complementary medicine in Africa and in the middle East. *Evidence-Based Complementary and Alternative Medicine,* 2013.

GAN, C., AMIRA, N. B. & ASMAH, R. 2013. Antioxidant analysis of different types of edible mushrooms (Agaricus bisporous and Agaricus brasiliensis). *International Food Research Journal,* 20**,** 1095.

GAO, J. M., WANG, C. Y., ZHANG, A. L. & LIU, J. K. 2001. A new trihydroxy fatty acid from the ascomycete, Chinese truffle Tuber indicum. *Lipids,* 36**,** 1365-1370.

GÜLSEN, T.-Ç., DEVECI, E., CAYAN, F. & DURU, M. E. 2018. Comparative assessment of phytochemical

composition, antioxidant and anticholinesterase activities of two Basidiomycota Truffle Fungi from Turkey. *Marmara Pharmaceutical Journal*, 22.

HAMZA, A., JDIR, H. & ZOUARI, N. 2016a. Nutritional, antioxidant and antibacterial properties of Tirmania nivea, a wild edible desert truffle from Tunisia arid zone. *Med. Aromat. Plants*, 5**,** 2167-0412.100.

HAMZA, A., ZOUARI, N., ZOUARI, S., JDIR, H., ZAIDI, S., GTARI, M. & NEFFATI, M. 2016b. Nutraceutical potential, antioxidant and antibacterial activities of Terfezia boudieri Chatin, a wild edible desert truffle from Tunisia arid zone. *Arabian Journal of Chemistry*, 9**,** 383-389.

HORWITZ, W. & LATIMER JR, G. 2006. Association of Official Analytical Chemists–AOAC. *Official methods of analysis of AOAC International. 18th ed. Gaithersburg: AOAC International*.

JULKUNEN-TIITTO, R. 1985. Phenolic constituents in the leaves of northern willows: methods for the analysis of certain phenolics. *Journal of agricultural and food chemistry*, 33**,** 213-217.

KAEWNARIN, K., SUWANNARACH, N., KUMLA, J. & LUMYONG, S. 2016. Phenolic profile of various wild edible mushroom extracts from Thailand and their antioxidant properties, anti-tyrosinase and hyperglycaemic inhibitory activities. *Journal of Functional Foods*, 27**,** 352-364.

KAGAN-ZUR, V. & ROTH-BEJERANO, N. 2008. Desert truffles. *Fungi*, 1**,** 32-37.

KELEŞ, A., KOCA, I. & GENÇCELEP, H. 2011. Antioxidant properties of wild edible mushrooms. *Journal of Food Processing & Technology*, 2**,** 2-6.

KHOJASTEH, S. M. B., AMIRI, L. & SHEIKHZADEH, F. 2013. Effect of the alcoholic extract of Terfezia boudieri on reproductive hormones in male rats. *Int J Pharm Bio Sci*, 3**,** 517-522.

MELLO, A., MURAT, C. & BONFANTE, P. 2006. Truffles: much more than a prized and local fungal delicacy. *FEMS Microbiology Letters*, 260**,** 1-8.

NEDELCHEVA, D., ANTONOVA, D., TSVETKOVA, S., MAREKOV, I., MOMCHILOVA, S., NIKOLOVA-DAMYANOVA, B. & GYOSHEVA, M. 2007. TLC and GC-MS Probes into the Fatty Acid Composition of some Lycoperdaceae Mushrooms. *Journal of liquid chromatography & related technologies*, 30**,** 2717-2727.

PATEL, S. 2012. Food, health and agricultural importance of truffles: a review of current scientific literature. *Current Trends in Biotechnology and Pharmacy*, 6**,** 15-27.

SEGNEANU, A., SFIRLOAGA, P., DAVID, I., BALCU, I. & GROZESCU, I. 2012. Characterisation of truffles using electrochemical and analytical methods. *Digest J. Nanomater Biostruct*, 7**,** 199-205.

SPLIVALLO, R., DEVEAU, A., VALDEZ, N., KIRCHHOFF, N., FREY-KLETT, P. & KARLOVSKY, P. 2015. Bacteria associated with truffle-fruiting bodies contribute to truffle aroma. *Environmental Microbiology*, 17**,** 2647-2660.

VAMANU, E. 2014. Antioxidant properties of mushroom mycelia obtained by batch cultivation and tocopherol content affected by extraction procedures. *BioMed research international*, 2014.

VETTER, J. 2007. Chitin content of cultivated mushrooms Agaricus bisporus, Pleurotus ostreatus and Lentinula edodes. *Food Chemistry*, 102**,** 6-9.

VETTER, J. & KRUZSELYI, D. 2014. Complex chemical evaluation of the summer truffle (Tuber aestivum Vittadini) fruit bodies. *Journal of Applied Botany and Food Quality*, 87.

WAHIBA, B., WAFAÀ, T., ASMAÀ, K., BOUZIANE, A. & MOHAMMED, B. 2016. Nutritional and antioxidant profile of red truffles (Terfezia claveryi) and white truffle (Tirmania nivea) from southwestern of Algeria. *Der Pharmacia Letter*, 8**,** 134-141.

WANG, S. & MARCONE, M. F. 2011. The biochemistry and biological properties of the world's most expensive underground edible mushroom: Truffles. *Food Research International*, 44**,** 2567-2581.

YAN, X., WANG, Y., SANG, X. & FAN, L. 2017. Nutritional value, chemical composition and antioxidant activity of three Tuber species from China. *AMB Express*, 7**,** 136.

YILDIZ, A., DÜNDAR, A., ACAY, H., AKYÜZ, M. & YEŞIL, Ö. 2006. Nutritive value of Pleurotus eryngii and Terfezia boudieri. The Scientific and Technological Research Council of Turkey, Agricultur.

ZANCO Journal of Pure and Applied Sciences
The official scientific journal of Salahaddin University-Erbil
https://zancojournals.su.edu.krd/index.php/JPAS

ISSN (print):2218-0230**, ISSN (online):** 2412-3986**, DOI: http://dx.doi.org/10.21271/zjpas**

RESEARCH PAPER

Succession Effect of Wheat Cultivation After Some Crops on Mycorrhizal Infection, Yield, and Quality of Wheat

Lubna Ahmed Abdulkarim[1], Bahar Jalal Mahmood[2], Azad Ahmad Abdullah[3]

1- Department Environmental Science, College of Science, Salahaddin University-Erbil, Kurdistan Region-Iraq
2- Department of field Crops, College of Agricultural Engineering Sciences, Salahaddin University-Erbil, Kurdistan Region-Iraq
3-Rresearcher at Ministry of Agriculture and Water Resources, Kurdistan Region-Iraq.

A B S T R A C T:
The present study was conducted during wheat growing season (from November to June 2017) at Grdmalla village, Qushtapa district, Erbil governorate with Global Positioning System (GPS) reading of 36^0 01 N , 44^0 01 E and 413.8m above sea level to study the impact of crop rotation or cultivation of wheat after some vegetable crops and wheat itself such as broccoli, tomato, pepper, cucumber, eggplant and wheat. The results showed that the lowest infection percentage was observed in case of cultivation of wheat after wheat which was 30% in case of cultivation of wheat after wheat, while this value raised to 70-90% in case of cultivation of wheat after the mentioned vegetables. The increase in infection percentage of plant roots with mycorrhizal fungi caused significant increase in wheat yield, phosphorus and protein content. The wheat yield increased from 2.50 Mega gram ha^{-1} to 4.86 Mega gram ha^{-1}(ton ha^{-1}) in case of cultivation wheat after wheat and broccoli respectively. On the other hand, the protein percentage was increased from 12.20 to 16.50% in case of cultivation of wheat after wheat and cultivation of wheat after broccoli respectively. The significant correlation was recorded between both of yield and protein content of wheat with mycorrhizal infection with correlation coefficient values of ($r=0.89^{**}$ and 0.99^{**}) respectively.

KEY WORDS: Crop rotation, mycorrhizal infection, protein content, wheat yield and protein content.
DOI: http://dx.doi.org/10.21271/ZJPAS.32.5.16
ZJPAS (2020) , 32(5);167-173 .

1. INTRODUCTION

Mycorrhiza is defined as a symbiotic association between the fungi organisms (specific for soil and plant life) and the plants root (or other substrate contacting parts) of a living plant which is primarily responsible for the transfer of the nutrients. Mycorrhizas in specialized organs of plant, where intimate communications formed from the coordinated development of plant-fungus (Brundrett, 2008).

Arbuscular mycorrhiza fungi (AMF) are a symbiotic relationship between soil fungi and terrestrial plants which the fungi supply the plant with water and nutrients in exchange for carbon, increasing plant growth and yield production. Several studies have reported to the important role of (AMF) in promoting (P) uptake by plant. Moreover, it is yet a matter of debate which how (AMF) affect soil (N) dynamic and as result plant (N) uptake. The important parts such affects by (AMF) are significance to health and productivity of the ecosystem (Miransari, 2012 and Miransari, 2017).

The infected plants with (AMF) are protected from salinity, drought condition, and also from excess phytotoxic elements **(**Ganugi et al; 2019**).**

* **Corresponding Author:**
Lubna Ahmed Abdulkarim[1]
E-mail: Lubna.abdulkarim@su.edu.krd
Article History:
Received: 02/02/2020
Accepted: 09/03/2020
Published: 13/10/2020

Enhancement of mycorrhizal inoculum potential by a given pre-crop may improve the mycorrhizal activity of a subsequent crop in the rotation (Barea et al., 1993). This is generally supposed to the fungi develop and sporulate most on the roots of those plant species which are most susceptible to mycorrhizal infection. Susceptible crops which, in the rotation, follow non-host plants (or plants which develop little mycorrhizal infection) may carry less infection than they would follow a strongly mycorrhizal crop (Ocampo and Hayman, 1981). Black and Tinker (1977) found fewer pores in soil kept fallow than in adjacent soil cropped with barley.

The (AMF) enhance the Chlorophyll concentration and photosynthetic rates. Phosphorus (P), and potassium (K) content in the plant parts (leaf, stem, and root), and nitrogen (N) content in the leaf and stem of arbuscular mycorrhizal seedlings were significantly more than in non- arbuscular mycorrhiza seedlings (Wang et al; 2019).

Howard, (1996) Indicated that crop rotation is a very ancient and cultural practice and has critical effect on soil microbial communities, soil structure, and organic matter. The main idea behind crop rotation practice is to disrupt disease cycle (Pierce and Rice, 1998). Few researches have been executed to distinguish mycorrhizal fungi community composition and diversity. The AMF spores' surveys as a baseline in the field soil to assess the impact of agricultural practice on mycorrhizosphere (Douds and Millner, 1999).

Agricultural practice management influence AM communities structure qualitatively and quantitatively (Miller et al., 1995). Crop rotation is known to affect AMF in the field. Crop rotation also affects species diversity, spore population of AMF in another crop-rotation management trial utilizing a maize-vegetable-small grain rotation and chemical fertilizer organic amendments as source of mineral nutrition (Douds. and. Schenck, 1990). Mycorrhiza are used as bio fertilizer and can decrease using of the chemical fertilizer especially phosphorus fertilizer (Ortas, 2012), therefore, they can significantly boost the phosphorus concentration in both root and shoot systems (Al-Hmoud and Al-Momany, 2017). It has been observed that AMF maintain P and N uptake ultimately helping in plant development at higher and lower P levels under different irrigation regimes (Liu et al., 2014; Liu et al., 2018). Lately, it has been found that treatments with native Vascular arbuscular mycorrhiza lead to produce significant change in the N in crop plants (Turrini et al., 2018).

The important role of (AMF) is to provid roots with phosphorus because element phosphor is an highly not mobile elements in soils (Turk et al. 2006). The phosphorus and nitrogen formed in shoots and dry mass of plants colonized with mycorrhiza were more than those of plants without mycorrhiza (Al-Amir et al. 2013).

The important limiting nutrient for plant growth is nitrogen (Sawers et al. 2008). Which is the major component of both protein and coenzymes, indeed nitrogen (N) is a major nutrient which enhance taking of nutrients from poor soils to roots which improved by arbuscular mycorrhizal colonization (Jin, et al., 2005). Nitrogen is obtained by the extraradical hyphae of AM fungi in different forms ranging from peptides, amino acids, (Ike-Izundu 2007 and Bago et al. 1996). Vascular arbuscular mycorrhiza eenhance taking of nitrogen by mycorrhizal plant compared to non-mycorrhizal plant. Vascular arbuscular mycorrhiza fungi is enhance the taking of ammonium NH_4^+ that their movement lower than nitrate NO_3^-, its uptake rate affected by low diffusion (Tobar et al., 1994). Since there are little or no studies about the role of plant rotation on mycorrhizal infection, phosphorus absorption, yield and protein content of wheat in calcareous soil.

2. MATERIALS AND METHODS

The field experiment was conducted from November to June 2017, which carried out in a clay loam soil in Grdmalla Village, Qushtapa, Erbil with Global Positioning System (GPS) reading of 36^0 01 N and 44^0 01 E, 413.8 m above sea level, to study the effect of sowing wheat after some other plants such as broccoli, tomato, cucumber, eggplant, and wheat.
Three plots were taken from each site of the field or the number of experimental units equal to 18 experimental units.

The area of each experimental unit was 6 m^2 (2m x 3 m) for wheat cultivated after each of the mentioned vegetables and wheat itself and the space between experimental unit was 1m for all sites as shown from the table below.

Table (1) explains the crop rotation of the studied crops.

Sites	Description	Number of Plots
Site number 1	Wheat cultivated after broccoli	3 plots
Site number 2	Wheat cultivated after tomato	3 plots
Site number 3	Wheat cultivated after pepper	3 plots
Site number 4	Wheat cultivated after cucumber	3 plots
Site number 5	Wheat cultivated after eggplant	3 plots
Site number 6	Wheat cultivated after wheat	3 plots

On 8th of June, 2017 the wheat (*Triticum aestivum* L) plants were harvested from all sites of the field and the root samples were taken to determine infection with mycorrhizal using the international method as mentioned by Troyvelote et al, (1986).

The total nitrogen and phosphorus were determined according to the standard methods as mentioned by Rowell (1996). The protein content of wheat seeds was calculated according to the equation mentioned by Darwesh (2007) as follow: Protein% = nitrogen % * 5.70.

Infection percentage:

In present study the method of Phillips and Hayman (1970) were applied to clearing and staining of roots colonized by (AMF). After removal of shoot, the root samples should be washed under running tap water. Washed roots were cut into 1cm pieces, 10 randomly chosen root segments were cleared with 10% KOH overnight, segments were placed in 10% HCl for 10 minutes for removing excess KOH, then washed with distilled water, after that 0.05% Trypan blu in lactophenol was used to staining of it and microscopically examined for (AMF) colonization. The intensity of the infected stained roots with mycorrhiza (M %) were determined according to Troyvelote et al., (1986). The percentage of fungus colonization was calculated as follow:

Fungus colonization% = (No. of root segments colonized / No. of total root segments examined) x 100.

3. RESULT AND DISCUSSION

Table (2) and figures (1-6) explain the infection percentage of wheat roots cultivated after some vegetable's crops such as tomato, cucumber, eggplant, pepper, broccoli, in additional to cultivation of wheat after wheat itself. Its appeared that the infection percent with mycorrhiza was ranged between (30 – 90) %. The lowest infection value was recorded form cultivation of wheat after wheat, while the infection was increased from cultivation of wheat after some vegetative plants from 30% to (70, 70, 80, 85, and 90)% for cultivation of wheat after tomato, cucumber, eggplant, pepper, and broccoli respectively, similar results was obtained by Bakhshandeh et al.,(2017). It means that the crop rotation plays an important role in increasing mycorrhizal root infection.

Table (2) Mycorrhizal infection percentage of wheat sowing after some crops

Treatments or Sowing wheat after	Infection %	Yield Mg ha^{-1} Or (Tons ha^{-1})	P %	Protein %
Tomato	70	3.91	0.23	12.90
Cucumber	70	3.50	0.26	13.00
Eggplant	80	3.30	0.27	14.10
Pepper	85	4.60	0.30	13.80
Broccoli	90	4.86	0.33	16.50
Wheat	30	2.50	0.20	12.20

Effect of root infection with mycorrhizae on wheat yield and quality:

As shown in table (2) the wheat yield increased from (2.50 Mg ha^{-1} in case of cultivation wheat after wheat to (3.91, 3.50, 3.30, 4.60, and 4.86) Mg ha^{-1} in case of crop rotation or cultivation of wheat after tomato, cucumber, eggplant, pepper, and broccoli respectively.

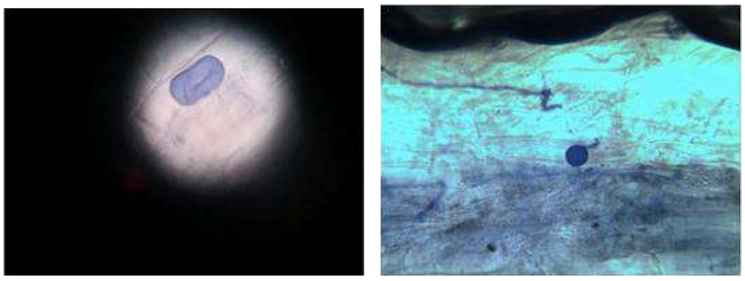

Figure 1: Long section for wheat roots infected with with AMF shown fungus arbuscules and hyphae cultured after Tomato (Magnification = 400X)

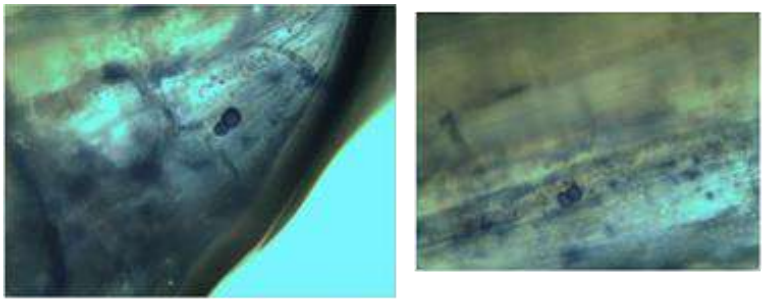

Figure 2: Long section for wheat roots infected with AMF shown fungus arbuscules and hyphae in cultured after Cucumber (Magnification = 400X).

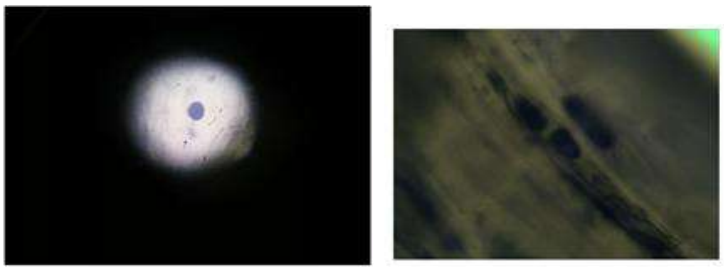

Figure 3: Long section for wheat roots infected with AMF shown fungus arbuscules and hyphae cultured by Eggplant (Magnification = 400X).

Figure 4: Long section for wheat roots infected with AMF shown fungus arbuscules and hyphae cultured after Pepper (Magnification = 400X).

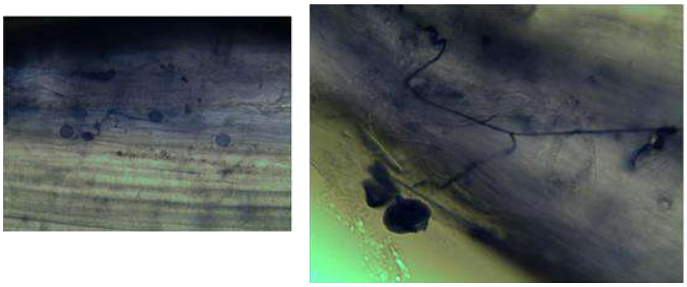

Figure 5 : Long section for wheat roots infected with AMF shown fungus arbuscules and hyphae cultured after broccoli (Magnification = 400X).

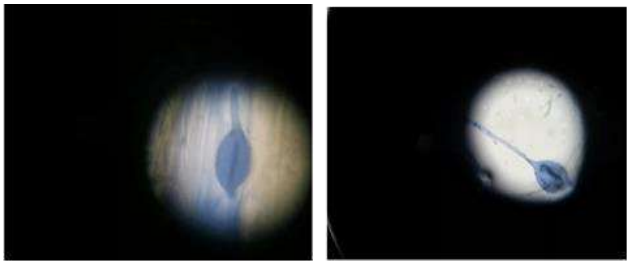

Figure 6 : Long section for wheat roots infected with AMF shown fungus arbuscules and hyphae cultured by Wheat (Magnification = 400X).

These explain the role of crop rotation in increasing mycorrhizal colonization which caused increase in nutrient uptake in a balance form (Bakhshandeh et al.; 2017).

On the other hand, figure (7) indicated to significant correlation coefficient between wheat yield and infection percentage of root `wheat with the correlation coefficient value of (r = 0.89**) this explains the role of mycorrhizal infection in increasing wheat yield.

It means wheat roots mycorrhizal infection caused increase in yield by (1.32 to 1.94) times, or caused (32 to 94 %) increase in wheat yield.

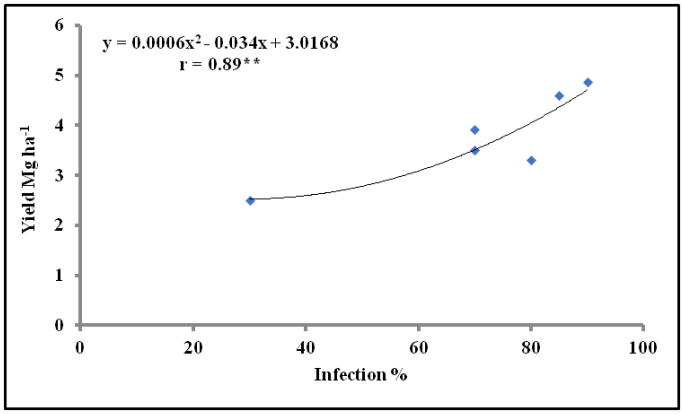

Figure 7: correlation between percentage of infection and yield

This increase in yield related to more uptake of phosphorus and availability which plays an important role in seed formation figure (8) support this result which indicated to significant correlation coefficient (r = 0.87**) between wheat yield and phosphorus content of wheat.

Infection with mycorrhiza caused increase in available phosphorus and its concentration in plant as shown from figure (9), the significant correlation coefficient between phosphorus concentration in plant and mycorrhizal infection of wheat roots with the correlation coefficient value of (r = 0.96**) support the above results.

Effect of mycorrhizal infection on wheat protein content

In current study table (2) and figure (10) showed that the mycorrhizal infection of wheat root with caused increase in protein content which was varied or depended on the type of plants used in crop rotation.

The protein content increased from 12.20% to (12.90, 13.00, 14.10, and 16.60) % for wheat cultivated after wheat, tomato, cucumber, eggplant, pepper, and broccoli respectively. The results of correlation coefficient explain the above results, since the significant correlation coefficient was recorded between wheat protein content and mycorrhizal infection percentage of wheat roots with the correlation coefficient value of (r = 0.95**) as shown from figure (10). Similar results were obtained by (Abdulkarim and Esmail, 2013).

Moreover, figure (11) indicated to significant effect of phosphorus concentration on protein content of wheat seeds this may due to the role of phosphorus in increase in root growth and absorption of nitrogen then increase in protein content as mentioned by (Esmail and Sharef, 2015).

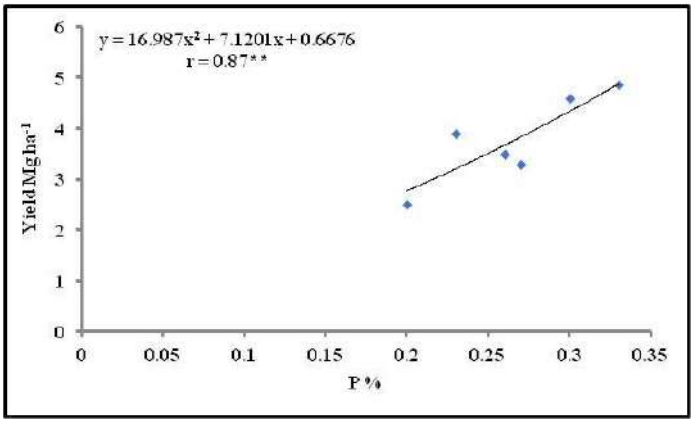

Figure 8: correlation between percentage of phosphorus and yield.

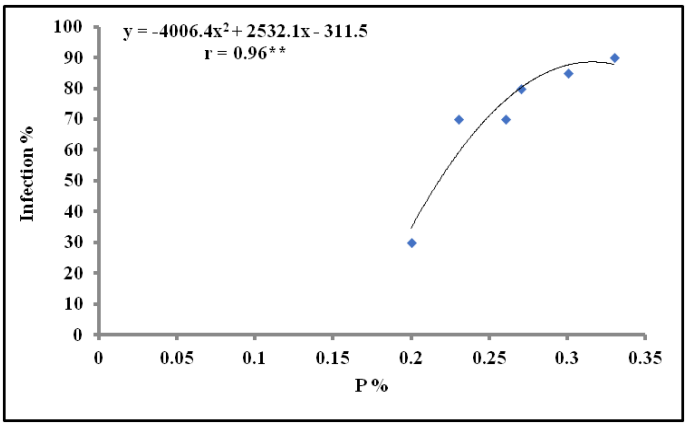

Figure 9: correlation between percentage of phosphorus and infection

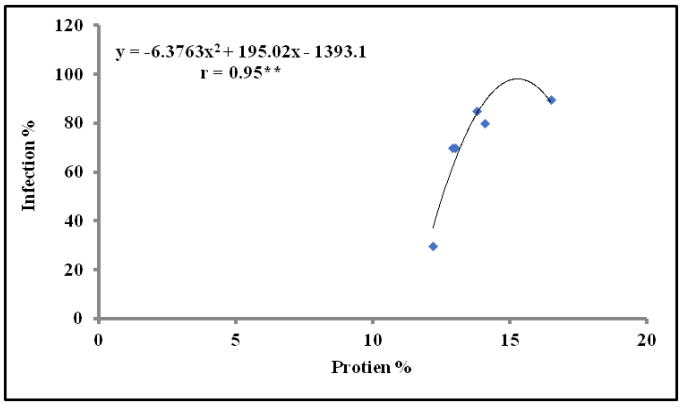

Figure 10: correlation between percentage of protein and infection

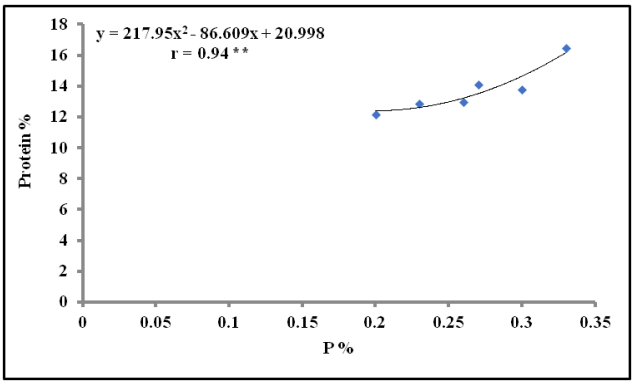

Figure 11: correlation between percentage of phosphorus and protein

The significant correlation coefficient between wheat protein content and concentration of phosphorus in wheat with the correlation coefficient value of (r = 0.94**) supported the above explanation.

4. CONCLUSION:

The interesting findings in this research points to the importance of selecting or choosing the type of vegetative crops in a rotation system, which have positive effect on wheat root infection with mycorrhizal colonies then increase in yield and quality of wheat.

REFRENCES

ABDULKARIM, L. A. & ESMAIL, A.O. 2013. Role of Mycorrhiza in availability of phosphorus and chlorophyll , carbohydrate and dry matter content of soy bean (Glycine max L.). University of Kirkuk, College of Agriculture. The 2nd international conference for agricultural scientific researches.30-31 October, Pp 11-22.

Al-HMOUD, G. & Al-MOMANY, A. 2017. Effect of four mycorrhizal products on squash plant growth and its effect on physiological plant elements. *Adv. Crop. Sci. Tech*. 5, 260.

AMIR, H., LAGRANGE, A., HASSAINE, N., & CAVALOC, Y. 2013. Arbuscular mycorrhizal fungi from New Caledonian ultramafic soils improve tolerance to nickel of endemic plant species. *Mycorrhiza*, 23, 585–595.

BAGO, B., VIERHEILIG, H., PICHI, Y. & AZCON – AGUILAR, C. 1996. Nitrate depletion and pH changes induced by the extraradical mycelium of the arbuscular mycorrhizal fungus Glomus intraradical grown in monoxenic culture . New Phytol, 133, 273–280.

BAKHSHANDEH, S., CORNEO, P.E., MARIOTTE, P., KERTESZ, M.A. & DIJKSTRA, F.A. 2017. Effect of crop rotation on mycorrhizal colonization and wheat yield under different fertilizer treatments. *Agriculture Ecosystems and Environment Journal* ,247(130-136).

BAREA , J.M., AZCON, R., & AZCON –AGUILAR, C. 1993. Mycorrhiza and crops. Advance in Plant Pathology, *London*, v.9, p.167-189.

BLACK , R.L.B. & TINKER, P.B. 1977. Interaction between effects of vesicular buscular mycorrhizae and phosphorus fertilizer on yields of potatoes in the field). *Nature. London*, 267, 510-511.

BRUNDRETT, M.C. 2008. Mycorrhizal Associations: The Web Resource. Date accessed. On August 2011 http://mycorrhizas.info/refs.html›.

DARWISH, D. A. 2007. The role of supplemental irrigation and fertilization treatment on yield, quality and nutrient balance of wheat using Modern DRIS methodology. PhD. Thesis, Salahuddin University, College of Agriculture.

DOUDS, Jr, D.D. & SCHENCK, N.C. 1990. Relationship of colonization and sporulation by VA mycorrhizal fungi to plant nutrient and carbohydrate contents. *New Phytology*, 116, 621-627.

DOUDS, J.D.D. & MILLNER, P.D. 1999. Biodiversity of Arbuscular mycorrhizal fungi in agroecosystems. Agric. *Ecol. Environ*, 47, 77-93.

ESMAIL, A.O. & SHIRREFF, S.F. 2017. Limitation of iron critical level for main agricultural soils cultivated with wheat (Triticum aestivum L.) in Sulaimani. 2nd scientific conference of Garmian University, *Journal of Garmian University, Special issue,2017*, page 375-394.

GANUGI, P., MASONI, A., PIETRAMELLARA , G. & BENEDETTELLI, S. 2019. A Review of Studies from the last twenty years on plant–arbuscular mycorrhizal Fungi Associations and Their Uses for Wheat Crops. *Agronomy journal*, 9, 840.

HOWARD, R.J. 1996. Cultural control of plant diseases: A historical perspective. *Canadian Journal of Plant pathology***,** 18, 145-150.

IkE-IZUNDU, N.E. 2007. Interaction between arbuscular mycorrhizal fungi and soil microbial populations in the rhizosphere. MSc Thesis. Rhodes University. Republic of South Africa, pp. 25-32.

JIN, J., WANG, G., LIU, X., PAN, X. & HERBERT, S.J. 2005. Phosphorus application affects the soybean root response to water deficit at the initial flowering and full pod stages. *Soil Sci Plant Nutrition*, 51, 953–960.

LIU, C., RAVNSKOV, S., LIU, F., RUBAEK, G. H. & ANDERSON, M. N. 2018. Arbuscular mycorrhizal fungi alleviate abiotic stresses in potato plants caused by low phosphorus and deficit irrigation/partial root-zone drying. J. *Agric. Sci*, 156, 46–58.

LIU, L. Z., GONG, Z. Q., ZHANG, Y. L. & LIi, P. J. 2014. Growth, cadmium uptake and accumulation of maize (Zea mays L.) under the effects of arbuscular mycorrhizal fungi. *Ecotoxicology*, 23, 1979–1986.

MIRANSARI, M. 2012. "Role of phytohormone signaling during stress," in Environmental Adaptations and Stress Tolerance of Plants in the Era of Climate Change, eds P. Ahmad and M. Prasad *(New York, NY: Springer)*, 381–393.

MIRANSARI, M. 2017. Arbuscular Mycorrhizal Fungi and Heavy Metal Tolerance in Plants. In book: Arbuscular Mycorrhizas and Stress Tolerance of Plants, pp.147-161.

OCAMPO, J.A. & HAYMANM D.S. 1981. Influence of plant interactions on vesicular-arbuscular mycorrhizal infections. II. Crop rotations and residual effects of non-host plants. *New Phytologist, Cambridge*, Vol.87, pp.333-343.

ORTAS, I. 2012. The effect of mycorrhizal fungal inoculation on plant yield, nutrient uptake and inoculation effectiveness under long-term field conditions. *Field Crops Res*. 125, 35–48.

PHILIPS, J.M. & HAYMAN, D.S. 1970. Improved procedure for clearing roots and staining parasitic and vesicular mycorrhizal fungi for rapid assessment of infection. Transactions of British Mycological Society, *Cambridge, Vol*. 55, Pp.158-160.

PIERCE, F.J. & RICE, C.W. 1998. Crop Rotation and its Impact on Efficiency of Water and Nitrogen Use. In: Cropping Strategies for Efficient Use of Water and Nitrogen, *Hargrove, W.L. (Ed.). American Society of Agronomy. Madison*, USA, Pp: 21-36.

ROWELL, D. L. 1996. Soil Science. Methods and application. Reading Univ. UK. JZS (Part-A).

SAWERS, RJH., GUITIJAHR, C. & PASZKOWSKI, U. 2008. Cereal mycorrhiza: an ancient symbiosis in modern agriculture. *Trends Plant Sci*, 13, 93–97.

TOBAR, R.M., AZCON, R., BAREA, J.M. 1994. Improved nitrogen uptake and transport from N15-labeled nitrate by external hyphae of arbuscular mycorrhiza under water-stressed conditions. *New Phytologist*, 126, 119–122.

TROUVELOT, A., KOUGH. J.L . & GIANINAZZI-PERSON, V. 1986. Mesure du taux de mycorhization VA d'un système radiculaire. Recherche de méthodes d'estimation ayant une signification fonctionnelle. In: Physiological and Genetical Aspects of Mycorrhizae, Gianinazzi-Pearson V. and S. Gianinazzi (eds.). *INRA Press, Paris*, pp. 217-221.

TURK, M. A., T. A. ASSAF., HAMEED, K. M. & Al-TAWAHA, A. M. 2006. Significance of Mycorrhizae. *World J. Agri. Sci*, 2, 16-20.

TURRINI, A., BEDINI, A., LOOR, M.B., SANTINI, G., SBRANA, C., GIOVANETTI, M., & AVIO, L. 2018. Local diversity of native arbuscular mycorrhizal symbionts differentially affects growth and nutrition of three crop plant species. *Biol Fertil Soils* 54, 203–217.

WANG, J., FU, Z.Y.; ZHNG, H., ZHU, L.J., YUAN, Y., XU, L., WANG, G.G., ZHAI, L., YANG, L. & ZHANG, J. 2019. Arbuscular Mycorrhizal Fungi Effectively Enhances the Growth of Gleditsia sinensis Lam. Seedlings under Greenhouse Conditions. *Forests*, 10, 567.

ZANCO Journal of Pure and Applied Sciences
The official scientific journal of Salahaddin University-Erbil
https://zancojournals.su.edu.krd/index.php/JPAS

ISSN (print):2218-0230**, ISSN (online):** 2412-3986**, DOI: http://dx.doi.org/10.21271/zjpas**

RESEARCH PAPER

Phytoremediation Efficiency of Some Evergreen Plant Genera for Lead Polluted Soil

Shilan Farhad Mamand, Nashmeel Saeed Khudhur and Dalshad Azeez Darwesh[1]

[1]Department of Environmental Science and Health, College of Science, Salahaddin University-Erbil, Kurdistan Region, Iraq

A B S T R A C T:

A pot experiment was performed to determine the efficiency of phytoremediation of some evergreen plants to lead in a polluted soil. The experiment was a factorial completely randomized design with three replications. The first factor was four evergreen plant genera involved *Dodonaea viscosa* L., *Myrtus communis* L., *Platycladus orientalis* L. and *Ficus benjamina* L. used as phytoremediators. Whereas, the second factor was different concentrations of lead (0, 100, 200 and 300 $mg.kg^{-1}$) which were prepared using laboratory grade $PbCl_2$. The results indicated that the highest bioaccumulation factor (BF) (39.15 and 19.39) were observed in *Dodonaea viscosa* and *Ficus benjamina* respectively. However, the maximum values of total Pb (127.53, 1084.96 and 106.99 $mg.kg^{-1}$) were detected in *Platycladus orientalis*, *Dodonaea viscosa* and *Myrtus communis* respectively. The values of BF and translocation factor (TF) showed that *Dodonaea viscosa* is the most effective phytoremediator among the other studied plants.

KEY WORDS: Lead, Phytoremediation, Soil, Pollution.
DOI: http://dx.doi.org/10.21271/ZJPAS.32.5.17
ZJPAS (2020), 32(5); 174-178.

1. INTRODUCTION

Recently, the type and content of heavy metals have gradually increased due to human activities, resulting in environmental deterioration. Heavy metals can enrich through food chains, thus they are highly hazardous to the environment and organisms (Jean-Philippe *et al.*, 2012; Sayadi and Rezaei, 2014). The most contaminant heavy metals are arsenic (As), cadmium (Cd), chromium (Cr), copper (Cu), lead (Pb), mercury (Hg) and nickel (Ni). Pb and Cd gained more attention because they are widely spread, highly toxic to plant functions (Verma and Dubey, 2003) and more persistence, so they cannot degrade naturally like other organic pollutants and they accumulate in different parts of food chains (Khudhur, *et al*., 2016).

Many studies showed that lead is one of the inhibitors of plant metabolic processes such as water uptake, nitrogen assimilation, respiration, photosynthesis and transcription. Lead may inactivate various enzymatic activities via binding to sulfhydryl (SH-) groups and intensifying reactive oxygen species (ROS) production leading to oxidative stress (Prasad *et al.*, 1999). Moreover, lead can negatively affect the structure of mitochondria through decreasing mitochondrial cristae and in turn lowering the capability of oxidative phosphorylation (Malecka *et al*., 2001).

Soils may be polluted with heavy metals due to their potential toxicity and high persistence, and represent serious environmental problems that require effective and reasonable solutions. Thus, phytoremediation, a remediation method of contaminated soils, has developed with more cost-effective and fewer side effects than chemical and physical approaches (Lone *et al.*, 2008). Phytoremediation is a diverse plant-based technologies used for cleaning contaminated soils by applying either naturally occurring or

* **Corresponding Author:**
Nashmeel Saeed Khudhur
E-mail: nashmeel.khudhur@su.edu.krd or nashmeel@gmail.com
Article History:
Received: 07/01/2020
Accepted: 03/0507/2020
Published: 13/10 /2020

genetically engineered plants (Flathman and Lanza, 1998).

There are several phytoremediation mechanisms like phytostabilization, phytovolatilization or phytoextraction of the heavy metals from plant harvesting sites. Phytoextraction is the most promising technique that has received increasing attention from researchers for remediating heavy metal polluted soils (Robinson *et al.*, 2009). Plant species that accumulate high concentrations of heavy metals in their shoots and produce large biomass after removing a great amount of metal should select for phytoremediation (Lone *et al.*, 2008). The rapid increases in population growth and industrial development in Kurdistan region of Iraq in the last fifteen years have resulted in increasing the demand of energy, specific translocation vehicles and building raw materials. For these purposes a large amount of several heavy metals particularly lead from various sources were discharged to the environment without any quality control, monitoring and prehistoric analyses, thus this study aimed to assess the phytoremediation efficiency of some evergreen plant genera to lead in polluted soil.

2. MATERIALS AND METHODS

2.1. Experimental design

A pot experiment was carried out to evaluate the phytoremediation efficiency of some genera of the evergreen plant to Pb in a polluted soil; the experiment was a factorial completely randomized design with three replications. The first factor was four evergreen plant genera, which involved *Dodonaea viscosa* L., *Myrtus communis* L., *Platycladus orientalis* L. and *Ficus benjamina* L. used as phytoremediators. Whereas, the second factor was different concentrations of lead (0, 100, 200 and 300 $mg.kg^{-1}$) which prepared by using laboratory-grade $PbCl_2$. Forty-eight experimental pots under sixteen combined treatments were tested each with three replications. Each pot packed with 16 Kg air-dried soil, after sieving via 4-mm sieve. Some physicochemical characteristics of the studied soil (table 1) were determined according to the described methods by (Richards,1954; Allen *et al*.,1974; Ryan *et al*., 2001 and Pansu and Gautheyrou, 2006). Three plants of each genera were planted in each pot. Plants were irrigated with water whenever needed to maintain soil moisture near field capacity by weighting methods and weeding done were needed.

Table 1: Physical and chemical characteristics of the studied soil.

Soil properties		Values
Particle size distribution (%)	Sand	63.0
	Silt	13.2
	Clay	23.8
Texture name		Sandy Clay Loam
Moisture content (%)		4.50
pH		7.56
Electrical conductivity (EC) ($dS.m^{-1}$)		0.40
Organic Matter (OM) (%)		0.61
Total nitrogen (N) (%)		0.11
Total phosphorus (P) (ppm)		23

2.2. Sampling and analyses of soil and plants

Soil samples were collected using core sampler (23 cm high and 4 cm in diameter) from the base of each uprooted plants, and packed in properly labeled polyethylene bags. Samples were oven-dried at 105 °C for 24 hours then sieved and kept in small containers until analyses. Plants were harvested six months after growth, each plant genera were separately collected and packed in properly labeled polyethylene bags. Plant samples were washed and cleaned with tap water, then oven dried at 70 °C for 24 hours, and ground into a powder and kept in small containers until analyses. Wet and dry weights of shoot and root systems were taken. Lead concentration in the soils and plant parts were determined using the XRF device (Genius 5000 XRF) (Khudhur, 2018).

2.3. Pollution quantification

The quantification of soil pollution was calculated through transfer factor (TF), plant bioaccumulation factor (BF), contamination factor (CF) and pollution load index (PLI).

2.3.1. Bioaccumulation factor (BF)

Bioaccumulation factor is the ratio of contaminant from the plant's root and shoot to soil, and used as a measure of plant effectiveness in concentrating pollutants into aerial part (Fayiga *et al*., 2004).

The following formula is used for calculation of bioaccumulation factor (BFs):

$$BF = \frac{M\ shoot}{M\ soil} \quad \ldots\ldots\ldots (1)$$

Where: M_{shoot} is the metal content in shoot (mg.kg^{-1} dry wt); M_{soil} is the total metal content in soil (mg.kg^{-1}). M_{soil} was determined by adding natural total soil content of metal with its applied content in soil.

2.3.2. Translocation factor (TF)

Translocation factor is used to calculate the efficiency of a plant in transferring a chemical from roots to shoots. It is the quotient of contaminant concentration in shoots to roots (Sun *et al*. 2011). Translocation factor (TFs) calculates by this formula:

$$TF = \frac{M\ shoot}{M\ root} \quad \ldots\ldots\ldots\ldots (2)$$

Where: M_{shoot} is the metal content in shoots (mg.kg^{-1} dry wt); M_{root} is the metal concentration in roots of the plants (mg.kg^{-1} dry wt).

2.3.3. The Contamination Factor (CF)

To assess the concentration of a metal, a normalization method has suggested by Simex and Helz (1981). By this study, CF normalized lead concentrations using Al and its background concentration was normalized in unaffected soil from the studied area (Khudhur *et al*., 2018). EF is calculated as follow:

$$CF = \frac{M\ sample}{M\ background} \quad \ldots\ldots\ldots\ldots (3)$$

2.3.4. Pollution Load Index (PLI)

PLI has calculated as n^{th} root of the product of the n CF, according to the equation adopted from (Muhammad *et al.*, 2013).

$$PLI = (CF_1 \times CF_2 \times CF_3 \times \cdots CFn)^{1/n} \quad \ldots\ldots (4)$$

2.4. Statistical Analyses

The experimental layout was a factorial completely randomized design (Factorial CRD). Data were statistically analyzed using SPSS version 23. All data expressed as mean value, the difference among the means of plant genera, lead concentration and their combination were compared by applying Duncan multiple comparison tests at the level of significant 5% (Townend, 2002).

3. RESULTS AND DISCUSSION

From the analysed data given in (table 2), the plant genera were significantly ($p \leq 0.05$) affected by the total concentration of lead in shoot, root and soil.

Table 2. Concentration of lead in shoot, root and soil of various plant genera.

Plant genera	Lead concentrations mg.kg^{-1}		
	Shoot	Root	Soil
Dodonaea viscosa	70.42^{b}	1084.96^{a}	96.77^{a}
Myrtus communis	69.75^{b}	326.69^{a}	106.99^{a}
Ficus benjamina	27.08^{c}	541.35^{a}	55.08^{a}
Platycladus orientalis	127.53^{a}	592.29^{a}	64.95^{a}

The maximum Pb values of 127.53, 1084.96 and 106.99 mg.kg^{-1} were recorded by *Platycladus orientalis*, *Dodonaea viscosa* and *Myrtus communis* respectively. The variation of Pb content in various plant genera is highly related to environmental factors in addition to variation in physiological and anatomical properties of roots. The results indicate that the higher concentration of pb recorded in the root system of all plants, and this may be related to the limited transfer of lead in plant, thus a great proportion is accumulated by roots and this result and interpretation agreed with those reported by (Kabata-Pendias and Pendias, 2001).

The data presented in (table 3) revealed that the application of different levels of lead significantly ($p \leq 0.05$) were affected the total concentration of lead in shoot, root and soil.

Table 3. Effect of different Pb doses on lead concentration in shoot, root and soil of various plant genera.

Pb Doses mg.kg^{-1}	Lead concentrations mg.kg^{-1}		
	Shoot	Root	Soil
D0(control)	50.39^{a}	35.96^{b}	11.01^{b}
D1(100)	64.17^{a}	215.19^{b}	66.16^{b}
D2(200)	90.72^{a}	860.37^{ab}	87.01^{ab}
D3(300)	89.49^{a}	1433.77^{a}	159.61^{a}

The highest value (90.72) and (1433.77, 159.61) mg.kg^{-1} were recorded in treatments that received (200) and (300) mg lead.kg^{-1} respectively. This may be due to the accumulation

of lead near the soil surface and mainly due to its sorption by clay mineral fraction particularly calcite, thus the availability of lead in this kind of soil decreased. The results indicate that the concentration of lead in shoot, root and soil increase with increasing the applied doses, and the reason behind the higher concentration of pb in root and shoot systems is that the absorption of Pb is passive thus the rate of its uptake from the soil is higher. This result and explanation are similar to those reported by (Kabata-Pendias and Pendias, 2001).

The application of Pb to soil significantly affects the plants BF and TF values (figure 1). According to the results, TF for all plant genera is < 1.

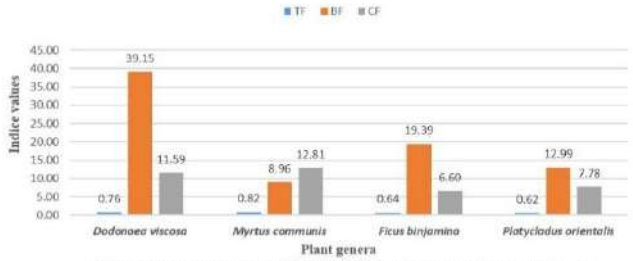

Figure 1. Transfer Factor, Bioaccumulation Factor and Contamination Factor of Pb in plant genera

This indicates the effective translocation of Pb from roots to shoot had the lowest TF. This demonstrates a lower ability to translocate Pb from the root to aboveground biomass and indicates the capability of these plants for absorbing and accumulating Pb in their roots. The highest BF values (39.15 and 19.39) were observed in *Dodonaea viscosa* and *Ficus benjamina* respectively, while the lowest BF values (12.99 and 8.96) were determined in *Platycladus orientalis* and *Myrtus communis* respectively. Although, these plants had high values of BF, they have the lowest TF in contrast. As well as, the CF in *Myrtus communis* and *Dodonaea viscosa* had the highest values with (12.81 and 11.59) respectively, and *Platycladus orientalis* and *Ficus benjamina* had the lowest value with (7.78 and 6.60) respectively.

The analysed data in (figure 2) showed that the value of BF and CF were increased with increasing the applied dose of lead. The maximum values (34.89 and 19.12) were observed in treatment that received 300 $mg.kg^{-1}$ of lead, while the result indicates that the value of TF decreased with increasing the lead doses. According to the values of BF and TF, *Dodonaea viscosa* was the most effective phytoremediator among all plant genera, and these results are similar to those reported by (Celebi *et al.*, 2017). However, pollution load index (PLI) of Pb concentrations was 4.95, which reveals high Pb contamination in soil (Muhammad *et al.*, 2013).

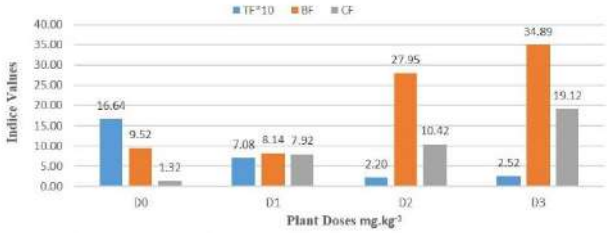

Figure 2. Effect of defferent levels of Pb on Transfer Factor, Bioaccumulation Factor and Contamination Factor.

These results and interpretations were confirmed by recording a significant positive correlation between Pb doses and its concentrations in shoot and root system of the plants with correlation coefficient R^2 = 0.939 and 0.978 respectively. (Figures 3 and 4). Similar results reported by (Muhammad *et al.*, 2013).

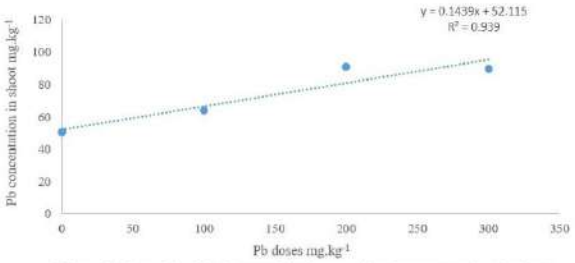

Figure 3. Correlatioship between Pb doses and lead concentration in shoot system

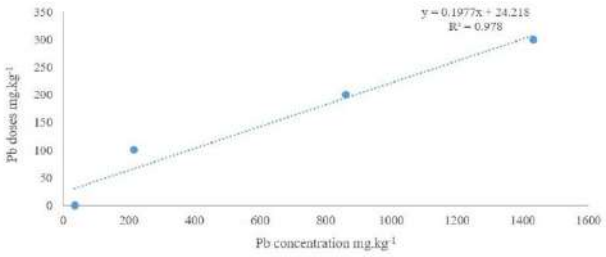

Figure 4. Correlationship between Pb doses and Pb concentarion in root system

4.Conclusion

By the present study, although, the soil was highly polluted by lead according to pollution load index value (4.95 > 1), *Dodonaea viscosa* showed the strongest tendency toward absorption and accumulation of lead in its tissues among the other

selected plants. This may be due to the root type of *D. viscosa*, which is fibrous and has a large surface area to cover and absorb more soil metals. By increasing Pb doses, a gradual increase of Pb concentrations is revealed in shoot and root systems, which suggests the plant efficiency to accumulate more heavy metals by time without damaging and affecting any of its tissues.

Conflict of Interest

The authors have no Conflict of Interest.

REFERENCES

Allen, S.E., Grimshaw, H.M., Parkinson, J.A. and Quarmby, C., 1974. Chemical Analysis of Ecological Materials. Blackwell Scientific Publications.

Çelebi, Ş.Z., Ekin, Z. and Eryiğit, T. 2017. Lead phytoremediation potential of hydroponically cultivated crop plants. *International Journal of Agriculture & Biology*, 19 (5): 1141-1148.

Fayiga, A.O., Ma, L.Q., Cao, X. and Rathinasabapathi, B., 2004. Effects of heavy metals on growth and arsenic accumulation in the arsenic hyperaccumulator *Pteris vittata* L. *Environmental pollution*, 132(2), 289-296.

Flathman, P.E. and Lanza, G.R., 1998. Phytoremediation: current views on an emerging green technology. *Journal of soil contamination*, 7(4), 415-432.

Jean-Philippe, S.R., Labbé, N., Franklin, J.A. and Johnson, A., 2012. Detection of mercury and other metals in mercury contaminated soils using mid-infrared spectroscopy. *Proceedings of the International Academy of Ecology and Environmental Sciences*, 2(3), p.139.

Kabata-Pendias, A. and Pendias H., 2001. Trace Elements in Soils and Plants. 3rd edition. CRC Press, Boca Raton, FL. pp. 413.

Khudhur, N.S., Khudhur, S.M. and Ameen, N.O.H., 2016. A study on soil bacterial population in Steel Company and some related area in erbil city in relation to heavy metal pollution. *ZANCO Journal of Pure and Applied Sciences*, 28(5), 101-116.

Khudhur, N.S., 2018. Effect of Kawrgosk Oil Refinery on some physicochemical characteristics, microbial population and biochemical properties of surface soils. *ZANCO Journal of Pure and Applied Sciences*, 30(1), 1-13.

Khudhur, N.S., Khudhur, S.M. and Ahmad, I.N., 2018. An assessment of heavy metal soil contamination in a Steel Factory and the surrounding area in Erbil City. *Jordan Journal of Earth and Environmental Sciences*, 9(1), 1-11.

Lone, M.I., He, Z.L., Stoffella, P.J. and Yang, X.E., 2008. Phytoremediation of heavy metal polluted soils and water: progresses and perspectives. *Journal of Zhejiang University Science B*, 9(3), 210-220.

Malecka, A., Jarmuszkiewicz, W. and Tomaszewska, B., 2001. Antioxidative defense to lead stress in subcellular compartments of pea root cells. *Acta Bioquimica Polonica*, 48(3), 687-698.

Muhammad, S., Shah, M.T., Khan, S., Saddique, U., Gul, N., Khan, M.U., Malik, R.N., Farooq, M. and Naz, A., 2013. Wild plant assessment for heavy metal phytoremediation potential along the mafic and ultramafic terrain in northern Pakistan. *BioMed research international*, 1-9.

Pansu, M. and Gautheyrou, J., 2006. Mineralogical Separation by Selective Dissolution. Handbook of Soil Analysis: Mineralogical, Organic and Inorganic Methods, pp.167-219.

Prasad, K.V., Saradhi, P.P. and Sharmila, P., 1999. Concerted action of antioxidant enzymes and curtailed growth under zinc toxicity in Brassica juncea. *Environmental and experimental Botany*, 42(1), 1-10.

Richards, L.A., 1954. Diagnosis and Improvement of Saline and Alkali Soils. Agriculture Handbook, 60. United State Department of Agriculture. 159pp.

Robinson, B.H., Bañuelos, G., Conesa, H.M., Evangelou, M.W. and Schulin, R., 2009. The phytomanagement of trace elements in soil. *Critical Reviews in Plant Sciences*, 28(4), 240-266.

Ryan, J., Estefan, G. and Rashid, A., 2001. Soil and Plant Analysis Laboratory Manual, International Centre for Agricultural Research in the Dry Areas (ICARDA). *Aleppo and National Agricultural Research Centre (NARC), Islamabad, Pakistan*.

Sayadi, M.H., and Rezaei, M. R., 2014. Impact of land use on the distribution of toxic metals in surface soils in Birjand city, Iran. *Proceedings of the international Academy of Ecology and Environmental Sciences*, 4(1), p.18.

Simex, S.A. and Helz, G.R., 1981. Regional geochemistry of trace elements in Chesapeake Bay. *Environmental Geology*, 3(6), 315-323.

Sun, Y., Zhou, Q., Xu, Y., Wang, L. and Liang, X., 2011. The role of EDTA on cadmium phytoextraction in a cadmium-hyperaccumulator Rorippa globosa. *Journal of Environmental Chemistry and Ecotoxicology*, 3(3), 45-51.

Townend, J. (2002). Practical Statistics for Environmental and Biological Science. John Wiley & Sons, Ltd. England.

Verma, S. and Dubey, R.S., 2003. Lead toxicity induces lipid peroxidation and alters the activities of antioxidant enzymes in growing rice plants. *Plant Science*, 164(4), 645-655.

ZANCO Journal of Pure and Applied Sciences
The official scientific journal of Salahaddin University-Erbil
https://zancojournals.su.edu.krd/index.php/JPAS

ISSN (print):2218-0230**, ISSN (online):** 2412-3986**, DOI: http://dx.doi.org/10.21271/zjpas**

RESEARCH PAPER

The effect of Diflubenzuron on Aphis fabae Scopoli and the vitality of their natural predator Coccinella septempunctat (L.)

Juhina Idrees Mohamad Ali *

Department of Plant Protection, College of Agricultural and Forestry, Mosul University, Mosul, Iraq

A B S T R A C T:

The results of the study of integration between the insect antimoulting compounds like diflubenzuron and the ladybird *Coccinella septempunctata* (L.) to control insects from the Black bean aphid, *Aphis fabae* Scopoli (Hemiptera: Aphididae). The results showed a good effect against insects Black bean aphid, *Aphis fabae* Scopoli. The results also revealed the existence of variation in a predation efficiency of male and female according the treatment method and Diflubenzuron concentration, the highest mean of males predation efficiency reached 52.7 ±4.7 % and for females 55.8 ±4.3 % when treating the plant leaf by Diflubenzuron concentration 0.15% respectively. The results also showed a variation in the mean mortality percentage of *Coccinella septempunctata* male and female and after 5 days from the treatment, highest mortality percentage in male and female were 65.4 ±3.8, 62.5 ±5.3 % respectively, when spraying at concentration of 0.5% on plant leaf with both prey and predator.

KEY WORDS: Insect, Pesticides, ladybird, Black bean aphid and plant production.
DOI: http://dx.doi.org/10.21271/ZJPAS.32.5.18
ZJPAS (2020), 32(5); 179-185.

1. INTRODUCTION

Black bean aphid, *Aphis fabae* Scopoli (Hemiptera: Aphididae) is generally considered a serious pest which cause damages in more than 200 leguminous plants and infesting all plant parts, particularly in northern Europe and worldwide, this pest has holocyclic life cycle with appear in early summer while disappear in winter and overwinter as eggs (Hansen et al., 2008) and (Barnea et al., 2005). This pest causes huge physiological changes in their hosts and reduce plant productivity in many cases (Minks et al., 1987). Many studies attempt to determine the rate of damage after the attacked by black bean aphid or other insect pests and recorded that yield losses can exceed 50% ((Hinz and Daebeler, 1981); (Shannag, 2007); (Ali, 2011) and (Sillero et al., 2017)).

Many Insecticides have been used for control of aphids on legume crops, for example in Iran insecticides like abamectin, imidacloprid and pymetrozine used to prevent these pests (Sabahi et al., 2011), while more recent investigations focused and used diflubenzuron as insecticide against black aphid (Bansal et al., 2012). Also, in Kurdistan region of Iraq crop production have been decreased due to insect pests, thus it is management is important (Ali, 2019). Direct relation present between plant infestation by aphids and predatory insects like *Coccinella septempunctata* which due to volatile compounds induce by plant host (Zhu and Park, 2005).

Diflubenzuron Dimilin is an insecticide of the benzoylurea class which widely have been used for selective control of insect pests (Subrero et al., 2019). A study by (Harðardóttir et al., 2019), explained the mechanism of diflubenzuron action on arthropod pests and confirmed that

* **Corresponding Author:**
Juhina Idrees Mohamad Ali
E-mail: juhinaisdreesali@gmail.com
Article History:
Received: 21/12/2020
Accepted: 15/06/2020
Published: 13/10 /2020

diflubenzuron inhibit the production of chitin which used by an insect to build its exoskeleton. Previous study concluded that antimoulting compounds like diflubenzuron and zertel showed a drastic effect on the bioactivity of entomophagous insect (Zaki and Gesraha, 1987). More-ever, diflubenzuron significantly reduce the growth of *Coccinella septempunctata* in cotton fields as has been shown by (Keever et al., 1977).
The present study aimed to determine rate and efficiency of diflubenzuron Dimilin with different concentration against *Aphis fabae* and predator *Coccinella septempunctata.*

MATERIALS AND METHODS

The present study was conducted during 2017 _2018 at the department of Plant Protection _ Faculty of Agriculture and Forestry University of Mosul and carried out under controlled condition (average temperature of 20+ 5 C° and relative humidity 45+ 5%) during the year 2017 - 2018.

Sample collection

The different ages of *Aphis fabae* and *Coccinella septempunctata* were collected from a pea filed (which located in), they were transferred to the laboratory via sterile plastic container with a diameter of 9 cm and examined daily to obtain adult insects of females and males.

Larvicidal activity of Diflubenzuron (Dimilin®) on *Aphis fabae*

Three different concentration of diflubenzuron (0.15, 0.3 and 0.5) have been used each with three replications on twenty immature insects of *Aphis fabae*, 2 ml of each concentration placed on the leaves of pea plant in a covered petri-dish and leaved for about 24 hours under laboratory conditions, finally mortality rate examined and recorded using Abbott equation (Bari et al., 2010).

The effect of diflubenzuron on the mortality of *Coccinella septempunctat*

Three types of treatment have been used each with three concentration of the insecticide diflubenzuron (Dimilin) (0.15, 0.3 and 0.5) on *Coccinella septempunctata*, in order to determine the best efficiency, first treatment included leaf plant, second treatment included leaf plant with the aphids and third treatment included sprinkles each of the plant leaf with both prey and predator. For each treatment 2 ml of each concentration prepared and sprayed. Ten replications of each concentration increased the rate of accuracy and also for the purpose of comparison control treatment has been sprayed with 2 ml of distal water. Finally, all data recorded after 5 days of treatment under laboratory condition and results corrected using Abbott equation. The results were analyzed using the complete global trial design and the Duncan test at a 5% probability level to determine differences between the average (O'Rourke et al., 2005).

RESULTS

Larvicidal activity of diflubenzuron Dimilin on *Aphis fabae*

The highest mortality rate of diflubenzuron Dimilin agansit *Aphis fabae* recorded at the concentration of 0.5 (76.4%), while the lowest effect of this pesticide recorded at the concentration of 0.15 (33.4%) as shown in (Table 1).

Table 1. Effect of the pesticide on *Aphis fabae*

Con.%	% Mortality	
	Rang	Mean ± S.E
0.15	20-53	33.4 ± 8.7 c
0.3	38-71	45.8 ± 7.4 b
0.5	67-92	76.4 ± 6.4 a

The effect of diflubenzuron on males of ladybird under different treatments

In leaf treatment, the results showed that diflubenzuron as an insecticide had a significant effect on efficiency of male ladybird, with increasing the concentration of this pesticide the efficiency of male ladybird decrease, for example the highest efficiency range (43.3-60.5) recorded at the concentration of 0.15. In second treatment when both leaf plant and aphids sprayed with the insecticide, result also showed that the efficiency range increase with the decrease of insecticide concentration as highest efficiency rang was (21.65-64.15) at the concentration of 0.15. this was correct for third treatment as well which

lowest concentration recorded highest efficiency rang (32.5-57.5) as has been shown in (Table 2).

Table 2. Effect of different concentrations of the insecticide and treatment method on predatory efficiency of male ladybird.

Treatments	% Con.	Efficiency		Treatments		Concentrations	
		Rang	Mean ± S.E	Rang	Mean ± S.E	Range	Mean ± S.E
first	0.15	43.3-60.5	52.7 ±4.7 a	40.8-57.75	50.2 ± 4.2 a	35.25-55.8	48.9 ± 4.1 a
	0.3	22.8-69.15	49.2 ±5.8 b				
	0.5	40.8-60.8	48.5 ±4.3 b				
second	0.15	21.65-64.15	43.9 ±5.8 c	13.6-64.15	41.3 ±5.9 b	22.5-56.65	47.65 ± 4.8 a
	0.3	19.15-69.15	45.4 ±6.7 cd				
	0.5	8.3-59.15	34.7 ±8.8 d				
third	0.15	32.5-57.5	50.1 ±5.7 ab	26.35-1.65	46.35 ±4.5 a	23.05-52.7	41.35 ± 6.8 b
	0.3	21.65-60	48.2 ±6.5 b				
	0.5	25-52.5	40.7 ±5.8 c				

* Numbers under the same letter or similar letters do not have significant differences according to Duncan polynomial test at a probability level of 5%

The effect of diflubenzuron on females of ladybird under different treatments

The result in (Table 3), illustrated that with decreasing the concentration of mentioned pesticide the efficiency rang increase. The highest recorded efficiency rang were (50-65.8), (45-57.5) and (43.3-64.15) at concentration of 0.15 for first, third and second type of treatment, respectively.

Table 3. Effect of different concentrations of insecticide and treatment method on predatory efficiency of female ladybird.

Treatments	% Con.	Efficiency		Treatments		Concentrations	
		Rang	Mean ± S.E	Rang	Mean ± S.E	Range	Mean ± S.E
First	0.15	50-65.8	55.8 ±4.3 a	49.1-63.3	54.2 ±3.2 a	48.6-60.5	54.1 ±1.8 a
	0.3	37.5-65.8	52.1 ±9.1 b				
	0.5	40.8-65.8	54.6 ±6.6 a				

Second	0.15	43.3-64.15	55 ±6.5 a	30.8-60.8	48.75±7.5 b	30-61.1	48.85 ± 8.8 b
	0.3	13.3-61.5	45.5 ±8.7 d				
	0.5	25.8-60.8	45.7 ±9.4 d				
Third	0.15	45-57.5	51.5 ±2.7 b	36.1-53.8	49.7 ±3.8 b	34.1-58.3	49.65 ±4.7 b
	0.3	34.15-57.5	48.9 ±5.8 c				
	0.5	24.15-60.8	48.9 ±6.1 c				

* Numbers under the same letter or similar letters do not have significant differences according to Duncan polynomial test at a probability level of 5%

The effect of diflubenzuron on males and females of ladybird under different treatments

The results in (Table 4 and 5) showed killing rate of this insecticides with different methods of treatment on the predatory efficiency of both males and females ladybird, killing rate increased with high concentration for all three treatment methods and there were significant differences in average mortality depending on the treatment method and the used concentration.

for male ladybird the highest mortality percentage was (57-71%) at the diflubenzuron concentration of 0.5 (third treatment methods), while for female ladybird mortality percentage was (42.5-71%) at same concentration of diflubenzuron (third treatment methods).

Table 4. Effect of different concentrations of insecticide and treatment method on the mortality of ladybirds' male

Treatments	**% Con.**	**Mortality%**		**Treatments**		**Concentrations**	
		Rang	**Mean ± S.E**	**Rang**	**Mean ± S.E**	**Range**	**Mean ± S.E**
First	0.15	0-28.5	17.1 ±4.2 h	19-33	26 ±2.8 c	14-42.5	30.2 ±5.25 c
	0.3	0-43.5	25.6 ±3.3 g				
	0.5	28.5-42.5	36.9 ±4.5 e				
second	0.15	0-28.5	22.8 ±2.5f	33-42.5	36.7 ±2.3 b	28-52	38.6 ±4.3 b
	0.3	14-57	39.7 ±6.5 d				
	0.5	42.5-57	48.3 ±4.1 c				
third	0.15	14-71	51.1 ±6.3 b	33-66	54.8 ±1.7 a	47-52	48.2 ±1.4 a
	0.3	28.5-71	51.1 ±5.1 b				
	0.5	57-71	65.4 ±3.8 a				

* Numbers under the same letter or similar letters do not have significant differences according to Duncan polynomial test at a probability level of 5%

Table 5. Effect of different concentrations of insecticide and treatment method on the mortality of ladybirds' female

Treatments	**% Con.**	**Mortality%**		**Treatments**		**Concentrations**	
		Rang	**Mean ± S.E**	**Rang**	**Mean ± S.E**	**Range**	**Mean ± S.E**
first	0.15	28.5-57	37 ±6.8 e	37.5-53	49.1 ±3.2 a	19-42.5	31 ±8.3 c
	0.3	14-71	45.5 ±9.5				

			d				
	0.5	27-71	45.4 ±3.8 b				
second	0.15	14-28.5	19.5 ±4.1 h	28-42.5	32 ±3.3 b	23.5-47	40.4 ±4.5 b
	0.3	14-42.5	28 ±3.5 g				
	0.5	28.5-71	48 ±7.6 c				
third	0.15	14-71	37 ±8.8 e	37.5-66	49 ±6.4 a	52-61.5	58.6 ±2.4 a
	0.3	42.5-57	48 ±4.2 c				
	0.5	42.5-71	62.5 ±5.3 a				

* Numbers under the same letter or similar letters do not have significant differences according to Duncan polynomial test at a probability level of 5%

DISCUSSION

Originally, insecticides have a great role in the managements of insect pests, however, the concentration and treatment methods of insecticide critical as adverse effects of insecticide on soil characteristics has been reported (Khudhur and Sarmamy, 2019). Diflubenzuron was first discovered as larvicidal after ingestion, however more comprehensive studies determined that this pesticide could also prevent hatching of eggs after direct contact of eggs or after treatment method of females (Grosscurt, 1976) and (Singh, 2015). A study by (Mulder and Gijswijt, 1973), explained the mechanism of action by diflubenzuron on larva and observed the histological changes could be resulted due to this insecticide which reported that diflubenzuron blocking of the formation of the cuticle (Mulder and Gijswijt, 1973). Additional biochemical studies resulted in a number of hypotheses about the primary mode of action of diflubenzuron in insects and explanations of the mode of action of diflubenzuron based on activation of chitinase, phenoloxidase, or on effects on ecdyson-metabolizing enzymes have probably to be considered as secondary (Verloop and Ferrell, 1977) and (Kumar et al., 2019). Many investigations have shown azadirachtin and diflubenzuron to be more toxic towards earlier instar larvae than later instar larvae when targeting a variety of other insect pests including semilooper, *Achaea janata* (Linnaeus), tobacco leaf eating caterpillar, *Spodoptera litura* (Fabricius), sweetpotato whitefly, *Bemisia tabaci* (Gennadius) and root weevil, Diaprepes abbreviates (Mule and Patil, 2000) and (Kumar et al., 2005).

From the present study highest mortality rate of diflubenzuron (Dimilin®) agansit *Aphis fabae* recorded at the concentration of 0.5 (76.4%), while the lowest effect recorded at the concentration of 0.15 (33.4%), thus with increasing concentration the effects of present pesticide has been increased directly on *Aphis fabae* and this result is agree with previous findings by Grosscurt (1978), which confirmed that insecticide action increase with increasing concentration of diflubenzuron. Another method to control fly, larvae by oral intake of diflubenzuron has been explained by (Grosscurt, 1978) , which mixed into poultry or cattle feed or into mineral blocks, in this application of diflubenzuron as a food additive, *Stomoxys calcitrans* seems to be more susceptible than *Musca domestica*.

In France a study done by Schwenke (1979), which concluded that difiubenzuron has been registered against *Thaumetopoea pityocampa* (Denis & Schiffermüller) at a concentration of 150 g considered as a great deal of field management for *T. pityocampa* . Other studies determined that some of the insecticides elicited a drastical reduction of the fecundity, especially in ladybirds fed with contaminated aphids (e.g. with teflubenzuron, fenoxycarb and flufenoxuron), moreover, chlorfluazuron was the most dangerous one for almost all larval stages (Olszak et al., 1994).

CONCLUSION

Concentration of the insecticide diflubenzuron was critical as highest mortality rate of

diflubenzuron on *Aphis fabae* recorded at the concentration of 0.5 (76.4%), while the lowest mortality rate recorded at the concentration of 0.15 (33.4%). The effects of diflubenzuron on ladybird were differ depended on treatment methods, concentration and sex of ladybird, for example highest recorded efficiency rang were (50-65.8), (45-57.5) and (43.3-64.15) at concentration of 0.15 for first, third and second type of treatment, respectively.

References

ALI, J. I. M. 2019. *Cydia pomonella* (L.)(Lepidoptera: Tortricidae) Larvae Infestation on Apple Trees According to Canopy Aspects. *ZANCO Journal of Pure and Applied Sciences,* 31**,** 135-142.

ALI, W. K. 2011. The level of sunn pest oophagous parasitoids (Hymenoptera: Scelionidae) in infested wheat fields of northern governorate in Iraq with an identification key of Trissolcus specis. *Bulletin of the Iraq Natural History Museum (P-ISSN: 1017-8678, E-ISSN: 2311-9799),* 11**,** 7-15.

BANSAL, R., MIAN, M. R., MITTAPALLI, O. & MICHEL, A. P. 2012. Characterization of a chitin synthase encoding gene and effect of diflubenzuron in soybean aphid, Aphis glycines. *International journal of biological sciences,* 8**,** 1323.

BARI, M., ISLAM, W. & KHAN, A. 2010. Pesticidal activity of Smilax zeylanica L. extracts on Cryptolestes pusillus (Schon.)(Coleoptera: Cucujidae). *Journal of Bangladesh Academy of Sciences,* 34**,** 205-208.

BARNEA, O., MUSTATA, M., MUSTATA, G. & SIMON, E. 2005. The parasitoids complex which control the Aphis fabae Scop. colonies installed on different crop species and spontaneous plants. *Lucrariles impozionului "Entomofagii si rolul lor ın pastrarea echilibrului natural" Al. I. Cuza" din Iasi***,** 99-110.

GROSSCURT, A. 1976. I OVICIDAL EFFECTS OF DIFLUBENZURON ON THE HOUSEFLY (MUSCA DOMESTICA). *hn< 9zci &107 O***,** 16.

GROSSCURT, A. C. 1978. Diflubenzuron: some aspects of its ovicidal and larvicidal mode of action and an evaluation of its practical possibilities. *Pesticide Science,* 9**,** 373-386.

HANSEN, L. M., LORENTSEN, L & .BOELT, B. 2008. How to reduce the incidence of black bean aphids (Aphis fabae Scop.) attacking organic growing field beans (Vicia faba L.) by growing partially resistant bean varieties and by intercropping field beans with cereals. *Acta Agriculturae Scandinavica Section B–Soil and Plant Science,* 58**,** 359-364.

HARÐARDÓTTIR, H. M., MALE, R., NILSEN, F. & DALVIN, S. 2019. Effects of chitin synthesis inhibitor treatment on Lepeophtheirus salmonis (Copepoda, Caligidae) larvae. *PloS one,* 14.

HINZ, B. & DAEBELER ,F. 1981. Harmful effects of the black bean aphid (Aphis fabae Scop.) on field beans. *Nachrichtenblatt fur den Pflanzenschutz in der DDR,* 35**,** 175-178.

KEEVER, D., BRADLEY JR, J. & GANYARD, M. 1977. Effects of diflubenzuron (Dimilin®) on selected beneficial arthropods in cotton fields. *Environmental entomology,* 6**,** 732-736

.

KHUDHUR, N. S. & SARMAMY, A.-G. O. I. 2019. the Determination of diazinon residues in artificially polluted soils. *ZANCO Journal of Pure and Applied Sciences,* 31**,** 1-8.

KUMAR, P., POEHLING, H. M. & BORGEMEISTER, C. 2005. Effects of different application methods of azadirachtin against sweetpotato whitefly Bemisia tabaci Gennadius (Hom., Aleyrodidae) on tomato plants. *Journal of Applied Entomology,* 129**,** 489-497.

KUMAR, R. P., BABU, K. D & .EVANS, D. 2019. Isolation, characterization and mode of action of a larvicidal compound, 22-hydroxyhopane from Adiantum latifolium Lam. against Oryctes rhinoceros Linn. *Pesticide biochemistry and physiology,* 153**,** 161-170.

MINKS, A. K., HARREWIJN, P. & HELLE, W. 1987. *Aphids: their biology, natural enemies and control*, Elsevier Amsterdam .

MULDER, R. & GIJSWIJT, M. J. 1973. The laboratory evaluation of two promising new insecticides which interfere with cuticle deposition. *Pesticide Science,* 4**,** 737-745.

MULE, R. & PATIL, R. 2000. Efficacy of diflubenzuron against tobacco leaf eating caterpillar. *Journal of Maharashtra Agricultural Universities,* 25**,** 23-26.

O'ROURKE, N., HATCHER, L. & STEPANSKI, E. J. 2005. *A step-by-step approach to using SAS for univariate & multivariate statistics*, SAS institute.

OLSZAK, R., PAWLIK, B. & ZAJAC, R. 1994. The influence of some insect growth regulators on mortality and fecundity of the aphidophagous coccinellids Adalia bipunctata L. and Coccinella septempunctata L.(Col., Coccinellidae). *Journal of Applied Entomology,* 117**,** 58-63.

SABAHI, Q., RASEKH, A. & MICHAUD, J. 2011. Toxicity of three insecticides to Lysiphlebus fabarum, a parasitoid of the black bean aphid, Aphis fabae. *Journal of Insect Science,* 11**,** 104.

SCHWENKE, W .1979 .Über die Rolle des Häutungshemmstoffes Dimilin im Waldschutz und

Waldökosystem. *Anzeiger für Schädlingskunde, Pflanzenschutz, Umweltschutz,* 52**,** 97-102.

SHANNAG, H. K. 2007. Effect of black bean aphid, Aphis fabae, on transpiration, stomatal conductance and crude protein content of faba bean. *Annals of applied biology,* 151**,** 183-188.

SILLERO, J. C., ÁVILA, C. M. & RUBIALES, D. 2017. Screening faba bean (Vicia faba) for resistance to aphids (Aphis fabae).

SINGH, S. 2015. Impact of new chemistry on biocontrol agents of major crop pests. *International Journal of Agricultural Science and Veterinary Medicine,* 3**,** 14-33.

SUBRERO, E., SFORZINI, S., VIARENGO, A. & CUCCO, M. 2019. Exposure to anti-mosquito insecticides utilized in rice fields affects survival of two non-target species, Ischnura elegans and Daphnia magna. *Paddy and Water Environment,* 17**,** 1-11.

VERLOOP, A. & FERRELL, C. Benzoylphenyl ureas--a new group of larvicides interfering with chitin deposition [in fungi and insects]. ACS Symposium Series American Chemical Society, 1977.

ZAKI, F. N. & GESRAHA, M. 1987. Evaluation of zertel and diflubenzuron on biological aspects of the egg parasitoid, Trichogramma evanescens Westw. and the aphid lion Chrysoperla carnea Steph. *Journal of Applied Entomology*.69-63 ,104 ,

ZHU, J. & PARK, K.-C. 2005. Methyl salicylate, a soybean aphid-induced plant volatile attractive to the predator Coccinella septempunctata. *Journal of chemical ecology,* 31**,** 1733-1746.

ZANCO Journal of Pure and Applied Sciences
The official scientific journal of Salahaddin University-Erbil
https://zancojournals.su.edu.krd/index.php/JPAS

ISSN (print):2218-0230**, ISSN (online):** 2412-3986**, DOI: http://dx.doi.org/10.21271/zjpas**

RESEARCH PAPER

Effect of Foliar Application of Some Micronutrients at Two Growth Stages on Growth, Yield and Yield Components of Two Bread Wheat (*Triticum aestivum L.)* Varieties

Dilan R. Hadi[1], Tareeq H. Kreem[2], Bahar J. Mahmood[3]

[1,3]Department of Field crops, College of Agricultural Engineering Sciences, Salahaddin University-Erbil, Kurdistan Region, Iraq
[2]Department of Soil and Water, College of Agricultural Engineering Sciences, Salahaddin University-Erbil, Kurdistan Region, Iraq

A B S T R A C T:

A field experiment was conducted during the growing season of 2018-2019 at the experimental farm of the college of Agricultural Engineering Sciences/ Salahaddin University- Erbil (Latitude 36˚4 N and Longitude 44˚2 E) to study the effect of Zn, Fe foliar application and their combination at two growth stages on growth and yield of two wheat varieties (*Triticum aestivum* L.). A factorial experiment (2×2×4) was conducted using randomized complete block design (RCBD) with three replicates. The research was included two wheat varieties (Hawler 2 and Hawler 4), foliar fertilization at two growth stages (Tillering GS Z25 and booting GS Z45) and four fertilizers treatments which include F_1(control), F_2 (134 mg/L) Fe as (FeSO4.7 H_2O), F_3 (270.01 mg/L Zn) as $ZnSO_4$ and F_4 ((134 mg/L Fe + 270.01 mg/L Zn) combination of (F_2.7H_2O + $ZnSO_4$). The results indicated that the treatment combination of $V_1 \times S_2 \times F_0$ recorded highest values for no. of spike plant^{-1}, no. of spikelet spike^{-1} and no. of seed spike^{-1} (4.25, 51.51 and 54.27) respectively. While the highest seed weight spike^{-1}, seed index (22.71and 45.41) were recorded for the combination treatment of $V_1 \times S_1 \times F_4$ the results also revealed that the treatment combinations ($V_2 \times S_1 \times F_4$) and ($V_1 \times S_1 \times F_1$) offered the highest and lowest seed yield respectively. The treatment combinations ($V_2 \times S_1 \times F_4$) resulted in higher seed yield by 69% compared to ($V_1 \times S_1 \times F_1$).

KEY WORDS: Wheat varieties, Foliar application, Micronutrients, stage of fertilization.
DOI: http://dx.doi.org/10.21271/ZJPAS.32.5.19
ZJPAS (2020), 32(5); 186-195.

1. INTRODUCTION

Wheat (Triticum aestivum L.) is an annual herbaceous crop which belongs to the poaceae

family it is regarded as one of the most important crop over the world and it is the third major

cereal produced after maize and rice (FAO, 2013). Wheat is the major source for human nutrition and a part of daily dietary need in different forms. According to FAO reports wheat contributes 28% of the world' s edible dry matter and 60% daily calorie intake in several developing countries.

The low wheat production is due to use of low seed quality, insufficient use of fertilizers, water shortage and no use of micronutrients (Khan et al., 1999). Micronutrients are playing a pivotal role in the yield improvement (Rehm and Sims, 2006).

Micronutrients play an important role in the increase of wheat production (Nadim et al., 2011). According to Narimani et al. (2010) lack of micronutrient effect on the quantity of wheat. Genetically cereals are low in Zn and Fe concentrations which caused reduce of bioavailability (Graham et al., 2001; Cakmak, 2002). In many Asian countries the deficiency of micronutrients is widespread because of the calcareous soils, low organic matter, high pH and high amount of bicarbonate in irrigation water

* **Corresponding Author:**
Dilan R. Hadi
E-mail: dilankhaffaf@gmail.com
Article History:
Received: 08/01/2020
Accepted: 20/06/2020
Published: 13/10 /2020

(Narimani et al., 2010). Foliar application of micronutrients increases the rate of absorption by leaf epidermis of plant and reach to other parts of plant through xylem and phloem (Hasslett et al., 2001).

Zinc is an essential micronutrient which has an important role in the growth of plants. It is required in many enzymatic reactions, metabolic processes and oxidation reduction reactions. According to Cakmak (2008) foliar application of Zn has an effective practice to improve production. Foliar application of Zn has significant effect on wheat grain yield (Bameri et al., 2012; El-Habbasha et al., 2015; Esfandiari et al., 2016).

Similarly, iron is one of the important micronutrients and considered the most abundant element on the earth as a whole. Iron is essentially participating in the process of plant photosynthesis and plays an important role in respiration, the oxidation process which releases energy from sugars and starches and the production of healthy green leaves. It also plays an essential role in metabolism of nucleic acid (Havlin et al., 2014). Since the soil of Iraqi Kurdistan region is calcareous which causes precipitation of micro nutrients (Zn and Fe) in the form of hydroxyl or carbonate which are un-available for plants at the same time soil application of them in a mineral form are useless, for this reason the foliar application of them was selected in order to study the effect of Zn, Fe and their combinations on wheat crop performance and grain yield quantity.

1. MATERIALS AND METHODS

The study was conducted at the experimental farm of the college of Agricultural Engineering Science at Grdarasha site (Latitude 36˚4 N and Longitude 44˚2 E) during the growing season of 2018-2019 to study the effect of foliar application of Zn, Fe and their combination at two growth stages on growth, yield and quality of two wheat varieties (*Triticum aestivum* L.).

A factorial experiment based on randomized completely block design (RCBD) with three replicates was used. The first factor comprised two varieties (Hawler 2 and Hawler 4) imported from Agriculture Research Center/ Erbil. The second factor included F_1 (control), F_2 (0.5 g) as ($FeSO_4.7H_2O$), F_3 (0.5 g) as ($ZnSO_4$) and F_4 (0.5+0.5 g) as (combination of $FeSO_4.7H_2O$ and $ZnSO_4$) per 750 ml distilled water for each experimental unit. The third factor included two growth stages (tillering and booting).

The field was first prepared by flooded up on 10th September, and subjected to evaporation the soil was plowed by mold board plow and rotivator to soften the soil. Table (1) exhibits some selected physical and chemical properties of the soil of the experimental site (Qadir, 2017).

Table (1): physical and chemical properties of the soil of the experimental site.

Site	Soil property		Unit	Average value
Grdarasha	Particle size distribution	Sand	g/kg	128.0
		Slit	g/kg	521.4
		Clay	g/kg	350.6
	Textural name			SiCL
	Organic matter content		g/kg	9.3
	ECe		dSm^{-1}	0.56
	pH			7.57
	Calcium carbonate equivalent		g/kg	339.0

The land was divided into plots, each block consisted of 16 experimental units, the dimensions of each unit was (1m×1m), each unit contained four rows, with row spacing of 20 cm. On 4th November, the seeds were sown manually at the rate of 100 kg ha-1 on a silty clay loam soil. Table (2) also shows some metrological parameters during the growing season.

Table (2): Metrological data for Grdarasha field during growing season of (2018-2019):

Month	Air temperature in (˚C)			Monthly precipitation (mm)	Relative humidity (%)
	Max	Min	Mean		
October	38.70	11.40	25.30	22.60	35.30
November	28.20	6.30	15.60	113.50	65.80
December	21.69	13.81	17.70	0.51	35.19
January	18.50	-0.90	8.60	96.30	71.70

February	18.50	2.80	10.00	42.40	69.30
March	21.54	0.48	11.01	173.60	72.25
April	26.62	3.51	15.06	105.50	69.57
May	39.70	10.80	25.90	5.80	39.30
Total	26.68	6.03	16.15	70.02	57.30

Studied Characters:

The studied characters included the following:

Characteristics that Studied at Flowering Stage:

Random representative samples of ten plants were used at full maturity stages from each experimental unit to stimulate the following characters:

- Total leaf area per plant (LA) cm^2:

Fifteen leaves were selected at each experimental unit to study the leaf area by the following formula:

$$\boldsymbol{Leaf\ area = (leaf\ length * leaf\ width * 0.905)}$$ (Kemp, 1960).

- Flag leaf area: Flag leaf area was determined from ten leaves of ten randomly selected plants at each experimental unit.
- Chlorophyll content:

The SPAD reading was recorded as an index of chlorophyll content three times with 10 days' interval using chlorophyll meter model (Vol 1.0) from five labeled plants at three locations on three leaves which equivalent to 45 readings for each experimental unit (Biber, 2007).

Measurements at maturity stage:

Representative samples were taken from the plants of the two inner rows from each experimental unit during physiological maturity stage. The samples were used to study the following characters:

Number of spike $plant^{-1}$, Number of spikelet $spike^{-1}$, Number of seed $spike^{-1}$: spikes were taken randomly from each experimental unit and shattered by hand then number of seeds per spike was calculated.

Weight of seed spike $^{-1}$ (g), Seed index: 1000-seed weight (g)

The wheat plant was harvested from the whole plot to determine:

Seed yield ($Mg\ ha^{-1}$): the seeds of harvested plants were threshed, cleaned and sieved to remove the impurities and weighed. The weight was converted to $Mg\ ha^{-1}$.

Statistical analysis:

The data were statistically analyzed according to the technique of analysis of variance (ANOVA) for randomized complete block design (RCBD) using SPSS program version (22) the difference among means of treatments were tested using Duncan's multiple range test at level of significant 5% 0.05 (Duncan, 1955).

2. RESULTS AND DISCUSSION

Effect of variety, growth stages, fertilizer and their treatment combinations on growth characteristics of wheat:

Leaf Area ($cm^2.Plant^{-1}$):

Table (3) Shows a significant effect of variety on plant leaf area. The highest leaf area (32.48) cm^2 was obtained from first variety (V_1). This result indicates that (V_1) is higher than (V_2) and this may be due to the genetic behavior of the variety and its adaptation to the local climatic conditions.

Additionally, Table (3) indicates that there was a positive influence of different fertilizer on leaf area of wheat. (F_3) treatment shows the highest leaf area (33.95) cm^2 than other fertilizer as well as F_1 treatment that obtained the smallest leaf area (29.09) cm^2.

F	S_1	S_2	Mean of Fertilizer
F_1	30.38 ab	27.79 b	29.09 b
F_2	31.38 ab	29.51 ab	30.44 ab
F_3	32.83 ab	35.08 a	33.95 a
F_4	32.09 ab	30.02 ab	31.06 ab

The statistical analysis of the data revealed that the combination treatment between variety and growth stage (V × S) had a significant influence on wheat leaf area. The largest leaf area (34.89) cm^2 attained from ($V_1 \times S_1$), and the minimum leaf area (28.45) cm^2 recorded from ($V_2 \times S_1$). These results obtained that there was no significant difference between the growth stages.

Leaf area was significantly affected by the combination treatment between variety and fertilizer (V × F). ($V_1 \times F_3$) treatment shows the maximum leaf area (35.05) cm^2 whereas the smallest leaf area

(27.28) cm^2 was recorded from V_2 at F_1 treatment. This differences may be due to the genetic background for the variety and its behavior under these conditions in which Zn foliar application effect on growth. The results are in accordance with El-Dahshouri (2018).

Furthermore, the impact of combination treatment between growth stage and fertilizer (S × F) was significant for this trait. (S_2 × F_3) performs the best results which was (35.08) cm^2 and the smallest leaf area (27.79) cm^2 was attained from (S_2 × F_1). This result shows that F3 fertilizer affects the leaf area at S2more than other treatments. The combination treatment among the three studied factor variety, growth stage and fertilizer (V × S × F) showed a positive effect on area of leaf. The maximum leaf area (37.73) cm^2 was recorded from the interaction (V_2 × S_2 × F_3) whereas the smallest leaf area (26.71) cm^2 was obtained from the interaction (V_2 × S_1 × F_2).

Table (3): Effect of variety, growth stage, fertilizer and their treatment combinations on Leaf Area (cm^2.$Plant^{-1}$):

Variety (V)	Fertilizer (F)	Growth stage (S)		Variety ×Fertiliz
		S_1	S_2	
V_1 (Hawler 2)	F_1	33.61 ab	28.19 b	30.90 ab
	F_2	36.05 ab	29.03	32.54 ab
	F_3	37.66 a	32.43	35.05 a
	F_4	32.24 ab	30.63	31.43 ab
V_2 (Hawler 4)	F_1	27.16 b	27.39 b	27.28 b
	F_2	26.71 b	29.98	28.35 ab
	F_3	27.99 b	37.73 a	32.86 ab
	F_4	31.94 ab	29.42	30.68 ab

V	S_1	S_2	Mean of Variety
V_1 (Hawler 2)	34.89 a	30.07 b	32.48 a
V_2 (Hawler 4)	28.45 b	31.13 ab	29.79 b
Mean of growth stages	31.67 a	30.60 a	

Flag Leaf Area (cm^2. $Plant^{-1}$):

Flag leaf contributes to most photosynthetic assimilates in wheat and thus it assumes greatest importance from grain yield. Figure (1) shows the combination treatment effect of the studied factors (V × S × F) on flag leaf, the highest value (57.48) cm^2 was obtained from the treatment combination (V_1 × S_2 × F_2) while the lowest value (33.43) cm^2 were recorded from the combination treatment treatments (V_2 × S_1 × F_1). Similar results were also obtained by Rawashdeh and Sala (2015). Fe when applied alone as foliar spray increased the area of flag leaf as well as broader flag leaves help in greater yield (Singh et al., 2015). This can be due to the positive effect of Fe foliar application and it can increase growth, thereby increase the length of flag leaf of wheat. Kahrariyan et al. (2013) reported the same results**.**

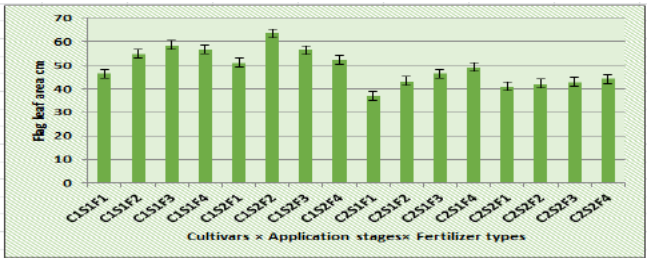

Figure (1) Effect of the treatment combinations among (V, S and F) on flag leaf cm^2.

Chlorophyll Content (SPAD):

Figure (2) presents the effect of treatment combination varieties, application stages and fertilizer types (V × S × F) on chlorophyll content the highest value (29.42 SPAD) was recorded from (V_1× S_1× F_3). While, the lowest value (20.50 SPAD) was obtained from (V_2 × S_1× F_1). This demonstrates the role of treatment combination in creating different conditions for plant growth.

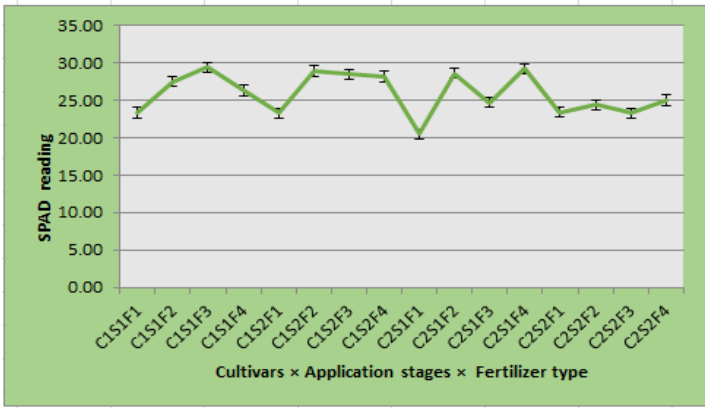

Figure (2): Leaf chlorophyll content as influenced by the interactions among (V× S ×F).

Effect of variety, growth stages, fertilizer and their treatment combinations on yield and yield parameters of wheat:

Spike Length (cm):

The results displayed in Table (4) indicates that the spike length was significantly affected by only

the combination treatment treatments (V × F × S), (F × S) and (V × S) were affected significantly on spike length. The highest and lowest values were (9.94, 10.03 and 10.23) cm which recorded from ($V_2 \times S_2$), ($S_2 \times F_4$) and ($V_2 \times S_2 \times F_4$) respectively, while the lowest values (9.14, 8.69 and 8.52) cm were obtained from ($V_2 \times S_1$), ($S_1 \times F_1$) and (($S_1 \times V_1 \times F_1$) respectively.

This may be due to the role of varieties, fertilization and stage of fertilization application in creating different growth conditions for plant growth as mentioned by Darwesh (2007) and Kahriyan et al. (2013).

Table (4): Effect of variety, growth stage, fertilizer and their treatment combinations on Spike Length (cm):

Variety (V)	Fertilizer (F)	Growth stages		Variety ×Fertilizer
		S_1	S_2	
V_1 (Hawler 2)	F_1	8.52 a	9.25 a	8.88 a
	F_2	9.21 a	9.34 a	9.28 a
	F_3	9.81 a	8.99 a	9.40 a
	F_4	9.18 a	9.83 a	9.51 a
V_2 (Hawler 4)	F_1	8.85 a	9.88 a	9.36 a
	F_2	9.29 a	9.55 a	9.42 a
	F_3	9.16 a	10.09 a	9.63 a
	F_4	9.25 a	10.23 a	9.74 a

F	S_1	S_2	Mean of Fertilizer
F_1	8.69 b	9.56 ab	9.12 a
F_2	9.25 ab	9.45 ab	9.35 a
F_3	9.49 ab	9.54 ab	9.51 a
F_4	9.21 ab	10.03 a	9.62 a

V	S_1	S_2	Mean of Variety
V_1 (Hawler 2)	9.18 ab	9.35 ab	9.27 a
V_2 (Hawler 4)	9.14 b	9.94 a	9.54 a
Mean of growth stages	9.16 a	9.64 a	

Number of Spike Plant $^{-1}$:

Data in table (5) explained that the number of spikes plant^{-1} was significantly affected by wheat varieties. The highest number of spike (3.67) was recorded from (V_1) variety. This result was in agreement with those reported by Ozturk et al. (2006), they concluded the maximum wheat yield is closely associated to the variety potential to give high number of spikes plant $^{-1}$. The results of the same table show that the significant differences of Zn and Fe spray on the number of spike plant^{-1}. The maximum amount of spike plant^{-1} (3.75) was obtained from the combination treatment of ($F_2 + F_3$) Whereas, the lowest number of spike (2.79) was recorded from F1 treatment.

Regarding the effect of combination treatment between variety and fertilizer (V × F) on the number of spike plant^{-1} it showed significant differences. V_1 variety and ($F_2 + F_3$) spraying showed the highest number of spike plant^{-1} (4.02) however, V_2 at F_1 treatment recorded the minimum amount of spike plant^{-1} (2.77). This may be due to the different growth characteristics and capabilities of high yielding quantity of varieties.

The same table also indicates to significant effect of combination treatment between growth stage × fertilizer (S × F) on the same trait. The largest amount of spike plant^{-1} (3.91) was obtained from ($S_2 \times F_2$) whereas the lowest amount of spike (2.74) noted from ($S_2 \times F_1$).

Furthermore, the combination treatment among the three studied factors variety, growth stage and fertilizer (V × S × F) had a positive combination treatment on number of spike plant^{-1}. ($V_1 \times S_2 \times F_2$) showed the highest amount of spike (4.25). The combination treatment among ($V_1 \times S_2 \times F_1$) recorded the smallest number of spike plant^{-1} (2.60). The results indicate that same variety at same growth stages by applying different fertilizer shows different amount of spike plant^{-1}. The present results are similar to that of Singh et al. (2015) in which they stated that maximum number of spikes per plant were obtained when $FeSO_4$ applied alone.

Table (5): Effect of variety, growth stage, fertilizer and their treatment combinations on Number of Spike Plant $^{-1}$:

Variety (V)	Fertilizer (F)	Growth stages (S)		Variety ×Fertilizer
		S_1	S_2	
V_1 (Hawler 2)	F_1	3.00 cde	2.60 e	2.80 c
	F_2	3.68 a-d	4.25 a	3.97 a
	F_3	3.96 ab	3.82 abc	3.89 ab
	F_4	4.04 ab	4.00 ab	4.02 a
V_2 (Hawler 4)	F_1	2.66 e	2.88 de	2.77 c
	F_2	3.38 a-e	3.31 b-e	3.34 bc
	F_3	3.85 abc	3.11 b-e	3.48 ab
	F_4	3.48 a-e	3.47 a-e	3.48 ab

F	S_1	S_2	Mean of Fertilizer
F_1	2.83 b	2.74 b	2.79 b
F_2	3.53 a	3.78 a	3.66 a
F_3	3.91 a	3.47 a	3.69 a
F_4	3.76 a	3.74 a	3.75 a

V	S_1	S_2	Mean of Variety
V_1 (Hawler 2)	3.67 a	3.68 a	3.67 a
V_2 (Hawler 4)	3.34 a	3.19 a	3.27 b
Mean of growth stages	3.51 a	3.43 a	

Number of Spikelet Spike $^{-1}$:

The presented results in the table (6) indicated to significant effect of Zn and Fe spraying on number of spikelet spike $^{-1}$. The highest number of spikelet (47.30) was obtained from F_3 fertilizer while the lowest number (40.48) was noted from F1 treatment. This is because $ZnSO_4$ is known to have an essential role as a metal component of enzymes or as a functional, structural or regulatory co-factor of a large number of enzymes (Hotz and Braun, 2004). Data in the same table illustrated that (V_1× F_2) treatment significantly had highest number of spikelet spike $^{-1}$. Whereas, the lowest number of spikelet spike $^{-1}$ (38.66) was attained from (V_1× F_1) treatment, it means that application of F_2 alone is more effective for this trait. This results are in accordance with those obtained by Zain et al. (2015) they reported that the application of Fe micronutrient substantially improved number of spikelet spike $^{-1}$. Although, there was a significant difference of combination treatment between the growth stage and fertilizer on the same trait. The largest number of spikelet spike $^{-1}$ (48.29) was noted from (S_1× F_3) combination treatment.

Furthermore, the combination treatment between the three factors Variety, growth stage and fertilizer (V × S × F) spraying affected positively on number the number of spikelet spike $^{-1}$. (V_1 × S_2 × F_2) was showed the highest number of spikelet (51.51) while the combination treatment (V_1 × S_2 × F_1) was recorded the minimum amount of spikelet spike^{-1} (37.09). The results are in accordance with those founded by Patel et al. (2009) they showed the increase in yield by spraying $FeSO_4$ as foliar application.

Table (6): Effect of variety, growth stage, fertilizer and their treatment combinations on Number of Spikelet Spike $^{-1}$:

Variety (V)	Fertilizer (F)	Growth stages (S)		Variety ×Fertilizer
		S_1	S_2	
V_1 (Hawler 2)	F_1	40.23 ab	37.09 b	38.66 c
	F_2	47.82 ab	51.51 a	49.66 a
	F_3	47.92 ab	45.74 ab	46.83 ab
	F_4	40.49 ab	42.11 ab	41.30 bc
V_2 (Hawler 4)	F_1	42.61 ab	41.99 ab	42.30 bc
	F_2	40.78 ab	43.95 ab	42.36 bc
	F_3	48.67 ab	46.88 ab	47.77 ab
	F_4	49.16 a	45.07 ab	47.12 ab

F	S_1	S_2	Mean of Fertilizer
F_1	41.42 ab	39.54 b	40.48 b
F_2	44.30 ab	47.73 a	46.01 a
F_3	48.29 a	46.31 ab	47.30 a

V	S_1	S_2	Mean of Variety
V_1 (Hawler 2)	44.11 a	44.11 a	44.11 a
V_2 (Hawler 4)	45.30 a	44.47 a	44.89 a
Mean of growth stages	44.71 a	44.27 a	
F_4	44.83 ab	43.59 ab	44.21 ab

Number of Seed Spike $^{-1}$:

Table (7) Explained that there was a significant difference between the varieties used in the study as well as the combination treatment between variety and growth stage on number of seed spike $^{-1}$. The highest number of seeds spike^{-1} (46.94) and (48.26) were attained from (V1) and the combination treatment of (V_1× S_2) respectively. While the minimum values (41.22) and (41.06) were recorded from (V_2) and (V_2× S_2) treatments. The results indicated to that the varieties used had different growth characteristics and ability of seed production

whereas there was no significant difference between the growth stages regarding the number of seed spike $^{-1}$.

The results revealed that combination treatment between variety and fertilizer spraying had significant influence on the same trait. (V_1) at (F_2) treatment obtained the maximum number of seed spike $^{-1}$ (51.65). In addition, the combination treatment among all the studied factor variety, growth stage and fertilizer (V × S × F) significantly different on the number of seed spike^{-1}, which were (54.27 and 36.00) seed spike $^{-1}$ for the combination treatment treatments ($V_1 \times S_2 \times F_2$) and ($V_2 \times S_1 \times F_2$) respectively. This shows that F_2 fertilizer was more effective when applied at booting and this may due to the favorable conditions at this stage and let the plants absorb it. The quantity of seed related to the number of spike plant $^{-1}$ (table 5) which shows that V_1 at S_2 with application of F_2 has significant effect regarding the spike production. The results of this study might be because of Fe had critical role in crop growth, involving in photosynthesis processes, respiration and other biochemical and physiological activates and thus their importance in achieving higher yields (Salih, 2013).

Table (7): Effect of variety, growth stage, fertilizer and their treatment combinations on Number of Seed Spike $^{-1}$:

Variety (V)	Fertilizer (F)	Growth stages (S)		Variety ×Fertilizer
		S_1	S_2	
V_1 (Hawler 2)	F_1	40.38 ab	46.93 ab	43.66 ab
	F_2	49.03 ab	54.27 a	51.65 a
	F_3	45.40 ab	48.70 ab	47.05 ab
	F_4	47.65 ab	43.13ab	45.38 ab
V_2 (Hawler 4)	F_1	39.43 b	41.68 ab	40.56 b
	F_2	36.00 b	42.35 ab	39.18 b
	F_3	45.55 ab	38.78 b	42.17 b
	F_4	44.55 ab	41.42 ab	42.98 ab

F	S_1	S_2	Mean of Fertilizer
F_1	39.91a	44.31 a	42.11 a
F_2	42.52 a	38.31 a	45.41 a
F_3	45.48 a	43.74a	44.61 a
F_4	46.10 a	42.27 a	44.19 a

V	S_1	S_2	Mean of Variety
V_1 (Hawler 2)	45.61 ab	48.26 a	46.94 a
V_2 (Hawler 4)	41.38 b	41.06 b	41.22 b
Mean of growth stages	43.50 a	44.66 a	

Seed Weight Spike $^{-1}$ (g):

Table (8) showed the existence of a significant effect of varieties on the seed weight spike $^{-1}$. (V_2) showed higher results (29.26) g than (V_1). It seems that (V_2) profit from existing conditions due to compatibility with climate of Kurdistan region which may cause increasing in seed weight spike $^{-1}$.

On the other hand, the seed weight spike $^{-1}$ significantly affected by the combination treatment (variety and growth stage) (V × S) and (Variety and fertilizer) (V × F). The maximum seed weight (29.61) g and (29.89) g were attained from ($V_2 \times S_1$) and ($V_2 \times F_2 + F_3$) combination treatment whereas, the lowest seed weight spike^{-1} (24.94) g and (24.39) g were recorded from ($V_1 \times S_2$) and ($V_1 \times F_2 + F_3$) combination treatment respectively.

This may be due to the foliar application with micronutrient (Fe+Zn) had critical role in crop growth, involving in photosynthesis, respiration, and other biochemical and physiological processes as well as their importance in achieving higher yields. The similar trend was also determined by Zeidan et al (2010).

As well as, the combination treatment between variety, growth stage and fertilizer (V × S × F) had a significant effect on the seed weight spike $^{-1}$. The highest seed weight (29.97) g was obtained from ($V_2 \times S_2 \times F_2 + F_3$) while the minimum seed weight (22.71) g was noted from ($V_1 \times S_2 \times F_2 + F_3$). This results indicated that there was no significant difference among the growth stages as well as fertilizers, the significance is due to the different varieties and this may be because of the genetic variation and the ability of the variety to produce high amount of seeds.

Table (8): Effect of variety, growth stage, fertilizer and their treatment combinations on Seed Weight Spike $^{-1}$ (g):

Variety (V)	Fertilizer (F)	Growth stages (S)		Variety ×Fertilizer
		S_1	S_2	
V_1 (Hawler 2)	F_1	24.30 bc	26.30 abc	25.30 c
	F_2	26.08 abc	24.98 abc	25.53 c
	F_3	26.48 abc	25.78 abc	26.13 bc
	F_4	26.08 abc	22.71 c	24.39 c
V_2 (Hawler 4)	F_1	29.67 a	29.21 ab	29.44 a
	F_2	29.59 a	28.43 ab	29.01 ab
	F_3	29.36 a	28.02 ab	28.69 ab
	F_4	29.82 a	29.97 a	29.89 a

F	S_1	S_2	Mean of Fertilizer
F_1	26.99 a	27.76 a	27.37 a
F_2	27.83 a	26.70 a	27.27 a
F_3	27.92 a	26.90 a	27.41 a
F_4	27.95 a	26.34 a	27.14 a

V	S_1	S_2	Mean of Variety
V_1 (Hawler 2)	25.74 b	24.94 b	25.34 b
V_2 (Hawler 4)	29.61 a	28.91 a	29.26 a
Mean of growth stages	27.67 a	26.92 a	

1000-Seed Weight (g):

As shown from table (9), the 1000 seed weight of V_2 (58.51g) was significantly higher than that of V_1 (50.68g). This result indicated that this difference may be due to the higher adaptation to the conditions of the study area. Zarin and Ehsan (2004) stated that there is genetic variation between wheat traits and in wheat breeding programs.

In addition, significant differences were observed from the treatment combinations (variety× growth stage) (V × S), (variety× fertilizer) (V × F) and (variety× growth stage× fertilizer) (V × S × F) on 1000- seed weight. The highest amounts (59.22, 59.79 and 59.93) g were obtained from the treatment combinations ($V_2 \times S_1$), ($V_2 \times F_4$) and ($V_2 \times S_2 \times F_4$). The mentioned treatment combinations may create the best environmental conditions for plant growth. The current results are in accordance to those reported by Habib (2012) in which it was stated that significant increase in 1000- seed weight when (Zn+Fe) applied on foliage at the late period of wheat growth. Additionally, Zeidan et al. (2010) recorded the same results they stated that there was a significant increase in all grain yield parameters when Zn + Fe were sprayed on foliage at tillering and booting stages.

Table (9): Effect of variety, growth stage, fertilizer and their treatment combinations on 1000-Seed Weight (g):

Variety (V)	Fertilizer (F)	Growth stages (S)		Variety ×Fertilizer
		S_1	S_2	
V_1 (Hawler 2)	F_1	48.61 bc	52.60 abc	50.60 c
	F_2	52.15 abc	49.95 abc	51.06 c
	F_3	52.97 abc	51.56 abc	52.26 bc
	F_4	52.15 abc	45.41 c	48.78 c
V_2 (Hawler 4)	F_1	59.34 a	58.42 ab	58.88 a
	F_2	59.17 a	56.85 ab	58.01 ab
	F_3	58.71 a	56.04 ab	57.38 ab
	F_4	59.64 a	59.93 a	59.79 a

F	S_1	S_2	Mean of Fertilizer
F_1	53.97 a	55.51 a	54.74 a
F_2	55.66 a	53.40 a	54.53 a
F_3	55.84 a	53.80 a	54.82 a
F_4	55.90 a	52.67 a	54.29 a

V	S_1	S_2	Mean of Variety
V_1 (Hawler 2)	51.47 b	49.88 b	50.68 b
V_2 (Hawler 4)	59.22 a	57.81 a	58.51 a
Mean of growth stages	55.34 a	53.85 a	

Seed Yield (Mg ha^{-1}):

The results in Table (10) indicate that the seed yield was significantly affected by type of applied fertilizer. The highest seed yield (2.58) *M*g ha^{-1} was obtained from (F_4) application. This support the fact that wheat crop was responded to application of both Fe and Zn nutrients.

As well as, the seed yield significantly affected by the combination treatment between variety and fertilizer (V × F) on this trait. Same variety at different fertilizer treatments gave different mean values of seed yield, (2.79 and 1.86) *M*g ha^{-1} were obtained from (F_4 and F_1) respectively. Broader flag leaves help in greater yield Singh et al. (2015) as well as it was observed from the flag leaf area (figure 1) of this investigation.

As shown in the table (10), there was a significant influence of combination treatment between growth stage and fertilizer (S × F) on seed yield. The maximum quantity of seed yield (2.81) *M*g ha^{-1} was

recorded from the combination treatment ($S_1 \times F_4$). Whereas the lowest seed yield of (2.10) *M*g ha^{-1} was attained from ($S_2 \times F_1$) treatment. Seed yield related to number of seed spike^{-1} (table 7) as well as seed weight spike^{-1} (table 8) that they had the highest mean value at S1 with combination of fertilizers (F_4). Although, the treatment combination of all studied factors variety, growth stage and fertilizer (V × S × F) had positive effect on seed yield. The highest seed yield (2.99) *Mg* ha^{-1} was recorded from ($V_1 \times S_1 \times F_4$). While the minimum amount of seed yield (1.77) *M*g ha^{-1} was achieved from ($V_1 \times S_1 \times F_1$), from the results we concluded that variety and growth stage had no significant effect on seed yield. Similarly, Zeidan et al. (2010) recorded the same results they stated that there was a significant increase in seed yield when (Zn + Fe) were sprayed on foliage at tillering stage.

Table (10): Effect of variety, growth stage, fertilizer and their treatment combinations on Seed Yield (*Mg* ha^{-1}):

Variety (V)	Fertilizer (F)	Growth stages (S)		Variety ×Fertilizer
		S_1	S_2	
V_1 (Hawler 2)	F_1	1.77 d	1.95 cd	1.86 d
	F_2	2.39 bc	2.58 ab	2.49 ab
	F_3	2.47 abc	2.56 ab	2.52 ab
	F_4	2.99 a	2.59 ab	2.79 a
V_2 (Hawler 4)	F_1	2.47 abc	2.24 b-d	2.36 bc
	F_2	2.40b c	2.17 b-d	2.29 bc
	F_3	1.95 cd	2.10 b-d	2.03 cd
	F_4	2.62 ab	2.10 b-d	2.36 bc

F	S_1	S_2	Mean of Fertilizer
F_1	2.12 b	2.10 b	2.11 c
F_2	2.40 ab	2.38 ab	2.39 ab
F_3	2.21b	2.33 b	2.27 bc
F_4	2.81 a	2.35 b	2.58 a

V	S_1	S_2	Mean of Variety
V_1 (Hawler 2)	2.41 a	2.42 a	2.41 a
V_2 (Hawler 4)	2.36 a	2.16 a	2.26 a
Mean of growth stages	2.38 a	2.29 a	

Conclusions:

Judging from seed yield, it can be concluded that the wheat crop grown in the calcareous soil responded to application of both Fe and Zn. The Hawler 2 variety performed better than Hawler 4. Additionally, it can be noticed that critical stage for foliar application of the applied nutrients is tillering stage.

References

Bameri, M., Abdolshahi, R., Mohammadi-Nejad, G., Yousefi, K., & Tabatabaie, S. M. (2012). Effect of different microelement treatment on wheat (*Triticum aestivum* L.) growth and yield. *International Research Journal of Applied and Basic Sciences*, *3*(1), 219-223.

Biber, K., Neumann, H., Inoue, K., & Boddeke, H. W. (2007). Neuronal 'On'and 'Off'signals F1 microglia. *Trends in neurosciences*, *30*(11), 596-602.

C.D. Kemp Methods of Estimating the Leaf Area of Grasses from L Vol. 24, No. 96 (October 1960), pp. 491-499.

Cakmak, I. (2002). Plant nutrition research: Priorities to meet human needs for food in sustainable ways. *Plant and soil*, *247*(1), 3-24.

Cakmak, I. (2008). Enrichment of cereal grains with zinc: agronomic or genetic biofortification? *Plant and soil*, *302*(1-2), 1-17.

Darwesh, D. A. (2007). *Role of supplemental irrigation and fertilizer treatments on yield and nutrients balance in wheat by using modified DRIS* (Doctoral dissertation, Ph. D. Thesis. College of Agriculture. University of Salahaddin/Erbil-Iraq).

Duncan, D. B. (1955). Multiple range and multiple F tests. *Biometrics*, *11*(1), 1-42.

El-Dahshouri, M. F. (2018). Effect of zinc foliar application at different physiological growth stages on yield and quality of wheat under sandy soil conditions. *Agricultural Engineering International: CIGR Journal*, *19*(5), 193-200.

El-Habbasha, E. S., Badr, E. A., & Latef, E. A. (2015). Effect of zinc foliar application on growth characteristics and Grain yield of some wheat varieties under Zn deficient sandy soil condition. *International Journal Chemtech Research*, *8*(6), 452-458.

Esfandiari, E., Abdoli, M., Mousavi, S. B., & Sadeghzadeh, B. (2016). Impact of foliar zinc application on agronomic traits and grain quality parameters of wheat grown in zinc deficient soil. *Indian Journal of Plant Physiology*, *21*(3), 263-270.

FAO Statistical (2013). World Food and Agriculture. Food and Agriculture Organization of the United Nations. Rome,pp 289.

Graham, R. D., Welch, R. M., & Bouis, H. E. (2001). Addressing micronutrient malnutrition through enhancing the nutritional quality of staple foods: principles, perspectives and knowledge gaps.

Habib, M. (2012). Effect of supplementary nutrition with Fe, Zn chelates and urea on wheat quality and quantity. *African Journal of Biotechnology*, *11*(11), 2661-2665.

Haslett, B. S., Reid, R. J., & Rengel, Z. (2001). Zinc mobility in wheat: uptake and distribution of zinc applied to leaves or roots. *Annals of Botany*, *87*(3), 379-386.

Havlin, J. L. (2014). Soil: Fertility and Nutrient Management. In *Encyclopedia of Natural Resources: Land* (pp. 460-469).

Hotz, C., & Brown, K. H. (2004). Assessment of the risk of zinc deficiency in populations and options for its F1.

Kahrariyan, B., Yeganehpoor, F., Beyginiya, V., & Samadiyan, F. (2013). Effect of Fe foliar application on morphological and physiological traits of different dryland wheat varietys. *International journal of Advanced Biological and Biomedical Research*, *1*(12), 1583-1589.

Khan, Z. A., Khan, M. A., & Baloch, M. S. (1999). Effect of different manures on the yield of wheat. *Scientific Khyber*, *12*(1), 41-46.

Nadim, M. A., Awan, I. U., Baloch, M. S., Khan, E. A., Naveed, K., Khan, M. A., ... & Hussain, N. (2011). Effect of micronutrients on growth and yield of wheat. *Pak. J. Agri. Sci*, *48*(3), 191-196.

Narimani, H., Rahimi, M. M., Ahmadikhah, A., & Vaezi, B. (2010). Study on the effects of foliar spray of micronutrient on yield and yield components of durum wheat. *Archives of Applied Science Research*, *2*(6), 168-176.

Ozturk, L., Yazici, M. A., Yucel, C., Torun, A., Cekic, C., Bagci, A., ... & Cakmak, I. (2006). Concentration and localization of zinc during seed development and germination in wheat. *Physiologia Plantarum*, *128*(1), 144-152.

Patel, M.M., Patel, I.C., Patel, P.H., Patel, A.G., Acharya, S. and Tikka, S.B.S. (2009). Impact of foliar nutrition of zinc and iron on the productivity of cowpea (*Vigna unguiculata* L.) under rain fed conditions. *J. Arid Legumes*, 6(1): 49-51.

Qadir, D. J. (2017). Soil physical properties, soil loss and runoff rate as influenced by rock fragments in Erbil province. MSc thesis. College of Agriculture, University of Salahaddin.

Rawashdeh, H. M., & Sala, F. (2015). Effect of some micronutrients on growth and yield of wheat and its leaves and grain content of iron and boron. *Bulletin of University of Agricultural Sciences and Veterinary Medicine Cluj-Napoca. Agriculture*, *72*(2), 503-508.

Rehm, G., & Albert, S. (2006). Micronutrients and Production of quality crop of sesame. *Minnesota Crop New*, 1-3.

Salih, H. O. (2013). Effect of foliar fertilization of Fe, B and Zn on nutrient concentration and seed protein of Cowpea "*Vigna unguiculata*". *Journal of Agriculture and Veterinary Science*, *6*(3), 42-46.

Shweta, M., & Agrawal, S. B. (2006). Interactive effects between supplemental ultra-violet -B radiation and heavy metals on the growth and biochemical characteristics of *Spinacia oleracea* L. *Brazilian Journal of Plant Physiology*, *18*(2), 307-314.

Singh, V., Ali, J., Kumar, A., & Chauhan, T. M. (2015). Productivity, nutrient uptake and economics of wheat (*Triticum aestivum*) under potassium and zinc nutrition. *Indian Journal of Agronomy*, *60*(3), 426-430.

Zadoks, J.C.., T.t. Chang and C.f. Zonzak. (1974). A decimal code for the growth stages of cereals. Weed Res. 14: 415 – 421).

Zain, M., Khan, I., Qadri, R. W. K., Ashraf, U., Hussain, S., Minhas, S., ... & Bashir, M. (2015). Foliar application of micronutrients

enhances wheat growth, yield and related attributes. *American Journal of Plant Sciences*, *6*(07), 864.

Zarin A. A., Ehsan Z. P. (2004). Growth, yield and yield components of three durum wheat genotypes under different planting densities in Isfahan. Science and Technology of Agriculture and Natural Resources, pp. 140-129.

Zeidan, M. S., Mohamed, M. F., & Hamouda, H. A. (2010). Effect of foliar fertilization of Fe, Mn and Zn on wheat yield and quality in low sandy soils fertility. *World J. Agric. Sci*, *6*(6), 696-699.

ZANCO Journal of Pure and Applied Sciences
The official scientific journal of Salahaddin University-Erbil
https://zancojournals.su.edu.krd/index.php/JPAS

ISSN (print):2218-0230**, ISSN (online):** 2412-3986**, DOI: http://dx.doi.org/10.21271/zjpas**

RESEARCH PAPER

Prospects of Potassium and Phosphate Solubilizing Bacteria for Nodulation Enhancement, growth and yield of Chickpea plant (*Cicer arientinum L.)*

Kwestan Jawhar Mustafa*, Aras.M. Khudhur*

*Department of Soil and Water, College of Agricultural Engineering Science, Salahaddin University-Erbil, Kurdistan Region-Iraq

A B S T R A C T:

Seventy one percent of the overall P and K in Erbil governorate soils are in inorganic forms which are unavailable for use in plants. As a result, chemical fertilizer is often used to supplement the nutrient for the growth crops. To reduce the addition of chemical fertilizer to agricultural soils, this research has been conducted to isolate naturally occurring potassium solubilizing microorganisms (KSB) and phosphate solubilizing microorganisms (PSB) from Erbil soil samples and use to improve chickpea growth. Thirty nine efficient PSB isolates were selected based on their ability to clear zone formation on Pikovskaya´s agar medium of and 26 efficient KSB isolates using Aleksandro medium. Depending on microscopical, cultural, and biochemical characteristics, PSB strains belonged to *Ps.putida* while KSB strains referred to *B.circulans*. All PSB and KSB strains were screened for their solubilization efficiency on both solid and liquid medium. Bh36 strain of *Ps.Putida* was the most efficient isolate in P solubilization (94.92%,117.78mg/ml) and the most efficient *B.circulans* strain in K solubilization was Q1 (87.01%,4.81mg/ml), and they were used for P and K biofertilizers preparation, respectively. Pot experiment showed that seed inoculation with *Ps.Putida*, *B.circulans*, and combined (*Ps.Putida*+ *B.circulans*) application significantly enhanced chickpea growth. Combined (*Ps.Putida*+ *B.circulans*) inoculation recorded the highest increase in shoot height (46.29cm), root length (37.84cm), shoot dry weight (4.28g/plant), number of seed (26.37seeds/plant), number of active nodules (11.56/plant) P (6.35g/plant) and K uptake (65.75g/plant), soil available phosphorus (17.21mg/kg) and soil available potassium (314.5mg/kg). It could be assumed that local *Ps.Putida* and *B.circulans* strain can be used as biofertilizer of P and K to improve plant growth and soil fertility.

KEY WORDS: *B.circulans*, Biofertilizer, Chickpea, K-solubilizing bacteria, P-solubilizing bacteria, *Ps.Putida*.
DOI: http://dx.doi.org/10.21271/ZJPAS.32.5.20
ZJPAS (2020) , 32(5);196-209 .

1. INTRODUCTION

Phosphorus (P) and potassium (K) are essential macro-nutrients that playing a significant role in plant growth and development. Plants usually need (P) for cellular bioenergetics, metabolic regulation, and vital components of essential bimolecular including RNA, DNA,ATP, phospholipids and sugar-phosphates (Plaxton and Lambers, 2015).

On the other hand, (K) plays a vital role in plant growth, metabolism and development, water retention, regulating opening, closing of stomata and enzyme activation (Pettigrew, 2008, Badr, 2006). Potassium also helps plants in faster growth, additionally to increasing plant resilience to pests, pathogens...etc (Rehm and Schmitt, 2002). Potassium deficiency causes decreased growth ,seed size and plant yield (Gupta et al., 2015). A great part of the total (P) in the soil is non-soluble and unavailable therefore cannot be utilize by plants. The major factors that hamper

* **Corresponding Author:**
Kwestan Jawhar Mustafa
E-mail: kwestan.jawher85@gmail.com
Article History:
Received: 02/04/2020
Accepted: 20/06 /2020
Published: 13/10/2020

crop production globally is a lack of soluble (P) in many agriculture soils (Panhwar et al., 2012, Pei-Xiang et al., 2012). A large portion of soil microbes, called phophate solubilizing microorganisms (PSM), these organisms have ability to dissolve insoluble inorganic phosphorus and make them available to plants by varies mechanisms such as production of organic acids and phosphatase enzymes (Shaikh et al., 2016). The quantity of soluble potassium which absorb by plant is very low, which represent 2% of total potassium, while large amount of it 90-98% is exist in insoluble form (Prajapati and Modi, 2012). Potassium solubilizing bacteria can solubilize K- bearing minerals, and increase it availability due to the production of some weak organic acids such as citric, tartaric...etc which causes in plant growth and yield (Maurya et al., 2014, Meena et al., 2014a). Phosphate and potassium solubilizing bacteria have a key role in soulubilization in organic and inorganic P and K in soil which can be used as biofertilizers, because biofertilizers are low-cost and environment-friendly plant nutrient source, which improves the availability of plant nutrients and enhancing the sustainability and the health of the soil (Singh et al., 2011). Biofertilizers have beneficial effect on crop production and increasing the uptake of nutrients by plants, when they use as inoculation in seeds and soils (Singh et al., 2011).

Since there are little studies about biofertilizers in Kurdistan region for this reason this study was selected and the objects are to isolation and characterization of phosphorus and potassium solubilizing bacteria in Erbil soil and preparation of biofertilizer from isolated strain, and then use for promotion plant growth and improving of some soil properties.

2. Materials and Methods

2.1. Collection of Samples

Fourteen soil samples collected in different geographical areas in Erbil governorate/Kurdistan region-Iraq included (Qushtapa, Salahaddin, Aski-Kalak, Girda-Rasha, Sami Abdul-Rahman park, Daratoo, Shanadar Park, Bastora, Smaqool, Ainkawa, Bahrka, Kawrgosk, Bnasllawa, and Kasnazan) in October 2018. The soils were brought to Microbiology laboratory, College of Agriculture Engineering Science, University of Salahaddin-Erbil.

2.2. Isolation, Purification and Identification of Phosphate Solubilizing Bacteria

Field moist soil samples were mixed with sterile sodium chloride solution of 0.85% and shackled for 20min, an aliquot dilutions were inoculated using NBRIP (national botanical research institute phosphorous) medium containing (0.1g $(NH_4)_2SO_4$, 5g $MgCl_2.6H_2O$, 10g glucose, 0.25g $MgSO_4.7H_2O$, 5g $Ca_3(PO_4)_2$, 0.2g KCl, in 1L distilled water) using pour plate method and incubated for five days at 28±2˚C. The colonies with clear halozone were considered to be phosphate solubilizing colonies. Purification of predominant colonies was performed using re-streaking on NBRIP agar. For further study, single colonies that appeared on NBRIP agar plates were transferred in to Pikoviskaya's liquid broth (PVK) and on agar slants.

Identification of isolated phosphate solubilizing strains was performed according to their microscopical, cultural, physiological and biochemical characteristics included: colonyshape, size, and color also known as pigmentation, colony texture, cell shape, arrangement, gram reaction, cell size, motility, spore formation, production of catalase, oxidase, and gelatin hydrolysis, growth at 37˚C, 4˚C and 44˚C, and carbohydrate fermentation patterns (Brenner et al., 2005).

2.3. Efficiency of Phosphate Solubilizing Bacteria in Phosphate Solubilization in Soil

Phosphate solubilizing activity of all phosphate solublizing isolates was assayed using plate screening method and broth culture method. All the suspended colonies were screened for phosphate solubilization efficiency on PVK ager medium containing (10g glucose, 0.002g $FeSO_4.7H_2O$, 0.1g $MgSO_4.7H_2O$, 0.5g$(NH_4)_2SO_4$, 0.002g $MnSO_4.H_2O$, 0.5g yeast extract, 0.2g NaCl, 5g$Ca_3(PO_4)_2$,and 0.2g KCl,). Spot inoculation was done at the center of PVK plate then the incubation was conducted at 28±2˚C. Clear halo diameter was successively measured after 24hr, up to 7 days. Phosphate solubilization efficiency (*Ps.putida*) of each isolates was evaluated depending on the following equation (Sarikhani et al., 2019).

$$PSE = \frac{\text{Solubilization Diameter}}{\text{Growth diameter}} \times 100$$

Broth culture method was also used to evaluate phosphate solubilizing activities for bacterial isolates. Hundred ml aliquots of PVK broth was transferred in to 250ml conical flask, after sterilization, tricalcium phosphate ($0.5g.100ml^{-1}$) were added. Each flask was inoculated with 1ml of active culture suspensions of each PSB isolate. For the control treatment a sterilized non-inoculated medium has been prepared. Then all inoculated treatments and non-inoculated control treatment were kept in shaker incubator for a week. After incubation period, all the broth culture was centrifuged at 11,000 rpm for 10 minutes remove bacterial cells and other insoluble materials. The supernatant was takento determine available phosphoroususing spectrophotometerat 882nm.

2.4. Isolation, Purification and Identification of Potassium Solublizing Bacteria

Potassium solublizing bacteria (KSB) can be isolated with a serial dilution method using modified Aleksandrov medium containing (0.5g $MgSO_4.7H_2O$; 2g $AlKO_6Si_2$; 0.1g $CaCO_3$; 0.006g $FeCl_3$; 2.0g $Ca_3(PO_4)_2$; 5.0g glucose; and 20.0g agar in 1L distilled water), the plates were incubated at 28±2˚C for 5 days. The bacterial isolates were maintained by periodic transfer on Aleksandrov agar medium slants and stored at 4˚C for further use. The identification of purified KSB bacteria was performed according to their microscopical, cultural, and biochemical properties included: colony size, shape, texture and pigmentation, cell shape, motility, gram stain, and endo-spore formation, oxidase, catalase, , gelatin liquefaction, urea hydrolysis, citrate hydrolysis and carbohydrate fermentation, according to Bergey´s Manual of Systematic Bacteriology (Brenner et al., 2005).

2.5. Efficiency of Potassium Solubilizing Bacteria in Potassium Solubilization in Soil

The efficiency of potassium solubilizing isolates was performed by spot inoculation on Aleksandrov agar medium. The plates were incubated at 28±2˚C, for 5 days, the colonies exhibiting clear zones and diameter of solubilization zone were calculated using following equation (Prajapati and Modi, 2012).

$$KSE = \frac{\text{Diameter of clearzone}}{\text{Growth diameter}} \times 100$$

Selected strains were further evaluated for their potassium solubilizing activity. Potassium soilubilizing ability of selected strains was quantitatively screened on 15ml of Aleksandrov broth medium amended with insoluble K sources (Potassium Aluminum Silicate) was taken in the volumetric flask having volume of 250ml and inoculated with KSB. The incubation was done using special shaker at about 28±2˚C for a week. When the incubation time has ended, culture filtrates were centrifuged at 8000rpm for 10min. The supernatants were subjected to estimation the release of potassium by KSB using a Flame photometer(Chitra and Sharavanan, 2014). The autoclaved medium without KSB inoculation was usedas a control.

2.6. Preparation of Biofertilizer

The most efficient isolate for each of potassium soilubilizing bacteria and phosphate soilubilizing bacteria were select for biofertilizer preparation. Biofertilizers was prepared by addition of 10ml of fresh broth culture ($35*10^7$cell/ml) to 100g carrier (%20 compost + %20 charcoal + %20 $CaCO_3^+$ %20 clay +%19 sand +%1 gum). Two types of biofertilizer were prepared included phosphate solubilizing biofertilizer PSB (*Ps.putida*) and potassium solubilizing biofertilizer KSB (*B.circulans*).

2.7. Pot Experiment

The pot experiment was carried out in Girda-Rasha field College of Agriculture Engineering Science, which is about 5 km to the southwest of Erbil city, during February 6, 2019 to May 20, 2019. The pots (45cm height, 30cm diameters) were filled with unsterilized soil (silty clay loam, pH 7.65, EC 1.23ds/m, total nitrogen 2.352mg/g, $CaCO_3$ 312g/kg, organic matter 11.765 g/kg, available phosphorus 3.423mg/g, soluble ions: HCO_3^- 13.22 mml/L, Mg^{2+} 1.88mml/L, Na^+ 11.07 mml/L, K^+ 29 mml/L, Ca^{2+} 1.21 mml/L, and Cl^- 1.7 mml/L. Growth promoting effects of prepared biofertilizers were studied on chickpea plant. The surface sterilized seeds of chickpea were inoculated with prepared biofertilizer (one gram freshly biofertilizer per 100g seed) before sowing (Milani and Anthofer, 2008). There were 4 treatments with four replications included: non inoculated control (without biofertilizer), PS biofertilizer (*Ps.putida*), KS biofertilizer

(*B.circulans*), and PS biofertliaer+ KS biofertilizer in combination. The experiment was set up in randomized complete design (CRD) using four replicates per treatment. Data was recorded for dry weight of shoots (the shoots were dried at 70°C for 72hr to calculate the dry matter), shoot height, number of seeds/plant, root length, number of active nodules/plant, P and K uptake of chickpea plant, and the available potassium and phosphorus of soil rhizosphere.

2.8. Statistical Analysis

In all cases, Duncan's H.S.D. multiple range tests were applied for comparing between mean of treatments by using SPSS 12.0 (Casanova et al., 2004).

3. Results and Discussion

3.1. Isolation and Identification of Phosphate Solubilizing Bacteria

Thirty nine isolates of phosphate solubilizing bacteria have been obtained and tested from various locations of rhizosphere soil in Erbil city (Qu1, Qu2, Qu3, Sa4, Sa5, Sa6, Sa7, Ka8, Ka9, Ga10, Ga11, Ga12, Ps13, Ps14, Ps15, Ps16, Da17, Da18, Da19, Psh20, Psh21, Psh22, Bs23, Bs24, Bs25, Bs26, Bs27, Sm28, Sm29, Sm30, An31, An32, Bh33, Bh34, Bh35, Bh36, Bh37, Kz38 and Kz39) and they had marked phosphate solubilizing abilities as visualized by developing halo zone around each colony after a week from incubation on a special medium (PVK). The soils showed variations in the appearance and growth of phosphate solubilizing bacterial strain. The highest population of PSB we observed in the soil samples of Bastora and Bahrka, while the lowest number was found in the soil samples of Aski-Kalak and Ainkawa.

These isolated strains were found to be quite similar in size, both in length and diameters. All isolates were gram negative, aerobic. Their colony on agar plate appeared as round and creamy, About 65% of 39 isolates were straight curve shape and 35% were rod shape, did not spore former and not motile, could not grow at 4˚C and 44˚C but could grow very well at 37˚C, and all isolates showed positive response to catalase and oxidase, but they showed negative response to gelatin and starch hydrolysis. All isolates could utilize glucose but did not utilize arabinose, lactose; mannitol and maltose, while they were differing from sucrose, rhibose, xylose, and rhamnose. depending on some morphological, culture, different biochemical analysis and using Bergey´s manual of determinative Bacteriology isolated bacterial strain are *Ps. putida* (Brenner et al., 2005).

3.2. Phosphate Solubilizing Activities

Phosphate solubilizng activity of all isolated strains was quantitatively and qualitatively determined using both broth and solid PVK media respectively. As they give clear zone, it can be assumed that these strains have activity for solubilizing phosphorus. The findings table (1) showed that on PKV agar media plates, all isolates have ability to solubilize phosphorus. The strain Bh36 showed the highest P-solubilizing activity (94.92%), while the lowest P-solubilizing activity (20.17%) were found in Bs24 treatment, which was significantly different from other isolates.

Results of evaluating P-solubilizing activity table (1) at the end of incubation time, in liquid PVK medium it was found that all isolates released P from tricalcium phosphate ranging from (27.62 to 117.78mg/ml) with variations among different isolates. Similarly to solid plate method, Bh36 released the maximum amount of soluble-P, while Bs24 recorded the minimum amount.

The results are in agreement with the finding of (Kumar et al., 2010, Dhandapani, 2011, Khudhur, 2017). The P-solubilizing activity is related to the microbial biochemical potential to produce and release organic acids which their carboxylic groups chelate the cations (mainly Ca) bound to phosphate converting them into soluble forms (Kpomblekou-a and Tabatabai, 1994), as well as the positive correlation between soluble phosphours content and titratable acid production, suggested that acidification of the medium could facilities solubilizng of phosphorus (Park et al., 2016).Based on above results the most effective isolate of *Pseudomonas putida* chosen for most experiment.

Table 1.Qualitative and Quantitative estimation of phosphate solubilization efficiency of isolated bacterial strains using Pikovskaya's media

Isolate	Bacterial	Phosphate solubilization on	Phosphate solubilization in

	genera	Agar %	Broth (mg/ml)
Qu1	*Ps.putida*	29.7^{y}	47.61^{w}
Qu2	*Ps.putida*	50.72^{g}	38.18^{x}
Qu3	*Ps.putida*	44.5^{t-u}	70.00^{n}
Sa4	*Ps.putida*	80.90^{f-e}	89.68^{g-f}
Sa5	*Ps.putida*	39.20^{w}	52.47^{t}
Sa6	*Ps.putida*	58.17^{o}	78.19^{j-k}
Sa7	*Ps.putida*	76.55^{h-g}	81.37^{i}
Ka8	*Ps.putida*	33.19^{x}	44.78^{x}
Ka9	*Ps.putida*	48.27^{t}	62.51^{q}
Ga10	*Ps.putida*	37.70^{x}	55.69^{s}
Ga11	*Ps.putida*	42.90^{u}	60.50^{r}
Ga12	*Ps.putida*	53.10^{q}	71.58^{m}
Ps13	*Ps.putida*	71.12^{l}	91.50^{fe}
Ps14	*Ps.putida*	28.64^{y}	37.12^{x}
Ps15	*Ps.putida*	63.42^{n}	79.14^{j}
Ps16	*Ps.putida*	51.01^{r}	68.20^{o}
Da17	*Ps.putida*	75.38^{i}	97.01^{d}
Da18	*Ps.putida*	65.23^{m}	82.71^{i}
Da19	*Ps.putida*	50.00^{g}	72.85^{m}
Psh20	*Ps.putida*	74.48^{j}	92.32^{e-d}
Psh21	*Ps.putida*	59.09^{o}	82.33^{i}
Psh22	*Ps.putida*	47.01^{t}	60.44^{r}
Bs23	*Ps.putida*	$31.\ 02^{y}$	31.10^{y}
Bs24	*Ps.putida*	20.17^{z}	27.62^{z}
Bs25	*Ps.putida*	48.105^{t}	50.51^{u}
Bs26	*Ps.putida*	55.51^{p}	71.81^{m}
Bs27	*Ps.putida*	37.90^{w}	49.01^{v}
Sm28	*Ps.putida*	81.45^{e}	98.70^{b}
Sm29	*Ps.putida*	76.87^{g}	83.39^{h}
Sm30	*Ps.putida*	52.02^{r}	68.49^{o}
An31	*Ps.putida*	37.80^{w}	51.18^{u}
An32	*Ps.putida*	65.93^{m}	77.01^{l-k}
Bh33	*Ps.putida*	47.30^{t}	70.54^{n}

Bh34	*Ps.putida*	87.39[d]	93.73[d]
Bh35	*Ps.putida*	90.48[b]	99.92[b]
Bh36	*Ps.putida*	94.92[a]	117.78[a]
Bh37	*Ps.putida*	89.98[c-b]	98.13[b]
Kz38	*Ps.putida*	73.14[k]	89.10[g-f]
Kz39	*Ps.putida*	41.10[v]	64.22[p]

*Similar letter or letters means non-significant difference

3.3. Isolation and Identification of Potassium Solubilizing Bacteria

Generally a total of 26 isolates of potassium solubilizing bacterial were recognized of different place in Erbil city (Qu1, Qu2, Qu3, Sa4, Sa5, Sa6, Ka7, Ga8, Ga9, Ga10, Ps11, Ps12, Da13, Da14, Da15, Psh16, Bs17, Bs18, Sm19, An20, An21, Ba22, Kw23, Kw24, Kw25 and Kz26) had marked potassium solubilizing abilities depending on the clear zone produced around the colonies of bacteria on Aleksandro agar medium after 7 days of incubation. The soil samples were differing in the number and growth of potassium solubilizing bacteria.

These isolated organisms when studied for morphological, cultural and biochemical characteristics barely was necessary for identification. The performed tests showed that all isolates were gram positive, rod shape, endospore producing, motile, aerobic, their colony on agar plate appeared as creamy, showed positive response to catalase, gelatinase and citrate ultilization, but they showed negative response to oxidase, urea hydrolysis, could utilize maltose, while they were differ from xylose, glucose, arabinose, mannitole and sucrose. According to the previous results and depending on Bergey´s manual of systematic Bacteriology(Brenner et al., 2005), The isolated bacterial strains were identified to the species *Bacillus circulans*.

Potassium solubilizing activities of selected strains were firstly screened for clear zone formation on Aleksandrov agar medium. All chosen strains, formed clear zone around the colonies. All the bacteria tested were capable to solubilizing potassium, but not always at the same extent table (2). The Qu1 strain had the most pronounced ability of potassium solubilization (87.01%), followed by Da15 (85.11%) and Ba22 (78.4%), while Sma19 (20%) and Ga9 (21.14%) showed the least solubilization activity.

All Potassium solubilizing strains was quantitatively determined in the Aleksandrov broth medium, added by PAS (Potassium Aluminum Silicate). The results in table (2) shows all the strains of KSB could solubilize insoluble PAS very effectively under in vitro condition. Likewise, Qu1 (4.8mg/ml) strain gave the highest amount of soluble K, and Da15 (4.2mg/ml) and Ba22 (3.9mg/ml), on the other hand, Sma19 (1.1mg/ml) and Ga9 (1.2mg/ml) were the lowest among all other strains.

This agree with the results recorded by (Mikhailouskaya and Tchernysh, 2005, Zhang and Kong, 2014). The ability of bacteria to release potassium greatly depends on the nature of the mineral compound (Iakhontova et al., 1987). The variability among the bacterial strain reveals the importance of exploration of different mineral potassium solubilizing bacteria and their solubilizing mechanisms. The key mechanism of potassium solubilization it is normally noted that the action of organic acids synthesized by KSB.

3.4. Potassium Solubilizing Activities

Table 2.Qualitative and Quantitative estimation of potassium solubilization efficiency of isolated bacterial strains using Aleksandrov media

Isolate	**Bacterial genera**	**Potassium solubilizationon Agar %**	**Potassium solubilizationin Broth (mg/ml)**

Qu1	*B.circulans*	87.01^{a}	4.8^{a}
Qu2	*B.circulans*	40^{l}	2^{g-i}
Qu3	*B.circulans*	69.98^{d-e}	3.2^{e-f}
Sa4	*B.circulans*	64.00^{e}	3^{g-e}
Sa5	*B.circulans*	54.23^{h}	2.2^{i-h}
Sa6	*B.circulans*	31^{n}	1.5^{k}
Ka7	*B.circulans*	48.12^{j}	2.4^{h}
Ga8	*B.circulans*	58.18^{g}	1.9^{g}
Ga9	*B.circulans*	21.14^{p}	1.2^{m-l}
Ga10	*B.circulans*	57.6^{g-h}	2.3^{h}
Ps11	*B.circulans*	35^{m}	1.4^{l-k}
Ps12	*B.circulans*	63.00^{e}	3^{ef}
Da13	*B.circulans*	73^{d}	3.4^{d}
Da14	*B.circulans*	26.33^{o}	1.3^{k}
Da15	*B.circulans*	85.11^{a}	4.2^{b}
Psh16	*B.circulans*	75^{dc}	3.7^{c}
Bs17	*B.circulans*	29.19^{n-o}	1.4^{l-k}
Bs18	*B.circulans*	62.75^{e}	3.3^{d-c}
Sm19	*B.circulans*	20^{p}	1.1^{n}
An20	*B.circulans*	26.07^{o}	3.4^{c}
An21	*B.circulans*	62.17^{e}	1.7^{g}
Ba22	*B.circulans*	78.4^{b}	3.9^{c}
Kw23	*B.circulans*	77.01^{c-b}	3.7^{c}
Kw24	*B.circulans*	43^{k-l}	2.8^{g}
Kw25	*B.circulans*	46^{j-k}	2.8^{g}
Kz26	*B.circulans*	52^{i-h}	3.1^{e-f}

*Similar letter or letters means non-significant difference

3.5. Pot Experiment

3.5.1. Plant Growth

The results illustrate that the seed inoculated with prepared biofertilizers significantly increased growth, yield and number of active nodules, phosphorus and potassium uptake, and availability of phosphorus and potassium in soil over non-inoculated control. As can be noticed in table (3), all the treatments improved root length over non-inoculated treatment. A significant variation in root length was observed in response to different bacterial inoculums. Co-inoculation with *Ps.putida+ B.circulans* (T3) produced the highest root length 37.84cm; it means that this inoculation treatment caused 43.76% increase in root length in comparing with non-inoculated treatment (control). *Pseudomonas putida* in combination with *B.circulans* was observed that the

mostefficient inoculums for enhancement of root length. Better root developmentmay be attributed to synergistic relationship of the inoculated bacteria for enhancing root length; *B.circulans* (T1) was the least effective inoculums but still it produced17% longer roots as compared to the non-inoculated treatment (control). Similar to these results, increasing of plant root length by phosphate solubilizing strain alone and in combination with potassium solubilizing also recorded by (Han and Lee, 2005, Chaiharn and Lumyong, 2011, Liu et al., 2016, Bakhshandeh et al., 2017). The strains of P- solubilizing bacteria causes increase in root length and growth regulators production which are causing increase in nutrient and water absorption by plants or host plants(Gupta et al., 2002, Barea et al., 2005). Potassium solubilizing microorganisms have been reported to be significant organisms for plant root establishment, prototypeof rootgrowth, plant nutrition andplant competitiveness, predominantlyunder abiotic and biotic stress and conditions of nutritional imbalances(Wu et al., 2005, Meena et al., 2014a, Meena et al., 2014b).

Healthy roots help the plant for absorption of soil water and uptake of major plant nutrients as well as results in good yield. The increase in plant root size and number or depletion zone of infected roots are leading to increase in nutrient absorption and water stress of plants, which in turn could be the major factors improving plant growth (Bai et al., 2003).

The results also indicatedthat the inoculated plants with different inoculums showed shoot height ranging from (34.31cm) up to (46.29cm). All produced biofertilizer exhibited significant increase in shoot height of chickpea over control, the maximum increase (46.29cm) was shown by co-inoculation of *Ps.putida*+ *B.circulans*, this increase may be attributed to the beneficial impact of bacterial inoculums in stimulating plant growth and increasing nutrient uptake, while the plants which treated by *B.circulans* alone was report the lowest value of shoot height (40.05cm). Phosphate and potassium solubilizing micro-organisms and other beneficial rhizobacteria cause the release of nutrients in plant utilizable form and have beneficial effect on the growth of plants (Sindhu et al., 2002, Glick, 1995,Marques et al., 2010).

Data regarding to dry weight of shoot as shown in table (3) revealed that application of prepared biofertilizer caused significant increase in weight of dry matter compared with control treatment. The highest shoot dry weight (4.28g/pot) was recorded in *Ps.putida*+ *B.circulans* followed by *Ps.putida* alone (2.83 g/pot) treatments. The treatment combinations caused 152%increase in weight of shoot. Here, control and *B.circulans* showed nearly similar results (1.70 and 1.98 g/pot). The increasing on shoot dry weight for inoculated treatments compared with control treatments might be attribute to the role of bacterial in stimulating absorption of macro-nutrients (N,P and K) and some trace elements, large rate of photosynthesis, which results in increasingleaf areaand nitrogen absorption could be expected (Basak and Biswas, 2010)and the effect of hormones (Silini-Cherif et al., 2012) and increase take of CO_2 (Dotaniya, 2015).

The seed yield values provided in table (3) showed that all the tested isolates had the capability to increase the seed yield of chickpea significantly as compared to control treatment. The highest seed yield (26.37seeds/plant) was obtained in pots which received *Ps.putida*+ *B.circulans* inoculation that were noticeably greater than any other treatments. While single inoculation of *B.circulans* showed the lowest value (16.62seeds/plant)behaved similar to that of *B.circulans* for root length shoot dry weight and plant height. Inoculation with either microbe enhanced the yield in chickpea but their interactive effect was more prominent. This is in agreement with the report of similar increase in plant seed yields due to inoculation of PSB and KSB strains were observed by (Pereira and Castro, 2014, Sarker et al., 2014, Sindhu et al., 2010).

In case number of active nodules of chickpea plants shown in table (3), pot experiment gave the highest average value and the lowest value. Highest active nodules (11.56 nodules/plant) was produced with co-inoculation *Ps.putida*+ *B.circulans* treatment, followed by *Ps.putida* inoculation (8.72nodules/plant), the leghemoglobin is responsible for a pink color of active nodules. On the other hand, the lowest values were found for both controls (5.98nodules/plant) and *B.circulans* (6.00nodules/plant), the active nodules have

important effect in the fixating of atmospheric nitrogen to beneficial form for fabaceae family. Inoculations alone (*Ps.putida*) or in combination produced higher number of active nodules. the results agree with (Gull et al., 2004), they show that the PSB affects nodule formation.

Table 3.Effect of single and co-inoculation of (*Pseudomonas putid*a and *Bacillus circulans*) biofertilizer on the growth and yield of Chickpea (*Cicer arientinum* L.) plant

Treatments	Root length cm	Shoot height cm	Shoot dry Weight g/plant	No.of Seeds/plant	No. of active Nodules /plant
T0 Control (withoutbacteria)	26.32^{d}	$34.31g^{h}$	1.70^{k}	10.00^{f}	5.98^{j}
T1*B.circulans*	30.82^{c}	40.05^{f}	1.98^{j}	16.62^{e}	6.00^{i}
T2 *Ps.putida*	34.67^{b}	45.12^{e}	2.83^{i}	19.00^{d}	8.72^{h}
T3*Ps.putida*+ *B.circulans*	37.84^{a}	$46.29b^{h}$	4.28^{h}	26.37^{c}	11.56^{g}

3.5.2. Phosphorus and Potassium Uptake in Plants

Findings indicated that inoculation with PSB and KSB or in combination significantly increased P and K uptake in chickpea plant table (4). The highest phosphorus and potassiumcontent generally occurred in combined treatment, this treatment combination caused increases in phosphorus and potassium content (6.35, 65.75 mg/plant respectively), while the lowest value (1.24, 16.32mg/plant respectively) were recorded in control. Combined inoculation treatments resulted in higher growth performances and P and K uptake than those from single inoculation, and either single treatment of inoculation resulted increase in content of both phosphorus and potassium to various degrees compared to control treatment (Figs.1 and 2). likewise, phosphorus and potassium solubilizing bacteria have also been found to play a significant role in plant nutrition by increasing phosphorus and potassium content by plants (Datta et al., 1982, Nianikova et al., 2002). Phosphate solubilizing bacteria besides having ability for phosphate solubilization is also capable of promoting growth through mechanisms such as production of plant growth hormone and vitamins, enhancement of plant nutrient uptake and the suppression of pathogenic or harmful organisms (O'sullivan and O'Gara, 1992) in the rhizosphere.

Phosphate solubilizing bacteria was a more effective phosphorus uptake than potassium solubiling bacteria. *Pseudomonas putida* is recognized to be good plant growth promotes by producing organic acids and phosphatase enzymes, increases the availability of plants to the soluble phosphorus (Khan et al., 2009). The results were identical with those findings (Shwetha and Lakshman, 2013, Walpola and Yoon, 2013, Khudhur, 2017). Additionally, single inoculations with KSB showed a better K-uptake, seeds and seedling inoculation of various plants with potassium solubilizing bacteria in general commonly showed significant enhancement of germination rate, seedling vigor, plant production, yield and the uptake of potassium by plants under greenhouse and fields conditions (Anjanadevi et al., 2016, Meena et al., 2014a, Zhang and Kong, 2014). Sheng and He (2006) in wheat plant showed that seeds inoculated with *B. edaphi-cus* had the superior of potassium uptake than the non-inoculated treatments which can be attributing to the produce of organic acids by these strain.

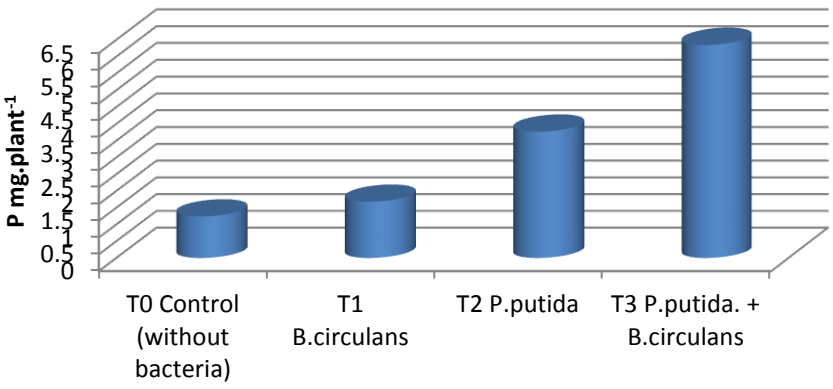

Fig.1. Effect of bacterial inoculation on Phosphorus content of chickpea plant

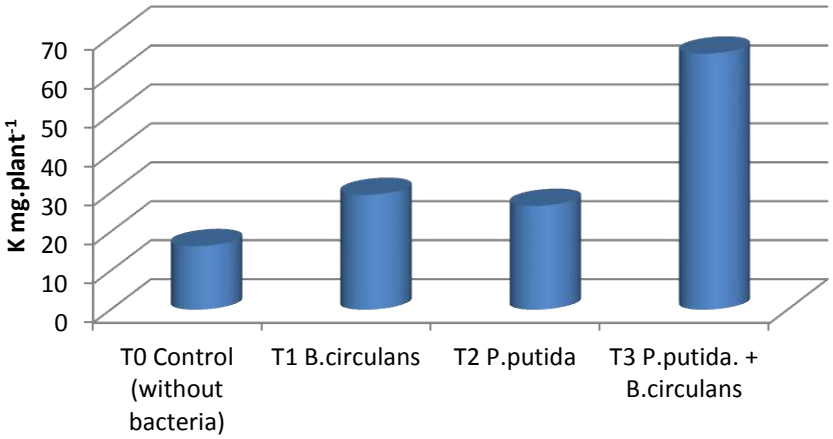

Fig.2. Effect of bacterial inoculation on Potassium content of chikpea plant

3.5.3. Available Phosphorus and Potassium Content of Cultivated Soil

The results in table (4) found that available phosphorus content of rhizosphere soil inoculated with PSB alone or in combination with KSB was found to be significantly higher than those in no – inoculated soil. The highest available P (17.21mg/kg) was obtained when *Ps.putida*+ *B.circulans* used for inoculation, while the least increase of available P-content (290.5 mg/kg) was recorded by *B.circulans* (Fig. 3). Khoshnaw and Esmail, (2020) were studied the phosphorus concentration and it balance in wheat plant, which caused an increase in grain yield and growth positively were cultivated at Girda-Rasha farm soil. therefore, PSB can also improve the availability of potassium in soil or potassium concentrations in plant tissues, additionally to increasing the availability and concentrations of phosphorus in soil and plant tissues (Bakhshandeh et al., 2017).

Potassium content of tested soil table (4) showed significant difference between treatments. The highest available K (403.5mg/kg) was recorded in the soil treated with mixture of *Ps.putida*+ *B.circulans* which was significantly higher than all other treatments. While the lowest value of available K was recorded by *Ps.putida* (279.9mg/kg) followed by non-inoculated treatment (174.8mg/kg) (Figs. 4). Inoculation with KSMs alone or co-inoculation with other plant growth promoting microorganisms (PGPMs)

enhanced K uptake, increased the availability of K in soil, and promoted growth of crops (Shrivastava et al., 2016). The results in agreement with the finding of Teotia et al. (2016) cleared that co-inoculation of PSB and KSB resulted in consistently higher P and K availability than in the control without bacterial inoculums.

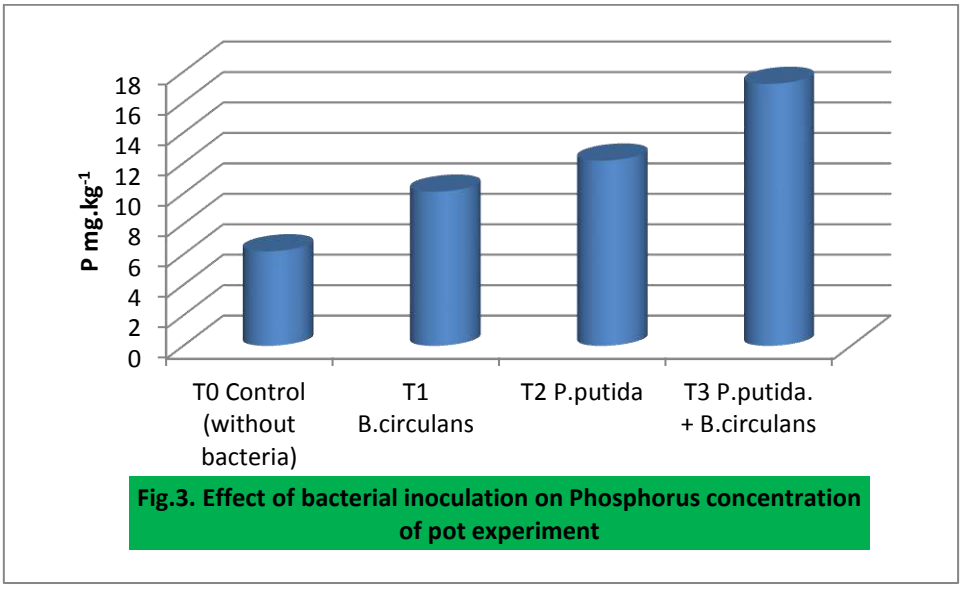

Fig.3. Effect of bacterial inoculation on Phosphorus concentration of pot experiment

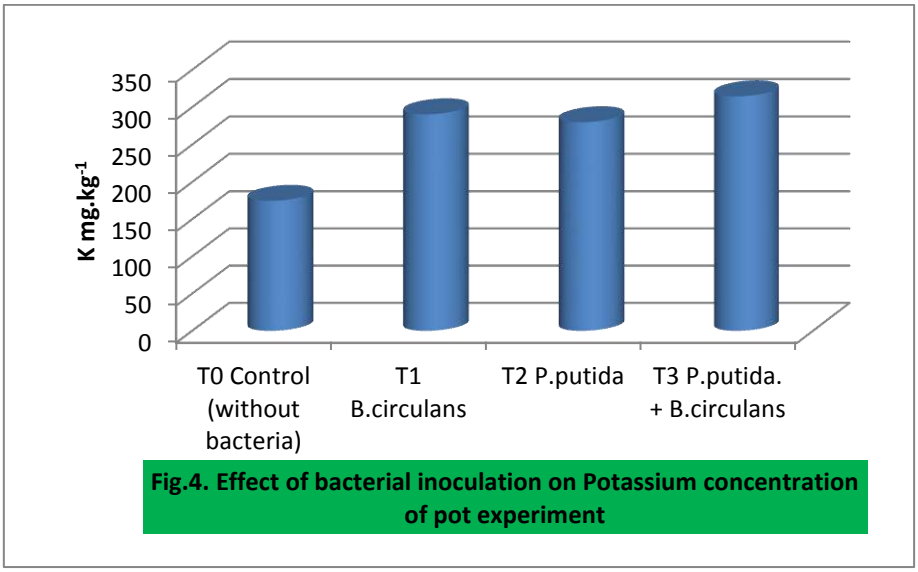

Fig.4. Effect of bacterial inoculation on Potassium concentration of pot experiment

Table 4.Effect of single and co-inoculation of (*Pseudomonas putida* and *Bacillus circulans*) biofertilizer on phosphorus and potassium uptake in Chickpea (*Cicer arientinum* L.) plant and on soil available phosphorus and potassium content

Treatments	P mg/plant	K mg/plant	P mg/kg	K mg/kg
T0 Control (withoutbacteria)	1. 24^{h}	16.32^{d}	6.21^{k}	174.8^{n}
T1*B.circulans*	1.628^{g}	29.48^{c}	10.13^{j}	290.5^{m}
T2 *Ps.putida*	3.77^{f}	26.65^{b}	12.17^{i}	279.9^{l}
T3*Ps.putida*+ *B.circulans*	6.35^{e}	65.75^{a}	17. 21^{h}	314.5^{k}

4. Conclusions

This study was conducted to prepare biofertilizer from local PSB and KSB strain and use to enhance plant growth and the nutrient uptake. Results suggested that prepared inoculums have a positive effect on chickpea plant growth and nutrient absorption when used as a single or combined inoculation of PSB and KSB. Specifically, inoculation increased several growth parameters (shoot dry weight, number of active nodules, shoot height, number of seedsand root length); the inoculation also improved available soil phosphorus and potassium, in addition to promotion of shoot phosphorus and potassium uptake compared to the non-inoculated treatments. *Pseudomonas putida* alone and in combination with *B.circulans* was found highly effective and significant enhancement in growth, nutrient content, increasing the plant available P and K in soil as well as the growth and yield of chickpea. Based on our results, local isolates of PSB and KSB can be used as biofertilizer to enhance soil fertility and plant growth.

5. References

ANJANADEVI, I. P., JOHN, N. S., JOHN, K. S., JEEVA, M. L. & MISRA, R. S. 2016. Rock inhabiting potassium solubilizing bacteria from Kerala, India: characterization and possibility in chemical K fertilizer substitution. *Journal of basic microbiology,* 56**,** 67-77.

BADR, M. 2006. Efficiency of K-feldspar combined with organic materials and silicate dissolving bacteria on tomato yield. *J Appl Sci Res,* 2**,** 1191-1198.

BAI, Y., ZHOU, X. & SMITH, D. L. 2003. Enhanced soybean plant growth resulting from coinoculation of Bacillus strains with Bradyrhizobium japonicum. *Crop science,* 43**,** 1774-1781.

BAKHSHANDEH, E., PIRDASHTI, H. & LENDEH, K. S. 2017. Phosphate and potassium-solubilizing bacteria effect on the growth of rice. *Ecological Engineering,* 103**,** 164-169.

BAREA, J.-M., POZO, M. J., AZCON, R. & AZCON-AGUILAR, C. 2005. Microbial co-operation in the rhizosphere. *Journal of experimental botany,* 56**,** 1761-1778.

BASAK, B. B. & BISWAS, D. R. 2010. Co-inoculation of potassium solubilizing and nitrogen fixing bacteria on solubilization of waste mica and their effect on growth promotion and nutrient acquisition by a forage crop. *Biology and Fertility of Soils,* 46**,** 641-648.

BRENNER, D. J., KRIEG, N. R., STALEY, J. T. & GARRITY, G. M. 2005. *Bergey's Manual® of Systematic Bacteriology: Volume Two: The Proteobacteria, Part A Introductory Essays*, Springer.

CASANOVA, E., VALDÉS, A. E., FERNÁNDEZ, B., MOYSSET, L. & TRILLAS, M. I. 2004. Levels and immunolocalization of endogenous cytokinins in thidiazuron-induced shoot organogenesis in carnation. *Journal of plant physiology,* 161**,** 95-104.

CHAIHARN, M. & LUMYONG, S. 2011. Screening and optimization of indole-3-acetic acid production and phosphate solubilization from rhizobacteria aimed at improving plant growth. *Current microbiology,* 62**,** 173-181.

CHITRA, K. & SHARAVANAN, P. 2014. Studies on Potassium Solubilizing Bacteria from Southern Indian Tea Soils. *Int. J. Curr. Microbiol. App. Sci,* 3**,** 1045-1052.

DATTA, M., BANIK, S. & GUPTA, R. 1982. Studies on the efficacy of a phytohormone producing phosphate solubilizingBacillus firmus in augmenting paddy yield in acid soils of Nagaland. *Plant and Soil,* 69**,** 365-373.

DHANDAPANI, P. 2011. Insoluble phosphate solubilization by bacterial strains isolated from rice rhizosphere soils from Southern India. *Int. J. Soil Sci,* 6**,** 134-141.

DOTANIYA, M. 2015. Impact of rising atmospheric CO2 concentration on plant and soil process. *Crop growth simulation modelling and climate change. Scientific Publisher, Jodhpur***,** 69-86.

GLICK, B. R. 1995. The enhancement of plant growth by free-living bacteria. *Canadian journal of microbiology,* 41**,** 109-117.

GULL, M., HAFEEZ, F., SALEEM, M. & MALIK, K. 2004. Phosphorus uptake and growth promotion of chickpea by co-inoculation of mineral phosphate solubilising bacteria and a mixed rhizobial culture. *Australian Journal of Experimental Agriculture,* 44**,** 623-628.

GUPTA, A., MEYER, J. M. & GOEL, R. 2002. Development of heavy metal-resistant mutants of phosphate solubilizing Pseudomonas sp. NBRI 4014 and their characterization. *Current Microbiology,* 45**,** 323-327.

GUPTA, G., PARIHAR, S. S., AHIRWAR, N. K., SNEHI, S. K. & SINGH, V. 2015. Plant growth promoting rhizobacteria (PGPR): current and future prospects for development of sustainable agriculture. *J Microb Biochem Technol,* 7**,** 096-102.

HAN, H. & LEE, K. 2005. Phosphate and potassium solubilizing bacteria effect on mineral uptake, soil availability and growth of eggplant. *Res J Agric Biol Sci,* 1**,** 176-180.

IAKHONTOVA, L., ANDREEV, P., IVANOVA, M. & NESTEROVICH, L. 1987. BACTERIAL DESTRUCTION OF SMECTITE MINERALS. *Doklady Akademii Nauk SSSR,* 296**,** 203-206.

KHAN, M. S., ZAIDI, A., WANI, P. A. & OVES, M. 2009. Role of plant growth promoting rhizobacteria in the

remediation of metal contaminated soils. *Environmental chemistry letters,* 7**,** 1-19.

KHOSHNAW, M., R.,A., & ESMAIL, A., O., 2020. Using Double Function Solubility Diagram to Study the Effect of Phosphorus Fertilizer on the Availability of Phosphorus in Different Soil Orders. *Zanco Journal of Pure and Applied Sciences.,* 32**,** 127-136.

KHUDHUR, A. M. 2017. Isolation and characterization of phosphate solubilizing bacteria in Erbil soil and study their effects on Cicer arietinum plant growth and phosphorus uptake. *Zanco Journal of Pure and Applied Sciences,* 29.

KPOMBLEKOU-A, K. & TABATABAI, M. 1994. Effect of organic acids on release of phosphorus from phosphate rocks1. *Soil Science,* 158**,** 442-453.

KUMAR, A., BHARGAVA, P. & RAI, L. C. 2010. Isolation and molecular characterization of phosphate solubilizing Enterobacter and Exiguobacterium species from paddy fields of Eastern Uttar Pradesh, India. *African Journal of Microbiology Research,* 4**,** 820-829.

LIU, M., LIU, X., CHENG, B.-S., MA, X.-L., LYU, X.-T., ZHAO, X.-F., JU, Y.-L., MIN, Z., ZHANG, Z. W. & FANG, Y. L. 2016. Selection and evaluation of phosphate-solubilizing bacteria from grapevine rhizospheres for use as biofertilizers. *Spanish journal of agricultural research,* 14**,** 26.

MARQUES, A. P., PIRES, C., MOREIRA, H., RANGEL, A. O. & CASTRO, P. M. 2010. Assessment of the plant growth promotion abilities of six bacterial isolates using Zea mays as indicator plant. *Soil Biology and Biochemistry,* 42**,** 1229-1235.

MAURYA, B., MEENA, V. S. & MEENA, O. 2014. Influence of Inceptisol and Alfisol's potassium solubilizing bacteria (KSB) isolates on release of K from waste mica. *Vegetos,* 27**,** 181-187.

MEENA, V., MAURYA, B. & BAHADUR, I. 2014a. Potassium solubilization by bacterial strain in waste mica. *Bangladesh Journal of Botany,* 43**,** 235-237.

MEENA, V. S., MAURYA, B. & VERMA, J. P. 2014b. Does a rhizospheric microorganism enhance K+ availability in agricultural soils? *Microbiological research,* 169**,** 337-347.

MIKHAILOUSKAYA, N. & TCHERNYSH, A. 2005. K-mobilizing bacteria and their effect on wheat yield. *Latvian Journal of Agronomy*.

MILANI, P. & ANTHOFER, J. 2008. Effect of Azotobacter and Azospirillum on the yield of wheat (Triticum aestivum) and barley (Hordeum vulgare) in Kermanshah and Lorestan, Iran. *Improving Water Productivity and Livelihood Resilience in Karkheh River Basin in Iran***,** 17.

NIANIKOVA, G., KUPRINA, E., PESTOVA, O. & VODOLAZHSKAIA, S. 2002. Immobilizing of Bacillus mucilaginosus--a producer of exopolysaccharides, on chitin. *Prikladnaia biokhimiia i mikrobiologiia,* 38**,** 300-304.

O'SULLIVAN, D. J. & O'GARA, F. 1992. Traits of fluorescent Pseudomonas spp. involved in suppression of plant root pathogens. *Microbiology and Molecular Biology Reviews,* 56**,** 662-676.

PANHWAR, Q. A., OTHMAN, R., RAHMAN, Z. A., MEON, S. & ISMAIL, M. 2012. Isolation and characterization of phosphate-solubilizing bacteria from aerobic rice. *African Journal of Biotechnology,* 11**,** 2711-2719.

PARK, J.-H., LEE, H.-H., HAN, C.-H., YOO, J.-A. & YOON, M.-H. 2016. Synergistic effect of co-inoculation with phosphate-solubilizing bacteria. *Korean Journal of Agricultural Science,* 43**,** 401-414.

PEI-XIANG, Y., LI, M., MING-HUI, C., JIA-QIN, X., FENG, H., CHANG-QUN, D., MING-HE, M., DUN-HUANG, F., YAN-QING, D. & FA-XIANG, Y. 2012. Phosphate solubilizing ability and phylogenetic diversity of bacteria from P-rich soils around Dianchi Lake drainage area of China. *Pedosphere,* 22**,** 707-716.

PEREIRA, S. I. & CASTRO, P. M. 2014. Phosphate-solubilizing rhizobacteria enhance Zea mays growth in agricultural P-deficient soils. *Ecological Engineering,* 73**,** 526-535.

PETTIGREW, W. T. 2008. Potassium influences on yield and quality production for maize, wheat, soybean and cotton. *Physiologia plantarum,* 133**,** 670-681.

PLAXTON, W. & LAMBERS, H. 2015. *Annual Plant Reviews, Phosphorus Metabolism in Plants*, John Wiley & Sons.

PRAJAPATI, K. & MODI, H. 2012. Isolation and characterization of potassium solubilizing bacteria from ceramic industry soil. *CIBTech J Microbiol,* 1**,** 8-14.

REHM, G. & SCHMITT, M. 2002. Potassium for crop production. *Retrieved February,* 2**,** 2011.

SARIKHANI, M. R., KHOSHRU, B. & GREINER, R. 2019. Isolation and identification of temperature tolerant phosphate solubilizing bacteria as a potential microbial fertilizer. . *World Journal of Microbiology and Biotechnology,,* 35**,** 126.

SARKER, A., TALUKDER, N. M. & ISLAM, M. T. 2014. Phosphate solubilizing bacteria promote growth and enhance nutrient uptake by wheat. *Plant Science Today,* 1**,** 86-93.

SHAIKH, S. S., SAYYED, R. Z. & REDDY, M. 2016. Plant growth-promoting rhizobacteria: an eco-friendly approach for sustainable agroecosystem. *Plant, Soil and Microbes.* Springer.

SHENG, X. F. & HE, L. Y. 2006. Solubilization of potassium-bearing minerals by a wild-type strain of Bacillus edaphicus and its mutants and increased potassium uptake by wheat. *Canadian journal of microbiology,* 52**,** 66-72.

SHRIVASTAVA, M., SRIVASTAVA, P. & D'SOUZA, S. 2016. KSM soil diversity and mineral solubilization, in relation to crop production and molecular mechanism. *Potassium solubilizing microorganisms for sustainable agriculture.* Springer.

SHWETHA, M. C. & LAKSHMAN, H. 2013. Effect of AM fungi, Azotobacter and Phosphate solubilizing bacteria in improvement of Amaranthus paniculatus L.-a leafy vegetable. *RESEARCH JOURNAL OF BIOTECHNOLOGY,* 8**,** 36-39.

SILINI-CHERIF, H., SILINI, A., GHOUL, M. & YADAV, S. 2012. Isolation and characterization of plant growth promoting traits of a rhizobacteria: Pantoea agglomerans lma2. *Pakistan Journal of Biological Sciences,* 15**,** 267.

SINDHU, S., SUNEJA, S., GOEL, A., PARMAR, N. & DADARWAL, K. 2002. Plant growth promoting effects of Pseudomonas sp. on coinoculation with Mesorhizobium sp. Cicer strain under sterile and "wilt sick" soil conditions. *Applied Soil Ecology,* 19**,** 57-64.

SINDHU, S. S., DUA, S., VERMA, M. & KHANDELWAL, A. 2010. Growth promotion of legumes by inoculation of rhizosphere bacteria. *Microbes for legume improvement.* Springer.

SINGH, J. S., PANDEY, V. C. & SINGH, D. 2011. Efficient soil microorganisms: a new dimension for sustainable agriculture and environmental development. *Agriculture, ecosystems & environment,* 140**,** 339-353.

TEOTIA, P., KUMAR, V., KUMAR, M., SHRIVASTAVA, N. & VARMA, A. 2016. Rhizosphere microbes: potassium solubilization and crop productivity–present and future aspects. *Potassium solubilizing microorganisms for sustainable agriculture.* Springer.

WALPOLA, B. C. & YOON, M.-H. 2013. Isolation and characterization of phosphate solubilizing bacteria and their co-inoculation efficiency on tomato plant growth and phosphorous uptake. *Afr J Microbiol Res,* 7**,** 266-275.

WU, S., CAO, Z., LI, Z., CHEUNG, K. & WONG, M. H. 2005. Effects of biofertilizer containing N-fixer, P and K solubilizers and AM fungi on maize growth: a greenhouse trial. *Geoderma,* 125**,** 155-166.

ZHANG, C. & KONG, F. 2014. Isolation and identification of potassium-solubilizing bacteria from tobacco rhizospheric soil and their effect on tobacco plants. *Applied Soil Ecology,* 82**,** 18-25.

ZANCO Journal of Pure and Applied Sciences
The official scientific journal of Salahaddin University-Erbil
https://zancojournals.su.edu.krd/index.php/JPAS

ISSN (print):2218-0230**, ISSN (online):** 2412-3986**, DOI: http://dx.doi.org/10.21271/zjpas**

RESEARCH PAPER

Evaluate the Quality of Some Imported Composts in Erbil Governorate

Shakar Jamal Aweez, Dalshad Azeez Darwesh, Faris Zaidan Jarjees

Department of Environmental sciences, College of Science, Salahaddin University-Erbil, Kurdistan Region, Iraq.

A B S T R A C T:

One of the main limitations concerning the use of compost as fertilizer materials is the uncertainty of nutrient availability to plants, especially Nitrogen (N) and Phosphorus (P), due to their presence in both organic and inorganic forms, which are not all immediately plant available. When a good quality compost is applied to an agricultural soil it could reconstitute soils and be an important fertilization backup. The present study was carried out to evaluate the quality of some imported composts in Erbil. The compost samples included 10 most common compost imported from different countries (Bulgari, Pakistan, Russia, Morocco, Egypt, Tabriz, Turkey, Poland, Malaysia, and Jordan) with five replications were bought in different local agrochemical market and shopping. Using a completely randomized design (CRD). The results revealed that the fertilizer index (FI) of imported compost was ranged from 4.42 to 4.92 while the clean index (CI) was ranged from 4.20 to 4.80, all composts have a fertilizer potential value >4. However, the clean index value of compost has medium-heavy metals content, the statistical analysis in the present study indicated that imported composts (Bulgari, Pakistan, Russia, Morocco, Egypt, Poland, Jordan) has a good quality, while (Tabriz, Turkey, Malaysia) are best and proper for agriculture land. In general, the mean concentrations of all heavy metals were lower than the permissible limit of Indian and German standards. However, the concentrations of Cd in Bulgaria, Pakistan, Morocco, Egypt, Tabriz, Poland, Jordan compost were higher than the permissible limit of Indian and Germany standards. In addition, the concentration of Ni in Bulgaria, Morocco, Turkey, Poland and Jordan higher than the Indian and Germany standards (Table 5 and 6).

KEY WORDS: Compost Quality; Fertilizer index; Clean index; Heavy Metals.
DOI: http://dx.doi.org/10.21271/ZJPAS.32.5.21
ZJPAS (2020) , 32(5);210-217 .

1. INTRODUCTION

Compost is resulted from the decomposition of organic matter. The compost involved garden waste, household solid waste, kitchen scraps, manure, leaves, grass clippings, and compost bears a little physical resemblance to the raw material from which it originated. Organic wastes can be degraded via a process called composting in order to divert its compounds into the more effective product which is appropriate to use for agricultural purposes. However, biodegradable wastes may contain pathogenic microorganisms, toxic elements and persistent organic compounds that may be toxic to the plants (Aweez and Darwesh, 2019).

Compost quality can be evaluated in terms of the presence of heavy metals because of their toxic potential to plant growths when incorporated into agricultural soil. High concentrations of heavy metals in compost can lead to phytotoxicity problems as well as may accumulate in the food chain and thus pose a health risk to both humans and the ecological food chain. In addition, high levels of heavy metals can have a profound impact on plant growth, morphology, and metabolism of soil microorganisms, and reduce both the population and activity of microbial pools, therefore decrease soil fertility. They bioaccumulate in ecological compartments when uptake by plants and transfer to humans through the food chain and thus human health problems

* **Corresponding Author:**
Shakar Jamal Aweez
E-mail: shakar.aweez@su.edu.krd
Article History:
Received: 04/03/2020
Accepted: 26/08 /2020
Published: 13/10/2020

and ecological concerns (Singh and Kalamdhad, 2012). Several studies were carried out around the world for assessing the compost quality index, especially the fertilizing and clean index by (Jalal, 2016; Jalal and Shekha 2019 and Aweez and Darwesh, 2019). Jalal and Shekha (2019) conducted a study on converting municipal solid wastes into compost which can be used as soil amendments. They evaluated the quality of several types of compost such as aerobic, anaerobic, pit and vermi-compost by measuring of selected several parameters. The composts are generally classified as extremely good quality according to CQI. Vaca et al., (2011) noted that soil amended with sewage sludge and sewage sludge compost increased organic matter (2.5-fold), phosphorus ($\geq$1.4-fold) and nitrogen content ($\geq$1.6-fold), as compared to the inorganically fertilized soil (N-P-K). Also they noticed that heavy metal such as Zn and Cu is an essential nutrient for plants which considered as present in sewage sludge. Angelova et al., (2013) reported that compost may increases heavy metals amount in the soil as it increases essential nutrients amount in soil, such as Pb, Cd, and Ni by compost. There are several parameters of compost quality that are well studied, but there are also new parameters that has been recently developed in order to make a better comparison among different types of composts. The quick increments in utilization in the application of compost to the soil especially in the nursery at 15 last years in Kurdistan region of Iraq expanding the interest composted. Many countries are now beginning to routinely publish compost guidelines with implied standards. A huge amount of several kinds of compost from different countries imported to this region without quality control and prehistoric analyses. Few data on the imported compost quality can be found. Moreover, there is a large demand of user for methods to assess the development and the quality of their composts. Since there are little or no studies about the quality of compost imported to Kurdistan region of Iraq for this reason this study aimed to evaluate the quality of some imported compost in the Erbil governorate.

2. Materials and methods:

2.1. Experimental design

This study was carried out in 2016 and 2017 to evaluate the quality of ten imported composts in the Erbil governorate**.** The composts were originally imported from Bulgari (C1), Pakistan (C2), Russia (C3), Morocco (C4), Egypt (C5), Tabriz (C6), Turkey (C7), Poland (C8), Malaysia (C9), and Jordan (C10) which were bought in different local agrochemical market and shopping. The samples collected and brought back to Environmental Sciences Department Laboratory, College of Science, Salahaddin University, where the laboratorial analyses carried out with five replications of each sample. Each sample was weighted in separate and then were dried at 65°C and then wet digested in the concentration of H_2O_2 and H_2SO4 acid (1/1, v/v) mixture using the producer of (Allen,1974). The samples were analyzed regarding these criteria: chemical criteria (organic carbon content), fertilizing parameters (total nitrogen, potassium, phosphorus), innocuousness parameters (heavy metals) and phytotoxicity parameters (germination index). The N content was measured by the distillation method of Ryan *et al.* (2001). The total phosphorus content was determined by the molybdenum blue colorimetric by spectrophotometric method (Olsen method), while the flame photometric method was used to determined potassium cations (Allen et al., 1974). The digested samples were used for determining the concentration of Cr, Cd, Pb, Cu, Ni and Zn by atomic absorption flame emission spectrophotometric and ICP (indicative coupled plasma) as described by (Pansu and Gautheyrou, 2006). Organic carbon from compost samples was determined by Walkely Black method using potassium dichromate procedure, the residual dichromate was titrated against ferrous sulfate as described by (Richards, 1954).

2.1.1 Germination index:

The germination test is a simple and reliable indicator of compost maturity. The seeds of wheat and chickpea were used for germination test, under three different compost extraction concentration were (30,60 and 100%). The germination tests included, the percentages of seed germination, root elongation and germination index (GI) after exposure to compost extracts were calculated according to Bera *et al.* (2013).as follow

$$\text{Seed germination \%} = \frac{\text{No. of seeds germinated in compost extract}}{\text{No. of seeds germinated in control}} * 100 \quad \ldots\ldots\ldots\ldots (1)$$

$$\text{Root elongation \%} = \frac{\text{Mean of root length in compost extract}}{\text{Mean of root length in control}} * 100 \quad \ldots\ldots\ldots\ldots\ldots\ldots (2)$$

$$\text{Relative germination index \%} = \frac{\text{Seed germination \%} - \text{Root elongation \%}}{10000} \ldots\ldots\ldots\ldots (3)$$

2.1.2. Fertilizing index:

The fertilizer index was calculated from the contents of the total organic compound (TOC), total organic nitrogen, total phosphorus (TP), soluble potassium (K) and C: N ratios as described by Saha *et al*., (2010). The MSW compost fertilization index is calculated using the formula:

$$\text{Fertilization index (FI)} = \sum \frac{S_i\, W_i}{W_i} \quad \ldots\ldots\ldots\ldots\ldots\ldots (4)$$

where 'Si' is a score value of analytical data, and 'Wi' is the weighing factor of the 'i'th fertility parameter (Table 1).

Table 1. Criteria for 'weighing factor' to fertility parameters and "score value" to compost (Saha*et al.*, 2010). Note: dm= dry matter.

Fertility	Score Value (Si)					Weight
Parameters (%dm)	5	4	3	2	1	Factor (Wi)
TOC	> 20.0	15.1-20.00	12.1-15	9.1-12	> 9.1	5
TN	> 1.25	1.01-1.25	0.81-1.0	0.51-0.80	> 0.51	3
TP	> 0.60	0.41-0.60	0.21-0.40	0.11-0.20	> 0.11	3
TK	> 1.00	0.76-1.00	0.51-0.75	0.26-0.50	> 0.26	1
C:N ratio	< 10.10	10.1-15	15.1-20	20.1-25	< 25	3

2.1.3. Clean index:

Calculation, heavy metal concentrations (Cr, Pb, Cd, Cu, Ni, and Zn) were used according to Mandal *et al*. (2014). The following formula was used to calculate the Clean Index value:

$$\text{Clean index (CI)} = \sum \frac{S_j\, W_j}{W_j} \quad \ldots\ldots\ldots\ldots\ldots\ldots\ldots (5)$$

where 'Sj' is the score value of analytical data, and 'Wj' is weighing factor of the 'j'th heavy metal (Table 2).

Table 2. Criteria for assigning 'weighing factor' to heavy metal parameters and 'score value' to analytical data (Saha*et al.*, 2010)

Heavy Metal	Score Value (Si)						Weighting
(mg kg^{-1} dm)	5	4	3	2	1	0	Factor (Wi)
Zn	< 151	151-300	301-500	501-700	701-900	> 900	1
Cu	< 51	51-100	101-200	201-400	401-600	> 600	2
Cd	< 0.3	0.3-0.6	0.7-1.0	1.1-2.0	2.0-4.0	> 4.0	5
Pb	< 21	51-100	101-150	151-250	251-400	> 400	3
Ni (mg/kg dm)	< 10.10	21-40	41-80	81-120	121-160	> 160	1
Cr (mg/kg dm)	< 51	51-100	101-150	151-250	251-350	> 350	3

2.1.4 Statistical analysis

The experiment was designed in a completely randomized design (CRD). Data were statistically analyzed using SPSS version 24. All data expressed as the mean value. The difference among the means of compost types was compared by applying Duncan multiple comparison tests at a level of a significant 5% (Steele and Torrie, 1969)

3. Results and discussion:

The portrayal of compost and its comparison with FCO (Fertilizer Control Order) standard endorsed by the Indian government and the standard of Hong Kong. The total organic matter (TOM) is important to compost quality parameters, generally the total organic carbon values in all imported compost is greater than the permissible limit of Hon Kong standard which is ≥20, the higher percentage is 33.31 estimated from Malaysia compost. Carbon and nitrogen ratios are very important characteristics for estimation the compost maturity with respect to the organic matter and the nitrogen cycle, the carbon-nitrogen ratio is directly related to the plant growth, because when the plant cultivated in soil amended with compost have higher carbon-nitrogen ratio the plant growth hinders and often yellow in color due to nitrogen deficiency arising out of nitrogen immobilization in that soil. Although the data analysis in this study refers to a significant difference among the studied compost the carbon and nitrogen ratio are less than the permissible limit of Indian standard which is <20. 6.5-7.5, as shown in (Table 7) the nitrogen phosphorus and potassium are important nutrients for plant growth, anyway assume an important role in compost quality determination. The statistical analysis shows a significant difference among the essential nutrients such as nitrogen, phosphorus, and potassium from the compost. It also shows that the higher values (2.92, 3.22 and 0.52%) for nitrogen, potassium and phosphorus were recorded in Egypt, Bulgaria and Pakistan compost respectively, the Nitrogen % is higher than the permissible limit of Indian standard, however, the K% was more than the permissible limit of Indian standard except in Malaysia compost was less, while the phosphorus% in all compost is lower than the permissible limit of Indian standard. Non-essential heavy metals detection in compost is greatly importance for the quality, not only because of these elements necessary to protect the soil and water resource from pollution, but also their impact on human health. In general, the mean concentrations of all heavy metals were lower than the permissible limit of Indian and German standards. However, the concentrations of Cd in Bulgaria, Pakistan, Morocco, Egypt, Tabriz, Poland, Jordan compost were higher than the permissible limit of Indian and Germany standards. Particularly it is concentration in Tabriz is very higher, thus its unsuitable to agriculture use because the exceeded heavy metals content limited the application of compost to the

agriculture soil. In addition, the concentration of Ni in Bulgaria, Morocco, Turkey, Poland and Jordan higher than the Indian and Germany standards (Table 5 and 6). The typical values of heavy metal concentrations and maximum concentration recommended for intensive compost are presented in Table (6). The impact of contaminated of compost by pollutants on environmental health is varies according to soil properties such as texture, cation exchange capacity of the soil (CEC), soil mineral types, the ability of soil to absorption of pollutants and the plant species (Zhao *et al.*, 2011).

The grades and marketability of compost depended largely on the germination, fertilizer index and clean index, also these three indices provide the information about the suitability of compost for a particular application. The germination index (GI) is the ratio of seeds that germinate and grow on an aqueous extract of compost compared to seeds that germinate and grow on water. With GI under 0.7, the compost aqueous extract is considered as phytotoxic for plant growth. Above 1.0, the compost aqueous extract proves to have a direct positive effect on plant growth. Data in the Table (3) showed that various sorts of compost were significantly at ($p \leq 0.05$) influenced the germination index of wheat and chickpea seed. The highest values (1.453 and 1.093) recorded in (Tabriz, Poland) treatment respectively. This result translated that the addition of organic matter to soil provide plant accessible supplement and expanded the wheat grain yield, besides an application of compost perhaps progress soil physical, chemical and biological properties such as water infiltration, water holding capacity, concentration of macro and micro nutrients, bulk density, cation exchange capacity and activity of microorganisms. The presence of essential micro and macronutrients is also important for plant growth and thus additionally diminished bulk density. These results are similar to those recorded by Youssef *et al.* (2013) who detailed that maximum wheat grain yield was recorded for the wheat plant treated with bio fertilizer such as effective microorganisms and tea compost. Akhtar *et al*., (2014) suggest the use of 5 tons ha^{-1} of mung bean residues with 2.5kg ha^{-1} of humic acid to improve. Iqbal (2014) take notes that all levels and sources of compost-based organic material had a significant effect on the yield and yield parameters of autumn maize. Data in Table (4) indicated that different composts dose was significantly at ($p \leq 0.05$) affected on germination of wheat and chickpea seed. The highest index values were (1.553 and 0.907) were recorded in (30 % and 60 %) compost doses respectively. This result appeared that an application organic matter improved soil with N, P, K, and other nutrients, expanded nutrient aggregation, improved nutrients uptake and yield components. These results agreed with those have been reported by Bekeko (2014). He found out than an application of farmyard manure alone or in combination with in organic fertilizer helps in proper doses replenishing of most deficient macro and micro nutrients which in turn help in getting the highest grain yield. Fertilizer index and clean index of imported compost are shown in Figure (1). The fertilizer index of compost was varied from 4.42 to4.92 whereas the clean index was varied from 4.20 to 4.80, all compost has a fertilizer potential value >4, however, the CI value of compost has medium-heavy metals content, the statistical analysis in the present study indicated that all imported compost are good while Tabriz, Turkey, and Malaysia consider as best quality.

Table 3. Effect of different types of compost on germination index of wheat and chickpea seeds

Compost types	Germination index of Wheat seed	Germination index of Chickpea seed
C1	1.443a	1.047a
C2	1.140a	0.590b
C3	1.403a	1.060a
C4	1.383a	0.943a
C5	1.146a	0.420b

C6	1.453a	1.017a
C7	1.423a	1.027a
C8	1.430a	1.093a
C9	1.430a	1.007a
C10	1.173a	0.507b

Table 4. Effect of compost dose on germination index of wheat and chickpea seeds

Compost doses%	Germination index of Wheat seed	Germination index of Chickpea seed
30	1.553a	0.870a
60	1.304b	0.907a
100	1.171b	0.836a

Table 5. The concentration of some heavy metals in different types of composts.

Heavy metal mg.kg^{1}	Types of imported composts									
	C1	**C2**	**C3**	**C4**	**C5**	**C6**	**C7**	**C8**	**C9**	**C10**
Pb	6.29c	19.60a	15.50b	7.52c	22.5a	6.33c	11.70b	7.71c	6.24c	15.30b
Cu	2.11c	2.73bc	3.18b	2.05c	5.06a	2.92bc	3.08bc	6.10a	2.03c	3.20b
Ni	**50.02b**	43.81c	35.80e	**60.20a**	42.98c	27.18d	**52.20b**	**71.8a**	48.70b	**52.30b**
Zn	25.60c	15.80d	45.70a	32.20b	20.30c	6.05e	22.80c	40.80a	23.80c	16.70d
Cr	30.36c	45.18a	20.18d	23.80d	35.25c	40.23bc	33.80c	22.30d	43.50a	10.80e
Cd	**6.52c**	**20.80a**	1.87d	**15.30b**	**5.40c**	**22.20a**	3.30cd	**9.04c**	1.56d	**5.89c**

Table 6. Recommended metal limits for heavy use rates of compost for vegetables, with typical soil levels (Brinton, 2000).

Heavy Metals	Standard Values		Maximum Concentration recommended for intensive compost	Typical values for soils mg.kg^{-1}
	Germany	India		

Pb	150	100	75	12 – 100
Cu	150	300	50	3 – 20
Ni	50	50	30	4 – 50
Zn	400	1000	200	14 – 125
Cr	150	50	75	5 – 100
Cd	3	5	0.75	0.3 – 0.7

Table 7. The fertility parameter values of different types of composts.

Fertility parameters %	**Types of composts**										**Standard values** (Germany ranges)
	C1	**C2**	**C3**	**C4**	**C5**	**C6**	**C7**	**C8**	**C9**	**C10**	
N	2.62a	2.87a	2.71a	1.98c	2.92a	1.68c	2.41b	2.01bc	1.23c	2.38b	1.66-1.77
K	3.22a	2.96a	3.08a	2.18bc	1.96c	1.72c	3.12a	2.08bc	0.90d	2.51b	0.60-1.14
P	0.18c	0.52a	0.31b	0.25c	0.36b	0.23c	0.10e	0.43a	0.32bc	0.20c	1.59-1.80
TOC	32.84a	32.75a	32.81a	33.05a	32.74a	33.15a	32.91a	33.04a	33.31a	32.92a	15.7-16.92
C:N	12.53c	11.41c	12.11c	16.69bc	11.21c	19.73b	13.65c	16.44bc	27.08a	13.83c	8.89-10.51

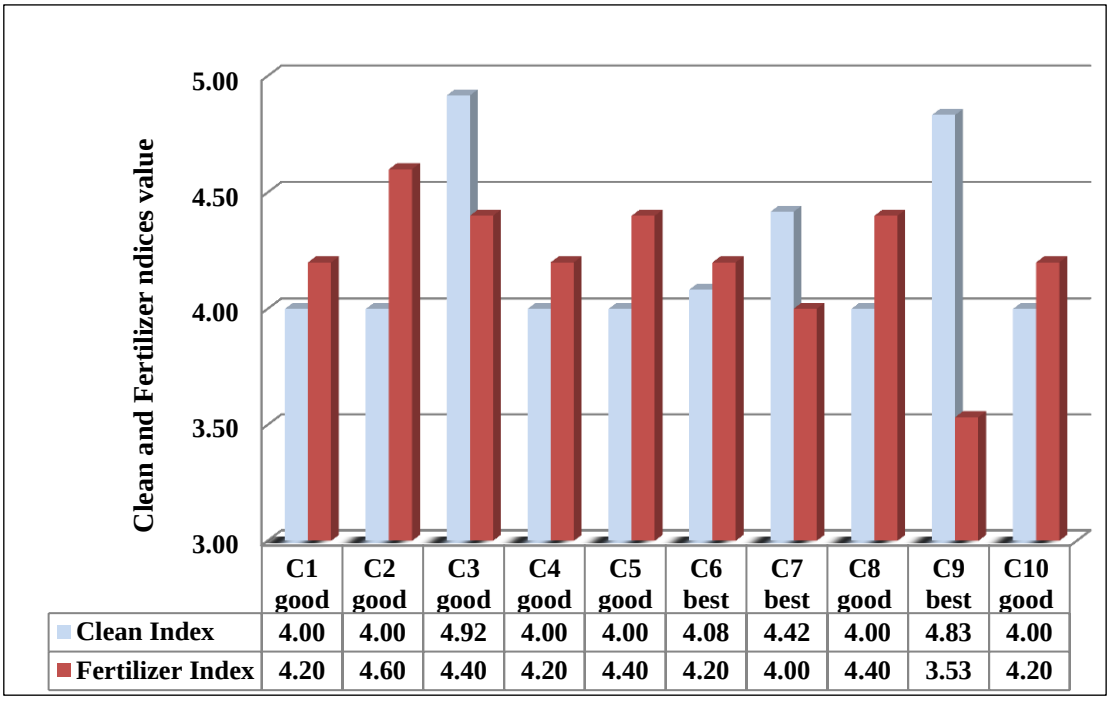

Figure 1. The Clean and fertilizers indices values of differences composts

4. Conclusion:

This study was aimed to evaluate the quality of ten imported composts from different countries in the Erbil governorate. The physic-chemical and phytotoxicity of the ten composts samples (five replications) demonstrated that the application of different types of compost with three different concentrations 30%, 60%, 100% significantly increase germination index of wheat and chickpea seeds. The highest values were found in Tabriz and Poland compost respectively. According to CI and FI (Tabriz, Turkey, Malaysia) consider the best quality, while (Bulgari, Pakistan, Russia, Morocco, Egypt, Poland, Jordan) have very good quality compost. In general, the mean concentrations of all heavy metals were lower than the permissible limit of Indian and Germany standards except Ni and Cd were higher than permissible levels in most imported composts. Phytotoxicity is generally related to the presence of phytotoxic molecules such as ammonia and easily biodegradable organic molecules such as volatile fatty acids. It underlines the fact that most imported composts are mainly mature and less biodegradable (stable). Further studies can investigate the correlation between physic-chemical characteristics of composts, sensory parameters such as (color, moisture and odors), biodegradation extent and phytotoxic effect of composts.

References

AWEEZ, SH. J., DARWESH, D. A. 2019. Assessment clean index and fertilizer index of some imported composts to Erbil city. Zanco Journal of Pure and Applied Sciences. 31(4):123-128.

ALLEN, S. E. 1974. Chemical analysis of ecological materials. Black well scientific publication Osney Mead, Oxford. pp: 64-214

BERA, R., DATTA, A., BOSE, S., DOLUI, A. K., CHATTERJEE, A. K., DEY, G. C., BARIK, A. K., SARKAR, R. K., MAJUMDAR, D. and SEAL, A. 2013. Comparative evaluation of compost quality, process convenience and cost under different composting methods to assess their large-scale adoptability potentials also complemented by compost quality index, International Journal of Scientific and Research Publications, 3(6): p.1-11.

BRINTON, W., 2000. *COMPOST QUALITY STANDARDS & GUIDELINES*. New York: Woods End Research Laboratory , Inc.

JALAL S. Y. 2016. Applied Compost Quality indices for Assessment Different Composting Methods by Using Household Solid Waste. M.Sc thesis of College of Science, Salahaddin University-Erbil.

JALAL S.Y., SHEKHA Y. A. 2019. Compost quality assessment for the household solid wastes of Erbil city. Zanco Journal of Pure and Applied Sciences.31.

MANDAL, P., CHATURVEDI, M. K., BASSIN, J. K., VAIDYA, A. N. and GUPTA, R. K. 2014. Estimating the quantity of solid waste generation in oyo, Int J Recycle Org Waste Agricult., 3: p.133139.

MORA, A. P.; BURGOS, P.; MADEJO'N, E.; CABRERA, R.; JAECKEL, P.; SCHLOTER, M. 2006. Microbial Community Structure and Function in a Soil Contaminated By Heavy Metals: Effects of Plant Growth and Different Amendments. Soil biology and biochemistry. 38:327-341.

PANSU, M, and GAUTHEYROU, J. 2006. Handbook of soil Analysis.Springer-velageBerlinHeidelberg.3:1-38.

RICHARDS, L. A. 1954. Diagnosis and Improvement of Saline and Alkaline Soils United States Salinity Laboratory Staff, USA. Hand Book No.60

SAHA, J. K., PANWAR, N. and SINGH, M. V. 2010. An assessment of municipal solid waste compost quality produced in different cities of India in the perspective of developing quality control indices, Waste Management, 30: p.192-201.

SINGH, J. and KALAMDHAD, A. S. 2012 . Reduction of Heavy Metals during Composting. International Journal of Environmental Protection. 2(9):36-43.

STEEL, R.G.D and TORRIE, J.H. 1969. Principle and Procedures of Statistics. McGraw Hill, New York.481pp

ZHAO S,I,JAN and, DUO,I. 2011. EDTA associated phytoextraction of heavy metals by turf grass from municipal solid waste compost using permeable barriers and potential leaching risk. Bioresour.Tech.102:621-626.

IQBAL, S. 2014. Impact of level and source compost based organic material on the productivity of Autumn Maize (Zea Mays L.). Pakistan journal of agricultural science.51 (1):1-7.

VACA, R., LUGO,J.MRTINEZ,R.,ESELLER,M.V.AND ZAVALETA.H.2011.Effects of sewage and sludge compost Amendment on soil properties and *Zea Mays* L.plants (Heavy Metals, Quality and Productivity). International contamination Ambienete.27 (4):303-311.

ZANCO Journal of Pure and Applied Sciences
The official scientific journal of Salahaddin University-Erbil
https://zancojournals.su.edu.krd/index.php/JPAS

ISSN (print):2218-0230**, ISSN (online):** 2412-3986**, DOI: http://dx.doi.org/10.21271/zjpas**

RESEARCH PAPER

Assessing Microbial and Biochemical Quality Indicators of Tanos Treated Soils

Hawser Khurshid Mawlood , Nashmeel Saeed Khudhur[1]

[1]Department of Environmental Science and Health, College of Science, Salahaddin University-Erbil, Kurdistan Region, Iraq

A B S T R A C T:

Different doses of tanos fungicide and two soil textures in combination (2×4: soil texture × fungicide doses) were studied in a pot experiment under chickpea cultivation to determine their effects on certain soil chemical, biochemical and microbiological properties. The main results showed that: clayey soil showed highest pH, enzymatic activities and microbial population during this study. Tanos doses showed significant changes in soil EC, reduced urease (R^2 = 0.9775), dehydrogenase (R^2 = 0.8806) and nitrate reductase (R^2 = 0.8541) activities. Whereas, significant increases in bacterial and fungal population in response to tanos doses were observed after two months. According to paired *t* test results, different tanos doses, as well as the combination effects between soil textures and tanos doses have significantly changed fungal population, urease, dehydrogenase and nitrate reductase activities after two months of experiment. The combined treatment S2D3 showed the lowest nitrate reductase activity, bacterial and fungal counts during the study. A significant correlation (R^2 = 0.8581) was observed between urease activity and bacterial population.

KEY WORDS: Soil Enzymes, Bacteria, Fungi, Fungicide, Tanos.
DOI: http://dx.doi.org/10.21271/ZJPAS.32.5.22
ZJPAS (2020), 32(5); 218-225.

1. INTRODUCTION

Soil is the vital component of natural environment and it is important as plants, animals, rocks, landforms and rivers that influences the distribution of plant species and provides habitat for a wide range of organisms. Soil controls the flow of water and chemicals between atmosphere and earth, acting as a source and storage of gasses in the atmosphere (Nortcliff *et al.*, 2006). Soil needs to be conserved and improved its performance and productive capacity. A wide range of pollutants, especially pesticides and heavy metals are stored in agricultural soils in several regions of the world (Bünemann *et al*., 2006).

Soil pollution by pesticides may relate to the accumulation of pesticides and chemical elements in the soil in a situation where they become more than natural (Usman *et al*., 2017).

The application of fungicides to soil to control plant diseases has become a common practice in crop production in many parts of the world. Fungicides are bio-toxicants which interfere not only with the biochemical and the physiological reactions of the target plant pathogens, but also influence population or activity of other non-target microorganisms in soil (Chen *et al*., 2001). Concern over the effects of fungicides on soil processes is because microbes mediate many of the reactions in nutrient cycling; there is also the possibility that fungicides can enter into the food chain and, thus, affect higher organisms including humans (Monkiedje and Spiteller, 2002).

Tanos 50WG is a double-component combined and systemic fungicide used to protect potatoes from potato blight and potato leaf spot caused by *Alternaria* sp., tomatoes from potato

* **Corresponding Author:**
Nashmeel Saeed Khudhur
E-mail: nashmeel.khudhur@su.edu.krd or nashmeel@gmail.com
Article History:
Received: 25/01/2020
Accepted: 03/05/2020
Published: 13/10 /2020

blight, cucumbers and zucchini from *Peronospora* cucumber, and vines from *Peronospora* soybean and chickpea. The active substance of Tanos is cymoxanil 250g.kg^{-1} [1-[(E/Z)-2-cyano-2-methoxyiminoacetyl]-3-ethylurea] and famoxadone 250g.kg^{-1} [(RS)-3-anilino-5-methyl-5-(4-phenoxyphenyl)-1,3- oxazolidine-2,4-dione]. It is formulated as: dispersible granule (Sasvary and Supinova, 2016).

Soil enzymes are considered as valuable parameters for assessing the side effects of pesticide treatments on soil microbial biomass and microbiological potential (Gundi *et al*., 2005). It has detected that some pesticides changed soil enzyme activity. Soil enzymes are essential in catalyzing reactions necessary for decomposition of organic matter and nutrient cycling because they are important in energy transfer, environmental quality and crop productivity. Enzymes are closely related to organic elements transformation which induced by microorganisms (Cycon *et al*., 2005).

Despite the good results of pesticides in agriculture and public health like increasing crop yield, economic boost, decreasing fatalities from pest-borne diseases; their use usually accompanied with undesirable environmental, health effects and crop production especially from repeated application. Thus, the present work aims to determine the effects of different doses of tanos fungicide on soil quality indicators regarding to enzymatic activities and microbial communities in two different textured soils under cultivated chickpea plant.

2. MATERIALS AND METHODS

2.1. Experimental layout and statistical analysis

Two different soil textures with no history of prior pesticide-use from Shaways (clayey) and Aski Kalak (sandy loam) were collected in May 2019 and brought to the greenhouse, where gravels and stones were separated, screened, crushed, air-dried, and 4-mm sieved. Tanos fungicide obtained from Dubbana Company was prepared on the base of its active ingredient as given by Hill (2008) at four different doses (D1, no tanos fungicide treatment; D2, recommended dose; D3, double and D4, ten-fold doses). The two soils were separately sprayed with tanos fungicide at its different doses, and left an overnight at room temperature.

Eight combined treatments were set up each with three replications in a factorial experiment (2×4, two soil textures and four different doses) combined with Completely Randomized Design (CRD).

The experiment last for two months and included two sampling periods. For this purpose 24 pre-labeled and similar plastic pots (with average diameter 27 cm and height 25 cm) were filled with 5 kg pesticide-treated soil and a sample was taken from each pot. The pots were provided by a below-container to collect the irrigation water and return-back to the pots as described by (Khudhur and Sarmamy, 2019). The pots were irrigated at 60% of field capacity. Statistical analysis was performed using SPSS version 23 and Microsoft Office Excel 2019 and the means were compared using Duncan's Multiple Range test at level of significant of 0.05. Paired t test was applied to find out the differences between the sampling periods.

2.2. Laboratory analyses

2.2.1. Soil chemical characteristics

Soil pH was assessed using standardized pH-meter with pH buffers (4, 7 and 9) and EC was detected by calibrated EC-meter with KCl solution in 1:1 (soil: water suspension). Soil organic matter was detected by Walkley-Black procedure as described by Ryan *et al*. (2001).

2.2.2. Estimation of soil enzymes

Urease activity was determined by the modified approach of Hoffmann and Teicher 1961 described by (Uzun and Uyanoz, 2011). After incubating urea-induced soils for 3 hours at 30°C, the formatted ammonium was observed spectrophotometrically at 636 nm (Bashour and Sayegh, 2007). Modified method of Casida 1977 given in Anjaneyulu *et al.*, (2011), was used for dehydrogenase estimation. Soils were introduced with 3% aqueous solution of triphenyl tetrazolium chloride (TTC) and incubated at 30°C for 24 hours. The produced triphenyl tetrazolium formazone was measured at 485 nm. Standard protocol for nitrite estimation in solutions was

followed for estimation of nitrate reductase as given by Nath and Samanta (2012). Soils were incubated in peptone water media with 1% KNO_3 at 30 °C for 3 hours and the supernatants were treated with sulphanilamide and the pink color solutions were estimated at 540 nm. The catalase enzyme was detected by $KMnO_4$ titration method as given by Kumar (2004). Soils were amended with H_2O_2 and the rest of the peroxide was balanced out by 3N H_2SO_4 and the aliquots were titrated with 0.1 N $KMnO_4$.

2.2.3. Microbial population counting

For bacterial counting from soil samples, 1g of soil was serially diluted in sterile distilled water and 1 ml of soil suspensions from 10^{-1} to 10^{-7} was spread on the nutrient agar plate. The growth of the bacterial colonies were observed after 24 hours of incubation at 30°C in inverted position (Khudhur *et al.*, 2016). For counting of total soil fungi, Sabouraud dextrose agar was prepared. Then 0.2 mg Chloramphinicol was added. Serial dilution was performed and 1 ml of 10^{-3} to 10^{-7} dilutions were poured in each Petri dish containing prepared medium (PDA + Chloramphinicol) by sterile pipette, each sample made by three replication plates and incubated at 25 °C for 10 days (Khudhur and Abdulla, 2016).

3. RESULTS AND DISCUSSION

Soil pH considered as an important soil quality indicator affecting on soil microorganisms and enzymatic activity (Martinez *et al.*, 2010). Soil pH values of clay-textured soil was highest during both sampling periods (8.48 ± 0.217^{a}) and (8.47 ± 0.074^{a}), however, soil pH showed no significant changes toward fungicide doses (Table 1) in the first sampling.

Table 1: Effect of soil texture, tanos doses and their combinations on soil chemical characteristics (Mean±S.D.).

Treatments	Soil pH		Soil EC (µS.cm^{-1})		Soil organic matter (%)	
	1st sampling	2nd sampling	1st sampling	2nd sampling	1st sampling	2nd sampling
S1	**8.47 ± 0.217^{a}**	**8.47 ± 0.074^{a}**	**284.25 ± 64.59^{b}**	**387.75 ± 85.63^{a}**	**0.69 ± 0.326^{b}**	1.25 ± 0.297
S2	**8.34 ± 0.189^{b}**	**8.33 ± 0.086^{b}**	**385.00 ± 120.4^{a}**	**229.91 ± 64.14^{b}**	**1.44 ± 0.302^{a}**	1.46 ± 0.656
t value	**1.000 (NS)**		**0.200 (NS)**		**-1.074 (NS)**	
D1	8.44 ± 0.278	**8.47 ± 0.082^{a}**	**247.83 ± 47.40^{c}**	348.16 ± 166.9^{a}	**1.18 ± 0.228^{a}**	1.51 ± 0.390
D2	8.31 ± 0.143	8.40 ± 0.079^{ab}	293.66 ± 58.15^{c}	**264.00 ± 97.72^{b}**	1.11 ± 0.287^{ab}	1.34 ± 0.483
D3	8.45 ± 0.255	**8.36 ± 0.126^{b}**	358.00 ± 95.03^{b}	**353.50 ± 80.42^{a}**	**0.89 ± 0.481^{b}**	1.48 ± 0.249
D4	8.43 ± 0.156	**8.36 ± 0.105^{b}**	**439.00 ± 117.5^{a}**	269.66 ± 51.99^{b}	1.09 ± 0.834^{ab}	1.09 ± 0.781
t value	**0.236 (NS)**		**0.813 (NS)**		**-2.352 (NS)**	
S1D1	8.24 ± 0.260^{c}	**8.53 ± 0.060^{a}**	254.33 ± 70.06^{cd}	**495.66 ± 62.18^{a}**	1.03 ± 0.137^{bc}	1.17 ± 0.069^{cd}
S1D2	8.42 ± 0.113^{bc}	8.45 ± 0.072^{ab}	266.33 ± 78.23^{cd}	329.66 ± 32.81^{bcd}	0.89 ± 0.182^{c}	**0.91 ± 0.105^{d}**
S1D3	**8.68 ± 0.056^{a}**	8.46 ± 0.060^{a}	277.00 ± 43.27^{cd}	420.66 ± 28.01^{ab}	0.51 ± 0.210^{d}	1.44 ± 0.344^{abc}
S1D4	8.54 ± 0.136^{ab}	8.43 ± 0.102^{ab}	339.33 ± 59.91^{c}	305.00 ± 13.23^{bcd}	**0.34 ± 0.137^{d}**	1.49 ± 0.173^{abc}
S2D1	8.63 ± 0.110^{ab}	8.42 ± 0.072^{ab}	**241.33 ± 24.11^{d}**	200.66 ± 22.30^{d}	1.33 ± 0.210^{b}	**1.86 ± 0.137^{a}**
S2D2	**8.21 ± 0.085^{c}**	8.36 ± 0.072^{ab}	321.00 ± 9.643^{cd}	**198.33 ± 99.29^{d}**	1.33 ± 0.173^{b}	1.77 ± 0.173^{ab}
S2D3	8.22 ± 0.032^{c}	**8.26 ± 0.086^{b}**	439.00 ± 31.95^{b}	286.33 ± 43.02^{cd}	1.28 ± 0.278^{b}	1.51 ± 0.182^{abc}
S2D4	8.31 ± 0.057^{c}	8.29 ± 0.036^{ab}	**538.66 ± 33.62^{a}**	234.33 ± 53.26^{abc}	**1.83 ± 0.210^{a}**	1.69 ± 1.000^{bc}
t value	**0.101 (NS)**		**0.420 (NS)**		**-1.171 (NS)**	
	NS: paired t value non-significant. **** : paired t value highly significant at $p \leq 0.001$.**					

Although the second sampling, showed changes in pH as the double and ten-fold doses of tanos has caused slight reductions in soil pH (8.36), but, these changes were not significant (*t* value = 0.236). Hicks *et al.* (1990) reported that pH affects the athletic behavior of the pesticide molecule on clay and organic surfaces and thus the chemical speciation, mobility and bioavailability of the molecule and this seem to confirm the present findings. Fungicide doses have showed significant changes in soil EC during both sampling periods (Table 1). In treatments received double and ten-fold dose, the EC values were 353.50 ± 80.42^{a} and 439.00 ± 117.5^{a} µS.cm^{-1} respectively, and the combined treatments S2D4 and S1D1 revealed highest soil EC (538.66 ± 33.62^{a} and 495.66 ± 62.18^{a} µS.cm^{-1}) respectively. Soil organic matter has significant effects on microbial activity due to its nature as a nutrient sink and a source that can enhance soil physical and chemical properties and promote biological activity (Fontaine *et al.*, 2003). Soil organic matter have been increased in the combinant treatment S2D4 (1.83 ± 0.210^{a}).

Soil enzymatic activity is an indication for living cell activity as well as the concentration of soil colloids and humic substances can be used as soil contamination indicators (Bello *et al.*, 2013). Urease is a soil enzyme that catalyzes urea hydrolysis into CO_2 and NH_3 and is a key component of the soil nitrogen content (Sarathchandra *et al.*, 1984). Clayey soil showed highest and significant urease activity during both sampling periods 78.705 ± 10.986^{a} and 112.005 ± 21.564^{a} µg N-NH_4^+.g^{-1}.$3h^{-1}$ respectively (Table 2).

Table 2: Effect of soil texture, tanos doses and combinations on soil urease and dehydrogenase activities (Mean±S.D.).

Treatments	Urease (µg N-NH_4^+.g^{-1}.$3h^{-1}$)		Dehydrogenase (TPF µg.g^{-1}.$24h^{-1}$)	
	1st sampling	2nd sampling	1st sampling	2nd sampling
S1	**78.705 ± 10.986^{a}**	**112.005 ± 21.564^{a}**	**609.792 ± 18.086^{a}**	19.722 ± 4.214
S2	**42.420 ± 11.372^{b}**	**88.915 ± 28.132^{b}**	**160.077 ± 73.210^{b}**	13.561 ± 6.374
t value	**-6.047 (NS)**		**1.661 (NS)**	
D1	**72.350 ± 20.917^{a}**	105.450 ± 10.612^{ab}	**450.187 ± 237.041^{a}**	17.182 ± 6.519^{ab}
D2	67.270 ± 18.864^{a}	97.450 ± 10.573^{ab}	424.852 ± 218.627^{b}	**20.208 ± 4.780^{a}**
D3	55.010 ± 21.583^{b}	**89.870 ± 38.629^{b}**	333.219 ± 258.362^{c}	16.326 ± 2.411^{ab}
D4	**47.620 ± 20.299^{c}**	**109.070 ± 37.724^{a}**	**331.479 ± 271.805^{c}**	**12.851 ± 8.359^{b}**
t value	**-5.504****		**12.381****	
S1D1	**90.380 ± 9.983^{a}**	96.600 ± 4.160^{cde}	**666.285 ± 18.086^{a}**	22.230 ± 1.459^{a}
S1D2	84.040 ± 4.014^{a}	88.680 ± 4.151^{de}	624.384 ± 4.057^{b}	**24.133 ± 2.792^{a}**
S1D3	74.300 ± 5.765^{b}	124.940 ± 4.607^{ab}	568.962 ± 12.352^{c}	15.928 ± 2.614^{b}
S1D4	66.100 ± 0.510^{b}	**137.800 ± 8.990^{a}**	579.538 ± 1.204^{c}	16.597 ± 2.464^{b}
S2D1	54.320 ± 4.350^{c}	114.300 ± 4.160^{bc}	234.089 ± 7.020^{c}	**12.133 ± 5.258^{b}**
S2D2	50.500 ± 5.466^{c}	106.220 ± 4.151^{bcd}	225.321 ± 6.311^{c}	16.283 ± 1.763^{b}
S2D3	35.720 ± 3.875^{d}	**54.800 ± 4.435^{e}**	97.476 ± 0.811^{d}	16.725 ± 2.687^{b}
S2D4	**29.140 ± 2.311^{d}**	80.340 ± 31.63^{e}	**83.420 ± 9.693^{d}**	21.87 ± 11.248^{a}
t value	**-2.416****		**4.264****	
	NS: paired t value non-significant. **** : paired t value highly significant at $p \leq 0.001$.**			

Tanos doses significantly affected urease activity (R^2 = 0.9775), it was observed that with increasing tanos dose will decrease urease enzyme activity (47.620 ± 20.299^{c}) µg N-NH_4^+.g^{-1}.$3h^{-1}$ as supported by (Figure 1).

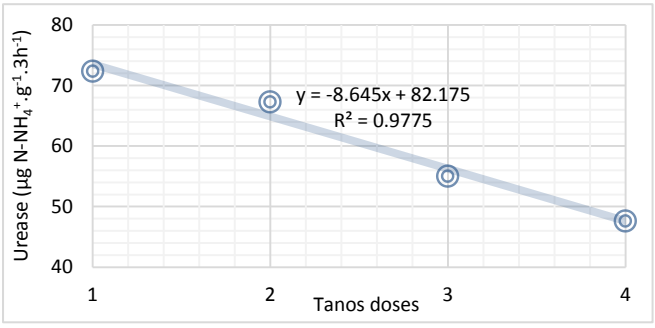

Figure 1: Correlation between tanos doses and urease activity during the first sampling.

Floch *et al.* (2011) stated that pesticides may have a direct impact on enzymes by inhibiting their catalytic ability, or by involving in the alteration of microbial activity and this may confirm this situation. Moreover, different tanos doses have significantly changed urease activity after two months of experiment according to *t* value (-5.504^{**}, $p \leq 0.001$) (Table 2). The combination effects of both soil texture and fungicide doses were significantly affected urease activity, the highest urease was observed in S1D1 (90.380 ± 9.983^{a}) and S1D4 (137.800 ± 8.990^{a}), whereas the lowest activities were detected in S2D4 (29.140 ± 2.311^{d}) and S2D3 (54.800 ± 4.435^{e}) during both sampling periods respectively. These decreases in urease activities may refer to reducing urea hydrolysis due to tanos fungicide use in accordance with (Antonious, 2003). Dehydrogenase activities were decreased as tanos doses increased during the studied periods (Table 2 and Figure 2).

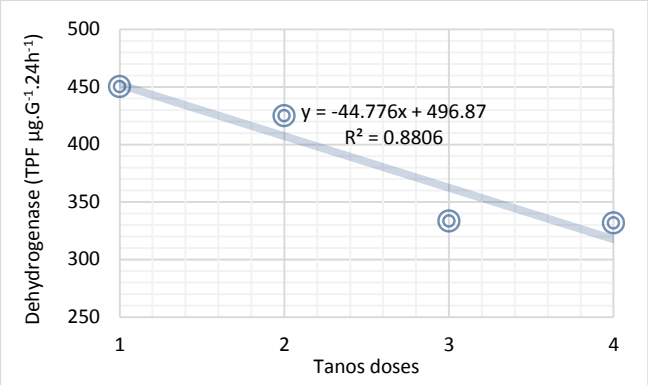

Figure 2: Correlation between tanos doses and dehydrogenase activity during the first sampling.

Its activity was sharply decreased during the second sampling period with the highest recorded *t* value (12.381**) (Figure 3).

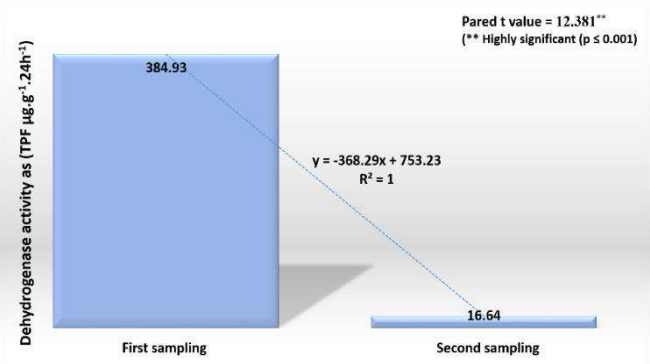

Figure 3: Dehydrogenase responses to different tanos doses during both sampling periods.

The reported sensitivity of dehydrogenase to the adverse effects of pesticides is consistent with many studies (Cycon *et al.*, 2005). Significant changes have observed between the sampling periods (*t* value of -5.132**) regarding to nitrate reductase activity (Table 3). During the second sampling, significant reduction has observed in responses to tanos doses as supported by (Figure 4).

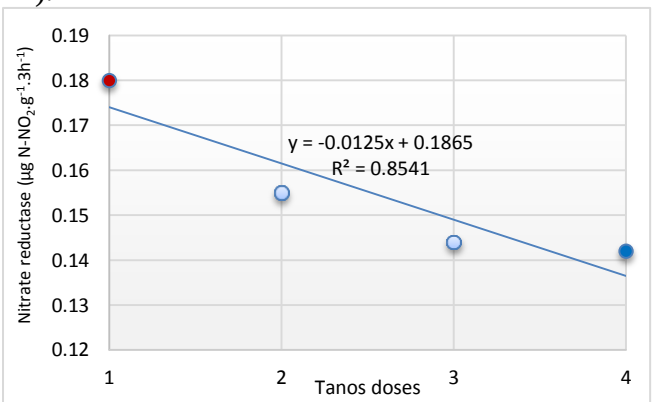

Figure 4: Correlation between tanos doses and nitrate reductase activity during the second sampling.

The combined treatment S2D3 showed the lowest value of nitrate reductase activity 0.061 ± 0.005^{f} and 0.106 ± 0.009^{e} (µg N-NO_2.g^{-1}.$3h^{-1}$) during both sampling periods respectively. While the highest activity was in control S2D1 (0.226 ± 0.0327^{a} µg N-NO_2.g^{-1}.$3h^{-1}$) during the second sampling. Catalase is an intracellular enzyme found in all aerobic bacteria and most facultative anaerobic bacteria, but not present in binding anaerobic agents (Trasar-Cepeda *et al.*, 2000). During the second sampling, catalase has increased slowly and the lowest value was recorded in control S2D1 (9.933 ± 0.351^{c} ml $KMnO_4$.g^{-1}.$20min^{-1}$) (Table 3).

Table 3: Effect of soil texture, tanos doses and combinations on nitrate reductase and catalase (Mean±S.D.).

Treat-ments	Nitrate reductase (µg N-NO_2.g^{-1}.$3h^{-1}$)		Catalase (ml $KMnO_4$.g^{-1}.$20min^{-1}$)	
	1st sampling	2nd sampling	1st sampling	2nd sampling
S1	**0.135 ± 0.032^{a}**	0.151 ± 0.023	**9.616 ± 0.032^{a}**	11.941 ± 0.023
S2	**0.073 ± 0.012^{b}**	0.159 ± 0.051	**11.708 ± 0.012^{b}**	11.541 ± 0.051
t value	-1.457 (NS)		-0.866 (NS)	
D1	0.110 ± 0.028^{b}	**0.180 ± 0.055^{a}**	**10.116 ± 1.149^{b}**	**10.566 ± 0.794^{b}**
D2	**0.132 ± 0.056^{a}**	0.155 ± 0.028^{b}	10.216 ± 1.227^{b}	**12.533 ± 1.318^{a}**
D3	0.089 ± 0.031^{c}	0.144 ± 0.044^{b}	**11.266 ± 1.148^{a}**	12.233 ± 1.543^{a}
D4	**0.085 ± 0.021^{c}**	**0.142 ± 0.015^{b}**	11.050 ± 2.044^{ab}	11.633 ± 0.999^{a}
t value	-5.132**		2.528 (NS)	
S1D1	0.135 ± 0.014^{b}	0.133 ± 0.012^{de}	9.633 ± 1.563^{d}	11.200 ± 0.500^{bc}
S1D2	**0.183 ± 0.017^{a}**	0.138 ± 0.014^{cde}	**9.200 ± 0.754^{d}**	13.400 ± 1.081^{a}
S1D3	0.117 ± 0.005^{c}	0.182 ± 0.021^{b}	10.333 ± 0.702^{cd}	11.033 ± 0.611^{bc}
S1D4	0.105 ± 0.001^{c}	0.152 ± 0.004^{bcd}	9.300 ± 1.081^{d}	12.133 ± 1.258^{ab}
S2D1	0.086 ± 0.009^{d}		10.600 ± 0.400^{cd}	**9.933 ± 0.351^{c}**
S2D2	0.082 ± 0.007^{de}	0.173 ± 0.028^{bc}	11.233 ± 0.305^{bc}	11.666 ± 0.960^{b}
S2D3	**0.061 ± 0.005^{f}**	**0.106 ± 0.009^{e}**	12.200 ± 0.435^{ab}	**13.433 ± 1.123^{a}**
S2D4	0.065 ± 0.000^{ef}	0.131 ± 0.016^{de}	**12.800 ± 0.0300^{a}**	11.133 ± 0.404^{bc}
t value	-2.566**		-1.640 (NS)	

NS: paired t value non-significant.
: paired t value highly significant at $p \leq 0.001$.

Moreover, the highest catalase values were in the combined treatments S2D3 (12.800±0.0300[a]) and S2D4 (13.433±1.123[a] ml $KMnO_4.g^{-1}.20min^{-1}$) respectively during both sampling periods, it is therefore difficult to detect a clear response of this enzymatic activity to pesticides, as this enzyme has received little attention in the last 10 years (Trasar-Cepeda *et al.*, 2000). According to the presented data in (Table 4), bacterial and fungal population were higher in clayey soil than the sandy loam soil during both sampling periods.

Table 4: Effects of soil texture, tanos doses and their combinations on soil total microbial population (Mean).

Treat-ments	Total bacteria×10^6 cfu.g^{-1} dry soil		Total fungi×10^5 cfu.g^{-1} dry soil	
	1st sampling	2nd sampling	1st sampling	2nd sampling
S1	**35.259[a]**	**35.490[a]**	**35.259[a]**	**35.490[a]**
S2	**2.011[b]**	**27.053[b]**	**2.011[b]**	**27.053[b]**
t value	**-1.019 (NS)**		**-1.614 (NS)**	
D1	27.027	31.027[b]	7.336[a]	**58.712[b]**
D2	28.058	**27.790[b]**	5.101[a]	59.835[b]
D3	4.818	30.780[b]	**1.180[b]**	117.613[ab]
D4	14.636	**35.488[a]**	**5.741[a]**	**152.510[a]**
t value	**-1.985 (NS)**		**3.926[**]**	
S1D1	**52.92[a]**	27.88[c]	**14.08[a]**	97.86[b]
S1D2	50.56[a]	24.96[c]	8.678[b]	98.01[b]
S1D3	9.448[b]	43.76[a]	2.319[c]	**225.5[a]**
S1D4	28.11[ab]	**45.35[a]**	11.34[b]	213.1[a]
S2D1	1.135[b]	34.173[b]	0.597[c]	19.56[b]
S2D2	5.561[b]	30.619[bc]	1.524[c]	21.66[b]
S2D3	**0.189[b]**	**17.797[d]**	**0.042[c]**	**9.702[b]**
S2D4	1.160[b]	25.622[c]	0.145[c]	91.90[b]
t value	**-1.475 (NS)**		**-3.200[**]**	
	NS: paired t value non-significant. **[**] : paired t value highly significant at $p \leq 0.001$.**			

Significant increase in bacterial population in response to tanos doses was observed during the second sampling, so the highest tanos dose (D4) showed highest bacterial population (35.488×10^6 cfu.g^{-1} dry soil) and fungal population (5.741×10^5 cfu.g^{-1} dry soil). This situation, as stated by (Kalia and Gosal, 2011), may refer to the ability of microorganisms to use pesticides as growth C source, a fraction of the used pesticide, as demonstrated in (Figure 5).

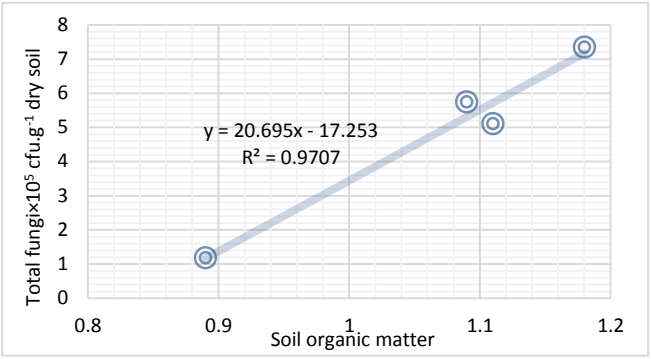

Figure 5: Correlation between soil organic matter and total fungal population during the study.

Moreover, it is well documented that with certain pesticides, repeated applications can promote microbial populations capable of selectively degrading that fungicide and various pesticides may degrade by bacterial isolates (Kanekar *et al.*, 2004). Furthermore, soil enzyme activities are greatly affected by organic matter content of the soil and often are used as indices of microbial activity, soil fertility and pollution (Cycon *et al.*, 2005). According to the observed data, a significant correlation (R^2 = 0.8581) was observed between urease activity and bacterial population (Figure 6).

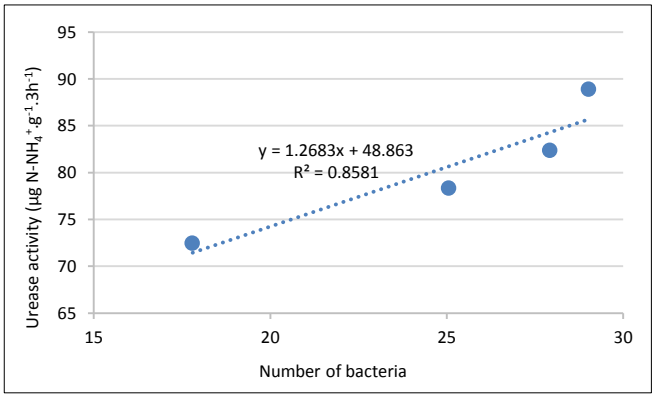

Figure 6: Correlation between bacterial population and urease activity during the second sampling.

However, the numbers of bacteria were directly proportional with urease enzyme activity in the soil. In this regard, Sarathchandra *et al*. (1984) stated that urease is producing by large number of bacteria. The highest tanos dose (D4) revealed the highest fungal population during both samplings (5.741 $\times 10^5$ cfu.g^{-1} dry soil) and (152.51 $\times 10^5$ cfu.g^{-1} dry soil) respectively (Figure 7) and the differences between the two sampling periods was significant (*t* value = 3.926** at $p \leq 0.001$).

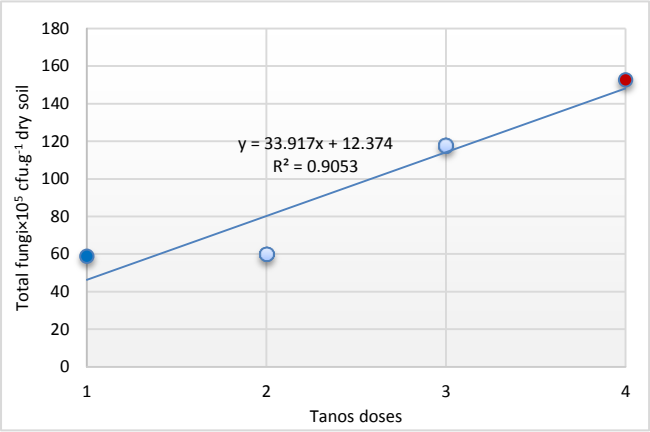

Figure 7: Correlation between tanos doses and soil fungi during the second sampling.

The statement of (Rajbongsh *et al.*, 2014) who state that the fungal population has typically decrease following fungicide application, but it slowly recover from the deleterious effect of fungicides applied to the soil over time, may confirm our findings. Although there were increases in bacterial and fungal population during the second sampling, but the combined treatment S2D3 showed the lowest bacterial number (0.189 and 17.797 $\times 10^6$ cfu.g^{-1} dry soil) and fungal count (0.042 and 9.702 $\times 10^5$ cfu.g^{-1} dry soil) during both sampling periods respectively. While, S1D3 showed the highest fungi number (225.5 $\times 10^5$ cfu.g^{-1} dry soil) during the second sampling. The combined effect of soil texture and pesticide doses showed significant differences between the two sampling periods (*t* value = -3.200** at $p \leq 0.001$).

4. CONCLUSIONS

Microbial and biochemical soil parameters are identified soil quality assessment indicators. From the results of this investigation we concluded that long-term and repeated fungicide applications interfere with soil biochemical balance, which can reduce soil fertility and productivity by affecting local metabolism and enzymatic activity especially the dehydrogenase, as shown by tanos doses especially double and tenfold doses. Tanos fungicides affect non-target and beneficial microorganisms and their behaviors, which are important for preserving soil fertility, as revealed during the first sampling, while a recovery of soil bacteria and fungi population was observed after two months of experiment.

Acknowledgements

The Authors acknowledge with many thanks to Mr. Dindar Fareeq Shex in the Ministry of Trade and Industry /Quality Control Center, who supported all laboratory works of the present study were performed in.

Conflict of Interest

The authors have no Conflict of Interest.

REFERENCES

Anjaneyulu, E., Ramgopal, M., Narasimha, G. and Balaji, M. 2011. Effect of pig iron slag particles on soil physico-chemical, biological and enzyme activities. *Iranica J. Energy & Environment*, 2(2): 161-165.

Antonious, G.F. 2003. Impact of soil management and two botanical insecticides on urease and invertase activity. *J. Environ. Sci. Health B*, 38, 479-488.

Bashour I.I. and Sayegh, A.H. 2007. Methods of Analysis for Soils of Arid and Semi-Arid Regions. Food and Agriculture Organization of the United Nations, Rome.

Bello, D., Trasar-Cepeda, C., Leirós M.C. and Gilsotres, F. 2013. Modification of enzymatic activity in soils of contrasting pH. *Soil Biol Biochem*, 56:80-86.

Bünemann, E., Schwenke, G., and Van Zwieten, L. 2006. Impact of agricultural inputs on soil organisms-a review. *Australian Journal of Soil Research*, 44(4), 379-406.

Chen, S.K., Edwards, C.A. and Sulber, S. 2001. Effects of the fungicides benomyl, captan and chlorothalonil on soil microbial activity and nitrogen dynamics in laboratory incubations. *Soil Biology and Biochemistry*, 33: 1971-1980.

Cycon, M., Kaczyñska, A. and piotrowska-Seget, Z. 2005. Soil enzyme activities as indicator of soil pollution by pesticides. *Pestycydy*, (1-2), 35-45. ISSN 0208-8703.

Floch, C., Chevremont, A.C., Joanico, K., Capowiez, Y. and Criquet, S. 2011. Indicators of pesticide contamination functional diversity of bacterial

communities via Biolog Ecoplates. *Eur J Soil Biol* 47: 256-263n.

Fontaine, S., Marotti, A. and Abbadie, L. 2003. The priming effect of organic matter: a question of microbial competition. *Soil Biology & Biochemistry*, 35: 837-843.

Gundi, V., Narasimha, G. and Reddy, B.R. 2005. Interaction Effects of soil insecticides on microbial populations and dehydrogenase activity in a black clay soil. *J. Environmental Science and Health, Part B*, 40(2): 269-283.

Hicks, R.J., Stotzky, G. and Voris, P.V. 1990. Review and evaluation of the effects of xenobiotic chemicals on microorganisms in soil. *Adv Appl Microbiol*, 35:195-253.

Hill, D.S. 2008. Pests of Crop in Warmer Climates and their Control. Springer Netherlands. XII Edition. 708pp.

Kalia, A. and Gosal, S.K. 2011. Effect of pesticide application on soil microorganisms. *Agronomy and Soil Science*, 57(6):569-596.

Kanekar, P.P., Bhadbhade, B., Deshpande, N.M. and Sarnai, S.S. 2004. Biodegradation of organophosphorus pesticides. *Proc. Indian Natl. Sci. Acad.*, Part B70 (1): 57-70.

Khudhur, N.S. and Abdulla, N.Q.F. 2016. Soil fungal population study related to oil pollution along different distances from Kawrgosk Oil Refinery of Erbil-Iraq. *Al-Anbar J. of Agr. Sci.*, 14(2): 1e-15e.

Khudhur, N.S. and Sarmamy, A.O.I. 2019. Determination of diazinon residues in artificially polluted soils. *ZANCO Journal of Pure and Applied Sciences*, 31(5): 1-8.

Khudhur, N.S., Khudhur, S.M. and Ameen, N.O.H. 2016. A Study on soil bacterial population in Steel Company and some related area in Erbil City in relation to heavy metal pollution. *ZANCO Journal of Pure and Applied Sciences*, 28(5): 101-116.

Kumar, A. 2004. Industrial pollution and management, In, Study of correlation of physical, chemical and biological characteristics with catalase activity in industrially polluted and unpolluted soils of Warangal (D.T.) A.P. by Kumari B.L. and Charya M.A., APH Publishing. New Delhi, pp. 134-138.

Martinez, M.M., Gutiérrez, V., Jannsens, M. and Ortega, R. 2010. Biological soil quality indicators: a review. Current Research, Technology and Education Topics in Applied Microbiology and Microbial Biotechnology, pp. 319-328.

Monkiedje, A. and Spiteller, M. 2002. Effects of the phenylamide fungicides, mefenoxam and metalaxyl, on the microbiological properties of a sandy loam and a sandy clay soil. *Biol Fertil Soils*, 35: 393-398.

Nath, R. and Samanta, R. 2012. Soil pH, microbial population, nitrate reductase and alkaline phosphatase activities of different environment of Dibrugarh district, Assam. *Advances in Applied Science Researc*h, 3(3): 1772-1775.

Nortcliff, S., Hulpke, H., Bannick, C.G., Terytze, K., Knoop, G., Bredemeier, M. and Schulte-Bisping, H. 2006. Soil, definition, function, and utilization of soil. Wiley-VCH Verlag GmbH & Co. KGaA, Weinheim, Vol. 33: 309-420. *DOI: 10.1002/14356007.b07_613.pub3*

Rajbongshi, P., Devashree, Y. and Kumardutta, B. 2014. A study on the effect of some fungicides on the population of soil microflora. *Journal of international academic research for multidisciplinary*, 1(12).

Ryan, J., Estefan, G. and Rashid, A. 2001. Soil and Plant Analysis Laboratory Manual. Second Edition. International Center for Agricultural Research in the Dry Areas (ICARDA), Aleppo, Syria. 172 pp.

Sarathchandra, S.U., Perrott, K.W. and Upsdell, M.P. 1984. Microbiological and biochemical characteristics of a range of New Zealand soils under established pasture. *Soil Biol. Biochem*. 16, 177-183.

Sasvary and Supinova 2016. Accidental Cymoxanil (TANOS) pesticide poisoning (Case report). *Clinical Social Work and Health Intervention*, 7(3): 27-31.

Trasar-Cepeda C., Leirós M.C., Seoane S. and Gil-Sotres F. 2000. Limitations of soil enzymes as indicators of soil pollution. *Soil Biology and Biochemistry*, 32: 1867–1875.

Usman, S., Kundiri, A.M. and Nzamouhe, M. 2017a. Effects of organophosphate herbicides on biological organisms in soil medium- A mini review. *Journal of Ecology and Toxicology*, 1(1):1-5.

Uzun, N. and Uyanoz, R. 2011. Determination of urease catalase activities and CO_2 respiration in different soils obtained from in semi-arid region Konya, Turkey. *Trends Soil Sci. Plant Nutr. J*., 2(1): 1-6.